UNIVERSITY OF SHEFFIELD
Department of Civil and Structural Engineering

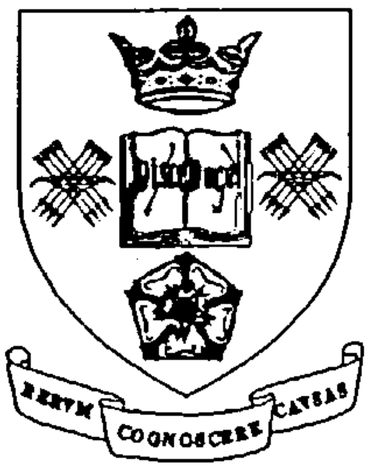

Developments in Modelling of Composite Building Structures in Fire

by ***Jun Cai***

January 2002

A thesis submitted in partial fulfilment of the requirements for the Degree of Doctor of Philosophy

Department of Civil and Structural Engineering
University of Sheffield
Sir Frederic Mappin Building
Mappin Street
Sheffield S1 3JD
United Kingdom

ABSTRACT

Some concern has been expressed that the load capacity of corner columns might be reduced in fire due to the expansion of unprotected fire-exposed connected beams, even through the columns themselves are protected from fire. A structural analysis program VULCAN has been used to perform a series of parametric studies on corner sub-frames. In order to obtain the best possible representation of the column cross-section, the formulation of beam-column elements was developed to allow the cross-section to be divided into large numbers of segments. The analyses indicate that the existing fire design codes, such as BS5950: Part 8, give an un-conservative result. The finite element method is shown to be capable of modelling this type of sub-frame, but is too complex to be used routinely. As an alternative, a generalised simplified approach to enable a rapid assessment of the sub-frame by hand or spreadsheet calculation has been developed. The results, in comparison with the finite element analyses, give some confidence in the use of this approach.

The beam-column elements of the program VULCAN were further developed to model the three-dimensional behaviour of asymmetric steel beams for fire conditions. The general approach, including the principles and details of the modifications to the formulation for asymmetric cross-sections, together with the refinement of the cross-section, are presented. The modified program has been validated by comparison with classical analytical results and test results at ambient and high temperatures.

A new generalised beam model has been developed, which can model not only reinforced concrete sections but also steel sections of different shapes including hollow sections, for three-dimensional composite structures at ambient and high temperatures. The method currently includes both geometrical and material non-

linearities and considers the cracking and crushing of concrete. Several material models have been included, especially for concrete in tension which shows significant effects on the results. The thermal expansion and degradation of both steel and concrete materials with elevated temperatures are also included. The cross-section is divided into an appropriate number of segments so that non-uniform temperature profiles, and variations of strain and stress across the section, can be represented with more accuracy. The formulation is used to further develop the program VULCAN, and is then validated by comparison with theoretical and experimental results.

CONTENTS

LIST OF FIGURES

List of Tables

NOTATION

(Only the general notations used during this thesis are presented here. Symbols which have only been used once and are of a more specific nature have been clearly explained where they arise in the text).

A	area of cross-section;
A_t, B_t, n_t	temperature-dependent constants;
$[\overline{A}]$	geometric description matrix;
$\langle \overline{B} \rangle$	non-linear strain-displacement vector;
$\langle B_0 \rangle$, $\langle \overline{B}_L \rangle$	small and large displacement strain-displacement vectors;
$\langle \overline{B}_{xz} \rangle$, $\langle \overline{B}_{yz} \rangle$	non-linear shear strain-displacement vectors;
[C]	constitutive matrix;
E_t	tangent modulus;
$f_{c,\theta}$, $f_{t,\theta}$	concrete compressive and tensile strengths at elevated temperatures;
f_x, f_y	shear forces parallel to x, y directions;
G	shear modulus;
I_x, I_y	first moments of area for an element;
I_{x2}, I_{y2}	second moments of area for an element;
I_{xy}	product second moment of area for an element;
I_{xn}, I_{yn}, I_{xnyn}	higher (n^{th} order) moments of area (Appendix);
$I_{\omega n}$, $I_{\omega xn}$, $I_{\omega yn}$	(n^{th} order) sectorial properties for an element;
J	St. Venant torsion constant;
$\overline{K}$	Wagner coefficient;
$[k_c]$	constant vector;
$[K_0]$	small linear displacement stiffness matrix;
$[K_L]$	large displacement stiffness matrix;
$[K_\sigma]$	geometric matrix;
$[K_t]$	element tangent stiffness matrix in local coordinates;
$[K_T]$	element tangent stiffness matrix in global coordinates;

m_x , m_y	stress resultants for internal moments about the x and y axes;
m_{x2} , m_{y2}	stress resultants for internal second moments about the x and y axes,
m_{z2}	stress resultant for torsional moment;
m_ω	stress resultant for warping bimoment;
n	stress resultant for internal axial force;
N	number of segments in either half-flange or half-web of the cross-section;
[N]	shape function matrix;
q_i	nodal displacement in local coordinates;
$\{\Delta q\}$	vector of incremental nodal displacements corresponding to unbalanced forces in local coordinates;
$\{Q\}$	vector of externally nodal forces in local coordinates;
$\{Q^R\}$	vector of internally nodal forces in local coordinates;
$\{\Delta Q\}$	load vector of nodal unbalanced forces in local coordinates;
$\{\Delta r\}$	vector of incremental nodal displacements corresponding to unbalanced forces in global coordinates;
{R}	vector of applied nodal loads in global coordinates;
$\{R^R\}$	vector of internally nodal forces in global coordinates;
$\{\Delta R\}$	load vector of nodal unbalanced forces in global coordinates;
T_ω , T_{sv}	twisting moments due to the warping shear stress and St. Venant shear stress;
T_σ	Wagner effect;
[T]	transformation matrix;
ΔT	increment in temperature;
u , v , w	displacements of an arbitrary point A in axes z, y, x;
u_0 , v_0 , w_0	displacements of the reference axis in axes z, y, x;
V_x , V_y	stress resultant for internal axial force;
W	virtual work;
x, y, z	local co-ordinates;
α	coefficient of thermal expansion;
ω	sectorial co-ordinate of the arbitrary point A;

ν	the Poisson's ratio;
$\varepsilon_{cr,\theta}$	concrete tensile strain at peak stress;
$\varepsilon_{cu,\theta}$	concrete strain corresponding to $f_{c,\theta}$;
ε_0, ε_L	axial strains under small and large displacements;
ε_z	axial strain at the arbitrary point A;
ε_{zt}	total axial strain;
ε_{zm}	mechanical axial strain;
ε_{zth}	thermally-induced axial strain;
ε_{zr}	residual axial strain;
θ_x, θ_y	rotations of infinitesimal segment about axes y, x;
θ_z	twist angle about reference axis z;
γ_{xz}, γ_{yz}	shear stains;
σ_z	axial stress;
τ_{xz}, τ_{yz}	shear stresses;
{ }	denotes a column vector;
< >	denotes a row vector;
[ ]	denotes a matrix;
$[\ ]^{-1}$	denotes a matrix inverse.

ACKNOWLEDGEMENT

The author would like to thank Prof. Ian Burgess and Prof. Roger Plank for their excellent supervision and kind help during this PhD study, and also to be grateful to his colleagues at the Steel Fire Research Group, especially to Dr. Zhaohui Hung, for their support and help. The financial support from SCI and Department of Civil & Structural Engineering, and Overseas Research Scholarship is greatly appreciated.

Finally, the author would like to express his gratitude to his wife, Minquan Feng, for her help and support both in life and academic aspect, and to his parents for their patience and encouragement from P. R. China.

DECLARATION

Except where specific reference has been made to the work of the work of others, this thesis is the result of my own work. No part of it has been submitted to any other University for a degree, diploma or other qualification.

Jun Cai

1. INTRODUCTION AND BACKGROUND

1.1 INTRODUCTION

Steel Structures are extensively used in Industrial and Civil Engineering due to steel's advantages as a relatively cheap material with fast erection, high strength and light weight. However, the big disadvantage of steel as a structural material is its vulnerability to elevated temperatures. Under fire conditions steel loses a considerable amount of strength and stiffness, so the fire resistance of steel framed buildings becomes important. Active and passive fire protection measures are normally adopted in buildings to reduce danger to persons and property. The former is used for fire detection and extinction; the latter is more common and covers the fire-resistant structural systems which include: applied fire insulation, bare steel designed to structural fire engineering principles, composite steel-concrete members (partially encased/concrete filled steel sections), integrated structural elements (steelwork built into walls, ceilings or floors), water cooled systems, etc[1].. At present the most common method of protecting the structure from the effects of fire is simply to apply a prescribed amount of thermal insulation. However, this method lacks systematic and in-depth analysis and is believed in many cases to be highly uneconomic. An analysis of UK fire statistics shows that the major causes of fatalities are smoke and burns, (which account for more than 97 percent of all deaths) -- not building collapse[2][3].

Two real fire incidents are given here as examples. One recent fire incident occurred in a partly completed 14 storey office block on the Broadgate Phase 8 development in London in 1990. Despite the lack of fire protection, there was no overall failure of structural elements and the floor slab maintained its integrity. Another fire incident occurred in the Mercantile Credit Insurance Building (twelve storeys) in Basingstoke

UK in 1991. The building was protected for 90 minutes' fire resistance. During the fire, the fire protection performed well and there was no permanent deformation to the steel frame. After the fire the fire protection was replaced, although visually it appeared undamaged, and the steel structure required no repair and was reused.

It is, therefore, becoming increasingly important and interesting to understand the behaviour of whole structures, especially that of bare-steel frames in fire. It is preferable from an engineering point of view to perform fire design without fire protection, by utilising any inherent fire resistance of the structural steel. An unprotected steel structure would have many economic advantages, which include eliminating the cost of protection, reduced construction time, simplified construction and greater ease of installation of building services[4]. It may even reduce the maintenance cost of the building. In recent years, six fire tests[5,6,7] have been carried out on an 8-storey composite steel framed building which had been constructed as a typical multi-storey office building at the Building Research Establishment's Cardington laboratory. The test results indicate that existing design codes may be over-conservative. This is because these codes have been based on the results of standard fire resistance tests, which are commonly conducted on single elements. The behaviour of these elements can be quite different compared with their performance as part of a complete frame. For example, some concern has been expressed by Bailey[8], based on evidence from one of the Cardington corner fire tests, that an additional bending moment may be induced in a corner column by the pushing-out of unprotected beams during thermal expansion. It is particularly important to know whether this push-out can lead to column buckling and give an un-conservative result in comparison with the current fire design codes. Further

research needs to be carried out to investigate its potential effect. Some background information related to this analysis is given in following sections.

Unfortunately realistic tests on whole structures are very expensive, and so computer modelling has become more important for investigating the behaviour of whole buildings. Two types of computer modelling exist for fire analysis. One is the fire simulation and heat transfer analysis model, which can simulate fire development and/or predict the temperature distribution histories within the components of the structure. This kind of modelling is often used for composite or concrete structures, whilst pure steel members are often assumed to have uniform temperature distribution since the thermal conductivity of steel is relatively high. This type of application is very useful, but is not detailed here since it exceeds the scope of this thesis. The other is well-known as structural fire modelling which is used to analyse the structural response based on known temperature distributions over the member cross-sections and lengths.

Interest in the performance of building construction elements in fire conditions can be traced back to the late nineteenth century, resulting from disastrous structural failures due to fire[9]. Numerical analysis has begun to attract attention, however, only within the past three decades. One of the earliest reports about the analysis of steel members in fire was presented by Witteveen in 1967[10]. Since then fire engineering has undergone enormous development, and many researchers have made significant contributions in this area. Structural fire modelling has been developed from simple isolated members to complicated frames, including two-dimensional and three-dimensional analysis of steel and composite structures. This work is continually being developed with the aim of simulating the behaviour of whole structures in real fires. However, a limited number of fire tests are still necessary

because the development of fire engineering should be based on both theory and experimental evidence. A brief review of analytical work based on numerical modelling under fire conditions is given here.

In 1972 Culver et al[11,12] used the finite difference method to investigate the buckling loads of an axially loaded unrestrained steel column subjected to fire. In his mathematical model the temperatures were assumed to be constant over the cross-section but to have a linear gradient along the length of the column. Thermal expansion was not included, but the effect of the residual stress was considered. In 1973 Ossenbruggen et al.[13] analysed similarly axially loaded steel columns subjected to thermal gradients across the cross-section and along the length of the column. The mathematical procedure used in his study was based on Newmark's numerical integration method[14]. The influences of residual stress, thermal stress and material degradation were included in his analysis. In 1974 Becker and Bresler[15] developed a finite element computer program, FIRES-RC, which could be used to analyse the structural response of reinforced concrete frames in fire. This 2D program was based on the work done by Bizri[16] and was defined as a one-dimensional stress analysis program. This program considered thermal expansion, material degradation, shrinkage and creep, but not geometric non-linearity. Later in 1991 Ellingwood and Lin[17] used a modified FIRES-RC to take into account the transient strain of concrete at elevated temperatures and to carry out structural analysis of reinforced concrete beams in fire. In 1975 Uddin et al[9] presented a comprehensive review, providing up to 219 articles, on analyses of the behaviour and strength of both steel and concrete structural members at elevated temperatures. In 1975 Cheng and Mak[18] conducted a general-purpose elastoplastic thermal creep analysis of the deformation behaviour of a steel frame in a typical fire compartment,

using a finite element displacement method. In the finite element model the structure was divided into a number of linear elements. The temperatures were assumed to have a linear distribution along the lengths of the members but to remain constant through the cross-sections. Both thermal strain and thermal creep strain were taken into account. In 1983 Jain and Rao[19] developed a numerical model for the analysis of plane steel frames subjected to fire based on using incremental and iterative procedures. The effects of creep and geometric non-linearity, a complex visco-plastic model, temperature dependence and an implicit scheme of time-marching were included in their model. In the same year (1983), Cheng[20] developed a 2D finite element program to investigate the behaviour of steel structures in an elevated-temperature environment. In 1990 Lie and Chabot[21] proposed a method to calculate the structural behaviour of plain concrete-filled columns exposed to fire. Later Lie[22], in 1994, extended this method to include bar-reinforced concrete-filled hollow structural section columns subjected to fire. In this method the cross-sectional area of the column was divided into a number of annular elements. The strength of the filled column could be calculated by a method based on a load-deflection or stability analysis. In 1996 Kodur and Lie[23] developed a model for predicting the behaviour of fibre-reinforced concrete-filled steel columns exposed to fire by using a similar numerical procedure to that presented for plain concrete-filled columns. In 1995 an inelastic semi-analytical finite strip method, which was originally presented by Cheung[24], was used to analyse the local buckling behaviour of cold-formed steel plates of composite steel-concrete structural elements at elevated temperature by Uy[25]. In his numerical model the element used was a lower-order strip element with two nodal lines and four degrees of freedom per nodal line. Also in 1995 Wang[26] developed a finite element computer program to predict

the three-dimensional structural behaviour of composite frames in fire. In his program a two-noded beam element with each node having six degrees of freedom was used as the basic building block. The second-order effects of large deflections are considered by the inclusion of a geometric stiffness matrix for each element. Both material non-linearity and flexible beam-column connections were considered. Concrete and steel/concrete composite members could also be analysed by the program. Almost at same time, Liu[33] developed a three-dimensional mathematical model to simulate the response of steel structures subjected to fire conditions. The model, which was based on a tangent stiffness approach, used eight-noded isoparametric shell finite elements, so that the behaviour of local buckling could be predicted. Both material plasticity and geometric non-linearity, and residual stresses, were included. In 1999 Bailey[28] developed a computer program to predict the structural response of asymmetric slimfloor steel beams, which are used with composite concrete floor slabs consisting of deep-profiled steel decking. Full composite bonding action between the steel and concrete encasement were assumed in Bailey's model. Many other finite element models have also been developed by researchers[29,30,31,32,33] and are continually being improved.

It is believed that this technology will be widely used for practical design in the future. The developments in analysis have enabled similar advances to be made in practical design tools, and there is an increasing awareness within the design profession of the opportunities which these offer. It is envisaged that computer programs could be used to assess the structural damage caused by a fire, and to determine the remaining structural capacity of a fire-damaged structure.

At the University of Sheffield the software VULCAN, which is described in the next chapter, has been developed[10,34] and has mainly concentrated on the overall

behaviour of steel frames. This finite element software is also capable of performing non-linear analysis on composite structures with concrete slabs, subjected to fire conditions. The limitation of the software prior to this work was that the beam cross-section was restricted to bi-symmetric I sections for which a fixed number of 12 segments was used for each section. In normal cases analytical results can be obtained with acceptable accuracy. However, it was considered necessary to have a more general form so that the Asymmetric Slimdek Beam with arbitrary cross-section division could be simulated in fire. A generalised beam element has therefore been developed for the beam member, with a cross-section composed of one or two materials. Validations have then been carried out for various members.

In the following sections some background material, especially for corner sub-frames, is introduced for further investigation.

1.2 FIRE TEST

In general, natural fire can be characterised into three phases, which can be defined as growth, full development and decay, as shown in Fig. 1-1. In the growth phase some combustible materials begin to burn and produce smoke and a relatively small amount of heat. Then the temperature rises rapidly to a peak value in the period following flashover, which defines the point at which all organic materials spontaneously combust, in the full development phase. In this phase, the temperature becomes practically uniform through the compartment, and the structural risk of collapse is high. After the combustible materials finish burning the temperature will decrease, in the cooling stage known as the decay phase.

The behaviour of a structural element subjected to fire is described in terms of its fire resistance, which is the period of time of exposure to fire in a standard test at which

failure occurs. The fire resistance of elements of building construction is assessed based on standard fire tests. The standard fire curves differ from code to code but the most widely used is the internationally agreed time-temperature curve defined in ISO 834,[35] (BS476[36] in the UK), which has been used in furnace testing of components, as also shown in Fig. 1-1.

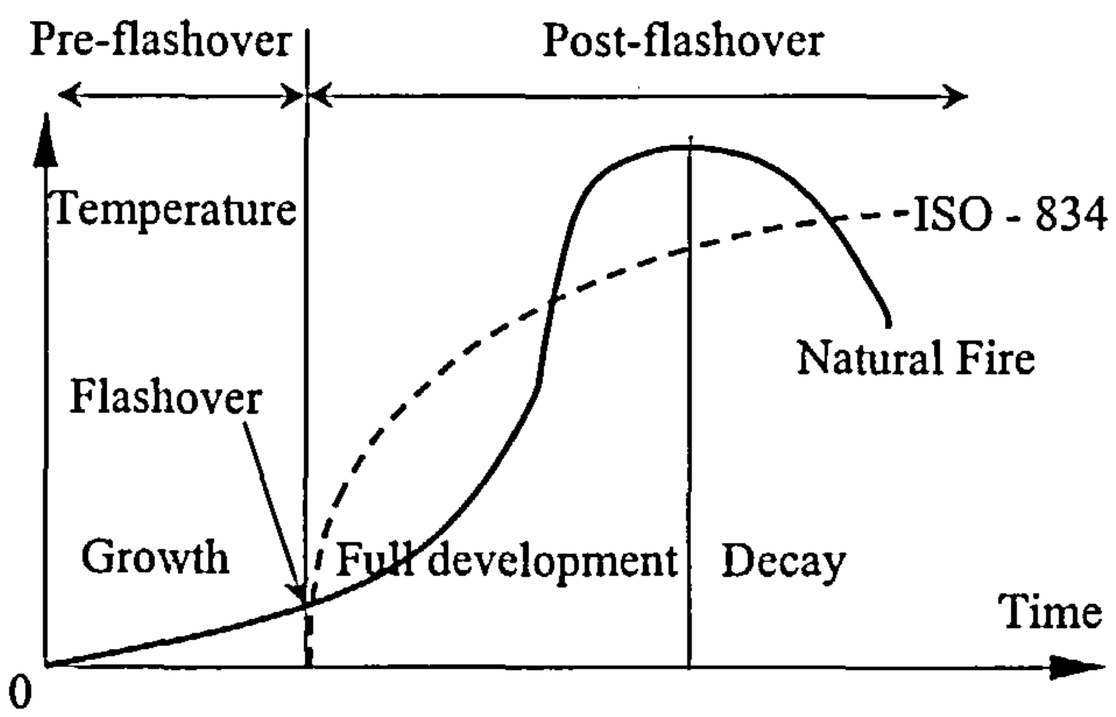

Fig. 1-1 Development of natural fire in a compartment, comparing with the ISO 834 standard fire curve

In the USA and Japan there are other curves such as ASTM-E.119[37] and JIS A 1304[38] available for fire tests. These standard fire curves are not designed for the purpose of representing any type of natural building fire, but are for convenient comparison between fire testing cases.

The fire resistance of an element is measured in units of time, and during this time the element must satisfy the criteria of load bearing capacity, integrity and insulation in a standard fire test. Structural elements can be classified as separating elements or non-separating elements, where non-separating elements only need to satisfy the criterion of load bearing capacity. The criterion of load bearing capacity imposed by BS476: Part 21[39] defines the failure of beams as either the deflection exceeding span/30 if the rate of the deflection (mm/min) exceeds $span^2/(9000 \times beam\ depth)$, or

the deflection exceeding span/20; for columns the failure will occur when the column cannot carry the applied load.

Beams are tested horizontally in a floor furnace, and are normally supported by rollers. Columns are tested in a cylindrical furnace subjected to constant load and are allowed free expansion at the top end. The specimens in tests are usually less than 5m long because of the sizes of standard furnaces. A large number of fire tests on isolated elements[17,40,41] have been conducted, but the behaviour of elements in buildings is critically different from the furnace tests.

Furnace testing using the standard fire curve is the traditional means of assessing the behaviour of frame elements in fire, but it is clear that it is difficult to conduct furnace tests of representative full-scale structural members under load. Full-scale fire tests can rarely be carried out on complete buildings and are very expensive. At present there is still very little data available from such tests. Most recently six scientifically monitored fire tests[5,6,7] have however been conducted. An eight-storey composite steel-framed test building was designed for the Building Research Establishment (BRE) and constructed at their Cardington laboratory, near Bedford in the UK, to represent a typical modern city centre office building. Composite action was achieved with the floor slab, as in conventional composite construction. On plan, the building covered an area of 21m x 45m with an overall height of 33m. The structural design was carried out in accordance with BS5950 Part 1 and also complied with Eurocodes EC3-1-1 and EC4-1-1. A total of six major fire tests were conducted on this frame between January 1995 and July 1996, four by British Steel and two by the Building Research Establishment. The layouts and locations of these fire tests are shown in Fig. 1-2. Most of the beams in these tests were unprotected, although columns were generally protected.

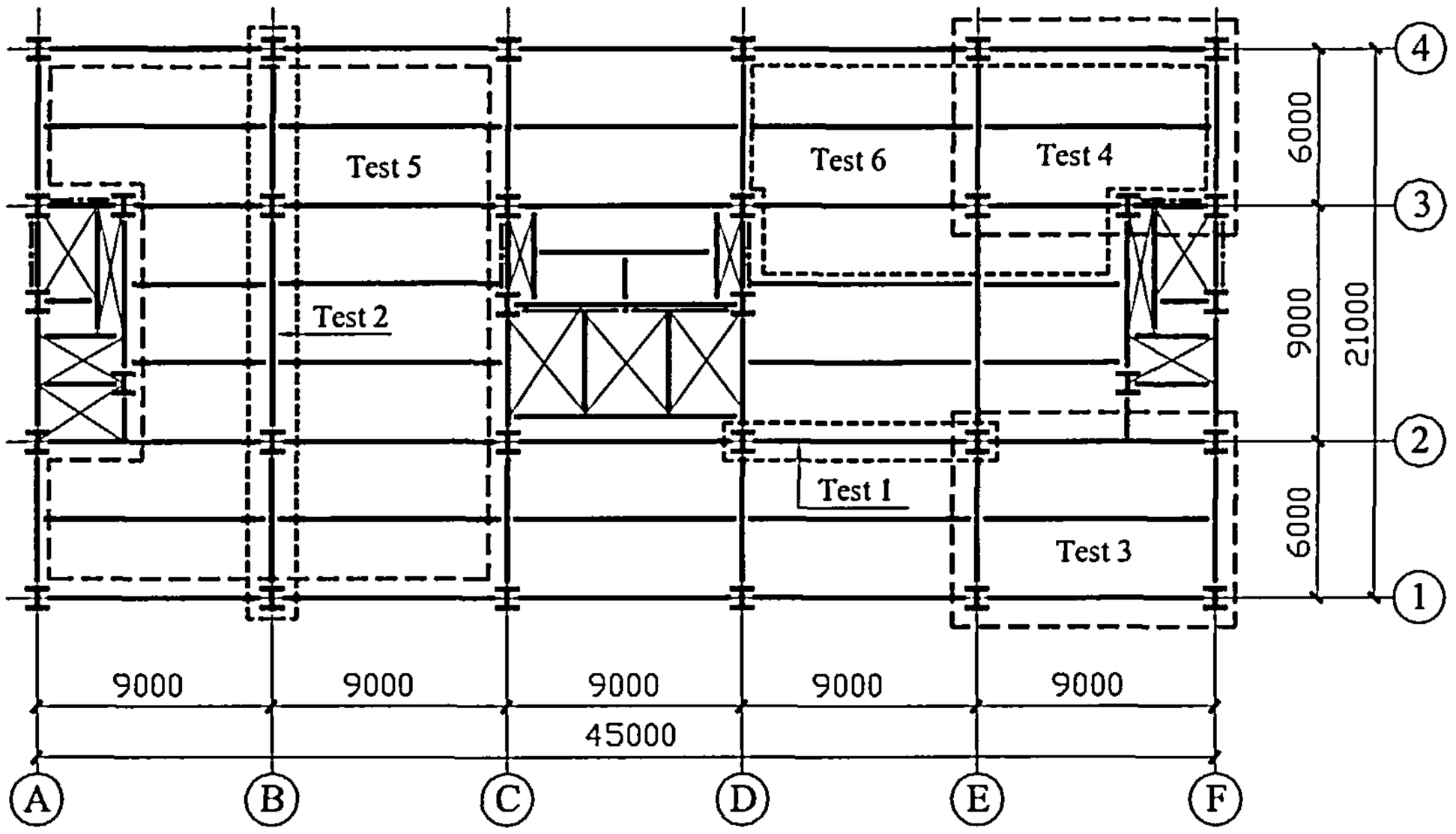

Test 1: Restrained beam (BS)
Test 2: Plane frame (BS)
Test 3: Corner (BS)
Test 4: Corner (BRE)
Test 5: Large compartment (BRE)
Test 6: Office demonstration (BS)

Fig. 1-2 The Cardington fire test locations

The first test, Test 1, the Restrained Beam Test, was carried out on the seventh floor using a purpose-built gas-fired furnace which heated the beam over the middle 8.0m of its 9.0m span. The maximum atmosphere and measured beam temperatures during this test were 913°C and 875°C respectively, the maximum measured vertical deflection was 232mm, with a residual deflection after cooling of 113mm. Test 2 is generally referred to as the Plane Frame Test, in which the primary beams and columns on one grid-line across the full width of the building on the fourth floor were heated using a gas furnace. The maximum beam temperature in the fire was 820°C and the maximum recorded deflection in the 9m span was 265mm. The first Corner Test, Test 3, was conducted in the corner of the building on the second floor where a compartment 10m x 7.6m was constructed using blockwork partition walls. The test fire was generated by burning wooden cribs with a fire load density of 45kg/m² of wood. The maximum steel temperature for the primary beam was in

excess of 1000°C and its maximum vertical deflection was 325mm. The maximum temperature recorded for the central secondary beam was 950°C with a maximum vertical deflection of 425mm. Tests 4 and 5 were carried out by the Building Research Establishment using the same fire load of 40kg/m² of timber. Test 4, referred to as the second Corner Fire Test, covered an area of 54m² and was located in the corner of the building, between the second and third floors. The maximum temperature on the unprotected secondary beam was 903°C with maximum atmosphere temperature in excess of 1000°C. The maximum vertical deflection in the centre of the slab was 269mm during the fire, returning to a final value of 160mm on cooling. Test 5, referred to as the Large Compartment Fire Test, was carried out in a large compartment between the second and third floors. This was claimed to be the largest ever monitored fire test in the world and covered an area of 340m². The maximum displacement recorded during the fire was 557mm, returning to a final value of 481mm. In Test 6, referred to as the Demonstration Office Furniture Test, real office furniture including modern furnishings, computers and filing systems were used to provide the fire load which was equivalent to 46kg/m² of wood. The compartment, with a floor area of 135m² was constructed between the first and second floors, using concrete blockwork. Columns and beam - to - column connections were protected, with the primary and secondary beams left exposed to the fire. The aim of this test was to examine whether the type of structural behaviour observed in the earlier tests would also occur when the building was subjected to a more realistic fire scenario. The Cardington test programme involved European co-operation and attracted the attention of fire researchers from all over the world. The aim of these tests was to study the structural response of a whole building when subjected to fire, and to provide comprehensive test data for validating computer

software. With the validated software, different structural and fire scenarios could then be investigated economically.

Following the Cardington fire test programme, further research is continuing to investigate whole-frame and structure behaviour under real fires, and to develop design guidance which will almost certainly involve using less applied protection and possibly greater use of active safety measures.

1.3 ANALYSIS

1.3.1 ANALYSIS OF THE BEHAVIOUR OF COLUMNS

To analyse the behaviour of isolated elements, the classical methods can be applied. The critical or Euler load of a pin-ended ideal elastic column subjected to axial load can be expressed by

$$P_{cr} = \frac{\pi^2 EI}{l^2} \qquad (1\text{-}1)$$

The above equation is based on small-deflection theory and assumes that the material follows Hooke's law. For columns with different support conditions it is still valid, using the concept of an effective length in which the actual length of the column is replaced by the length of an equivalent pin-ended column. The behaviour of the column is represented by the Euler curve. However, if the column is short or its compressive stress exceeds the proportional limit σ_{pr} of the material, the critical load will be less than that calculated by Eqn. (1-1), as demonstrated in Fig. 1-3.

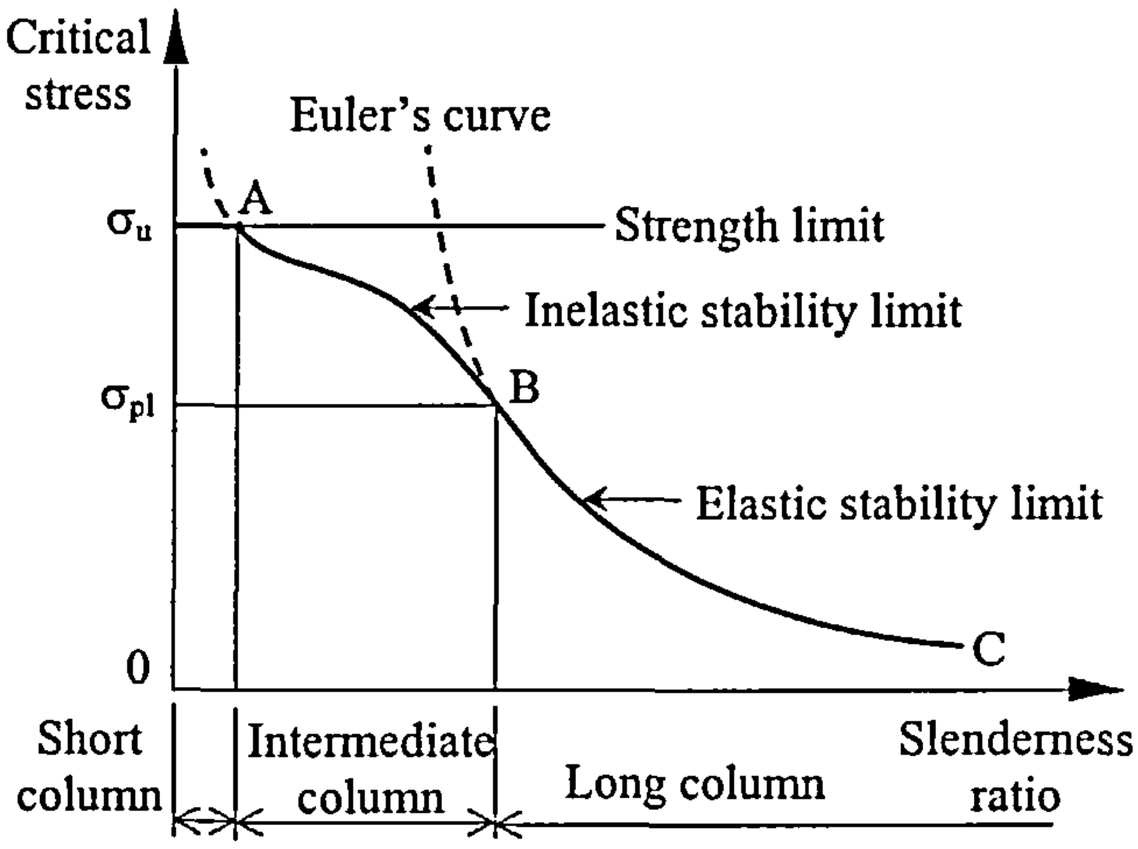

Fig. 1-3 Diagram of critical stress versus slenderness ratio (L/r)

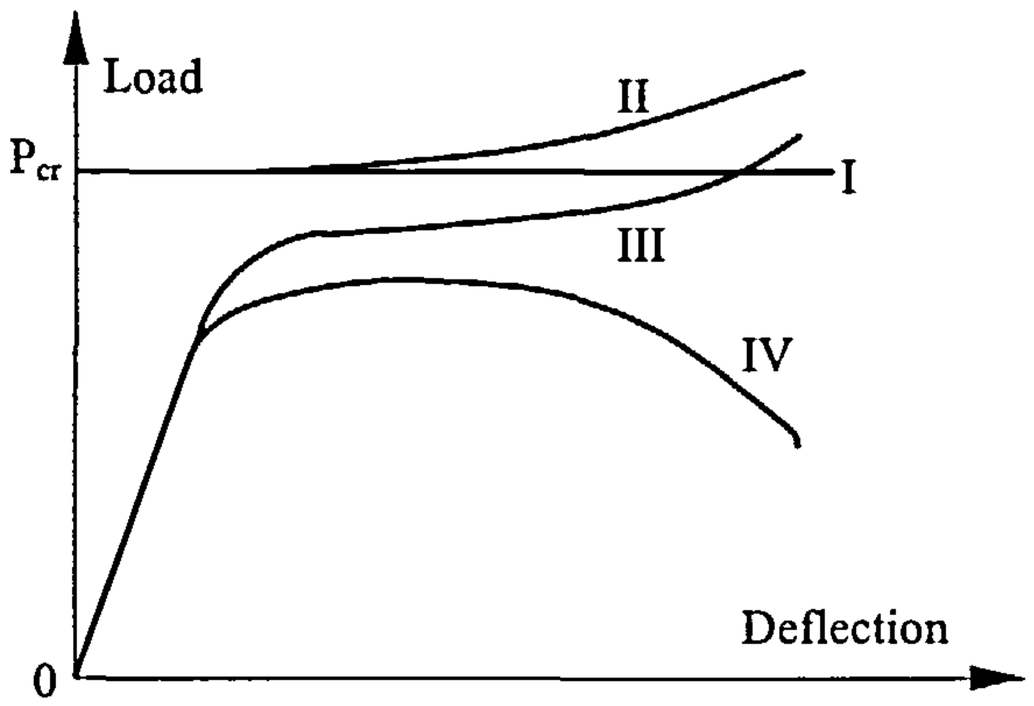

Fig. 1-4 Load-deflection diagram for columns: I for ideal elastic column with small deflections; II for ideal elastic column with large deflections; III for elastic column with imperfections; IV for inelastic column with imperfections.

For intermediate columns, from A to B in Fig. 1-3, instability will be accompanied by yielding. Current methods typically used for solving this inelastic buckling are based on the tangent-modulus theory or the reduced-modulus theory[43]. For very short columns, collapse is due to material yielding. If we consider large-deflection effects and the column being imperfect, the behaviour is again different as illustrated in Fig. 1-4. More detail concerning large-deflection behaviour is given in Ref. [44].

Columns generally include imperfections, such as initial out-of-straightness, eccentricity of the axial thrust and residual stresses. All the imperfections can be

regarded as an equivalent initial out-of-straightness. An analysis developed by Perry indicated that for a long pin-ended column with an initial imperfection of $y_0 = a_0 \sin\frac{\pi x}{l}$, the initial deflection of the column ($\mathbf{y_0}$) would be increased by an amplification factor of $\mathbf{1/(1-P/P_e)}$ due to the axial load $\mathbf{P}$, where $\mathbf{P_e}$ is Euler buckling load. The deflection and the critical stress of the column are given by,

$$y = \frac{y_0}{1 - P/P_e} \tag{1-2}$$

$$\sigma_{cr} = \frac{f_y + \sigma_e(1+\eta)}{2} - \sqrt{\left(\frac{f_y + \sigma_e(1+\eta)}{2}\right)^2 - f_y\sigma_e} \tag{1-3}$$

where f_y is yield strength of the column, σ_e is Euler buckling stress, η is the imperfection ratio which is equal to $a_0 c/r^2$ (where c and r are the distances from the neutral axis to the point of maximum compressive stress and the minimum radius of gyration of the section respectively). Eqn. (1-3) is known as the Perry equation, and is based on the assumption that failure of the column occurs by the material reaching a 'first yield'. When a concentrated lateral load is applied at the centre of an axially loaded pin-ended column, the maximum deflection and bending moment are given by[24],

$$\delta_{max} = \frac{Ql^3}{48EI}\frac{3(\tan u - u)}{u^3} \tag{1-4}$$

$$M_{max} = \frac{Ql}{4}\frac{\tan u}{u} \tag{1-5}$$

where, Q is the concentrated lateral load and $u = \frac{kl}{2} = \frac{l}{2}\sqrt{\frac{P}{EI}}$. In both equations, the first factor on the right-hand side gives the deflection and bending moment under

lateral load Q alone, and the second factor represents the influence of the axial load **P**.

The more general situation of an elastically restrained column is shown in Fig. 1-5. If the two coefficients of end restraint are α and β , the equations for the end moments ($M_a = -\alpha\theta_a$ and $M_b = -\beta\theta_b$) are given by Timoshenko[44] as follows:

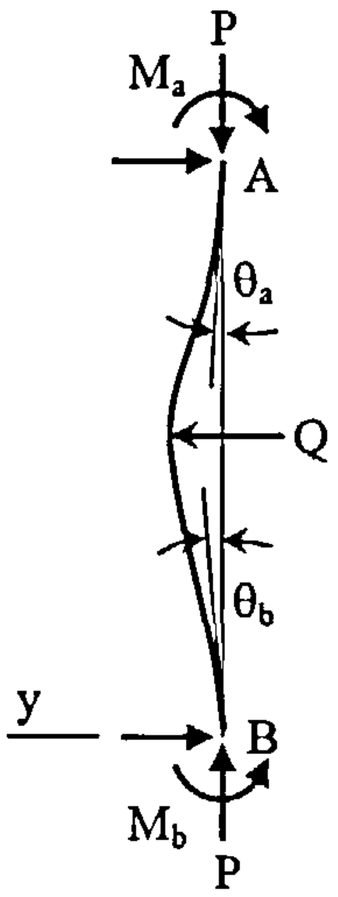

Fig. 1-5 Column with elastic restraints

$$\left.\begin{aligned} -\frac{M_a}{\alpha} &= \theta_{0a} + \frac{M_a l}{3EI}\psi(u) + \frac{M_b l}{6EI}\phi(u) \\ -\frac{M_b}{\beta} &= \theta_{0b} + \frac{M_b l}{3EI}\psi(u) + \frac{M_a l}{6EI}\phi(u) \end{aligned}\right\} \qquad (1\text{-}6)$$

where θ_{0a} and θ_{0b} are the angles of rotation calculated for pin-ends, and

$$\psi(u) = \frac{3}{2u}\left(\frac{1}{2u} - \frac{1}{\tan 2u}\right), \quad \phi(u) = \frac{3}{u}\left(\frac{1}{\sin 2u} - \frac{1}{2u}\right).$$

The equation for determining the critical load is,

$$\left[\frac{1}{\alpha} + \frac{l}{3EI}\psi(u)\right]\left[\frac{1}{\beta} + \frac{l}{3EI}\psi(u)\right] - \left[\frac{l}{6EI}\phi(u)\right]^2 = 0 \qquad (1\text{-}7)$$

Once the equations for columns at ambient temperature are determined, the high temperature forms can be obtained by replacing the modulus, the yield strength and the Euler critical load with the corresponding reduced temperature-dependent values. The effect of thermal elongation is ignored.

1.3.2 ANALYSIS OF THE BEHAVIOUR OF SUB-FRAME

When we investigate the behaviour of a structure by hand, the structure is usually separated into sub-frames for the sake of simplification (Fig. 1-6). Each sub-frame may contain only one beam or column, which is then treated as an isolated individual member with elastic restraints.

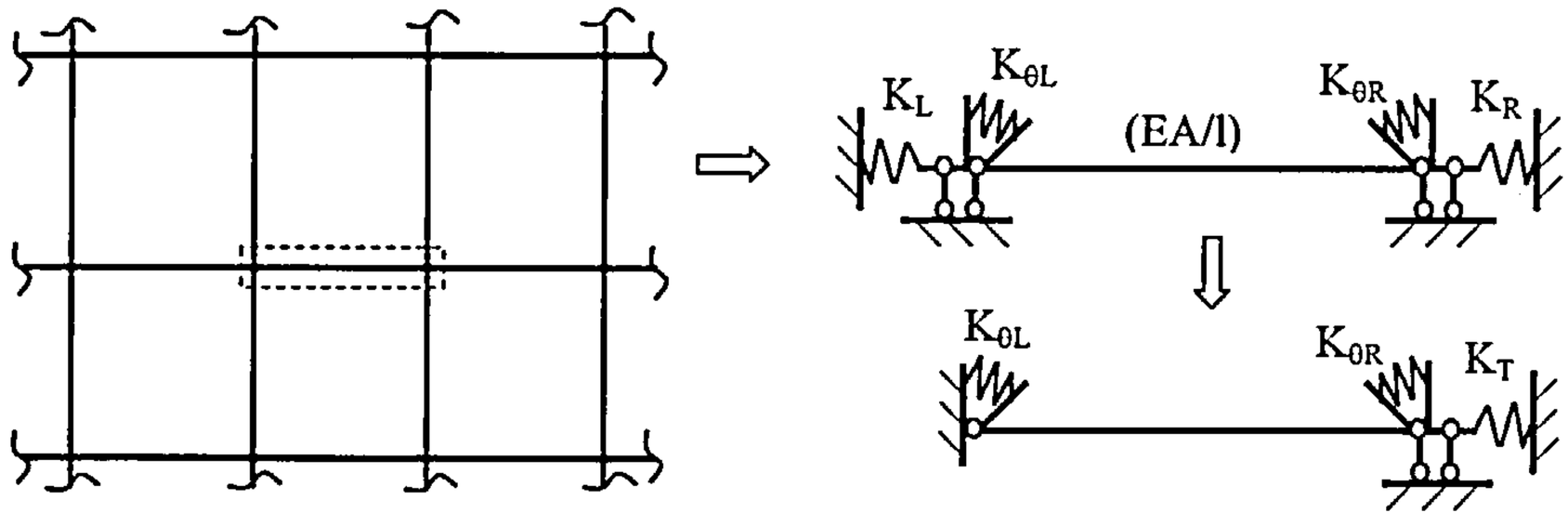

Fig. 1-6 Separation of the structure

The restraints derive from the surrounding structure, and include both translation and rotation stiffnesses, and relate to the position of the member and the stiffness of the adjacent members. Li, et al[45] developed very detailed formulations to calculate these elastic restraints, which were based on a typical plane frame as shown in Fig. 1-7 and are given below.

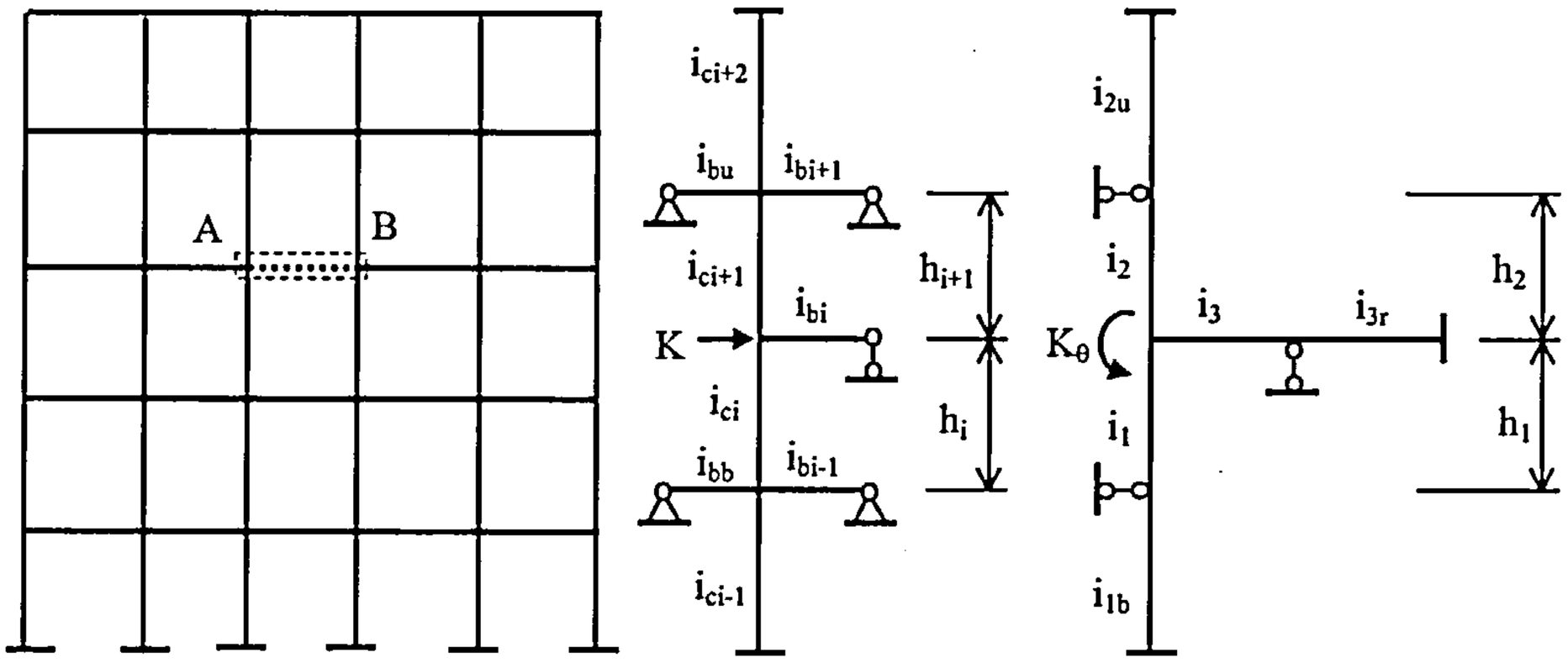

(a) Frame for restraint stiffness calculation

(b) Model for axial stiffness calculation

(c) Model for rotational stiffness calculation

Fig. 1-7 Model for stiffness calculation

The axial stiffness at the end **A** or **B**, is given by:

$$K = \left\{ \left[12 + \frac{18\left(h_i \bar{i}_{ci+1} - h_{i+1} \bar{i}_{ci}\right)}{h_{i+1}\left[2\left(\bar{i}_{ci} + \bar{i}_{ci+1}\right) + 6 i_{bi}\right]} \right] \frac{\bar{i}_{ci}}{h_i^2} + \left[12 + \frac{18\left(h_i \bar{i}_{ci+1} - h_{i+1} \bar{i}_{ci}\right)}{h_i\left[2\left(\bar{i}_{ci} + \bar{i}_{ci+1}\right) + 6 i_{bi}\right]} \right] \frac{\bar{i}_{ci+1}}{h_{i+1}^2} \right\} \psi \tag{1-8}$$

where,

$\bar{i}_{ci} = \alpha_1 \alpha_3 i_{ci}, \quad \bar{i}_{ci+1} = \alpha_2 \alpha_4 i_{ci+1},$

$$\alpha_1 = \frac{1}{4}\left(1 + \frac{3}{1 + \dfrac{i_{ci}}{i_{ci-1} + 3 i_{bi-1} + 1.5 i_{bb}}} \right), \quad \alpha_2 = \frac{1}{4}\left(1 + \frac{3}{1 + \dfrac{i_{ci+1}}{i_{ci+2} + 3 i_{bi+1} + 1.5 i_{bu}}} \right),$$

$$\alpha_3 = \frac{1}{2}\left(1 + \frac{1}{1 + \dfrac{i_{ci}}{i_{ci-1} + 3 i_{bi-1} + 1.5 i_{bb}}} \right), \quad \alpha_4 = \frac{1}{2}\left(1 + \frac{1}{1 + \dfrac{i_{ci+1}}{i_{ci+2} + 3 i_{bi+1} + 1.5 i_{bu}}} \right),$$

$i = EI / l,$

ψ is the reduction factor considering the effect of the axial deformation of the member; values are tabulated in Ref. [45].

The total axial restraint of the member will be,

$$K_T = \frac{1}{\dfrac{1}{K_A} + \dfrac{1}{K_B}} \tag{1-9}$$

The rotational stiffness at the end **A** or **B** of an edge span is given by:

$$K_\theta = 4\left(\bar{i}_1 + \bar{i}_2 + \bar{i}_3\right) - \frac{3\left(h_1 \bar{i}_2 - h_2 \bar{i}_1\right)^2}{h_1^2 \bar{i}_2 + h_2^2 \bar{i}_1} \tag{1-10}$$

Otherwise, for an internal span,

$$K_\theta = 4\left(\bar{i}_1 + \bar{i}_2 + \bar{i}_3\right) \tag{1-11}$$

where,

$\bar{i}_1 = \beta_1 i_1, \qquad \bar{i}_2 = \beta_2 i_2, \qquad \bar{i}_3 = \beta_3 i_3,$

$$\beta_1 = \frac{1}{4}\left(3 + \frac{1}{1 + i_1 / i_{1b}}\right), \qquad \beta_2 = \frac{1}{4}\left(3 + \frac{1}{1 + i_2 / i_{2u}}\right),$$

$$\beta_3 = \frac{1}{4}\left(3 + \frac{1}{1 + i_3 / i_{3r}}\right).$$

Details of the coefficients in Eqns. (1-8) to (1-11) can be found in Ref. [45].

When the elastic restraints of a member are known, a normal analysis can be carried out on the "individual member". This can include the effect of temperature. Failure of the structure can be defined by any of the members exceeding the prescribed limit state according to standard codes[39] or being unable to carry the applied load.

1.4 DESIGN CODES

Fire engineering designs are normally performed by an engineer according to prescriptive fire design guidance[46,47,48], rather than by carrying out complicated analyses. For columns, two design codes, BS5950: Part 8 and Eurocode 3: Part 1.2, have been considered in this thesis. Both are based on the results of standard fire-resistance tests, which are commonly conducted on single elements.

1.4.1 BS5950 PART 8 FOR COLUMNS

BS5950 Part 8: Code of Practice for fire resistant design[47], which was one of the first structural fire design codes in the world, was published in 1990, and treated fire as an accidental limit state. For a column exposed to fire, the Limiting Temperature Method can be used. The limiting temperature of a member is based on its load ratio, which is the ratio of the load carried during the fire to the member resistance at 20°C, which is tabulated against limiting temperature in Table 1-1.

Table 1-1 Limiting temperature for design of column

Member in compression, for a slenderness λ	Limiting temperature at load ratio of: (°C)					
	0.7	0.6	0.5	0.4	0.3	0.2
≤ 70	510	540	580	615	655	710
> 70 but ≤ 180	460	510	545	590	635	635

For columns in simple construction designed in accordance with the recommendations of BS 5950: Part1, the load ratio is either

$$R = \frac{F_f}{A_g P_c} + \frac{M_{fx}}{M_b} + \frac{M_{fy}}{P_y Z_y}$$ for columns in simple construction (1-12a)

or

$$R = \frac{F}{A_g P_y} + \frac{M_{fx}}{M_{cx}} + \frac{M_{fy}}{M_{cy}}$$ or $$R = \frac{F}{A_g P_c} + \frac{mM_{fx}}{M_b} + \frac{mM_{fy}}{P_y Z_y}$$, whichever is the greater, for columns in continuous construction (1-12b,c)

where,

A_g is the gross area;

P_c is the compressive strength;

P_y is the design strength of steel;

Z_y is the elastic modulus about the minor axis;

M_b is the buckling resistance moment;

F_f is the axial load at the fire limit state;

M_{fx}, M_{fy} are the maximum moments about the major and minor axes at the fire limit state respectively;

M_{cx}, M_{cy} are the moment capacities of the section about the major and minor axes in the absence of axial load;

m is the equivalent uniform moment factor.

The limiting temperature determined as above is then compared with the design temperature, which is the temperature the steel column may be expected to reach at the end of the prescribed fire resistance period. Values for the design temperature are tabulated in BS5950. If the design temperature is less than the limiting temperature no fire protection is necessary. If not, then some fire protection must be applied.

1.4.2 EUROCODE 3 PART 1.2 FOR COLUMN

EC3 Part 1.2[46] treats the design of steel structures for fire as an accidental situation (the fire limit state). Three levels of calculation method are allowed: tabular methods, simple calculation models and advanced calculation models. The tabular methods are based on simple design tables. The simple calculation models are suitable for calculation by hand and are based on conservative assumptions. Advanced calculation methods are generally appropriate for computer analyses. The general equation, which should be satisfied for a member or structure during a fire, is given as:

$$E_{fi,d} \leq R_{fi,d,t} \qquad (1\text{-}13)$$

where,

$E_{fi,d}$ is the design effect of actions for the fire situation, determined in accordance with ENV 1991-2-2, including the effects of thermal expansion and deformations;

$R_{fi,d,t}$ is the corresponding design resistance of the steel member in fire.

The critical temperature of a steel column subjected to fire can be conveniently obtained by using the simple calculation model (or tabular methods). For a column with a uniform temperature distribution, the critical temperature ($\theta_{a,cr}$) is given by,

$$\theta_{a,cr} = 39.19 ln\left[\frac{1}{0.9674\mu_0^{3.833}} - 1\right] + 482 \qquad (1\text{-}14)$$

For members with a Class1, Class 2 or Class 3 cross-section, the degree of utilisation μ_0 at time t = 0 may be defined by:

$$\mu_0 = E_{fi,d} / R_{fi,d,0} \qquad (1\text{-}15)$$

in which $R_{fi,d,0}$ is the value of $R_{fi,d,t}$ for time t =0.

A design table (Table 1-2), which defines the critical temperature ($\theta_{a,cr}$) according to the utilisation factor μ_0 based on Eqn. (1-14), is also given in EC3 Part 1.2 as,

Table 1-2 Critical temperature $\theta_{a,cr}$ for values of the utilisation factor μ_0

μ_0	0.22	0.24	0.26	0.28	0.30	0.32	0.34	0.36	0.48	0.40
$\theta_{a,cr}$ (°C)	711	698	685	674	664	654	645	636	628	620
μ_0	0.42	0.44	0.46	0.48	0.50	0.52	0.54	0.56	0.58	0.60
$\theta_{a,cr}$ (°C)	612	605	598	591	585	578	572	566	560	554
μ_0	0.62	0.64	0.66	0.68	0.70	0.72	0.74	0.76	0.78	0.80
$\theta_{a,cr}$ (°C)	549	543	537	531	526	520	514	508	502	496

1.5 MATERIAL CHARACTERISTICS

1.5.1 STEEL PROPERTIES AT ELEVATED TEMPERATURE

Structural steel, generally mild steel or low-carbon steel, is the most widely used in steel construction. It has high strength, light weight and good ductility. However, when exposed to fire, its material properties are changed and thermal expansion is induced. The typical mechanical properties of this steel in tension at ambient temperature are well known. They can be found in many standard books on mechanics or materials and are based on data determined from tests on small specimens of the material. In engineering practice, the strain-stress relationship, as shown in Fig. 1-8, is normally idealised as an elastic-perfectly plastic material by using a bilinear curve, as shown in Fig. 1-9, or a tri-linear curve to account approximately for the strain hardening of the material. Most of steel's material properties are temperature-dependent. From 300°C steel begins to lose its strength and stiffness, and continues to lose strength at a fast rate until 750°C. Beyond this temperature, steel continues to lose its remaining strength at a slower rate until reaching its melting point (approximately 1500°C). Only 23% of the ambient-temperature strength remains at 700°C, and at 800°C this has reduced to 11% and at 900°C to 6%. The elastic modulus of steel also decreases when the temperature rises. At elevated temperature the stiffness decreases and its bi-linear nature is lost. This leads to difficulty in recognising the yield point and elastic modulus clearly. Therefore, 0.5%, 1.5% and 2.0% strain limits are defined by design codes[46,47] for the fire limit state. Based on these straight-line relationships, some mathematical models for steel at elevated temperature have been suggested[49,50,51]. However, the bilinear model has proved to be unsatisfactory for accurate analysis, even though it is quite adequate for most design purposes. More complex continuous models[10,52,4,46]

have therefore been developed, and two typical examples currently used in analysis, are the Ramberg-Osgood[4,10] and EC3 models[46]. Both are suitable for representing tension and compression. The Ramberg-Osgood model is expressed as:

$$\varepsilon_T = \frac{\sigma_T}{A_T} + 0.01\left(\frac{\sigma_T}{B_T}\right)^{n_T}$$

where,

ε_T, σ_T are strain and stress at temperature T respectively.

A_T, B_T and n_T are temperature-dependent constants whose variation is detailed in Ref. [10].

EC3: Part 1.2 presents the stress-strain relationship of structural steel at elevated temperature as a set of linear-elliptical curves as shown in Fig. 1-10. The form of the curve is divided into four ranges as summarised in Table 1-3

Table 1-3

Strain range	Stress σ	Tangent modulus
I elastic $(\varepsilon \le \varepsilon_{p,\theta})$	$E_{a,\theta} \cdot \varepsilon$	$E_{a,\theta}$
II transit elliptical $(\varepsilon_{p,\theta} \le \varepsilon \le \varepsilon_{y,\theta})$	$\frac{b}{a}\sqrt{a^2 - (\varepsilon_{y,\theta} - \varepsilon)^2} + f_{p,\theta} - c$ with $a^2 = (\varepsilon_{y,\theta} - \varepsilon_{p,\theta})(\varepsilon_{y,\theta} - \varepsilon_{p,\theta} + c / E_{a,\theta})$ $b^2 = E_{a,\theta}(\varepsilon_{y,\theta} - \varepsilon_{p,\theta})c + c^2$ $c = \frac{(f_{y,\theta} - f_{p,\theta})^2}{E_{a,\theta}(\varepsilon_{y,\theta} - \varepsilon_{p,\theta}) - 2(f_{y,\theta} - f_{p,\theta})}$	$\frac{b(\varepsilon_{y,\theta} - \varepsilon)}{a\sqrt{a^2 - (\varepsilon_{y,\theta} - \varepsilon)^2}}$
III plastic $(\varepsilon_{y,\theta} \le \varepsilon \le \varepsilon_{t,\theta})$	$f_{y,\theta}$	0
IV decreasing $(\varepsilon_{t,0} \le \varepsilon \le \varepsilon_{u,\theta})$	$f_{y,\theta}[1 - (\varepsilon - \varepsilon_{t,\theta})/(\varepsilon_{u,\theta} - \varepsilon_{t,\theta})]$	--

Where,

$f_{y,\theta}$ is the effective yield strength;

$f_{p,\theta}$ is the proportional limit;

$E_{a,\theta}$ is the slope of the linear elastic range;

$\varepsilon_{p,\theta}$ is the strain at the proportional limit;

$\varepsilon_{y,\theta}$ is the yield strain;

$\varepsilon_{t,\theta}$ is the limiting strain for yield strength;

$\varepsilon_{u,\theta}$ is the ultimate strain.

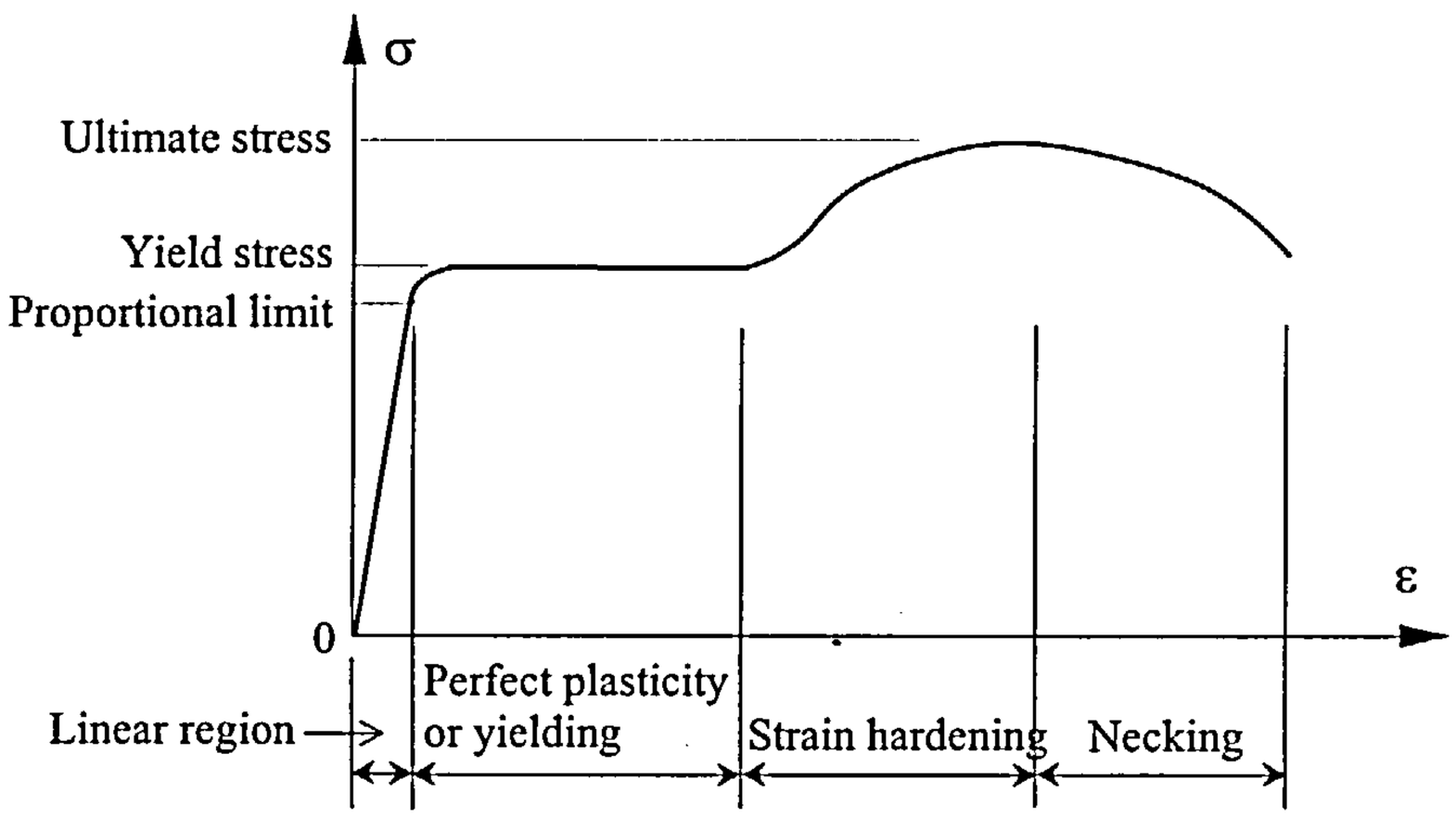

Fig. 1-8 Stress-strain relationship at ambient temperature for a typical structural steel in tension

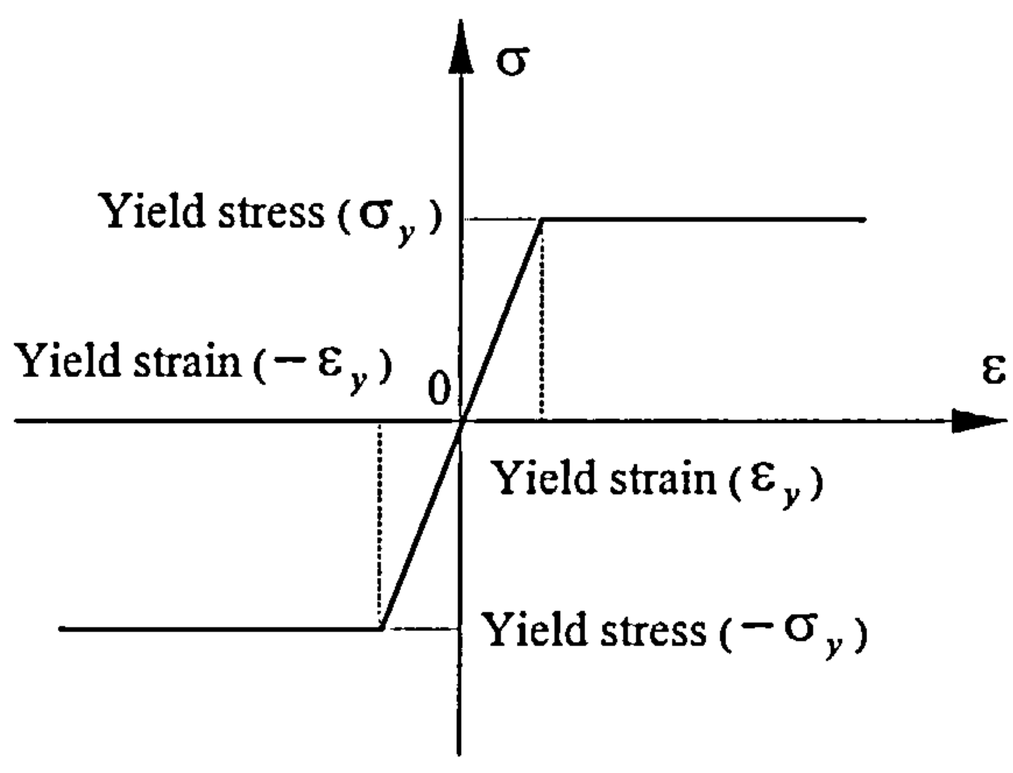

Fig. 1-9 Idealised ambient temperature Stress-strain Diagram

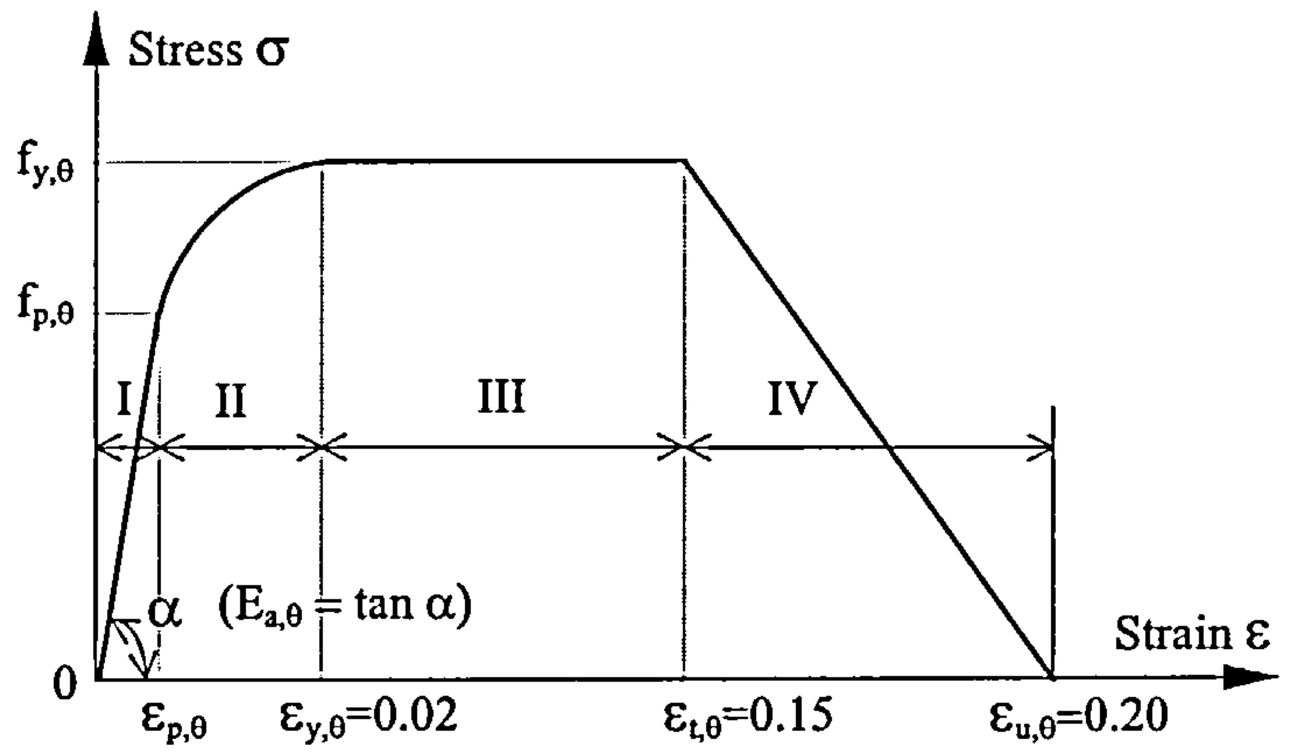

Fig. 1-10 Stress-strain relationship for structural steel at elevated temperature according to EC3.

The rate of thermal expansion of steel changes at high temperatures. EC3 part 1.2[46] defines three ranges to model this, although more simplified virtually linear models are available[47,52]. The details of the EC3 model are as follows:

$$\Delta l / l = 1.2 \times 10^{-5} \theta_a + 0.4 \times 10^{-8} \theta_a^2 - 2.416 \times 10^{-4} \quad \text{-- for } 20°C \le \theta_a < 750°C$$

$$\Delta l / l = 1.1 \times 10^{-2} \quad \text{-- for } 750°C \le \theta_a \le 860°C$$

$$\Delta l / l = 2 \times 10^{-5} \theta_a - 6.2 \times 10^{-3} \quad \text{-- for } 860°C < \theta_a \le 1200°C$$

where,

l is the length at 20°C;

Δl is the temperature-induced expansion;

θ_a is the steel temperature (°C).

Creep strain is considered to be essentially non-recoverable, and normally depends on applied stress σ, time **t** and temperature θ. Due to the short duration of typical building fire scenarios (usually being no more than a few hours), the effect of time t may be neglected. Previous research has indicated that creep of steel is unimportant below 550°C. A comprehensive creep model, based on the Dorn θ concept of temperature-compensated time, was generally used[52,53,54]. However, in some

experimentally-based models, for example EC3's model which requires the heating rates to be limited to between 2°C and 50°C/min, its effect has been approximately included.

There are two kinds of reinforcing steels used in reinforced concrete construction, (i.e. hot-rolled and cold-worked steel). The characteristics of hot-rolled reinforcement are similar to those of structural steel. However, cold-worked reinforcing steel is "cold formed", and this changes the microstructure of the steel so that it exhibits a higher strength and its properties are therefore slightly different from those of structural steel. At elevated temperature, EC4: Part 1.2[48] assumes the same thermal expansion characteristics for all structural and reinforcing steels but provides different reduction factors for the stress-strain relationships for cold-worked reinforcement.

1.5.2 CONCRETE PROPERTIES AT ELEVATED TEMPERATURE

Concrete is generally understood to mean a mixture composed of cement, which principally combines lime (**CaO**) with silica (SiO_2), alumina (Al_2O_3) and ferric oxide (Fe_2O_3), various aggregates and water. This hardens at ambient temperatures and is designed to achieve a specified compressive strength after 28 days[55]. Light-weight concrete is often defined as having a dry density of 1600 to 2000 kg/m^3 whilst that of normal-weight concrete is approximately 2400 kg/m^3. Because concrete is of a heterogeneous nature, including pores which contain a large proportion of water of various forms including chemically combined water, adsorbed water and capillary water, it is difficult to establish an accurate mechanical model at elevated temperature, especially using a uniaxial model to describe the behaviour under multi-axial stress. Different experimental techniques may give conflicting

results. At high temperatures, concrete releases most of the contained water, producing a physico-chemical change. In physical terms, when the temperature increases the coefficient of thermal expansion of concrete increases but its conductivity decreases. These properties are mainly influenced by the aggregates used and by evaporation of water. Differential dilatation between the cement paste and the aggregates easily lead to the destruction of the concrete. The physical loss of moisture and shrinkage (especially at lower temperatures) both give a decrease in the coefficient of expansion, but as temperature increases their effects diminish.

The mechanical properties of concrete also degrade with increase in temperature, being influenced by the loss of both the combined and free moisture, and disintegration of concrete with chemical transformation, for example from $Ca(OH)_2$ (decomposition) or $CaCO_3$ (de-carbonation) into $CaO + H_2O$. At a certain temperature local degradation occurs in the form of cracking or crushing of the concrete. The rates of shrinkage and creep normally increase with an increase in temperature. The effect of high temperature on the properties introduced above have been well documented in Refs. [15], [16] and [54] to [57]; these references also present a number of models.

In this study the uniaxial mathematical models for concrete suggested by EC4 part 1.2[48] are used consistently. The thermal expansion model is given by:

For normal-weight concrete:

$$\Delta l / l = -1.8\times10^{-4} + 9\times10^{-6}\theta_c + 2.3\times10^{-11}(\theta_c)^3 \quad \text{-- for } 20°C \le \theta_c \le 700°C$$

$$\Delta l / l = 14\times10^{-3} \quad \text{-- for } 700°C < \theta_c \le 1200°C$$

For light-weight concrete:

$$\Delta l / l = 8.1\times10^{-6}(\theta_c - 20)$$

The mechanical model for concrete in compression is given by a set of stress-strain relationships with a shape as specified in Fig. 1-11 and Table 1-4,

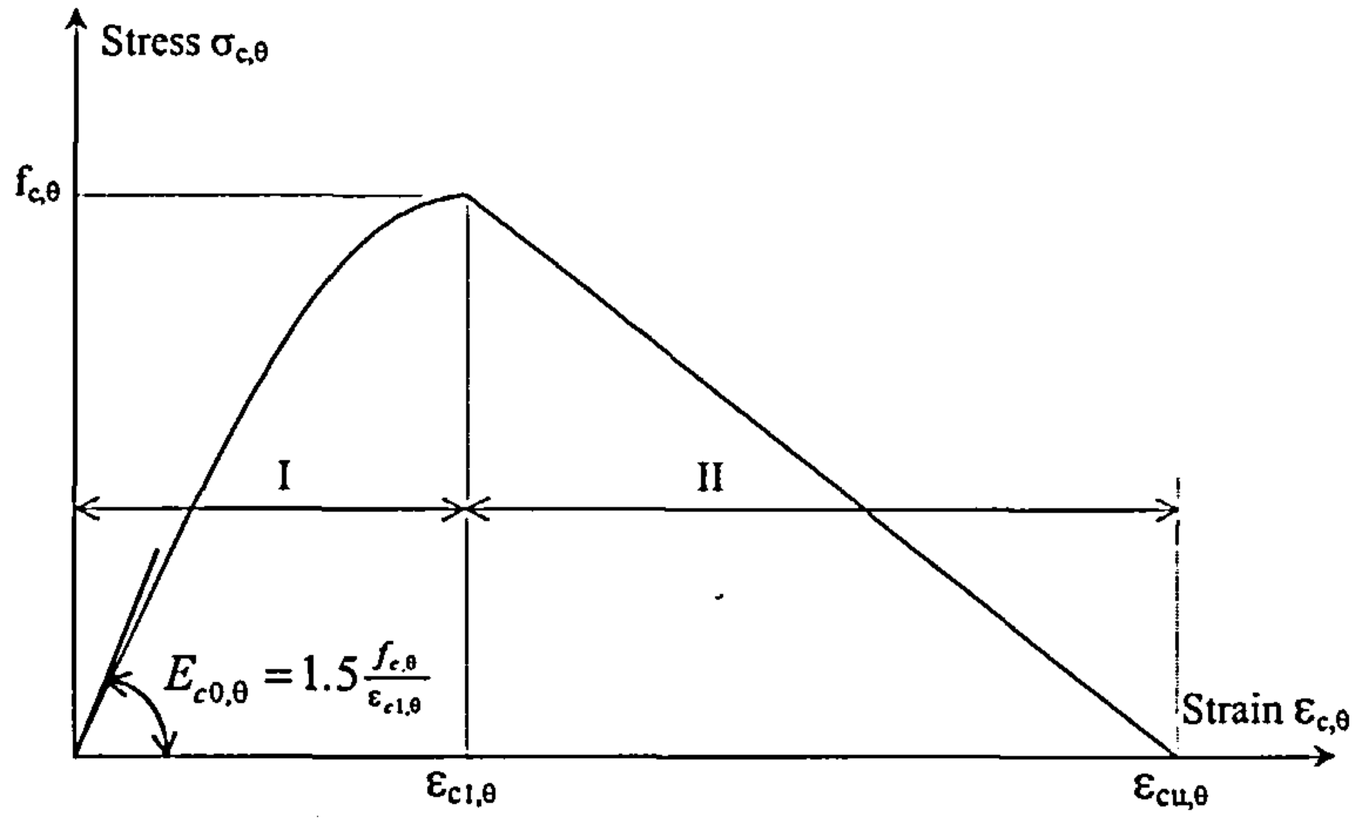

Fig. 1-11 Stress-strain relationship of concrete at elevated temperature

Table 1-4

Strain range	Stress $\sigma_{c,\theta}$	Tangent modulus
I $(\varepsilon_{c,\theta} \le \varepsilon_{c1,\theta})$	$f_{c,\theta}\left(\frac{3d}{2+d^3}\right)$ with $d=\frac{\varepsilon_{c,\theta}}{\varepsilon_{c1,\theta}}$	$\frac{f_{c,\theta}}{\varepsilon_{c1,\theta}}\left(\frac{3}{2+d^3}\right)\left(1-\frac{3d^3}{2+d^3}\right)$ with $d=\frac{\varepsilon_{c,\theta}}{\varepsilon_{c1,\theta}}$
II $(\varepsilon_{c1,\theta} \le \varepsilon_{c,\theta} \le \varepsilon_{cu,\theta})$	$f_{c,\theta}\left(1-\frac{\varepsilon_{c,\theta}-\varepsilon_{c1,\theta}}{\varepsilon_{cu,\theta}-\varepsilon_{c1,\theta}}\right)$	--

where,

$f_{c,\theta}$ is the compressive strength of concrete;

$\varepsilon_{c1,\theta}$ is the strain corresponding to $f_{c,\theta}$;

$\varepsilon_{cu,\theta}$ is the ultimate strain of concrete -- recommended values are given in EC4 part 1.2[48].

In engineering design the tensile stress of concrete is often ignored. This is both convenient and safe. It is recognised that tensile and flexural strength is more

sensitive than compressive strength to the effects of temperature, and the rate of reduction of tensile strength is greater than that of compressive strength when temperatures increase. EC4 part 1.2 suggests that, if tensile strength is taken into account, it should not exceed 10% of the corresponding compressive strength. No explicit expression is provided. However, an accurate analysis may require the effect of tension to be considered. At low levels of tension, concrete usually shows linear elastic behaviour until cracking occurs (reaching its ultimate tensile strength). When a region cracks, concrete cannot fully resist the subsequent tension and the effective tensile stress decreases. However, the amount and rate of these decreases seem still to be matters of controversy. Vecchio, et al.[58] proposed an equation to model the tensile strain-softening as.

$$f_t = \frac{f_t^{'}}{1.0 + \sqrt{200\varepsilon_{ct}}}$$

in which f_t, $f_t^{'}$ and ε_{ct} are the tensile stress, strength and strain, respectively.

However Rots, et al.[59] presented what they claimed to be a more simple and realistic model as illustrated in Fig. 1-12.

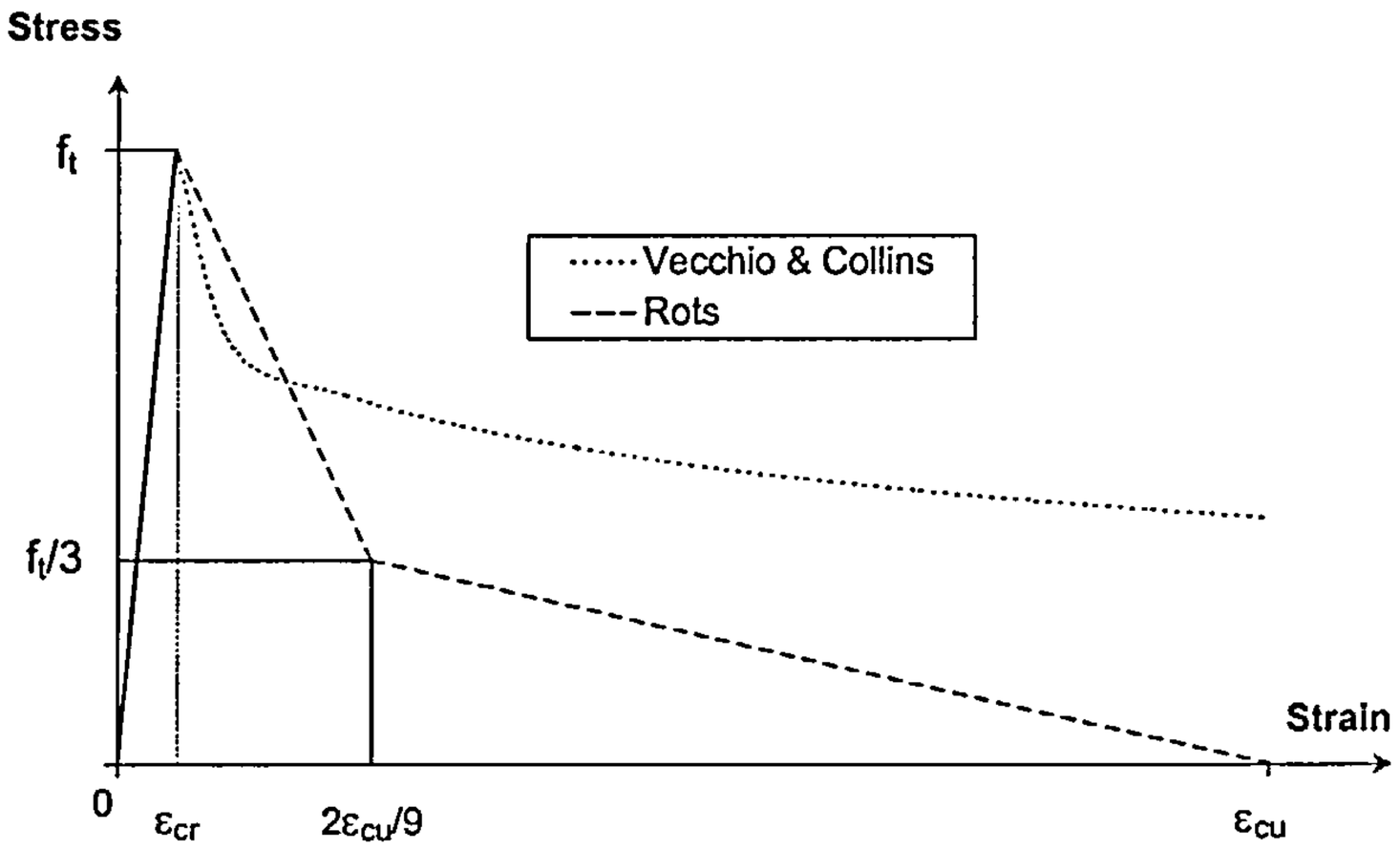

Fig. 1-12 Stress-strain relationship of concrete in tension at elevated temperature

1.6 THE OBJECTIVE AND SCOPE OF THE RESEARCH WORK

The main objective of this research is to develop the capability of the structural software VULCAN to perform non-linear analysis of three-dimensional composite structures subjected to fire conditions, and to carry out the investigations on composite structures, especially on the behaviour of corner sub-frames for fire conditions. This includes developing a more generalised beam-column model suitable not only for pure steel but also for reinforced concrete members and different section shapes under fire conditions. This chapter and the next outlines the background to the research work and the software VULCAN. Chapter 3 investigates the corner sub-frame based on the observed behaviour of the Cardington BRE corner test compared with 2D plane, 3D skeletal and composite frame analysis using VULCAN, and calculations according to fire design codes. These design codes are based on simplified assumptions and are normally considered as over conservative. One aim of this comparison was therefore to study the degree of conservatism of the design methods for the special corner column sub-frame. In Chapter 4 a generalised simplified approach is developed for corner sub-frames in fire. This is different from the complex finite element approach, being based on classical analysis and much simpler in its analytical solution. This sub-frame approach allows a quick approximate assessment of the behaviour to be performed. In Chapters 5 and 6, the development of the software VULCAN to improve the accuracy of the solution by using the member cross-section refinement is described. Chapter 6 also introduces a new type of steel beam cross-section into VULCAN. This is the Asymmetric Slimflor® Beam (ASB) which was developed for use with composite floors with deep steel decking. The principles and details of the modifications to the formulations together with software validations are included. In Chapter 7 a

generalised beam element has been developed to perform non-linear analysis for not only pure steel but also reinforced concrete beams in fire. Detailed formulations are given, followed by validations for various section types and materials. Chapter 8 presents the generalised conclusions for this research, with recommendations for further studies. Appendix **A** lists a post-processing programme, which can extract useful nodal displacement and force information from the VULCAN output file (**S.1**). This programme is written in standard Fortran and C++ languages, respectively, and is very easy to operate. Appendix **C** defines the data format for the input file of the generalised concrete beam member.

2. INTRODUCTION OF THE FINITE ELEMENT SOFTWARE VULCAN

In the course of several research projects at the University of Sheffield, the structural analysis software VULCAN has been well developed and is capable of modelling three-dimensional frames and sub-frames subjected to fire conditions. This chapter briefly introduces the development history of the software and its main principles.

2.1 HISTORY OF SOFTWARE VULCAN

In 1985, the fire research group at the University of Sheffield, which was led by Prof. Roger Plank and Prof. Ian Burgess, launched its work in numerical modelling, starting from simulating isolated steel members in furnace tests. In that time, Olawale[60] firstly used the finite strip method to analyse uniformly heated columns in fire. In his studies, the degradation of structural properties of the material was taken into account by considering the stress-strain-temperature relationship as a series of Ramberg-Osgood equations. In 1990, Saab[61,62] developed the two-dimensional non-linear finite element software INSTAF, which was based on EI-Zanaty and Murray's work[63,64], and this was extended by including temperature to investigate plane steel frames in fire. The original software covered both geometric and material non-linearities for steel beam/column members. Their stress-strain relationship was assumed to be temperature dependent only. The effects of thermal strains and residual stresses were also considered, and the cross-section of a member was intentionally divided into six sub-segments so that the variation of stress and non-linear distribution of temperature could be approximately modelled, even though within each of the sub-segments both were represented as linear distributions. In 1994, Najjar[34,65] extended this software to three-dimensions to analyse three-dimensional skeletal frames in fire, and named it

3DFIRE. Several different material models had been adopted in Najjar's model, and the cross-section was supposed to be divided into twelve sub-segments. Shortly afterwards, the further work had been done by Bailey[10] to develop the numerical model to include semi-rigid connection characteristics, lateral-torsional buckling and a 4-noded linear plate-element which could represent slab continuity. The unloading behaviour of steel-framed buildings in the cooling phase of a fire had also been addressed in Bailey's studies. This was the original version of the software VULCAN. In 1996, Shepherd[66] rewrote this software using structured standard Fortran language. Based on this version Huang[67,68] developed it to include a layered slab which addressed cracking behaviour. Since that time, Huang[74,75] has extended the 4-noded plate element to a 9-noded formulation in which both the geometric and material non-linearities for reinforced concrete slabs have been included. At present VULCAN has been developed to be able to perform non-linear analysis of three-dimensional composite structures in fire. The finite element approach currently includes both beam-column and flat-shell slab elements and is continually being developed by fire research group members.

2.2 BASIC PRINCIPLES AND FORMULATIONS

VULCAN is three-dimensional non-linear finite element analysis software. This software is intended to perform highly non-linear analysis for composite and steel-framed buildings under fire conditions. As shown in Fig. 2-1, the numerical model currently includes three different kinds of elements -- two-noded one-dimensional beam elements, four-noded/or nine-noded concrete slab elements and two-noded special elements (shear connector and spring elements). All these elements are related

to a reference plane but not necessarily simultaneously. Within this software certain assumptions are important

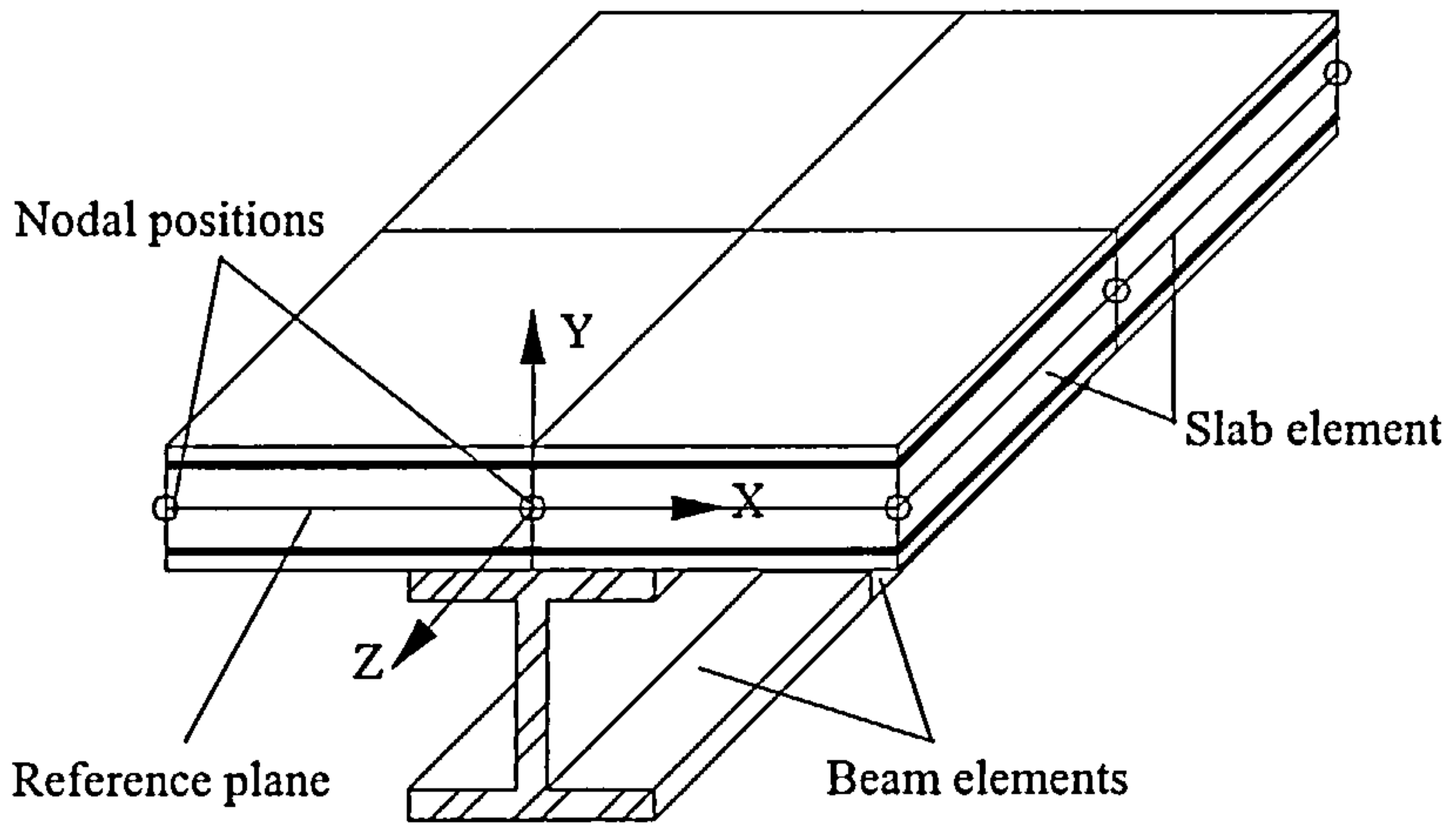

Fig 2-1 Normal composite structure division

- The common reference plane is assumed to coincide with the mid-surface of the concrete slab element when a slab element is represented, otherwise it should be at the centroid of the steel beam/column element.
- The beam/column element is straight, prismatic and symmetric about both the x-axis and y-axis, and its plane cross-section remains plane under flexural deformation. There is no distortion in cross-section and no shear deformation.
- The slab element is layered and there is no slip between adjacent layers. Concrete layers of the slab are in a state of plane stress, and concrete is considered to be orthotropic after cracking. Reinforcing steel bar is assumed to be modelled as an equivalent steel layer in which stiffness exists only along the reinforcement direction.
- There is no relative movement between the beam and slab elements unless shear connector elements have been included, and it is assumed that in the shear connector elements only relative movements parallel to slab plane have been

considered (i.e. the longitudinal and transverse slips between beam and slab element have been allowed, but uplift and other relative movements are prevented).

Based on these assumptions, the basic finite element stiffness equation for an element can be obtained through numerical manipulations

$$[K_t^e]\{\Delta q\} = \{\Delta Q\} \quad \text{or} \quad [K_t^e]\{\Delta q\} = \{Q\} - \{Q^R\} \tag{2-1a}$$

In global coordinates Eqn. (2-1a) can be rewritten as

$$[K_T^e]\{\Delta r\} = \{\Delta R\} \tag{2-1b}$$

Where,

$[K_t^e]$ is the incremental tangent stiffness matrix in local coordinates.

$[K_T^e]$ is tangent stiffness matrix in global coordinates and $[K_T^e] = [T]^T [K_t^e][T]$

in which [T] is a transformation matrix and has been defined by

$$\{\Delta q\} = [T]\{\Delta r\} \tag{2-2}$$

we also have Eqn. (2-3) for the globally unbalanced nodal force vector

$$\{\Delta R\} = [T]^T\{\Delta Q\} \tag{2-3}$$

The beam/column element is represented by a two-noded one-dimensional line element, and each of its nodes has eight degrees of freedom in local coordinates as shown in Fig. 2-2. In order to assemble the elements in the structure these local degrees of freedom need to be transformed into eleven global degrees of freedom by using the transformation matrix $[T]^{-1}$ which has been readily defined in Eqn. (2-2) and is detailed elsewhere[34]. It is evident that a beam node has the greatest number of degrees of freedom, and these numbers are regarded as common nodal degrees of freedom in spite of slab and special elements. Therefore the slab element has to extend

its nodal degrees of freedom to meet the common node's -- that is -- eleven degrees of freedom.

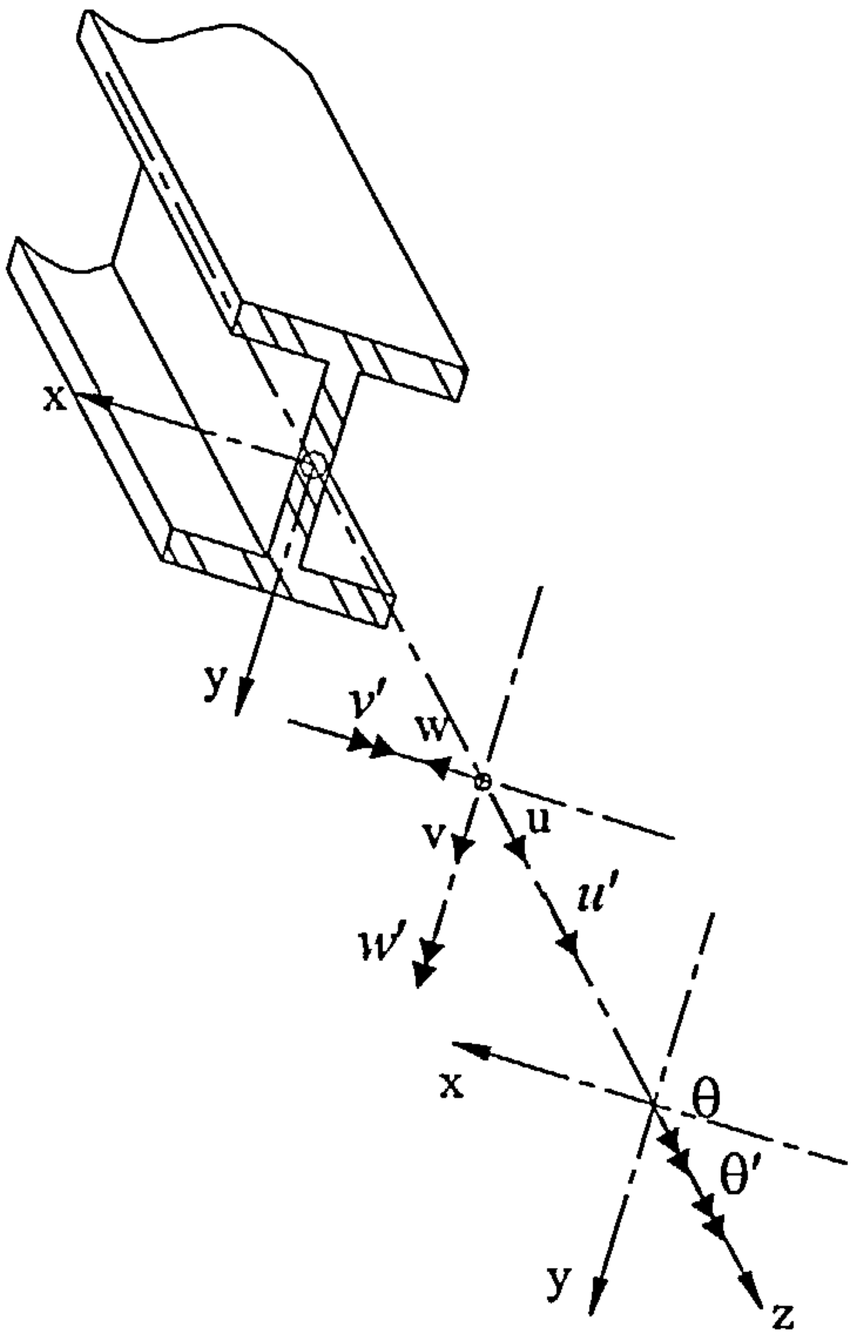

(a) Nodal degrees of freedom in local Coordinates (eight D.O.F)

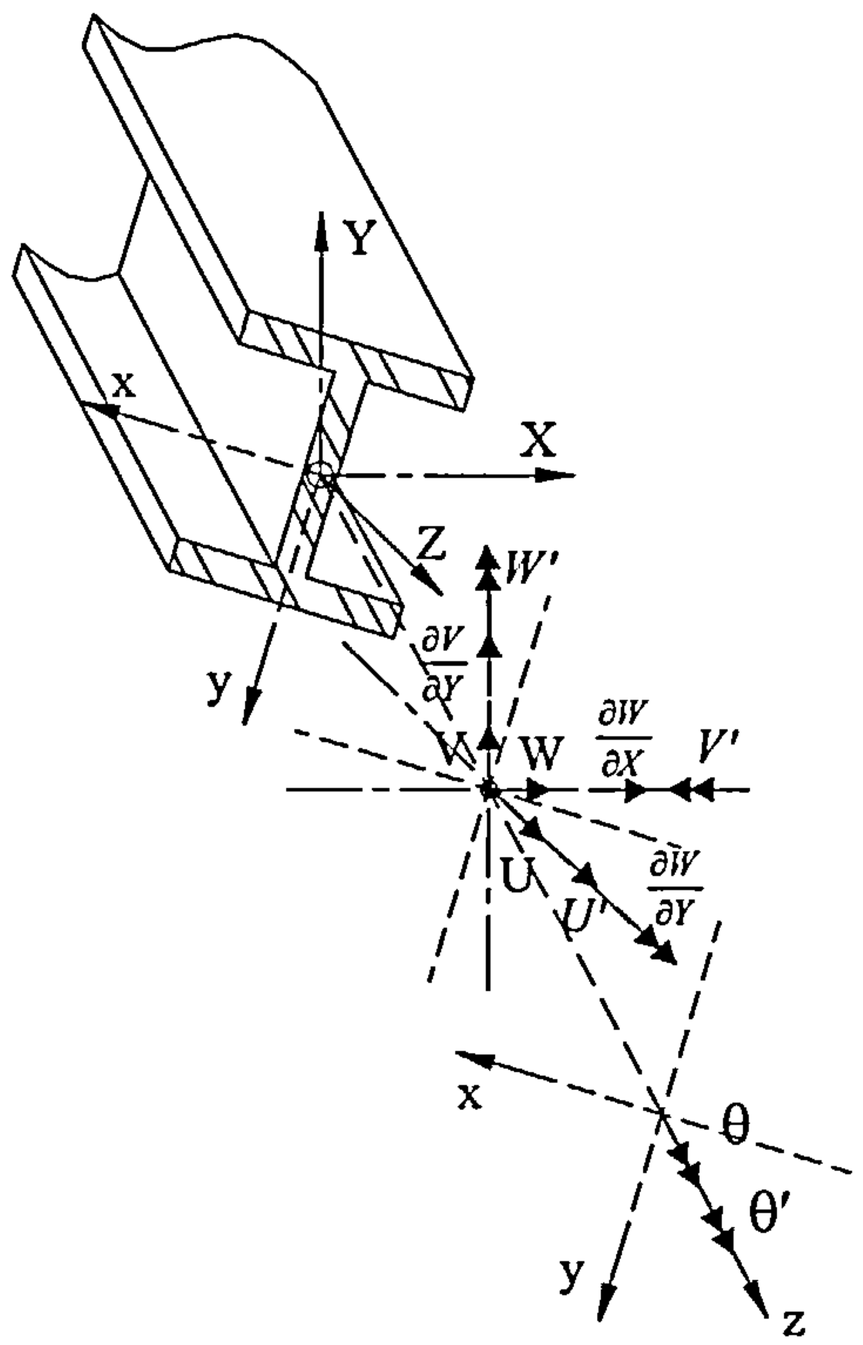

(b) Nodal degrees of freedom in global coordinates (eleven D.O.F)

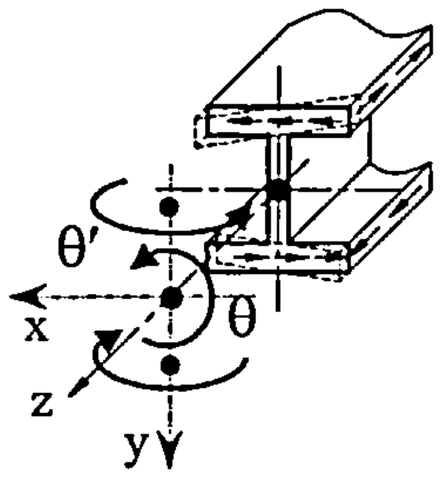

(c) Twisting and warping degrees of freedom

Fig. 2-2 Nodal Degrees of freedom in local and global coordinates

After assembling all the elements in global coordinates, the basic equation for the whole structure can finally be obtained as

$$[K_T]\{\Delta r\} = \{\Delta R\} \qquad \text{or} \qquad [K_T]\{\Delta r\} = \{R\} - \{R^R\} \qquad (2\text{-}4)$$

Where ,

$\{\Delta r\}$ is the assembled nodal displacement vector,

$\{\Delta R\}$ is the assembled unbalanced nodal force vector,

$\{R\}$ is the applied load vector in global coordinates,

$\{R^R\}$ is the assembled resisting force (internal nodal forces) vector, and is

$$[R^R] = \sum_{i=1}^{N_{beam}} [R^e_{beam}] + \sum_{i=1}^{N_{slab}} [R^e_{slab}] + \sum_{i=1}^{N_{shear}} [R^e_{shear}] + \sum_{i=1}^{N_{spring}} [R^e_{spring}] \qquad (2\text{-}5)$$

$[K_T]$ is the assembled incremental tangent stiffness matrix, and can be expressed by

$$[K_T] = \sum_{i=1}^{N_{beam}} [K^e_{beam}] + \sum_{i=1}^{N_{slab}} [K^e_{slab}] + \sum_{i=1}^{N_{shear}} [K^e_{shear}] + \sum_{i=1}^{N_{spring}} [K^e_{spring}] \qquad (2\text{-}6)$$

A brief view of these of three kinds of element can be given as follows.

2.2.1 BEAM ELEMENT MODELLING

The steel beam element is a two-noded line element with each node having eight degrees of freedom (as already shown in Fig. 2-2). Within this beam element, the displacements at any point on the reference axis between two end nodes can be expressed by

$$\{u_0\} = [N]\{q\} \qquad (2\text{-}7)$$

Where [N] is a cubic shape function matrix and {q} is the nodal displacement vector in local coordinates.

If a cross-section of the beam element cuts across the reference axis at this point, the displacements of an arbitrary point **A** on this cross-section can be obtained in terms of the reference axis displacements, according to the geometric description, as

$$\{u\} = [A]\{u_0\} + \{k_c\} \qquad (2\text{-}8)$$

where [A] is the geometric description matrix, $\{k_c\}$ is a constant vector and $\{u\}^T = \langle u, v, w \rangle$.

The general definition of axial strain at any arbitrary point in the beam element can be found from the large displacement equations[69] as

$$\varepsilon_z = < S > \{u\} \tag{2-9}$$

where <S> is a suitable operator vector. Since Eqn. (2-9) represents the highly non-linear strain-displacement relationship, the vector <S> contains displacements and their derivative terms. Thus Eqn. (2-9) may be rewritten in terms of the infinitesimal and large displacement components by

$$\varepsilon_z = \varepsilon_0 + \varepsilon_L = < B_0 > \{q\} + \frac{1}{2}\{u'\}^T\{u'\} \tag{2-10}$$

where $\{u'\}^T = \langle u', v', w' \rangle$ and $< B_0 >$ is the usual small displacement stain-displacement vector.

From Eqn. (2-10) it is implicit that $\varepsilon_L = \frac{1}{2}\{u'\}^T\{u'\}$ and thereby we have

$$d\varepsilon_L = \frac{1}{2}\{du'\}^T\{u'\} + \frac{1}{2}\{u'\}^T\{du'\} = \{u'\}^T\{du'\} = < B_L > \{dq\} \tag{2-11}$$

Then there is

$$d\varepsilon_z = d\varepsilon_0 + d\varepsilon_L = \langle B_0 \rangle \{dq\} + \langle B_L \rangle \{dq\} \tag{2-12a}$$

in which only $\langle B_L \rangle$ depends on the displacement.

Denoting $< \overline{B} > = < B_0 > + < B_L >$ Eqn. (2-12a) becomes

$$d\varepsilon_z = \langle \overline{B} \rangle \{dq\} \tag{2-12b}$$

where $\langle \overline{B} \rangle$ is the non-linear stain-displacement vector.

Based on this stain-displacement relationship, the principle of virtual work can be applied,

$$\delta W = \int_V \delta\varepsilon_z^T \sigma_z dV - \{\delta q\}^T \{Q\} = 0 \tag{2-13}$$

where ε_z expresses the mechanical axial strain such that

$$\varepsilon_{zm} = \varepsilon_z - \varepsilon_{zth} - \varepsilon_{zr}$$

On substitution of Eqn. (2-12b), Eqn. (2-13) can be rewritten as

$$\delta W = \int\int_A \{\delta q\}^T \{\overline{B}\} \sigma_z dA dz - \{\delta q\}^T \{Q\} = 0 \qquad (2\text{-}14)$$

The stress is related to strain by using the constitutive matrix [C]. However, since a two-noded one-dimensional line beam element is used here, the relationship can be simplified as

$$\delta\sigma_z = E_t \delta\varepsilon_z \qquad (2\text{-}15)$$

Equilibrium requires

$$\psi_i = \frac{\partial W}{\partial q_i} = 0 \qquad (2\text{-}16)$$

Where the range **i** is equal to the number of local nodal displacements, and

$$\{\psi\} = \int\int_A \{\overline{B}\} \sigma_z dA dz - \{Q\}$$

in which $\{\psi\}$ represents the sum of external and internal generalised forces.

If this equation is not satisfied exactly, the Newton-Raphson iteration will be applied to yield

$$\Delta\psi_i = \frac{\partial \psi_i}{\partial q_j} \Delta q_j = -\psi_i \qquad (2\text{-}17)$$

So that

$$\int\int_A \left(\left[\frac{\partial (B_L)_i}{\partial q_j} \right] \sigma_z + \{\overline{B}\} E_t \{\overline{B}\}^T \right) dA dz \cdot \{\Delta q\} = \{Q\} - \int\int_A \{\overline{B}\} \sigma_z dA dz \qquad (2\text{-}18)$$

Substituting $< \overline{B} > = < B_0 > + < B_L >$ into Eqn. (2-18) and rearranging produces

$$([K_\sigma] + [K_0] + [K_L])\{\Delta q\} = \{\Delta Q\} \qquad (2\text{-}19)$$

in which

$[K_\sigma]$ represents the geometric matrix and $[(K_\sigma)_{ij}]=\int\int_A\left[\frac{\partial(B_L)_i}{\partial q_j}\right]\sigma_z dAdz$

$[K_0]$ represents the small displacement stiffness matrix and

$$[K_0]=\int\int_A\{B_0\}E_t\{B_0\}^T dAdz$$

$[K_L]$ represents the large displacement matrix and

$$[K_L]=\int\int_A(\{B_0\}E_t\{B_L\}^T+\{B_L\}E_t\{B_0\}^T+\{B_L\}E_t\{B_L\}^T)dAdz$$

This is often written in symbolic form as

$$[K_t]\{\Delta q\}=\{\Delta Q\} \qquad (2\text{-}1)$$

in which $[K_t]$ is know as tangential stiffness matrix.

The detailed formulations of the beam element have been given by Najjar[34]. One can also consult chapter 7 of this thesis for reference.

2.2.2 SLAB ELEMENT MODELLING

Reinforced concrete slab elements can be represented by over-lapped four-noded Mindlin plate elements and four-noded plane stress elements. Each of their nodes has five degrees of freedom (three translations and two rotations) in local coordinates. For the sake of compatibility with the beam element, which has eleven nodal degrees of freedom, six additional dummy degrees of freedom are introduced for the slab. These are for convenience in combining the different elements and contribute nothing to the stiffness matrix. The following brief introduction to the slab formulations concerns only five basic nodal degrees of freedom.

As shown in Fig. 2-3, a typical slab shell element is considered as a plate bending element (with 3 degrees of freedom each node) superimposed on a plane stress membrane element (with 2 degrees of freedom each node). Since a node of the plate

bending element has only one transverse displacement and two rotations, the displacements at any point within the plate element can be expressed by

$$\{u_{plate}\} = [A_{plate}][N_{plate}]\{q_{plate}\} \tag{2-20}$$

Where $[N_{plate}]\{q_{plate}\}$ expresses the displacements at reference plane, and $[A_{plate}]$ is geometric description matrix, and $\{u_{plate}\}^T = \langle u, v, w \rangle$

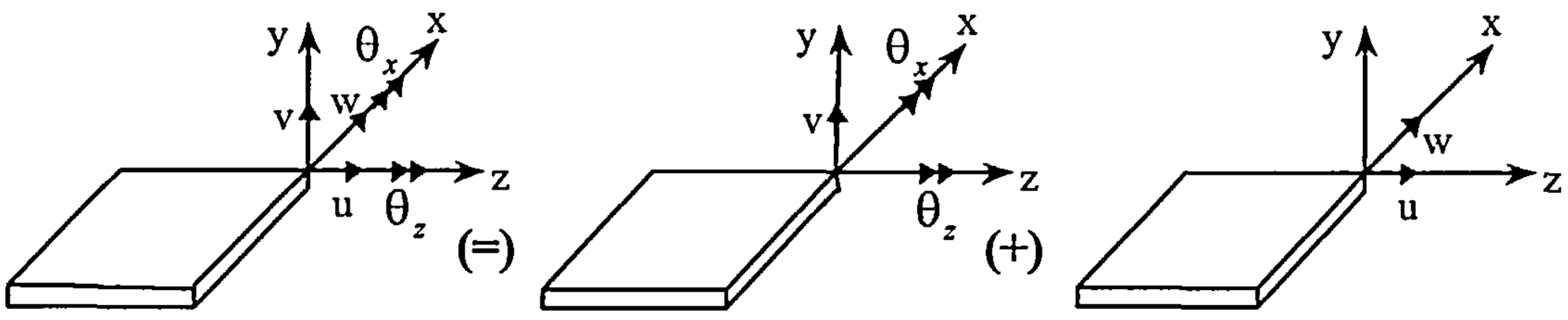

Slab element **Plate element** **Plane stress element**

Fig. 2-3 Concrete shell element

The general strain at any arbitrary point in the plate element can be obtained by

$$\{\varepsilon_{plate}\} = [S]\{u_{plate}\} \tag{2-21}$$

in which [S] is a suitable operator matrix and $\{\varepsilon_{plate}\}^T = \langle\langle \varepsilon_{bend} \rangle, \langle \gamma_{shear} \rangle\rangle$.

Substituting Eqns. (2-20) into Eqn. (2-21) and writing in symbolic form, we have

$$\{\varepsilon_{plate}\} = [B_{plate}]\{q_{plate}\} \tag{2-22}$$

in which $[B_{plate}]$ is the strain-displacement matrix, $[B_{plate}] = \begin{bmatrix} y[B_{bend}] \\ [B_{shear}] \end{bmatrix}$.

The stress resultants are related to strains and can be obtained by using the constitutive matrix [C]

$$\{\sigma_{plate}\} = [C_{plate}]\{\varepsilon_{plate}\} \tag{2-23}$$

where

$$\{\sigma_{plate}\}^T = \langle\langle \sigma_{bend} \rangle, \langle \tau_{shear} \rangle\rangle \text{ and } [C_{plate}] = \begin{bmatrix} [C_{bend}] & [0] \\ [0] & [C_{shear}] \end{bmatrix}$$

Applying the principle of virtual work[16],

$$\delta W = \int_V \{\delta q_{plate}\}^T [B_{plate}]^T [C_{plate}][k_1][B_{plate}]\{q_{plate}\} dV - \int_A \{\delta q_{plate}\}^T [N_{plate}]^T \{k_2\} p dA = 0$$

(2-24)

where $[k_1]$ is a constant factor matrix in which the actual non-uniformity of the shearing stress has been considered[73], $[k_1] = \begin{bmatrix} [I] & [0] \\ [0] & \frac{5}{6}[I] \end{bmatrix}$, and $\{k_2\}^T = \langle 0,0,1 \rangle$.

It is requires $\psi_i = \dfrac{\partial W}{\partial q_i} = 0$ (here **i** has the range of the number of local degrees of freedom for the plate element):

$$\int [B_{plate}]^T [C_{plate}][B_{plate}][k_1] dV \{q_{plate}\} - \{Q\} = 0 \qquad (2\text{-}25)$$

where $\{Q\}$ is the vertical load intensity and is given by: $\{Q\} = \int_A [N_{plate}]^T \{k_2\} p dA$.

If Eqn. (2-25) is not satisfied, the Newton-Raphson iteration method may be applied producing

$$[K_{plate}]\{\Delta q_{plate}\} = \{\Delta Q_{plate}\} \qquad (2\text{-}26)$$

in which $[K_{plate}] = [K_{bend}] + [K_{shear}]$,

$$[K_{bend}] = \int_A [B_{bend}]^T \left(\int_t y^2 [C_{bend}] dy \right) [B_{bend}] dA$$

$$[K_{shear}] = \int_A [B_{shear}]^T \left(\int_t \frac{5}{6} [C_{shear}] dy \right) [B_{shear}] dA$$

Within the plane stress membrane element, it is considered that there are two horizontal displacements at each node. The displacement will be

$$\{u_m\} = [N_m]\{q_m\} \qquad (2\text{-}27)$$

where the subscript m identifies the membrane element.

The strain can therefore be obtained by

$$\{\varepsilon_m\} = [S]\{u_m\} = [B_m]\{q_m\} \tag{2-28}$$

Using the principle of virtual work

$$\delta W = \int \{\delta q_m\}^T [B_m]^T [C_m][B_m]\{q_m\} dV - \{\delta q_m\}^T \{F\} = 0 \tag{2-29}$$

Finally we have

$$[K_m]\{\Delta q_m\} = \{\Delta Q_m\} \tag{2-30}$$

where $[K_m] = \int_A [B_m]^T (\int_t [C_m] dy)[B_m] dA$ and $[C_m] = [C_{bend}]$

By combining the plate element and the plane stress membrane element, the complete formulation for a reinforced concrete slab element can be written as

$$[K_{slab}]\{\Delta q_{slab}\} = \{\Delta Q_{slab}\} \tag{2-31}$$

where,

$$[K_{slab}] = \begin{bmatrix} [K_{plate}] & [0] \\ [0] & [K_m] \end{bmatrix}, \{\Delta q_{slab}\} = \begin{Bmatrix} \Delta q_{plate} \\ \Delta q_m \end{Bmatrix} \text{ and } \{\Delta Q_{slab}\} = \begin{Bmatrix} \Delta Q_{plate} \\ \Delta Q_m \end{Bmatrix}$$

Further details about this slab formulation can be found in references [67,68].

2.2.3 SPECIAL ELEMENT MODELLING

Some special elements, such as spring element and shear connector element, have been developed in the software. The spring element is a special beam element with zero length and can represent a semi-rigid connector between beam and column. The shear connector element is used to model the shear stud connection between the steel beam and the concrete slab.

The spring element is similar to the beam element but has zero length. The typical equation for this kind of element can be expressed by

$$[K_{sp}]\{q\} = \{Q\} \tag{2-32a}$$

which for non-linear behaviour becomes

$$\lfloor K_{sp} \rfloor \{\Delta q\} = \{\Delta Q\} \tag{2-32b}$$

as illustrated in Fig. 2-4.

Within the stiffness matrix $\lfloor K_{sp} \rfloor$, all the parameters are assumed to be independent. At present the spring element is assumed to be rigid in the lateral direction and the corresponding stiffness coefficients are therefore set to very large values. The in-plane parameters (K_u, K_v') of the stiffness matrix are normally obtained from experimental data. A formulation to calculate the rotation stiffness parameter K_v' at various temperatures was introduced by Bailey[10]. He suggested using a Ramberg-Osgood expression to fit the moment-rotation-temperature curve, and gave a set of temperature-dependent factors for a particular extended end-plate connection. He also considered the unloading behaviour of the connections in his program. The Ramberg-Osgood expressions are

$$\theta = \frac{M}{A} + 0.01(\frac{M}{B})^n \tag{2-33}$$

and thus

$$K_v' = \frac{dM}{d\theta} = \frac{1}{\frac{1}{A} + 0.01(\frac{M}{B})^{n-1}\frac{n}{B}} \tag{2-34}$$

where θ is the relative rotation (rads/1000), M is the moment (kNm) and A, B, n are temperature-dependent factors.

The shear connector element is also a two-noded element of zero length, each node having eight degrees of freedom in local coordinates. It is assumed that there is no relative vertical displacement or rotation between the beam and slab at common nodes. The tangent stiffness approach can be used to determine the relation between nodal

forces and nodal displacements for the connector, based on an empirical shear-slip relationship[70,71] given by

$$F = a(1 - e^{-b\lambda}) \tag{2-35}$$

in which F is the shear force, λ is the longitudinal slip and a, b are experimental constants which depend on the dimension and strength of the connector, surrounding concrete and temperature.

The longitudinal translation stiffness (tangent stiffness) can be evaluated by differentiating Eqn. (2-35) with respect to horizontal slip (λ) producing

$$K_i = \frac{dF_i}{d\lambda_i} = abe^{-b\lambda_i} \qquad (i = u, w) \tag{2-36}$$

where $\lambda_u = u$ and $\lambda_w = w$

Then, the basic equation for a shear connector element is given by

$$[K_{sh}]\{\Delta q\} = \{\Delta Q\} \tag{2-37}$$

as illustrated in Fig. 2-5. It should be noted that because Eqn. (2-37) is based on the assumption that there is no vertical uplift, or relative rotation between the beam and slab, the corresponding stiffness matrix coefficients will have infinite magnitude. Further details for the shear connector element is given by Huang et al.[72]

$$
\begin{bmatrix}
K_u & 0 & 0 & 0 & 0 & 0 & 0 & 0 & -K_u & 0 & 0 & 0 & 0 & 0 & 0 & 0 \\
0 & K_u' & 0 & 0 & 0 & 0 & 0 & 0 & 0 & -K_u' & 0 & 0 & 0 & 0 & 0 & 0 \\
0 & 0 & K_v & 0 & 0 & 0 & 0 & 0 & 0 & 0 & -K_v & 0 & 0 & 0 & 0 & 0 \\
0 & 0 & 0 & K_v' & 0 & 0 & 0 & 0 & 0 & 0 & 0 & -K_v' & 0 & 0 & 0 & 0 \\
0 & 0 & 0 & 0 & K_w & 0 & 0 & 0 & 0 & 0 & 0 & 0 & -K_w & 0 & 0 & 0 \\
0 & 0 & 0 & 0 & 0 & K_w' & 0 & 0 & 0 & 0 & 0 & 0 & 0 & -K_w' & 0 & 0 \\
0 & 0 & 0 & 0 & 0 & 0 & K_0 & 0 & 0 & 0 & 0 & 0 & 0 & 0 & -K_0 & 0 \\
0 & 0 & 0 & 0 & 0 & 0 & 0 & K_0' & 0 & 0 & 0 & 0 & 0 & 0 & 0 & K_0' \\
-K_u & 0 & 0 & 0 & 0 & 0 & 0 & 0 & K_u & 0 & 0 & 0 & 0 & 0 & 0 & 0 \\
0 & -K_u' & 0 & 0 & 0 & 0 & 0 & 0 & 0 & K_u' & 0 & 0 & 0 & 0 & 0 & 0 \\
0 & 0 & -K_v & 0 & 0 & 0 & 0 & 0 & 0 & 0 & K_v & 0 & 0 & 0 & 0 & 0 \\
0 & 0 & 0 & -K_v' & 0 & 0 & 0 & 0 & 0 & 0 & 0 & K_v' & 0 & 0 & 0 & 0 \\
0 & 0 & 0 & 0 & -K_w & 0 & 0 & 0 & 0 & 0 & 0 & 0 & K_w & 0 & 0 & 0 \\
0 & 0 & 0 & 0 & 0 & -K_w' & 0 & 0 & 0 & 0 & 0 & 0 & 0 & K_w' & 0 & 0 \\
0 & 0 & 0 & 0 & 0 & 0 & -K_0 & 0 & 0 & 0 & 0 & 0 & 0 & 0 & K_0 & 0 \\
0 & 0 & 0 & 0 & 0 & 0 & 0 & -K_0' & 0 & 0 & 0 & 0 & 0 & 0 & 0 & K_0'
\end{bmatrix}
\bullet
\begin{Bmatrix}
u_i \\ u_i' \\ v_i \\ v_i' \\ w_i \\ w_i' \\ \theta_{zi} \\ \theta_{zi}' \\ u_j \\ u_j' \\ v_j \\ v_j' \\ w_j \\ w_j' \\ \theta_{zj} \\ \theta_{zj}'
\end{Bmatrix}
=
\begin{Bmatrix}
Fz_i \\ Fz_i' \\ Fy_i \\ My_i \\ Fx_i \\ Mx_i \\ Mz_i \\ Mz\omega_i \\ Fz_j \\ Fz_j' \\ Fy_j \\ My_j \\ Fx_j \\ Mx_j \\ Mz_j \\ Mz\omega_j
\end{Bmatrix}
$$

Fig. 2-4 Illustration of typical equation for a spring element in local coordinates

Note: Since lateral displacements have been prevented, the lateral parameters will be

$$K_v = K_u' = K_w = K_w' = K_\theta = K_\theta' = 10^{20}$$

$$
\begin{bmatrix}
K_u & 0 & 0 & 0 & 0 & 0 & 0 & 0 & -K_u & 0 & 0 & 0 & 0 & 0 & 0 & 0 \\
0 & 0 & 0 & 0 & 0 & 0 & 0 & 0 & 0 & 0 & 0 & 0 & 0 & 0 & 0 & 0 \\
0 & 0 & K_v & 0 & 0 & 0 & 0 & 0 & 0 & 0 & -K_v & 0 & 0 & 0 & 0 & 0 \\
0 & 0 & 0 & K_v' & 0 & 0 & 0 & 0 & 0 & 0 & 0 & -K_v' & 0 & 0 & 0 & 0 \\
0 & 0 & 0 & 0 & K_w & 0 & 0 & 0 & 0 & 0 & 0 & 0 & -K_w & 0 & 0 & 0 \\
0 & 0 & 0 & 0 & 0 & K_w' & 0 & 0 & 0 & 0 & 0 & 0 & 0 & -K_w' & 0 & 0 \\
0 & 0 & 0 & 0 & 0 & 0 & 0 & 0 & 0_f & 0 & 0 & 0 & 0 & 0 & 0 & 0 \\
0 & 0 & 0 & 0 & 0 & 0 & 0 & 0 & 0 & 0 & 0 & 0 & 0 & 0 & 0 & 0 \\
-K_u & 0 & 0 & 0 & 0 & 0 & 0 & 0 & K_u & 0 & 0 & 0 & 0 & 0 & 0 & 0 \\
0 & 0 & 0 & 0 & 0 & 0 & 0 & 0 & 0 & 0 & 0 & 0 & 0 & 0 & 0 & 0 \\
0 & 0 & -K_v & 0 & 0 & 0 & 0 & 0 & 0 & 0 & K_v & 0 & 0 & 0 & 0 & 0 \\
0 & 0 & 0 & -K_v' & 0 & 0 & 0 & 0 & 0 & 0 & 0 & K_v' & 0 & 0 & 0 & 0 \\
0 & 0 & 0 & 0 & -K_w & 0 & 0 & 0 & 0 & 0 & 0 & 0 & K_w & 0 & 0 & 0 \\
0 & 0 & 0 & 0 & 0 & -K_w' & 0 & 0 & 0 & 0 & 0 & 0 & 0 & K_w' & 0 & 0 \\
0 & 0 & 0 & 0 & 0 & 0 & 0 & 0 & 0 & 0 & 0 & 0 & 0 & 0 & 0 & 0 \\
0 & 0 & 0 & 0 & 0 & 0 & 0 & 0 & 0 & 0 & 0 & 0 & 0 & 0 & 0 & 0
\end{bmatrix}
\bullet
\begin{Bmatrix}
u_i \\ u_i' \\ v_i \\ v_i' \\ w_i \\ w_i' \\ \theta_{zi} \\ \theta_{zi}' \\ u_j \\ u_j' \\ v_j \\ v_j' \\ w_j \\ w_j' \\ \theta_{zj} \\ \theta_{zj}'
\end{Bmatrix}
=
\begin{Bmatrix}
Fz_i \\ Fz_i' \\ Fy_i \\ My_i \\ Fx_i \\ Mx_i \\ Mz_i \\ Mz\omega_i \\ Fz_j \\ Fz_j' \\ Fy_j \\ My_j \\ Fx_j \\ Mx_j \\ Mz_j \\ Mz\omega_j
\end{Bmatrix}
$$

Fig. 2-5 Illustration of typical equation for a shear connector element in local coordinates

Note: Since there are no uplift and no relative rotation between beam and slab, the corresponding vertical and rotation parameters will be

$$K_v = K_v' = K_w' = 10^{20}$$

2.3 SOLUTION PROCEDURE

The finite element software VULCAN has been developed for the large deflection analysis of three-dimensional composite structures in fire conditions. This software considers both geometric and material non-linearities. As outlined above the governing equation gave

$$[K_T]\{\Delta r\} = \{\Delta R\} \quad \text{or} \quad [K_T]\{\Delta r\} = \{R\} - \{R^R\} \tag{2-4}$$

In order to perform the integration described above, the two-point formula and four-point formula of Gauss quadrature are employed for slab element and beam element respectively. Within the software the Newton-Raphson iteration procedure, which is probably the most rapidly convergent process for the solution of non-linear problems, is adopted for solving the nonlinear equilibrium equation Eqn. (2-4). During this process, the external loads and temperatures are assumed to remain constant within any single step. Loads or temperatures are only changed at the beginning of the subsequent step. This numerical procedure can be demonstrated by Fig. 2-6:

(1) At room temperature $\mathbf{T_0}$ the stiffness matrix $[\mathbf{K_T}]$ can be established based on displacements $\mathbf{r}$ (initially assumed to be zero), and the set of unbalanced forces $\Delta\mathbf{R_i}$ evaluated.

(2) Based on the stiffness matrix $[\mathbf{K_T}]$ and unbalanced forces $\Delta\mathbf{R_i}$ the incremental displacements $\Delta\mathbf{r_i}$ can be obtained by using the equilibrium equation of Eqn. (2-4), and the displacements are updated by adding incremental displacements $\Delta\mathbf{r_i}$ to previous displacements.

(3) Steps (1) and (2) are repeated until the real solution point **A** has been approached with both the unbalanced forces and incremental displacements being sufficiently

small.

(4) The temperature is increased to T_1, and the structure is reanalysed by repeating steps (1) to (3) based on the initial point **B** until the solution converges on point **C**.

By repeating this for each temperature increment, the complete deformation history is obtained.

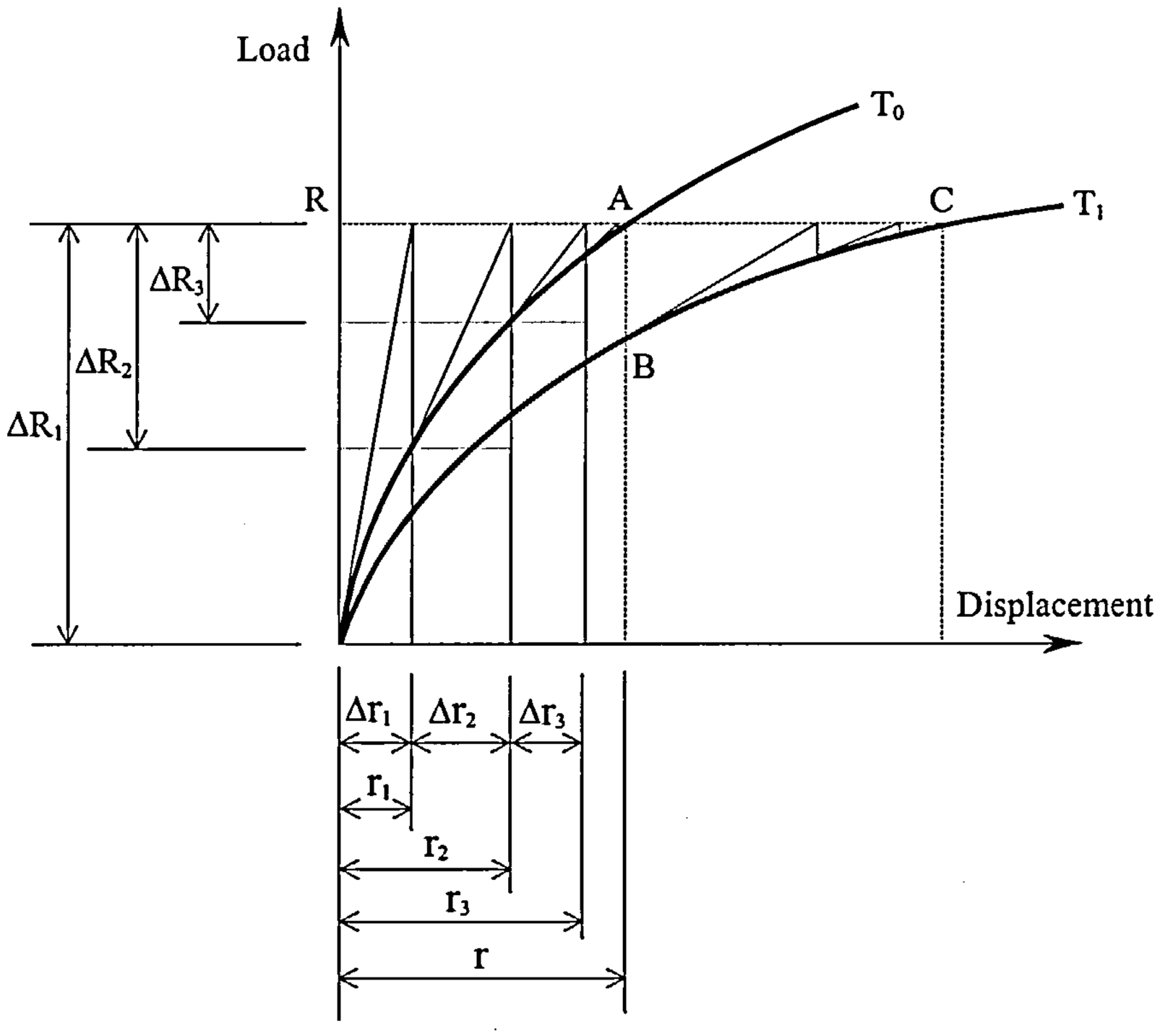

Fig. 2-6 Schematic representation of Newton-Raphson solution process (Temperature $T_1 > T_0$)

2.4 SHORTCOMINGS OF VULCAN

So far the basic formulations and principles of the original VULCAN have been introduced in this chapter. All the works introduced above have already been done by the group researchers[10,34,68]. Further developments based on the author's research work will be presented in the following chapters. Since the beam element in the original version of VULCAN is limited to a bi-symmetric I-section divided into twelve segments, it is necessary to develop a more generalised version for asymmetric

members with arbitrary section divisions. These modifications also allow the more accurate solution and highly non-linear distributions of temperatures and stresses across the cross-section to be represented. These developments are described in Chapters 3 and 6. In chapter 7 a new generalised beam element is described, capable of representing reinforced concrete members as well as steel sections of solid, open thin-walled, or hollow section. This enables the slimedek® floor system to be modelled. All these software developments are presented in detail the following chapters.

3. REFINEMENT OF BEAM-COLUMN ELEMENT CROSS-SECTION FOR SOFTWARE VULCAN

As introduced in the preceding chapter, for reasons of computational efficiency the software VULCAN uses two noded one-dimensional beam elements for prismatic members. The cross-section of these members is automatically divided into several segments by VULCAN. However, no deep study has been conducted until now to establish how refined this division should be to fully represent the behaviour of such members, especially at higher temperatures, even though Najjar[34] presented a preliminary study on it. His study used 12, 24, 36, 48, 60 and 72 segments and only two simple examples of a simply supported beam and a single column, were given. No detailed formulation was given. In this chapter, a general approach for refining the cross-section of a member and the formulations for its properties are developed. The results obtained using different segmentations are compared with original segmentations.

3.1 INTRODUCTION

The finite element software VULCAN has been developed at the University of Sheffield over many years to perform non-linear analysis of three-dimensional frames and sub-frames in fire. The software uses two-noded one-dimensional elements for beam/column members, with element nodes located at the reference axis, and it is at only these node positions that strain and stress are needed to perform the finite element analysis. However, in order to represent the true behaviour of the whole section and the variations of strain and stress, several sampling points are considered. Najjar[34,65] first developed the three-dimensional formulation of the beam-column elements as bi-symmetric thin-walled I- or H-section, whose cross-section was divided into twelve

segments, as shown in Fig 3-1, so that displacements and stresses are defined at thirteen points. This allows a considerable variation of stress through the cross-section.

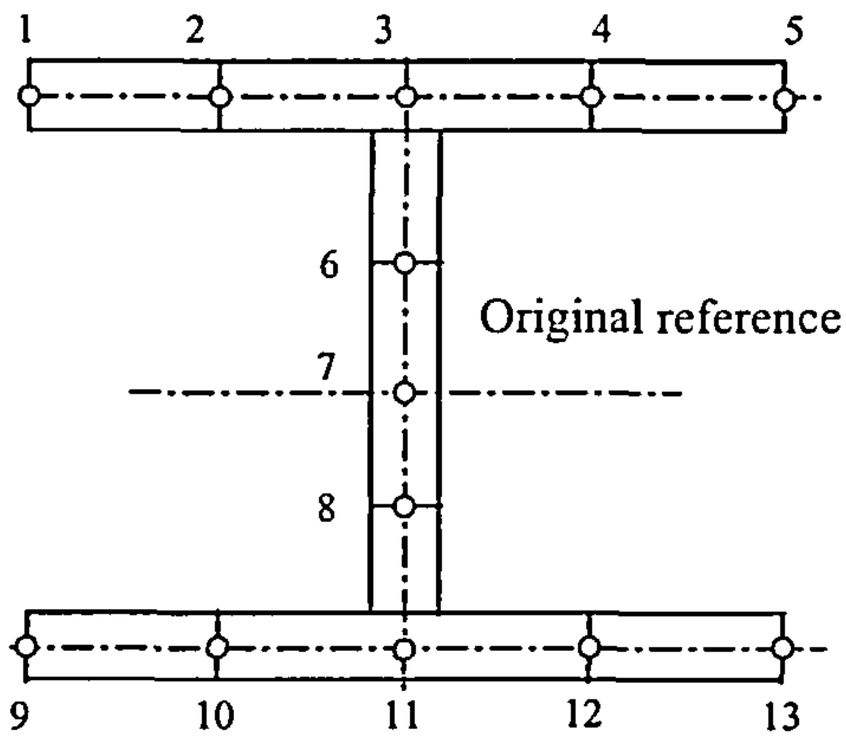

Fig. 3-1 Original Segmentation of a Beam-Column Element

From the non-linear axial stain-displacement equation (2-9), the axial strain at any arbitrary point on the cross-section can be expressed in terms of the displacement of the reference axis, which was originally sited at the centroid of the cross-section. The sectional properties and stress resultants can also be specified according to the formulations which were given by Najjar [34] and are not repeated here. However, there are some detailed changes in the exact expressions for certain properties resulting from the current more generalised approach, and these are listed. These are expressed on the basis of the assumption that the reference axis is at the centroid of the cross-section, for the case of symmetric section considered here, this coincides with the mid-depth and is consistent with Najjar's development. No studies have been undertaken to determine the optimum number of segments to maximise accuracy while keeping runtimes to a reasonable level, but it is no doubt that using more segments will produce more accurate results. This chapter concerns a re-formulation of part of the program in order to obtain a more accurate representation, in particular, of warping effects in unrestrained beams or columns, and comparisons are made based on uniform and non-uniform temperature profiles.

3.2 MEMBER CROSS-SECTION REFINEMENT

In order to refine the cross-section representation, the program has been upgraded so that the cross-section can be divided as finely as necessary. A new variable N has been included which defines half of the number of segments in either flange or the web of the cross-section. This means that the cross-section contains (6N+1) sampling points, as is shown in Fig 3-2.

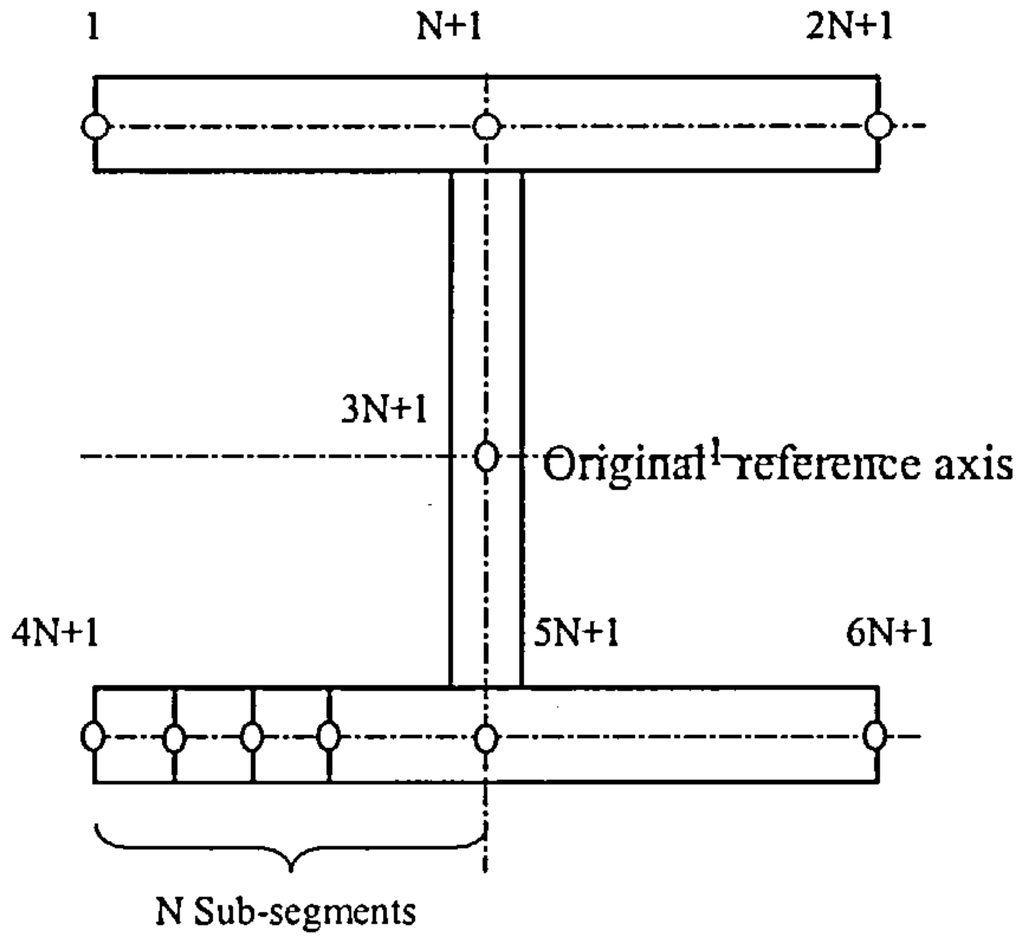

Fig. 3-2 The Refined Symmetric Cross-section

Although the number of segments of the cross-section can be varied in this way, the basic formulation and section properties are unchanged. However the detailed equations for the section properties and stress resultants are rewritten as follows.

Section properties:

$$A = \sum_{k=1}^{6N} A_k$$

$$I_x = \sum_{k=1}^{6N} A_k \Delta x$$

$$I_y = \sum_{k=1}^{6N} A_k \Delta y$$

$$I_{x2} = \sum_{k=1}^{6N} I_{yy} + \sum_{k=1}^{6N} A_k \Delta x^2$$

$$I_{y2} = \sum_{k=1}^{6N} I_{xx} + \sum_{k=1}^{6N} A_k \Delta y^2$$

$$I_{x3} = \sum_{k=1}^{6N} 3I_{yy} \Delta x + \sum_{k=1}^{6N} A_k \Delta x^3$$

$$I_{y3} = \sum_{k=1}^{6N} 3I_{xx} \Delta y + \sum_{k=1}^{6N} A_k \Delta y^3$$

$$I_{x4} = \sum_{k=1}^{6N} I_{4yy} + \sum_{k=1}^{6N} 6I_{yy} \Delta x^2 + \sum_{k=1}^{6N} A_k \Delta x^4$$

$$I_{y4} = \sum_{k=1}^{6N} I_{4xx} + \sum_{k=1}^{6N} 6I_{xx} \Delta y^2 + \sum_{k=1}^{6N} A_k \Delta y^4$$

$$I_{xy} = \sum_{k=1}^{6N} A_k \Delta x \Delta y$$

$$I_{x2y} = \sum_{k=1}^{6N} I_{yy} \Delta y + \sum_{k=1}^{6N} A_k \Delta x^2 \Delta y$$

$$I_{xy2} = \sum_{k=1}^{6N} I_{xx} \Delta x + \sum_{k=1}^{6N} A_k \Delta x \Delta y^2$$

$$I_{x2y2} = \sum_{k=1}^{6N} I_{xx} \Delta x^2 + \sum_{k=1}^{6N} I_{yy} \Delta y^2 + \sum_{k=1}^{6N} A_k \Delta x^2 \Delta y^2 + \sum_{k=1}^{6N} I_{xxyy} \quad (3\text{-}1)$$

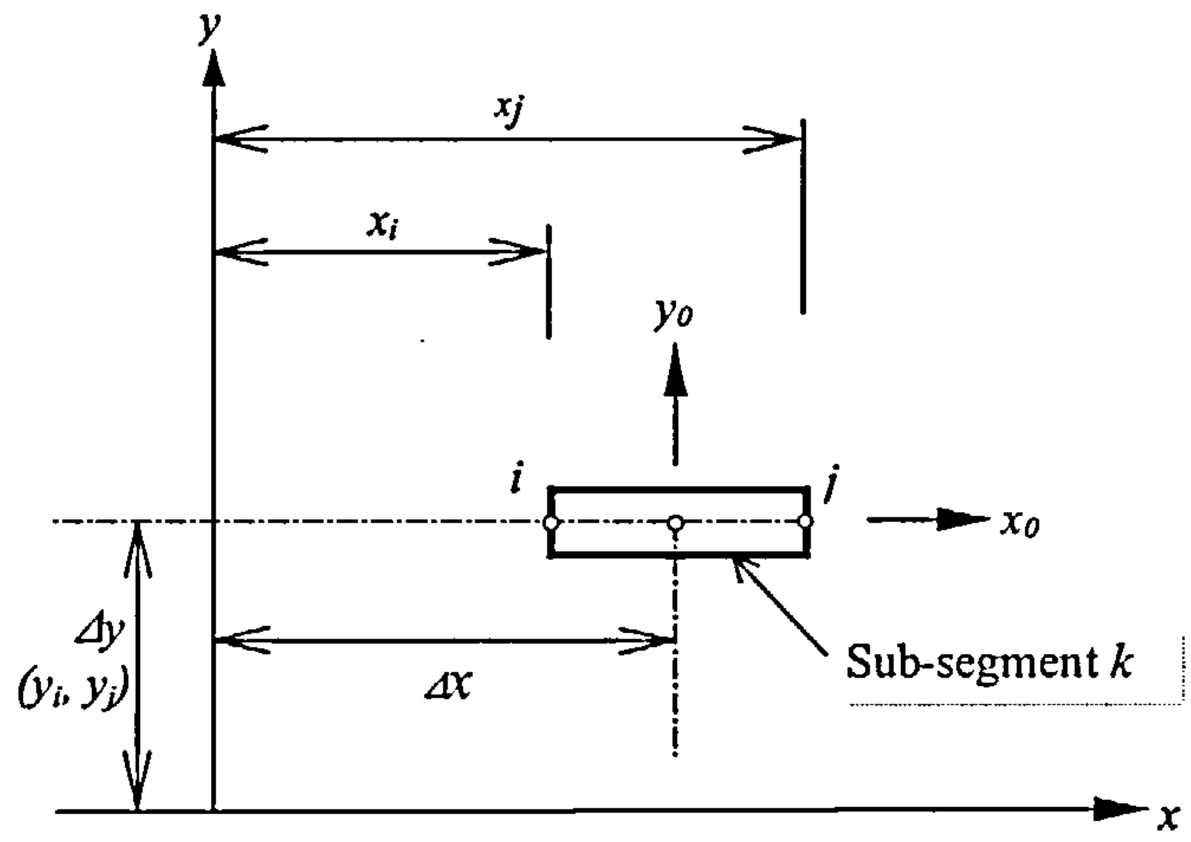

Fig 3-3 Co-ordinate system for segments.

where $I_{xxyy}=\frac{b^3h^3}{144}$, $I_{4xx}=\frac{bh^5}{80}$, $I_{4yy}=\frac{hb^5}{80}$, $I_{xx}=\frac{bh^3}{12}$, $I_{yy}=\frac{hb^3}{12}$ and the co-ordinates are defined in Fig 3-3. Here **b** is the side length of a segment measured in the x-direction, and **h** is its side length in the y-direction.

Sectorial properties are

$$I_\omega=\sum_{k=1}^{6N}\frac{lt}{2}(\omega_i+\omega_j)$$

$$I_{\omega x}=\sum_{k=1}^{6N}\frac{lt}{6}[\omega_i(x_j+2x_i)+\omega_j(x_i+2x_j)]$$

$$I_{\omega x2}=\sum_{k=1}^{6N}\frac{lt}{12}\{\omega_i[4x_i^2+2x_j^2+\frac{t^2}{2}-(x_j-x_i)^2(1+\frac{t^2}{2l^2})]+\omega_j[4x_j^2+2x_i^2+\frac{t^2}{2}-(x_j-x_i)^2(1+\frac{t^2}{2l^2})]\}$$

$$I_{\omega y}=\sum_{k=1}^{6N}\frac{lt}{6}[\omega_i(y_j+2y_i)+\omega_j(y_i+2y_j)]$$

$$I_{\omega y2}=\sum_{k=1}^{6N}\frac{lt}{12}\{\omega_i[4y_i^2+2y_j^2+\frac{t^2}{2}-(y_j-y_i)^2(1+\frac{t^2}{2l^2})]+\omega_j[4y_j^2+2y_i^2+\frac{t^2}{2}-(y_j-y_i)^2(1+\frac{t^2}{2l^2})]\}$$

$$I_{\omega 2}=\sum_{k=1}^{6N}\frac{lt}{3}(\omega_i^2+\omega_i\omega_j+\omega_j^2) \tag{3-2}$$

where ω is the sectorial co-ordinate of the corresponding point.

Stress resultants are

$$n=\sum_{k=1}^{6N}\frac{lt}{2}(\sigma_i+\sigma_j)$$

$$m_x=\sum_{k=1}^{6N}\frac{lt}{6}[\sigma_i(y_j+2y_i)+\sigma_j(y_i+2y_j)]$$

$$m_{x2} = \sum_{k=1}^{6N} \frac{lt}{12}\{\sigma_i[4y_i^2 + 2y_j^2 + \frac{t^2}{2} - (y_j - y_i)^2(1 + \frac{t^2}{2l^2})]$$
$$+ \sigma_j[4y_j^2 + 2y_i^2 + \frac{t^2}{2} - (y_j - y_i)^2(1 + \frac{t^2}{2l^2})]\}$$

$$m_y = \sum_{k=1}^{6N} \frac{lt}{6}[\sigma_i(x_j + 2x_i) + \sigma_j(x_i + 2x_j)]$$

$$m_{y2} = \sum_{k=1}^{6N} \frac{lt}{12}\{\sigma_i[4x_i^2 + 2x_j^2 + \frac{t^2}{2} - (x_j - x_i)^2(1 + \frac{t^2}{2l^2})]$$
$$+ \sigma_j[4x_j^2 + 2x_i^2 + \frac{t^2}{2} - (x_j - x_i)^2(1 + \frac{t^2}{2l^2})]\}$$

$$m_\omega = \sum_{r=1}^{3} \frac{lt}{6}[\sigma_i(\omega_j + 2\omega_i) + \sigma_j(\omega_i + 2\omega_j)]$$

$$m_{z2} = \sum_{k=1}^{6N} \frac{lt}{12}\theta_z'\{\sigma_i[4(x_i^2 + y_i^2) + 2(x_j^2 + y_j^2) + \frac{t^2}{2} - l^2]$$
$$+ \sigma_j[4(x_j^2 + y_j^2) + 2(x_i^2 + y_i^2) + \frac{t^2}{2} - l^2]\} \qquad (3\text{-}3)$$

where **l** and **t** are the breadth and thickness of any plate segment in the section (which means that **l** is an *x*-measurement in flanges and a *y*-measurement in the web). There is an exact match between **b** and **l** (and **h** and **t**) in a flange, but the correspondence is reversed for segments of a web. All calculations are based on the transformed section, that is $t_t = t\frac{E_t}{E}$, in which t_t is the transformed thickness of the plate segment, E_t is the average tangent modulus of the material within the segment, t is the original thickness of the plate segment, and E is the original Young's Modulus of material within the segment.

Applying these steps within the program, a more exact result can be obtained when a large number for the sub-segment variable **N** is set. The results also show some improvement in convergence behaviour, since the refinement to the cross-section gives a smoother variation of stress resultants.

3.3 PROGRAM VULCAN MODIFICATIONS

The following subroutines of the program VULCAN have been modified to take account of the re-formulation presented above:

- SUBROUTINE MAINMG
- SUBROUTINE STIFF
- SUBROUTINE STEP
- SUBROUTINE STEPF
- SUBROUTINE GET_TEMP
- SUBROUTINE INPUT1
- SUBROUTINE INPUT2
- SUBROUTINE GET_INFO
- SUBROUTINE GET_RES
- SUBROUTINE GET_DPLY

In order to validate the modified program, several analyses were carried out by using the same sectional representation of sub-segments as in the original program (N=2, i.e. twelve sub-segments), for both restrained and unrestrained members. All the results showed an identical comparison with the original program, indicating that the modifications had been correctly implemented.

3.4 COMPARISON STUDIES (VALIDATION STUDIES)

To generalise the study of the effect of section refinement three cases have been considered. The first two were based on a simply supported beam with different temperature profiles, and the last one was based on a more realistic sub-frame.

The first case was a simply supported beam of 1000mm span and 356x171x51UB symmetric section, loaded by a central point load of 1000KN. The material for this beam was S355 steel and it was uniformly heated up to failure. Five different levels of section refinements, that is 6, 12, 30, 60 and 600 segments respectively, were used through this analysis. The results for mid-span deflections (horizontal and vertical) at increasing temperature for the different refinements are tabulated in Table 3-1. Fig 3-4 shows the displacement profile along the length of the beam at the predicted failure temperature of 582°C. It can be seen from Table 3-1that at ambient temperature there is no difference between results, regardless of how the section is divided, but as the temperature rises deviations develop. For vertical displacements these show a difference of 37% between 6-segment and 600-segment at 570°C but less than 5% difference between 12-segment and 600-segment at the predicted failure temperature of 582°C. The differences in horizontal displacements between 6-segment with 600-segment and 12-segment with 600-segment were both less than 5% at a beam temperature of 570°C.

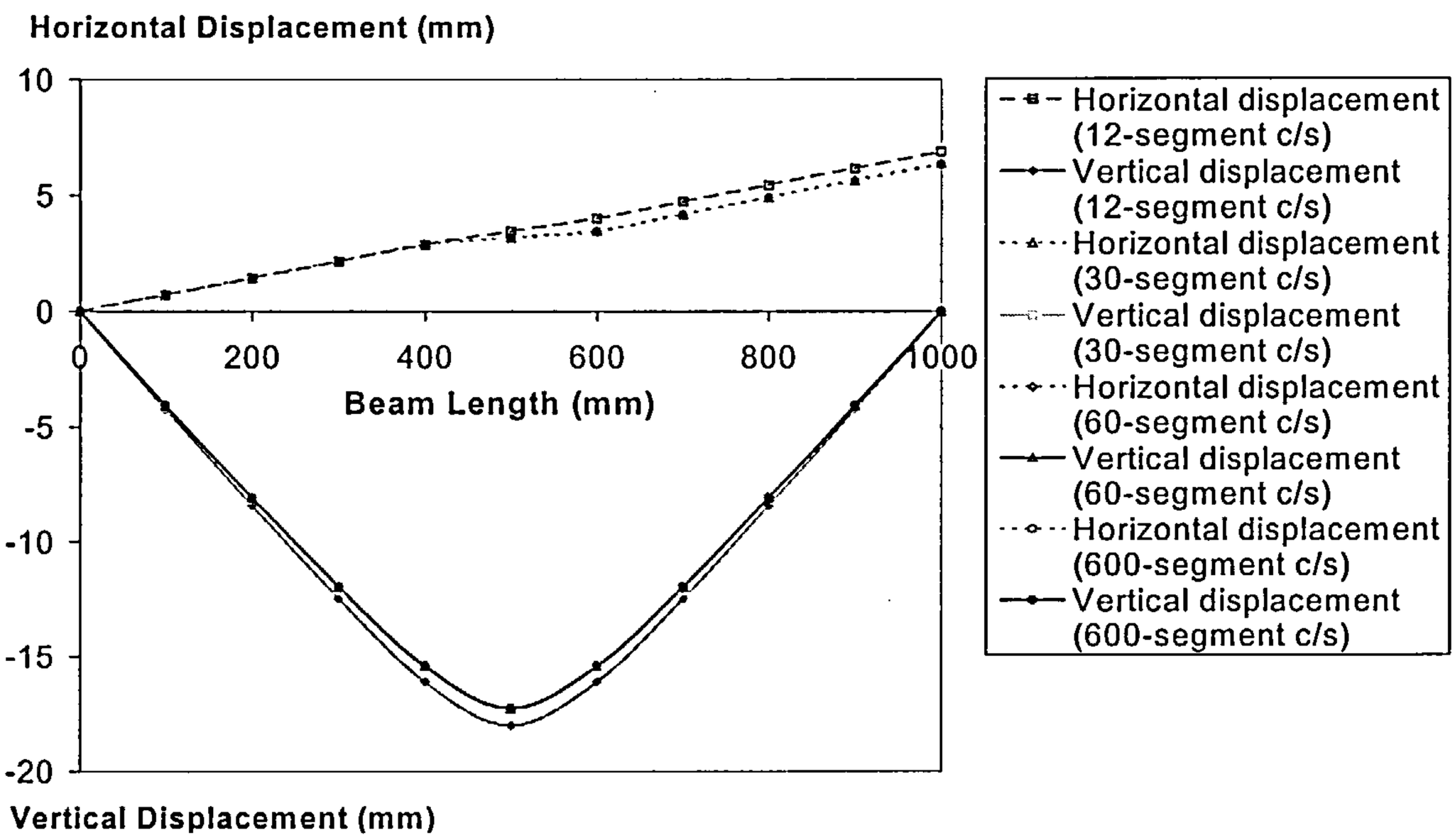

Fig 3-4 Displacement of steel beam at 582°C

Beam temperature (°C)	Horizontal displacement (mm)					Vertical displacement (mm)				
	6-segment	12-segment	30-segment	60-segment	600-segment	6-segment	12-segment	30-segment	60-segment	600-segment
20	-0.001	-0.001	-0.001	-0.001	-0.001	-0.7019	-0.7019	-0.7019	-0.7019	-0.7019
70	0.3072	0.3072	0.3072	0.3072	0.3072	-0.701	-0.701	-0.701	-0.701	-0.701
120	0.625	0.6251	0.6251	0.6251	0.6251	-0.7112	-0.7112	-0.7112	-0.7112	-0.7112
170	0.9526	0.9526	0.9526	0.9526	0.9526	-0.7395	-0.7395	-0.7395	-0.7395	-0.7395
220	1.2898	1.2898	1.2898	1.2898	1.2898	-0.7763	-0.7756	-0.7751	-0.775	-0.7749
270	1.6362	1.6363	1.6363	1.6363	1.6363	-0.8889	-0.8714	-0.865	-0.8642	-0.8639
320	1.9915	1.9919	1.9919	1.992	1.992	-1.1585	-1.0871	-1.0752	-1.0734	-1.0728
370	2.3568	2.3572	2.3574	2.3574	2.3574	-1.3663	-1.2676	-1.2516	-1.2493	-1.2485
420	2.7309	2.7316	2.7318	2.7318	2.7318	-1.6724	-1.5213	-1.4975	-1.4942	-1.4931
470	3.1083	3.1099	3.1102	3.1104	3.1104	-2.6975	-2.328	-2.2657	-2.259	-2.2567
520	3.463	3.4713	3.467	3.4666	3.467	-5.7545	-4.6593	-4.4537	-4.4331	-4.4268
570	3.5349	3.6238	3.5088	3.4817	3.4875	-16.97	-13.0785	-12.4342	-12.3966	-12.3698
573.125	3.4973	--	--	--	--	-18.3893	--	--	--	--
574.688	3.4739	--	--	--	--	-19.1562	--	--	--	--
575.078	3.4674 *	--	--	--	--	-19.3541 *	--	--	--	--
576.25	--	3.5601	3.3787	3.3583	3.3629	--	-15.3426	-14.6805	-14.6212	-14.592
579.375	--	3.5017	3.2796	3.2659	3.2696	--	-16.6827	-16.0338	-15.9546	-15.9244
580.938	--	3.4622	3.2191	3.2093	3.2126	--	-17.4181	-16.7819	-16.6901	-16.6591
581.719	--	3.439	3.1857	3.1778	3.181	--	-17.8046	-17.176	-17.0774	-17.0459
582.109	--	3.4265 *	3.1682 *	3.1612 *	3.1644 *	--	-18.003 *	-17.3785 *	-17.2763 *	-17.2445 *

Table 3-1 Analysis results at mid-span for different cross-section divided
(Note: Displacements at predicted failure temperature have been marked with asterisk *)

The above example was re-analysed using a different temperature profile. The layout and temperature distribution are shown in Fig 3-5, where the top and bottom flange temperatures are increased in steps of 20°C and 50°C respectively. The results of the analyses are illustrated in Fig 3-6 and Fig 3-7.

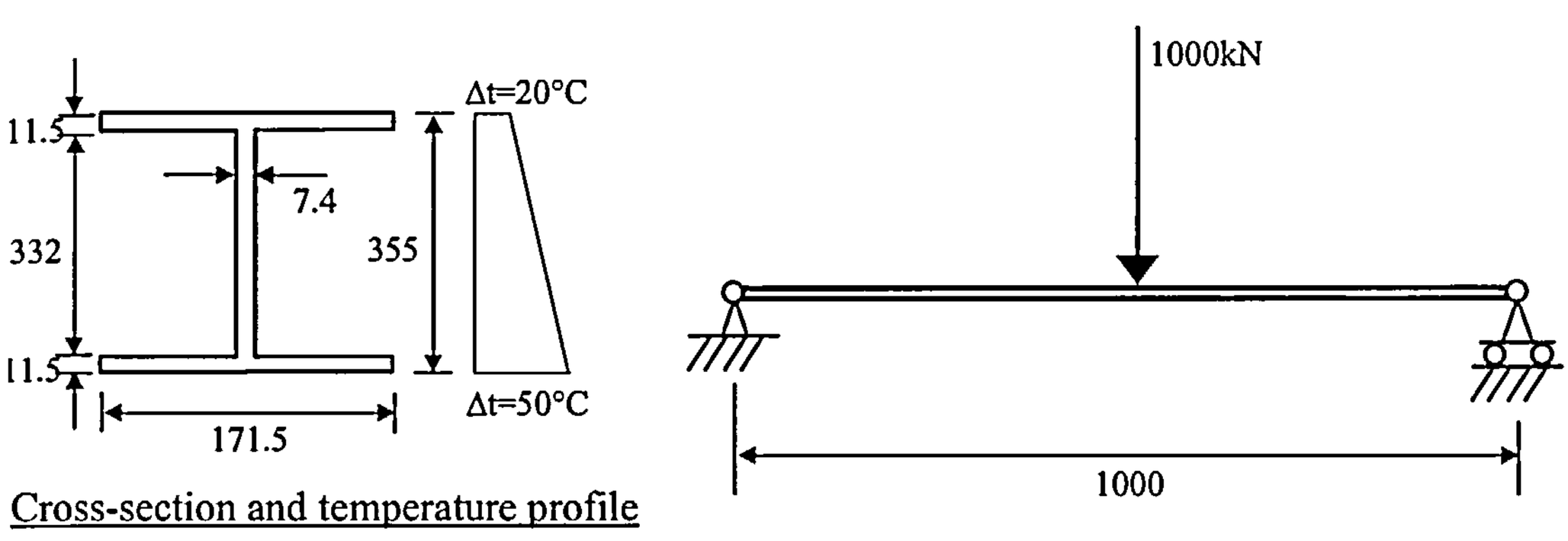

Fig. 3-5 Simply supported symmetric beam (356x171x51UB) example

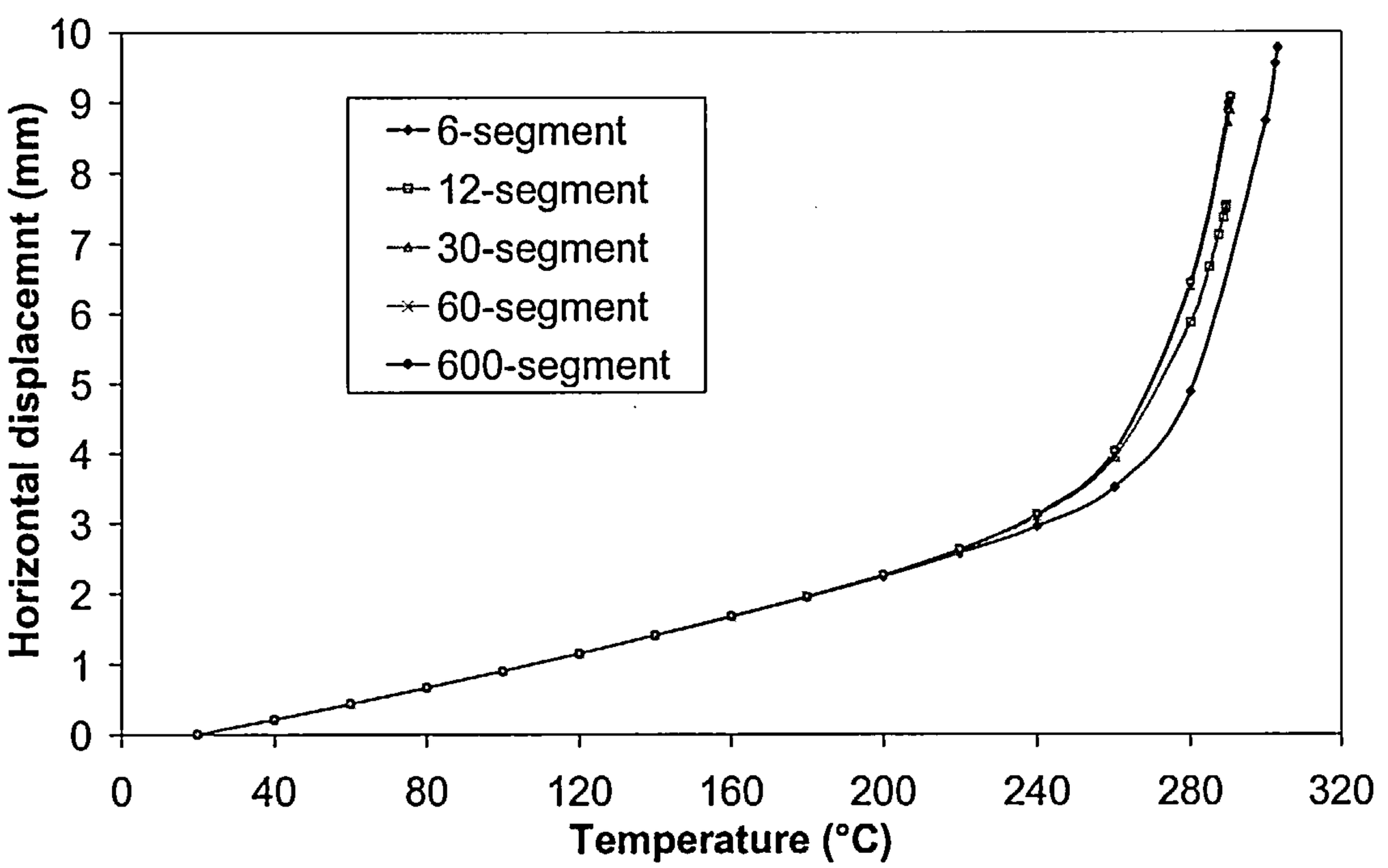

Fig. 3-6 Horizontal displacement at mid-span for a simply supported symmetric beam (356x171x51UB)

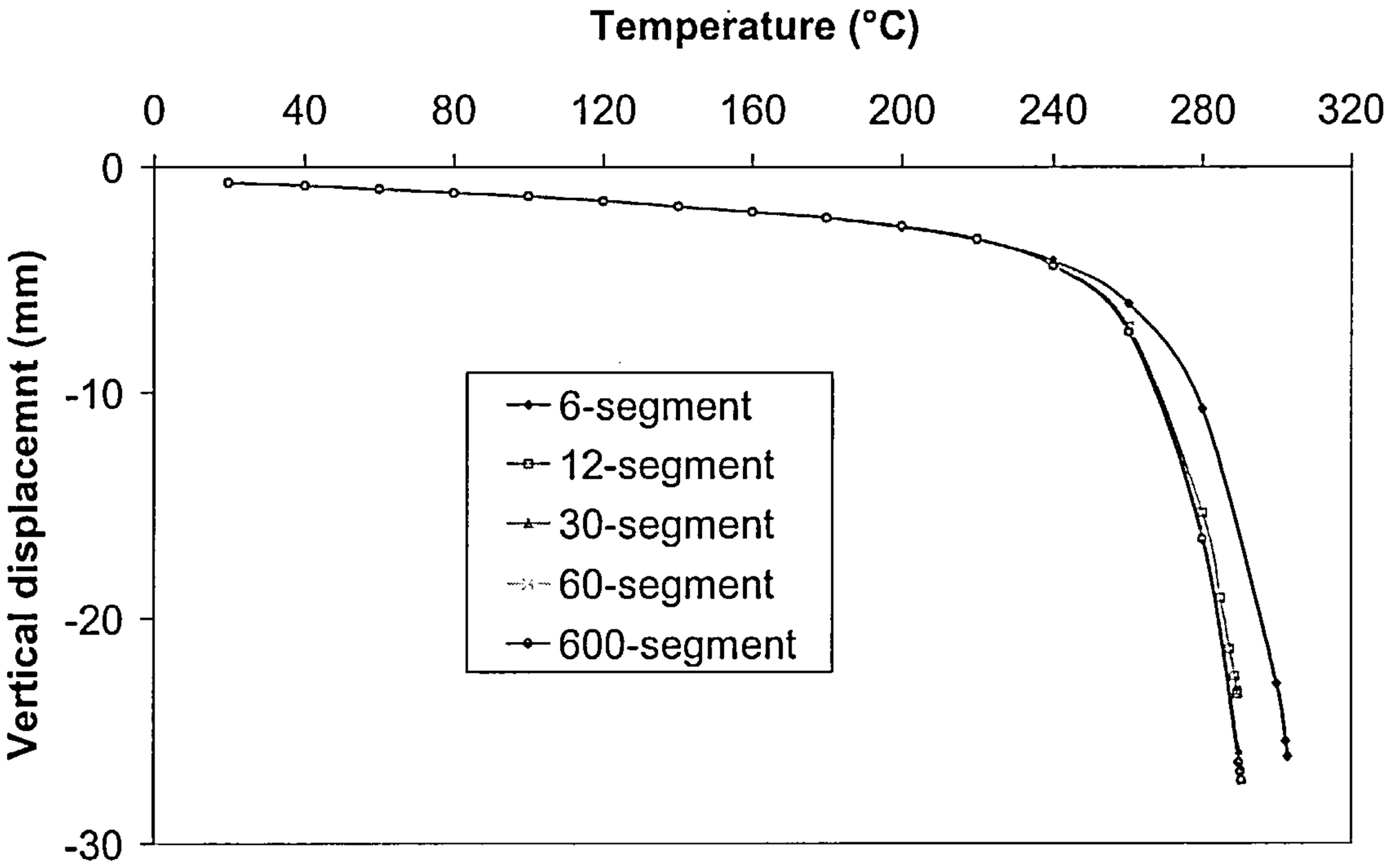

Fig. 3-7 Vertical displacement at mid-span for a simply supported symmetric beam (356x171x51UB)

From these it can be seen that there is more than 32% difference in horizontal displacement and 54% difference in vertical displacement between 6-segment and 600-segment when the beam temperature exceeds 280°C, but the 12-segment model gives results which are almost identical to those for more refined sections.

In order to investigate further the influence of section refinement, a more complex case was analysed using the original program and its re-formulation. This was a simple sub-frame as shown in Fig 3-8 for which the column length was 8370mm, and the lengths of beams 1 and 2 were 6000mm and 9000mm respectively. The column used was a 305x305x137UC (S355 steel) symmetric section and beams 1 and 2 were 356x171x51UB S355 section. An axial load of 2684KN (load ratio=0.55) was imposed at the top of column, and the lower column and both beams were uniformly heated at the same rate, with the upper column being kept cool.

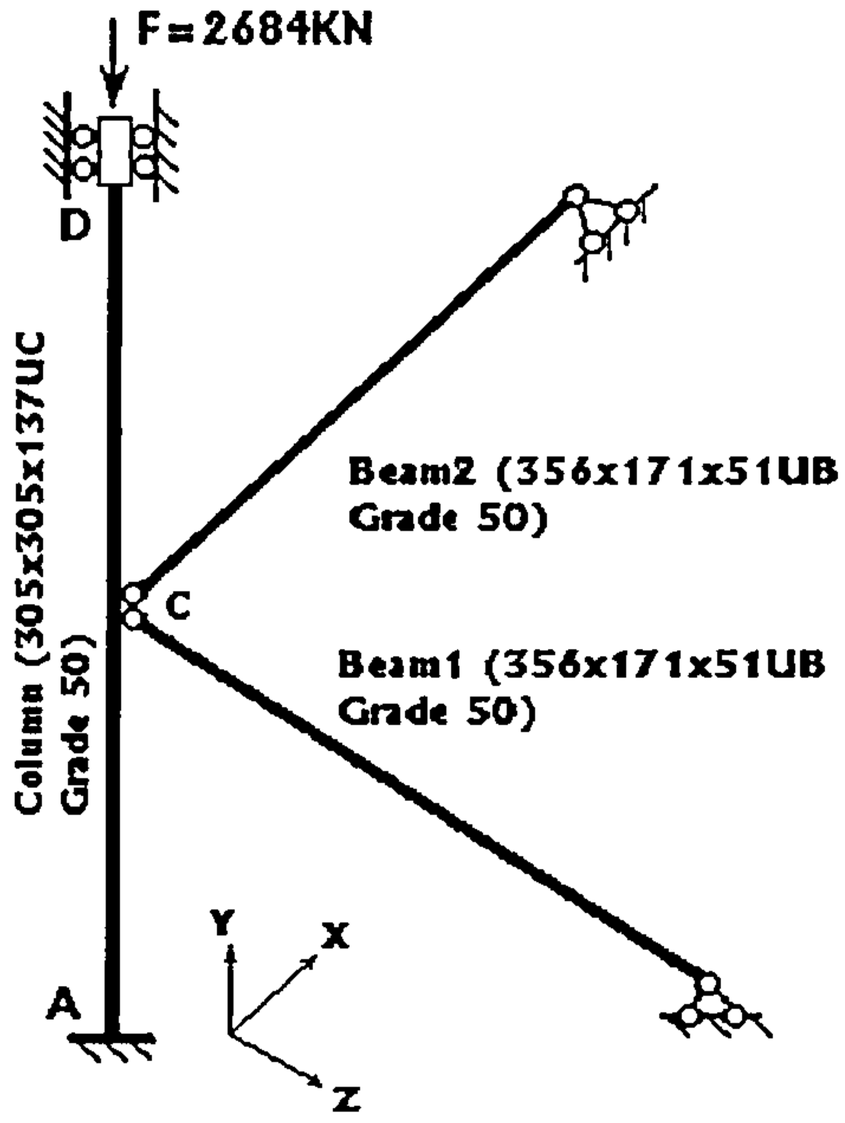

Fig 3-8 Skeletal sub-frame used for validation

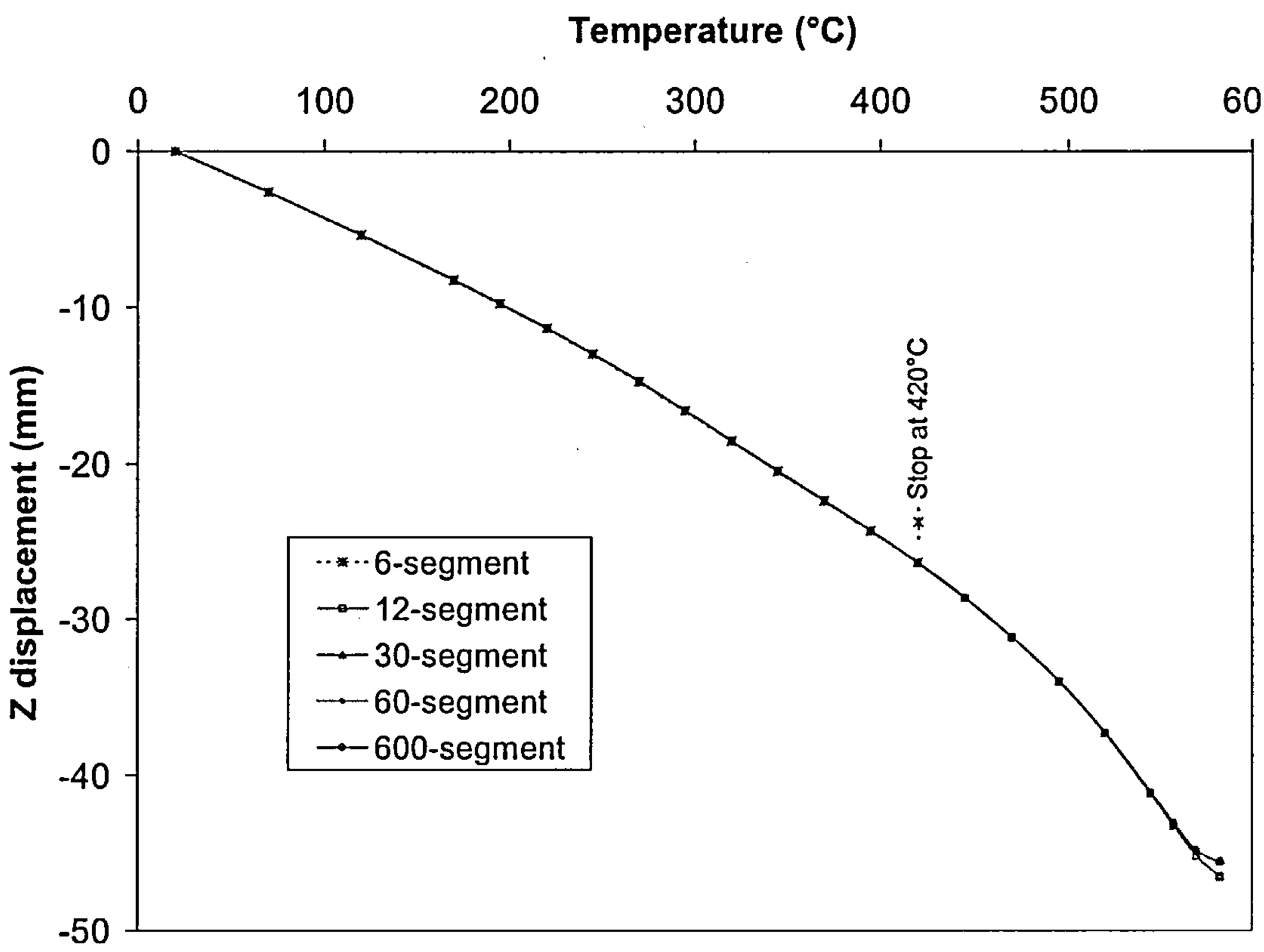

Fig 3-9 Horizontal Z displacements at 14/20 of lower column

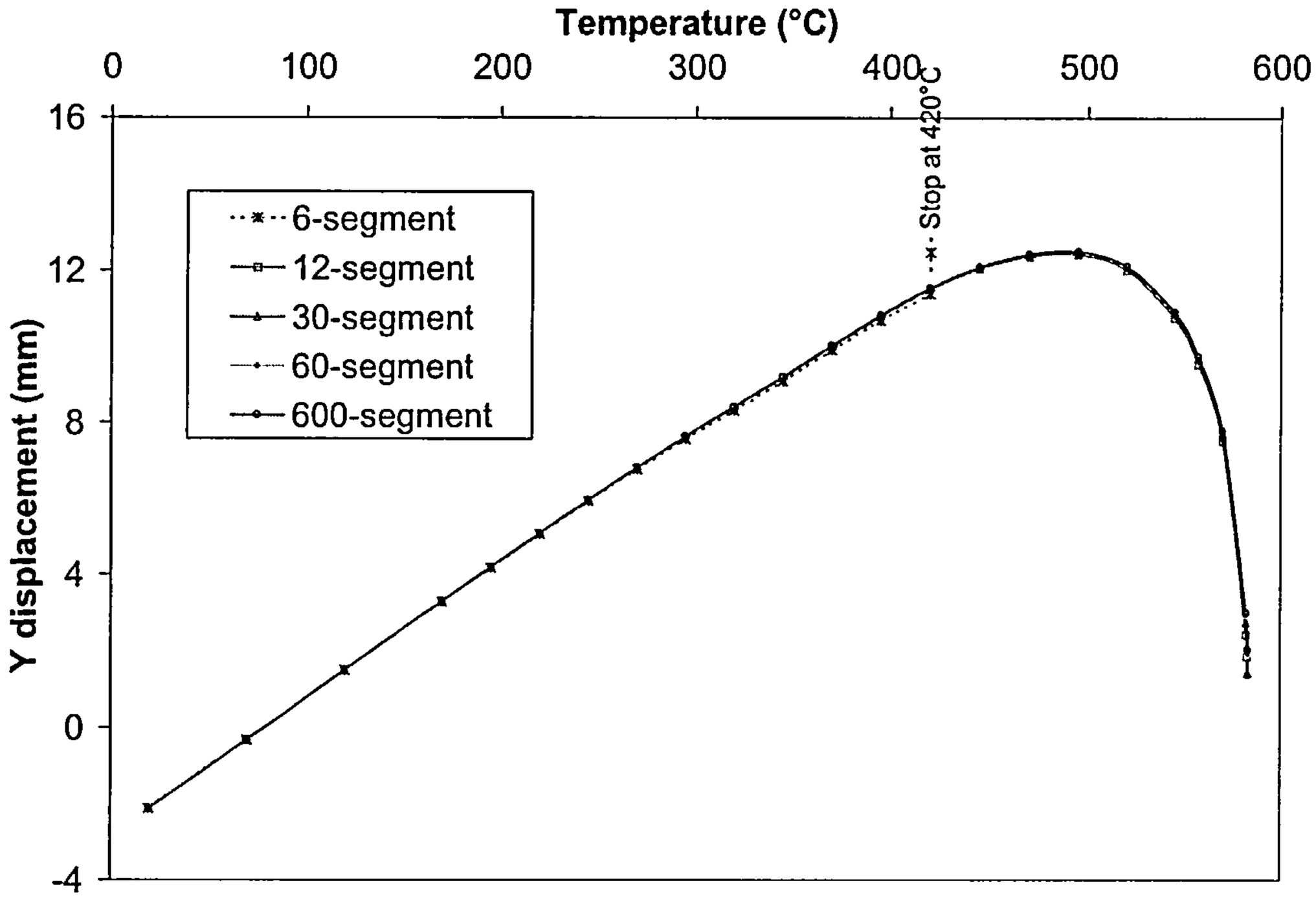

Fig 3-10 Vertical Y displacements at 14/20 of lower column

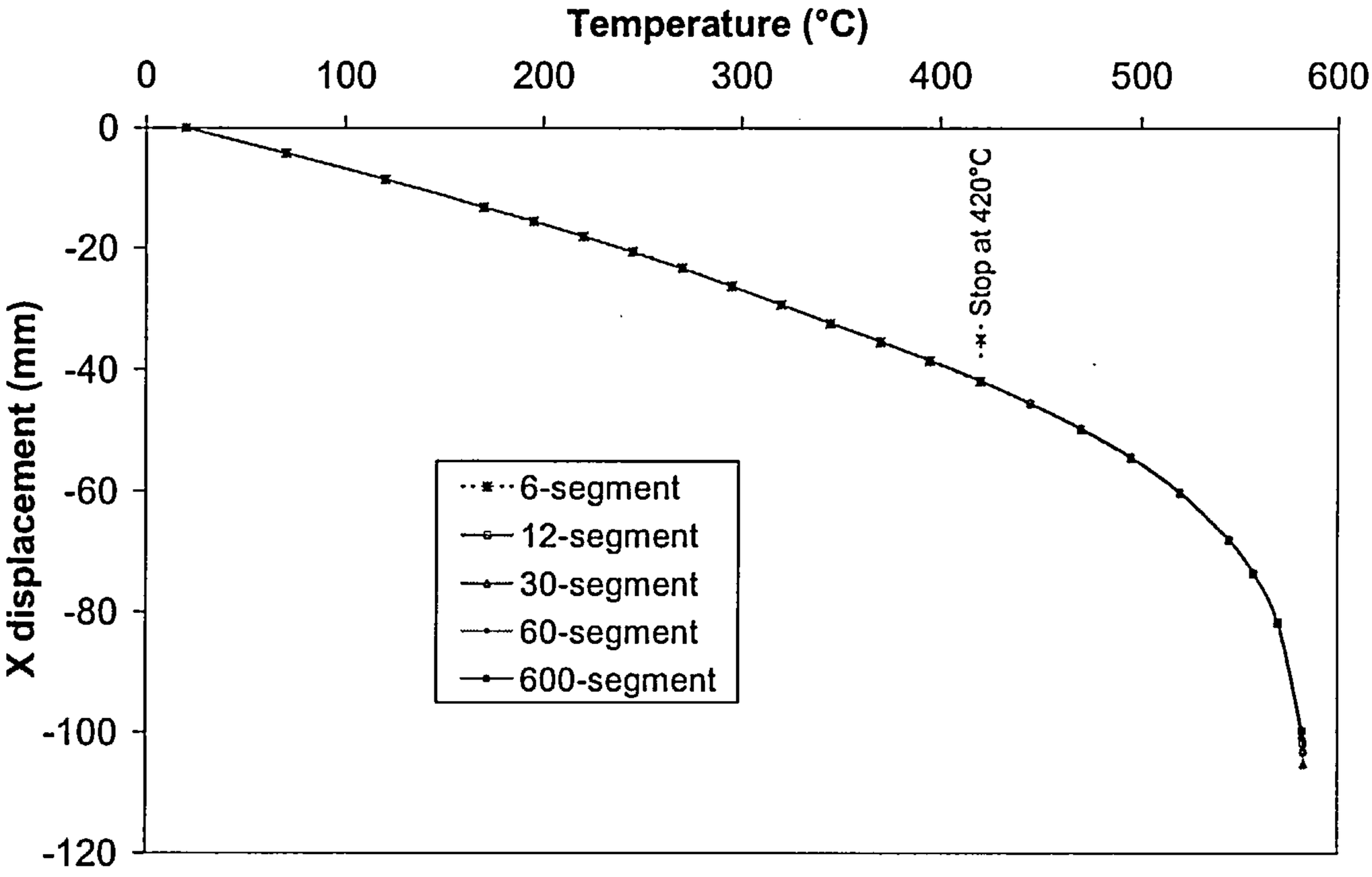

Fig 3-11 Horizontal X displacements at 14/20 of lower column

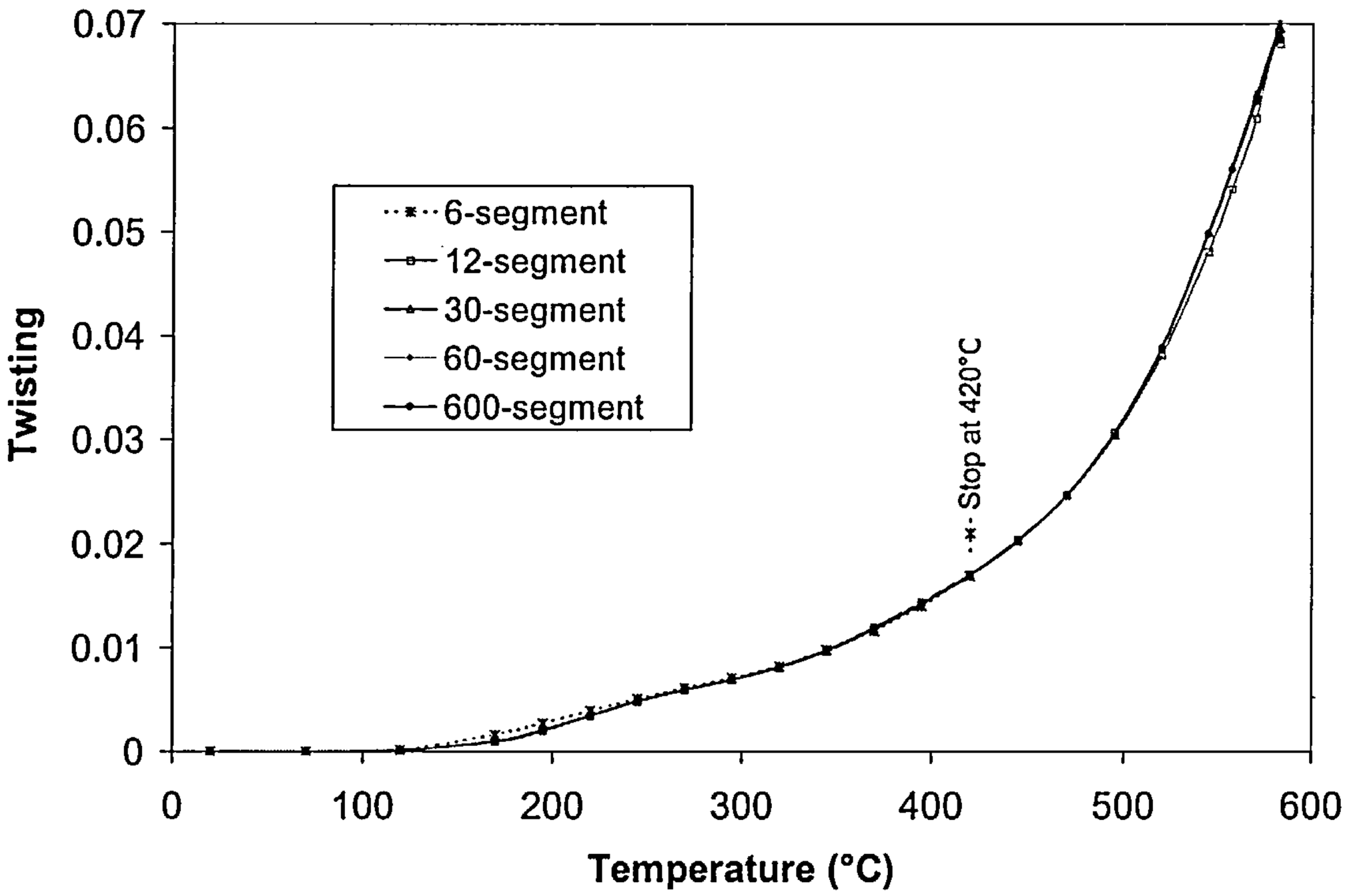

Fig 3-12 Twisting displacements at 14/20 of lower column

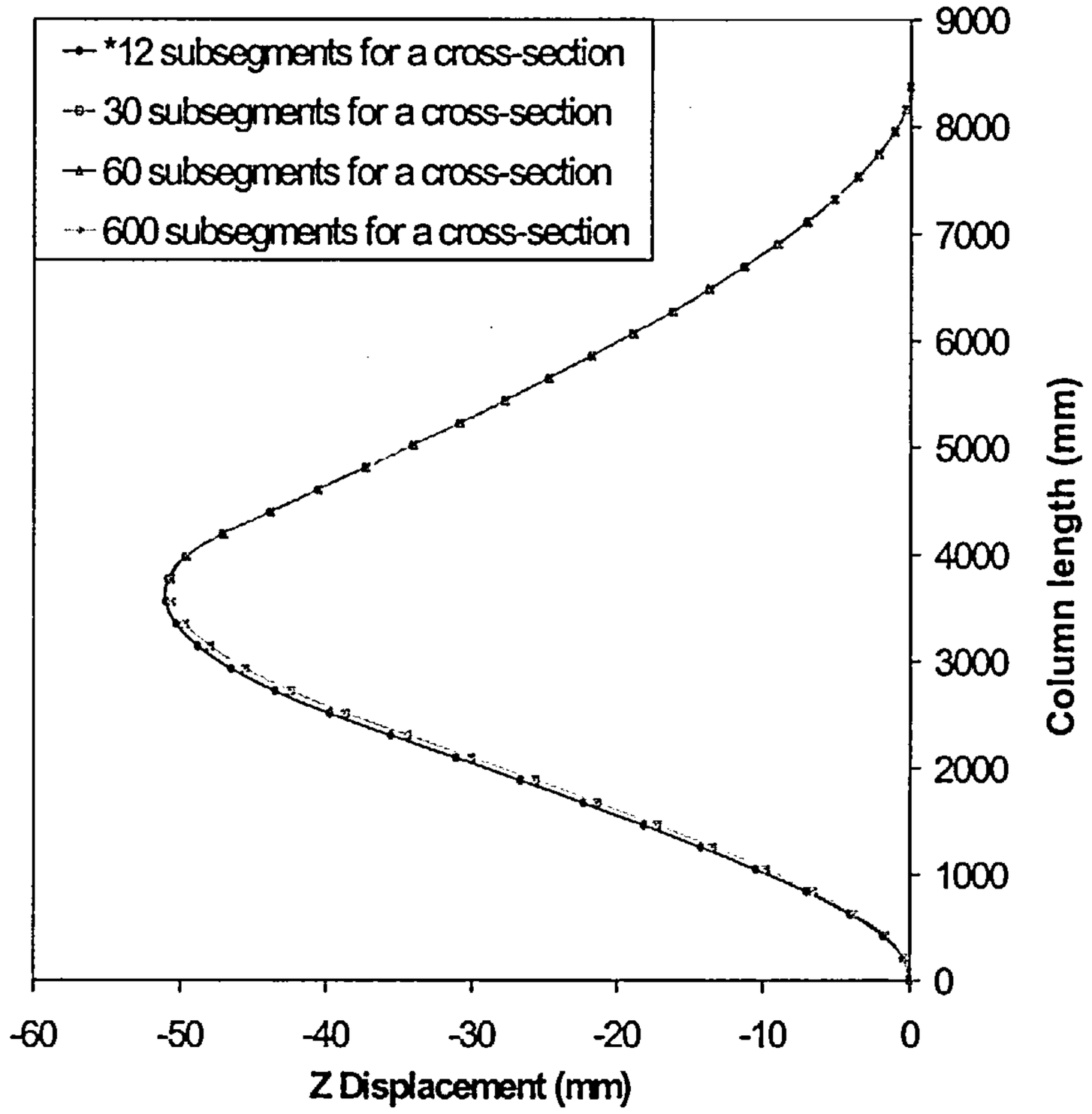

Fig 3-13 Horizontal Z-displacement of Column at 582.89°C

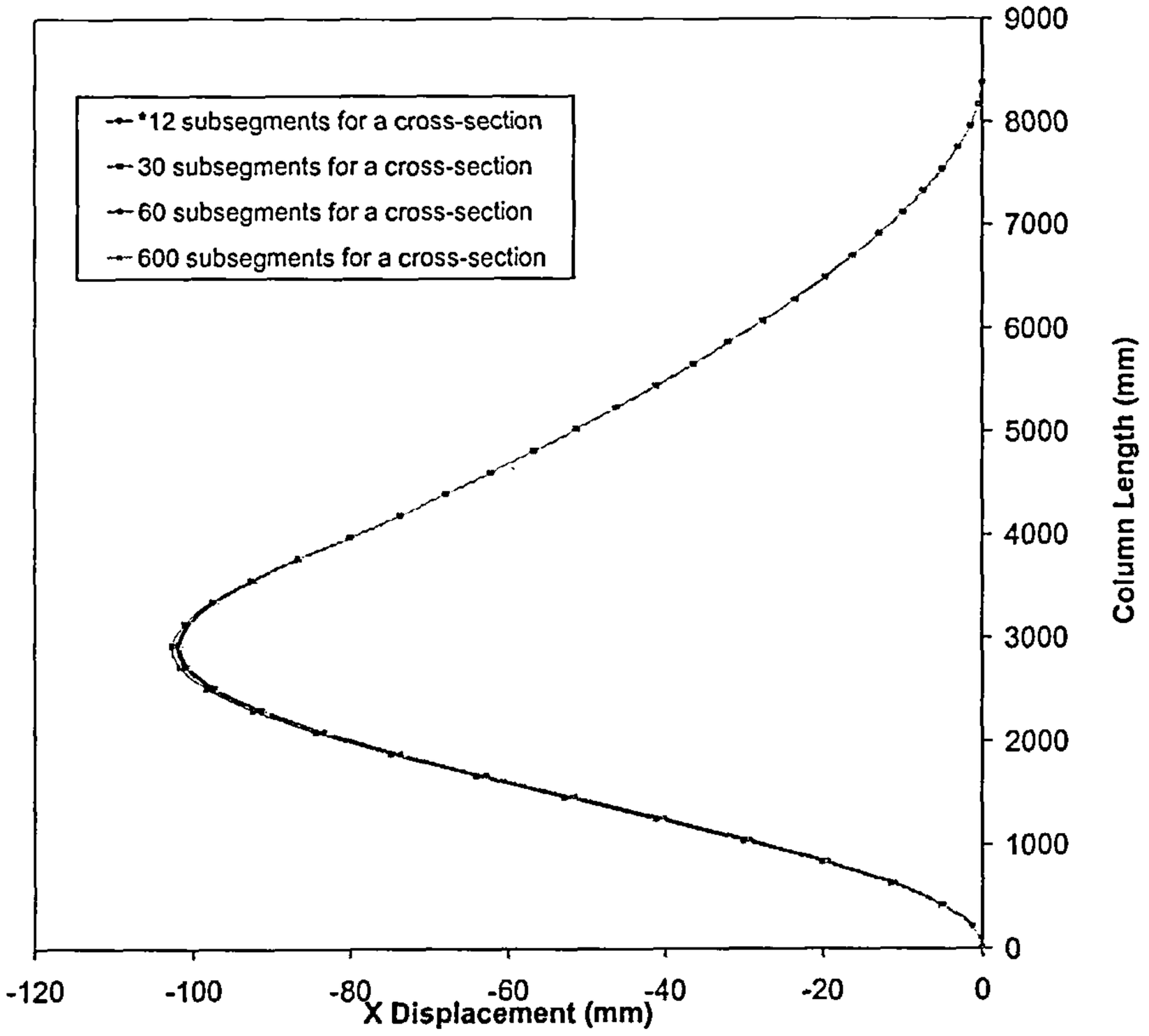

Fig 3-14 Horizontal X-displacement of Column at 582.89°C

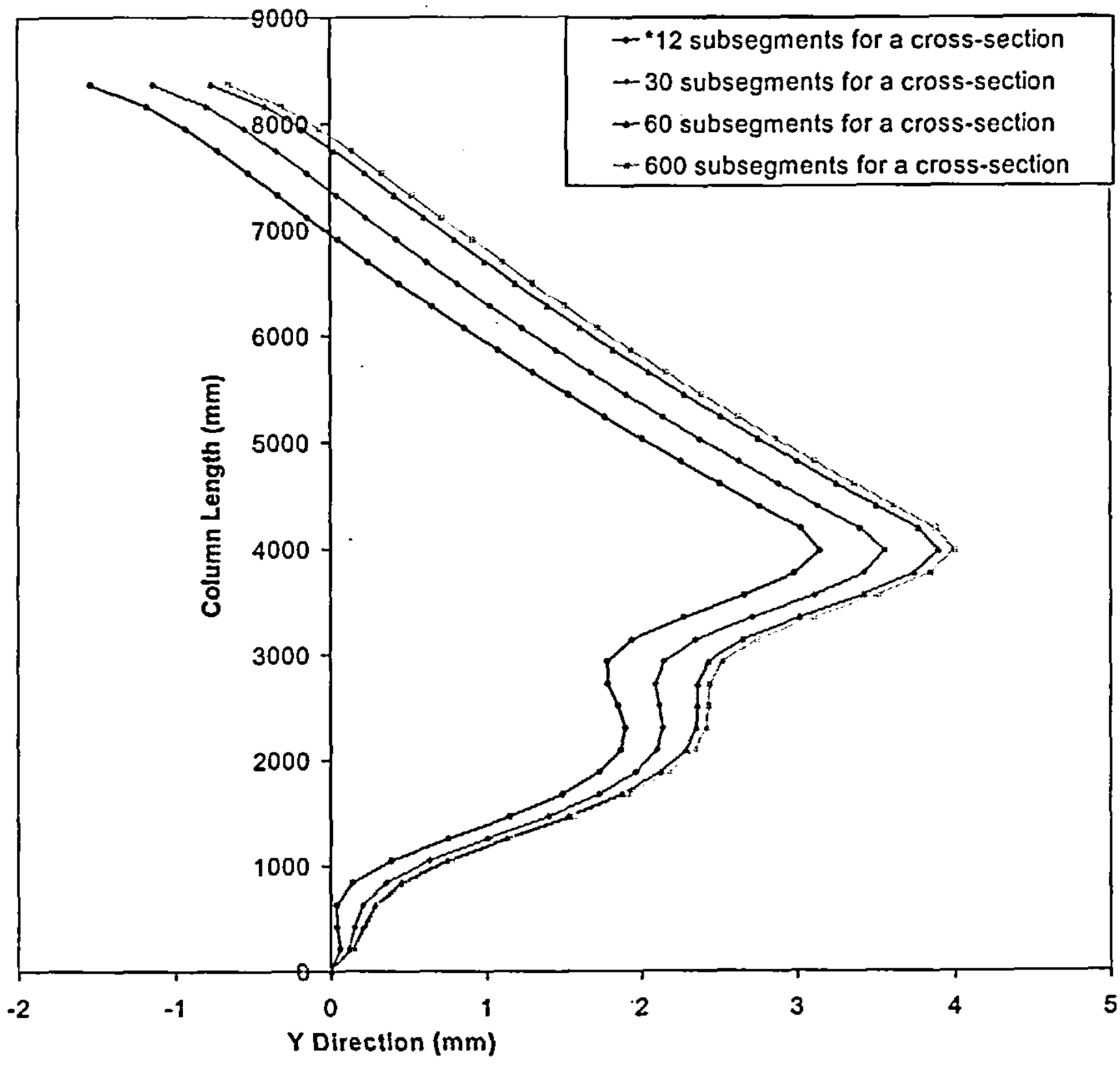

Fig 3-15 Vertical Y-displacement of Column at 582.89°C

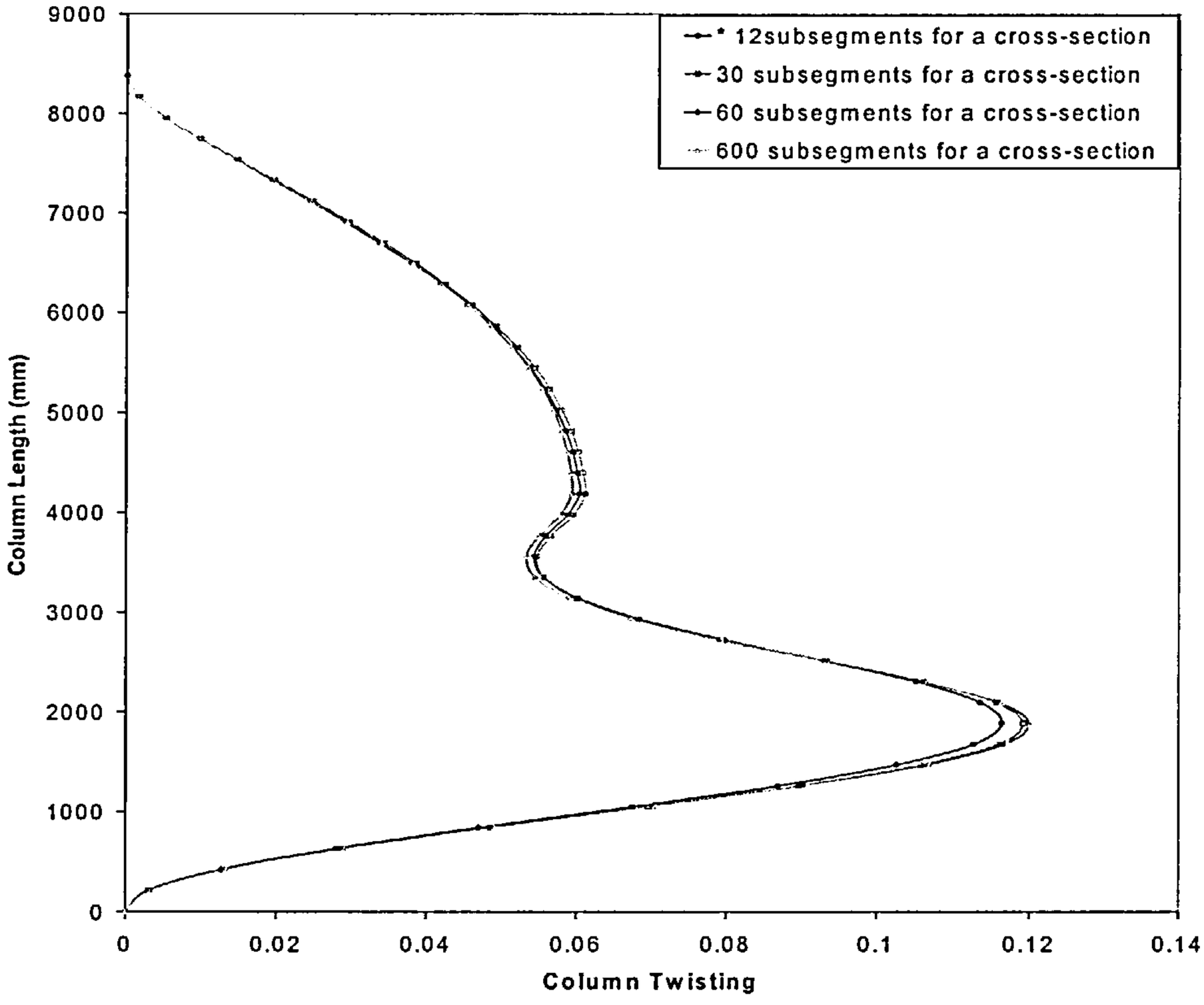

Fig 3-16 Twisting of Column at 582.89°C

Note: asterisk expresses reaching the predicted final temperature.

The z, x, y and twisting deformations at 14/20 of lower column where the maximum horizontal x displacement occurred are shown in Figs 3-9, 3-10, 3-11 and 3-12 respectively, for different numbers of sub-segments. Since the warping effects according to the computer predictions were very small and showed no variation with number of segments in this study, these effects are not plotted here. It can be seen that VULCAN stopped at 420°C when a 6-segment model was used. This was because of numerical instability of the program, the iterative processes not converging. Beam displacements were well represented by 12 segments. Figs. 3-13 to 3-16 show the displacement profile for the column at 582.89°C (the failure temperature when cross-section was divided into 12 sub-segments). The results show little difference for the z and x deformation, but there is some difference for the y deformation. However, the

general pattern of deformation is consistent and in any case the deformations are very small, suggesting that the original division of the section into twelve segments was quite reasonable.

3.5 DISCUSSION

The results from the three cases considered indicate that 6-segment division is too crude to represent the cross-section in VULCAN but 12-segment is appropriate, nevertheless more refinement provides marginal improvement. Although this study considered only three simple cases, the conclusion can be drawn that the original division of the section into twelve segments was quite reasonable for most analytical purposes. In the case of symmetric members, it is therefore suggested that the cross-section should be divided into at least twelve segments, since a more coarse division of the cross-section, for example into six segments, can cause either big errors or numerical instability. However, in some special case, such as beams using Asymmetric Slimflor® Beam (ASB) with highly non-linear temperature distribution, the situation will be more complicated, the cross-section may really need to be divided into more than 18 segments. This new asymmetric beam (ASB) forms part of slim-floor system and have a number of advantage for fire resistance, which will be introduced in chapter 6.

4. ANALYSES OF COLUMN SUB-FRAMES

There has been some concern[8,76] that column distortion due to the expansion of beams exposed to fire may reduce the axial load capacity to such an extent that failure occurs in the column, even if it is protected from the fire. In this chapter and the next the structural analysis software VULCAN has been used to predict the behaviour of a range of column sub-frames in fire scenarios. The effect of thermal expansion of unprotected beams on the critical temperatures of edge columns has been studied for different levels of axial load.

4.1 INTRODUCTION

In current structural fire engineering design practice it is usual to use some method of fire-protection for steel columns because they play a key role in carrying loads back to foundations. Failure of columns, as distinct from beams, may cause widespread rather than localised collapse of the structure. However, some concern has been expressed[8], partly based on observation of the recent fire tests on a full-scale composite building at Cardington, that increased bending moments may be induced in the perimeter columns because of the pushing-out of unprotected beams due to thermal expansion. Internal columns, although often subject to higher loads, are generally unaffected by this because the effects of thermal expansion either side of the column are approximately balanced. No column failures were seen as a result of this push-out, but the phenomenon clearly merits investigation.

The concerns expressed have questioned whether existing specifications for fire-protection of columns are sufficient to ensure their stability, since this column distortion will lead to additional secondary bending stresses and cause a reduction in load capacity. The benefits of continuity due to cool upper and lower columns are

already allowed for in EC3 Part 1.2[46] by the use of effective length factors of 0.5, thus removing one inherent safety factor which might otherwise have compensated for this reduction. In this chapter, a series of parametric studies, based on a column sub-frame of the Cardington BRE corner fire test, have been carried out to investigate the potential effects of thermal expansion of unprotected beams on the critical temperatures of edge columns.

4.2 PARAMETRIC STUDIES

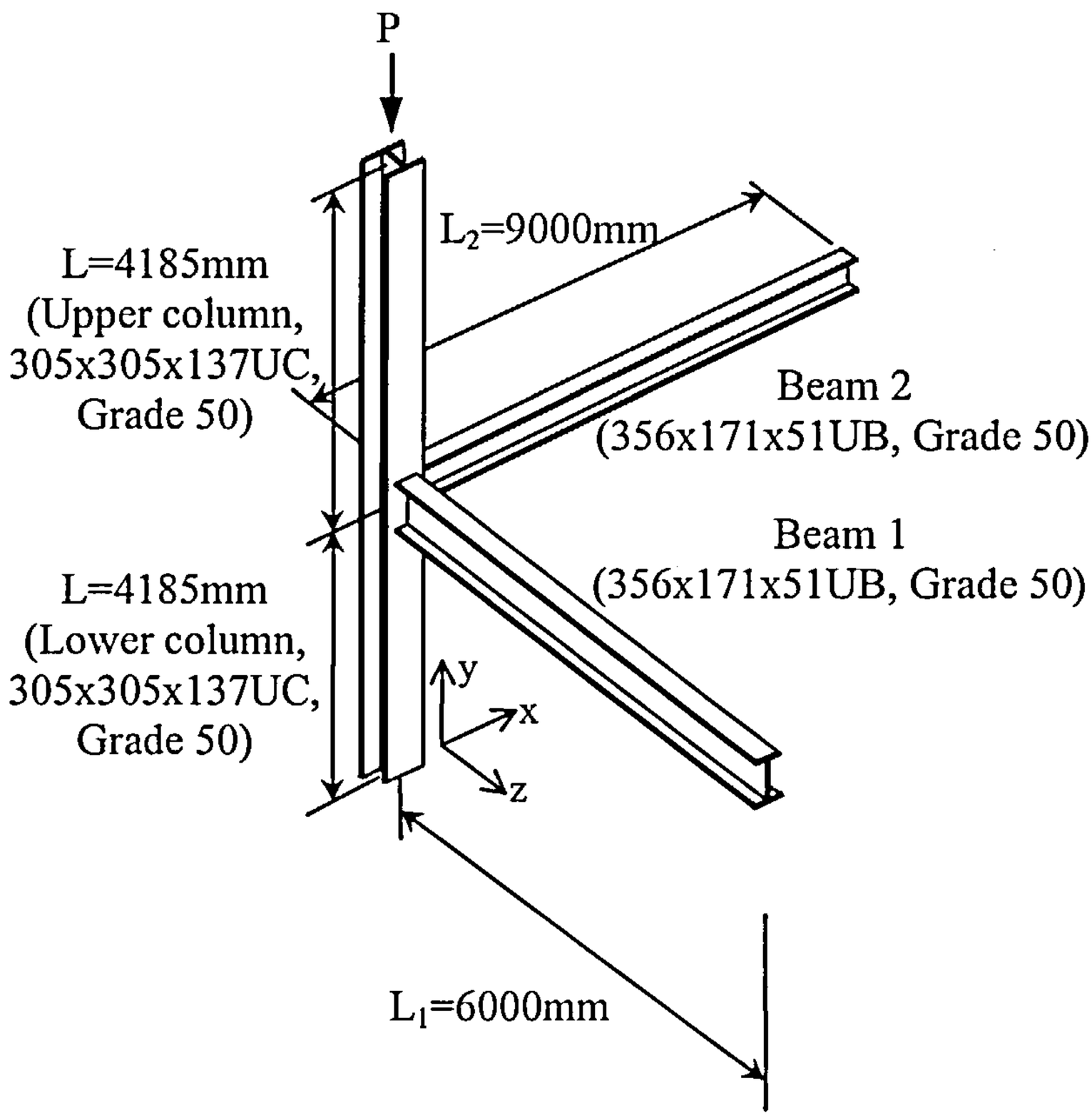

Fig. 4-1 Corner sub-frame used for studies

A simple sub-frame, shown in Fig. 4-1, was used to simulate the corner frame of the Cardington test building, representing the worst case of column push-out. In this model, two orthogonal beams, both of 356x171x51UB (S355) section, one 6000mm long, the other 9000mm, are pinned to the mid-point of a 305x305x137UC (S355)

column of 8370mm length. A constant axial load (**P**) is imposed at the top of the column, and it is assumed that the beams are unloaded. The beams and lower column are exposed to fire whilst the upper column is kept cool.

4.2.1 CASE STUDY 1

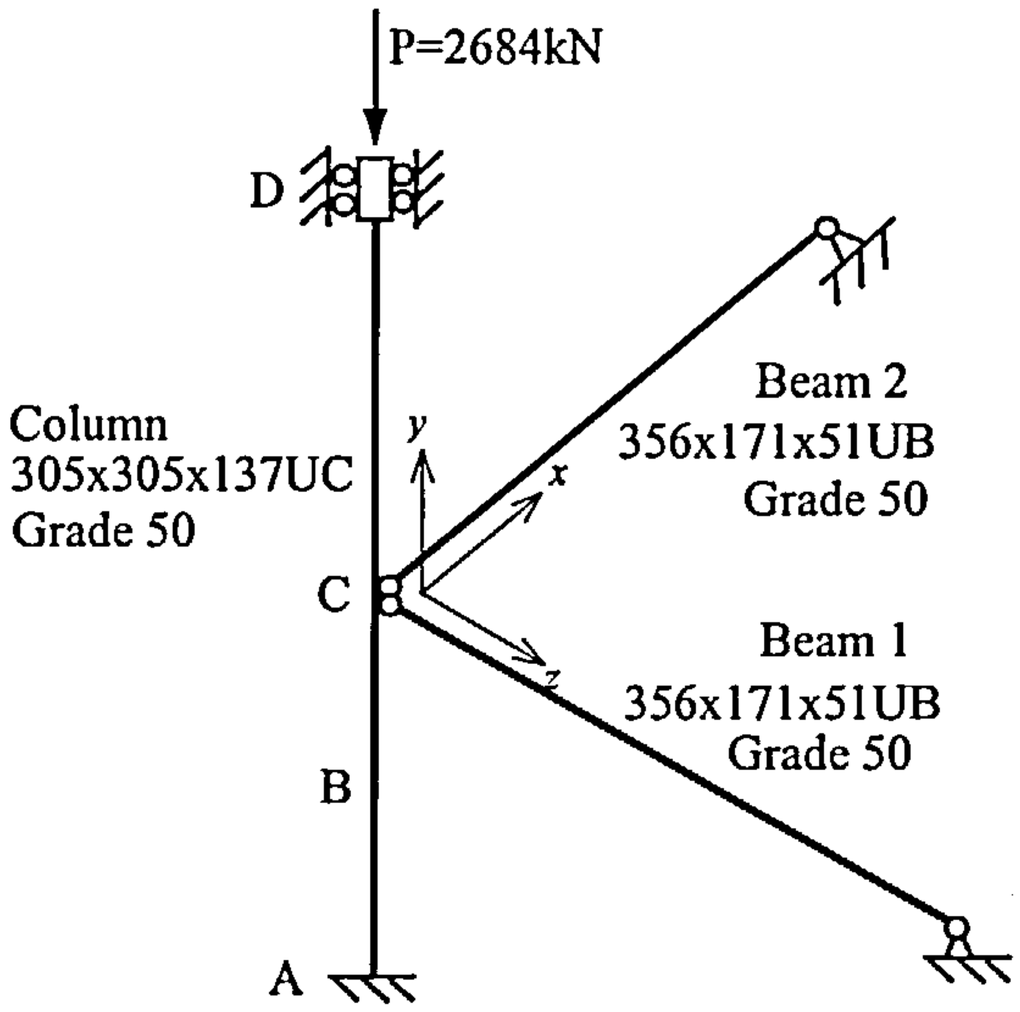

Fig. 4-2 Three-dimensional model for analysis

As an initial study, the column is subjected to an axial load (**P**) of 2684kN. This gives a load ratio of 0.5 when an effective length factor of 0.7 is assumed. Since columns are normally fire protected, the lower column was assumed to remain below 550°C. In the analysis it was uniformly heated up to 540°C and then held constant. Both beams were uniformly heated until instability occurred. The column is divided into 40 finite elements with the beams each divided into 8 elements so that reasonably accurate results can be expected. The structure and its boundary conditions are shown in Fig. 4-2. The computer predictions indicate that failure occurs when the beams reach 646 °C. The maximum lateral deflection of the column is at 17/20 of the lower column (point **B**) which is 627.75mm below the beam connection (point **C**) and the maximum deflections of beams are near the mid-span (but not exactly at mid-span since out-of-

plane action of the joint is assumed to be rigid). The results are shown in Figs. 4-3 to 4-8. Figs. 4-3 and 4-4 present the horizontal displacements of the column, and it is evident that the column does not buckle. Fig. 4-5 shows the total out-of-plane deflection for the beams. This is partly due to the horizontal deflection at the supporting, and partly due to the relative deformation of the beam between the two ends. Fig. 4-7 gives the bending moment at the central point (C) of the column. The relative lateral deflections of the beams can be obtained by subtracting the effect of the column push out, as follows.

The relative deflection = The total deflection – 1/2 deflection at the mid-point of column.

The results are given in Fig. 4-6.

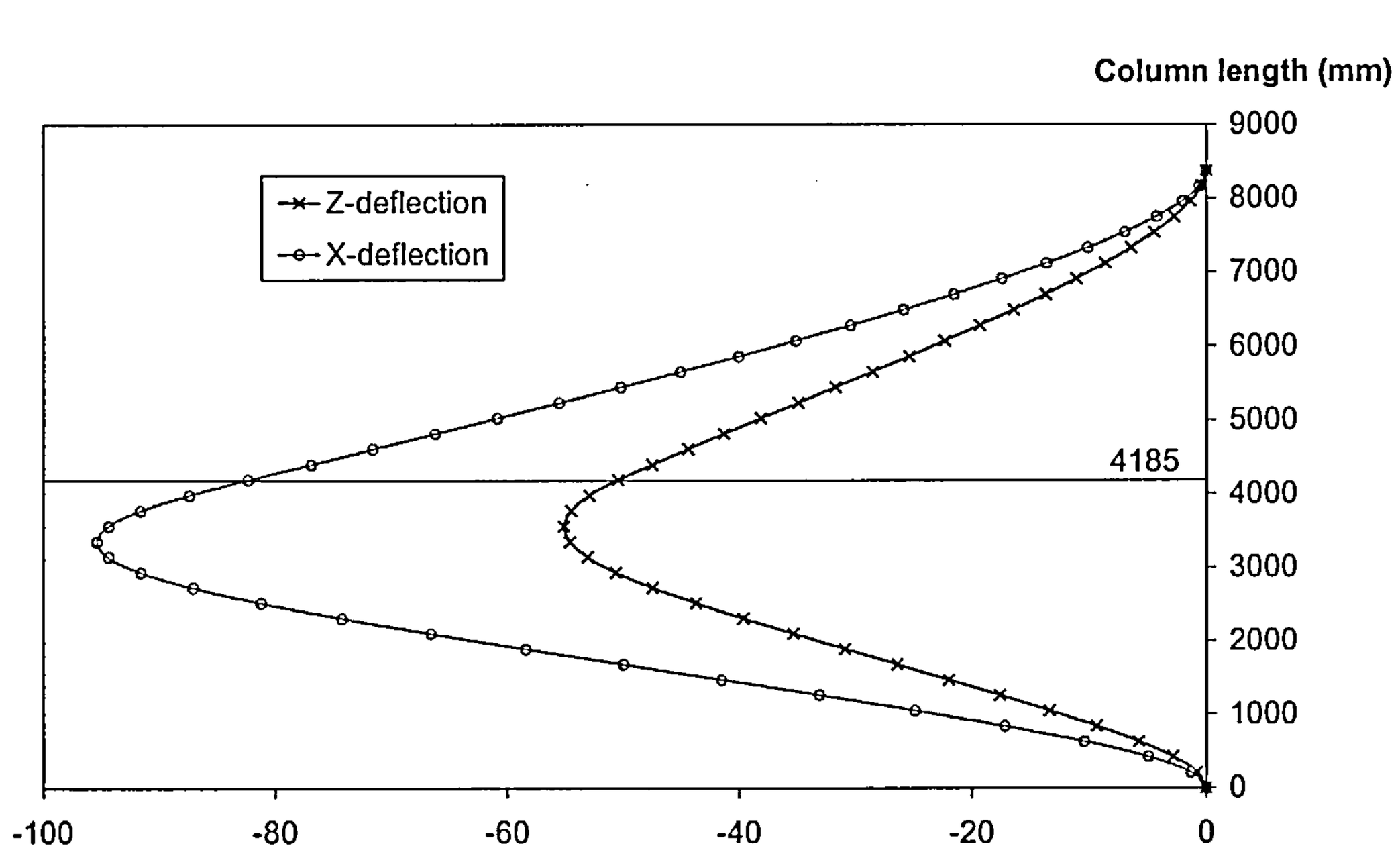

Fig. 4-3 Column horizontal deflections at beam temperature of 646.660°C (Lower column 540°C, P=2684kN)

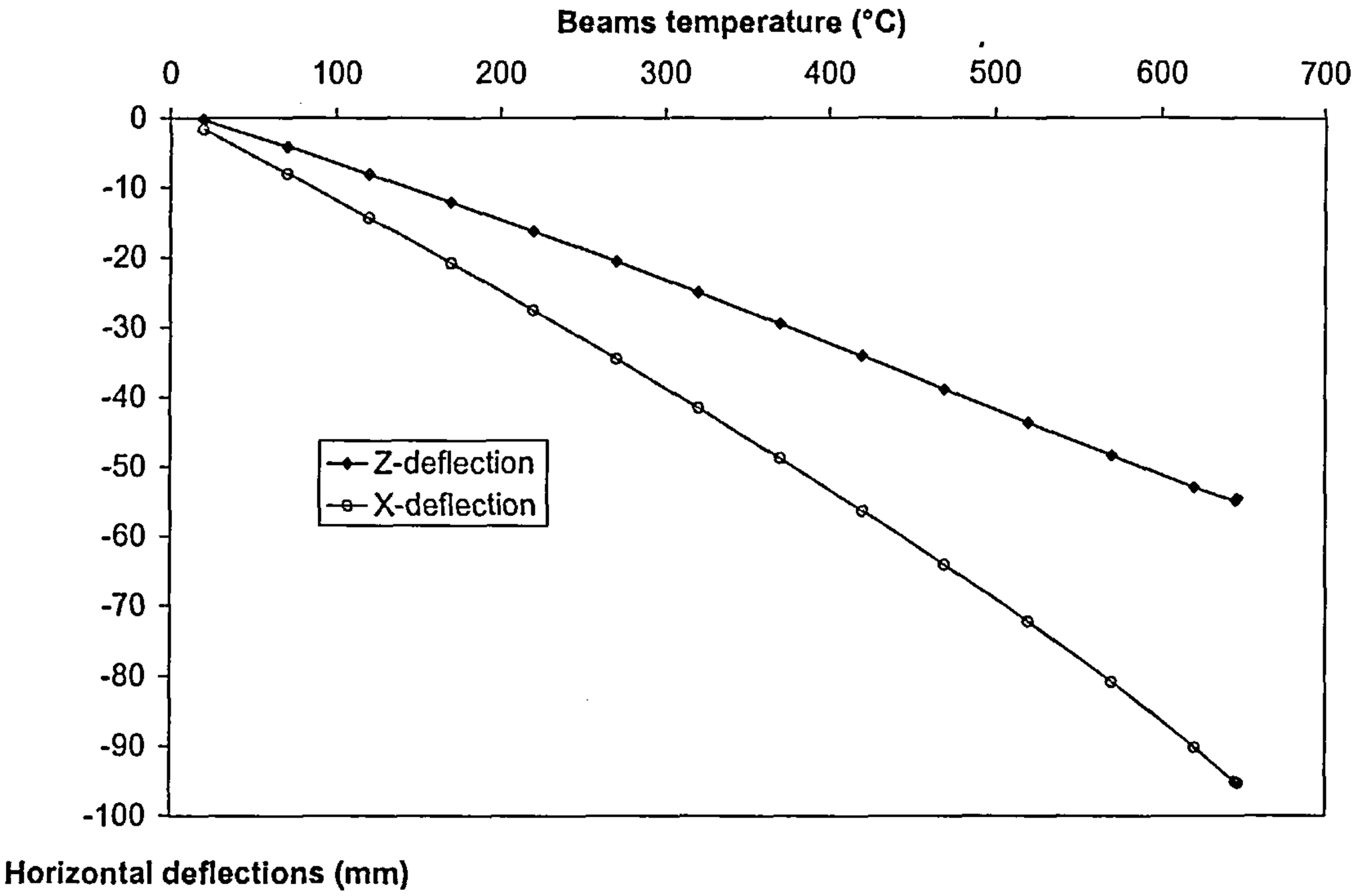

Fig. 4-4 The horizontal deflections at 17/20 of lower column

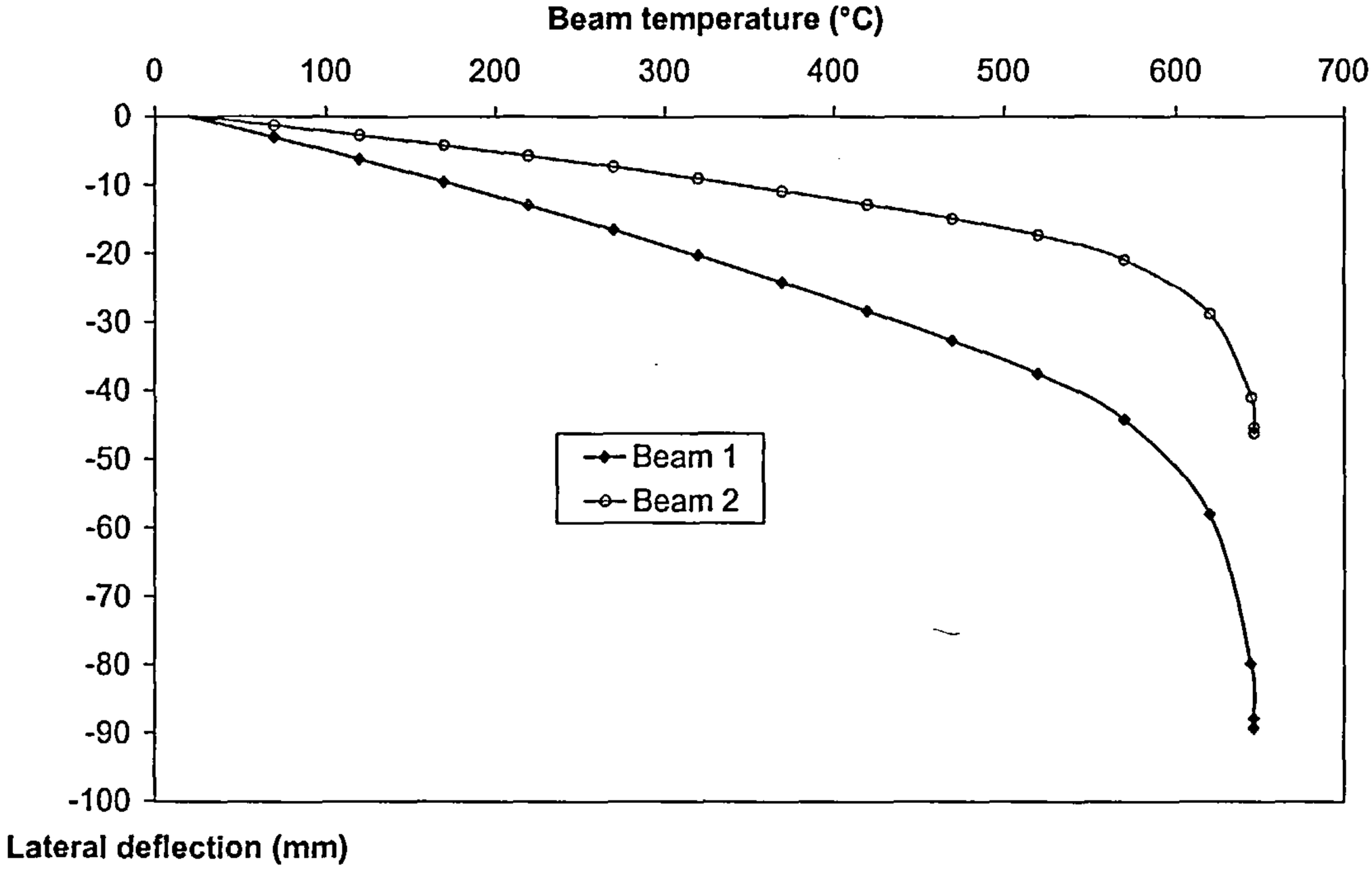

Fig. 4-5 The total lateral horizontal deflections at the mid-point of the beams

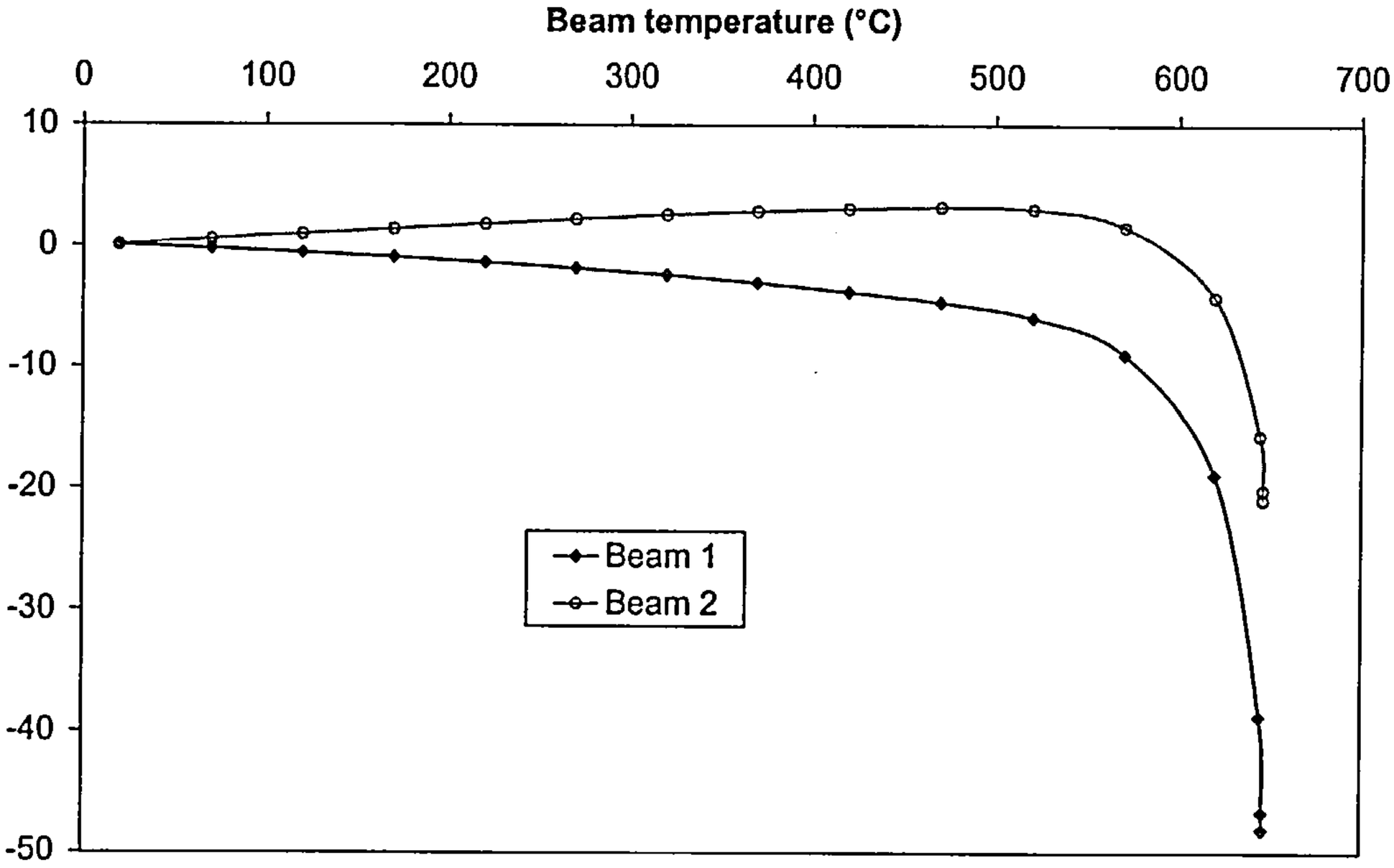

Fig. 4-6 The relative lateral horizontal deflections at the mid-point of the beams

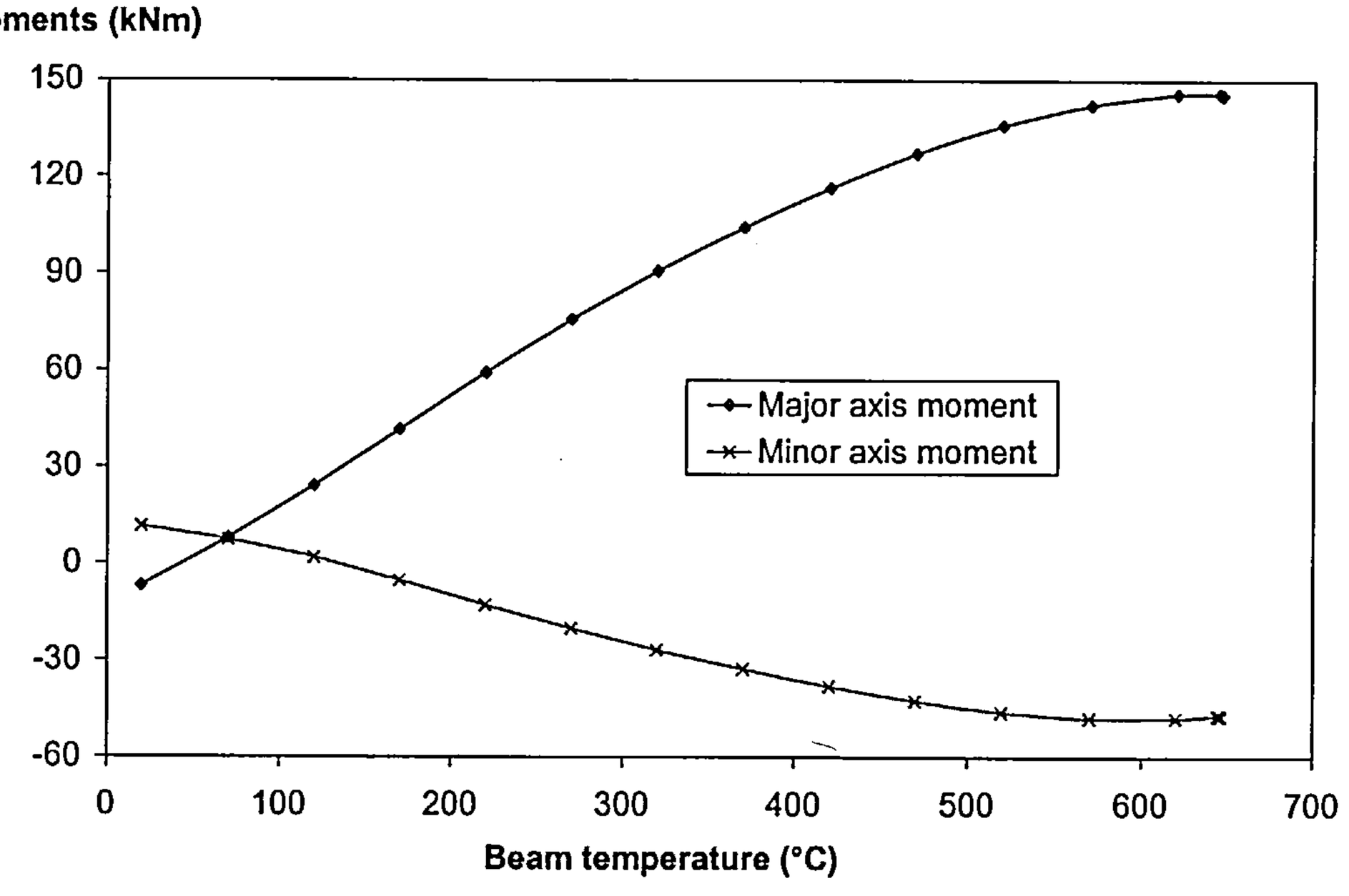

Fig. 4-7 Induced bending moment at the central point C of the column

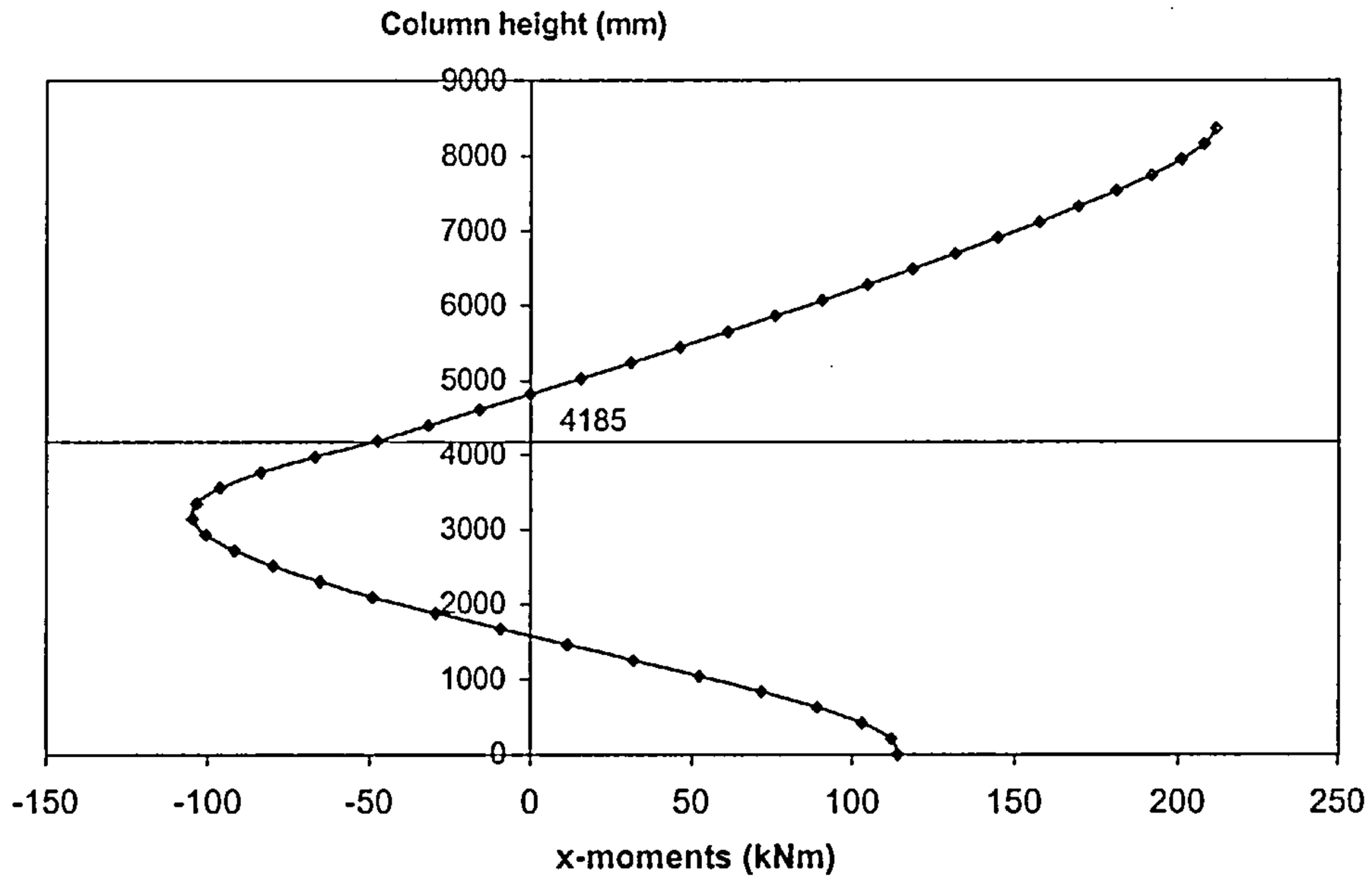

Fig. 4-8 Column minor axis bending moments at the beam temperature of 646.660°C (Lower column 540°C, P=2684kN)

From Figs. 4-5 and Fig. 4-6, it is clear that the deflections of both beams accelerate rapidly at temperatures in excess of 600°C, giving a strong indication of actual beam failure rather than numerical instability and column failure. In this case, even though some bending moments have been induced in the column as shown in Fig. 4-7, their effects are limited and do not change the conventional critical temperature for the column since the beams are the critical members. However, if the lower column temperature is allowed to rise to 550°C, the structure fails by column instability when the beam temperature reaches 671.367°C. The results for the case are shown in Figs. 4-9 to 4-13. The maximum column deflection about the minor axis is found to be at 15/20 of the lower column (point **B**), which is 3138.75mm above the bottom of the column, as shown in Fig. 4-9. This accelerates at temperatures above 500°C, indicating failure of the column. It is interesting to see from Fig. 4-13 that beam 2 is always in tension for the duration of the heating. This is because, at the connection point **C**, the deflection caused by **P-Δ** effect is bigger than that produced by thermal

expansion of the beam so that beam 2 holds the column back in the minor axis direction. However, failure of the column was still associated with the connection point C moving out in spite of this restraining effect from the beam. The column temperature at failure (550°C) is 30°C less than that calculated according to BS5950: Part 8[47], which gives a critical temperature of 580°C based on a load ratio of 0.5 (an effective length factor of 0.7 being assumed). This result suggests that the existing code rules although based on conservative assumptions, may be under un-conservative for the case of corner columns. If we assume that point C is free to move in position but effectively restrained against rotations, the effective length factor becomes 1.2, giving a load ratio of 0.66. Based on this load ratio, BS5950: part 8 gives a conservative critical temperature of 522°C for the column which is 28°C less than the failure temperature (550°C) observed.

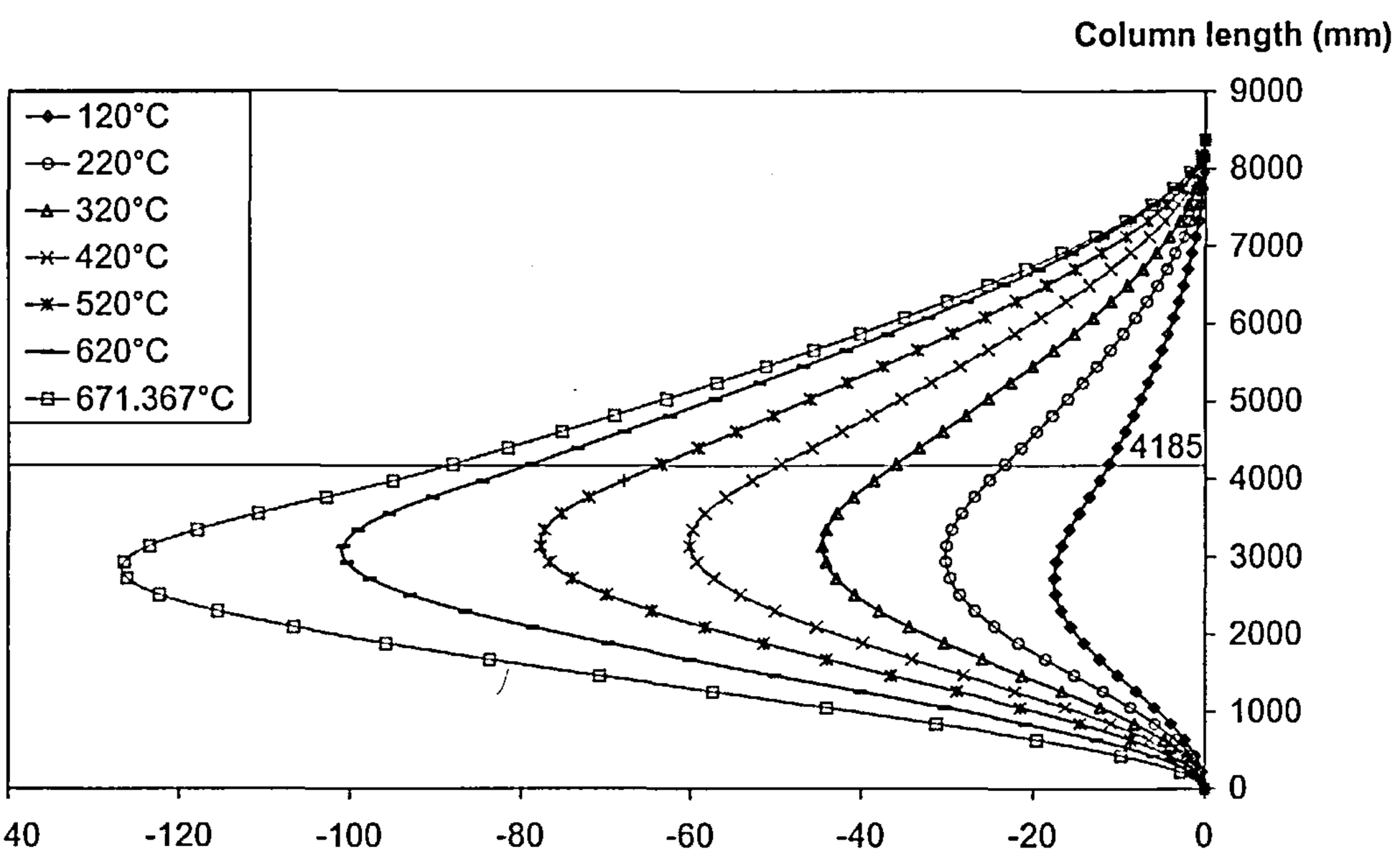

Fig. 4-9 Column out of plane displacement at different beam temperature (Lower column 550°C, P=2684kN)

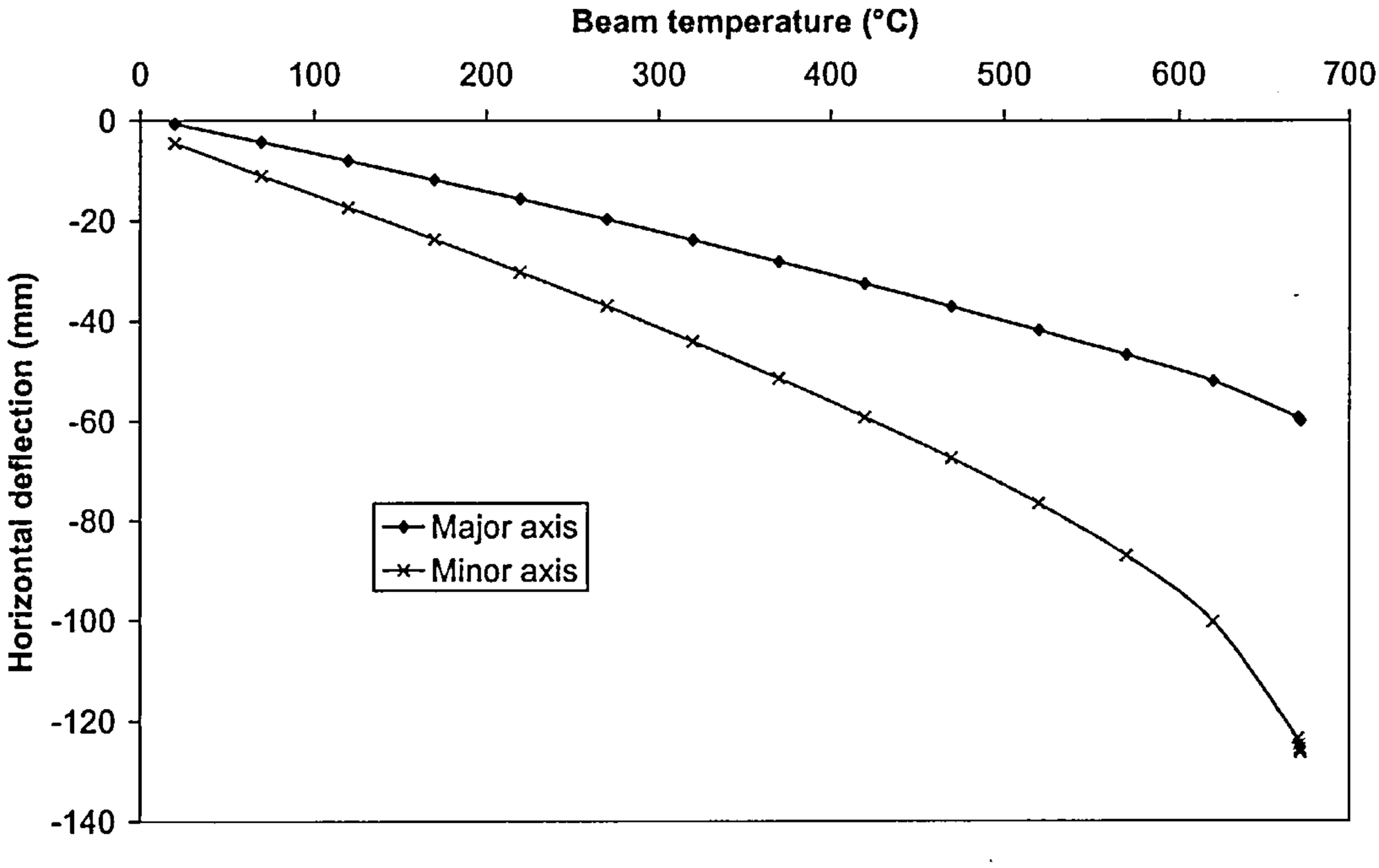

Fig. 4-10 The horizontal deflections at 15/20 of lower column

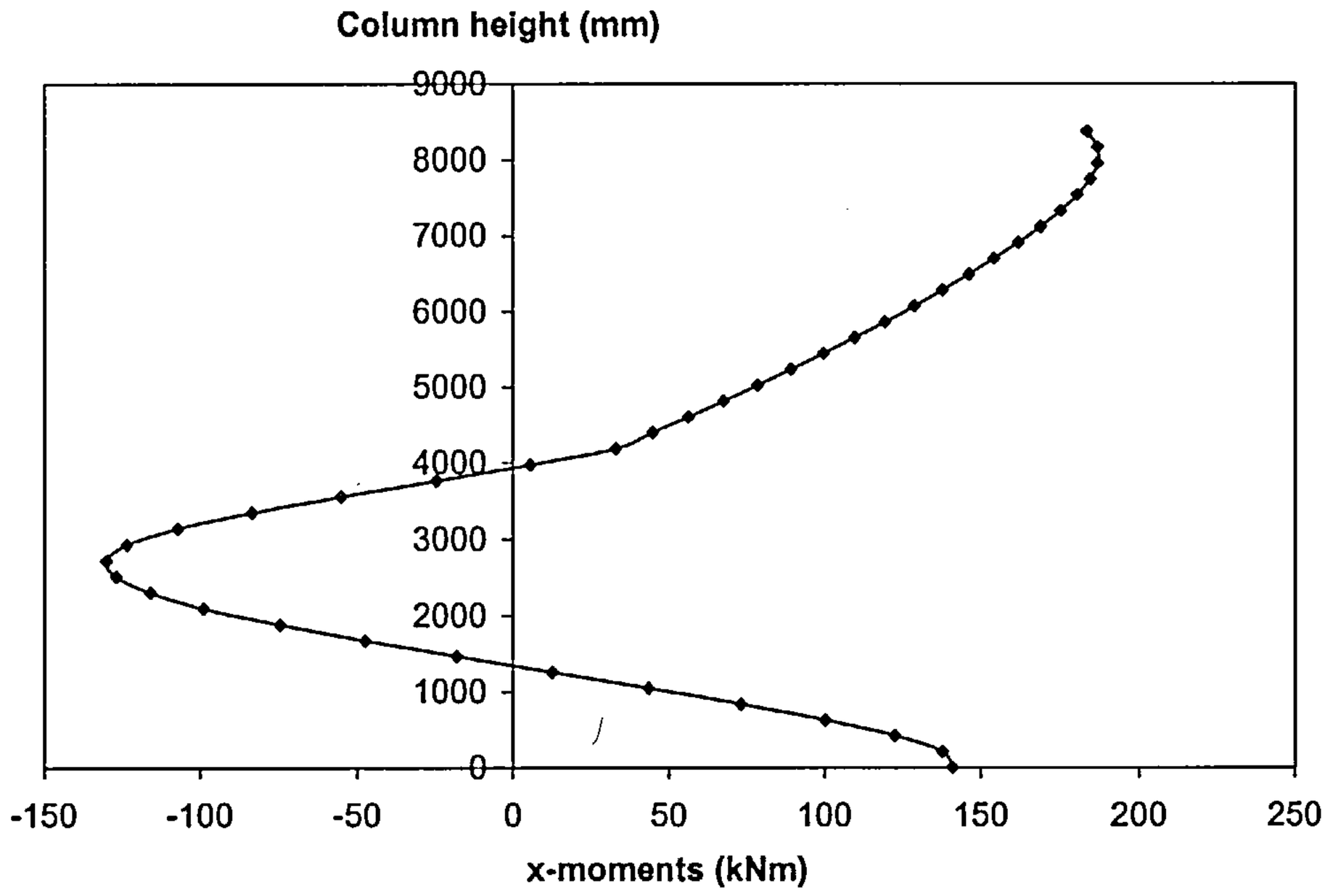

Fig. 4-11 Column minor axis bending moments at the beam temperature of 671.367°C (Lower column 550°C, P=2684kN)

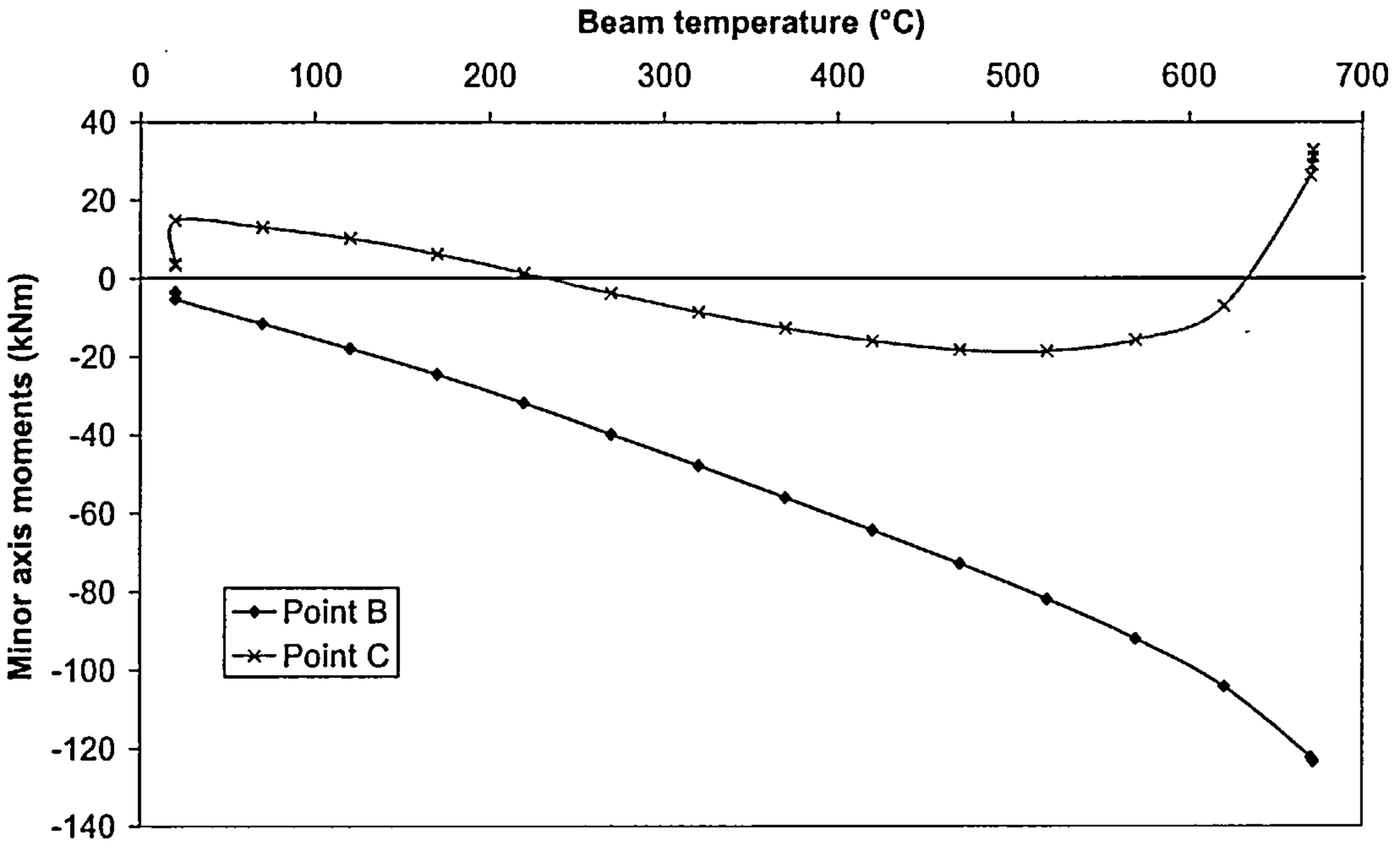

Fig. 4-12 The bending moment for the column

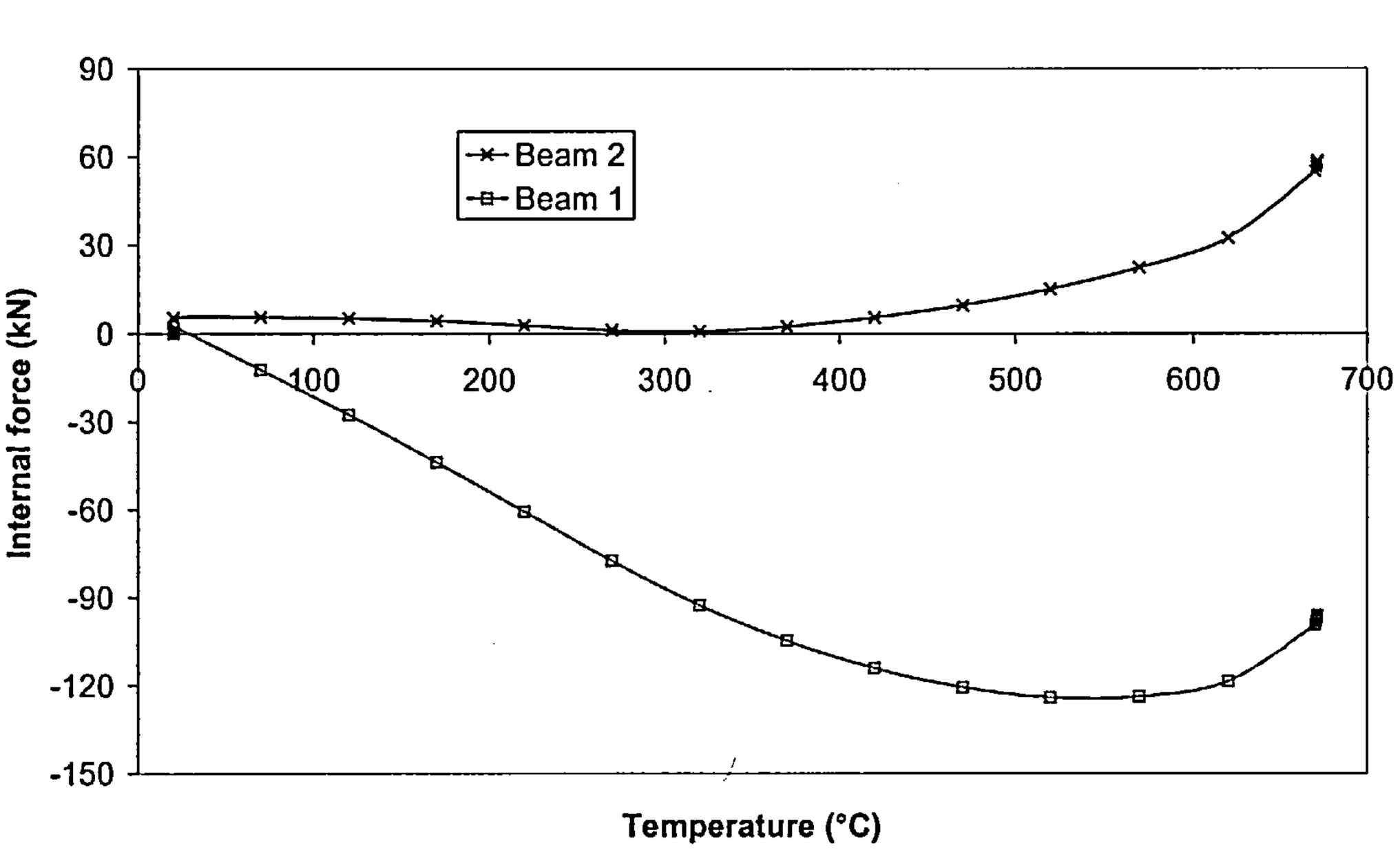

Fig. 4-13 Beams internal forces (Negative sign expresses compression)

The above case has been re-analysed by considering the lower column unprotected, i.e. the column and both beams are uniformly heated at the same rate. The analysis

predicts instability of the structure at 560°C with the maximum horizontal deflection of the lower column about its minor axis at 14/20 of its length (point **B**), which is 2929.5mm above the bottom of the column, as shown in Fig. 4-14. The horizontal deflections and moments in the column and the internal forces in the beams are summarised in Figs. 4-14 to 4-17. It is obvious from Fig. 4-14 that instability occurs in the column since the minor axis deflection of the column tends towards infinity, and it is interesting from Fig. 4-15 that the position of extreme minor column moment is very close to the one of extreme deflection. It can be seen from Figs. 4-16 and 4-17 that both the column moments and internal forces in beam 2 (x-direction) have reversed in sign, in contrast to those shown in Fig. 4-13. It is clear that the thermal expansions firstly push the column out and induce additional bending moments in the column (Point **C**), but as the failure temperature is approached the moments and expansion forces reverse sign to restrain column buckling. Because of the **P-Δ** effect the point of maximum deflection has dropped down towards the central point B, almost coinciding with the position of maximum column moment as shown in Fig. 4-15. It is to be noted that if both beams and upper column are kept cool whilst only the lower column is uniformly heated, instability will occur when the column reaches 577°C (Fig. 4-18). This is less than the critical temperature (580°C) according to BS5950: Part 8 based on an effective length factor of 0.7, suggesting an effective length factor of 0.85 is more suitable for this no beam push-out case. This case implies that the beam push-out caused by thermal expansion does not affect the column critical temperature too much as we imagined, giving a difference of 17°C by comparison with the above beam heated case. It is also evident that the lower the stiffness of beams the smaller will be the thermal expansion forces, and hence the critical temperature of the column will be greater. In order to investigate further the behaviour of edge columns, three cases -- a

2D plane frame, a 3D skeletal frame, and a 3D composite frame including floor slabs - - are analysed with different levels of axial load.

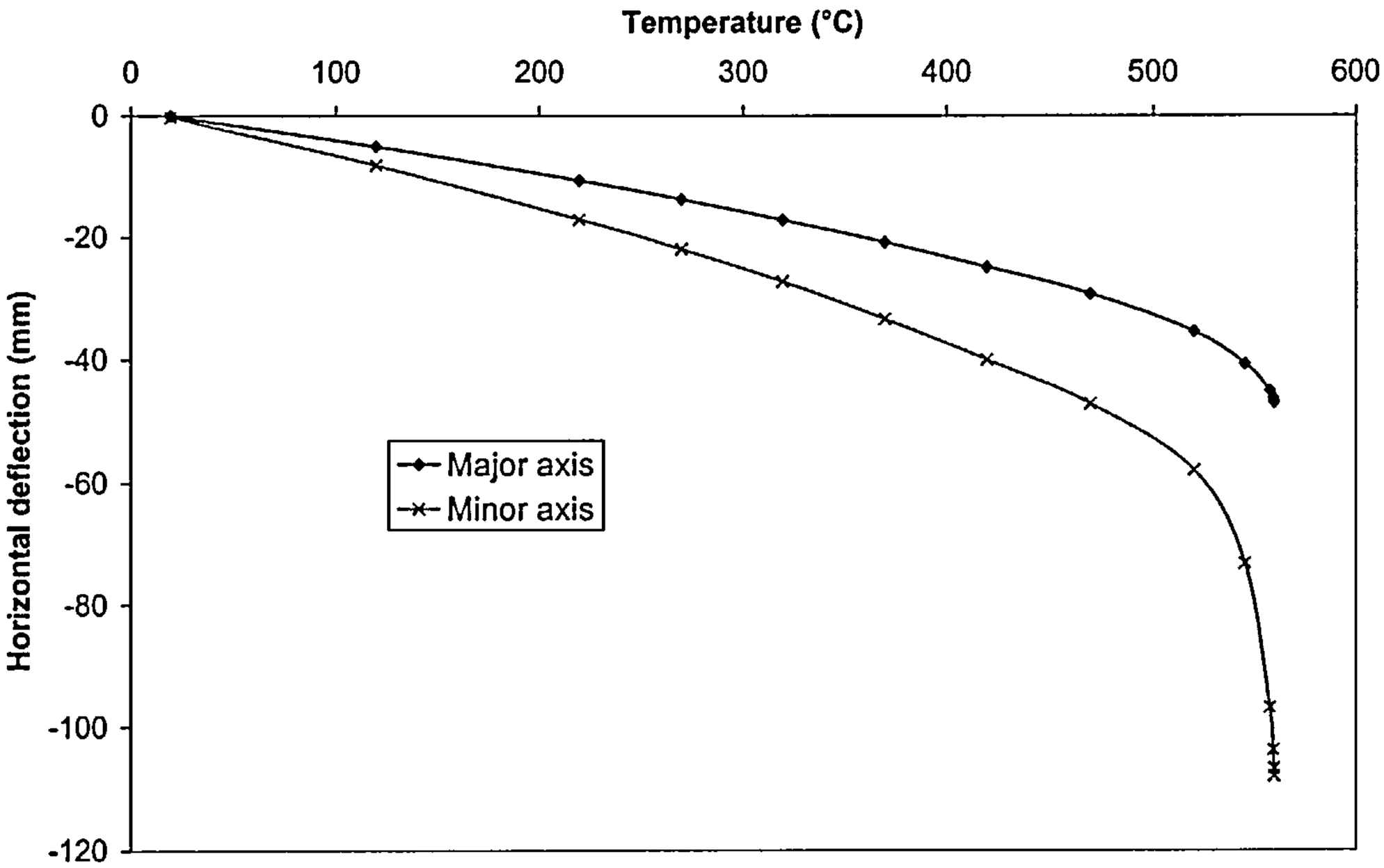

Fig. 4-14 The horizontal deflections at 14/20 of lower column

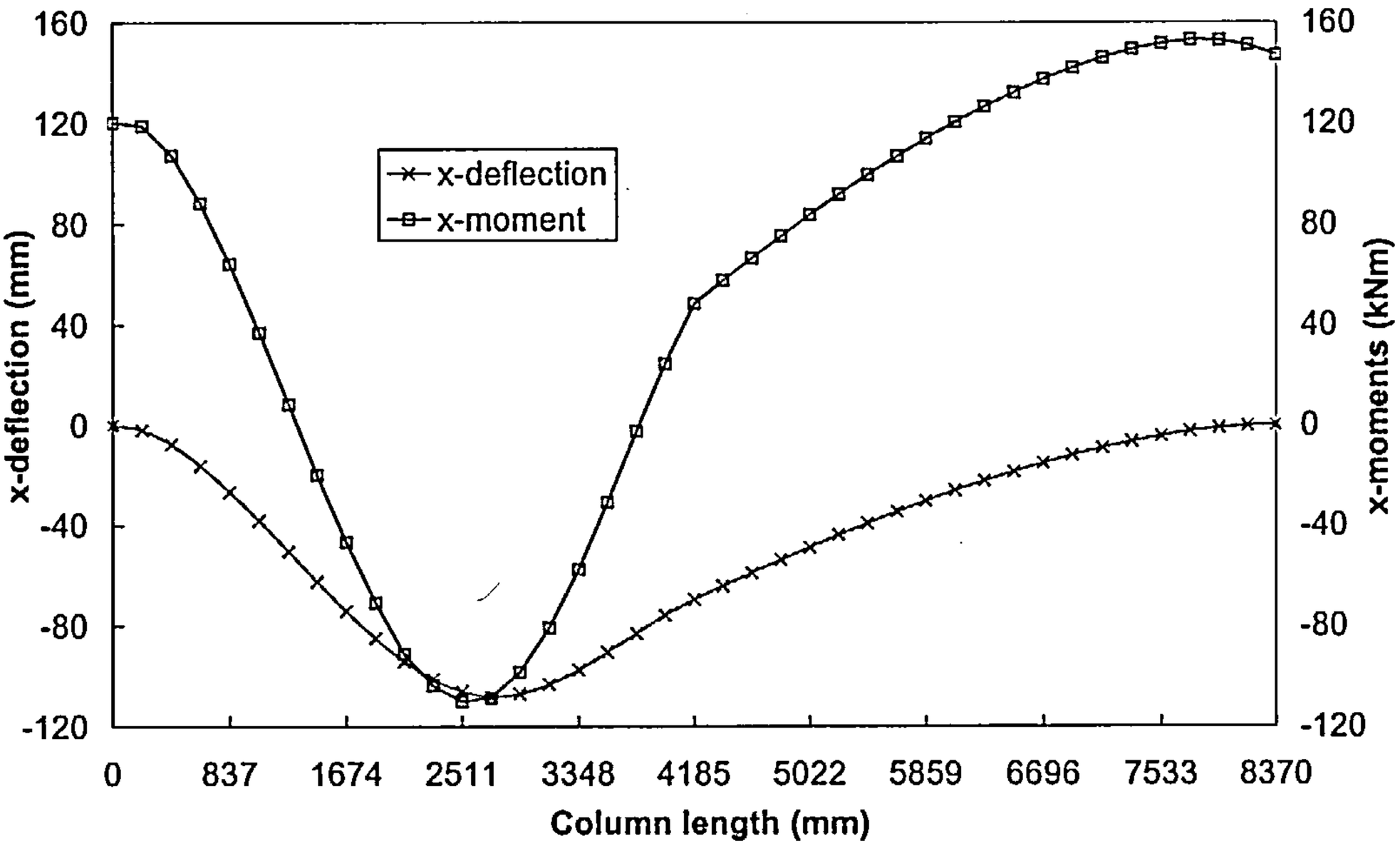

Fig. 4-15 Column minor axis deflections and bending moments at 559.551°C (P=2684kN)

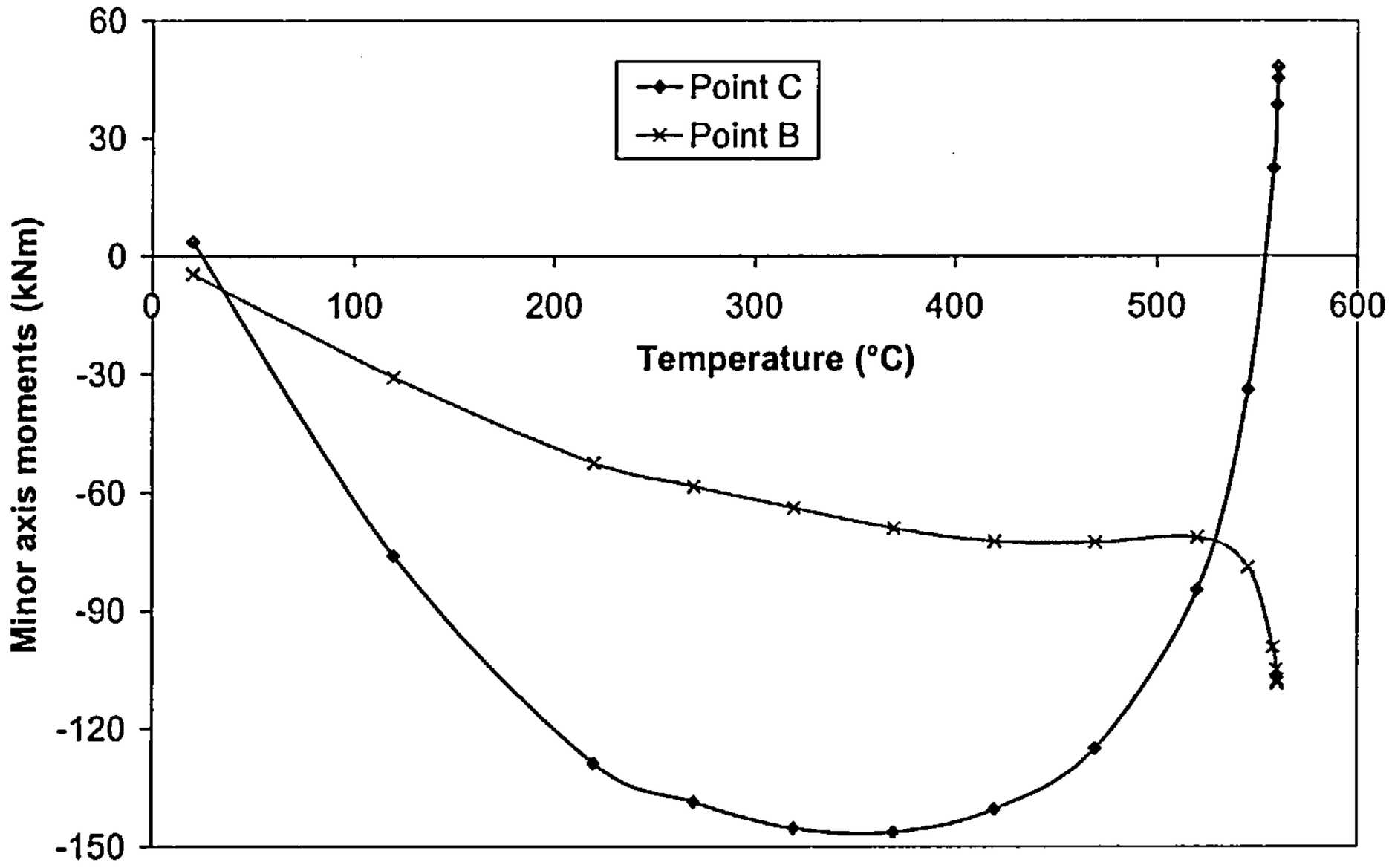

Fig. 4-16 Minor axis column bending moments at the floor level (Point C) and 14/20 of lower column (Point B).

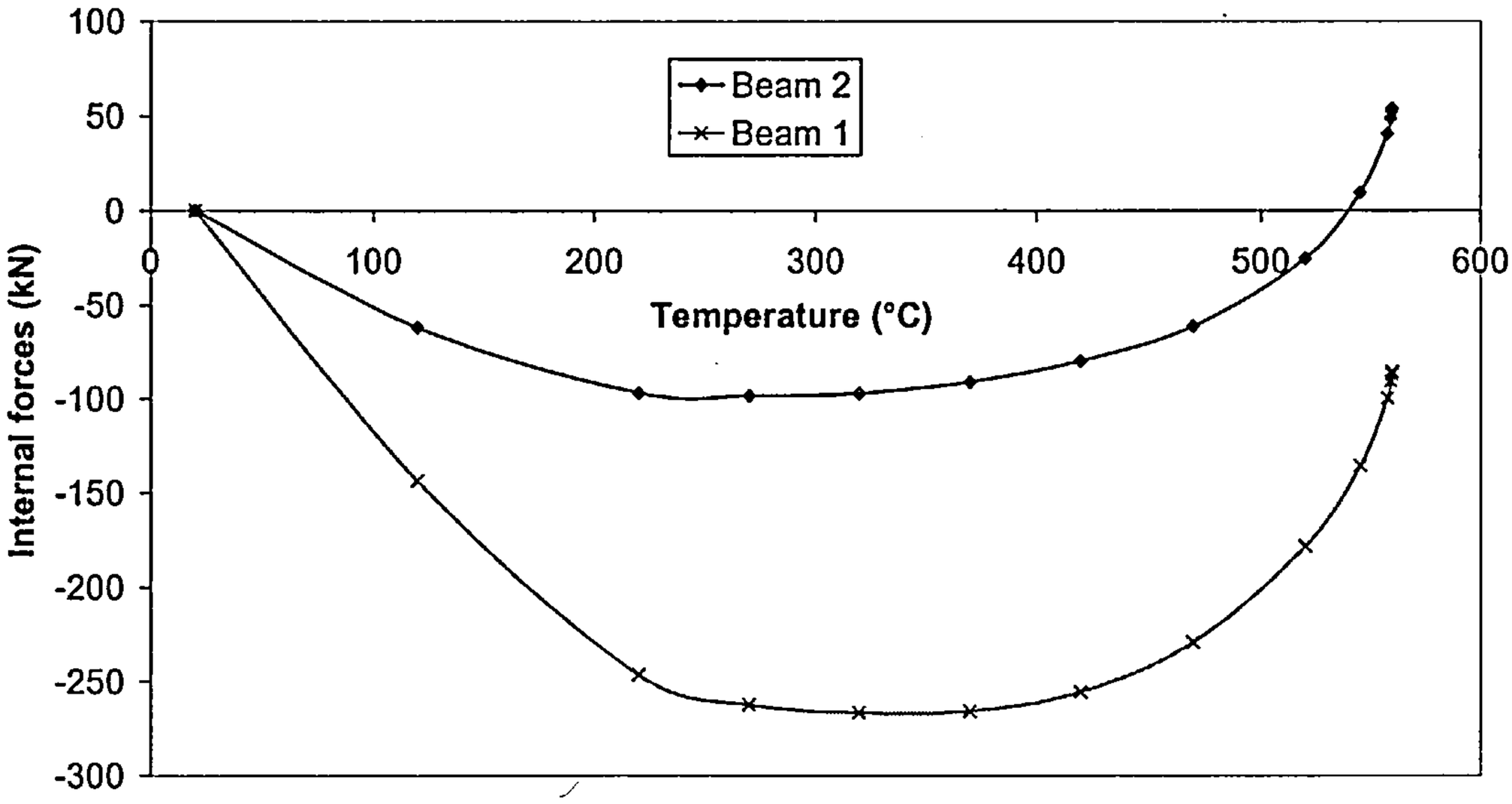

Fig. 4-17 Beams internal forces (Negative sign expresses compression)

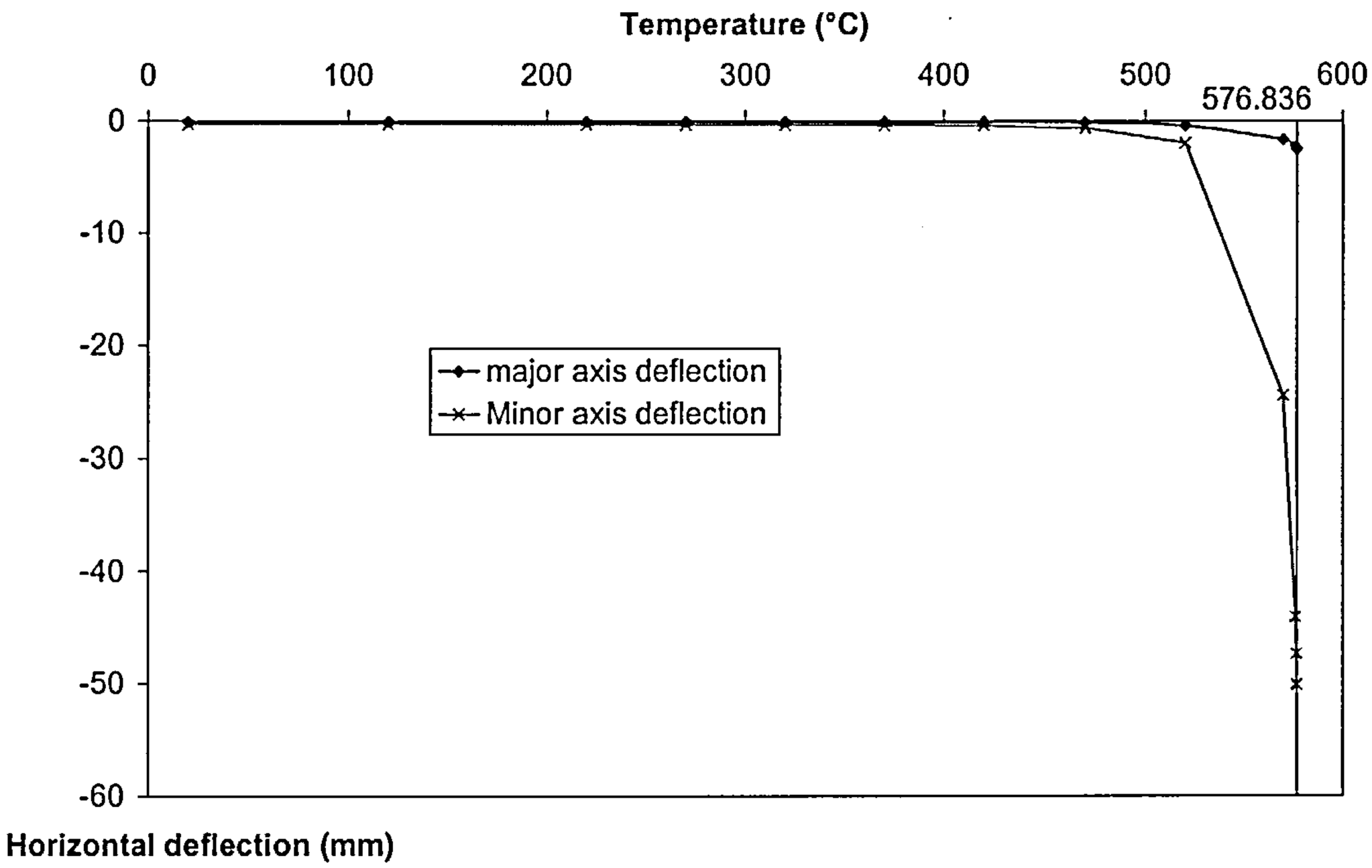

Fig. 4-18 The horizontal deflection at 11/20 of lower column (Maximum horizontal deflection) for the case of only the lower column being uniformly heated (P=2684kN)

4.2.2 CASE STUDY 2 -- 2D PLANE FRAME

The 3D sub-frame described above has been further simplified to investigate the accuracy of using a 2D representation. A simple plane sub-frame with the column bent about its minor axis (Fig. 4-1) has been analysed with different levels of axial load ranging from 2000kN to 5000kN. Two models (model 1 and model 2 as shown in Fig. 4-19) are used to represent the braced and unbraced structure respectively. For the unbraced model (model 2) an axial spring is included at the remote end of the beam to simulate the axial stiffness of a total of six columns, giving a horizontal restraint of 22015 N/mm as demonstrated in Fig. 4-19a. The lower columns in both models are protected to different level of 400°C, 450°C, 500°C and 550°C respectively, whilst the beams are uniformly heated. This allows more systematic studies to be implemented. Again the column is divided into 40 elements with 4 elements used for each beam member. The VULCAN results are shown in Figs. 4-20 to 4-26.

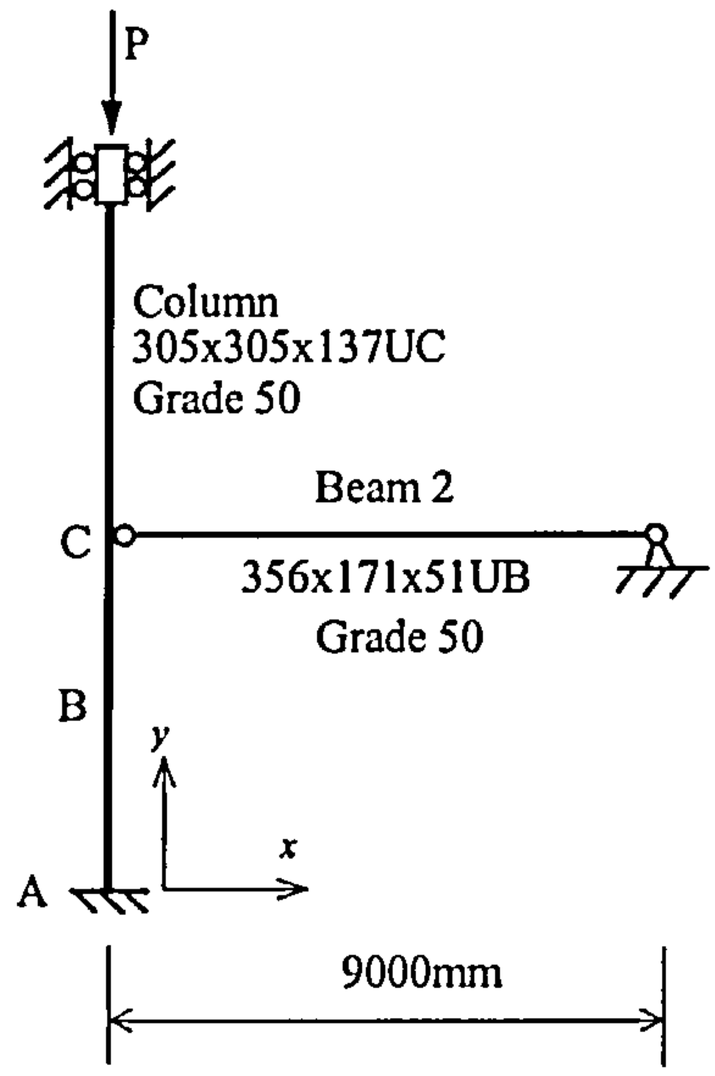

(a) Model 1
(Braced frame: pin end)

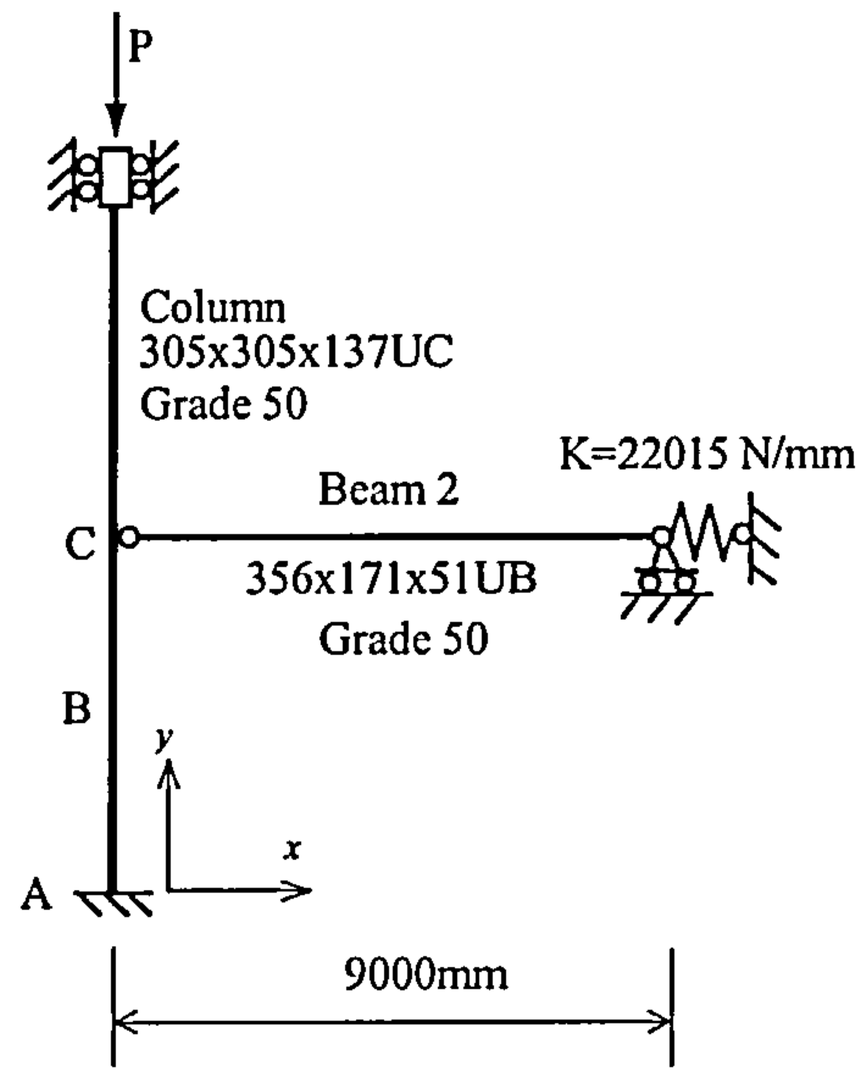

(b) Model 2
(Unbraced frame: spring end)

Fig. 4-19 x-y plane sub-frame models

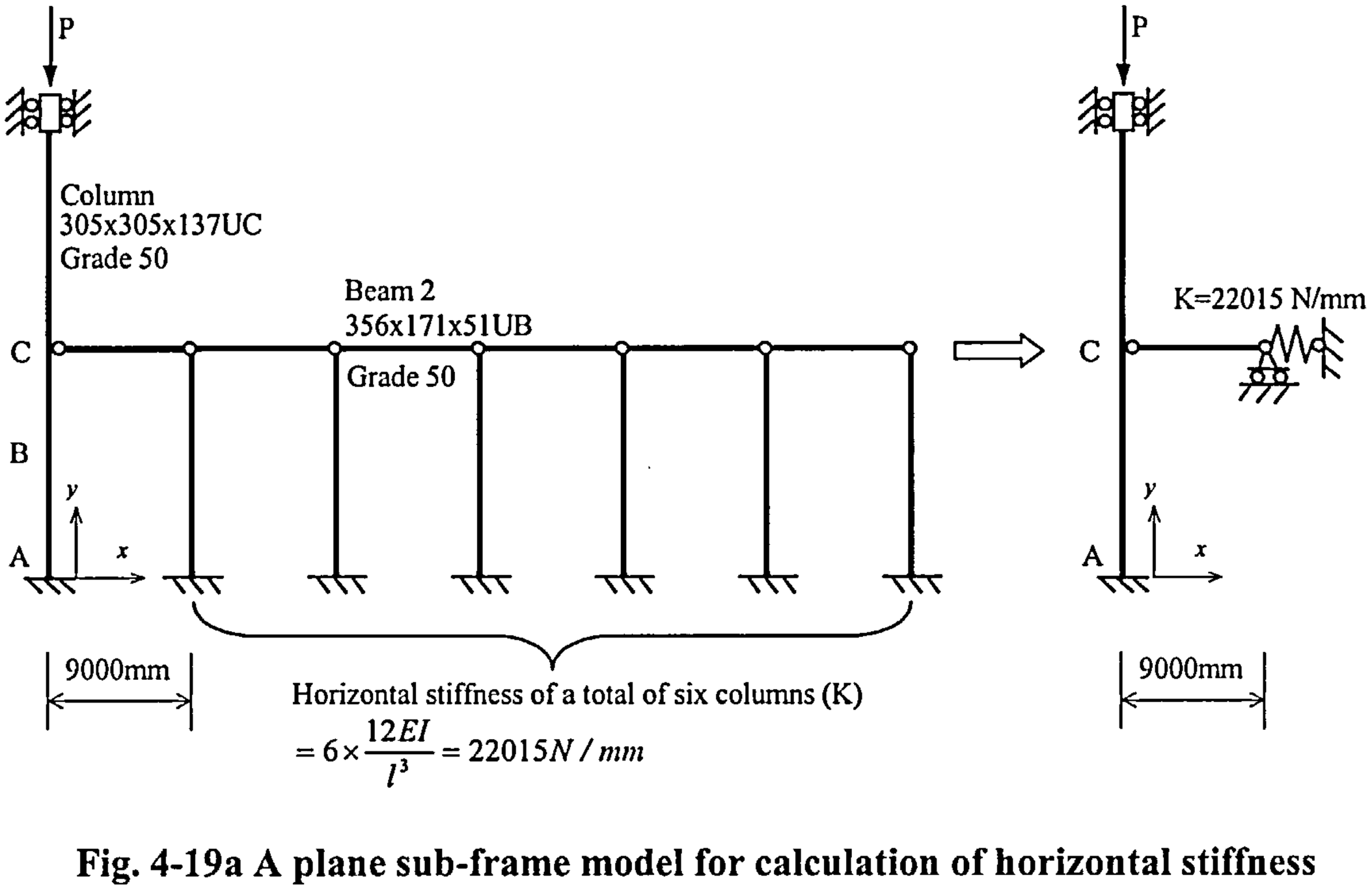

Fig. 4-19a A plane sub-frame model for calculation of horizontal stiffness

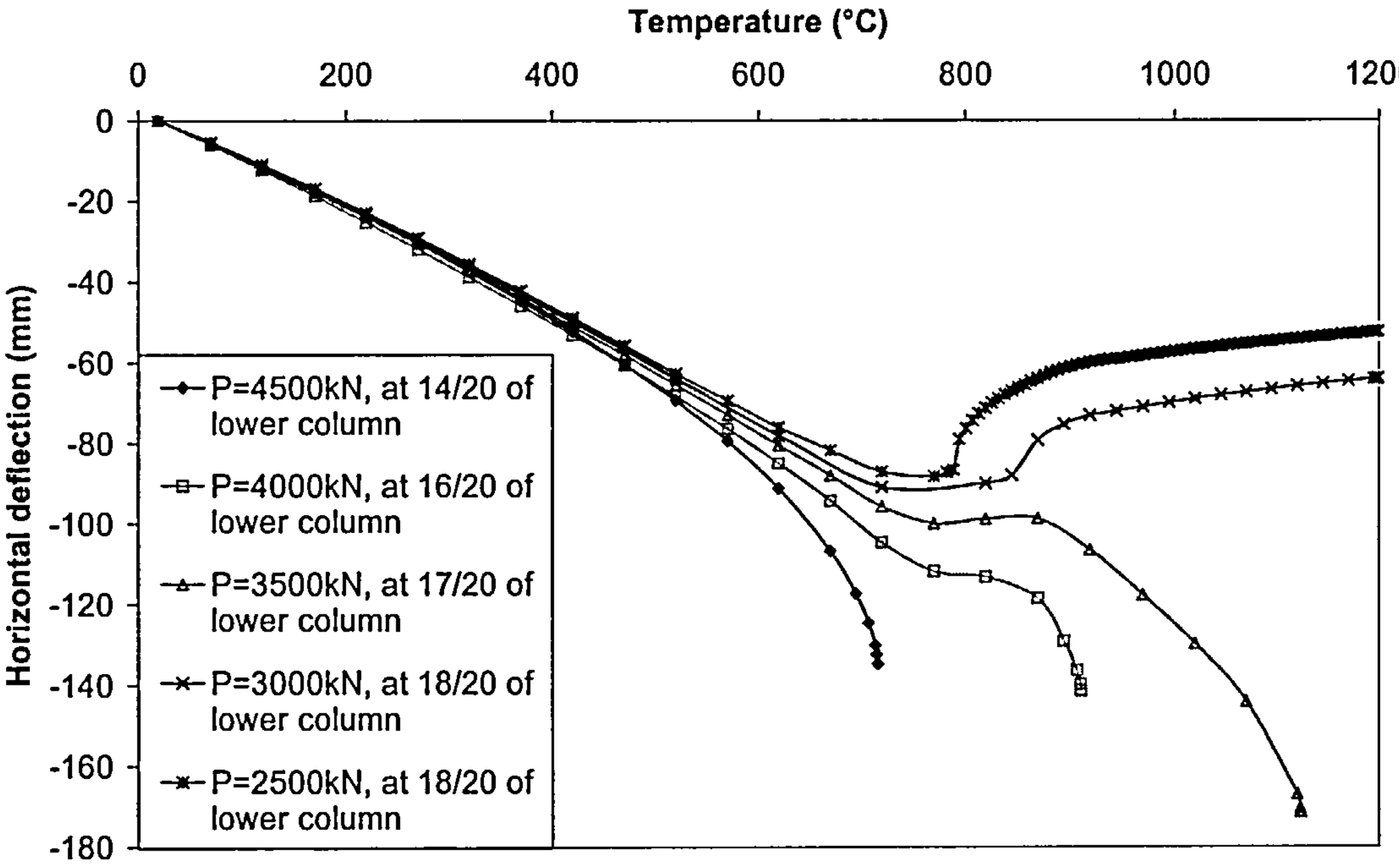

Fig. 4-20 Maximum column x-deflection for x-y plane sub-frame model 1 (Lower column 400°C, pin end)

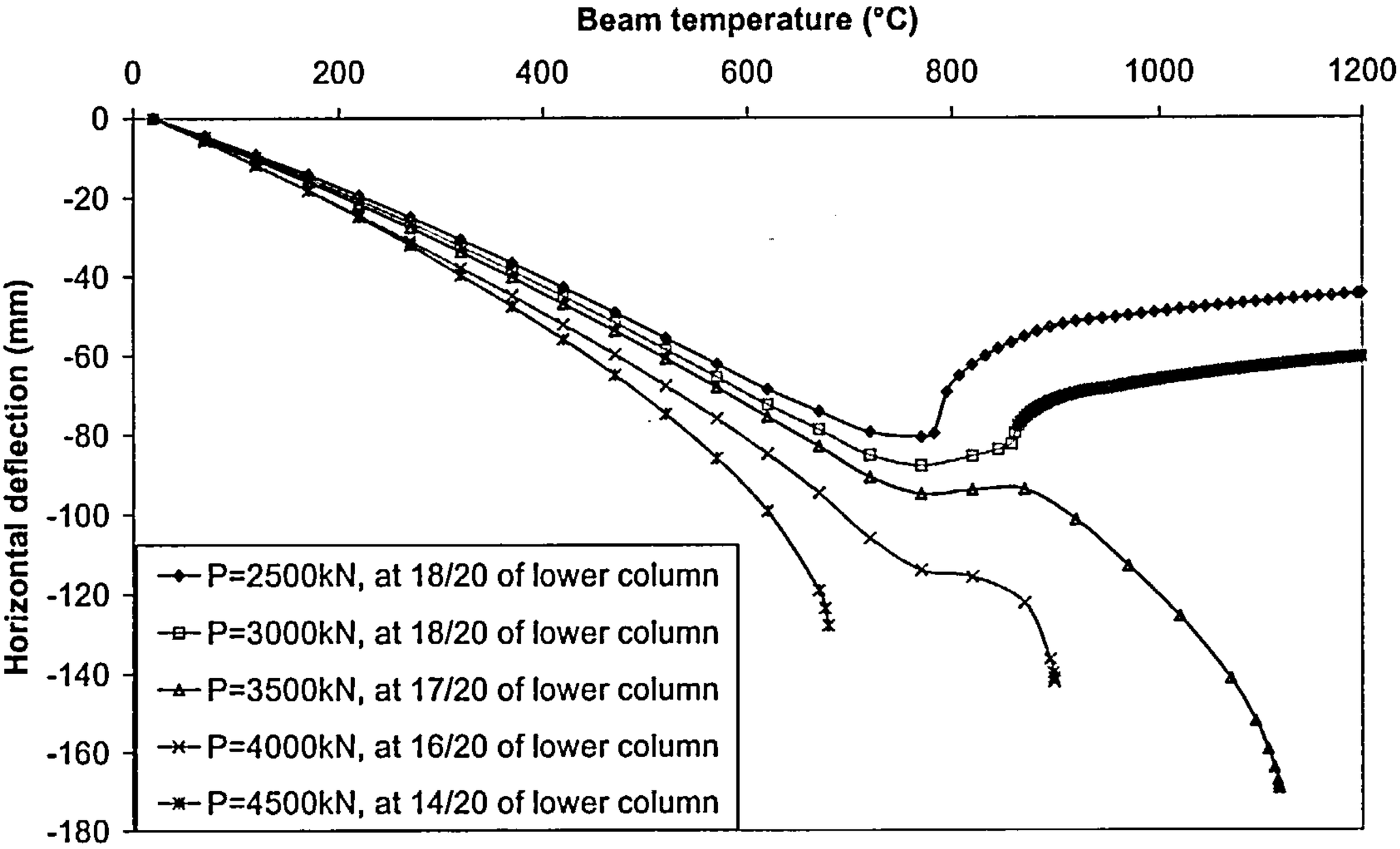

Fig. 4-21 Maximum column x-deflection for x-y plane sub-frame model 2 (Lower column 400°C, spring end)

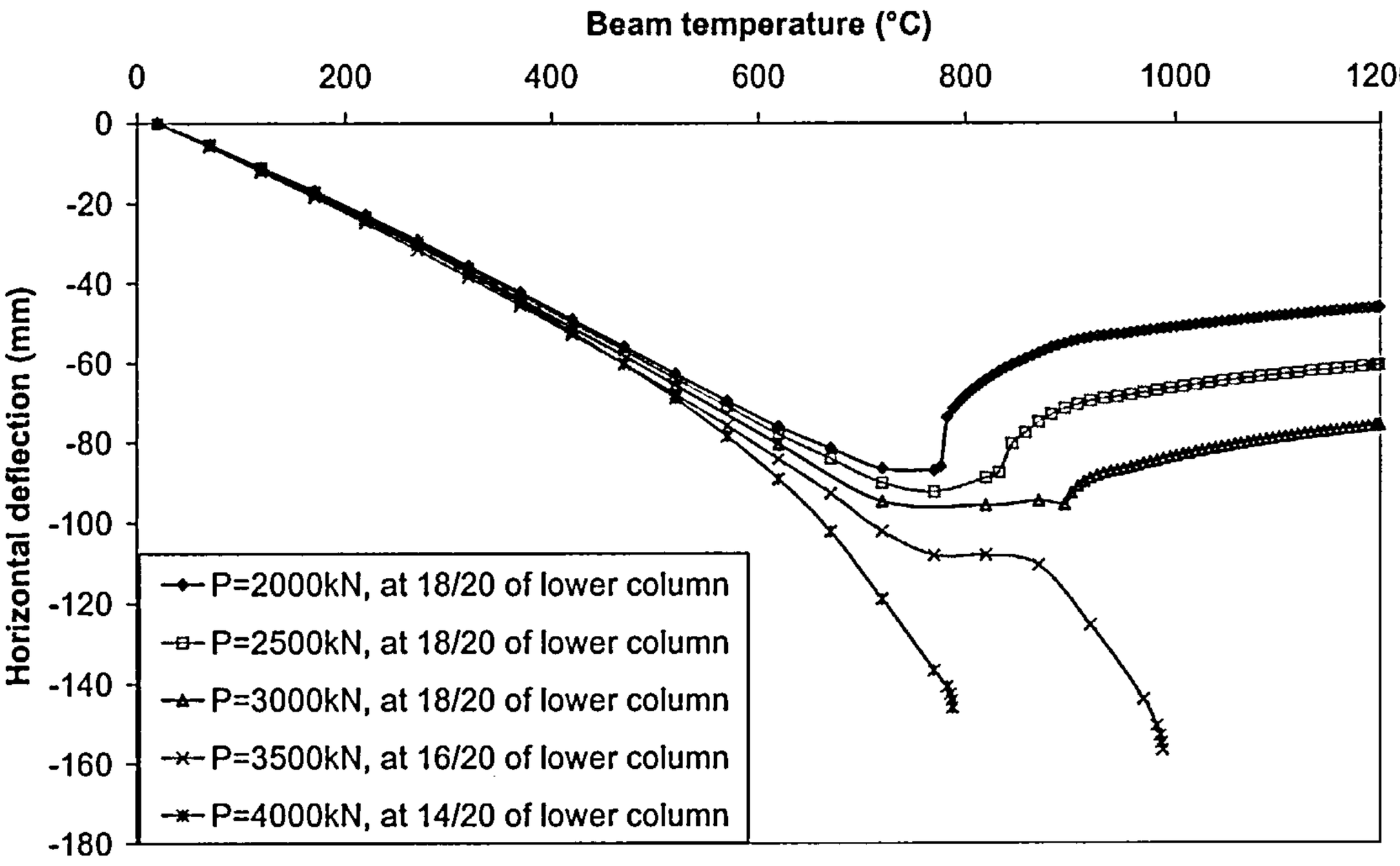

Fig. 4-22 Maximum column x-deflection for x-y plane sub-frame model 1 (Lower column 450°C, pin end)

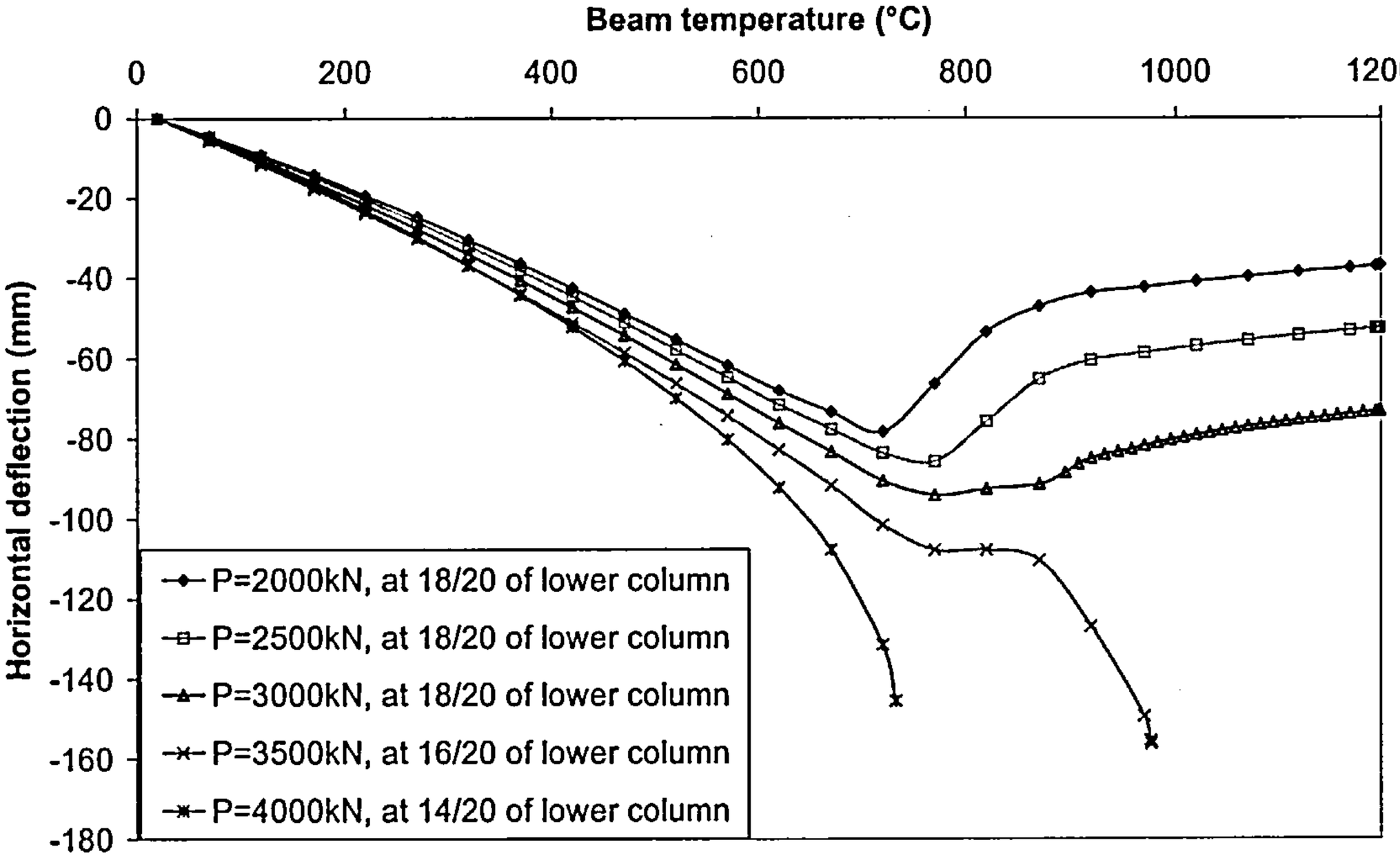

Fig. 4-23 Maximum column x-deflection for x-y plane sub-frame model 2 (Lower column 450°C, spring end)

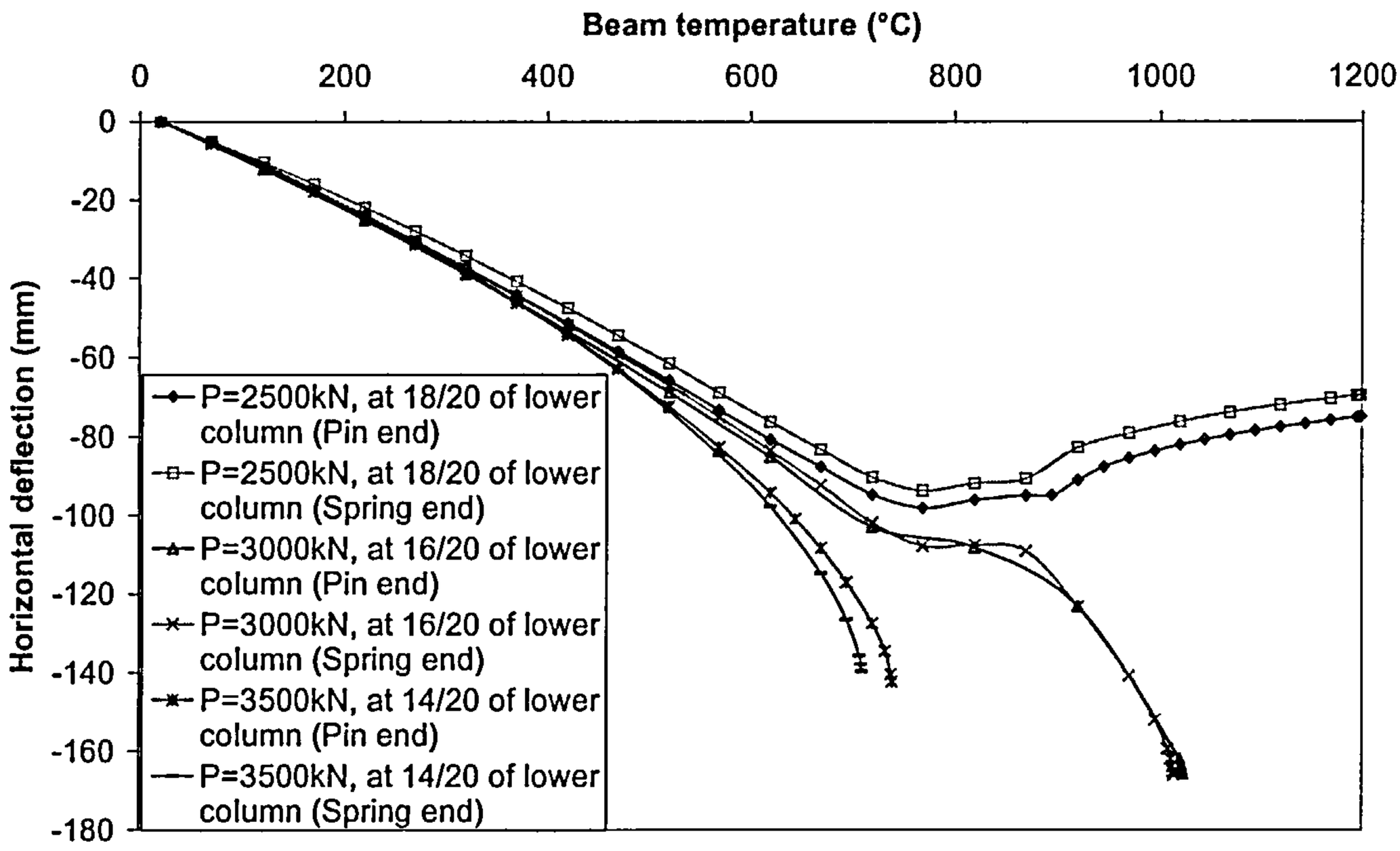

Fig. 4-24 Maximum column x-deflection for x-y plane sub-frame model 1 and model 2 (Lower column 500°C)

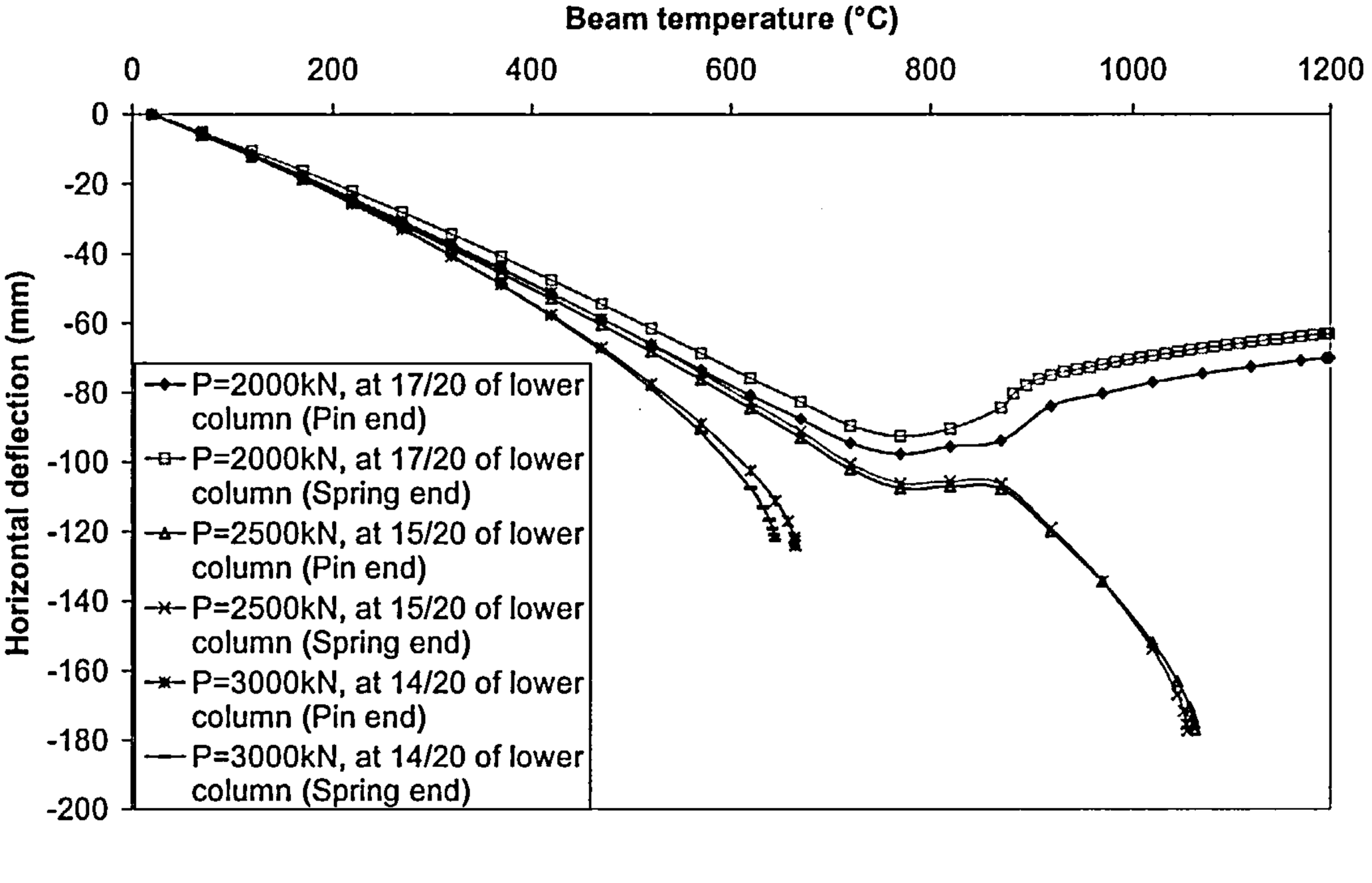

Fig. 4-25 Maximum column x-deflection for x-y plane sub-frame model 1 and model 2 (Lower column 550°C)

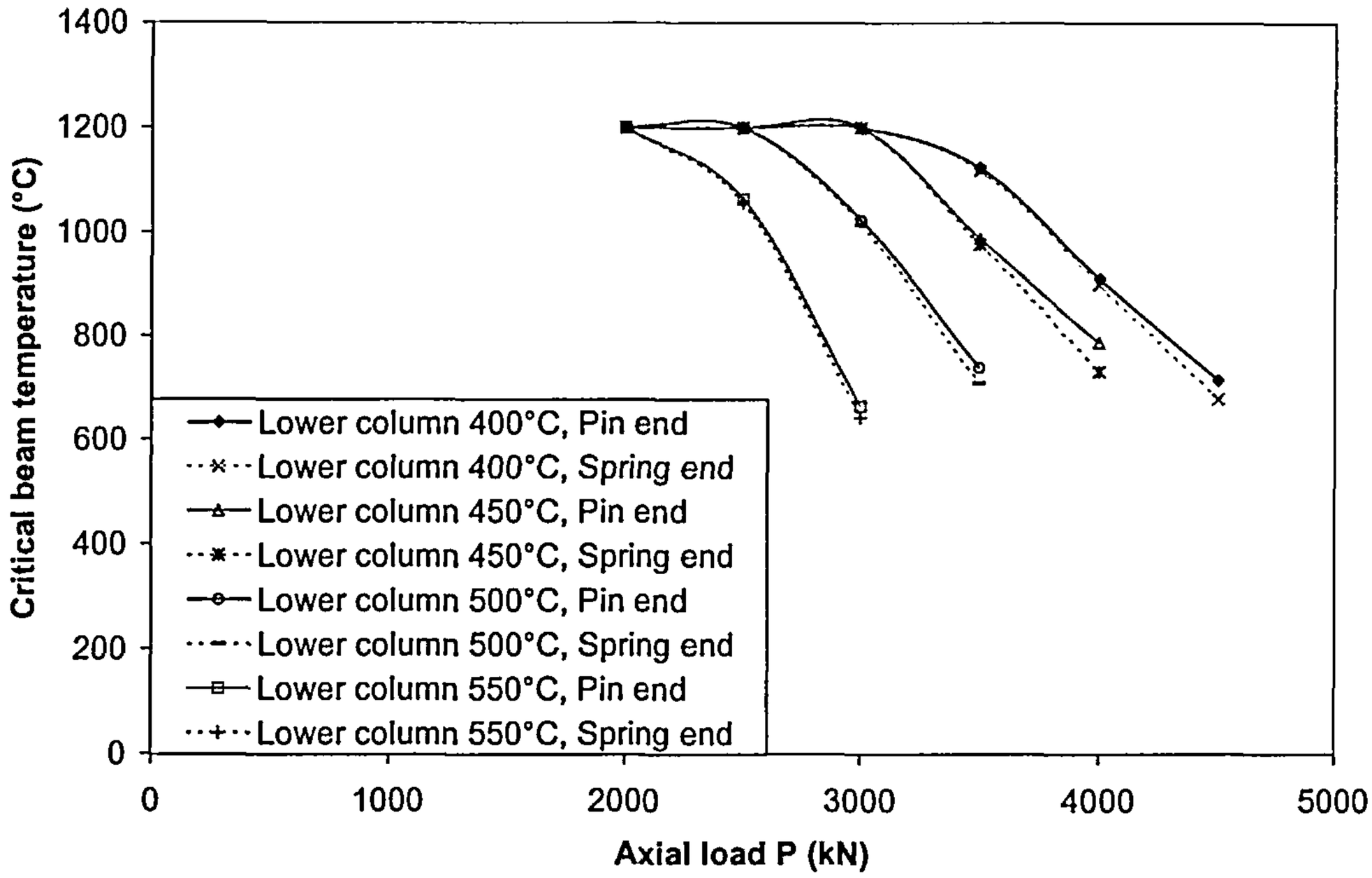

Fig. 4-26 The critical temperature under different level of axial load for x-y plane sub-frame model 1 and model 2

From the analyses it can be seen that, because of beam buckling, some curves, especially with low axial load, reverse their directions. Nevertheless, the structure retains its stability until 1200°C (at which point the steel is considered to have lost all of its stiffness). It is of interest to see that there is negligible difference between the results for pin and spring ends for the same axial load and temperature. When the temperature approaches failure the internal force in the beam reverses direction to restrain column buckling. However the axial spring softens this restraining force. For this reason all the critical temperatures for cases including axial springs are slightly less than those obtained for pin end cases, with a maximum difference of 55°C at an axial load of 4000kN for the lower column of 450°C as shown in Fig. 4-26 with the sway (unbraced) frame performing a little worse than the braced frame. It is noted that in VULCAN the thermal elongation of steel is assumed to be constant between 750°C

and 860°C, and as the column temperature is constant there is no column instability likely in this range.

4.2.3 CASE STUDY 3 -- 3D SKELETAL FRAME

The above case has been extended to 3-dimension skeletal sub-frame as shown in Fig. 4-27. The springs K_1 and K_2 represent the horizontal stiffness of six columns for the minor axis of the sub-frame column and three columns for the major axis, to simulate the sway (unbraced) structure. In this case, the lower column and both the beams are uniformly heated at the same rate until reaching a prescribed temperature level (400°C, 500°C and 550°C). The column temperature then remains constant while the beam temperatures continues to rise. The results are shown in Figs. 4-28 to 4-30. Figs. 4-31 and 4-32 also show the results for the same 3D structure but re-run by using different heating scheme as described in 2D cases, indicating little difference in critical temperature compared with those based on a 2D sub-frame for an equivalent heating scheme, and by comparison with Figs 4-29 and 4-30 respectively there is less effect from using the two heating schemes.

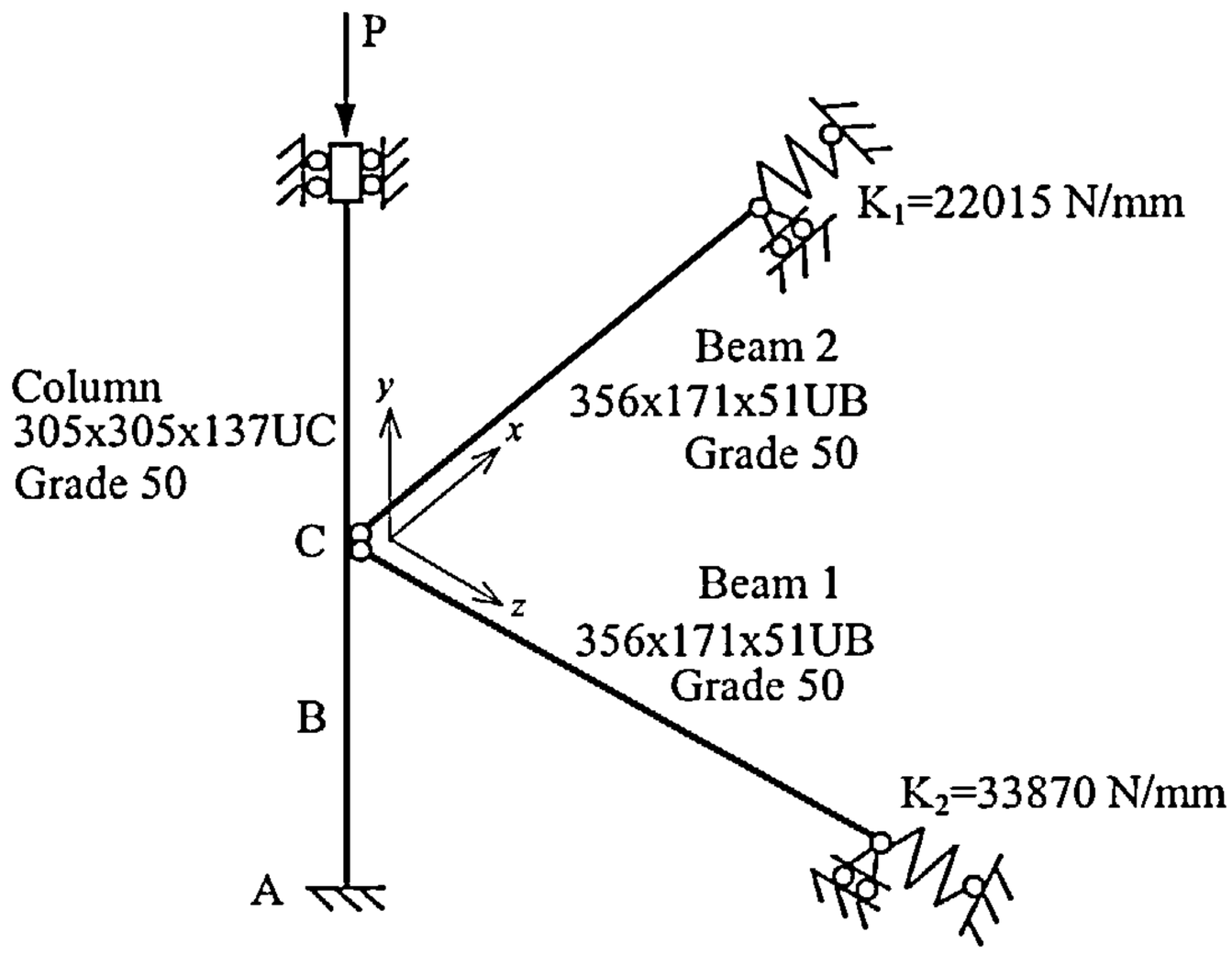

Fig. 4-27 Three-dimensional skeletal sub-frame

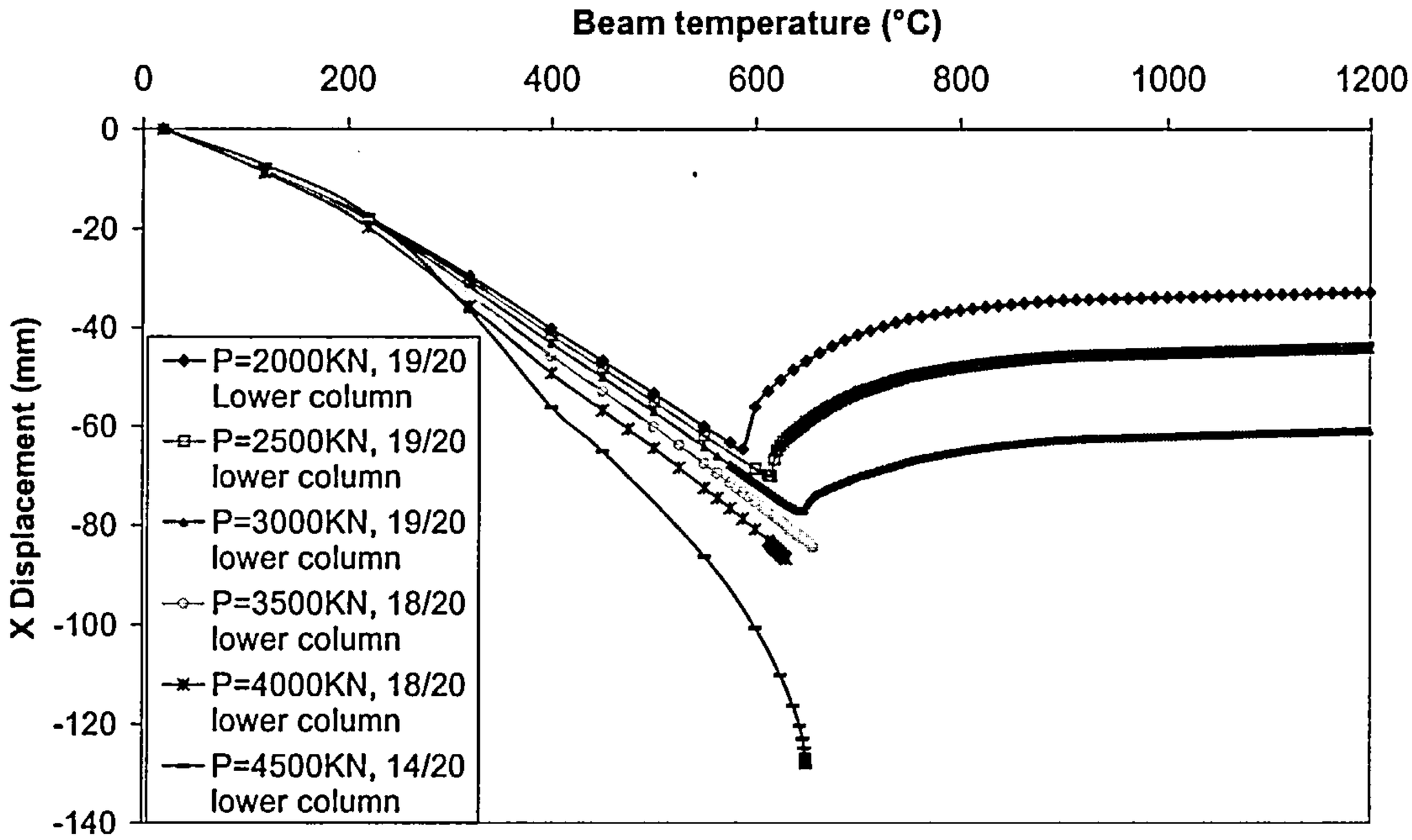

Fig. 4-28 Maximum column x-deflection for 3D sub-frame case (Lower column 400°C)

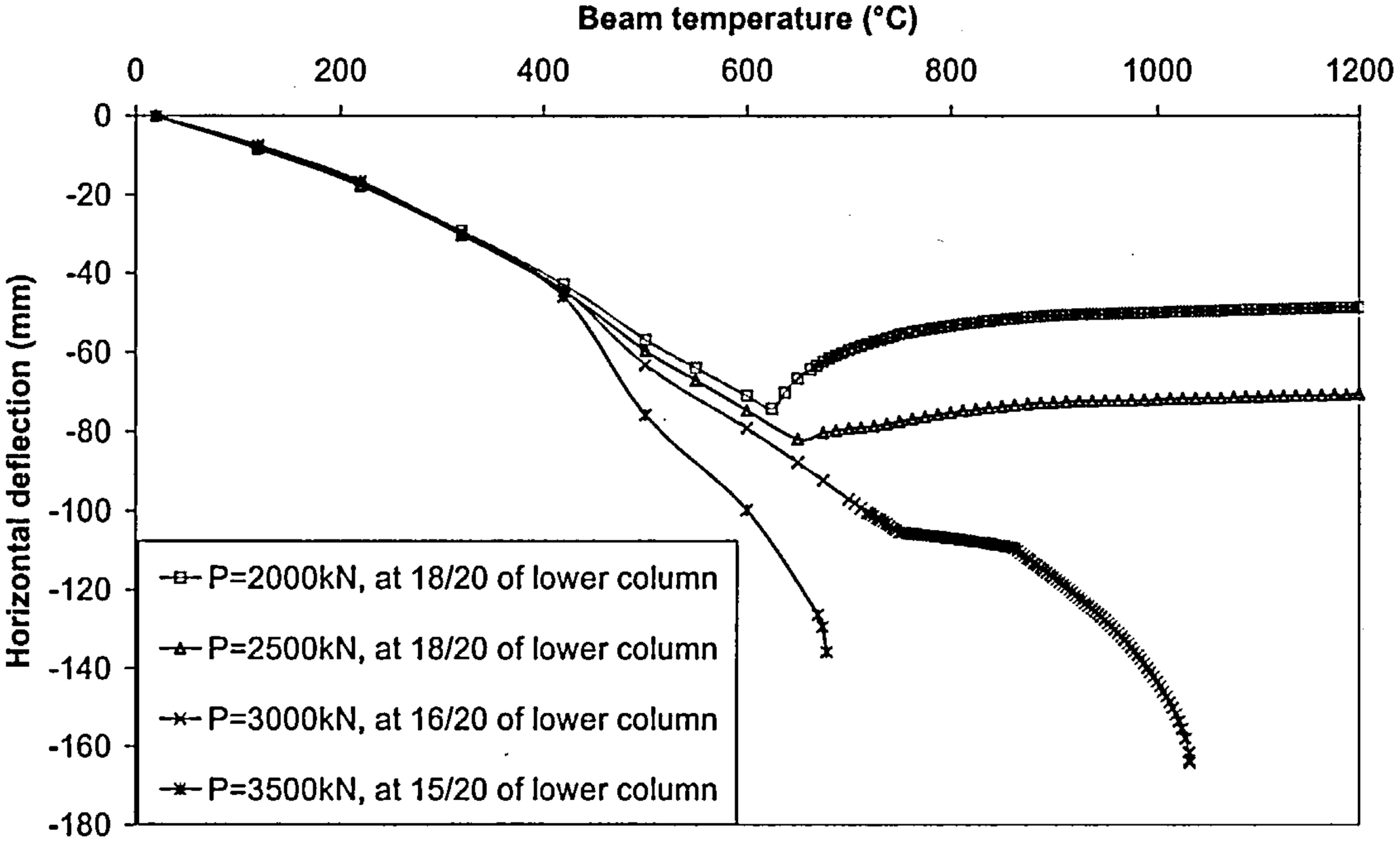

Fig. 4-29 Maximum column x-deflection for 3D sub-frame case (Lower column 500°C)

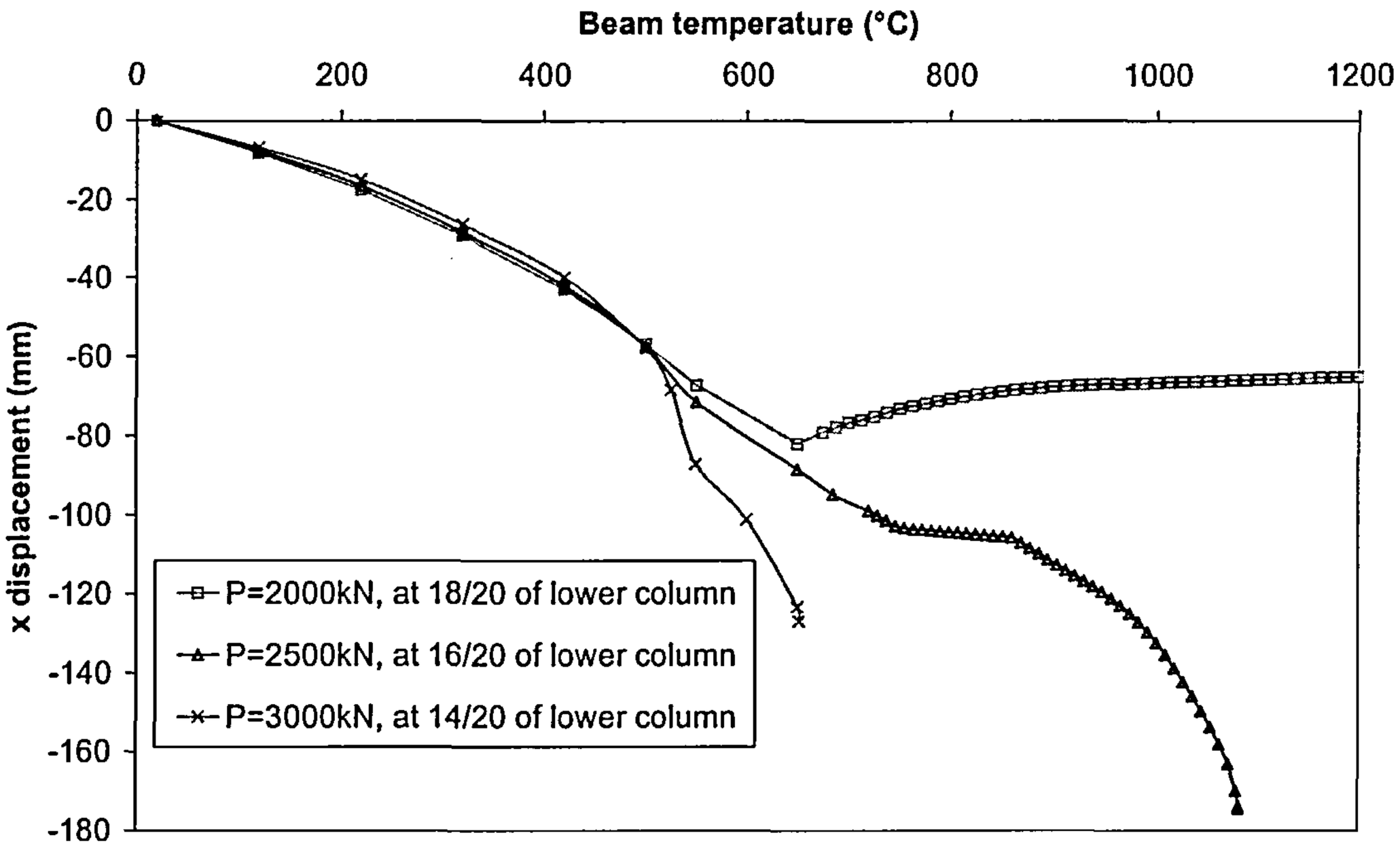

Fig. 4-30 Maximum column x-deflection for 3D sub-frame case (Lower column 550°C)

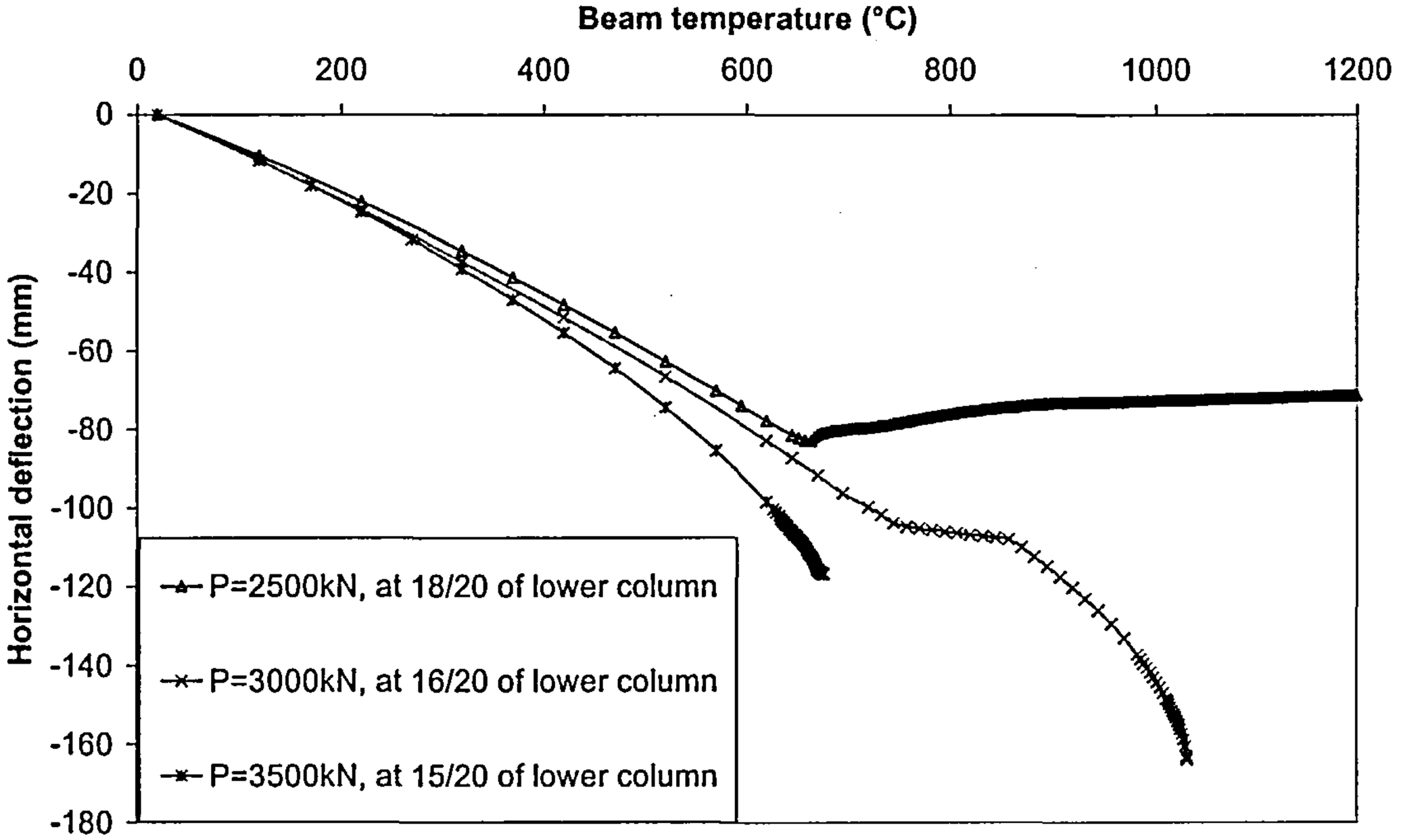

Fig. 4-31 Maximum column x-deflection for 3D sub-frame case at lower column 500°C (Heating scheme is same as 2D sub-frame case)

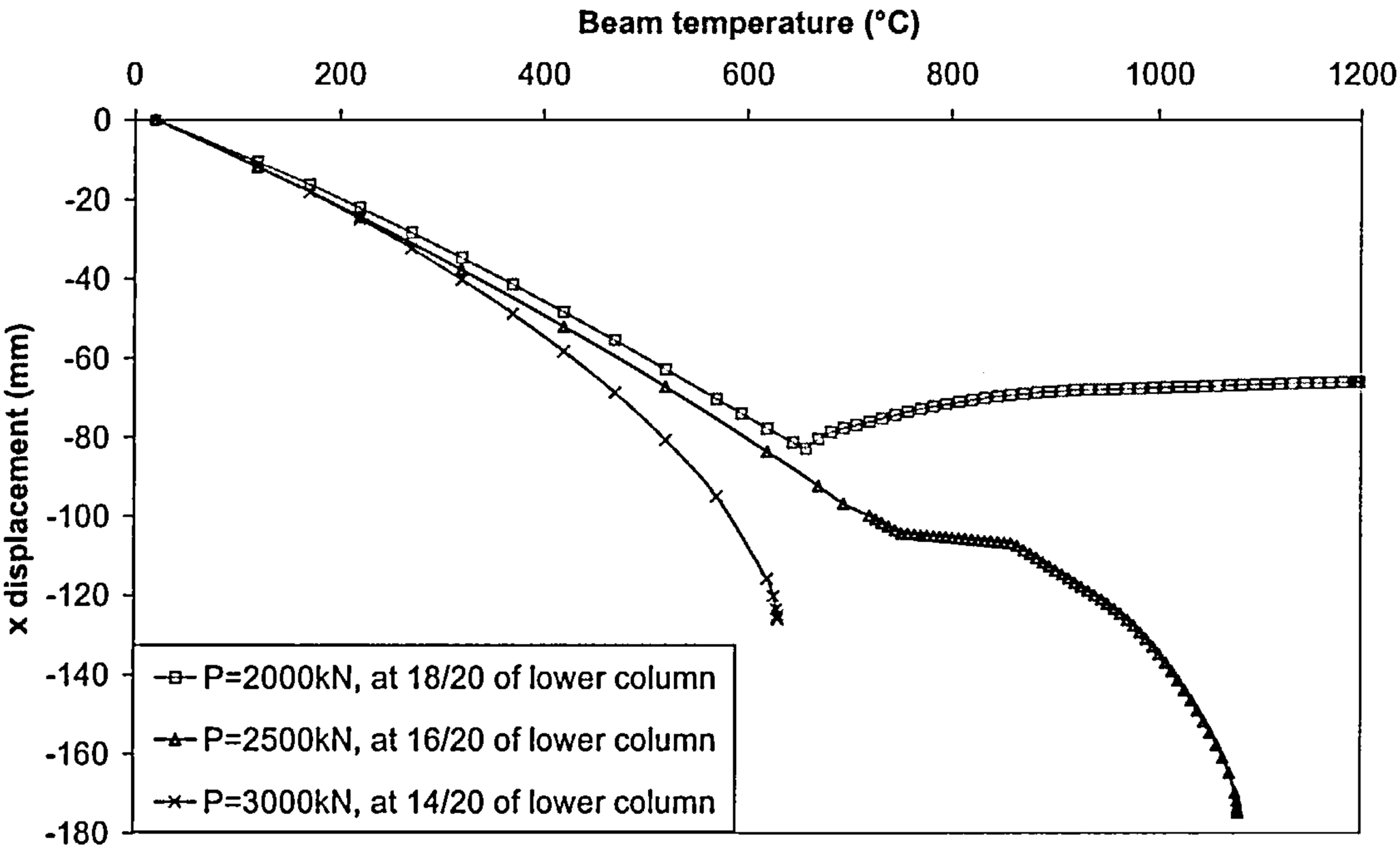

Fig. 4-32 Maximum column x-deflection for 3D sub-frame case at Lower column 550°C (Heating scheme is same as 2D sub-frame case)

4.2.4 CASE STUDY 4 -- 3D FRAME WITH FLOOR SLABS

A more complicated composite frame case, which is based on the above 3D skeletal frame but extended to include a concrete slab of 70mm thickness (Fig. 4-33), has been analysed. In this case the concrete slab is divided into 16 elements and is assumed to be fully connected to the beams. The slab, beams and lower column are uniformly heated up to 400°C and 500°C respectively. The column temperature is then kept constant whilst the beams and slab continue to be heated until structural instability occurs. Four springs were used to model the column stiffnesses of a 3 (row) x 6 (column) structure as illustrated in Fig. 4-33a. Because of the effect of the slab, the behaviour of the frame shows some differences compared with the skeletal frame, and all the critical temperatures are less than 1000°C due to either beam buckling or column buckling. The results of the analyses are shown in Figs 4-34 to 4-37. Some curves reverse their directions because of beam buckling or slab failure since it can be observed from Figs. 4-35 and 4-37 to give infinite tendencies of beam vertical

displacements, and their reversing actions are not too sharp as presented above for the skeletal case because of the inclusion of the slab. The horizontal deflection of the column is less than for the skeletal frame and the beam reaches a higher temperature before buckling. This is because the slab restrains the thermal expansion of the beam and prevents lateral buckling of the beam.

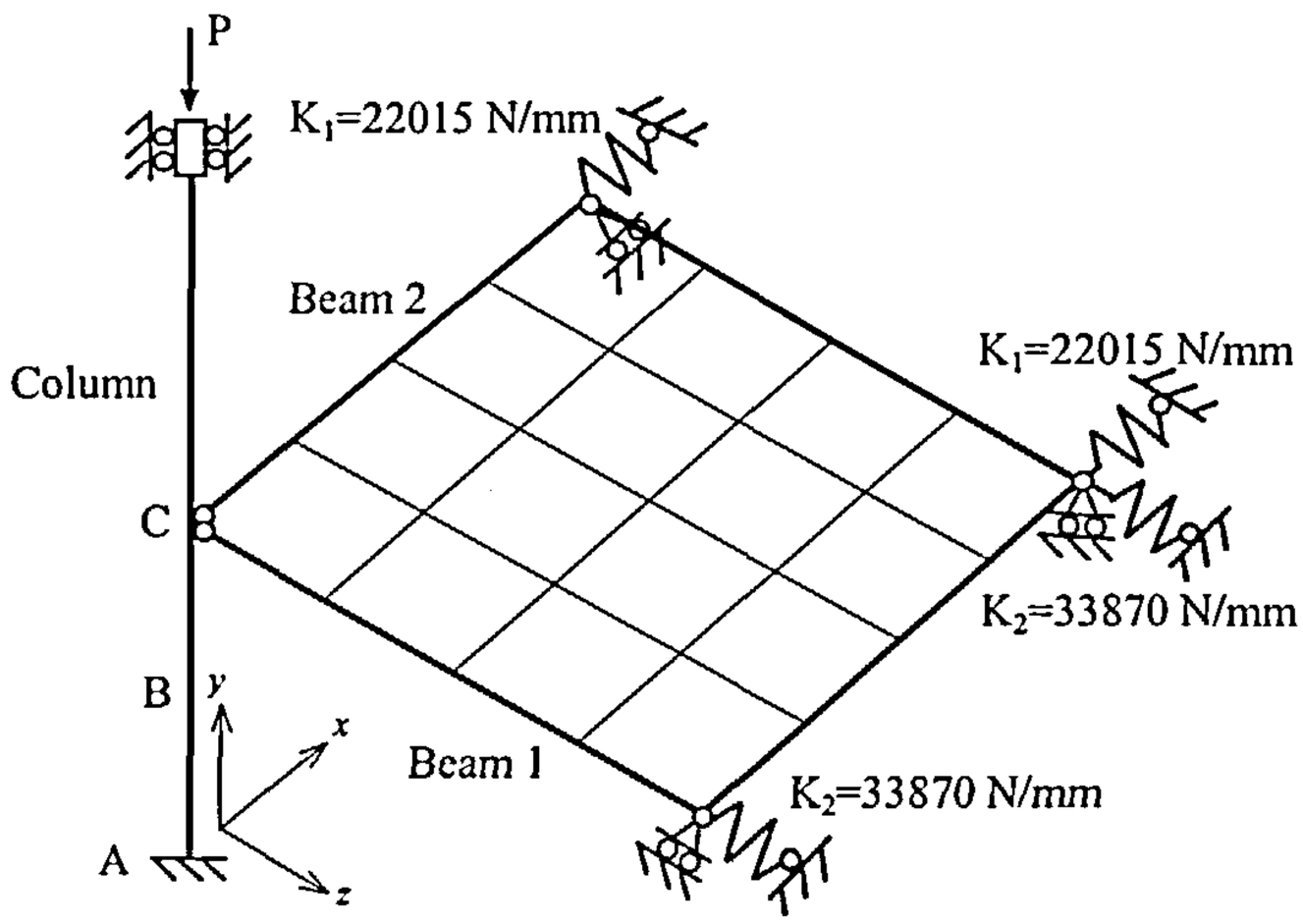

Fig. 4-33 Three-dimensional composite sub-frame including floor slabs

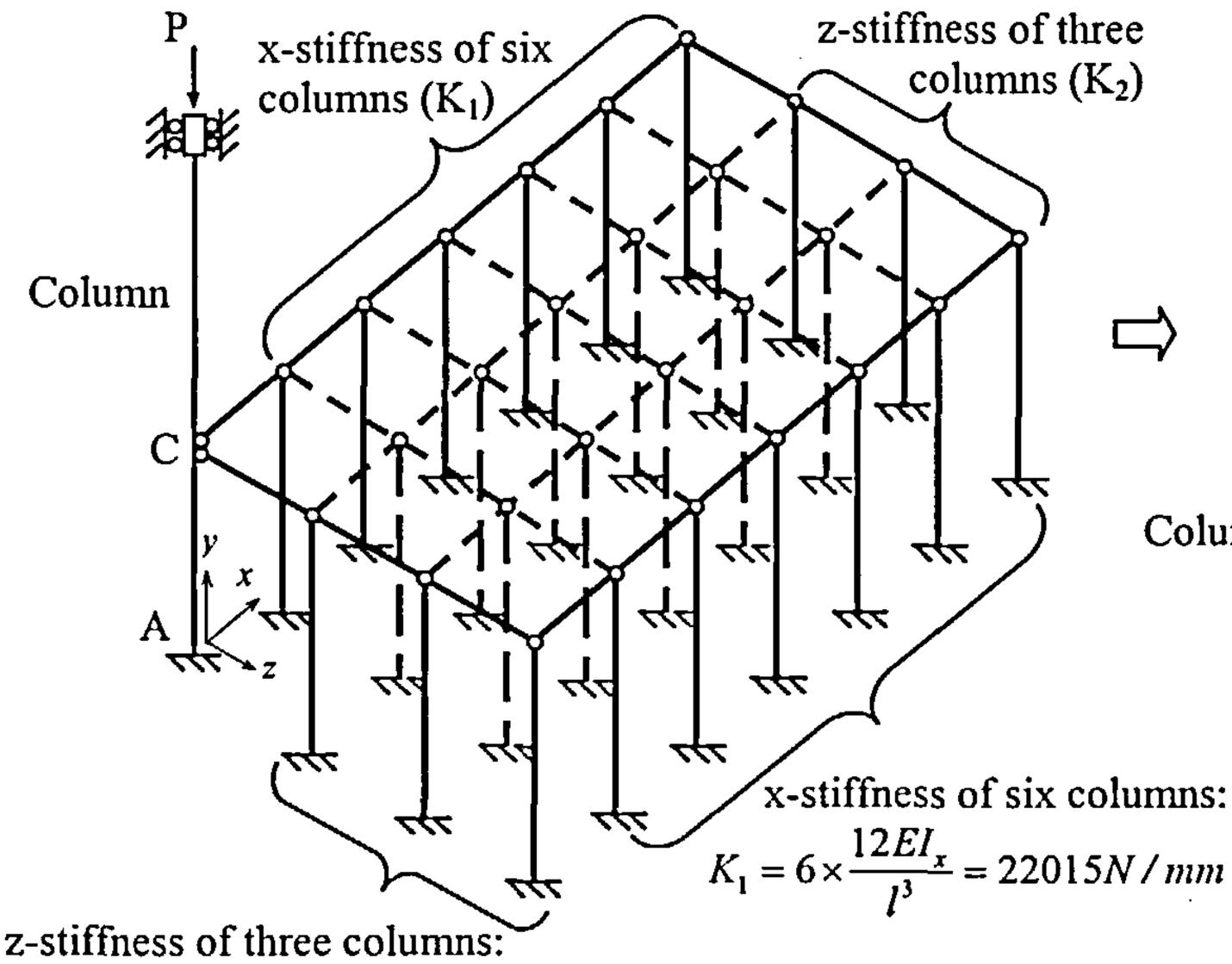

x-stiffness of six columns:

$$K_1 = 6 \times \frac{12EI_x}{l^3} = 22015N/mm$$

z-stiffness of three columns:

$$K_2 = 6 \times \frac{12EI_z}{l^3} = 33870N/mm$$

Fig. 4-33a Three-dimensional composite sub-frame model for calculation of horizontal stiffness

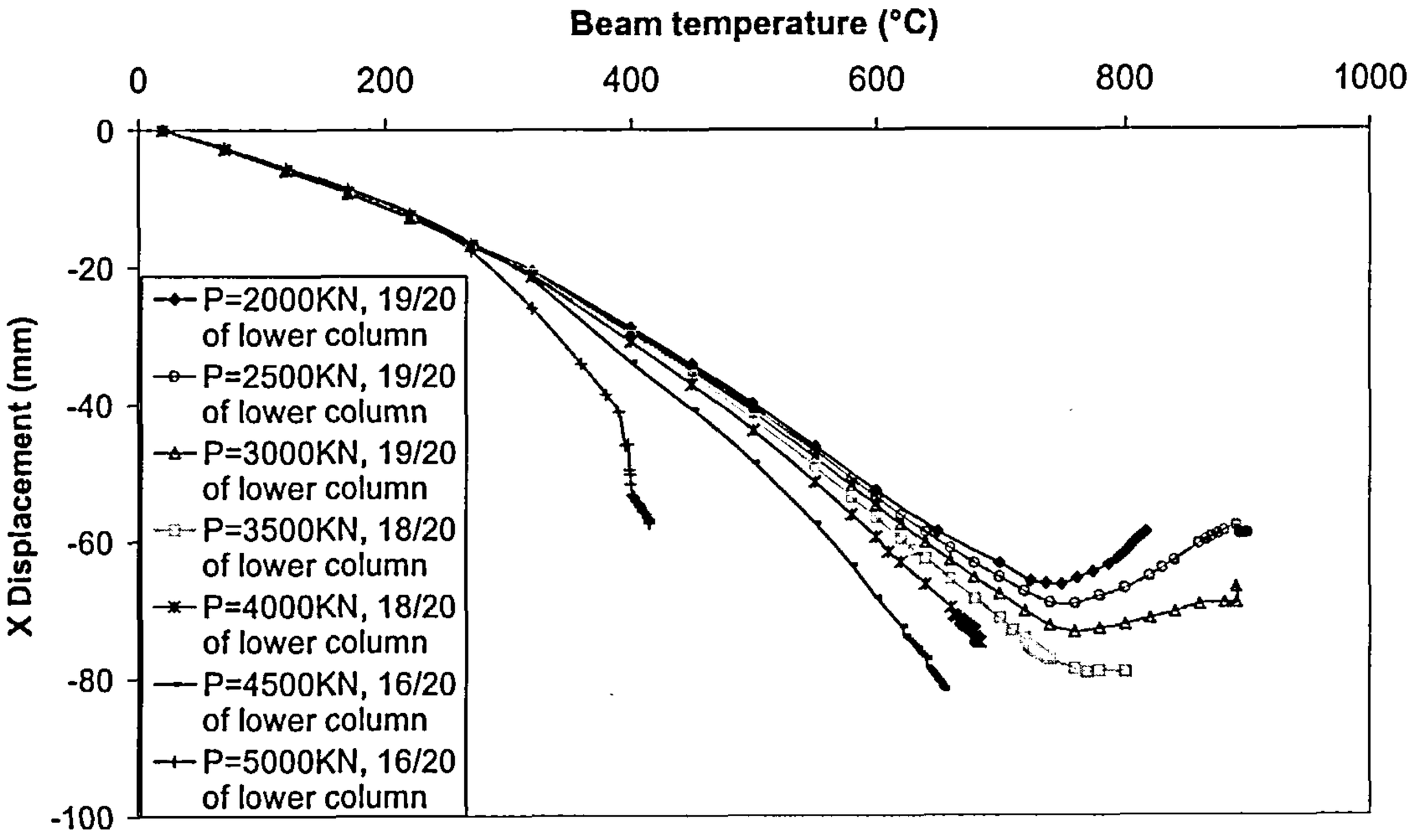

Fig. 4-34 Maximum column x-deflection at lower column 400°C

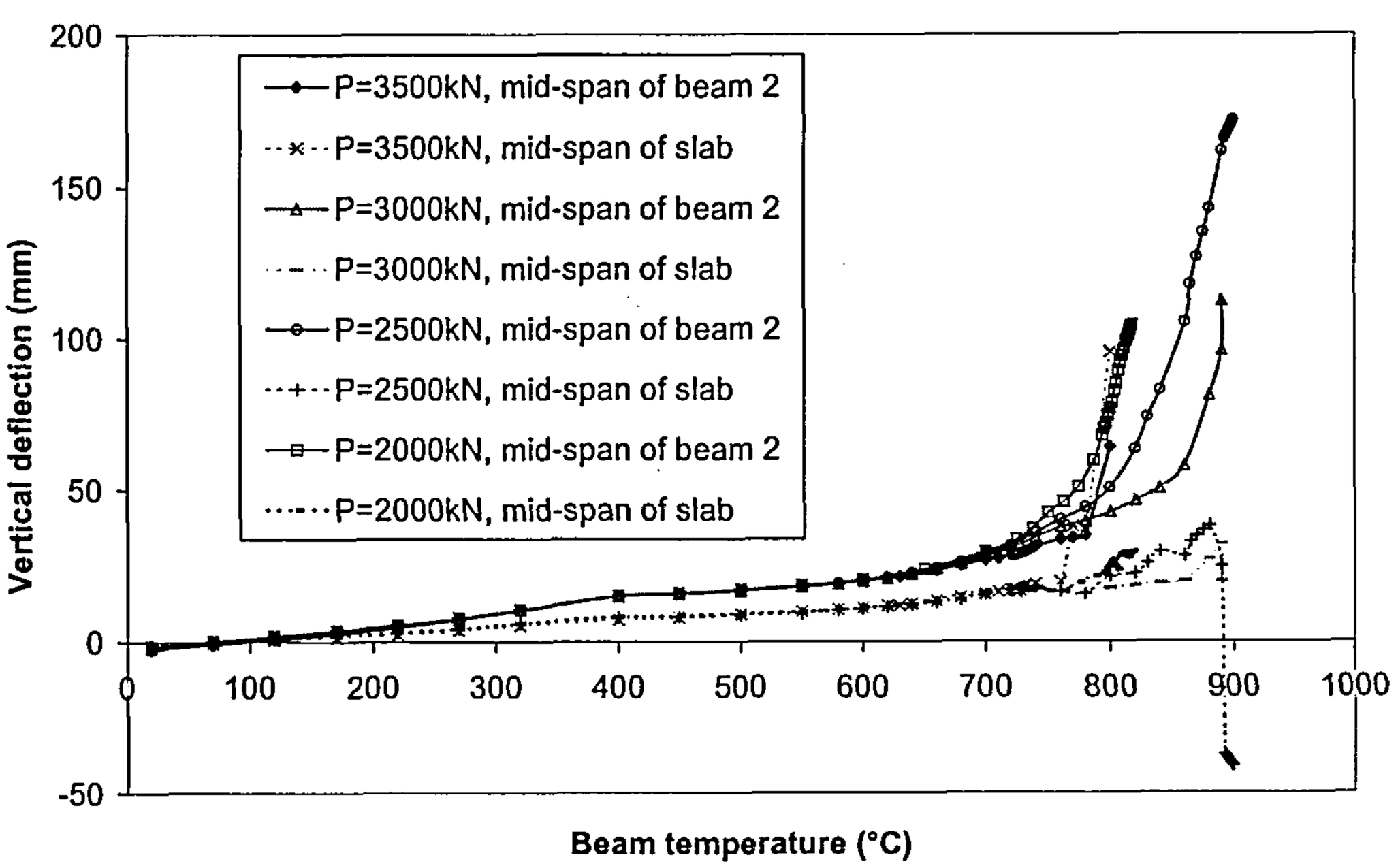

Fig. 4-35 Vertical deflections of beam and slab at lower column being 400°C

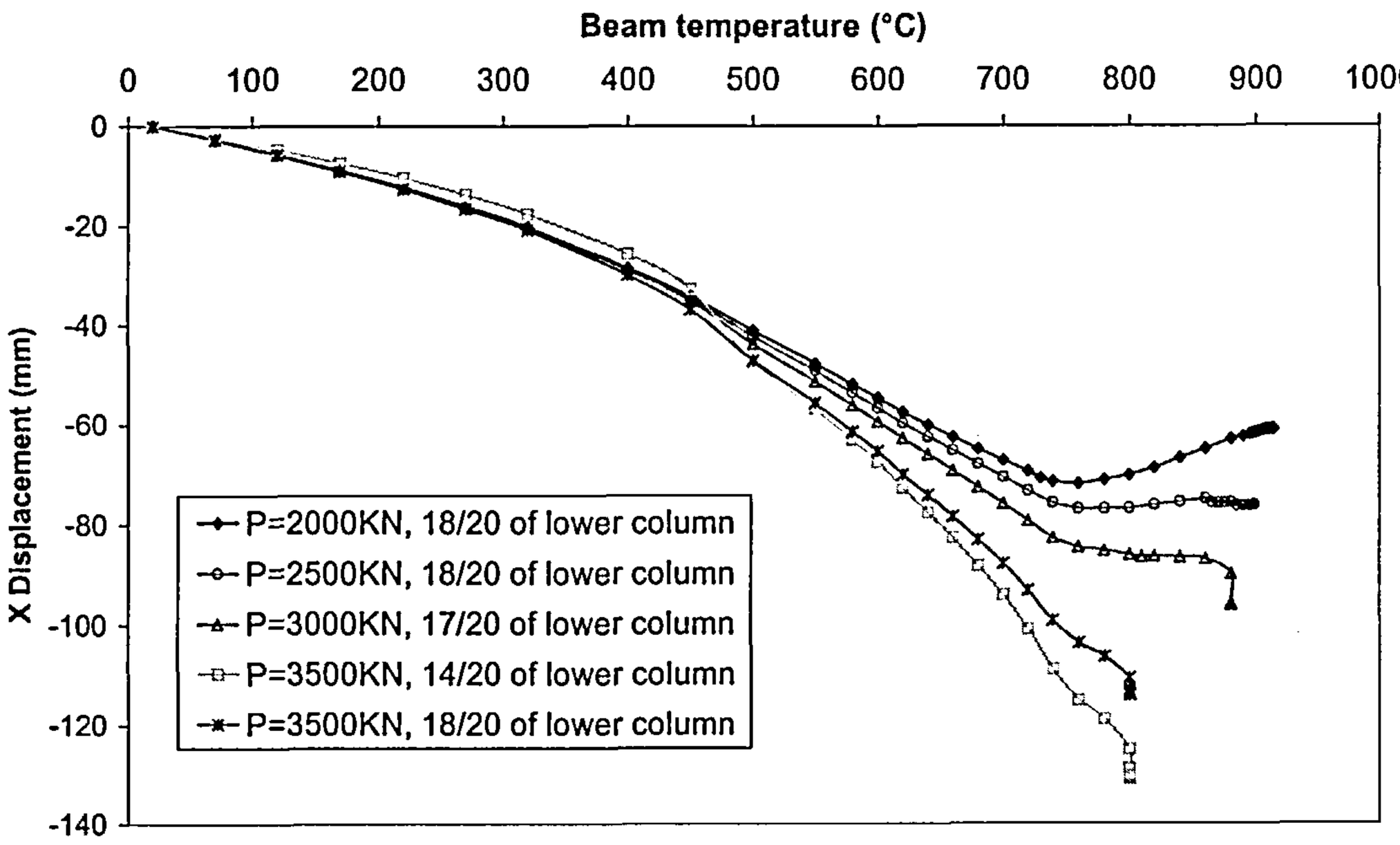

Fig. 4-36 Maximum column x-deflection at lower column being 500°C

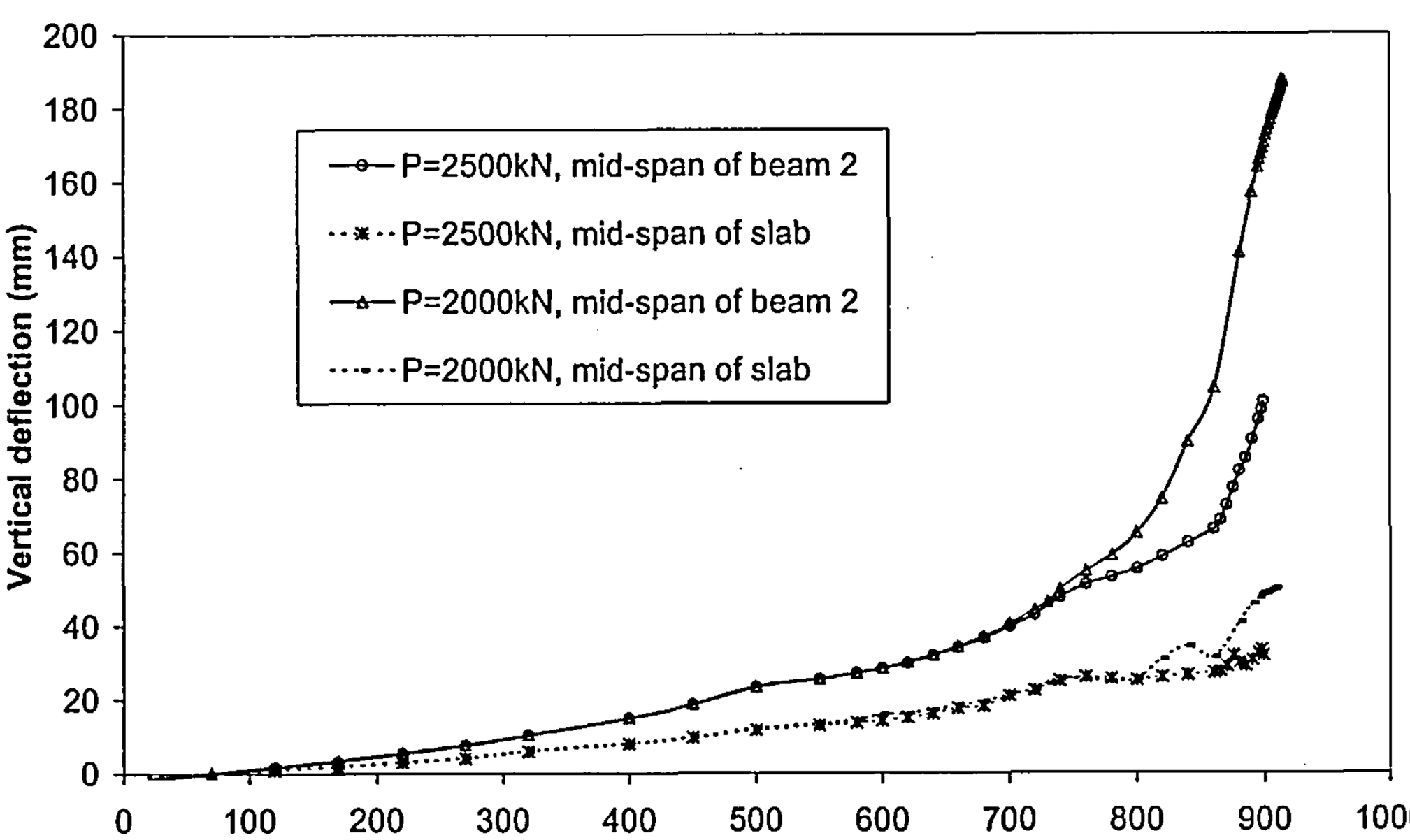

Fig. 4-37 Vertical deflections of beam and slab at lower column being 500°C

4.3 CONCLUSIONS

4.3 CONCLUSIONS

In this study, a series of analyses have been carried out based on a corner sub-frame which involved 2D and 3D composite models. The results indicate that the most important factor reducing the survival temperature of columns is the **P-Δ** effect. The thermal expansion of unprotected beams induces extra bending moments in the column, as the failure temperature of the column is approached the effect reverses and becomes a restraining force. The slab also has a significant influence in reducing the effect of beam expansion. The pull-in effect, which is normally caused by bending of the beams, is of benefit to the survival of the column but is relatively small compared with the effect of thermal expansion which is the primary influence for the **P-Δ** effect. The analyses also point out that the existing fire design codes, such as BS5950: Part 8, can be unsafe. To calculate the critical temperature of the column based on these design codes, a modified effective length factor of 1.2 should be taken into account, and whether the structure is braced or not, the factors for a sway frame should be considered. These preliminary results indicate that the reduction in column capacity is not critical if a modified effective length is taken into account, particularly when a composite frame is used. Since the 2D frame does not present much difference in critical temperature from the 3D frame, it is suggested that designers use simplified 2D calculations to model the structural instability. These calculation methods will be introduced in chapter 5.

5. THE EFFECT OF PUSH-OUT OF PERIMETER BUILDING COLUMNS ON THEIR SURVIVAL IN FIRE

In this chapter a generalised simplified approach suitable for hand calculation to enable a quick assessment of perimeter building columns is presented.

5.1 INTRODUCTION

Current fire design codes, such as BS5950: Part 8[47] and EC3: Part 1.2[46], typically consider the structure as a series of individual members ignoring the effect of adjacent members. Whilst this is generally a conservative assumption, it may not give a safe representation for the corner column as described in the preceding chapter. In chapter 4, the particular case of a 305x305x137UC column with two 356x171x51UB beams connected was analysed, and an effective length factor of 1.2 suggested for the column when designed according to BS5950: Part 8[47]. However, if different sizes of columns or beams (including cross-section size and length) are used, the analyses have to be repeated to obtain a new effective length factor. It is clear that the longer and stiffner the beam is, the bigger thermal elongation of the beam and therefore the more induced bending moments we obtain, this could lead a less critical column temperature. A generalised simplified approach, as an alternative to complex finite element analysis (for example using software such as VULCAN), will enable a quick assessment of these problems by designers. This chapter describes such an approach.

For a general member with large deflections, the differential equation for linear elastic bending ignoring buckling can be expressed as

$$\frac{\frac{d^2y}{dx^2}}{\left[1+\left(\frac{dy}{dx}\right)^2\right]^{3/2}} = -\frac{M}{EI} \qquad (5\text{-}1)$$

Considering a column subjected to an axial load **P** with a small deflection **y**, which implies that $\left(\frac{dy}{dx}\right)^2$ is small and is negligible by comparison with unity, the governing differential equation for stability of a long column can be simplified from Eqn. (5-1) for all boundary conditions as

$$EI\frac{d^4y}{dx^4}+P\frac{d^2y}{dx^2}=0 \qquad (5\text{-}2)$$

where the deflection **y** of the column at any point at distance **x** from the origin is the displacement of that point in the y direction, measured from **x** axis to the deflection curve as illustrated as the right.

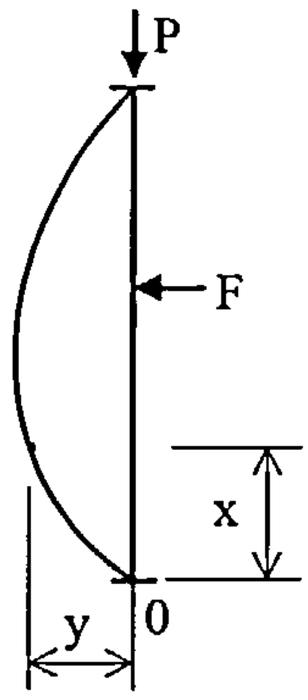

The general solution of Eqn. (5-2) will be

$$y=C_1\sin Kx+C_2\cos Kx+C_3x+C_4 \qquad (5\text{-}3)$$

Taking account of the influence of axial shortening[77] on the column, Eqn. (5-2) may be written

$$\frac{EI}{\left(1-\frac{P}{EA}\right)}\frac{d^4y}{dx^4}+P\frac{d^2y}{dx^2}=0 \qquad (5\text{-}4)$$

where **EA** is the axial rigidity. However, the effect of axial shortening is usually negligible in the case of a long column.

A simple corner sub-frame as shown in Fig. 5-1 is used for this study. In this sub-frame the lower column and both beams are assumed to be uniformly heated, with the upper column being kept cool. In order to perform the analysis, the following assumptions are made,

- The material is linearly elastic and there is uniform temperature distribution across the section;
- The column is long (large slenderness ratio) with $\lambda \geq \pi\sqrt{\frac{E}{\sigma_{cr}}}$;
- Small deflection theory for simple bending is applicable and shear may be neglected;
- No buckling (local or lateral) occurs;
- The effect of axial shortening on the column is negligible;
- The thermal expansion of the column is ignored, and the reduction factors for strength presented in EC3: Part 1.2 are adopted.

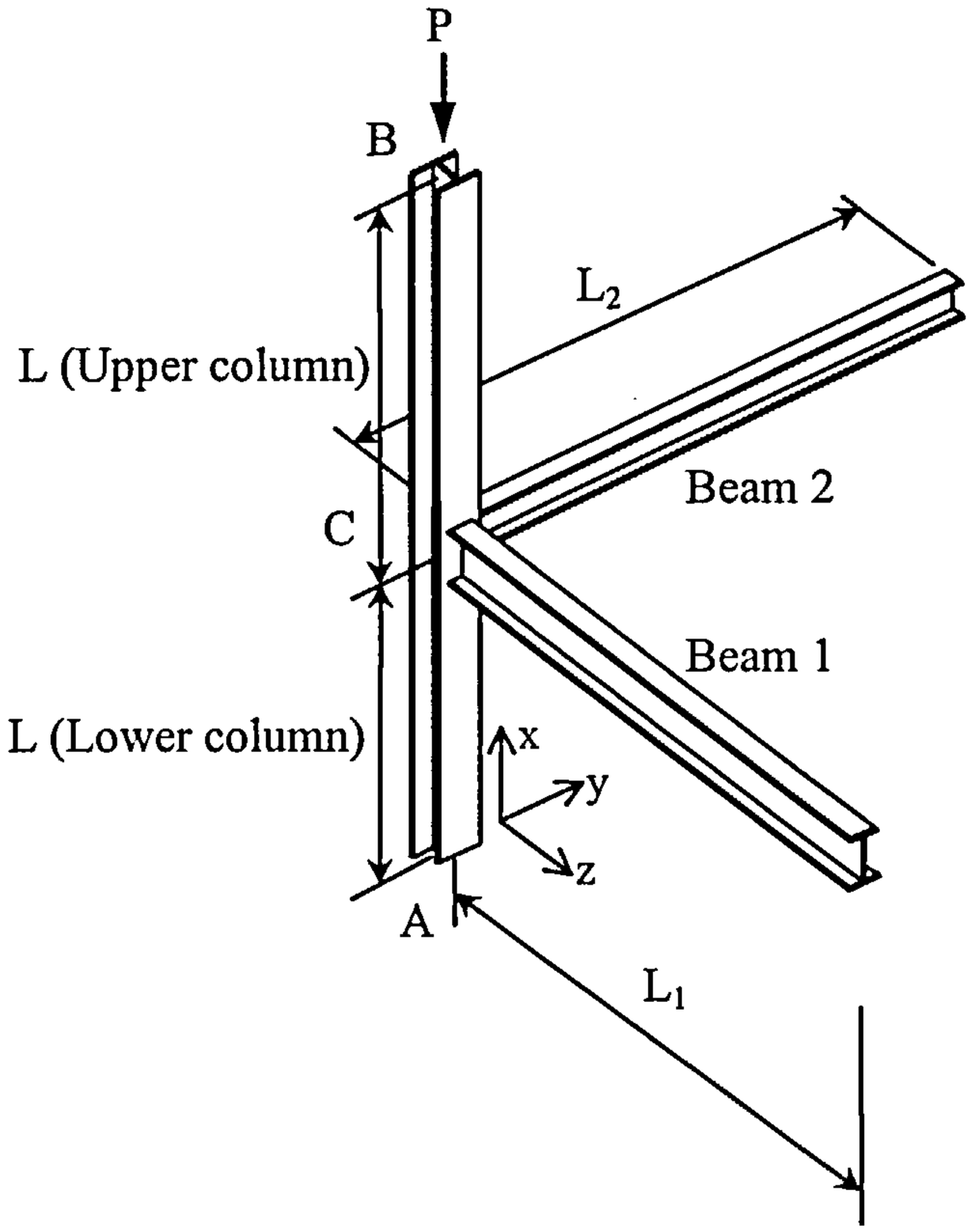

Fig. 5-1 Corner sub-frame used for calculation

Based on Fig. 5-1, several 2D models have been developed for hand analyses.

5.2 HAND CALCULATION USING CLASSICAL METHOD BASED ON TWO DIMENSION MODEL

5.2.1 CALCULATION MODEL 1 – THE EFFECT OF THERMAL EXPANSION AS A HORIZONTAL FORCE

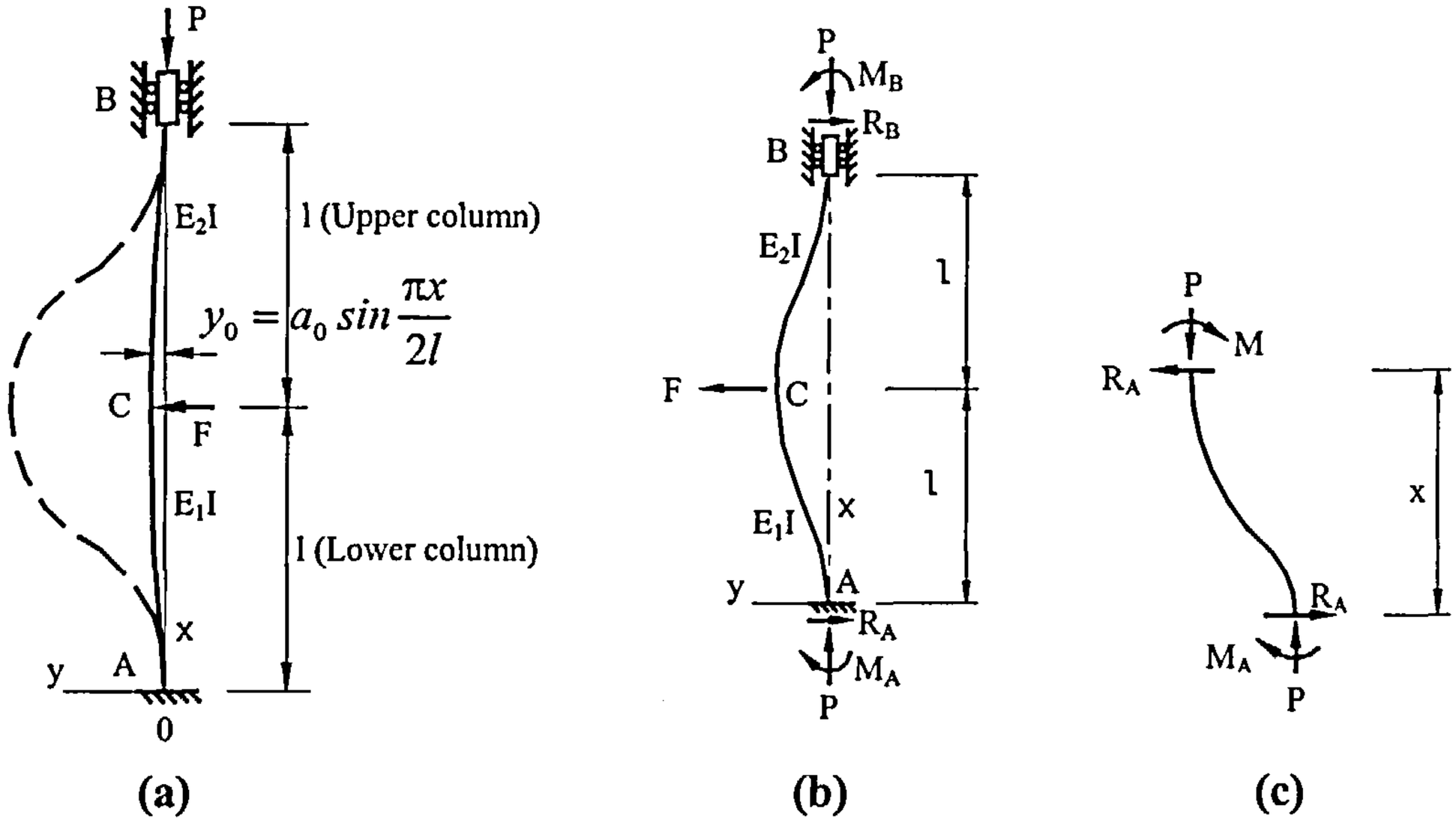

Fig. 5-2 Two-dimensional model 1 for calculation
(The effect of thermal expansion being represented as a horizontal force F)

For the basic investigation, a simplified model of a plane sub-frame was used. This assumes that the effect of thermal expansion is represented as a horizontal force (F) acting at floor level (point C) and is shown in Fig. 5-2. If we assume that initial out of straightness of the column is $y_0 = a_0 \sin\frac{\pi x}{2l}$, where a_0 is the amplitude, the equations for the deflected shape of the column can be obtained from Eqn. (5-3) by applying the appropriate boundary conditions. However, this equation is not always easy to solve as it is based on a fourth-order differential equation (Eqn. (5-2)). Therefore the second-order equation is expected to be used since its general solution is the simplest. From static equilibrium as shown in Fig 5-2(c), the differential equations for

the deflected shape of the column are

$$\left.\begin{aligned} E_1 I\frac{d^2 y_l}{dx^2} &= M_A - P(y_l + y_0) - R_A x && (0 \le x \le l) \\ E_2 I\frac{d^2 y_u}{dx^2} &= M_A - P(y_u + y_0) - R_A x + F(x-l) && (l \le x \le 2l) \end{aligned}\right\} \qquad (5\text{-}5a)$$

where y_l and y_u are the horizontal deflections for the lower and upper column respectively. Introducing the notation $\alpha_1^2 = \frac{P}{E_1 I}$ and $\alpha_2^2 = \frac{P}{E_2 I}$, Eqn. (5-5a) becomes

$$\left.\begin{aligned} \frac{d^2 y_l}{dx^2} + \alpha_1^2 y_l &= \frac{\alpha_1^2 M_A}{P} - \frac{\alpha_1^2 R_A}{P}x - \alpha_1^2 a_0 \sin\frac{\pi x}{2l} && (0 \le x \le l) \\ \frac{d^2 y_u}{dx^2} + \alpha_2^2 y_u &= \frac{\alpha_2^2 M_A}{P} - \frac{\alpha_2^2 R_A}{P}x + \frac{\alpha_2^2}{P}F(x-l) - \alpha_2^2 a_0 \sin\frac{\pi x}{2l} && (l \le x \le 2l) \end{aligned}\right\} \qquad (5\text{-}5b)$$

The general solutions of the equations are

$$\left.\begin{aligned} y_l &= A_1 \cos\alpha_1 x + B_1 \sin\alpha_1 x + \frac{M_A}{P} - \frac{R_A}{P}x + \frac{\alpha_1^2}{\frac{\pi^2}{4l^2} - \alpha_1^2} a_0 \sin\left(\frac{\pi x}{2l}\right) && (0 \le x \le l) \\ y_u &= A_2 \cos\alpha_2 x + B_2 \sin\alpha_2 x + \frac{M_A}{P} - \frac{R_A}{P}x + \frac{F}{P}(x-l) + \frac{\alpha_2^2}{\frac{\pi^2}{4l^2} - \alpha_2^2} a_0 \sin\left(\frac{\pi x}{2l}\right) && (l \le x \le 2l) \end{aligned}\right\} \qquad (5\text{-}6)$$

and we also have,

$$\left.\begin{aligned} y_l' &= -A_1\alpha_1 \sin\alpha_1 x + B_1\alpha_1 \cos\alpha_1 x - \frac{R_A}{P} + \frac{\alpha_1^2 \frac{\pi}{2l}}{\frac{\pi^2}{4l^2} - \alpha_1^2} a_0 \cos\left(\frac{\pi x}{2l}\right) && (0 \le x \le l) \\ y_u' &= -A_2\alpha_2 \sin\alpha_2 x + B_2\alpha_2 \cos\alpha_2 x - \frac{R_A}{P} + \frac{F}{P} + \frac{\alpha_2^2 \frac{\pi}{2l}}{\frac{\pi^2}{4l^2} - \alpha_2^2} a_0 \cos\left(\frac{\pi x}{2l}\right) && (l \le x \le 2l) \end{aligned}\right\} \qquad (5\text{-}7)$$

Letting $y_T = y + y_0$, the total deflection at distance x will be

$$\left.\begin{aligned} y_{lT} &= A_1 \cos\alpha_1 x + B_1 \sin\alpha_1 x + \frac{M_A}{P} - \frac{R_A}{P}x + \frac{\left(\frac{\pi}{2l}\right)^2}{\frac{\pi^2}{4l^2} - \alpha_1^2} a_0 \sin\left(\frac{\pi x}{2l}\right) \quad (0 \le x \le l) \\ y_{uT} &= A_2 \cos\alpha_2 x + B_2 \sin\alpha_2 x + \frac{M_A}{P} - \frac{R_A}{P}x + \frac{F}{P}(x-l) + \frac{\left(\frac{\pi}{2l}\right)^2}{\frac{\pi^2}{4l^2} - \alpha_2^2} a_0 \sin\left(\frac{\pi x}{2l}\right) \\ &\qquad (l \le x \le 2l) \end{aligned}\right\} \quad (5\text{-}8)$$

where A_1, A_2, B_1 and B_2 are arbitrary constants, which can be evaluated from the boundary conditions. Applying the boundary conditions $y_l = 0$, $y_l' = 0$ at $x = 0$, from Eqns. (5-6) and (5-7) gives

$$A_1 = -\frac{M_A}{P}$$

and

$$B_1 = \frac{R_A}{PK_1} - \frac{\alpha_1 \frac{\pi}{2l}}{(\frac{\pi}{2l})^2 - \alpha_1^2} a_0 .$$

The boundary conditions at the mid-point **C** of column are $y_{uT} = y_{lT}$ and $y_{uT}' = y_{lT}' = \theta_{TC}$, and at top-point **B** of column are $y_u = 0$, $y_u' = 0$. Thus the following equations can be obtained

$$\begin{cases} -\dfrac{M_A}{P}\cos\alpha_1 l+\left[\dfrac{R_A}{P\alpha_1}-\dfrac{\dfrac{\pi}{2l}\alpha_1}{(\dfrac{\pi}{2l})^2-\alpha_1^2}a_0\right]\sin\alpha_1 l+\dfrac{\left(\dfrac{\pi}{2l}\right)^2}{\left(\dfrac{\pi}{2l}\right)^2-\alpha_1^2}a_0 \\ =A_2\cos\alpha_2 l+B_2\sin\alpha_2 l+\dfrac{\left(\dfrac{\pi}{2l}\right)^2}{\left(\dfrac{\pi}{2l}\right)^2-\alpha_2^2}a_0 \end{cases} \quad (5\text{-}9a)$$

$$\begin{cases} \dfrac{M_A}{P}\alpha_1\cos\alpha_1 l+\left[\dfrac{R_A}{P\alpha_1}-\dfrac{\dfrac{\pi}{2l}\alpha_1}{\left(\dfrac{\pi}{2l}\right)^2-\alpha_1^2}a_0\right]\alpha_1\sin\alpha_1 l \\ =-A_2\alpha_2\sin\alpha_2 l+B_2\alpha_2\cos\alpha_2 l+\dfrac{F}{P} \end{cases} \quad (5\text{-}9b)$$

$$A_2\cos(2\alpha_2 l)+B_2\sin(2\alpha_2 l)+\frac{M_A}{P}-2\frac{R_A l}{P}+\frac{Fl}{P}=0 \quad (5\text{-}9c)$$

$$-A_2\alpha_2\sin(2\alpha_2 l)+B_2\alpha_2\cos(2\alpha_2 l)-\frac{R_A}{P}+\frac{F}{P}-\frac{\dfrac{\pi}{2l}\alpha_2^2}{\left(\dfrac{\pi}{2l}\right)^2-\alpha_2^2}a_0=0 \quad (5\text{-}9d)$$

Solving this series of equations gives,

$$A_2=A_{2s}+b_1a_0;\qquad B_2=B_{2s}+b_2a_0;\qquad R_A=R_{As}+b_3a_0;\qquad M_A=M_{As}+b_4a_0$$

where,

$$A_{2s}=\frac{(a_2a_5-a_4a_6)}{(a_2a_3-a_1a_4)}\frac{F}{P};\qquad B_{2s}=\frac{(a_1a_5-a_3a_6)}{(a_2a_3-a_1a_4)}\frac{F}{P};$$

$$R_{As}=[\frac{a_1a_5-a_3a_6}{a_2a_3-a_1a_4}\alpha_2\cos(2\alpha_2 l)-\frac{a_2a_5-a_4a_6}{a_2a_3-a_1a_4}\alpha_2\sin(2\alpha_2 l)+1]F;$$

$$M_{As}=\left\{[2l\alpha_2\cos(2\alpha_2 l)-\sin(2\alpha_2 l)]\frac{a_1a_5-a_3a_6}{a_2a_3-a_1a_4}-[2l\alpha_2\sin(2\alpha_2 l)+\cos(2\alpha_2 l)]\frac{a_2a_5-a_4a_6}{a_2a_3-a_1a_4}+l\right\}F;$$

$$b_1 = \frac{a_2 a_8 - a_4 a_7}{a_2 a_3 - a_1 a_4}; \qquad b_2 = \frac{a_1 a_8 - a_3 a_7}{a_2 a_3 - a_1 a_4};$$

$$b_3 = [\frac{a_1 a_8 - a_3 a_7}{a_2 a_3 - a_1 a_4}\cos(2\alpha_2 l) - \frac{a_2 a_8 - a_4 a_7}{a_2 a_3 - a_1 a_4}\sin(2\alpha_2 l) - \frac{\alpha_2 \frac{\pi}{2l}}{(\frac{\pi}{2l})^2 - \alpha_2^2}]\alpha_2 P;$$

$$b_4 = \left\{[2l\alpha_2 \cos(2\alpha_2 l) - \sin(2\alpha_2 l)]\frac{a_1 a_8 - a_3 a_7}{a_2 a_3 - a_1 a_4} - [2l\alpha_2 \sin(2\alpha_2 l) + \cos(2\alpha_2 l)]\frac{a_2 a_8 - a_4 a_7}{a_2 a_3 - a_1 a_4} - \frac{\pi\alpha_2^2}{(\frac{\pi}{2l})^2 - \alpha_2^2}\right\} P;$$

$$a_1 = \sqrt{\frac{E_1}{E_2}}\sin\alpha_1 l \sin(2\alpha_2 l) - 2\alpha_2 l \cos\alpha_1 l \sin(2\alpha_2 l) - \cos\alpha_1 l \cos(2\alpha_2 l) + \cos\alpha_2 l;$$

$$a_2 = \sqrt{\frac{E_1}{E_2}}\sin\alpha_1 l \cos(2\alpha_2 l) - 2\alpha_2 l \cos\alpha_1 l \cos(2\alpha_2 l) + \cos\alpha_1 l \sin(2\alpha_2 l) - \sin\alpha_2 l;$$

$$a_3 = \sqrt{\frac{E_2}{E_1}}[\sin\alpha_1 l \cos(2\alpha_2 l) + 2\alpha_2 l \sin\alpha_1 l \sin(2\alpha_2 l)] + \cos\alpha_1 l \sin(2\alpha_2 l) - \sin\alpha_2 l;$$

$$a_4 = \sqrt{\frac{E_2}{E_1}}[2\alpha_2 l \sin K_1 l \cos(2\alpha_2 l) - \sin\alpha_1 l \sin(2\alpha_2 l)] + \cos\alpha_1 l \cos(2\alpha_2 l) - \cos\alpha_2 l;$$

$$a_5 = \frac{1}{\alpha_2}(\cos\alpha_1 l + \alpha_1 l \sin\alpha_1 l - 1);$$

$$a_6 = \frac{1}{\alpha_1}\sin\alpha_1 l - l\cos\alpha_1 l;$$

$$a_7 = \frac{\pi\alpha_2^2 \cos\alpha_1 l}{(\frac{\pi}{2l})^2 - \alpha_2^2} - \frac{\frac{\pi}{2l}\alpha_1 \sin\alpha_1 l}{(\frac{\pi}{2l})^2 - \alpha_1^2} - \sqrt{\frac{E_1}{E_2}}(\frac{\pi}{2l})\frac{\alpha_2 \sin\alpha_1 l}{(\frac{\pi}{2l})^2 - \alpha_2^2} + \frac{(\frac{\pi}{2l})^2}{(\frac{\pi}{2l})^2 - \alpha_1^2} - \frac{(\frac{\pi}{2l})^2}{(\frac{\pi}{2l})^2 - \alpha_2^2};$$

$$a_8 = \frac{-\pi\alpha_1\alpha_2 \sin\alpha_1 l}{(\frac{\pi}{2l})^2 - \alpha_2^2} - \frac{\alpha_2 \cos\alpha_1 l}{(\frac{\pi}{2l})^2 - \alpha_2^2}(\frac{\pi}{2l}) - \sqrt{\frac{E_2}{E_1}}(\frac{\pi}{2l})\frac{\alpha_1 \cos\alpha_1 l}{(\frac{\pi}{2l})^2 - \alpha_1^2}$$

Therefore, the deflections of the column will be

$$y_{lT} = \frac{F}{P}\left\{\left[\alpha_2 \cos(2\alpha_2 l)\frac{a_1a_5 - a_3a_6}{a_2a_3 - a_1a_4} - \alpha_2 \sin(2\alpha_2 l)\frac{a_2a_5 - a_4a_6}{a_2a_3 - a_1a_4} + 1\right]\left(\frac{\sin\alpha_1 x}{\alpha_1} - x\right) - \right.$$
$$\left[(2l\alpha_2 \cos(2\alpha_2 l) - \sin(2\alpha_2 l))\frac{a_1a_5 - a_3a_6}{a_2a_3 - a_1a_4} - (2l\alpha_2 \sin(2\alpha_2 l) + \cos(2\alpha_2 l))\frac{a_2a_5 - a_4a_6}{a_2a_3 - a_1a_4}\right.$$
$$\left.\left. + l\right](\cos\alpha_1 x + 1)\right\} + C_1 a_0 \qquad (0 \le x \le l)$$

$$y_{uT} = \frac{F}{P}\left\{[\sin\alpha_2 x - \alpha_2 x\cos(2\alpha_2 l) + 2l\alpha_2 \cos(2\alpha_2 l) - \sin(2\alpha_2 l)]\frac{a_1a_5 - a_3a_6}{a_2a_3 - a_1a_4} + [\cos\alpha_2 x + \right.$$
$$\left.\alpha_2 x \sin(2\alpha_2 l) - 2l\alpha_2 \sin(2\alpha_2 l) - \cos(2\alpha_2 l)]\frac{a_2a_5 - a_4a_6}{a_2a_3 - a_1a_4}\right\} + C_2 a_0 \quad (l \le x \le 2l)$$

(5-10a)

or more concisely:

$$y_{lT} = -\frac{M_{As}}{P}\cos\alpha_1 x + \frac{R_{AS}}{P\alpha_1}\sin\alpha_1 x - \frac{R_{AS}}{P}x + \frac{M_{As}}{P} + C_1 a_0 \qquad (0 \le x \le l))$$

$$y_{uT} = A_{2s}\cos\alpha_2 x + B_{2s}\sin\alpha_2 x - \frac{R_{As}}{P}x + \frac{F}{P}(x - l) + \frac{M_{As}}{P} + C_2 a_0 \quad (l \le x \le 2l)$$

(5-10b)

The last term on the right-hand side of the equations represents the effect of the column imperfection, and its magnitude is

$$C_1 = \alpha_2\left[\cos(2\alpha_2 l)\frac{a_1a_8 - a_3a_7}{a_2a_3 - a_1a_4} - \sin(2\alpha_2 l)\frac{a_2a_8 - a_4a_7}{a_2a_3 - a_1a_4} - \frac{\alpha_2\left(\frac{\pi}{2l}\right)}{\left(\frac{\pi}{2l}\right)^2 - \alpha_2^2}\right]\left(\frac{\sin\alpha_1 x}{\alpha_1} - x\right) +$$

$$\left\{[2l\alpha_2 \cos(2\alpha_2 l) - \sin(2\alpha_2 l)]\frac{a_1a_8 - a_3a_7}{a_2a_3 - a_1a_4} - [2l\alpha_2 \sin(2\alpha_2 l) + \cos(2\alpha_2 l)]\frac{a_2a_8 - a_4a_7}{a_2a_3 - a_1a_4}\right.$$
$$\left. - \frac{\pi\alpha_2^2}{(\frac{\pi}{2l})^2 - \alpha_2^2}\right\}(1 - \cos\alpha_1 x) - \frac{\frac{\pi}{2l}}{\left(\frac{\pi}{2l}\right)^2 - \alpha_1^2}\left(\frac{\pi}{2l}\sin\frac{\pi x}{2l} - \alpha_1 \sin\alpha_1 x\right)$$

$$C_2 = \frac{a_1 a_8 - a_3 a_7}{a_2 a_3 - a_1 a_4}\left[\sin\alpha_2 x - \alpha_2 x\cos(2\alpha_2 l) + 2l\alpha_2\cos(2\alpha_2 l) - \sin(2\alpha_2 l)\right]$$
$$+ \frac{a_2 a_8 - a_4 a_7}{a_2 a_3 - a_1 a_4}\left[\cos\alpha_2 x + \alpha_2 x\sin(2\alpha_2 l) - 2l\alpha_2\sin(2\alpha_2 l) - \cos(2\alpha_2 l)\right]$$
$$+ \frac{\pi}{\left(\frac{\pi}{2l}\right)^2 - \alpha_2^2}\left(\frac{\pi}{(2l)^2}\sin\frac{\pi x}{2l} + \alpha_2^2\frac{x}{2l} - \alpha_2^2\right)$$

The bending moment at an arbitrary point along the column can also be determined by

$$M = -EIy''$$

5.2.2 CALCULATION MODEL 2 – A MORE COMPLICATED MODEL

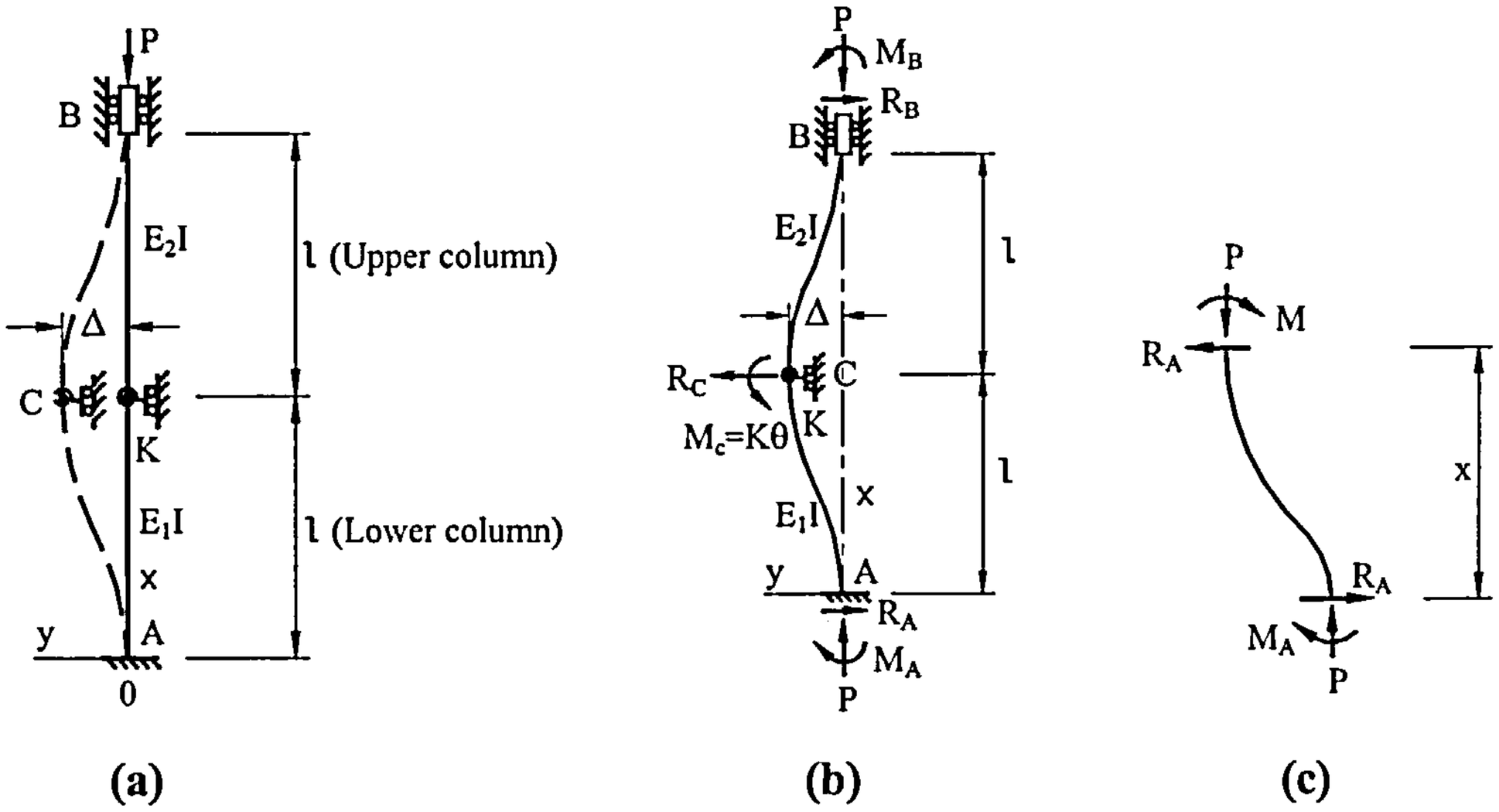

Fig. 5-3 Two-dimensional model 2 for calculation
(The effect of thermal expansion being represented as a thermal elongation Δ)

If we assume that the effect of the pushing-out of the unprotected beam is represented as a thermal elongation Δ and the semi-rigid connection between the column and beam as a spring of rotational stiffness **K** at floor level (point **C**), a 2D model, as shown in Fig. 5-3, can be established. Moment equilibrium gives

$$\left.\begin{aligned} -E_1 I\frac{d^2 y_l}{dx^2} &= Py_l + R_A x - M_A && \text{for lower column} \\ -E_2 I\frac{d^2 y_u}{dx^2} &= Py_u + R_A x - M_A - R_C(x-l) + M_C && \text{for upper column} \end{aligned}\right\} \quad (5\text{-}11a)$$

Introducing the notation $\alpha_1^2 = \frac{P}{E_1 I}$ and $\alpha_2^2 = \frac{P}{E_2 I}$, Eqn. (5-11a) becomes

$$\left.\begin{aligned} &\frac{d^2 y_l}{dx^2} + \alpha_1^2 y_l = \frac{\alpha_1^2 M_A}{P} - \frac{\alpha_1^2 R_A}{P} x && (0 \le x \le l) \\ &\frac{d^2 y_u}{dx^2} + \alpha_2^2 y_u = \frac{\alpha_2^2 M_A}{P} - \frac{\alpha_2^2 R_A}{P} x + \frac{\alpha_2^2 R_C}{P}(x-l) - \frac{\alpha_2^2 M_C}{P} && (l \le x \le 2l) \end{aligned}\right\} \quad (5\text{-}11b)$$

The general solutions for deflection (y) are

$$\left.\begin{aligned} &y_l = A_1 \cos\alpha_1 x + B_1 \sin\alpha_1 x + \frac{M_A}{P} - \frac{R_A}{P} x && (0 \le x \le l) \\ &y_u = A_2 \cos\alpha_2 x + B_2 \sin\alpha_2 x + \frac{M_A}{P} - \frac{R_A}{P} x + \frac{R_C}{P}(x-l) - \frac{M_C}{P} && (l \le x \le 2l) \end{aligned}\right\} \quad (5\text{-}12)$$

We also have,

$$\left.\begin{aligned} &y_l' = -A_1\alpha_1 \sin\alpha_1 x + B_1\alpha_1 \cos\alpha_1 x - \frac{R_A}{P} && (0 \le x \le l) \\ &y_u' = -A_2\alpha_2 \sin\alpha_2 x + B_2\alpha_2 \cos\alpha_2 x - \frac{R_A}{P} + \frac{R_C}{P} && (l \le x \le 2l) \end{aligned}\right\} \quad (5\text{-}13)$$

At the bottom of the column ($x = 0$) the boundary conditions require $y_l = 0$ and $y_l' = 0$. Substituting into Eqns. (5-12) and (5-13) produces

$$A_1 = -\frac{M_A}{P}$$

and

$$B_1 = \frac{R_A}{\alpha_1 P}.$$

The boundary conditions at mid-column ($x = l$) and top of the column ($x = 2l$) are $y_l = y_u = \Delta$, $y_l' = y_u' = \theta$ and $y_u = 0$, $y_u' = 0$ respectively, and noting that $M_c = K\theta$, a series of equations can be obtained as

$$\begin{cases}
\Delta = -\frac{M_A}{P}\cos\alpha_1 l + \frac{R_A}{\alpha_1 p}\sin\alpha_1 l + \frac{M_A}{P} - \frac{R_A}{P} l & \text{(5-14a)} \\
\Delta = A_2\cos\alpha_2 l + B_2\sin\alpha_2 l + \frac{M_A}{P} - \frac{R_A}{P} l - \frac{K\theta}{P} & \text{(5-14b)} \\
\theta = \frac{M_A}{P}\alpha_1\sin\alpha_1 l + \frac{R_A}{P}\cos\alpha_1 l - \frac{R_A}{P} & \text{(5-14c)} \\
\theta = -A_2\alpha_2 \sin\alpha_2 l + B_2\alpha_2 \cos\alpha_2 l - \frac{R_A}{P} + \frac{R_C}{P} & \text{(5-14d)} \\
0 = A_2\cos(2\alpha_2 l) + B_2\sin(2\alpha_2 l) + \frac{M_A}{P} + \frac{R_C}{P} l - \frac{2R_A}{P} l - \frac{K\theta}{P} & \text{(5-14e)} \\
0 = -A_2\alpha_2 \sin(2\alpha_2 l) + B_2\alpha_2 \cos(2\alpha_2 l) - \frac{R_A}{P} + \frac{R_C}{P} & \text{(5-14f)} \\
M_A - 2R_A l + R_C l - K\theta - M_B = 0 & \text{(5-14g)} \\
R_C = R_A + R_B & \text{(5-14i)}
\end{cases}$$

Solving these equations gives

$$A_2 = \frac{a_4a_7a_9 - a_4a_5a_{10} - a_6a_9 + a_5a_8}{a_3a_6a_9 - a_3a_5a_8}\Delta;$$

$$B_2 = \frac{a_7a_9 - a_5a_{10}}{a_6a_9 - a_5a_8}\Delta; \qquad R_A = \frac{a_6a_{10} - a_7a_8}{a_6a_9 - a_5a_8}\Delta;$$

$$M_A = (a_2 + a_1\frac{a_6a_{10} - a_7a_8}{a_6a_9 - a_5a_8})\Delta;$$

$$R_C = \frac{\Delta}{a_6a_9 - a_5a_8}\left[\frac{\alpha_2}{a_3}(a_4a_7a_9 - a_4a_5a_{10} - a_6a_9 + a_5a_8)\sin(2\alpha_2 l)P - (a_7a_9 - a_5a_{10})\alpha_2\cos(2\alpha_2 l)P + a_6a_{10} - a_7a_8\right];$$

$$\theta = \frac{\Delta}{P}\left[\left(a_2 + a_1\frac{a_6a_{10} - a_7a_8}{a_6a_9 - a_5a_8}\right)\alpha_1\sin\alpha_1 l + \frac{a_6a_{10} - a_7a_8}{a_6a_9 - a_5a_8}(\cos\alpha_1 l - 1)\right];$$

$$M_B = M_A - 2R_A l + R_C l - K\theta;$$

$$R_B = R_C - R_A$$

where,

$$a_1 = \frac{l - \dfrac{\sin \alpha_1 l}{\alpha_1}}{1 - \cos \alpha_1 l}; \qquad a_2 = \frac{P}{1 - \cos \alpha_1 l}$$

$$a_3 = \alpha_2 l \sin(2\alpha_2 l) + \cos(2\alpha_2 l) - \cos \alpha_2 l;$$

$$a_4 = \alpha_2 l \cos(2\alpha_2 l) + \sin \alpha_2 l - \sin(2\alpha_2 l);$$

$$a_5 = \frac{a_1}{P} + \frac{K}{P^2} - \frac{K\alpha_1 \sin \alpha_1 l}{P^2} a_1 - \frac{l}{P} - \frac{K \cos \alpha_1 l}{P^2};$$

$$a_6 = \frac{a_4}{a_3} \cos \alpha_2 l + \sin \alpha_2 l;$$

$$a_7 = 1 + \frac{\cos \alpha_2 l}{a_3} + \frac{K\alpha_1 a_2 \sin \alpha_1 l}{P^2} - \frac{a_2}{P};$$

$$a_8 = \alpha_2 \left\{ \frac{a_4}{a_3} [\sin \alpha_2 l - \sin(2\alpha_2 l)] + \cos(2\alpha_2 l) - \cos \alpha_2 l \right\};$$

$$a_9 = \frac{a_1 \alpha_1 \sin \alpha_1 l}{P} + \frac{\cos \alpha_1 l}{P} - \frac{1}{P};$$

$$a_{10} = \frac{\alpha_2}{a_3} \sin \alpha_2 l - \frac{\alpha_2}{a_3} \sin(2\alpha_2 l) - \frac{a_2 \alpha_1}{P} \sin \alpha_1 l$$

Finally, the deflected shape can be obtained by substituting these coefficients into equation (5-12) giving the expressions

$$\left.\begin{aligned} y_l &= -\frac{M_A}{P} \cos \alpha_1 x + \frac{R_A}{\alpha_1 P} \sin \alpha_1 x - \frac{R_A}{P} x + \frac{M_A}{P} && (0 \le x \le l) \\ y_u &= A_2 \cos \alpha_2 x + B_2 \sin \alpha_2 x + \frac{R_C}{P}(x - l) - \frac{R_A}{P} x + \frac{M_A}{P} - \frac{K\theta}{P} && (l \le x \le 2l) \end{aligned}\right\} \quad (5\text{-}15)$$

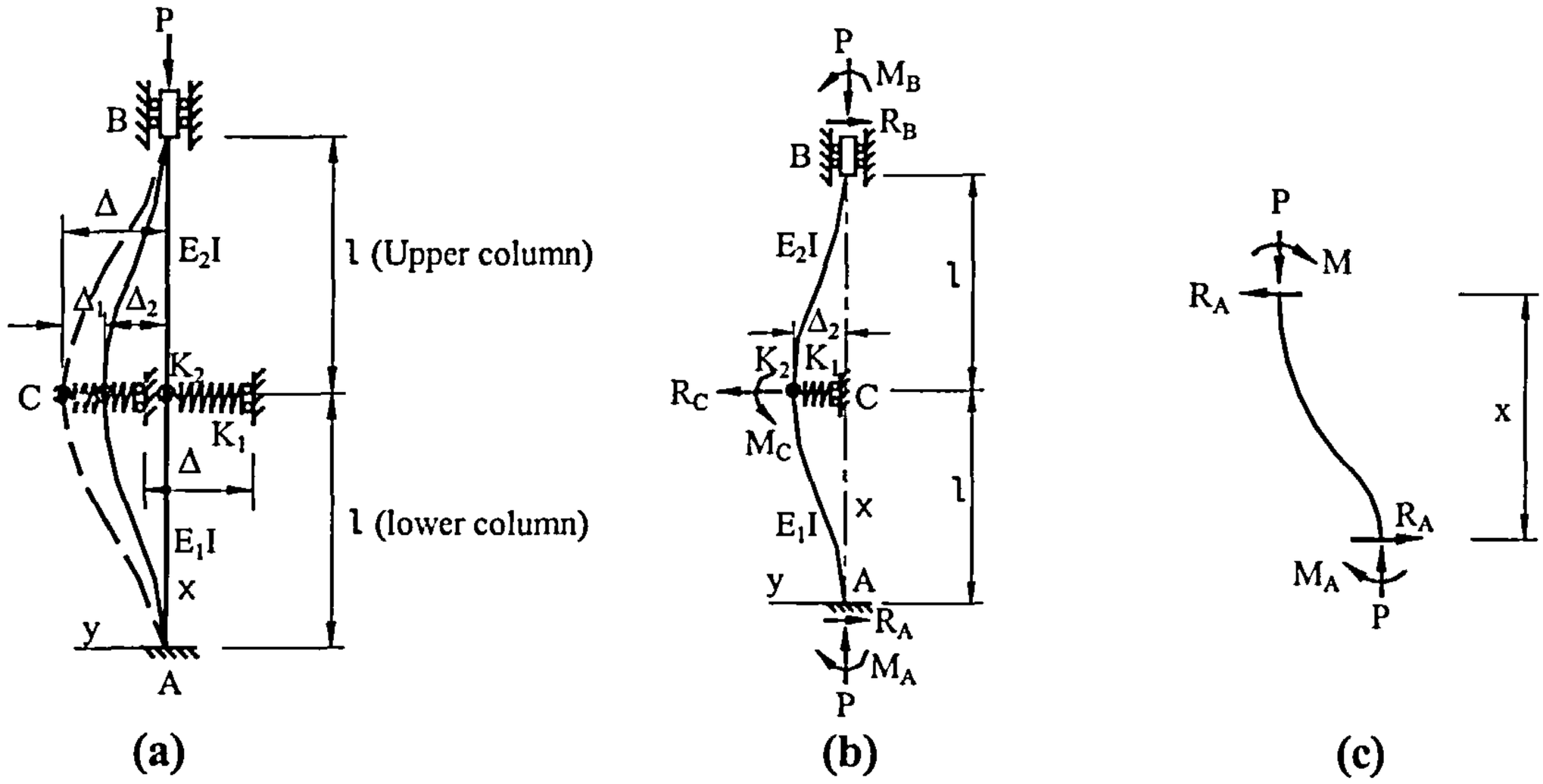

(a) (b) (c)

Fig. 5-4 Two-dimensional model 3 for calculation (A more generalised case)

The above analytical model (as illustrated in Fig. 5-3) has been extended into a more generalised case in which the axial stiffness of beam is taken into account. In this generalised model (Fig. 5-4), K_1 represents the horizontal stiffness of beam and K_2 is the rotational stiffness of connection between the beam and column at floor level (point C). Both K_1 and K_2 are assumed to remain constant. The thermal elongation due to beam expansion is Δ. By considering the effect of beam softening, which is simulated by the axial stiffness K_1, the actual deflection of the column at the floor level point **C** becomes Δ_2. The reaction R_c at this point **C** should be $K_1\Delta_1$, giving $\Delta_1 = \frac{R_c}{K_1}$. Hence, from Fig. 5-4(a), we have $\Delta_2 = \Delta - \Delta_1 = \Delta - \frac{R_c}{K_1}$. If we assume that the rotation of the column at point **C** is θ, the restraint to the column provided by the rotational spring K_2 will be $M_c = K_2\theta$. From the free-body diagram of the column (Fig. 5-4(c)) the basic governing differential equations are the same as those presented above, giving

$$\left.\begin{aligned} -E_1 I\frac{d^2 y_l}{dx^2} &= Py_l + R_A x - M_A && \text{for the lower column } (0 \le x \le l) \\ -E_2 I\frac{d^2 y_u}{dx^2} &= Py_u + R_A x - M_A - R_C(x-l) + M_C && \text{for the upper column } (l \le x \le 2l) \end{aligned}\right\} \quad (5\text{-}16a)$$

Using the notation $\alpha_1^2 = \frac{P}{E_1 I}$ and $\alpha_2^2 = \frac{P}{E_2 I}$, Eqn. (5-16a) can be rewritten in the form

$$\left.\begin{aligned} \frac{d^2 y_l}{dx^2} + \alpha_1^2 y_l &= \frac{\alpha_1^2 M_A}{P} - \frac{\alpha_1^2 R_A}{P} x && (0 \le x \le l) \\ \frac{d^2 y_u}{dx^2} + \alpha_2^2 y_u &= \frac{\alpha_2^2 M_A}{P} - \frac{\alpha_2^2 R_A}{P} x + \frac{\alpha_2^2 R_C}{P}(x-l) - \frac{\alpha_2^2 M_C}{P} && (l \le x \le 2l) \end{aligned}\right\} \quad (5\text{-}16b)$$

The general solutions for deflections (y) are

$$\left.\begin{aligned} y_l &= A_1 \cos\alpha_1 x + B_1 \sin\alpha_1 x + \frac{M_A}{P} - \frac{R_A}{P} x && (0 \le x \le l) \\ y_u &= A_2 \cos\alpha_2 x + B_2 \sin\alpha_2 x + \frac{M_A}{P} - \frac{R_A}{P} x + \frac{R_C}{P}(x-l) - \frac{M_c}{P} && (l \le x \le 2l) \end{aligned}\right\} \quad (5\text{-}17)$$

and,

$$\left.\begin{aligned} y_l' &= -A_1\alpha_1 \sin\alpha_1 x + B_1\alpha_1 \cos\alpha_1 x - \frac{R_A}{P} && (0 \le x \le l) \\ y_u' &= -A_2\alpha_2 \sin\alpha_2 x + B_2\alpha_2 \cos\alpha_2 x - \frac{R_A}{P} + \frac{R_C}{P} && (l \le x \le 2l) \end{aligned}\right\} \quad (5\text{-}18)$$

At $x = 0$ the boundary conditions are $y_l = 0$ and $y_l' = 0$, hence there are

$$A_1 = -\frac{M_A}{P} \quad \text{and} \quad B_1 = \frac{R_A}{\alpha_1 P}.$$

The boundary conditions at the mid-column $(x = l)$ are $y_l = y_u = \Delta_2$ and $y_l' = y_u' = \theta$, and at the top of column $(x = 2l)$ are $y_u = 0$ and $y_u' = 0$, respectively. The following equations can then be obtained according to these conditions as

$$\begin{cases}
\Delta_2 = \Delta - \dfrac{R_C}{K_1} = -\dfrac{M_A}{P}cos\,\alpha_1 l + \dfrac{R_A}{\alpha_1 p}sin\,\alpha_1 l + \dfrac{M_A}{P} - \dfrac{R_A}{P}l & \text{(5-19a)} \\
\Delta_2 = \Delta - \dfrac{R_C}{K_1} = A_2\,cos\,\alpha_2 l + B_2\,sin\,\alpha_2 l + \dfrac{M_A}{P} - \dfrac{R_A}{P}l - \dfrac{K_2\theta}{P} & \text{(5-19b)} \\
\theta = \dfrac{M_A}{P}\alpha_1 \sin\alpha_1 l + \dfrac{R_A}{P}\cos\alpha_1 l - \dfrac{R_A}{P} & \text{(5-19c)} \\
\theta = -A_2\alpha_2\,sin\,\alpha_2 l + B_2\alpha_2\,cos\,\alpha_2 l - \dfrac{R_A}{P} + \dfrac{R_C}{P} & \text{(5-19d)} \\
0 = A_2\,cos(2\alpha_2 l) + B_2\,sin(2\alpha_2 l) + \dfrac{M_A}{P} + \dfrac{R_C}{P}l - \dfrac{2R_A}{P}l - \dfrac{K_2\theta}{P} & \text{(5-19e)} \\
0 = -A_2\alpha_2\,sin(2\alpha_2 l) + B_2\alpha_2\,cos(2\alpha_2 l) - \dfrac{R_A}{P} + \dfrac{R_C}{P} & \text{(5-19f)}
\end{cases}$$

Solving these equations gives

$$M_A = \frac{a_1c_1c_7 - K_1a_3}{a_2a_3 - a_1a_4}\Delta$$

$$R_A = \frac{a_2c_1c_7 - K_1a_4}{a_2a_3 - a_1a_4}\Delta$$

$$R_c = \frac{a_1c_1c_3c_7 + a_2c_1c_2c_7 - K_1a_3c_3 - K_1a_4c_2}{c_1(a_2a_3 - a_1a_4)}\Delta$$

$$\theta = \left[\frac{a_1c_1c_7 - K_1a_3}{a_2a_3 - a_1a_4}\alpha_1\,sin\,\alpha_1 l + \frac{a_2c_1c_7 - K_1a_4}{a_2a_3 - a_1a_4}(cos\,\alpha_1 l - 1)\right]\frac{\Delta}{P}$$

$$B_2 = \frac{1}{b_2}\left\{\frac{[sin\,\alpha_2 l - cos\,\alpha_1 l\,sin(2\alpha_2 l)](a_2c_1c_7 - K_1a_4) - \alpha_1\,sin\,\alpha_1 l\,sin(2\alpha_2 l)(a_1c_1c_7 - K_1a_3)}{\alpha_2 P(a_2a_3 - a_1a_4)}\right.$$
$$\left. + \frac{[sin(2\alpha_2 l) - sin\,\alpha_2 l]\left(a_1c_3c_7 + a_2c_2c_7 - K_1a_3\dfrac{c_3}{c_1} - K_1a_4\dfrac{c_2}{c_1}\right)}{\alpha_2 P(a_2a_3 - a_1a_4)}\right\}\Delta$$

$$A_2 = \frac{1}{\alpha_2 P \sin(2\alpha_2 l)(a_2 a_3 - a_1 a_4)}\left\{\frac{\cos(2\alpha_2 l)}{b_2}\left[(\sin\alpha_2 l - \cos\alpha_1 l \sin(2\alpha_2 l))(a_2 c_1 c_7 - K_1 a_4)\right.\right.$$
$$-\alpha_1 \sin\alpha_1 l \sin(2\alpha_2 l)(a_1 c_1 c_7 - K_1 a_3) + (\sin(2\alpha_2 l) - \sin\alpha_2 l)(a_1 c_3 c_7 + a_2 c_2 c_7$$
$$\left.\left. - K_1 a_3 \frac{c_3}{c_1} - K_1 a_4 \frac{c_2}{c_1}\right)\right] + a_1 c_3 c_7 + a_2 c_2 c_7 - K_1 a_3 \frac{c_3}{c_1} - K_1 a_4 \frac{c_3}{c_1} - a_2 c_1 c_7 + a_4 K_1 \Bigg\}\Delta$$

where,

$$a_1 = \frac{c_2}{c_1} + \frac{K_1}{\alpha_1 P}\sin\alpha_1 l - \frac{K_1 l}{P}$$

$$a_2 = \frac{K_1}{P}(\cos\alpha_1 l - 1) - \frac{C_3}{C_1}$$

$$a_3 = c_4 c_2 - c_1 c_6$$

$$a_4 = c_1 c_5 - c_3 c_4$$

$$c_1 = b_1[\sin(2\alpha_2 l) - \sin\alpha_2 l] + b_2[\cos(2\alpha_2 l) + \alpha_2 l \sin\alpha_2 l]$$

$$c_2 = b_1[\cos\alpha_1 l \sin(2\alpha_2 l) - \sin\alpha_2 l] + b_2\left[\cos\alpha_1 l \cos(2\alpha_2 l) + 2\alpha_2 l \sin\alpha_2 l + \frac{K_2\alpha_2}{P}\sin\alpha_2 l(\cos\alpha_1 l - 1)\right]$$

$$c_3 = b_1\alpha_1 \sin\alpha_1 l \sin(2\alpha_2 l) + b_2\left[\alpha_1 \sin\alpha_1 l \cos(2\alpha_2 l) + \alpha_1\alpha_2 \frac{K_2}{P}\sin\alpha_1 l \sin\alpha_2 l - \alpha_2 \sin\alpha_2 l\right]$$

$$c_4 = b_3 K_1[\sin(2\alpha_2 l) - \sin\alpha_2 l] - b_2 K_1[\cos(2\alpha_2 l) - \cos\alpha_2 l] - b_2\alpha_2 \sin(2\alpha_2 l)(K_1 l - P)$$

$$c_5 = b_3\alpha_1 K_1 \sin\alpha_1 l \sin 2\alpha_2 l$$

$$c_6 = b_3 K_1[\cos\alpha_1 l \sin(2\alpha_2 l) - \sin\alpha_2 l] + b_2 K_1[\cos\alpha_2 l - \cos(2\alpha_2 l)] - b_2 K_1\alpha_2 l \sin(2\alpha_2 l)$$

$$c_7 = b_2 K_1\alpha_2 P \sin(2\alpha_2 l)$$

$$b_1 = \cos\alpha_2 l \cos(2\alpha_2 l) + \sin\alpha_2 l \sin(2\alpha_2 l)$$

$$b_2 = \sin\alpha_2 l \cos(2\alpha_2 l) - \cos\alpha_2 l \sin(2\alpha_2 l)$$

$$b_3 = \sin(2\alpha_2 l)(\sin\alpha_2 l - \sin(2\alpha_2 l)) + \cos(2\alpha_2 l)[\cos\alpha_2 l - \cos(2\alpha_2 l)]$$

Therefore, the deflection of the column can be written

$$\left.\begin{aligned} y_l &= -\frac{M_A}{P}\cos\alpha_1 x + \frac{R_A}{\alpha_1 P}\sin\alpha_1 x - \frac{R_A}{P}x + \frac{M_A}{P} && (0 \le x \le l) \\ y_u &= A_2\cos\alpha_2 x + B_2\sin\alpha_2 x + \frac{R_c}{P}(x-l) - \frac{R_A}{P}x + \frac{M_A}{P} - \frac{K_2\theta}{P} && (l \le x \le 2l) \end{aligned}\right\} \quad (5\text{-}20)$$

The bending moment in the lower column will be

$$M = -EIy'' = -EI\left(\frac{M_A}{P}\alpha_1^2\cos\alpha_1 x - \frac{R_A}{P}\alpha_1\sin\alpha_1 x\right)$$

The extreme bending moment (maximum or minimum) in the lower column may occur at the position of $\frac{dM}{dx} = 0$, which gives:

$$x = \frac{1}{\alpha_1}arctg\left(-\frac{R_A}{M_A\alpha_1}\right)$$

5.2.3 CALCULATION MODEL 3 – THE SIMPLEST MODEL OF A CORNER COLUMN SUB-FRAME

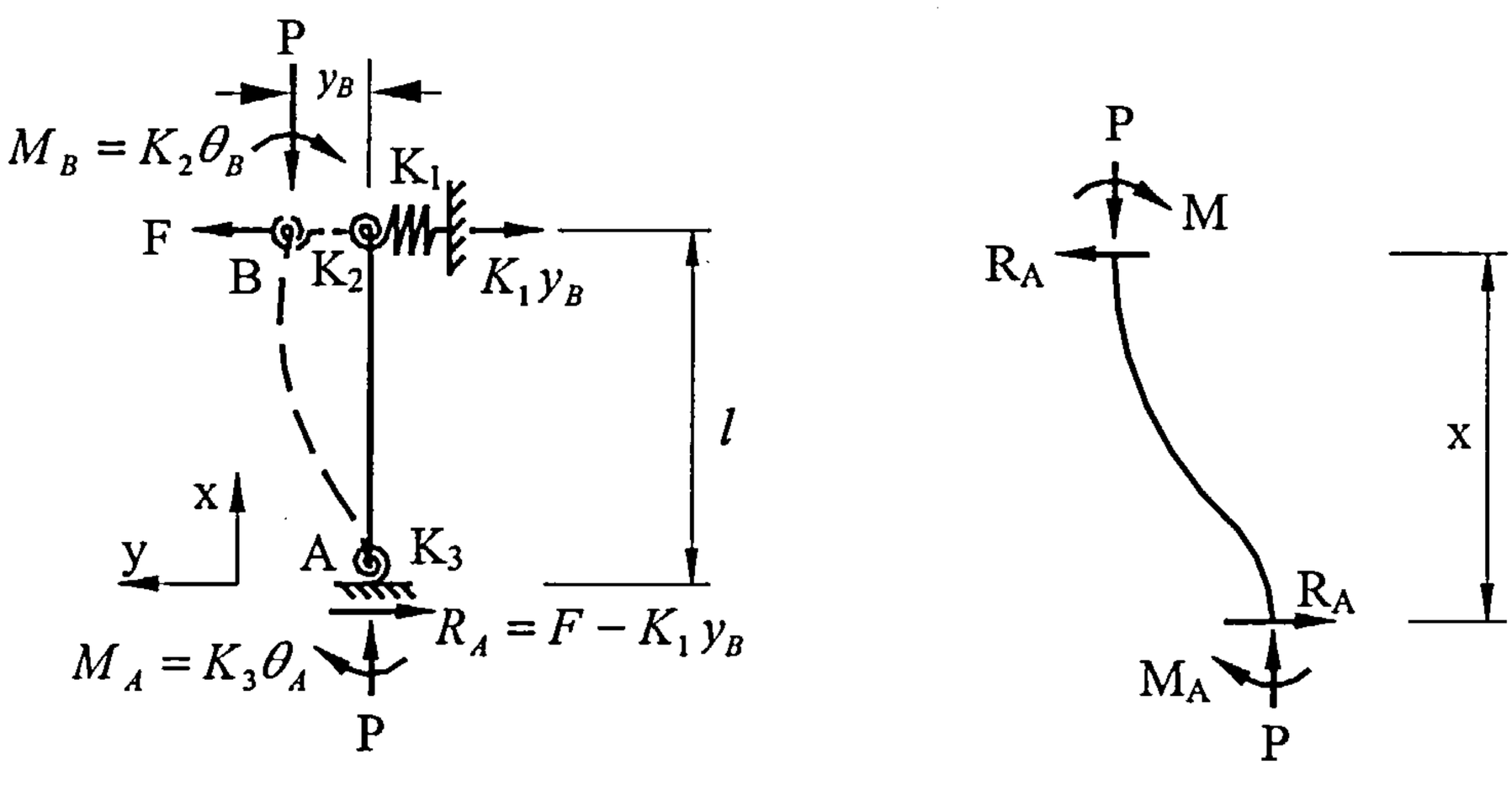

(a) 2D model for analysis **(b) Free body diagram**

Fig. 5-5 2D model for column subjected to thermal force F

The above two-storey column models may be further simplified to include only the lower-storey column with appropriate boundary conditions (Fig. 5-5). In this model,

the column is partially restrained against rotation at each end and against horizontal translation at the top of the column by considering the effect of adjacent members as a series of appropriate stiffnesses $\mathbf{K_1}$, $\mathbf{K_2}$ and $\mathbf{K_3}$. $\mathbf{K_1}$ and $\mathbf{K_2}$ at the top of the lower column represent the restraint stiffnesses from the upper column. In this analysis these stiffnesses ($\mathbf{K_1}$, $\mathbf{K_2}$, $\mathbf{K_3}$) are assumed to be constant although in practice they are temperature-dependent. For the first case, we consider the thermal expansion force **F** as a known parameter. From Fig. 5-5(b) the bending moment at a distance **x** from the bottom is

$$M = -EI\frac{d^2y}{dx^2} = R_A x + Py - M_A \qquad (5\text{-}21a)$$

Let $\alpha^2 = \frac{P}{EI}$ and $EI = \frac{P}{\alpha^2}$, then the differential equation becomes

$$\frac{d^2y}{dx^2} + \alpha^2 y = -\frac{R_A\alpha^2}{P}x + \frac{M_A\alpha^2}{P} \qquad (5\text{-}22b)$$

It is evident from Fig. 5-5(a) that $M_A = K_3\theta_A = K_3 y_A' = (F - K_1 y_B)l + Py_B - M_B$ and $R_A = F - K_1 y_B$. Hence Eqn. (5-22b) can be rewritten as

$$\frac{d^2y}{dx^2} + \alpha^2 y = -\frac{(F - K_1 y_B)\alpha^2}{P}x + \frac{K_3\theta_A\alpha^2}{P} \qquad (5\text{-}22c)$$

The solution of homogeneous equation is

$$y_h = A\cos\alpha x + B\sin\alpha x$$

where **A** and **B** are arbitrary constants to be evaluated from the boundary conditions, and the particular solution is

$$y_p = \frac{K_1 y_B - F}{P}x + \frac{K_3\theta_A}{P}$$

Therefore the general solution of Eqn. (5-22c) can be obtained by combining the two solutions

$$y = A\cos\alpha x + B\sin\alpha x + \frac{K_1 y_B - F}{P}x + \frac{K_3\theta_A}{P} \tag{5-23}$$

and also

$$y' = -A\alpha\sin\alpha x + B\alpha\cos\alpha x + \frac{K_1 y_B - F}{P} \tag{5-24}$$

The boundary conditions are $y = 0,\ y' = \theta_A$ at $\mathbf{x} = 0$, from which

$$A = -\frac{K_3\theta_A}{P} \quad \text{and} \quad B = \frac{1}{\alpha}(\theta_A + \frac{F - K_1 y_B}{P}).$$

and at the top of column ($x = l$) $y = y_B$ and $y' = y_B' = \theta_B$. Therefore a set of equations can be established based on these conditions as

$$\begin{cases} \theta_B = \dfrac{K_3}{P}\theta_A\alpha\sin\alpha l + \left(\theta_A + \dfrac{F - K_1 y_B}{P}\right)\cos\alpha l + \dfrac{K_1 y_B - F}{P} & \text{(5-25a)} \\ y_B = -\dfrac{K_3}{P}\theta_A\cos\alpha l + \dfrac{1}{\alpha}\left(\theta_A + \dfrac{F - K_1 y_B}{p}\right)\sin\alpha l + \dfrac{K_3}{P}\theta_A + \dfrac{K_1 l}{P}y_B - \dfrac{F}{P}l & \text{(5-25b)} \\ K_3\theta_A = (F - K_1 y_B)l + P y_B - K_2\theta_B & \text{(5-25c)} \end{cases}$$

Solving these equations we have

$$y_B = \frac{a_3 a_5 + a_1 a_6}{a_1 a_4 - a_2 a_5}F$$

$$\theta_A = \frac{a_2 a_6 + a_3 a_4}{a_1 a_4 - a_2 a_5}F$$

where,

$$a_1 = K_3 + \frac{K_2 K_3}{P}\alpha\sin\alpha l + K_2\cos\alpha l;$$

$$a_2 = \frac{K_1 K_2}{P}\cos\alpha l + P - K_1 l - \frac{K_1 K_2}{P};$$

$$a_3 = l + \frac{K_2}{P} - \frac{K_2}{P}\cos\alpha l;\ a_4 = 1 + \frac{K_1\sin\alpha l}{\alpha P} - \frac{K_1 l}{P};$$

$$a_5 = \frac{\sin \alpha L}{\alpha} + \frac{K_3}{P} - \frac{K_3}{P}\cos \alpha l \; ; \; a_6 = \frac{\sin \alpha l}{\alpha P} - \frac{l}{P}.$$

The deflected shape of the column can be represented as

$$y = \left[-\frac{a_2 a_6 + a_3 a_4}{a_1 a_4 - a_2 a_5} K_3 \cos \alpha x + \frac{1}{\alpha}\left(1 + \frac{a_2 a_6 + a_3 a_4}{a_1 a_4 - a_2 a_5} P - K_1 \frac{a_3 a_5 + a_1 a_6}{a_1 a_4 - a_2 a_5} \right) \sin \alpha x \right.$$
$$\left. + \left(\frac{a_3 a_5 + a_1 a_6}{a_1 a_4 - a_2 a_5} K_1 - 1 \right) x + \frac{a_2 a_6 + a_3 a_4}{a_1 a_4 - a_2 a_5} K_3 \right] \frac{F}{P} \qquad (5\text{-}26a)$$

or in a more concise form

$$y = -\frac{K_3}{P}\theta_A \cos \alpha x + \frac{1}{\alpha}\left(\theta_A - \frac{K_1 y_B - F}{P} \right) \sin \alpha x + \frac{K_1 y_B - F}{P} x + \frac{K_3}{P}\theta_A \qquad (5\text{-}27)$$

The bending moment in the column will be

$$M = -EI\left[\frac{K_3}{P}\theta_A \alpha^2 \cos \alpha x - \alpha\left(\theta_A - \frac{K_1 y_B - F}{P} \right) \sin \alpha x \right]$$

If we know that the thermal elongation is Δ and rotational stiffnesses $\mathbf{K_1}$ and $\mathbf{K_2}$ at the top and bottom of the column respectively, the analytical model will be illustrated as shown in Fig. 5-6.

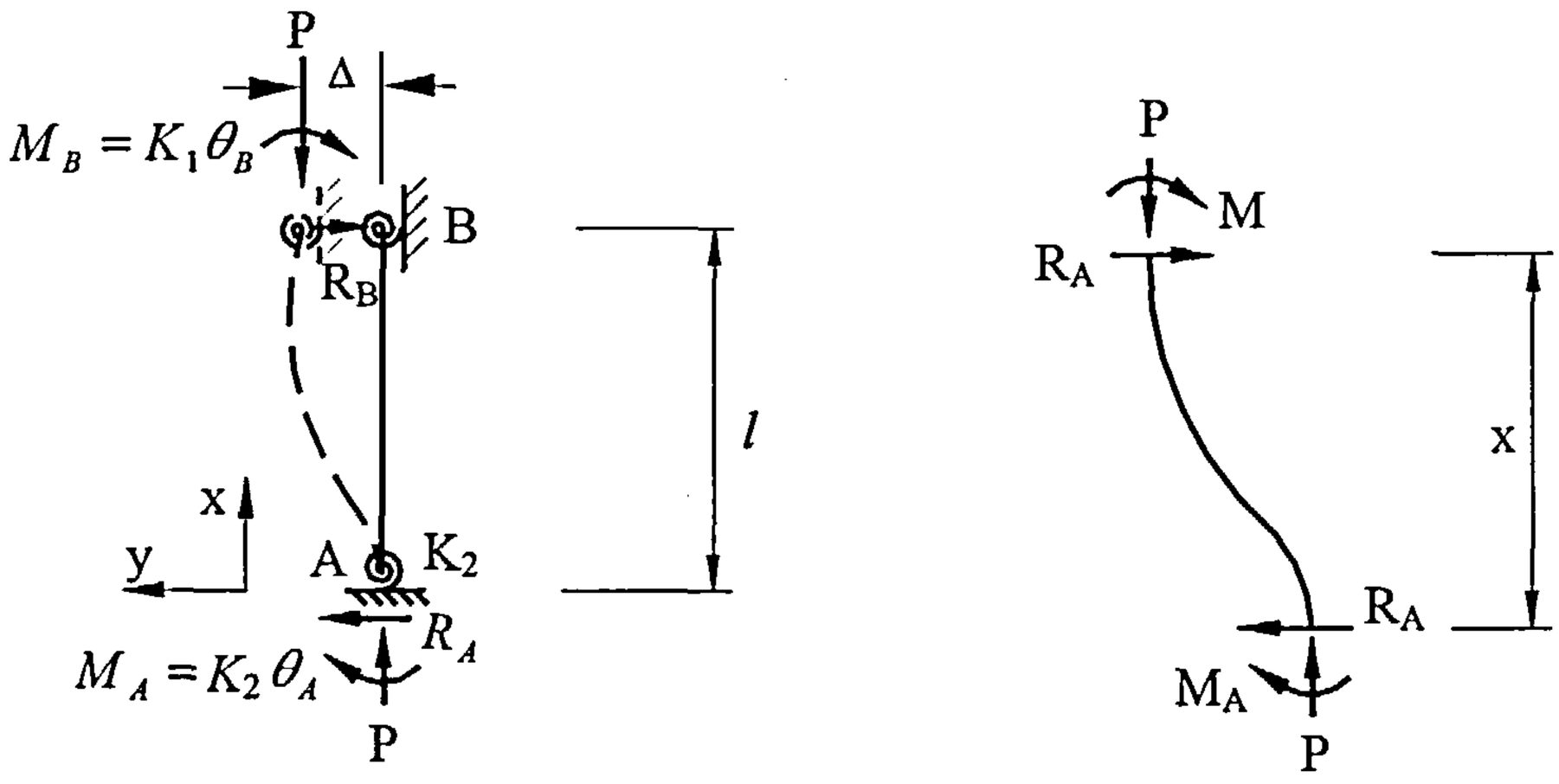

(a) 2D model for analysis **(b) Free body diagram**

Fig. 5-6 Simplest 2D model for calculation

From the free body diagram the differential equation will be

$$EI\frac{d^2y}{dx^2}+Py=R_Ax+M_A \tag{5-28a}$$

Let $\alpha^2=\frac{P}{EI}$, then Eqn (5-28a) becomes

$$\frac{dy^2}{dx^2}+\alpha^2y=\frac{\alpha^2R_A}{P}x+\frac{\alpha^2M_A}{P} \tag{5-28b}$$

The general solution is

$$y=A\cos\alpha x+B\sin\alpha x+\frac{R_A}{P}x+\frac{M_A}{P} \tag{5-29}$$

and,

$$y'=-A\alpha\sin\alpha x+B\alpha\cos\alpha x+\frac{R_A}{P} \tag{5-30}$$

where **A** and **B** are arbitrary constants which can be evaluated from the boundary conditions. From the boundary conditions $y=0,\ y'=\theta_A$ at $x=0$, we have

$$A=-\frac{M_A}{P}$$

and

$$B=\frac{\theta_A-\frac{R_A}{P}}{\alpha},$$

From the boundary conditions that $y=\Delta$ and $y'=\theta_B$ at $x=l$, there are

$$\begin{cases}\Delta=-\dfrac{K_2\theta_A}{P}cos\,\alpha l+\left(\dfrac{\theta_A}{\alpha}-\dfrac{R_A}{\alpha P}\right)sin\,\alpha l+\dfrac{R_A}{P}l+\dfrac{K_2\theta_A}{P} & (5\text{-}31a)\\ \theta_B=\dfrac{K_2\theta_A}{P}\alpha\,sin\,\alpha l+\left(\theta_A-\dfrac{R_A}{P}\right)cos\,\alpha l+\dfrac{R_A}{P} & (5\text{-}31b)\\ K_2\theta_A=P\Delta-K_1\theta_B-R_Al & (5\text{-}31c)\end{cases}$$

Solving the above Eqns (5-31a) to (5-31c) produces

$$R_A = R_B = \frac{a_1 - a_3 P}{a_2 a_3 - a_1 a_4}\Delta$$

$$\theta_A = \frac{a_2 - a_4 P}{a_2 a_3 - a_1 a_4}\Delta$$

$$\theta_B = \frac{K_2\theta_A}{P}\alpha \sin\alpha l + (\theta_A - \frac{R_A}{P})\cos\alpha l + \frac{R_A}{P}$$

where

$$a_1 = \frac{K_1 K_2 \alpha \sin\alpha l}{P} + K_1 \cos\alpha l + K_2;$$

$$a_2 = \frac{K_1 \cos\alpha l}{P} - \frac{K_1}{P} - l;$$

$$a_3 = \frac{K_2}{P} + \frac{\sin\alpha l}{\alpha} - \frac{K_2 \cos\alpha l}{P}; \qquad a_4 = \frac{\sin\alpha L}{\alpha P} - \frac{l}{P}$$

The deflected shape will be

$$y = -\frac{K_2\theta_A}{P}\cos\alpha x + (\frac{\theta_A}{\alpha} - \frac{R_A}{\alpha P})\sin\alpha x + \frac{R_A}{P}x + \frac{K_2}{P}\theta_A \qquad (5\text{-}32)$$

Therefore, the bending moment in the column at an arbitrary point can be obtained by

$$M = -EI\left[\frac{K_2\theta_A\alpha^2}{P}\cos\alpha x - \alpha\left(\theta_A - \frac{R_A}{P}\right)\sin\alpha x\right]$$

where the extreme bending moment may occur at $x = \frac{1}{\alpha} arctg\left(\frac{R_A - \theta_A P}{K_2\theta_A\alpha}\right)$

5.3 VALIDATION AND PARAMETRIC STUDIES

Form the equations presented above it is obvious that the factors affecting deflection are: Young's modulus of the column (**E**) including lower column $\mathbf{E_1}$ and upper column $\mathbf{E_2}$ if a two-storey column is considered, its second moment of area (**I**), column length (**L**), axial load in the column (**P**) and the effect of thermal expansion including thermal force **F** or thermal elongation Δ. There is a linear relationship between the deflection

and the thermal expansion force (**F**) or thermal elongation (Δ). It is also clear that the only parameter which varies with temperature is Young's modulus, **E** (or $\mathbf{E_1}$ for the lower column). In order to validate the analyses, a corner sub-frame as shown in Fig. 5-1 has been analysed with the two ends of the column being fully restrained against rotation and horizontal translation. For calculation a 2D sub-frame consisting of a 305x305x137UC S355 column bending about its minor axis is considered. If the effect of thermal expansion of the beam is represented as a horizontal expansion force (**F**) of 100kN and the column is subject to an axial load (**P**) of 3000kN (a load ratio of 0.59 if an effective length factor of 0.7 is assumed), and the reduction factor[46] for $\mathbf{E_1}$ at elevated temperature is taken into account, the results of the classical analysis from Eqn. (5-10) are as shown in Figs. 5-7 and 5-8. Also shown are results from the software VULCAN,

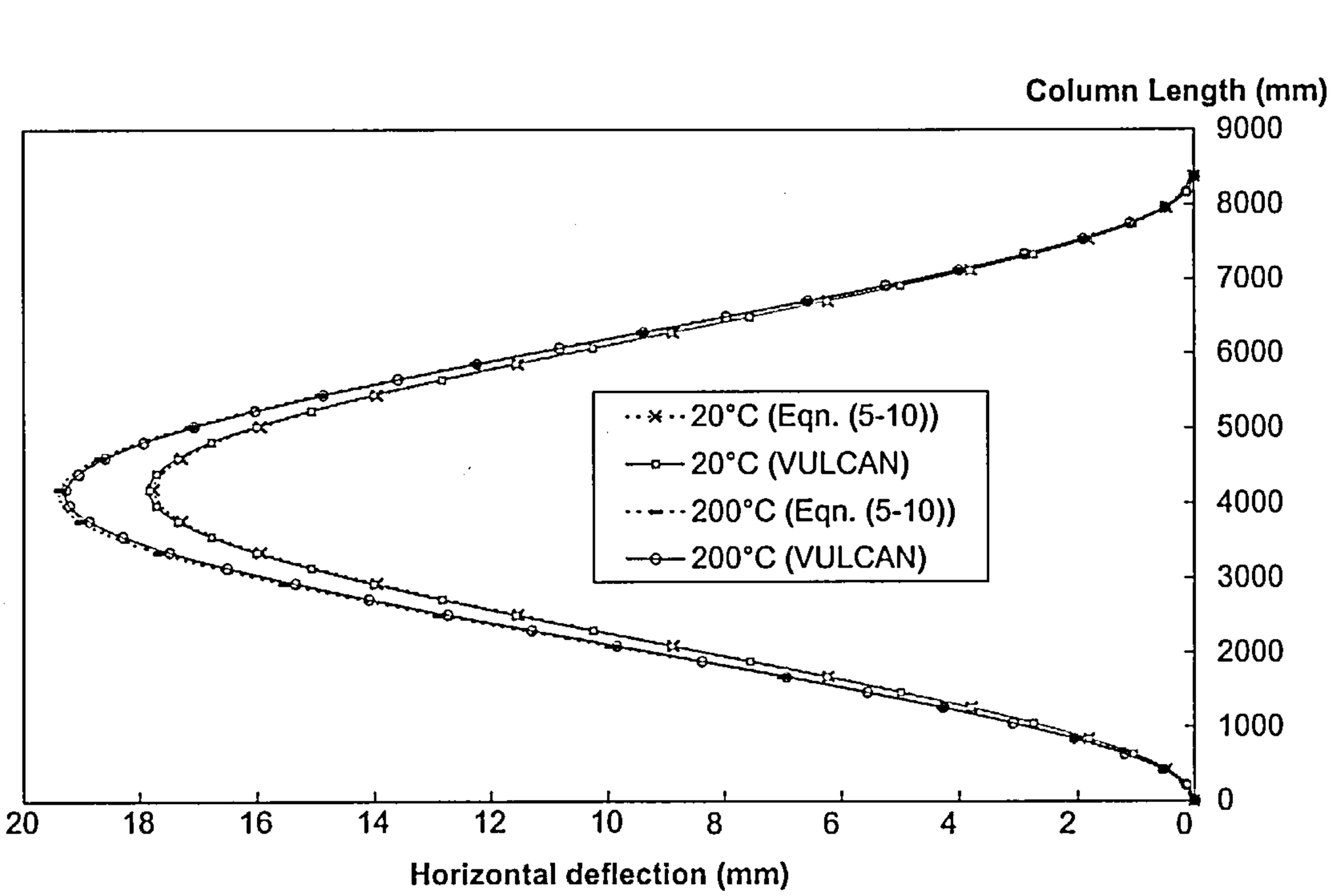

Fig. 5-7 Column horizontal deflection (P = 3000kN, F = 100kN)

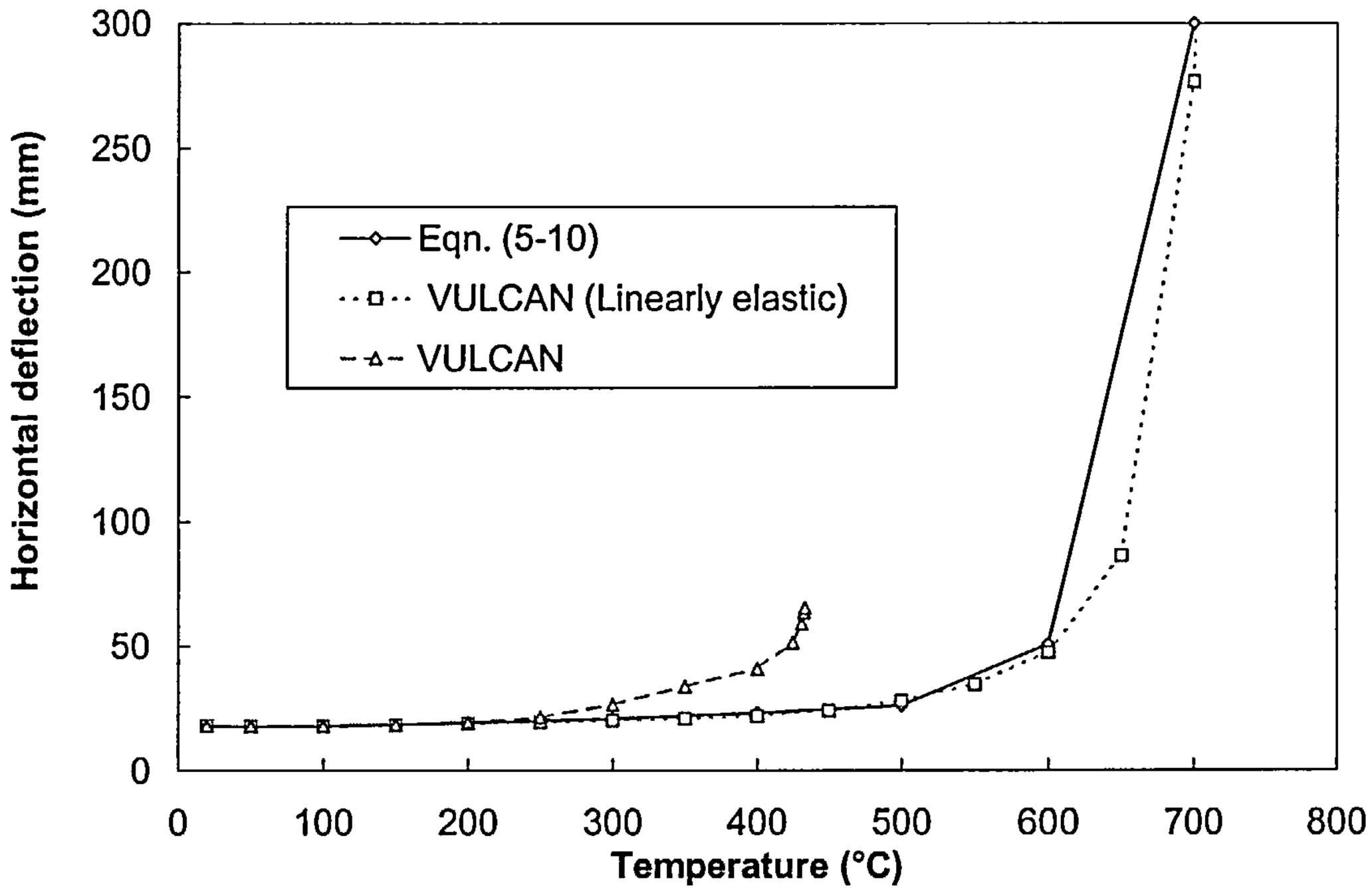

Fig. 5-8 Deflection-temperature plot for floor level point C. (Axial load P = 3000kN, thermal expansion force F=100kN)

It is of interest to note that when VULCAN uses linear-elastic material properties it is in close agreement with the classical analysis. However when more realistic properties are used the two diverge significantly beyond 250°C because of the material yielding which is important for columns of medium or low slenderness[78].

The effects of thermal force, axial load and imperfection have been studied by using Eqn. (5-10) and the results are summarised in Figs. 5-9, 5-10 and 5-11. It may be seen from Fig. 5-10 that keeping the lower column temperature below 500°C is beneficial since there is only a relatively small change in behaviour at lower temperatures. Fig. 5-9 indicates that the deflection is proportional to the thermal force when axial load is constant. Fig. 5-11 indicates that at a low load ratio the magnitude of imperfections has negligible effect.

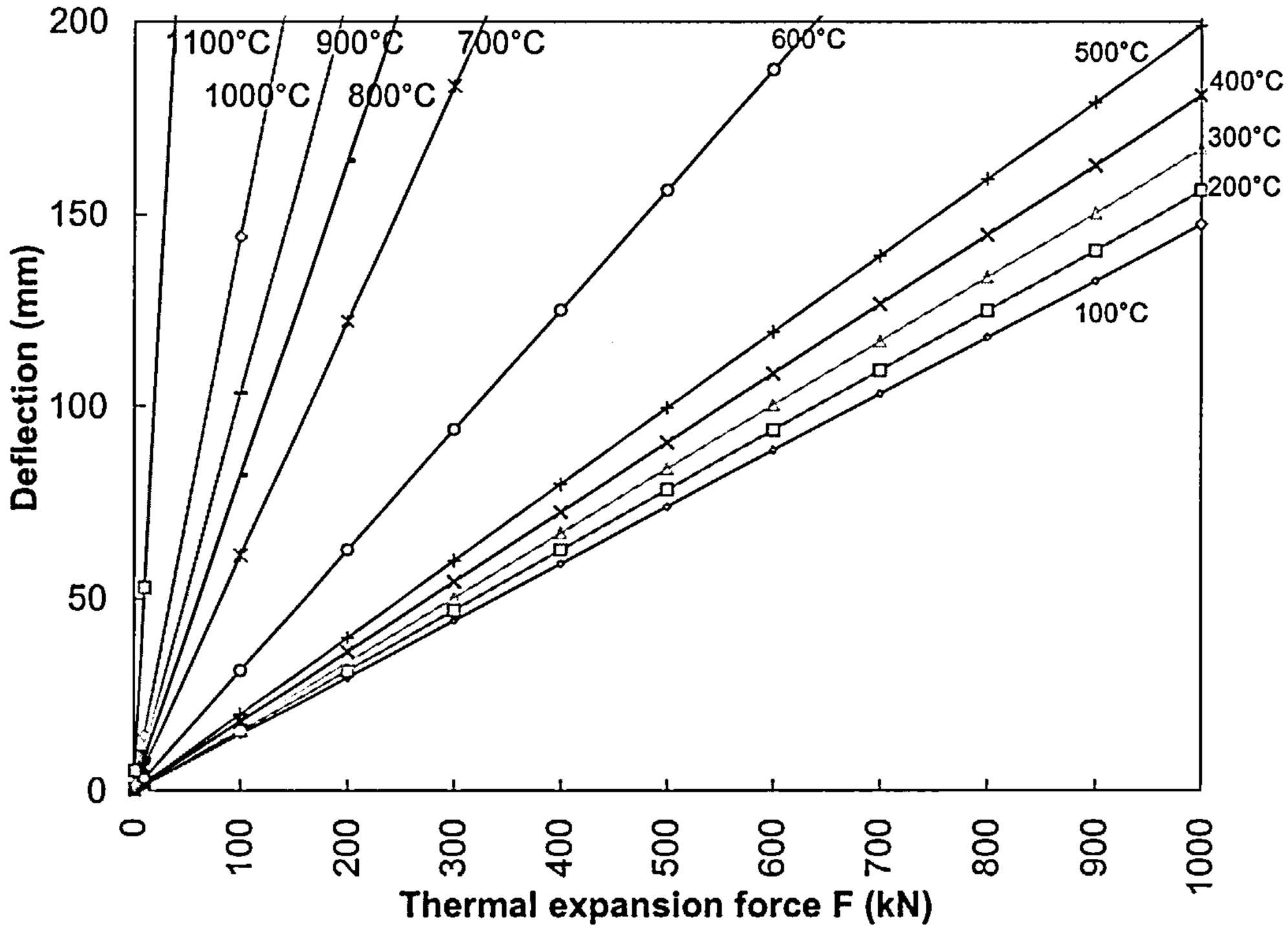

Fig. 5-9 Deflection-Thermal Force plot at floor level point C. (Axial load P = 1000kN)

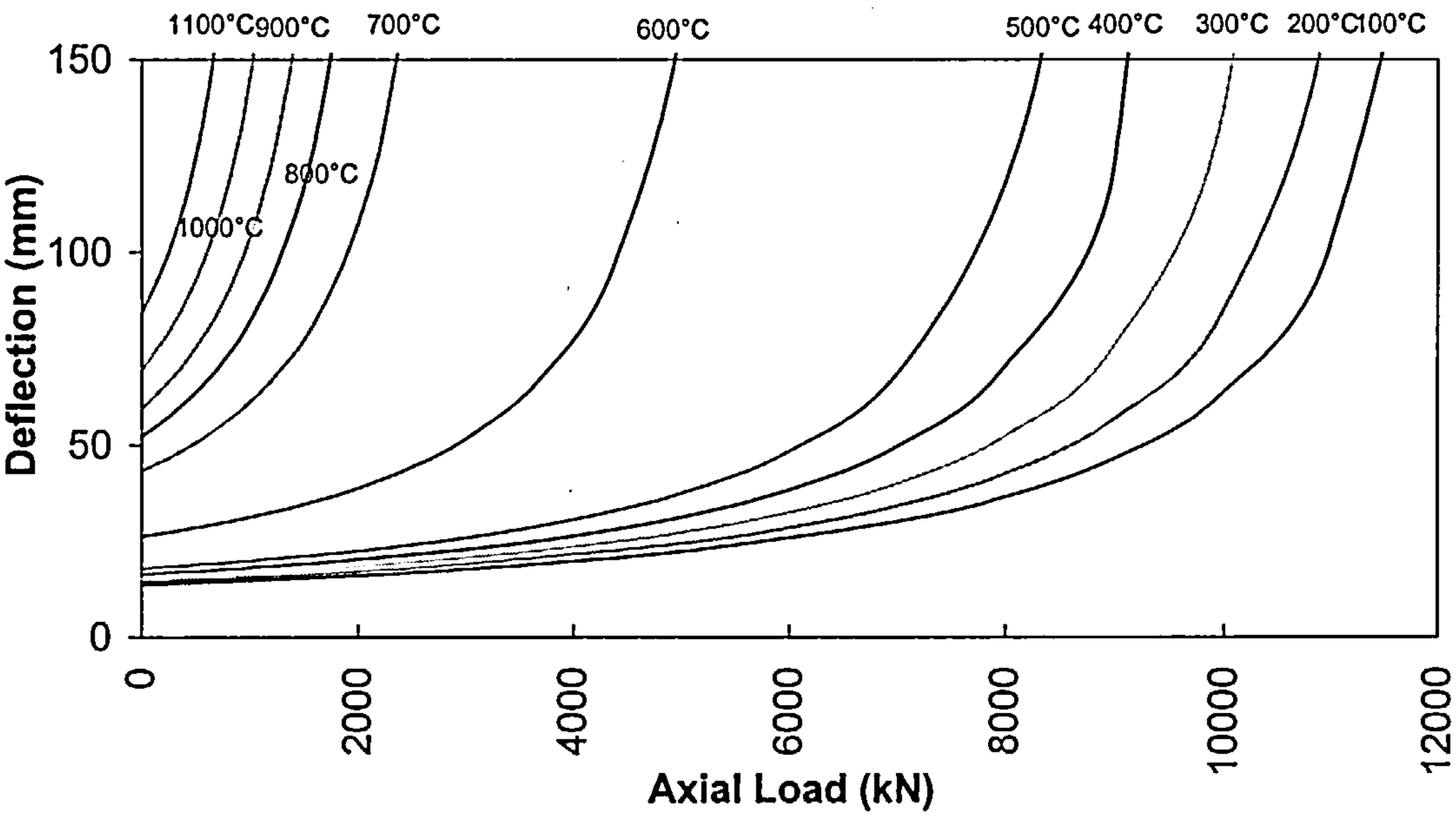

Fig. 5-10 Deflection-Axial load plot (Thermal expansion force F =100kN)

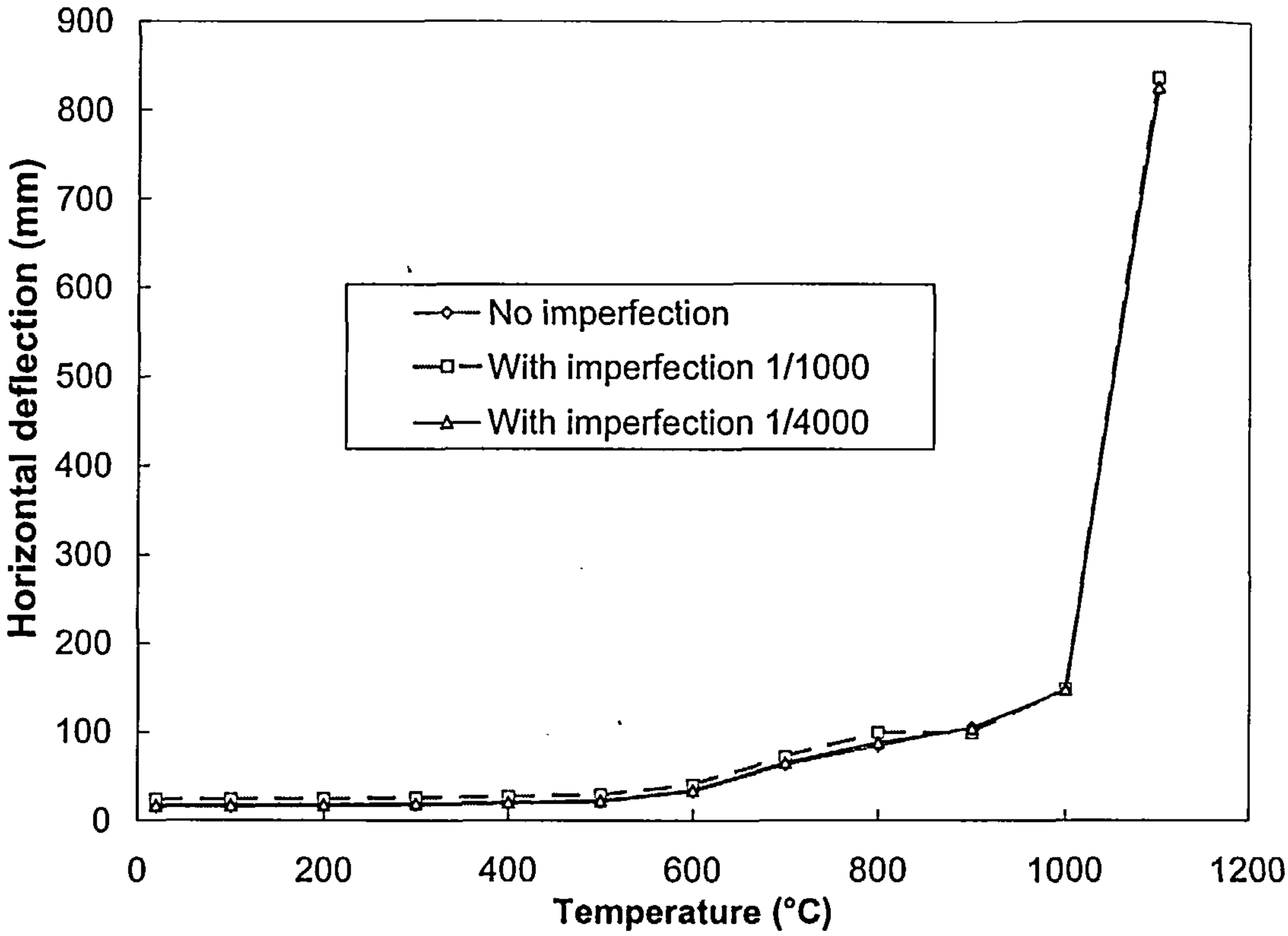

Fig. 5-11 Effect of imperfection on column with axial load 1000kN, thermal expansion force 100kN

If this case is analysed by using the simplest model -- Eqn. (5-27) -- and assuming that the restraining axial and rotational stiffnesses afforded by the upper column are $K_1 = \frac{12E_2I_2}{l^3} = 3669.1N/mm$ and $K_2 = \frac{4E_2I_2}{l} = 2.142x10^{10}Nmm$ respectively, the result is as shown in Fig. 5-12. It can be seen that there are some differences between the results of Eqn. (5-10) and Eqn. (5-27). This may be because the lateral and rotational restraints from the upper column are represented in a simplified manner in Eqn. (5-27) as $Q = \frac{12EI}{l^3}\Delta$ and $M = \frac{4EI}{l}\theta$. The full expressions for restraint are in fact $Q = \frac{12EI}{l^3}\Delta + \frac{6EI}{l^2}\theta$ and $M = \frac{4EI}{l}\theta + \frac{6EI}{l^2}\Delta$, ignoring the second term in each case causes the discrepancy shown in Fig. 5-12. This represents a maximum error of

9.18% in horizontal displacement at ambient temperature. This error may be even more pronounced at high temperature.

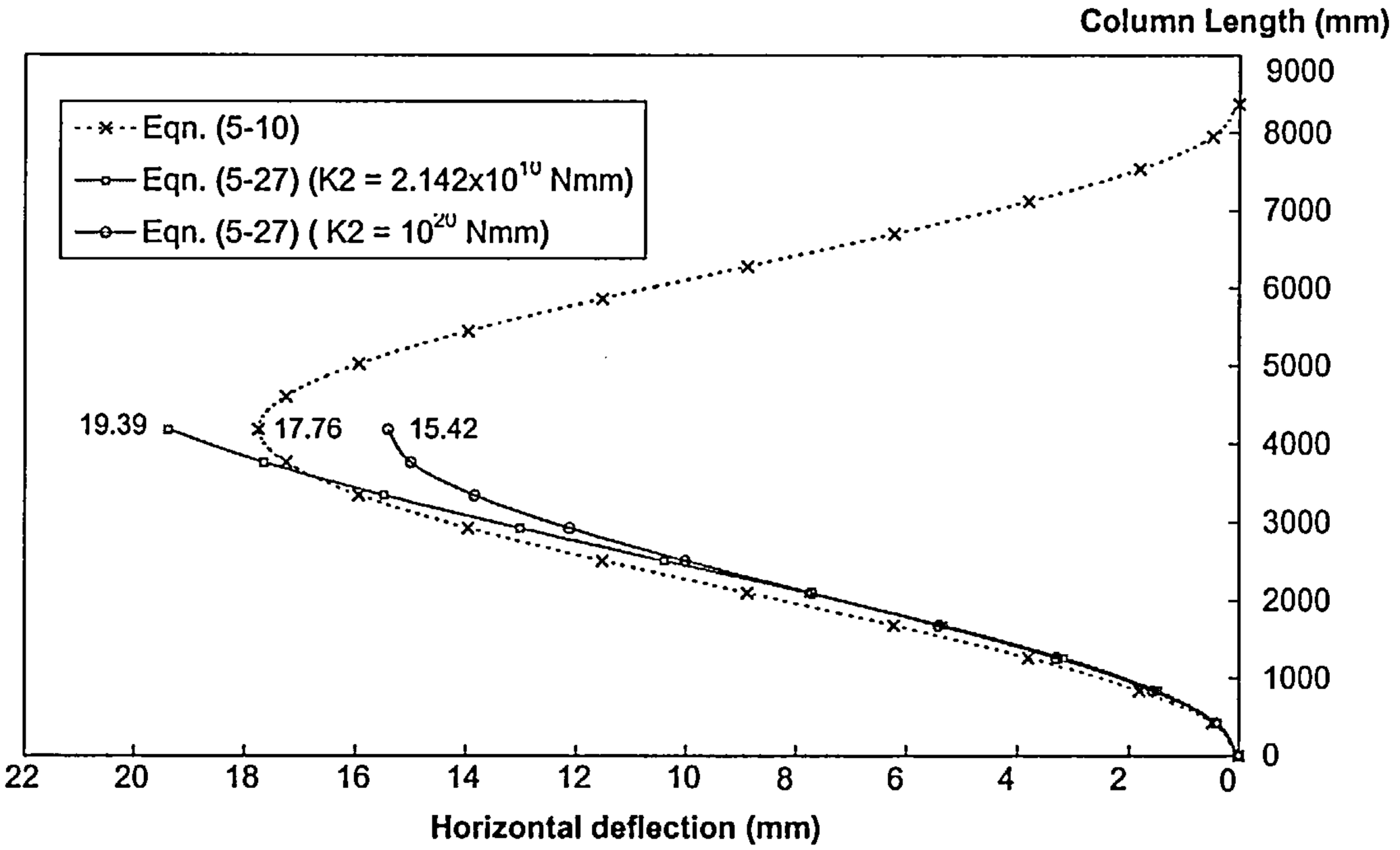

Fig. 5-12 Comparison between Eqn. (5-10) and Eqn. (5-27) for horizontal deflection at ambient temperature (P = 3000kN, F = 100kN, K_1=3669.1N/mm, K_3=10^{20} Nmm)

If we consider the column is subjected to an axial load (**P**) of 3000kN, with the thermal effect being a horizontal elongation (Δ) of 67.25mm at floor level (point **C**), the classical calculation results (from Eqns. (5-15) and (5-20)) compared with VULCAN results are as illustrated in Figs. 5-13 and 5-14. It is evident that the results obtained by using the different calculation mode (Eqns. (5-15) and (5-20)) are identical, and they are very close to those predicted by VULCAN. However, the effect of material yielding clearly starts to be important just beyond 400°C. It is to be noted that in Fig. 5-14 the curve corresponding to Eqn. (5-15) reverses in direction at temperature over 900°C. This is because the formulations include all possible deformation shapes. This reversal corresponds to a higher order mode of buckling as shown in Fig. 5-15, and is of no practical importance. Figs. 5-16 and 5-17 show the

external reaction force ($\mathbf{R_C}$) and rotation (θ) at floor level (point **C**). It is clear that the reaction force changes sign to restrain the instability at temperatures beyond 700°C and approaching the critical temperature which is defined by direction reversal in Figs. 5-14, 5-16 and 5-17. This is consistent with the observations in chapter 4. Fig. 5-18 shows a linear relationship between the horizontal deflection and thermal elongation.

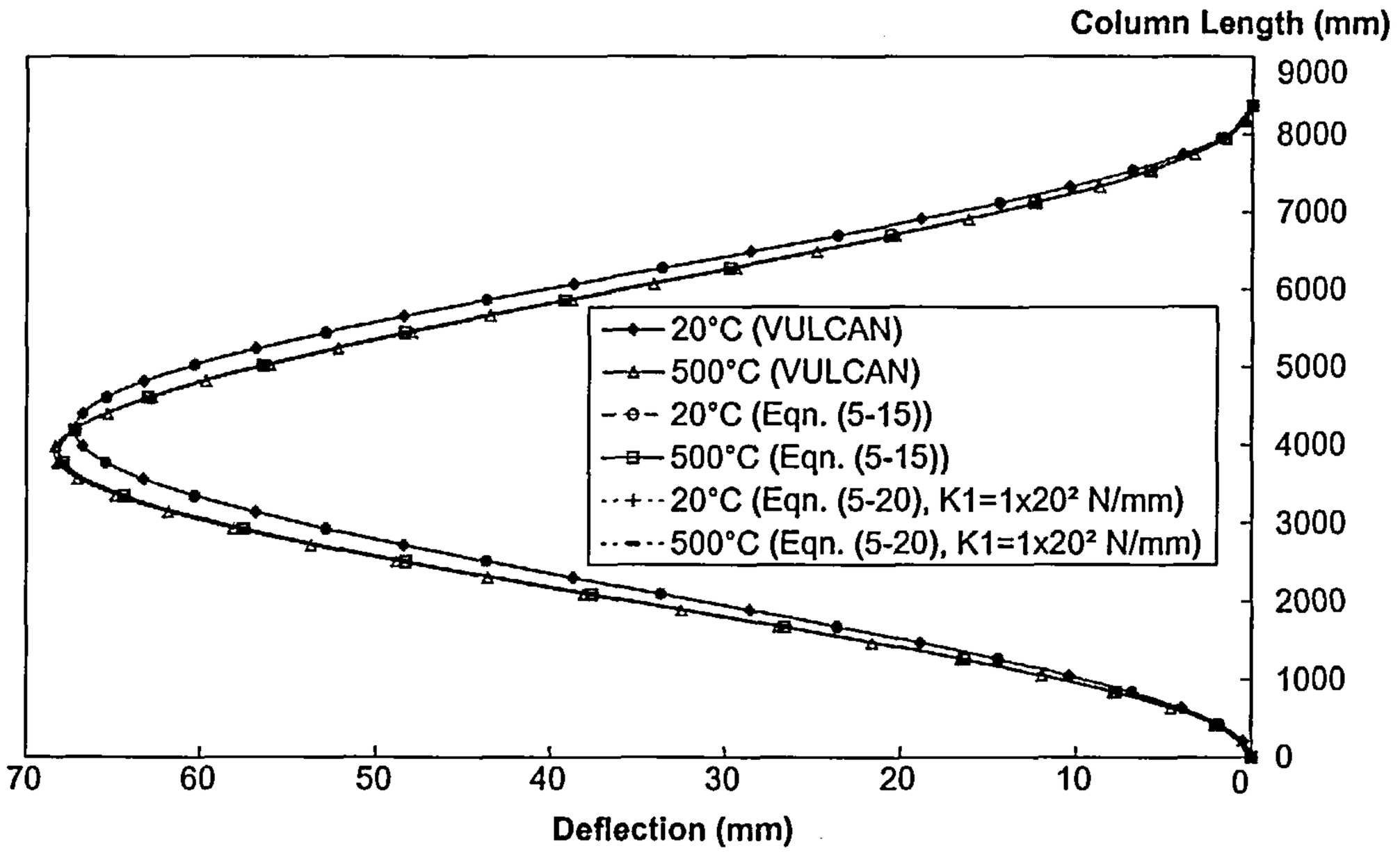

Fig. 5-13 Column horizontal deflection (Axial load P = 3000kN, thermal elongation Δ = 67.25mm, rotation stiffness K = 0)

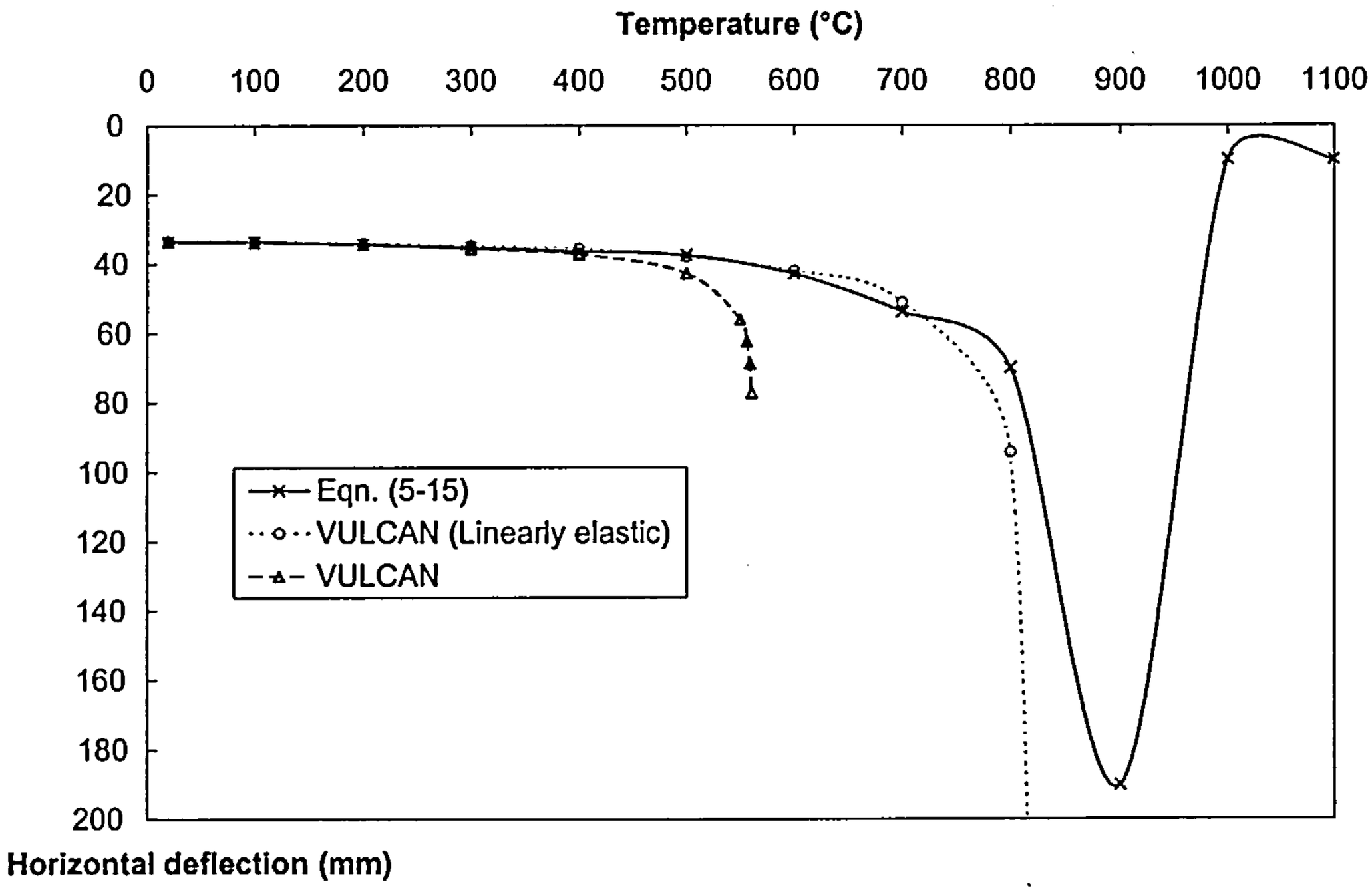

Fig. 5-14 Horizontal deflection-temperature plot at mid-point of the lower column. (Axial load P = 3000kN, thermal elongation Δ=67.25mm)

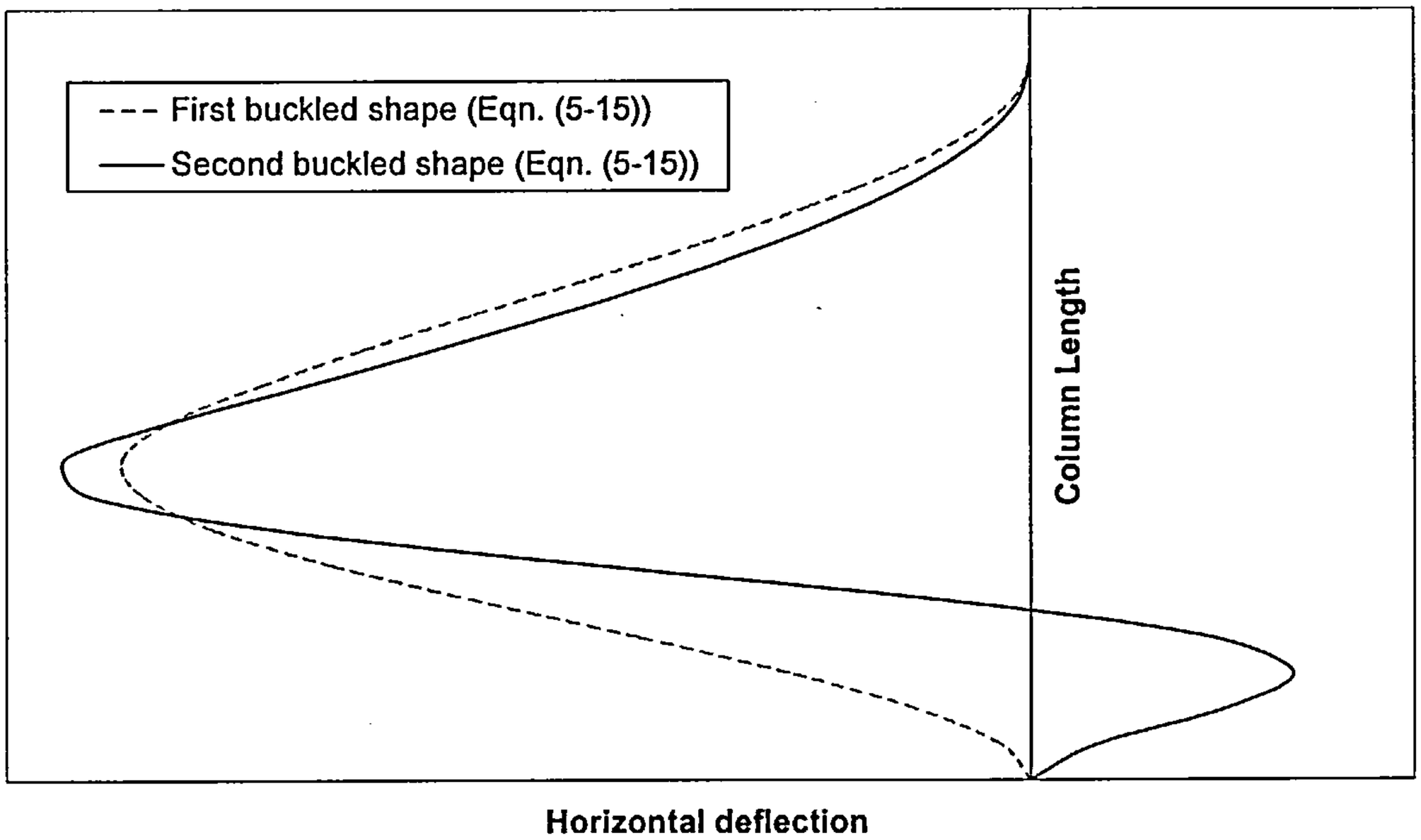

Fig. 5-15 Deformation shapes of the column (Axial load P = 3000kN)

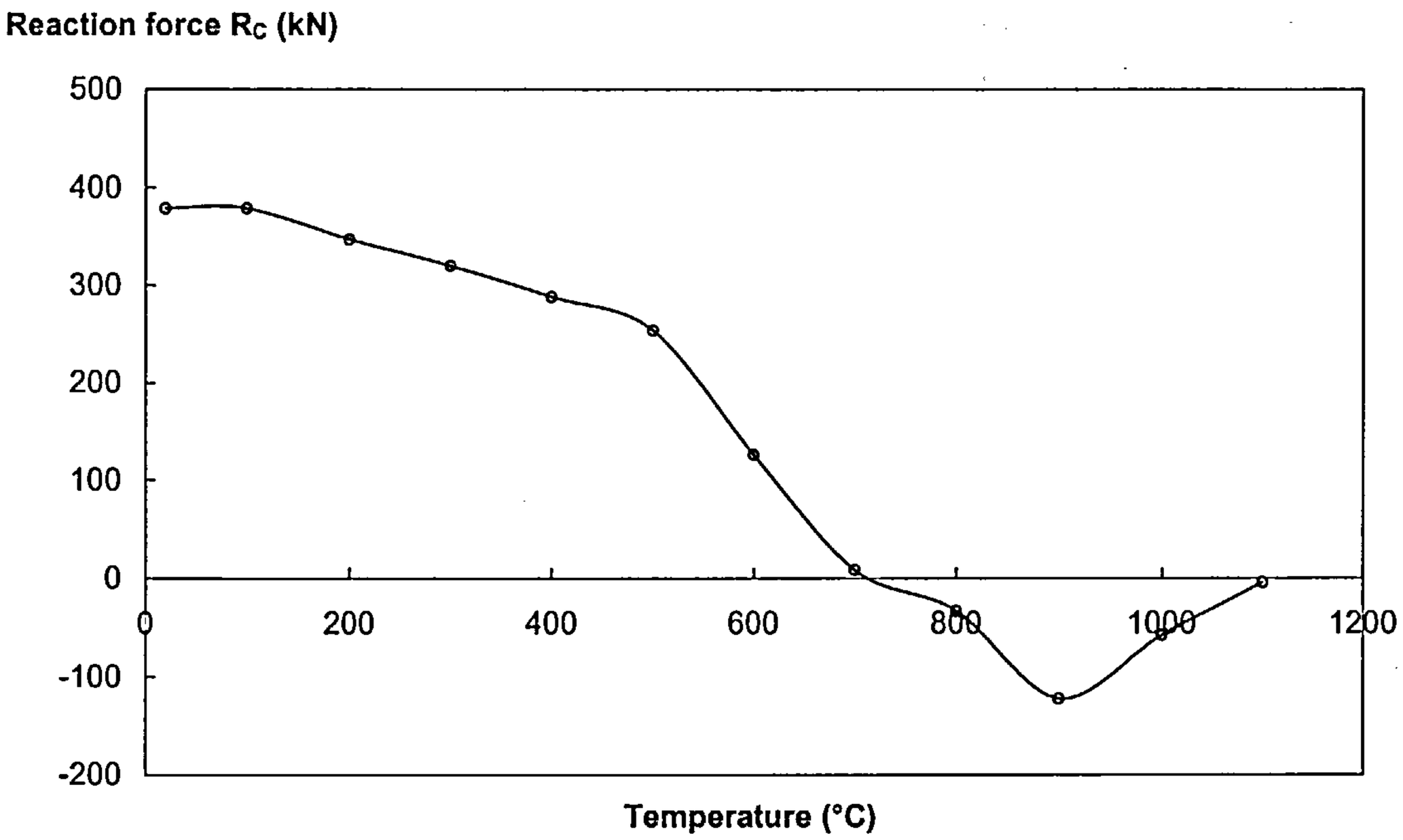

Fig. 5-16 Reaction (R_C) at floor level (point C). (Axial load P = 3000kN, thermal elongation Δ=67.25mm)

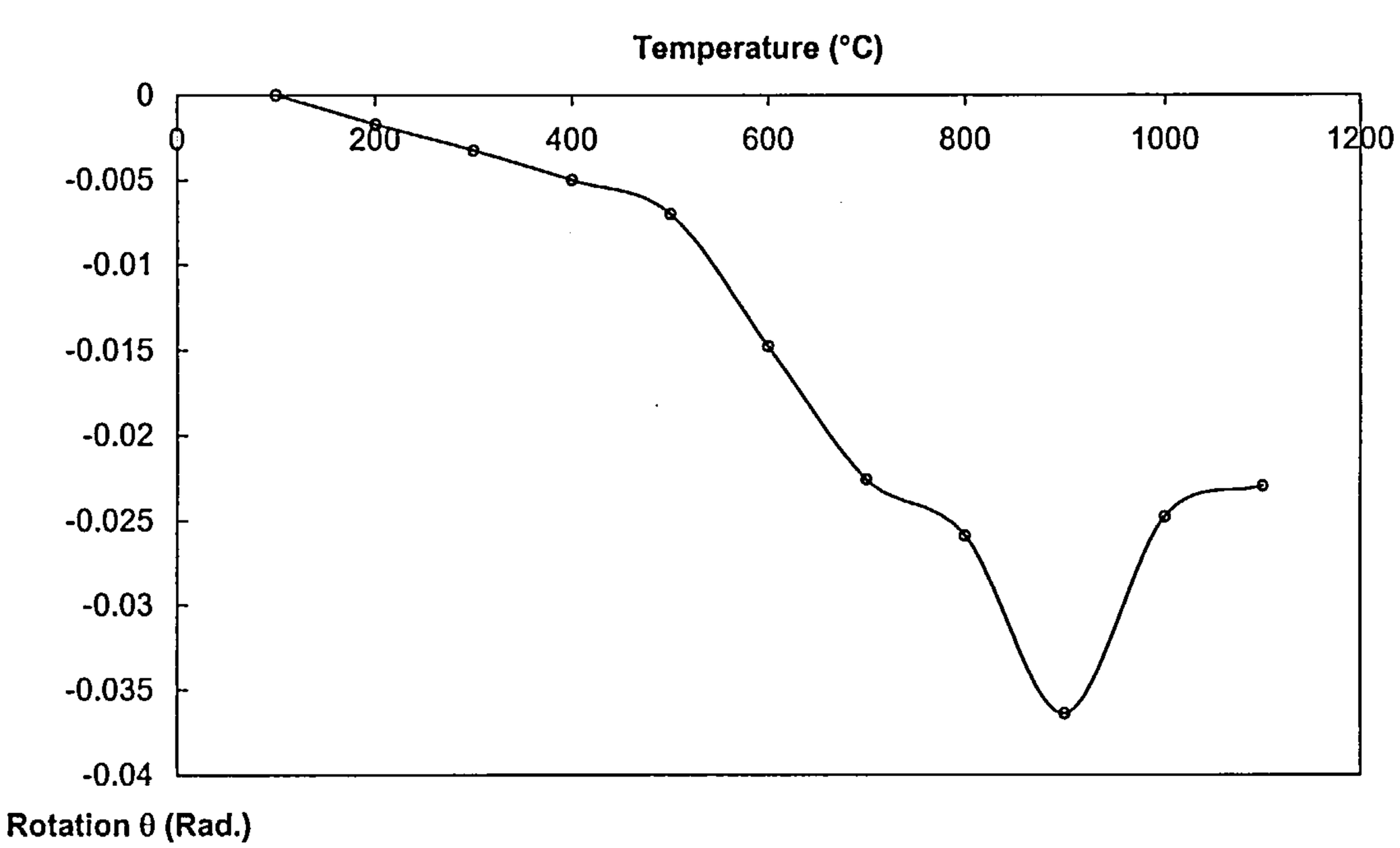

Fig. 5-17 Rotation of the mid-point of the column (point C). (Axial load P = 3000kN, thermal elongation Δ = 67.25mm)

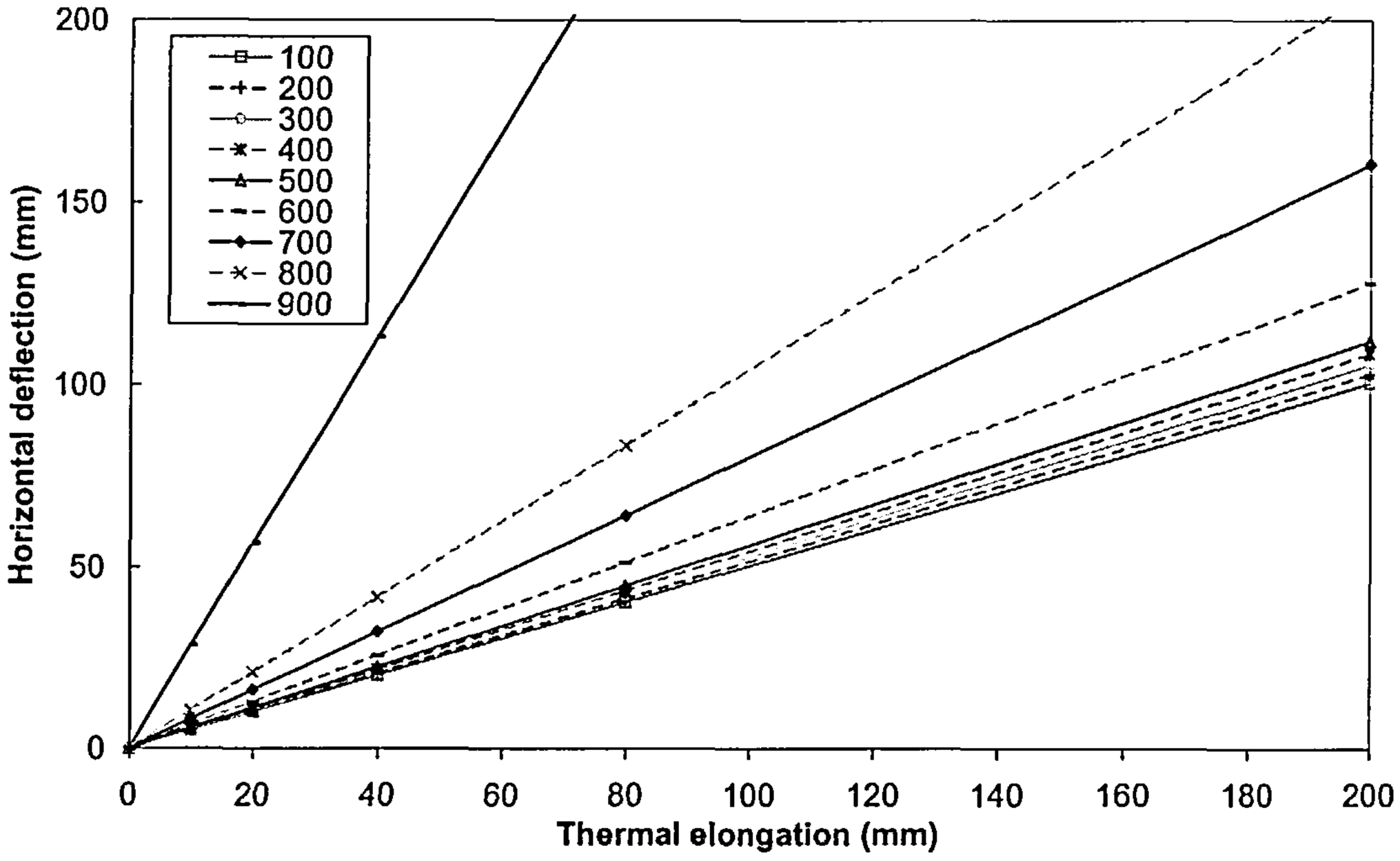

Fig. 5-18 Horizontal deflection-thermal elongation plot at mid-point of the lower column. (Axial load P = 3000kN)

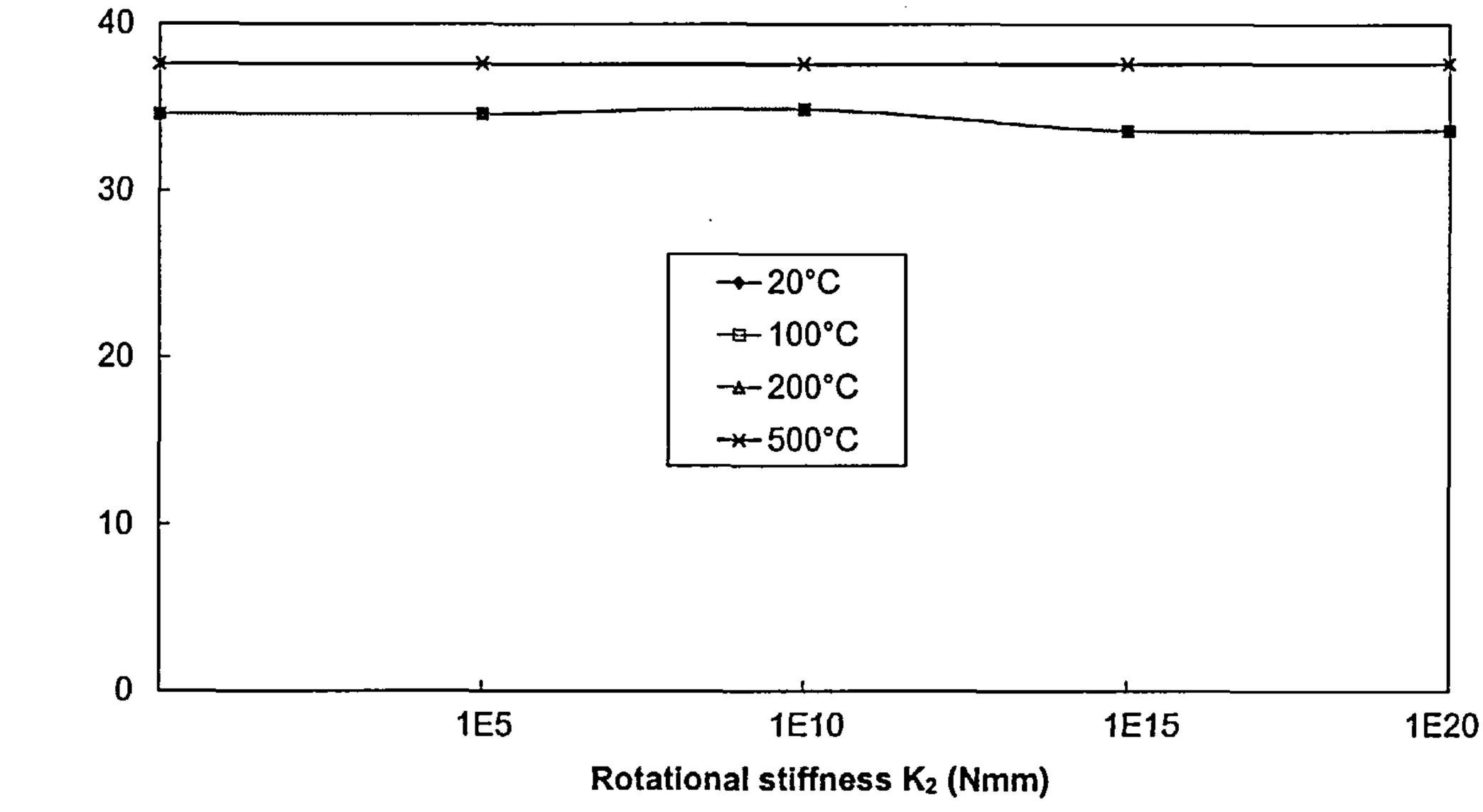

Fig. 5-19 Horizontal deflection-rotational stiffness plot at mid-point of the lower column. (Axial load P = 3000kN, thermal elongation Δ = 67.25mm, axial stiffness $K_1 = 10^{20}$Nmm)

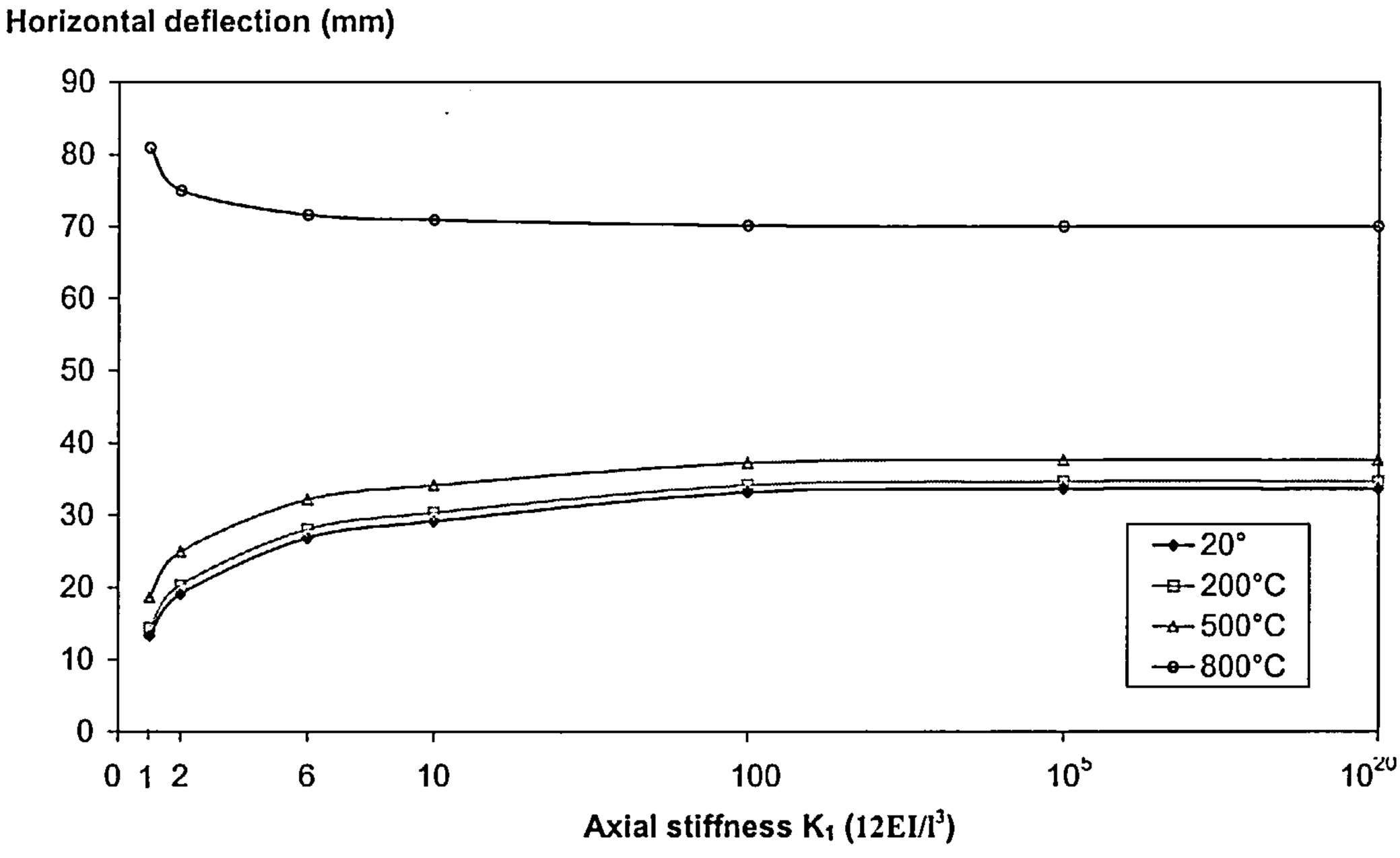

Fig. 5-20 Horizontal deflection-axial stiffness plot at mid-point of the lower column. (Axial load P = 3000kN, thermal elongation Δ = 67.25mm, rotational stiffness $K_2 = 0$, $E = 2.05 \times 10^5 N/mm^2$, $I = 1.067 \times 10^8 mm^4$, l = 4185mm)

In order to investigate the effects of axial and rotational stiffness of the beam at floor level (point **C**), some parametric studies have been performed based on Eqn. (5-20) for the special sub-frame case. The analytical results are shown in Figs. 5-19 and 5-20. From Fig. 5-19 it is clear that the rotation stiffness has negligible effect when the column temperature is below 500°C, and it is recognised that when the beam reaches a high temperature it loses the stiffness and cannot provide significant rotational restraint. Fig. 5-20 indicates that there is only a small change in deflection once the axial stiffness exceeds $6\frac{12EI}{l^3}$ (i.e. the stiffness of six columns). Therefore, the effects of rotation stiffness from the beams may be less important. However, the axial stiffness cannot be ignored, especially for those exceeding $6\frac{12EI}{l^3}$ where the axial stiffness could be regarded as infinite in magnitude.

If the above case is analysed by using the simplest model and we assume the rotational stiffness provided by the upper column is $K_1 = \frac{4EI}{l} = 2.142x10^{10} Nmm$, the deflections can be calculated by using Eqn. (5-32). The results are compared with those obtained by Eqn. (5-15) and show some differences especially in high temperatures (Fig. 5-21). Fig. 5-21 also includes the case of full rotational restraint ($K_1=10^{20}$). It is clear that even though the column is fully restrained at the top, the deflection is still less than those calculated by Eqn. (5-15). This indicates that the bending moment produced by the upper column cannot be ignored. If we include this moment in, Eqn. (5-32) can be rewritten according to Fig.5-22 as

$$y = -\frac{K_2\theta_A}{P}\cos\alpha x + (\frac{\theta_A}{\alpha} - \frac{R_A}{\alpha P})\sin\alpha x + \frac{R_A}{P}x + \frac{K_2}{P}\theta_A \qquad (5\text{-}33)$$

where,

$$R_A = R_B = \frac{(a_1 - a_3 P)\Delta + a_3 M_U}{a_2 a_3 - a_1 a_4}; \qquad \theta_A = \frac{(a_2 - a_4 P)\Delta + a_4 M_U}{a_2 a_3 - a_1 a_4};$$

$$\theta_B = \frac{K_2\theta_A}{P}\alpha\sin\alpha l + (\theta_A - \frac{R_A}{P})\cos\alpha l + \frac{R_A}{P}; \qquad \alpha^2 = \frac{P}{EI};$$

$$a_1 = \frac{K_1 K_2 \alpha \sin\alpha l}{P} + K_1\cos\alpha l + K_2; \qquad a_2 = \frac{K_1\cos\alpha l}{P} - \frac{K_1}{P} - l;$$

$$a_3 = \frac{K_2}{P} + \frac{\sin\alpha l}{\alpha} - \frac{K_2\cos\alpha l}{P}; \qquad a_4 = \frac{\sin\alpha L}{\alpha P} - \frac{l}{P}.$$

Therefore, the bend moment of the column is

$$M = \frac{\theta_A P - R_A}{\alpha}\sin\alpha x - K_2\theta_A\cos\alpha x \qquad (5\text{-}34)$$

The extreme bending moment occurs at

$$x_m = \frac{1}{\alpha} arctg\left(\frac{R_A - \theta_A P}{K_2\theta_A\alpha}\right) \qquad (5\text{-}35)$$

and its value will be

$$M_m = \frac{\theta_A P - R_A}{\alpha} sin\left(arctg \frac{R_A - \theta_A P}{K_2 \theta_A \alpha} \right) - K_2 \theta_A cos\left(arctg \frac{R_A - \theta_A P}{K_2 \theta_A \alpha} \right) \qquad (5\text{-}36)$$

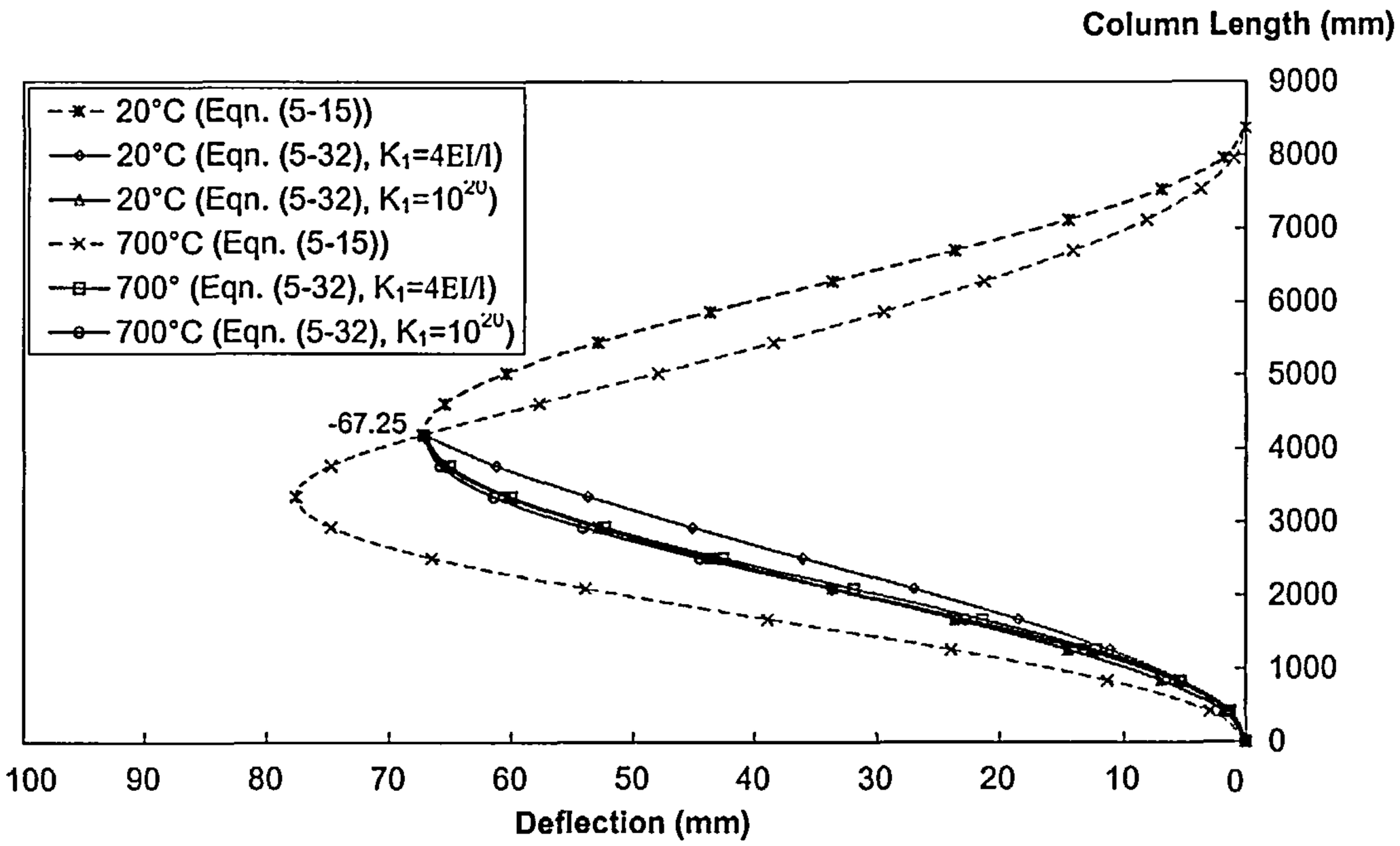

Fig. 5-21 Comparison between Eqn. (5-15) and Eqn. (5-32) for horizontal deflection (P = 3000kN, Δ = 67.25mm, K_2=10^{20} Nmm, E = 2.05x10^5N/mm^2, I = 1.067x10^8mm^4, l = 4185mm)

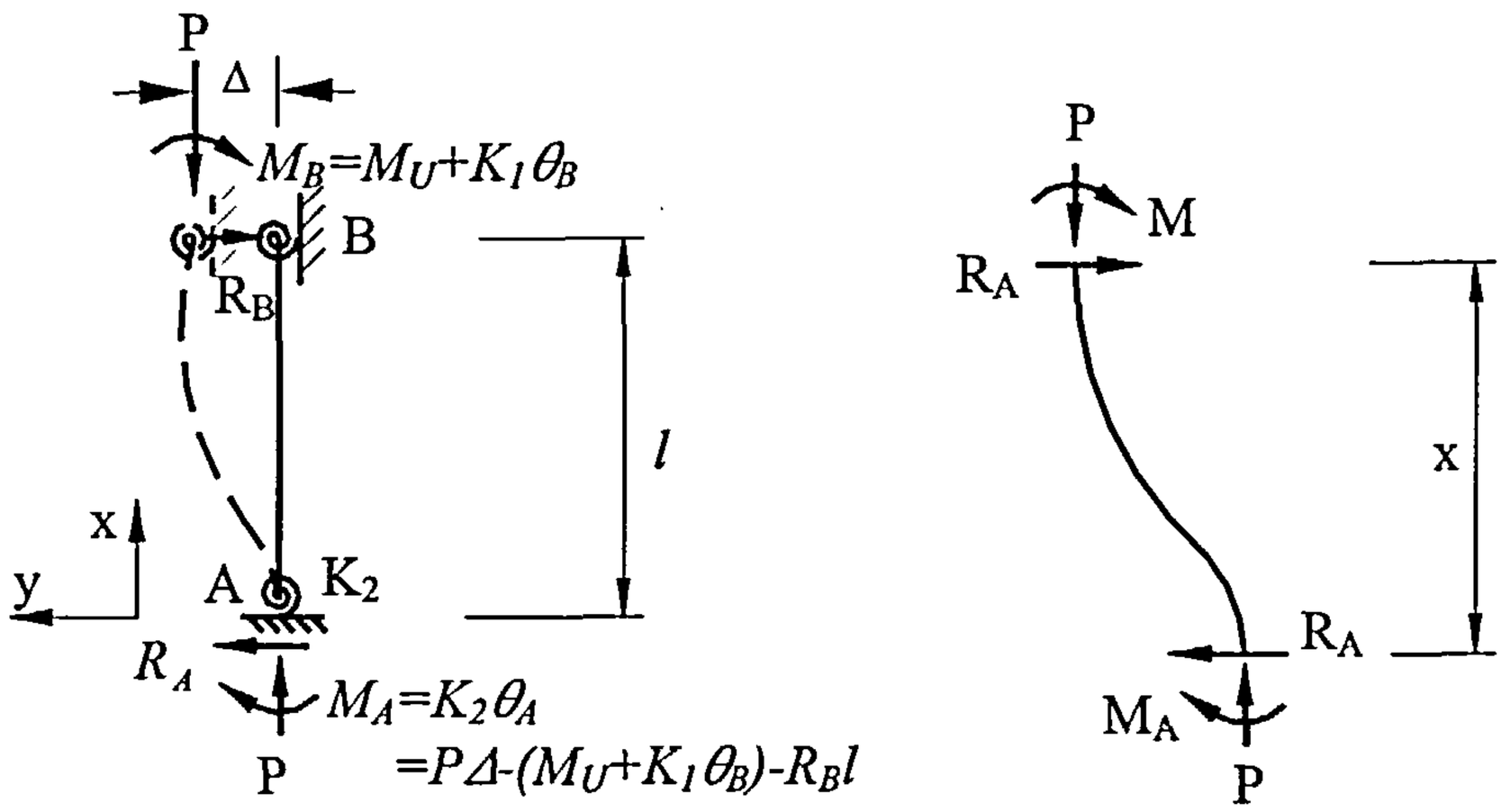

(a) 2D model for analysis **(b) Free body diagram**

Fig. 5-22 Modified simplest 2D model for calculation

Based on Eqn. (5-33) and assuming that the rotational stiffness is $K_1 = \frac{4EI}{l} = 2.142x10^{10}\,Nmm$ and the induced bending moment from the upper column is $M_U = \frac{6EI}{l^2}\Delta = 5.1632x10^{8}\,Nmm$, the deflected shape of the one-storey column can be obtained (Fig. 5-23) and is very close to those calculated from Eqn. (5-15) which is based on two-storey sub-frame, indicating that the simple one-storey model (Fig. 5-22 and Eqn. (5-33)) is capable of modelling the corner sub-frame of a building.

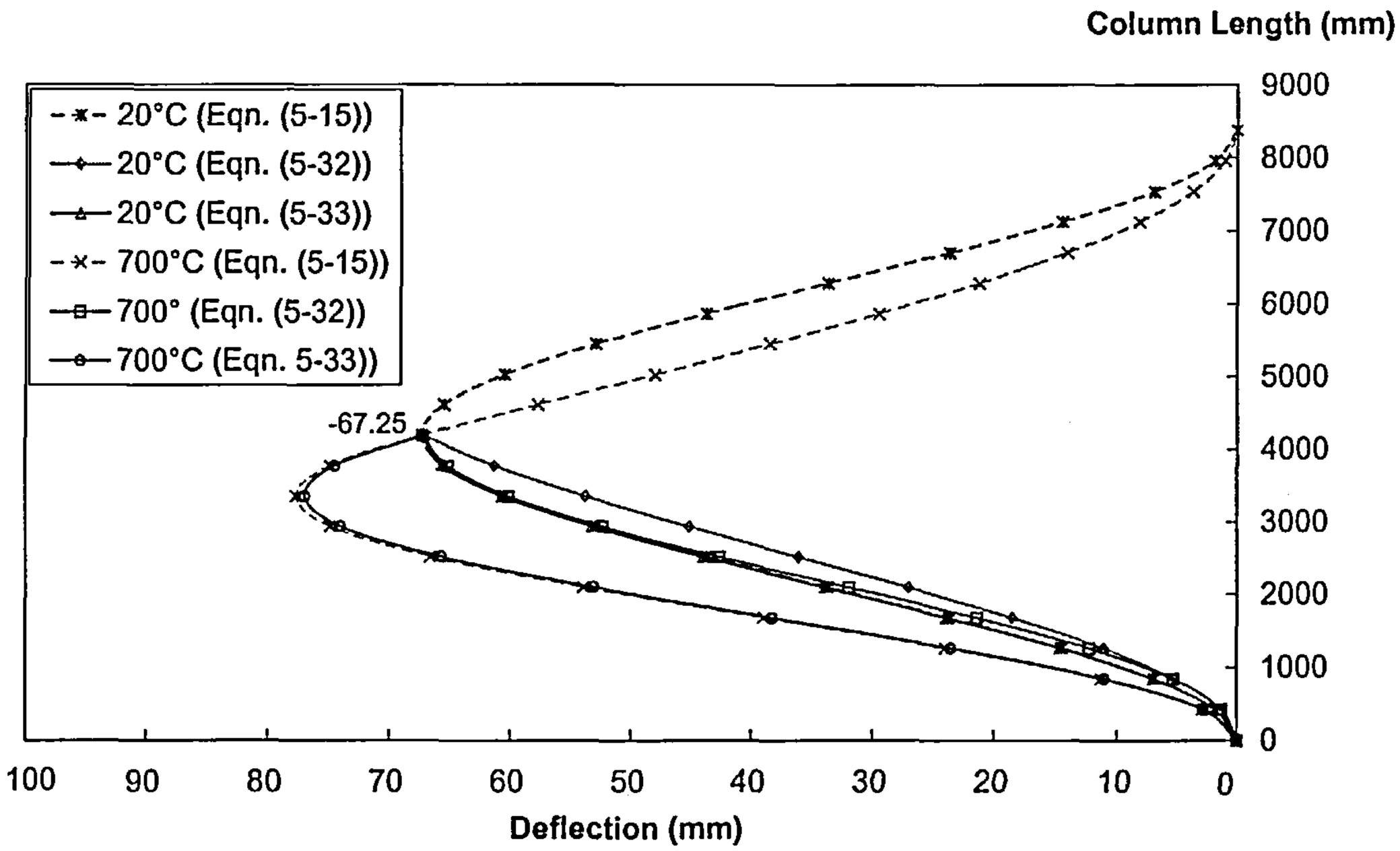

Fig. 5-23 Comparison between Eqn. (5-15) and Eqn. (5-33) for horizontal deflection (P = 3000kN, Δ = 67.25mm, K_2=10^{20} Nmm, E = 2.05x10^5N/mm^2, I = 1.067x10^8mm^4, l = 4185mm)

5.4 CONCLUSION

In this chapter, a series of classical buckling calculations have been developed for a column based on the assumption that thermal expansion of a floor beam can be expressed as a horizontal force or elongation acting at floor level. The results indicate that the effects of thermal expansion of unprotected beams reduce the survival

temperature of the column. This is associated with the $P-\Delta$ effect and causes a significant reduction of the survival temperature for high axial loads but is less important for low axial loads. Both the effects of thermal expansion and axial load should be taken into account in designs and it is suggested that designers use simplified calculation in two dimensions to provide a quick approximate assessment of the structural instability. The general formulations for this purpose are given by

$$y = -\frac{M_A}{P}cos\,\alpha x + \frac{R_A}{\alpha P}sin\,\alpha x - \frac{R_A}{P}x + \frac{M_A}{P} \qquad \text{for horizontal deflection;}$$

$$M = \frac{R_A}{\alpha}sin\,\alpha x - M_A\,cos\,\alpha x \qquad \text{for bending moment}$$

where, $\alpha^2 = \frac{P}{EI}$. Other parameters, such as M_A and R_A, are detailed in this chapter. The critical load or temperature may therefore be determined conservatively by using the equation and defining failure as the first occurrence of material yielding

$$\sigma_m = \frac{P}{A} \pm \frac{M_m}{S} \leq \sigma_y$$

in which **S** is the section moduli of the cross-sectional area, $\mathbf{M_m}$ is the extreme bending moment (maximum or minimum) in the column and σ_y is the yield stress.

6. MODELLING OF ASYMMETRIC CROSS-SECTION MEMBERS FOR FIRE CONDITIONS

This chapter describes a general approach for modelling the three-dimensional behaviour of asymmetric steel beam-columns under fire conditions using two-noded one-dimensional beam elements.

6.1 INTRODUCTION

Recently a new type of steel beam, known as the Asymmetric Slimflor Beam (ASB), which was developed for use with composite floors with deep steel decking, has been introduced in the UK. The web of the ASB is thicker than that of the flanges, which significantly improves its fire resistance properties as part of a slim-floor system. In order to analyse this type of composite construction the software VULCAN, which has been shown to compare well with test data for symmetric beams and columns, has now been extended, and this chapter outlines the basic principles and formulations associated with this. The modified software is then validated by comparison with classical analytical results for idealised conditions at ambient temperature, and with the results of two tests at high temperature.

6.2 BASIC PRINCIPLES AND FORMULATION FOR THE ASYMMETRICAL BEAM-COLUMN CROSS-SECTION

For modelling the behaviour of asymmetric steel members (ASB) in a frame exposed to fire, a set of highly non-linear formulations has been adopted, so that accurate large-deflection solutions can be reached. These formulations are based on the work of Najjar[34,65] and Bailey[10] who extended EI-Zanaty and Murray's[63,64] 2-dimensional formulations to include three-dimensional behaviour and slab elements. These earlier details can be found elsewhere[10,34,65] and are not repeated here except where basic

concepts and appropriate developments are concerned. In order to formulate the governing equations for an asymmetric member, the following assumptions are made:

- The member is straight, prismatic and symmetric about the y-axis. (though not necessarily about the x-axis)
- Plane cross-sections of the plate elements of the thin-walled open member remain plane after loading.

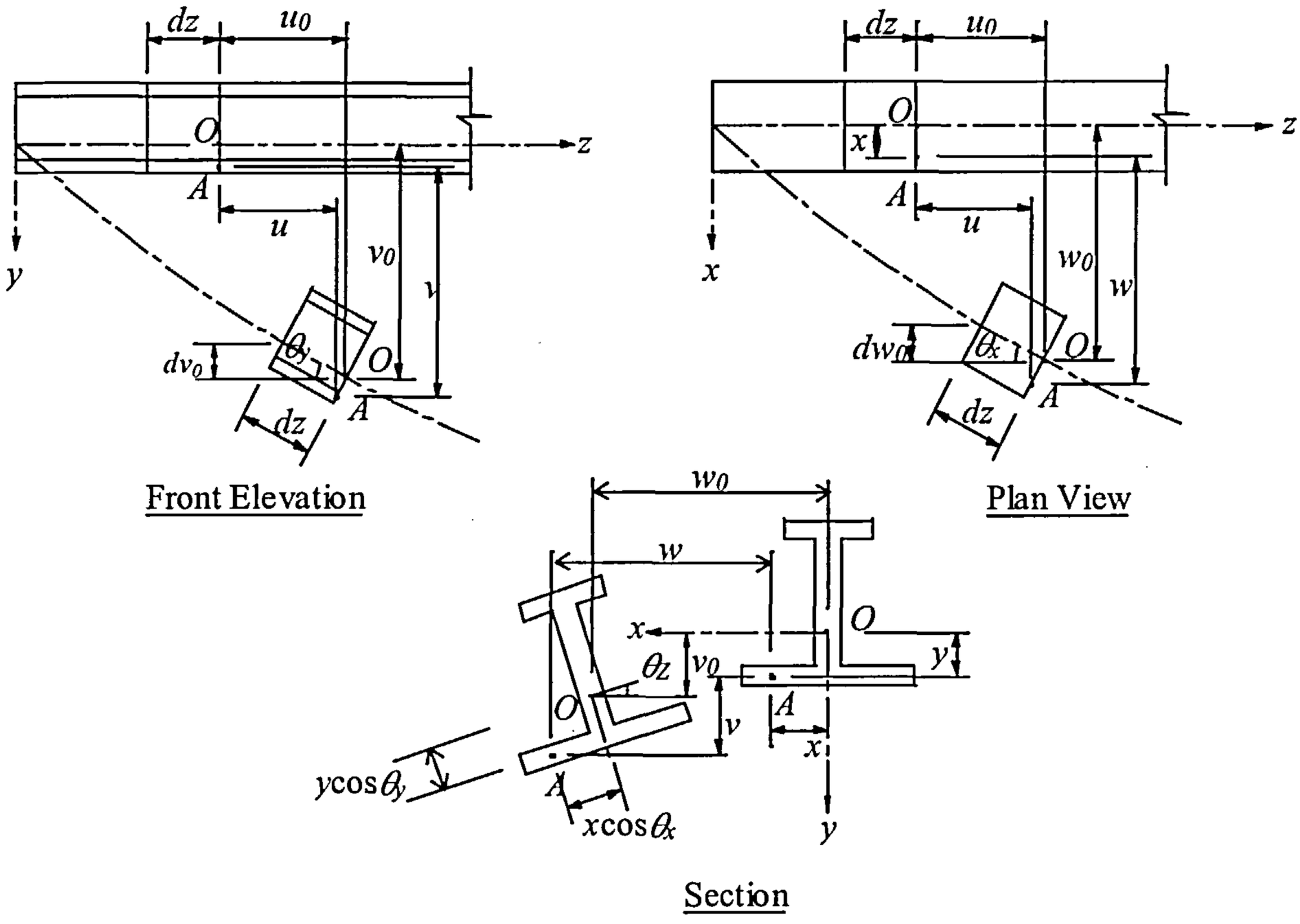

Fig. 6-1 Definition of the displacement of an arbitrary point on the asymmetric cross-section

Based on the above assumptions the displacements u, v, w of an arbitrary point A on the asymmetric beam cross-section (Fig. 6-1) can be derived from geometry and expressed in terms of the displacement of the reference axis by the following expressions,

$$u = u_0 - (y \sin\theta_y + x \sin\theta_x) \tag{6-1a}$$

$$v = v_0 - y + (y \cos\theta_y \cos\theta_z + x \cos\theta_x \sin\theta_z) \tag{6-1b}$$

$$w = w_0 - x + (x \cos\theta_x \cos\theta_z - y \cos\theta_y \sin\theta_z) \tag{6-1c}$$

in which x and y are the co-ordinates of point A. The reference axis for displacements is the axis of the undeformed elements.

From the above assumptions the slope of the member in the x and y-directions respectively is given by:

$$w_0' = \sin\theta_x \tag{6-2a}$$

$$v_0' = \sin\theta_y \tag{6-2b}$$

Although the slopes could be represented by tangents, the sine assumption gives a better representation for large-displacement problems.

The twist angle θ_z is small, so that

$$\sin\theta_z = \theta_z \tag{6-3a}$$

and

$$\cos\theta_z = 1 \tag{6-3b}$$

Then Eqns. (1) can be rewritten as:

$$u = u_0 - (y v_0' + x w_0') \tag{6-4a}$$

$$v = v_0 - y + (y \cos\theta_y + x\theta_z \cos\theta_x) \tag{6-4b}$$

$$w = w_0 - x + (x \cos\theta_x - y\theta_z \cos\theta_y) \tag{6-4c}$$

Eqn. (6-4a) is based on the assumption that plane sections remain plane after deformation so that it only represents the axial deformation. However for thin-walled

beams it is necessary to take account of the effect of warping[79]. Adding the warping term, Eqn. (6-4a) becomes:

$$u = u_0 - yv_0' - xw_0' + \omega\theta_z' \tag{6-5}$$

where ω is the sectorial co-ordinate of the arbitrary point A as illustrated in Fig. 6-2.

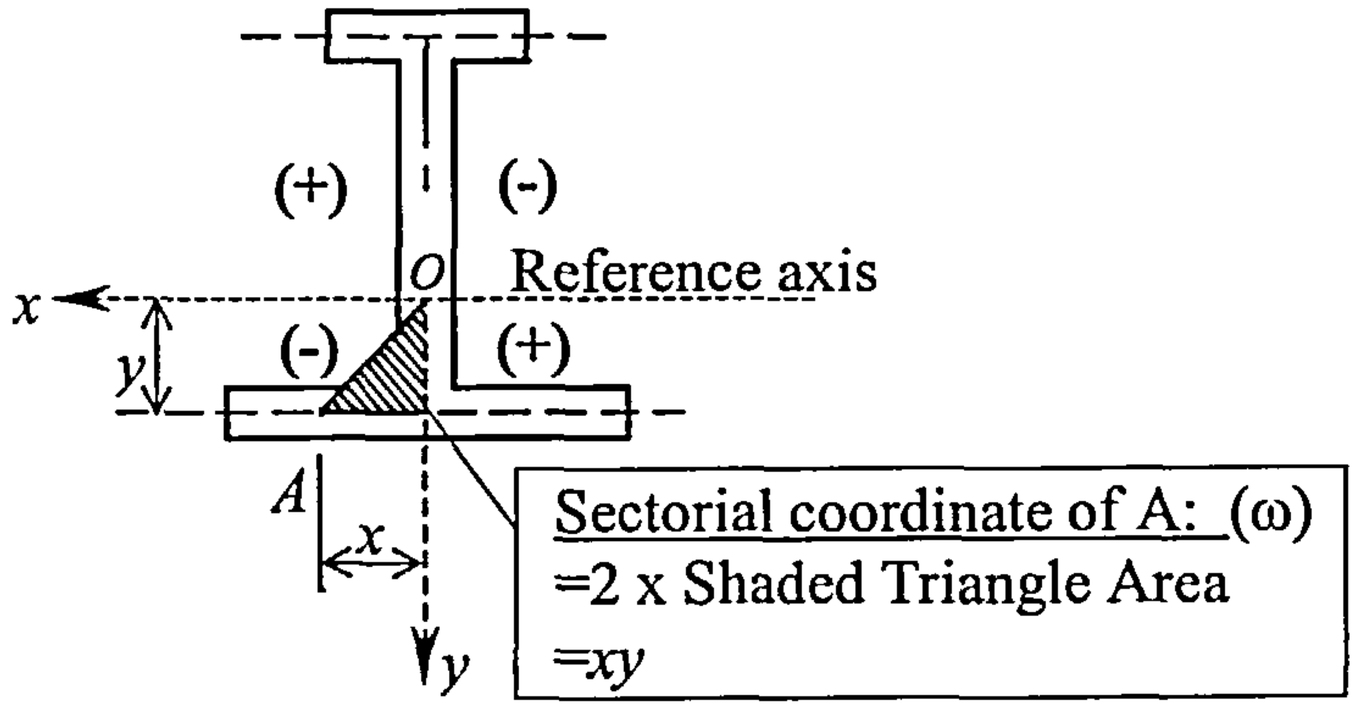

Fig. 6-2 Definition of sectorial co-ordinate of the arbitrary point *A*

For thin-walled beams, the axial strain ε_z at any arbitrary point A can be obtained from the large strain-displacement relationship[69,80] in terms of the derivatives of displacements of the reference axis from:

$$\varepsilon_z = u' + \frac{1}{2}[(u')^2 + (v')^2 + (w')^2] \tag{6-6}$$

Substituting Eqns. (6-4b), (6-4c) and (6-5) into (6-6), and letting $\cos\theta_y = \sqrt{1-(v_0')^2}$, $\cos\theta_x = \sqrt{1-(w_0')^2}$, $v_0'' = \cos\theta_y \frac{d\theta_y}{dz}$, and $w_0'' = \cos\theta_x \frac{d\theta_x}{dz}$ produces

$$\varepsilon_z = u_0' - yv_0'' - xw_0'' + \omega\vartheta_z'' + \frac{1}{2}(u_0')^2 - yu_0'v_0'' - xu_0'w_0'' + \omega u_0'\theta_z'' + \frac{1}{2}(yv_0'')^2 + \frac{1}{2}(xw_0'')^2$$
$$+\frac{1}{2}(v_0')^2 - \frac{yv_0''(v_0')^2}{\sqrt{1-(v_0')^2}} + v_0'x\theta_z'\sqrt{1-(w_0')^2} + \frac{1}{2}y^2\frac{(v_0')^2(v_0'')^2}{1-(v_0')^2}$$
$$\frac{1}{2}x^2(\theta_z')^2(1-(w_0')^2) + \frac{1}{2}(w_0')^2 - \frac{xw_0''(w_0')^2}{\sqrt{1-(w_0')^2}} - w_0'y\theta_z'\sqrt{1-(v_0')^2}$$

$$+\frac{1}{2}x^2\frac{(w_0')^2(w_0'')^2}{1-(w_0')^2}+\frac{1}{2}y^2(\theta_z')^2(1-(v_0')^2) \tag{6-7}$$

For the shear stain, the non-linear shear strain-displacement relationships[69,80] are given by

$$\gamma_{xz}=\frac{\partial u}{\partial x}+\frac{\partial w}{\partial z}+(\frac{\partial w}{\partial x}\cdot\frac{\partial w}{\partial z}+\frac{\partial v}{\partial x}\cdot\frac{\partial v}{\partial z}+\frac{\partial u}{\partial x}\cdot\frac{\partial u}{\partial z}) \tag{6-8a}$$

and,

$$\gamma_{yz}=\frac{\partial u}{\partial y}+\frac{\partial v}{\partial z}+(\frac{\partial w}{\partial y}\cdot\frac{\partial w}{\partial z}+\frac{\partial v}{\partial y}\cdot\frac{\partial v}{\partial z}+\frac{\partial u}{\partial y}\cdot\frac{\partial u}{\partial z}) \tag{6-8b}$$

Ignoring higher-order terms, the above shear strains can simply be expressed as:

$$\gamma_{xz}=v_0'\theta_z \tag{6-9a}$$

and

$$\gamma_{yz}=-w_0'\theta_z \tag{6-9b}$$

Applying the principle of virtual work over the length of the asymmetric member,

$$\delta W=\int_v(\sigma_z\delta\varepsilon_z+\tau_{xz}\delta\gamma_{xz}+\tau_{yz}\delta\gamma_{yz})dv-<Q>\{\delta q\}=0 \tag{6-10}$$

in which $\delta\varepsilon_z$ is the incremental variation in axial strain, and $\delta\gamma_{xz},\delta\gamma_{yz}$ are the incremental variations in shear strain, $\{\delta q\}$ is the column vector of incremental deformations.

Because strains can be expressed in terms of a discrete set of nodal displacement co-ordinates q_i through shape functions, Eqn. (6-10) may be written for the stationary state as[8, 9]

$$\psi_i = \frac{\partial W}{\partial q_i} = 0 \tag{6-11a}$$

where i has the range N (the number of local degrees of freedom per node),

and $$\psi_i = \int_l \int_A (\sigma_z \frac{\partial \varepsilon_z}{\partial q_i} + \tau_{xz} \frac{\partial \gamma_{xz}}{\partial q_i} + \tau_{yz} \frac{\partial \gamma_{yz}}{\partial q_i}) dA dz - Q_i \tag{6-11b}$$

If Eqn. (6-11b) is not satisfied exactly, it may be solved using a numerical method (such as the Newton-Raphson method)[69], and therefore the following equation can be obtained:

$$\Delta \psi_i = \frac{\partial \psi_i}{\partial q_j} \Delta q_j = -\psi_i \tag{6-12}$$

where the repeated-index summation convention is used and j also has a range of N.

Substituting Eqn. (6-11b) into Eqn. (6-12) for repeated indices j and i produces

$$\int_l \int_A (\frac{\partial \sigma_z}{\partial q_j} \frac{\partial \varepsilon_z}{\partial q_i} + \frac{\partial \tau_{xz}}{\partial q_j} \frac{\partial \gamma_{xz}}{\partial q_i} + \frac{\partial \tau_{yz}}{\partial q_i} \frac{\partial \gamma_{yz}}{\partial q_i}) dA dz \cdot \Delta q_j$$

$$= Q_i - \int_l \int_A (\sigma_z \frac{\partial \varepsilon_z}{\partial q_i} + \tau_{xz} \frac{\partial \gamma_{xz}}{\partial q_i} + \tau_{yz} \frac{\partial \gamma_{yz}}{\partial q_i}) dA dz \tag{6-13}$$

Finally, we have the basic finite element formulation[10,63] as follows:

$$[K_T]\{\Delta q\} = \{\Delta Q\} \tag{6-14}$$

where $[K_T]$ is the element tangent stiffness matrix, given by

$$(K_T)_{ij} = \int_l \int_A (\frac{\partial \sigma_z}{\partial q_j} \frac{\partial \varepsilon_z}{\partial q_i} + \frac{\partial \tau_{xz}}{\partial q_j} \frac{\partial \gamma_{xz}}{\partial q_i} + \frac{\partial \tau_{yz}}{\partial q_i} \frac{\partial \gamma_{yz}}{\partial q_i}) dA dz$$

$\{\Delta Q\}$ is the load vector of unbalanced forces, given by

$$\Delta Q_i = Q_i - \int_l \int_A (\sigma_z \frac{\partial \varepsilon_z}{\partial q_i} + \tau_{xz} \frac{\partial \gamma_{xz}}{\partial q_i} + \tau_{yz} \frac{\partial \gamma_{yz}}{\partial q_i}) dA dz$$

and $\{\Delta q\}$ is the vector of incremental displacements.

The external virtual work done by the applied loads balances the virtual work of the internal stresses. In the fire condition, this means that the internal work should exclude other influences, such as thermal effects caused by the heating scheme and residual stresses from manufacturing processes. So the internal stresses (σ_z) should include only those stresses due to external load. The analysis requires the relationship between stress and strain to be specified as a function of temperature. Various representations, such as those specified in EC3 Part 1.2[46] (Fig. 6-3) and BS5950 Part 8[47], can be used. Alternatively, a mathematical relationship, such as a modified Ramberg-Osgood equation [4,83], can be fitted to the basic high-temperature data for the material.

It is evident that at each sampling point the strains use axial mechanical strains which can be obtained by

$$\varepsilon_{zm} = \varepsilon_{zt} - \varepsilon_{zr} - \varepsilon_{zth} \qquad (6\text{-}15)$$

In this chapter, since two-noded one-dimensional elements are used to model asymmetric members, it is assumed that the shear strains caused by thermal expansion are equal to zero. The effect of thermal axial strains is modelled using the relationship defined in Eurocode 3 Part 1.2[46] as shown in Fig. 6-4, although a constant coefficient of thermal expansion may also be used, giving[84]

$$\varepsilon_{zth} = \int_{T_1}^{T_2} \alpha(t) dt \qquad \text{or} \qquad \varepsilon_{zth} = \alpha(\Delta T) \qquad (6\text{-}16)$$

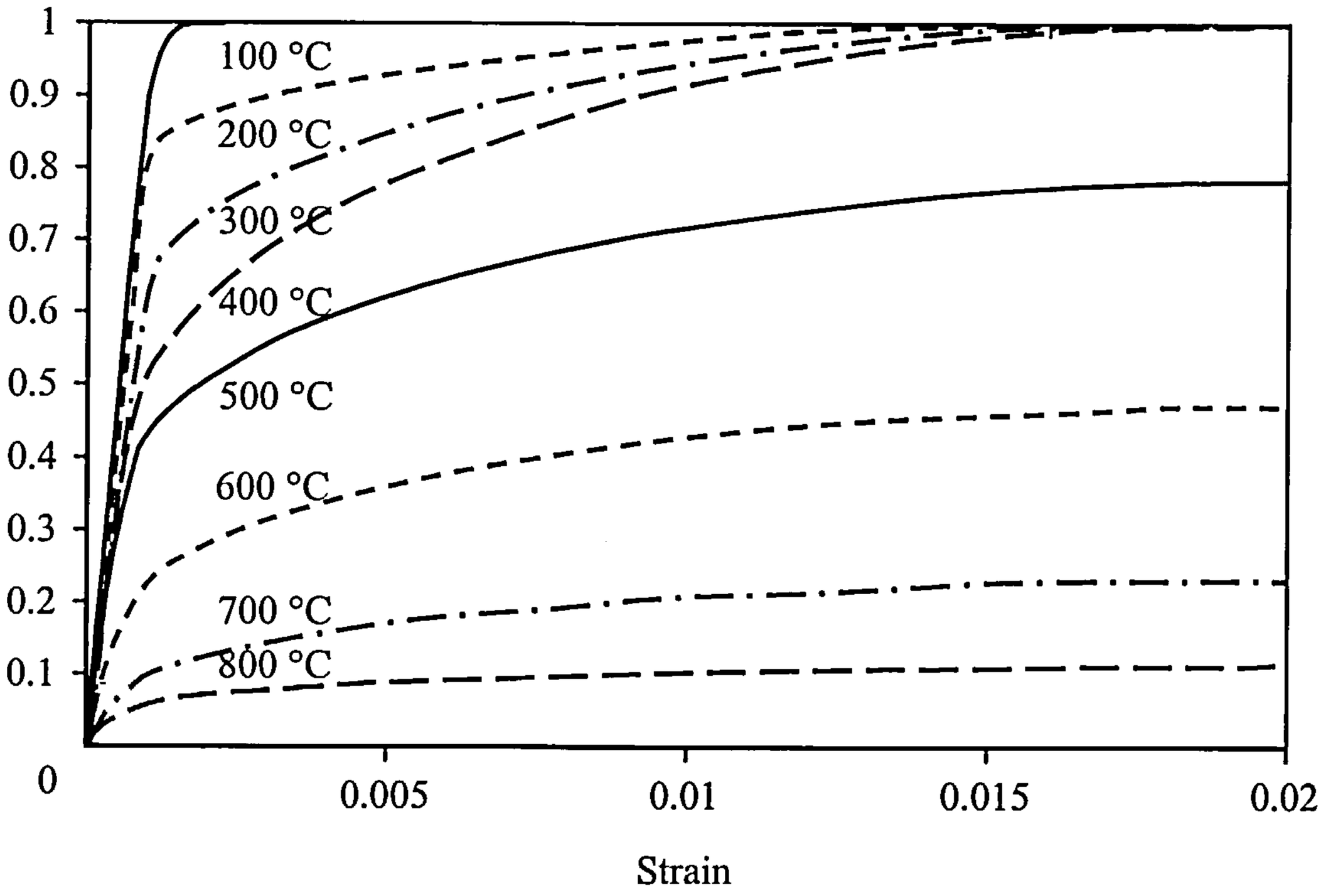

Fig. 6-3 Stress-strain relationships of structural steel at elevated temperatures; strain-hardening not included.

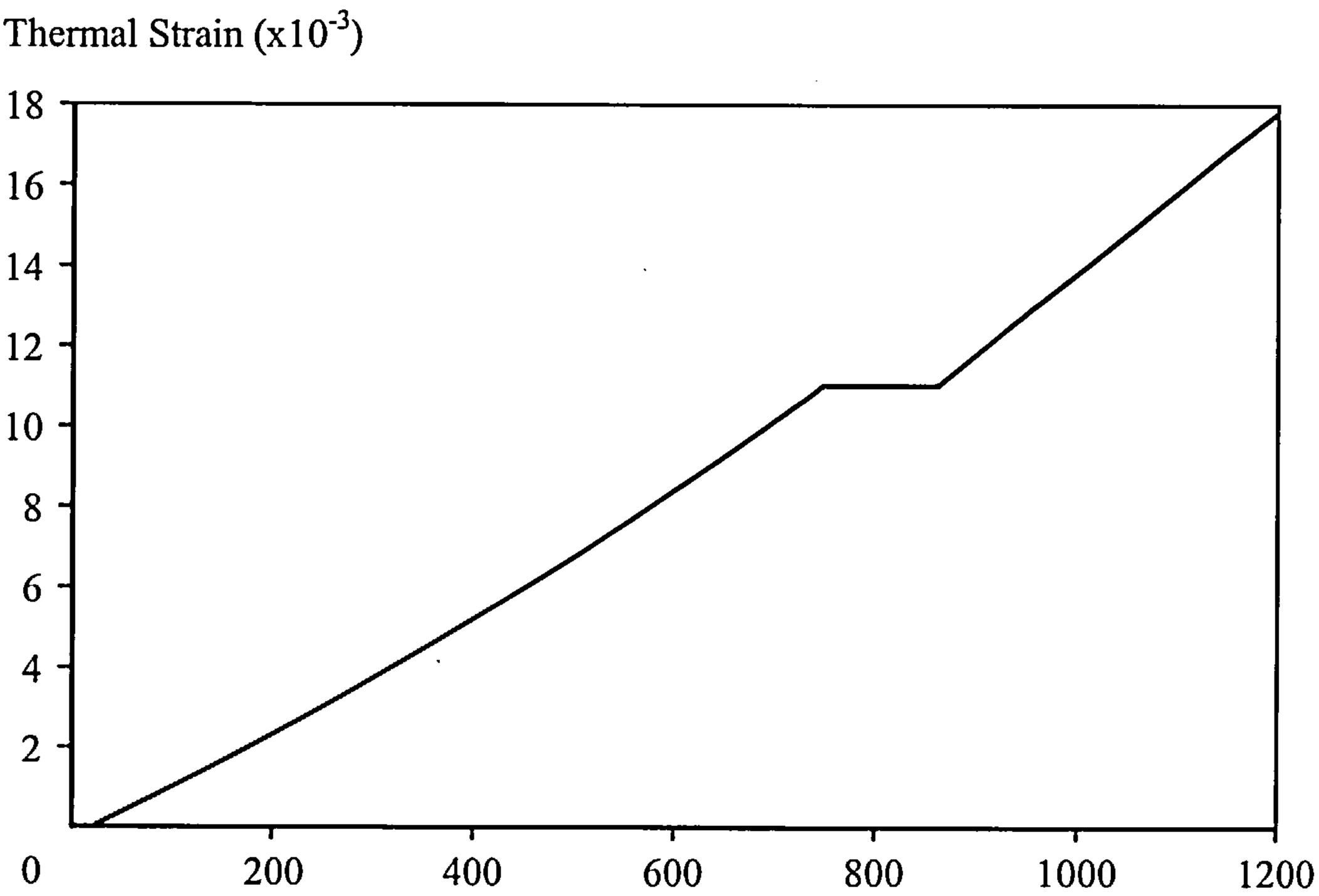

Fig. 6-4 Thermal strain of steel as a function of temperature.

6.3 MEMBER REFINEMENT AND NUMERICAL SOLUTION

In this study, two-noded one-dimensional elements are used for computational efficiency. The cross-section can be divided into segments as finely as necessary. This allows a more accurate representation of the structural behaviour of the section and enables non-linear temperature distributions to be modelled. The cross-section contains (6N+1) sampling points. The section properties and stress resultants are specified according to the formulations which have been given here for an asymmetric member.

6.3.1 SECTION PROPERTIES AND STRESS RESULTANTS

From Fig. 6-5 the section properties and stress resultants can be obtained.

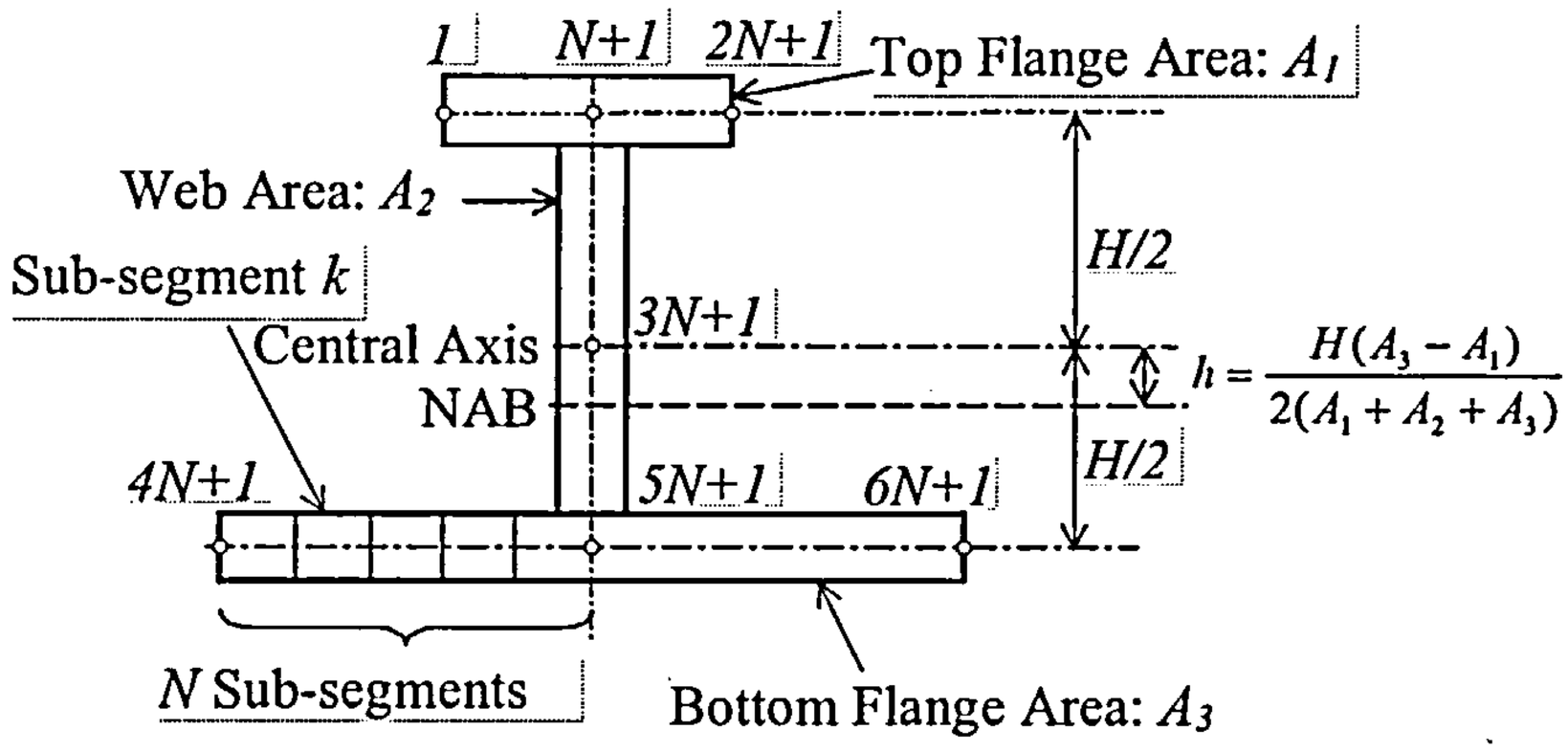

Fig. 6-5 Division of asymmetric beam-column cross-section.

Section properties:

$$A = \int_A dA = \sum_{r=1}^{3}\sum_{k=1}^{2N} A_{rk} \tag{6-17a}$$

$$I_x = \int_A (x_0 + \Delta x)dA = \int_{A_1+A_2+A_3} (x_0 + \Delta x)dA = \sum_{r=1}^{3}\sum_{k=1}^{2N} (A_{rk}\Delta x) \tag{6-17b}$$

$$I_y = \int_A (y_0 + \Delta y)dA = \int_{A_1+A_2+A_3} (y_0 + \Delta y)dA = \sum_{r=1}^{3}\sum_{k=1}^{2N} (A_{rk}\Delta y) \tag{6-17c}$$

$$I_{x2} = \int_A (x_0 + \Delta x)^2 dA = \int_{A_1+A_2+A_3} (x_0 + \Delta x)^2 dA = \sum_{r=1}^{3} \sum_{k=1}^{2N} (Iyy_{rk} + A_{rk} \Delta x^2) \qquad (6\text{-}17d)$$

$$I_{y2} = \int_A (y_0 + \Delta y)^2 dA = \int_{A_1+A_2+A_3} (y_0 + \Delta y)^2 dA = \sum_{r=1}^{3} \sum_{k=1}^{2N} (Ixx_{rk} + A_{rk} \Delta y^2) \qquad (6\text{-}17e)$$

$$I_{x3} = \int_A (x_0 + \Delta x)^3 dA = \int_{A_1+A_2+A_3} (x_0 + \Delta x)^3 dA = \sum_{r=1}^{3} \sum_{k=1}^{2N} (3Iyy_{rk} \Delta x + A_{rk} \Delta x^3) \qquad (6\text{-}17f)$$

$$I_{y3} = \int_A (y_0 + \Delta y)^3 dA = \int_{A_1+A_2+A_3} (y_0 + \Delta y)^3 dA = \sum_{r=1}^{3} \sum_{k=1}^{2N} (3Ixx_{rk} \Delta y + A_{rk} \Delta y^3) \qquad (6\text{-}17g)$$

$$I_{x4} = \int_A (x_0 + \Delta x)^4 dA = \int_{A_1+A_2+A_3} (x_0 + \Delta x)^4 dA = \sum_{r=1}^{3} \sum_{k=1}^{2N} (I_4 yy_{rk} + 6Iyy_{rk} \Delta x^2 + A_{rk} \Delta x^4)$$

(6-17h)

$$I_{y4} = \int_A (y_0 + \Delta y)^4 dA = \int_{A_1+A_2+A_3} (y_0 + \Delta y)^4 dA = \sum_{r=1}^{3} \sum_{k=1}^{2N} (I_4 xx_{rk} + 6Ixx_{rk} \Delta y^2 + A_{rk} \Delta y^4)$$

(6-17i)

$$I_{xy} = \int_A (x_0 + \Delta x)(y_0 + \Delta y) dA = \int_{A_1+A_2+A_3} (x_0 + \Delta x)(y_0 + \Delta y) dA = \sum_{r=1}^{3} \sum_{k=1}^{2N} (A_{rk} \Delta x \Delta y)$$

(6-17j)

$$I_{x2y} = \int_A (x_0 + \Delta x)^2 (y_0 + \Delta y) dA = \int_{A_1+A_2+A_3} (x_0 + \Delta x)^2 (y_0 + \Delta y) dA$$

$$= \sum_{r=1}^{3} \sum_{k=1}^{2N} (Iyy_{rk} \Delta y + A_{rk} \Delta x^2 \Delta y) \qquad (6\text{-}17k)$$

$$I_{xy2} = \int_A (x_0 + \Delta x)(y_0 + \Delta y)^2 dA = \int_{A_1+A_2+A_3} (x_0 + \Delta x)(y_0 + \Delta y)^2 dA$$

$$= \sum_{r=1}^{3} \sum_{k=1}^{2N} (Ixx_{rk} \Delta x + A_{rk} \Delta x \Delta y^2) \qquad (6\text{-}17l)$$

$$I_{x2y2} = \int_A (x_0 + \Delta x)^2 (y_0 + \Delta y)^2 dA = \int_{A_1+A_2+A_3} (x_0 + \Delta x)^2 (y_0 + \Delta y)^2 dA$$

$$= \sum_{r=1}^{3} \sum_{k=1}^{2N} (Ixx_{rk} \Delta x^2 + Iyy_{rk} \Delta y^2 + A_{rk} \Delta x^2 \Delta y^2 + Ixxyy_{rk}) \qquad (6\text{-}17m)$$

where the co-ordinate system is defined in Fig. 6-6. Also, defining l and t as the breadth and thickness of any plate segment in the section (which means that l is an x-measurement in the flanges and a y-measurement in the web), the sectorial properties are

$$I_{\omega} = \int_{A_1+A_2+A_3} \omega dA = \sum_{r=1}^{3}\sum_{k=1}^{2N} \frac{lt}{2}(\omega_{i_{rk}} + \omega_{j_{rk}}) \qquad (6\text{-}17n)$$

$$I_{\omega x} = \int_{A_1+A_2+A_3} \omega x dA = \sum_{r=1}^{3}\sum_{k=1}^{2N} \frac{lt}{6}[\omega_{i_{rk}}(x_{j_{rk}} + 2x_{i_{rk}}) + \omega_{j_{rk}}(x_{i_{rk}} + 2x_{j_{rk}})] \qquad (6\text{-}17o)$$

$$I_{\omega x2} = \int_{A_1+A_2+A_3} \omega x^2 dA = \sum_{r=1}^{3}\sum_{k=1}^{2N} \frac{lt}{12}\{\omega_{i_{rk}}[4x_{i_{rk}}^2 + 2x_{j_{rk}}^2 + \frac{t^2}{2} - (x_{j_{rk}} - x_{i_{rk}})^2(1 + \frac{t^2}{2l^2})]$$

$$+ \omega_{j_{rk}}[4x_{j_{rk}}^2 + 2x_{i_{rk}}^2 + \frac{t^2}{2} - (x_{j_{rk}} - x_{i_{rk}})^2(1 + \frac{t^2}{2l^2})]\} \qquad (6\text{-}17p)$$

$$I_{\omega y} = \int_{A_1+A_2+A_3} \omega y dA = \sum_{r=1}^{3}\sum_{k=1}^{2N} \frac{lt}{6}[\omega_{i_{rk}}(y_{j_{rk}} + 2y_{i_{rk}}) + \omega_{j_{rk}}(y_{i_{rk}} + 2y_{j_{rk}})] \qquad (6\text{-}17q)$$

$$I_{\omega y2} = \int_{A_1+A_2+A_3} \omega y^2 dA = \sum_{r=1}^{3}\sum_{k=1}^{2N} \frac{lt}{12}\{\omega_{i_{rk}}[4y_{i_{rk}}^2 + 2y_{j_{rk}}^2 + \frac{t^2}{2} - (y_{j_{rk}} - y_{i_{rk}})^2(1 + \frac{t^2}{2l^2})]$$

$$+ \omega_{j_{rk}}[4y_{j_{rk}}^2 + 2y_{i_{rk}}^2 + \frac{t^2}{2} - (y_{j_{rk}} - y_{i_{rk}})^2(1 + \frac{t^2}{2l^2})]\} \qquad (6\text{-}17r)$$

$$I_{\omega 2} = \int_{A_1+A_2+A_3} \omega^2 dA = \sum_{r=1}^{3}\sum_{k=1}^{2N} \frac{lt}{3}(\omega_{i_{rk}}^2 + \omega_{i_{rk}}\omega_{j_{rk}} + \omega_{j_{rk}}^2) \qquad (6\text{-}17s)$$

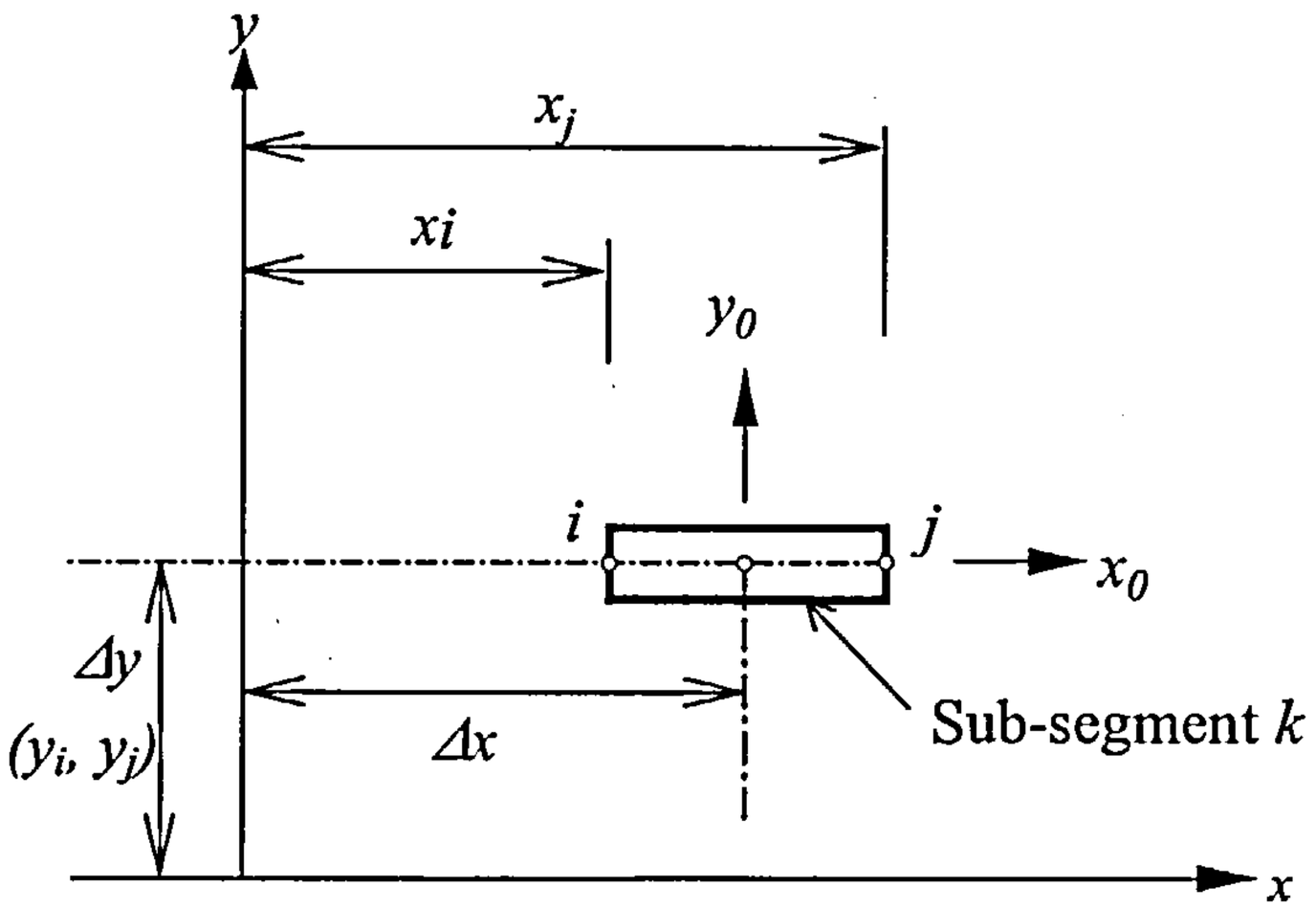

Fig. 6-6 Co-ordinate system for segments

Stress resultants:

$$n = \int_{A_1+A_2+A_3} \sigma_z dA = \sum_{r=1}^{3}\sum_{k=1}^{2N} \frac{lt}{2}(\sigma_{i_{rk}} + \sigma_{k_{rk}}) \qquad (6\text{-}18a)$$

$$m_x = \int_{A_1+A_2+A_3} \sigma_z y dA = \sum_{r=1}^{3}\sum_{k=1}^{2N} \frac{lt}{6}[\sigma_{i_{rk}}(y_{j_{rk}} + 2y_{i_{rk}}) + \sigma_{j_{rk}}(y_{i_{rk}} + 2y_{j_{rk}})] \qquad (6\text{-}18b)$$

$$m_{x2} = \int_{A_1+A_2+A_3} \sigma_z y^2 dA = \sum_{r=1}^{3}\sum_{k=1}^{2N} \frac{lt}{12}\{\sigma_{i_{rk}}[4y_{i_{rk}}^2 + 2y_{j_{rk}}^2 + \frac{t^2}{2} - (y_{j_{rk}} - y_{i_{rk}})^2(1+\frac{t^2}{2l^2})]$$

$$+\sigma_{j_{rk}}[4y_{j_{rk}}^2 + 2y_{i_{rk}}^2 + \frac{t^2}{2} - (y_{j_{rk}} - y_{i_{rk}})^2(1+\frac{t^2}{2l^2})]\} \qquad (6\text{-}18c)$$

$$m_y = \int_{A_1+A_2+A_3} \sigma_z x dA = \sum_{r=1}^{3}\sum_{k=1}^{2N} \frac{lt}{6}[\sigma_{i_{rk}}(x_{j_{rk}} + 2x_{i_{rk}}) + \sigma_{j_{rk}}(x_{i_{rk}} + 2x_{j_{rk}})] \qquad (6\text{-}18d)$$

$$m_{y2} = \int_{A_1+A_2+A_3} \sigma_z x^2 dA = \sum_{r=1}^{3}\sum_{k=1}^{2N} \frac{lt}{12}\{\sigma_{i_{rk}}[4x_{i_{rk}}^2 + 2x_{j_{rk}}^2 + \frac{t^2}{2} - (x_{j_{rk}} - x_{i_{rk}})^2(1+\frac{t^2}{2l^2})]$$

$$+\sigma_{j_{rk}}[4x_{j_{rk}}^2 + 2x_{i_{rk}}^2 + \frac{t^2}{2} - (x_{j_{rk}} - x_{i_{rk}})^2(1+\frac{t^2}{2l^2})]\} \qquad (6\text{-}18e)$$

$$m_\omega = \int_{A_1+A_2+A_3} \sigma_z \omega dA = \sum_{r=1}^{3}\sum_{k=1}^{2N} \frac{lt}{6}[\sigma_{i_{rk}}(\omega_{j_{rk}} + 2\omega_{i_{rk}}) + \sigma_{j_{rk}}(\omega_{i_{rk}} + 2\omega_{j_{rk}})] \qquad (6\text{-}18f)$$

$$m_{z2} = \int_{A_1+A_2+A_3} \sigma_z (x^2+y^2)\theta_z' dA = \sum_{r=1}^{3}\sum_{k=1}^{2N} \frac{lt}{12}\theta_z'\{\sigma_{i_{rk}}[4(x_{i_{rk}}^2 + y_{i_{rk}}^2) + 2(x_{j_{rk}}^2 + y_{j_{rk}}^2) + \frac{t^2}{2} - l^2]$$

$$+\sigma_{j_{rk}}[4(x_{j_{rk}}^2 + y_{j_{rk}}^2) + 2(x_{i_{rk}}^2 + y_{i_{rk}}^2) + \frac{t^2}{2} - l^2]\} \qquad (6\text{-}18g)$$

$$f_x = \int_{A_1+A_2+A_3} \tau_{xz} dA = \sum_{r=1}^{3}\sum_{k=1}^{2N} \frac{lt}{2}(\tau_{xzi_{rk}} + \tau_{xzj_{rk}}) \qquad (6\text{-}18h)$$

$$f_y = \int_{A_1+A_2+A_3} \tau_{yz} dA = \sum_{r=1}^{3}\sum_{k=1}^{2N} \frac{lt}{2}(\tau_{yzi_{rk}} + \tau_{yzj_{rk}}) \qquad (6\text{-}18i)$$

where all calculations are based on the transformed section so that, taking into account material non-linearity and thermal effects, the thickness of each of segment is transformed by $t_t = t\left[\frac{E_t}{E}\right]$, in which t_t is the transformed thickness of the plate segment, E_t is the average tangent modulus of the material within the segment at the appropriate temperature, t is the original thickness of the plate segment, and E is the original Young's Modulus of the material within the segment at ambient temperature. By reducing the thickness of each plate segment but not its length, the original mid-

surface contour is maintained; this is very important. Certain sectional moments of area related to the segment centroids are included in these equations as follows:

$$I_{xxyy} = \int_{A_0} y_0^2 x_0^2 dA = \frac{t^3 l^3}{144} \tag{6-19a}$$

$$I_{4xx} = \int_{A_0} y_0^4 dA = \frac{bh^5}{80} \tag{6-19b}$$

$$I_{4yy} = \int_{A_0} x_0^4 dA = \frac{hb^5}{80} \tag{6-19c}$$

$$I_{xx} = \int_{A_0} y_0^2 dA = \frac{bh^3}{12} \tag{6-19d}$$

$$I_{yy} = \int_{A_0} x_0^2 dA = \frac{hb^3}{12} \tag{6-19e}$$

Where, b is the side length of a segment measured in the x-direction, and h is its side length in the y-direction.

6.3.2 MEMBER REFINEMENT AND NUMERICAL SOLUTION

The finite element software VULCAN has been extended using the above formulation to include asymmetric members. For the sake of efficiency of the program, the length of each beam element is divided into three sub-elements, one at each end and a central sub-element, representing 10% and 80% respectively of the element length. The cross-section of each sub-element is divided into 6N sub-segments, as shown in Fig. 6-5, each of the flanges and the web containing 2N. Increasing the number of sub-segments increases the accuracy of the results, and also has the advantage of allowing a better representation of the temperature distribution within the cross-section. It was shown in chapter 3 that, for symmetric section beams, using N = 2 (dividing the cross-section into 12 sub-segments) gives sufficiently accurate results. Using the above principles and formulations the displacements, strains and stresses at each "Gauss

point" along the sub-elements can be interpolated at each of the (6N+1) sampling points within the cross-section using the cubic shape functions. Four Gauss points have been used along the length of each sub-element. For the whole beam element a static condensation scheme is applied to eliminate the internal degrees of freedom. The whole structure can be represented by assembling all the member stiffnesses in the usual manner, and imposing external boundary conditions. Standard solution procedures can then be used to determine the nodal displacements. Since the formulations are highly non-linear, in both geometric and material terms, a numerical solution procedure must be used. The Newton-Raphson method, which is probably the most rapidly convergent process for solving such non-linear problems, has been adopted here. The following subroutines were mainly involved in this program development:

- SUBROUTINE MAINMG;
- SUBROUTINE STIFF;
- SUBROUTINE STEP;
- SUBROUTINE STEPF;
- SUBROUTINE GET_INFO;
- SUBROUTINE INPUT2;
- SUBROUTINE GET_SECT;
- SUBROUTINE GET_MEMB.

6.3.3 POSITION OF REFERENCE AXIS

In the software the default beam reference axis, which is the nodal position within the cross-section, is assumed to be at the Neutral Axis for Elastic Bending (**NAB**). Since the shift of the reference axis from its neutral position may induce an additional

moment and it is known that only the moment causes the curvature or bending of the member, the different reference axis position will lead to a different vertical deflection except the pinned support at which no moment is provided. Due to the significant effect of the reference axis, determining its position is one of the most important steps in the process.

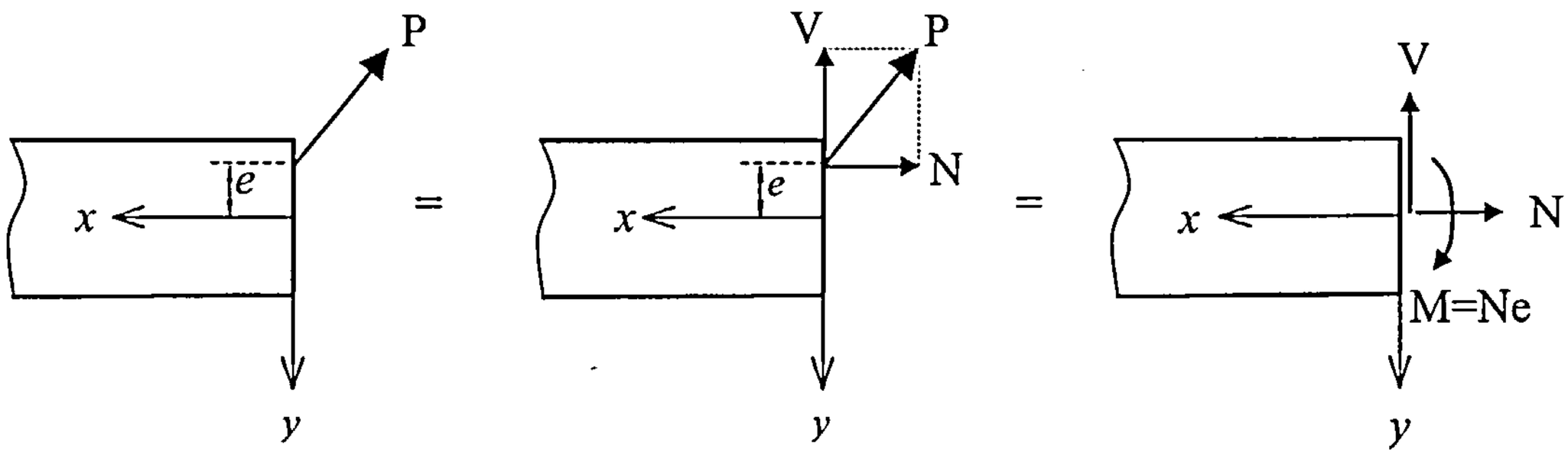

Fig. 6-7 Forces decomposed (where *x*-axis is NAB, *e* is eccentricity from NAB)

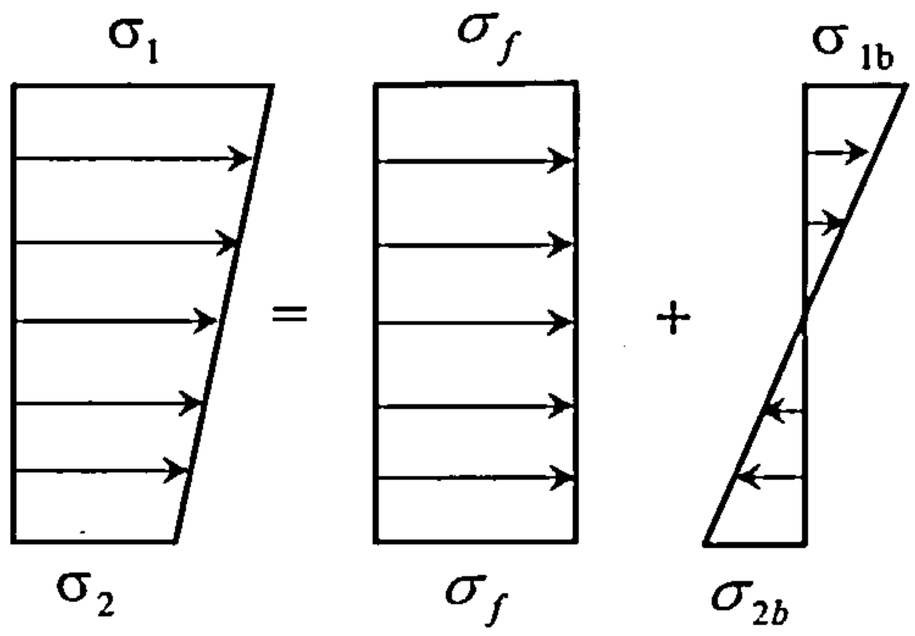

(a) Normal stress (b) Axial (c) bending

Fig. 6-8 Normal stresses decomposed for elastic phase.

Let us consider a normal situation, any resultant force **P** acting upon the section can be decomposed into three components; namely an axial force **N** at the **NAB**, a bending moment **M** about the **NAB** and a shear force **V** across the section, as shown in Fig. 6-7. The actual position of zero axial strain is not at the **NAB**, except in the case of pure bending action. For elastic behaviour the bending moment **M** produces a linearly varying stress σ_b. Thus the final distribution of normal stress σ caused by axial

force **N** and bending moment **M** is obtained by combining the averaged axial stress ($\sigma_f = N/A$) and bending stress ($\sigma_b = My/I$) as illustrated in Fig. 6-8.

Hence

$$\sigma = \sigma_f + \sigma_b = \frac{N}{A} + \frac{My}{I} \tag{6-20}$$

The shear stress is

$$\tau = VQ / Ib \tag{6-21}$$

where Q is the first moment of the area of the cross-section.

Hence, we can use bending stresses to determine the **NAB**. The resultant axial force due to bending stresses should be zero, and this is expressed by

$$\int_A \sigma_b dA = \int_{A_a} \sigma_{1b} dA + \int_{A_b} \sigma_{2b} dA = 0 \tag{6-22}$$

If the material is at room temperature and linear-elastic, Hooke's law for uniaxial stress ($\sigma = E\varepsilon$) can be used to obtain

$$\sigma_b = E\varepsilon = -Eky \tag{6-23}$$

where strain $\varepsilon = -\frac{y}{\rho} = -ky$ and $k = \frac{1}{\rho}$, if ρ is the radius of curvature, as shown in Fig. 6-9.

Substituting Eqn. (6-23) into Eqn. (6-22) produces

$$-\int_A Ekydy = -\int_{A_a} Eky_1 dA - \int_{A_b} Eky_2 dA = 0 \tag{6-24}$$

Because the curvature k and modulus of elasticity E are constants for the cross section:

$$\int_A ydA = 0 \quad \text{or} \quad \int_{A_a} y_1 dA + \int_{A_b} y_2 dA = 0 \tag{6-25}$$

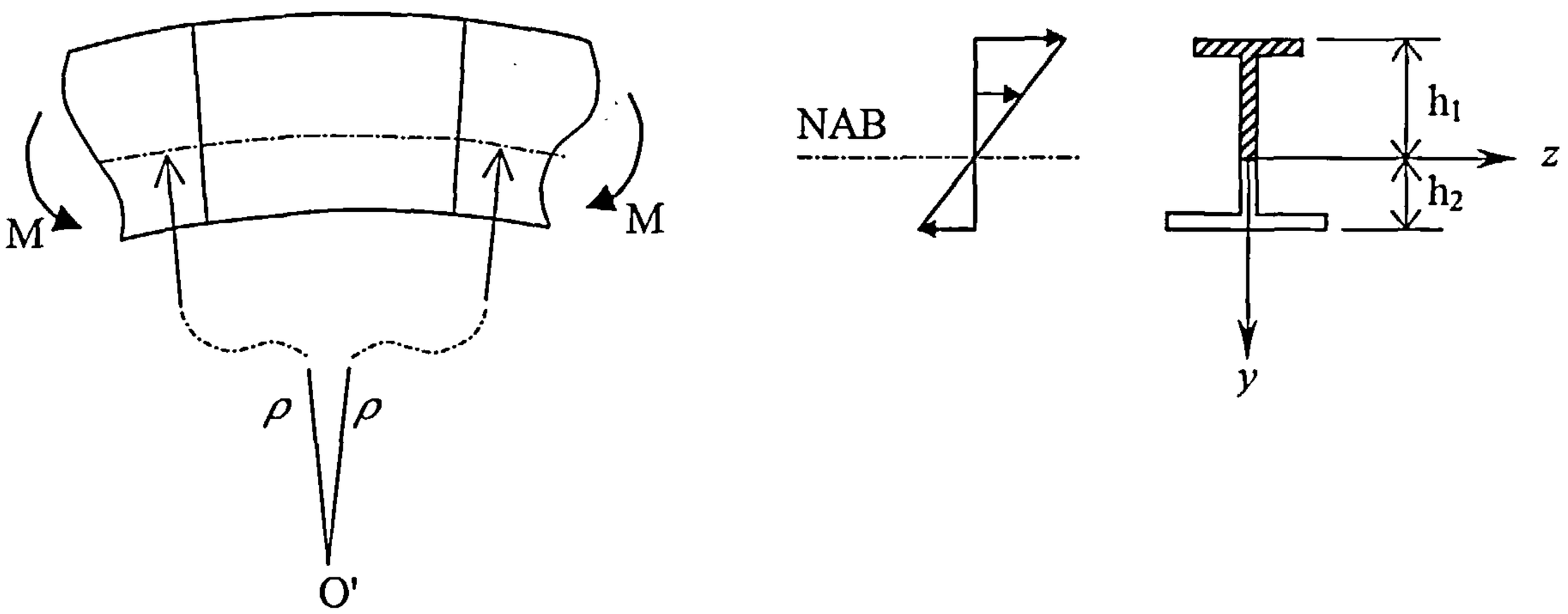

Fig. 6-9 Deformation of beam due to bending stresses

If $S_1 = \int_{A_a} y_1 dA$ and $S_2 = \int_{A_b} y_2 dA$, where S_1 and S_2 are the first moments of the area above and below the NAB respectively, evidently $S_1 + S_2 = 0$ which means that the NAB coincides with the geometric centroid. From Eqn. (6-25):

$$A_1(\frac{H}{2}+h)+A_2h-A_3(\frac{H}{2}-h)=0 \qquad (6\text{-}26)$$

The distance between the mid-depth of the cross section and the **NAB** in the elastic phase is therefore, as shown in Fig. 6-5,

$$h=\frac{H(A_3-A_1)}{2(A_1+A_2+A_2)} \qquad (6\text{-}27)$$

For a beam in the plastic phase, the stress-strain diagram for an homogenous elastic-plastic material has the same yield stress σ_y and the same modulus of elasticity E in both tension and compression as shown in Fig. 10[84].

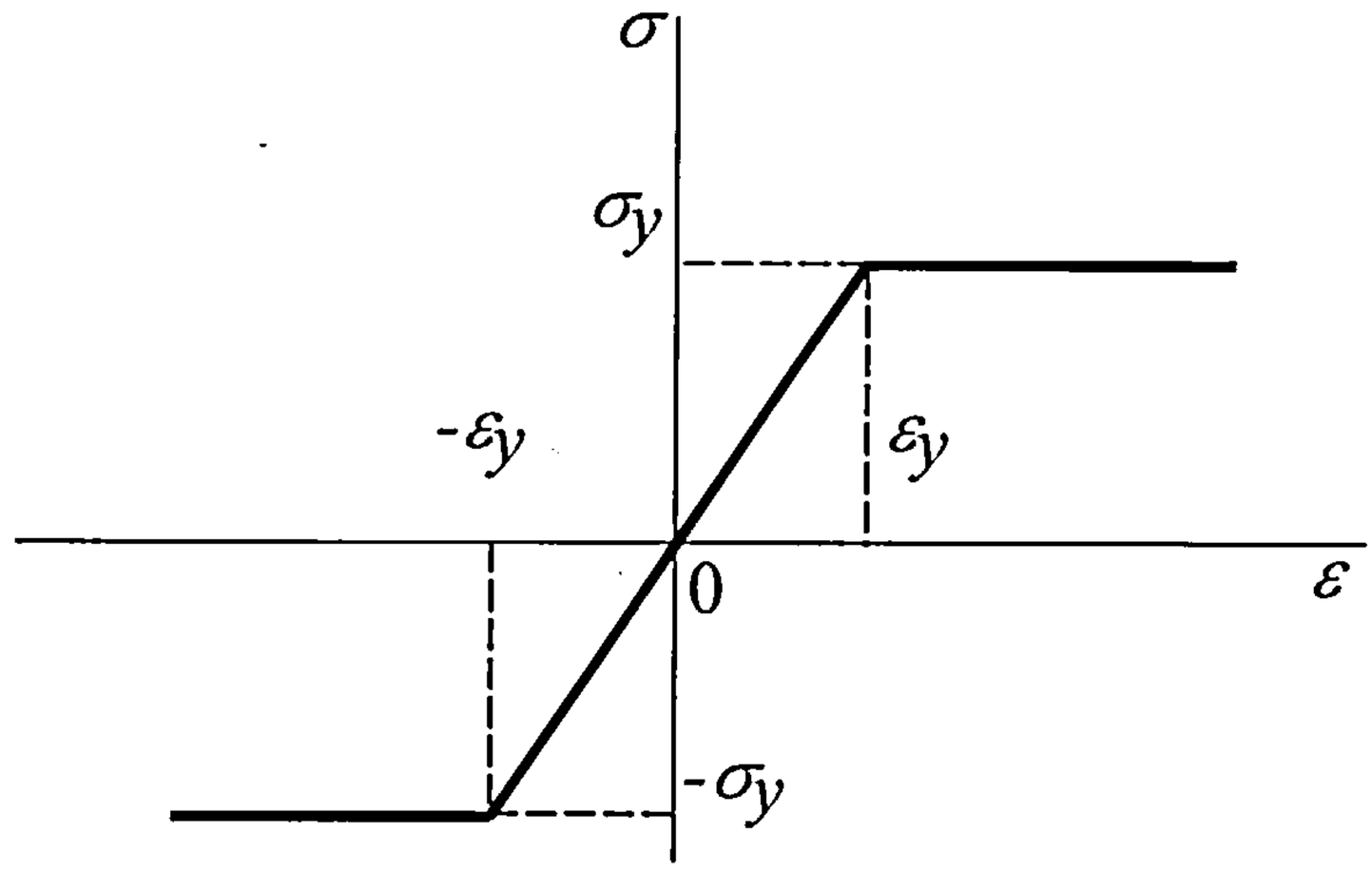

Fig. 6-10 Stress-strain diagram for an elastic-plastic material at room temperature

From equation (6-22)

$$\int_A \sigma_b dA = \int_{A_a} \sigma_y dA - \int_{A_b} \sigma_y dA = 0 \qquad (6\text{-}28)$$

Integrating equation (6-28) we get

$$\sigma_y A_a - \sigma_y A_b = 0 \quad \text{or} \quad \frac{A_a}{A_b} = 1 \qquad (6\text{-}29)$$

For thin flanges (i.e. $A_b >> A_3$ and $A_a >> A_1$) and with reference to Fig. 6-11, equation (6-29) can be written:

$$\sigma_y A_a + \sigma_y T_w \frac{Y}{2} - \sigma_y A_b - \sigma_y T_w \frac{Y}{2} = 0$$

and then there is,

$$A_a + T_w \frac{Y}{2} - A_b - T_w \frac{Y}{2} = 0 \qquad (6\text{-}30)$$

in which T_w is the thickness of the web and the areas A_a and A_b are defined in Fig. 11. So the following equation can be obtained.

$$A_1 + T_w(\frac{H}{2} - \frac{T_{f1}}{2}) + T_w h - A_3 - T_w(\frac{H}{2} - \frac{T_{f2}}{2}) + T_w h = 0 \qquad (6\text{-}31)$$

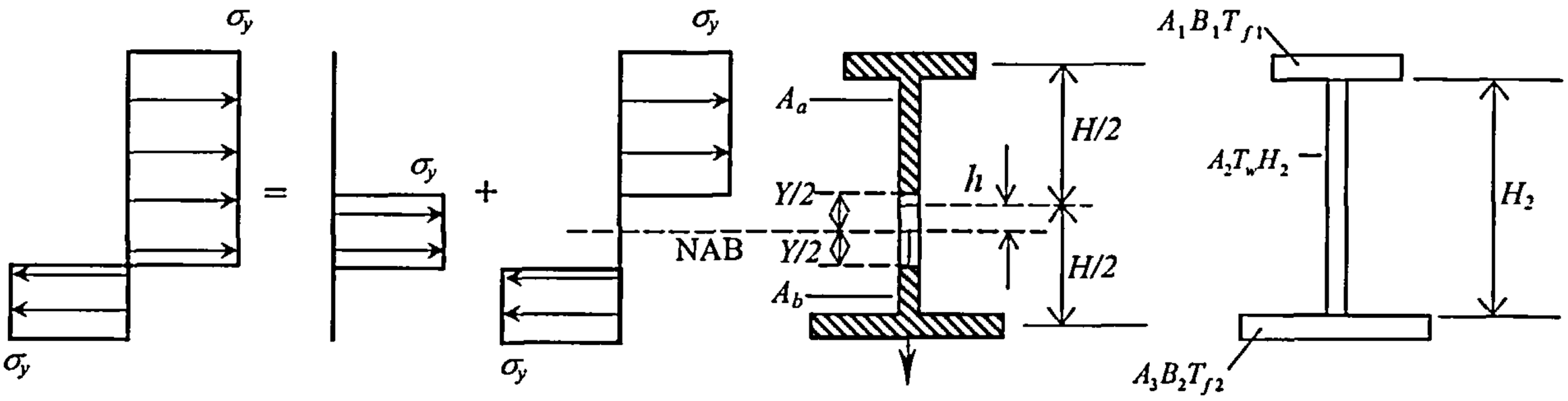

Fig. 6-11 Normal stresses decomposed for plastic phase

From this, the distance between the mid-depth of the cross section and the **NAB** is obtained as

$$h = \frac{A_3 - A_1}{2T_w} + \frac{T_{f1} - T_{f2}}{4} \qquad (6\text{-}32)$$

for the plastic phase.

In the elastic-plastic phase the situation is more complex. The position of the reference axis varies between it is in elasticity and plasticity. Referring to Fig 6-12 and again using the condition that the resultant axial forces due to bending stresses should be zero, we have

$$\int_A \sigma_b dA = \int_{A_{a1}} (\sigma_y - \sigma_f) dA + \int_{A_{a2}} \sigma_b dA + \int_{A_{b1}} \sigma_b dA + \int_{A_{b2}} (\sigma_y + \sigma_f) dA = 0 \qquad (6\text{-}33)$$

so

$$(\sigma_y - \sigma_f) A_{a1} - (\sigma_y + \sigma_f) A_{b2} - Ek \int_{A_{a2}} y dA - Ek \int_{A_{b1}} y dA = 0 \qquad (6\text{-}34)$$

or

$$(\sigma_y - \sigma_f) A_{a1} - (\sigma_y + \sigma_f) A_{b2} - Ek S_{elastic} = 0 \qquad (6\text{-}34a)$$

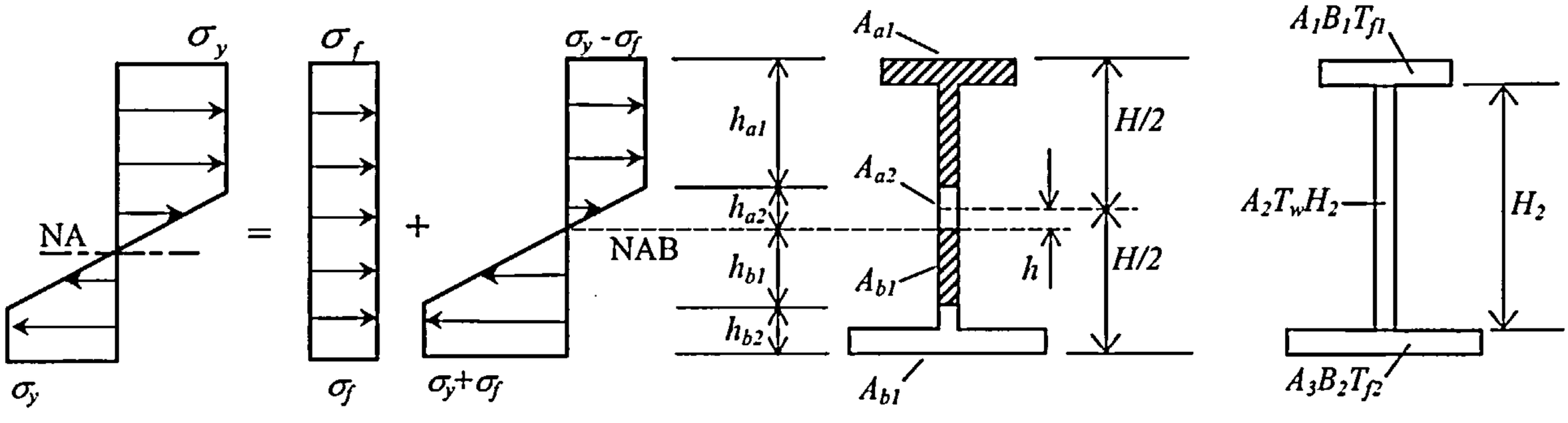

Fig. 6-12 Normal stresses decomposed for elastic-plastic phase (B_1, B_2 and T_{f1}, T_{f2} are top flange, bottom flange width and thickness respectively)

It can be observed that in eqn. (6-34) the first two terms represent the resultant forces ($F_{plastic}$) for the plastic area and the next two items express the resultant forces ($F_{elastic}$) for the elastic zone. For pure bending these must be equal in magnitude but opposite in direction:

$$F_{plastic} = -F_{elastic} \tag{6-35}$$

At present, for different structural elements the reference axis may differ; for example it is usually placed at the mid-depth for a concrete slab. When connecting elements with different reference axis positions an offset must therefore be used[85].

6.4 PROGRAM VALIDATION

As an initial validation, a self-consistency check was performed by analysing a number of problems (based on a simply supported asymmetric beam) in each case using three different assumed positions for the reference axis. These positions were: at the mid-height of cross-section, at the NAB and 1000mm above mid-height. The results were found to be identical.

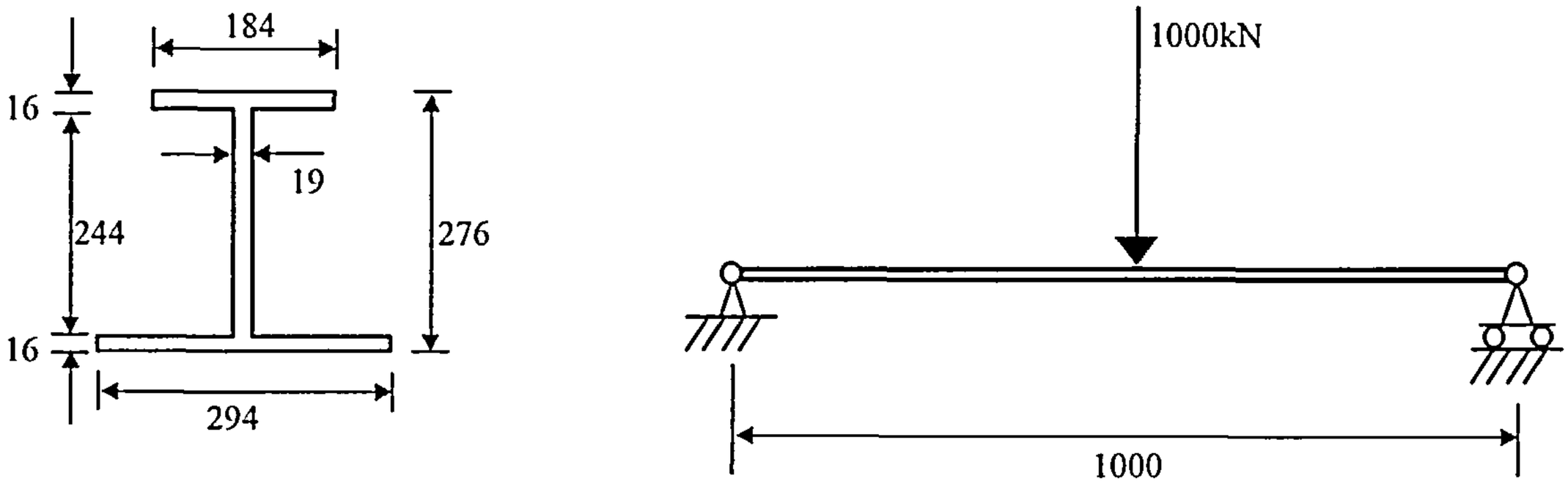

Fig. 6-13 Simply supported asymmetric beam (280ASB100) example

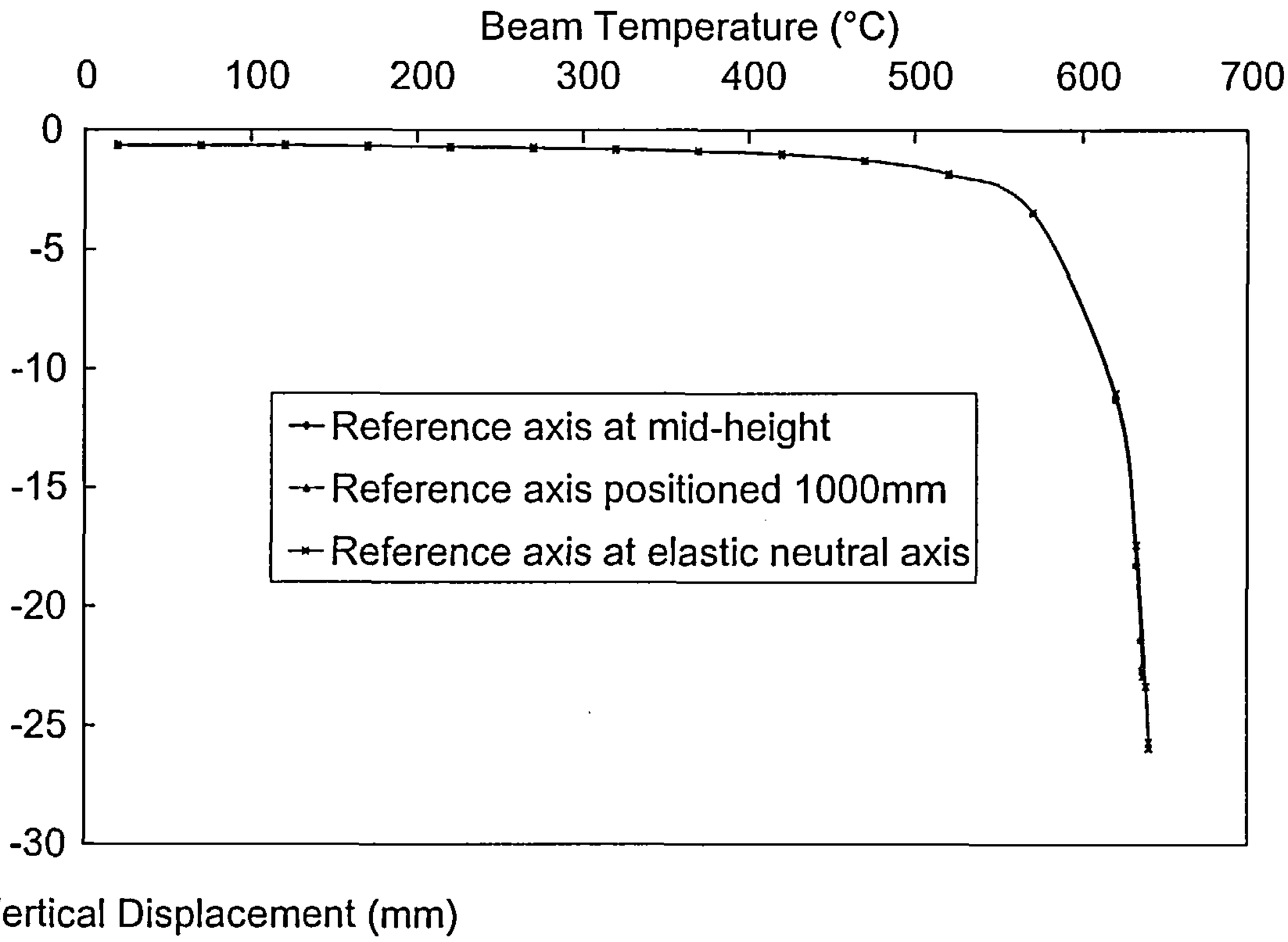

Fig. 6-14 Vertical mid-span displacement of uniformly heated beam of Fig. 6-13

Fig 6-13 shows one of those cases -- a uniformly heated simply supported beam (280 ASB 100, S355 grade steel) of 1000mm span with a concentrated load of 1000kN applied at the mid-span. The results shown in Fig 6-14 showed identical vertical deflections at the mid-span for all three analyses, indicating that the assumed position

of the reference axis does not affect the mid-span deflections of simply supported members and the software modifications had been implemented correctly.

More formal validation was then carried out by comparison with classical analysis at ambient temperature and test data for high temperatures. These are described briefly below.

6.4.1 AMBIENT-TEMPERATURE VALIDATIONS

VULCAN was used to model the behaviour of two simple cases at ambient temperature. The first was a simply supported beam under self-weight loading only, so that the assumption of linear elastic behaviour is satisfied, allowing deflections to be calculated by hand. The results from VULCAN were identical to those obtained using the elastic approach. The second was a classical case for large deflections for which theoretical solutions are well established[84,86].

A simply supported asymmetric beam (280ASB100) of S355 (Grade 50) steel spanning 5000 mm was analysed for a uniform load of 1.003N/mm representing the self-weight only. For these conditions, the vertical deflections can be calculated by using small-deflection elastic theory[87] ($y = \frac{qx}{24EI}(L^3 - 2Lx^2 + x^3)$). Fig 6-15 shows the result of this hand calculation compared with the computer prediction. The two sets of deflections were found to be identical.

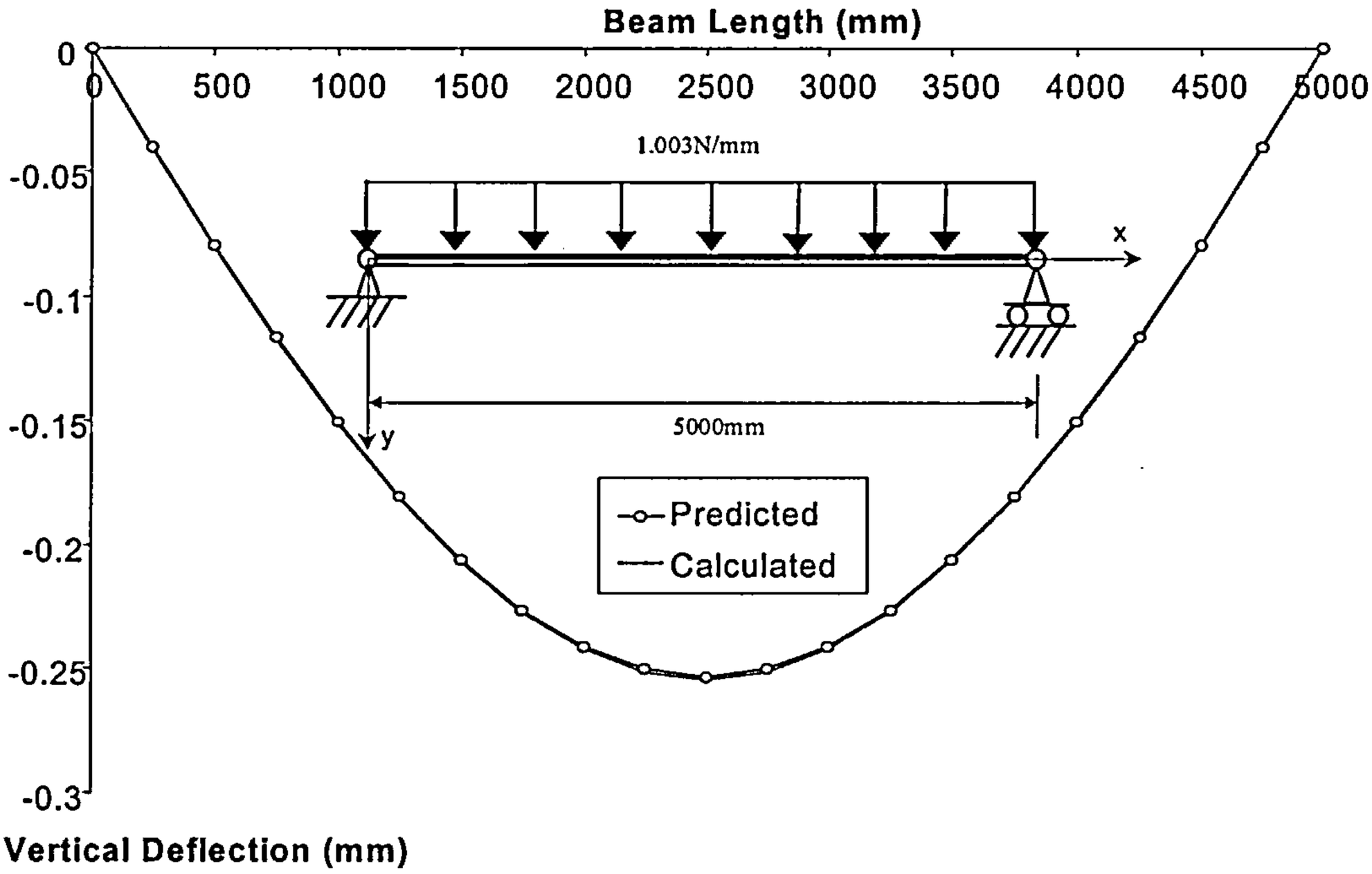

Fig. 6-15 Vertical displacement for a simply supported asymmetric beam (280ASB100) at ambient temperature (20°C)

Under fire conditions structural members may undergo very large deformations, so it is very important to check the representation of geometrical non-linearity. To do this, the classical example of an ambient-temperature elastic cantilever loaded at its free end was used (Fig. 6-16). The material properties were the same as for the above case. The reference axis of the beam was assumed to be at the NAB. The applied load (P) was gradually increased up to a value of $\frac{1.8EI}{L^2}$ producing a maximum deflection at the free end of the cantilever equal to almost half of its span.

Theoretical solutions for this example are readily available [84] for comparison. Figs. 6-17 and 6-18 show the results for the vertical and horizontal displacements at the free end. Fig. 6-17 also includes the results for vertical displacement according to small-deflection theory.

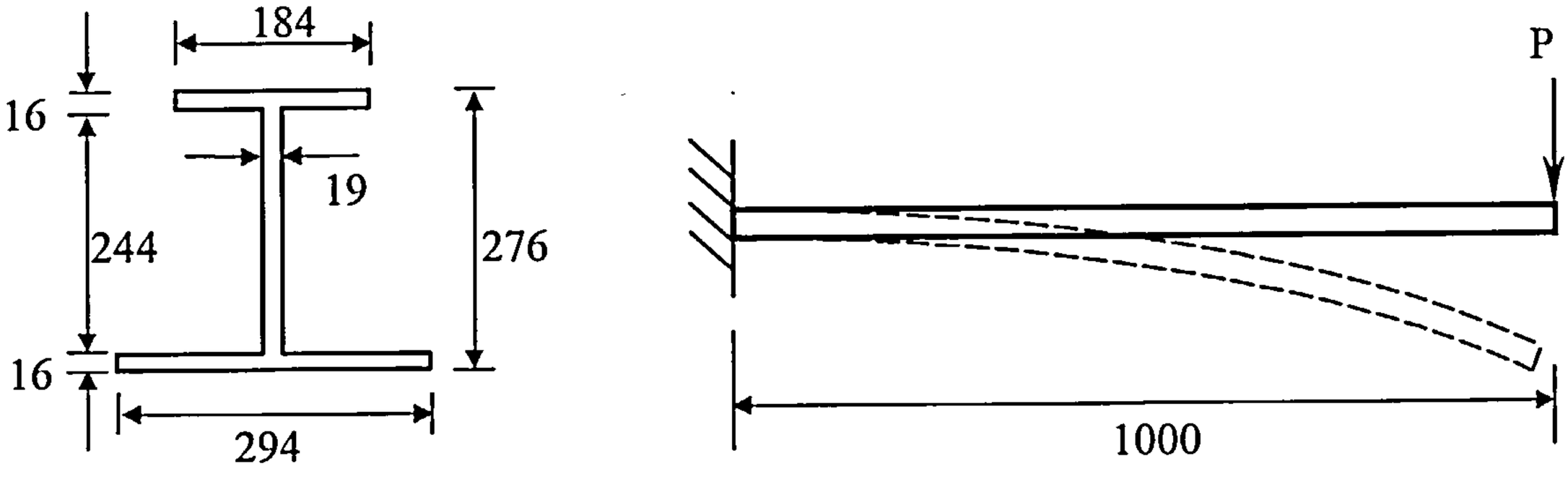

Cross-section

Fig. 6-16 Cantilever beam (280ASB100) ambient-temperature example.

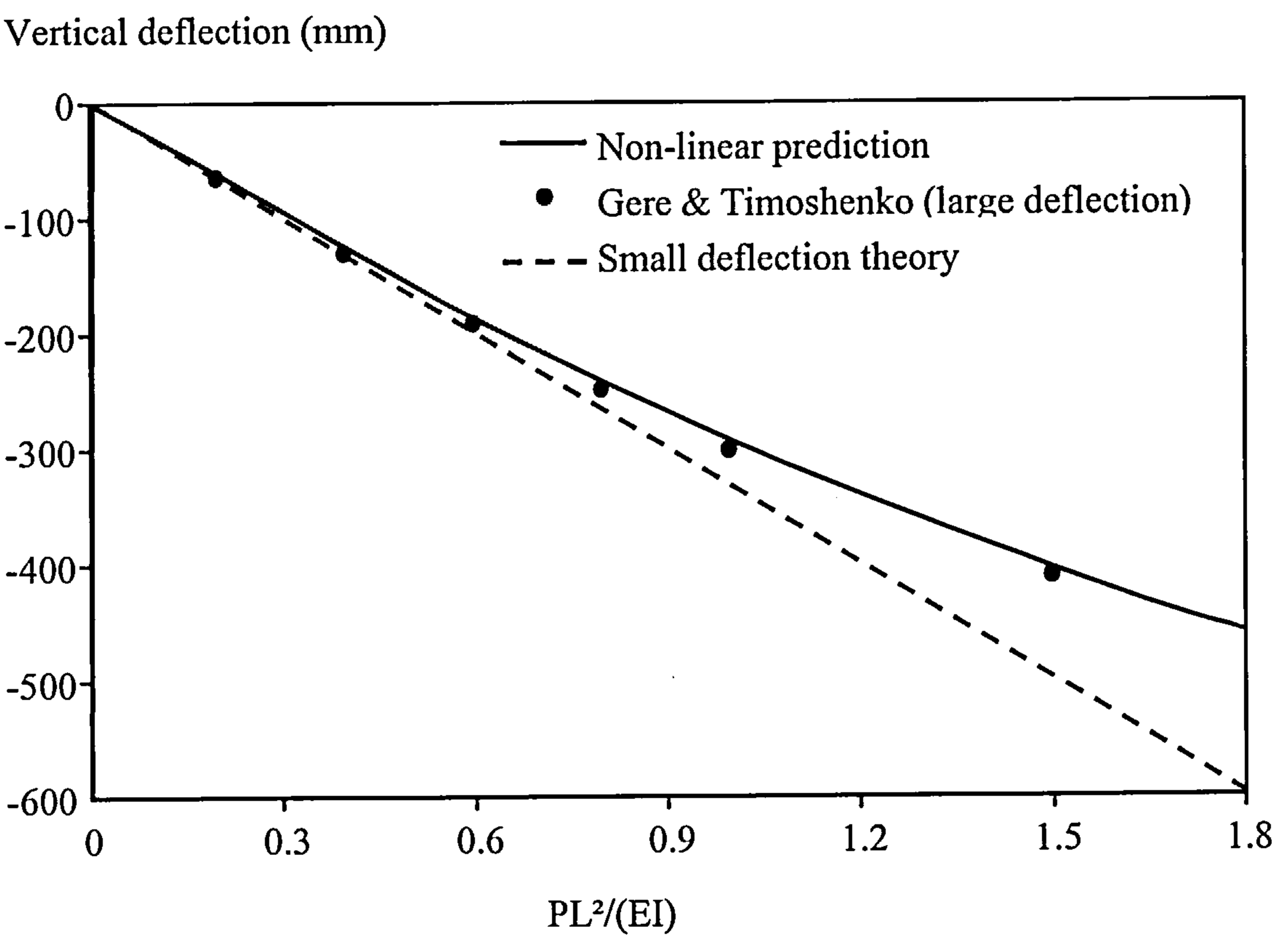

Fig. 6-17 Vertical deflection at free end of elastic cantilever beam.

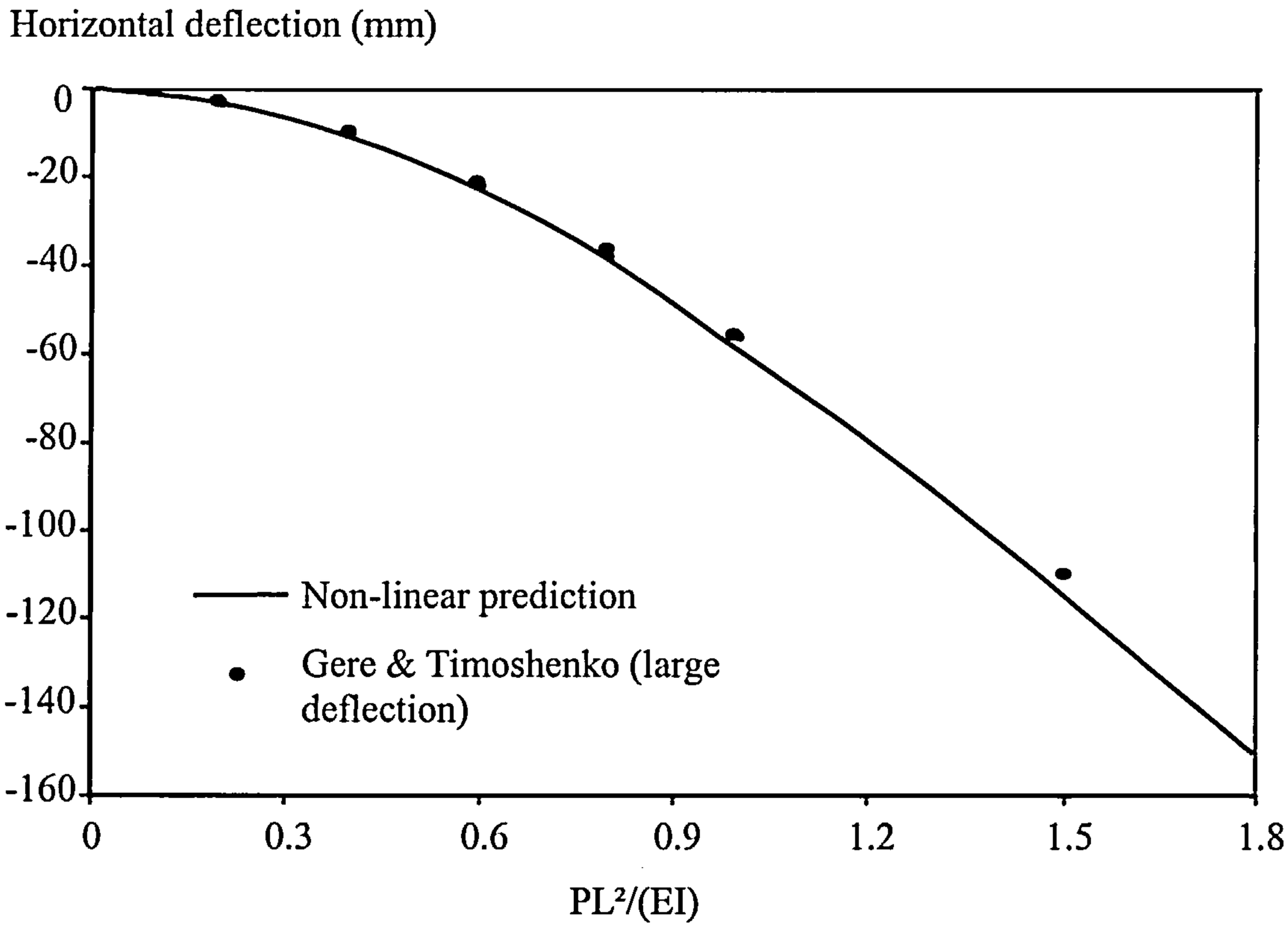

Fig. 6-18 Horizontal deflection at free end of elastic cantilever beam.

It is clear that, for small vertical deflections, the classical analyses for both large and small deflection theory are very close and the predictions are almost identical. However for larger deflections the two classical curves diverge illustrating the importance of geometrical non-linearity in the analysis of such conditions. The results from VULCAN are very close to those of the classical non-linear analysis, indicating satisfactory representation of this behaviour.

6.4.2 HIGH-TEMPERATURE VALIDATIONS

Only a very small number of high-temperature tests have been performed on asymmetric beam sections. Two of these have been used to check the ability of VULCAN to model the behaviour of such sections in fire.

6.4.2.1 STANDARD FIRE RESISTANCE TEST ON ASB BEAM

The first high-temperature comparison is for a standard fire resistance test[40] on a slim-floor beam, conducted at the Warrington Fire Research Centre in 1996. The test specimen consisted of a simply supported composite 280ASB100 asymmetric beam (depth 279mm, flanges 280mm and 183mm as shown in Table 6-1) with normal-weight Grade 30 concrete cast onto deep-deck profiled sheeting with an A142 mesh. The yield stress of the steel, measured by tensile tests on coupons, was 402N/mm². The cross-section and layout are shown in Fig. 6-19. The span of the beam was 4500mm, with four loads of 84.6kN applied at the 1/8, 3/8, 5/8, and 7/8 points of the span. The beam was exposed to the ISO834 standard time-temperature curve (Fig 6-20).

POSITION/ORIENTATION			NOMINAL (mm)	ACTUAL (mm)
Beam Depth			280	279
Beam Width	-- Upper Flange		180	183
	-- Lower Flange		280	280
Flange Thickness	-- Upper	Left Side	18	16.0
	-- Lower	Right Side	18	17.3
		Mean Value	18	16.6
Flange Thickness	-- Lower	Left Side	18	18.9
	-- Lower	Right Side	18	18.0
		Mean Value	18	18.4
Web Thickness			18	19.5
Between Flanges		Left Side		245.0
		Right Side		244.7
		Mean Value		244.9

Table 6-1 Dimensional Data for the Steel Section Used in the Fire Resistance at the Warrington Fire Research Centre (WFRC 66162).

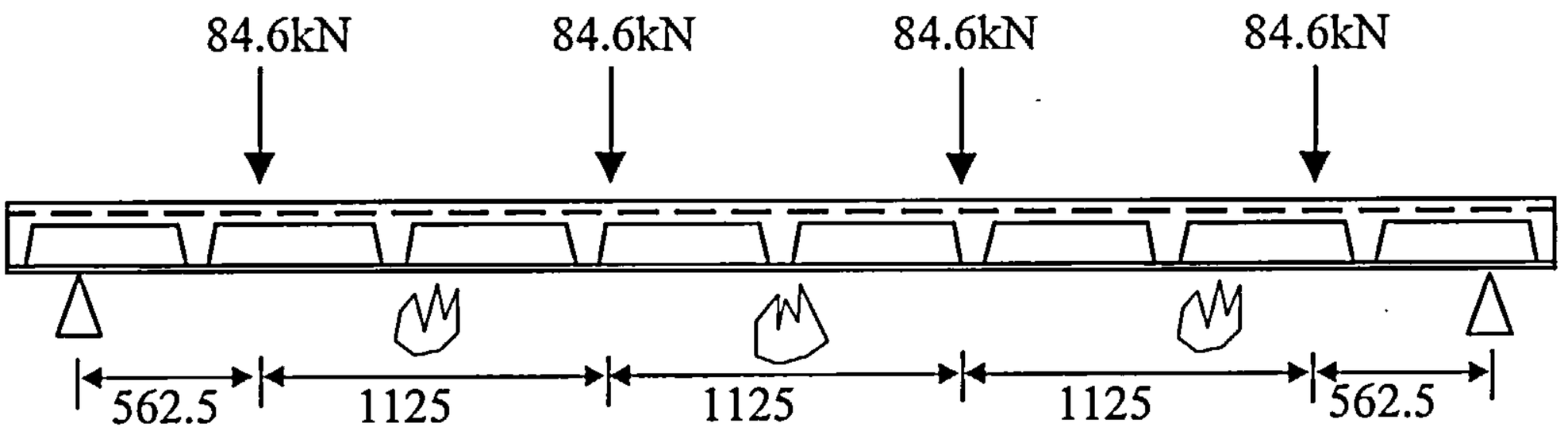

Elevation

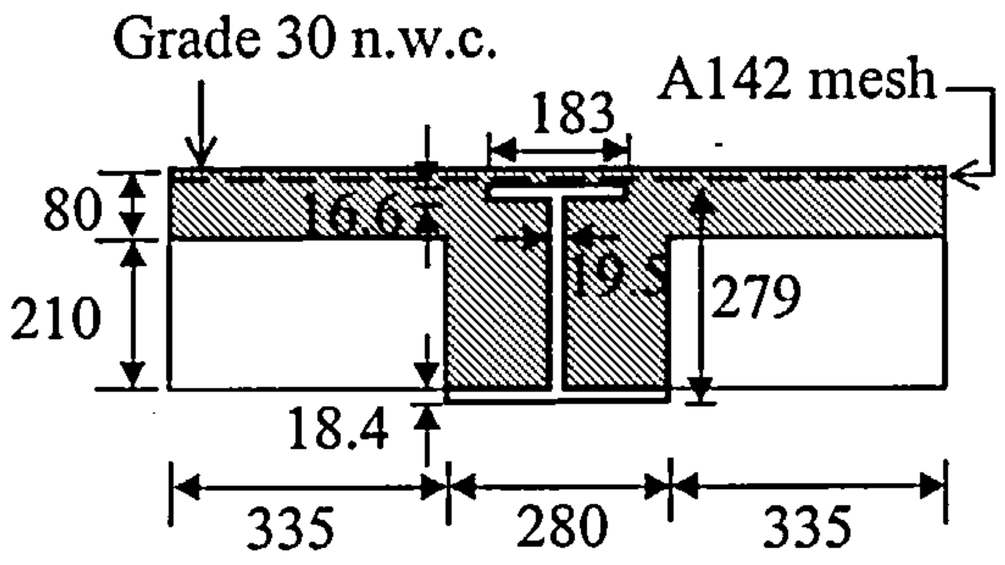

Composite ASB cross-section

Fig. 6-19 Setup of fire resistance test [40] on a deep-deck ASB composite beam conducted at the Warrington Fire Research Centre.

Fig. 6-20 Comparison of average furnace atmosphere temperature and the standard temperature / time curve

Two analyses have been carried out using VULCAN to compare with the test results, one using a pure steel beam model (neglecting the effect of the slab completely) and the other using a composite beam model in which Huang's[68] layered slab formulation has been included. The beam was divided into 20 finite elements and the cross-section into 12 segments and 60 segments for comparson. In order to compare directly with the test, the measured material properties and the recorded temperature profiles were used in the analysis. The comparisons of mid-span deflections are shown in Figs 6-21 to 6-23, where Fig 6-23 presents the same results as Fig 6-22, but plotted in terms of the mid-span deflection versus time.

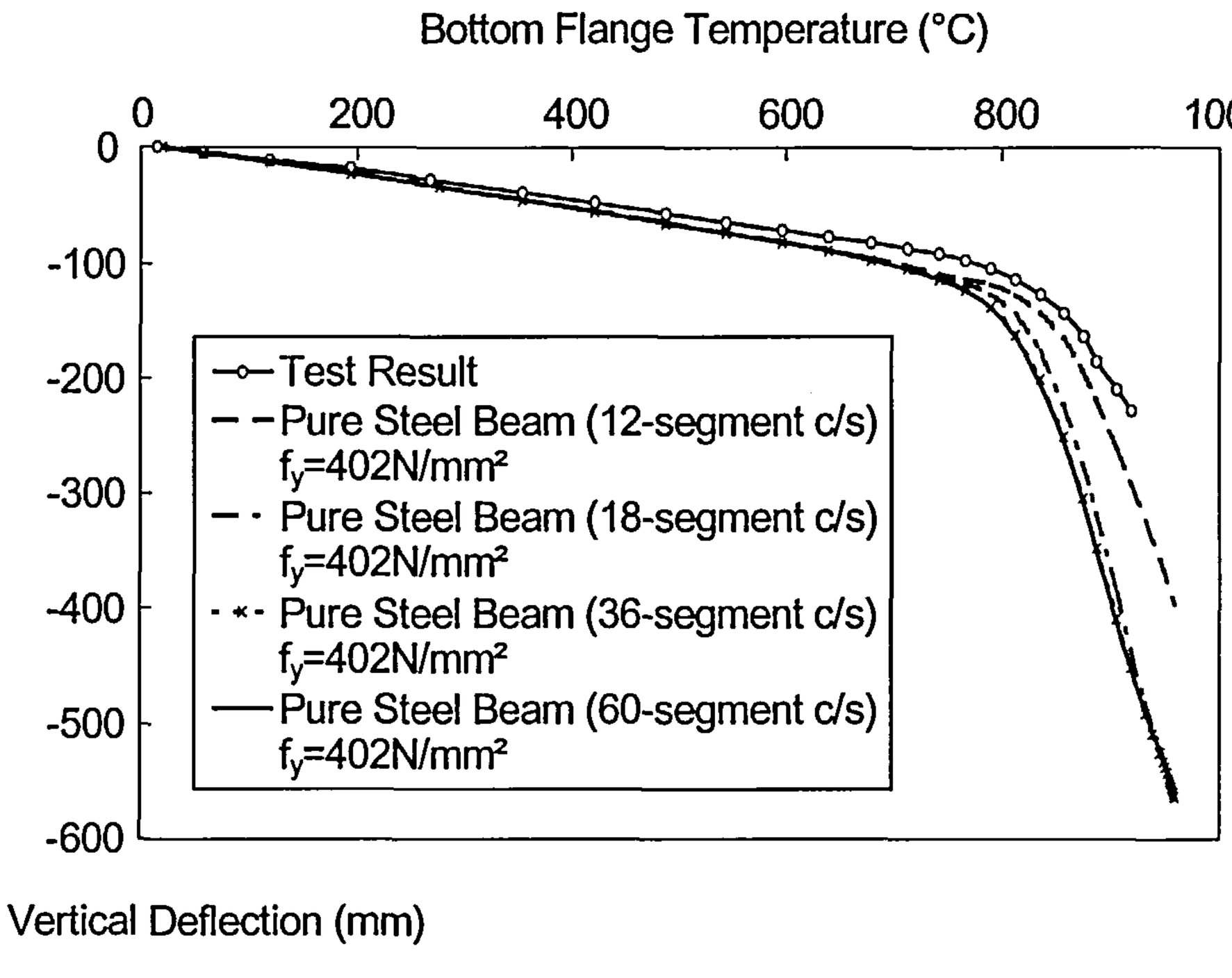

Fig. 6-21 Displacement-temperature plot for the pure steel beam model at mid-span.

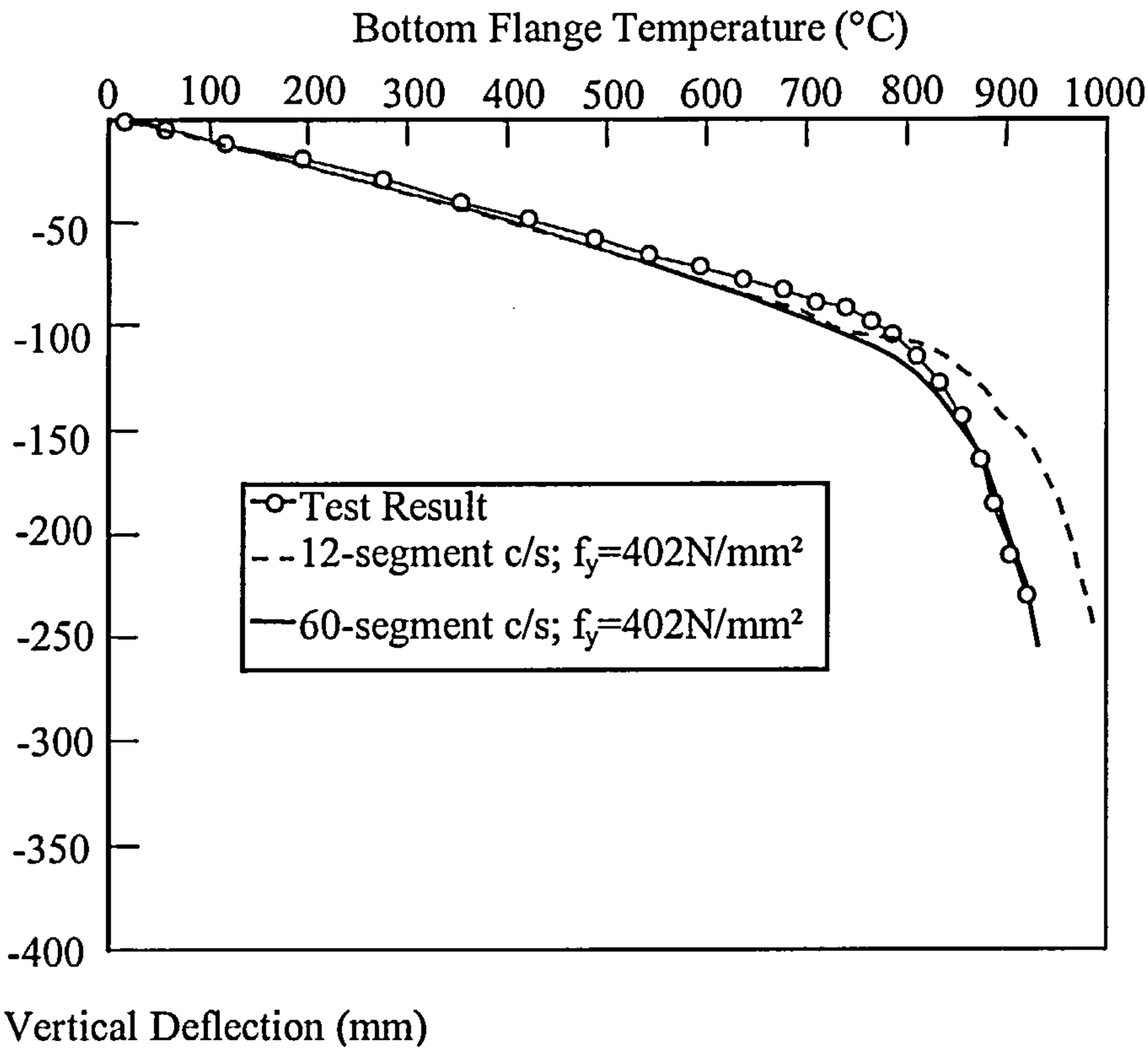

Fig. 6-22 Displacement-temperature plot for the deep-deck ASB composite beam at mid-span.

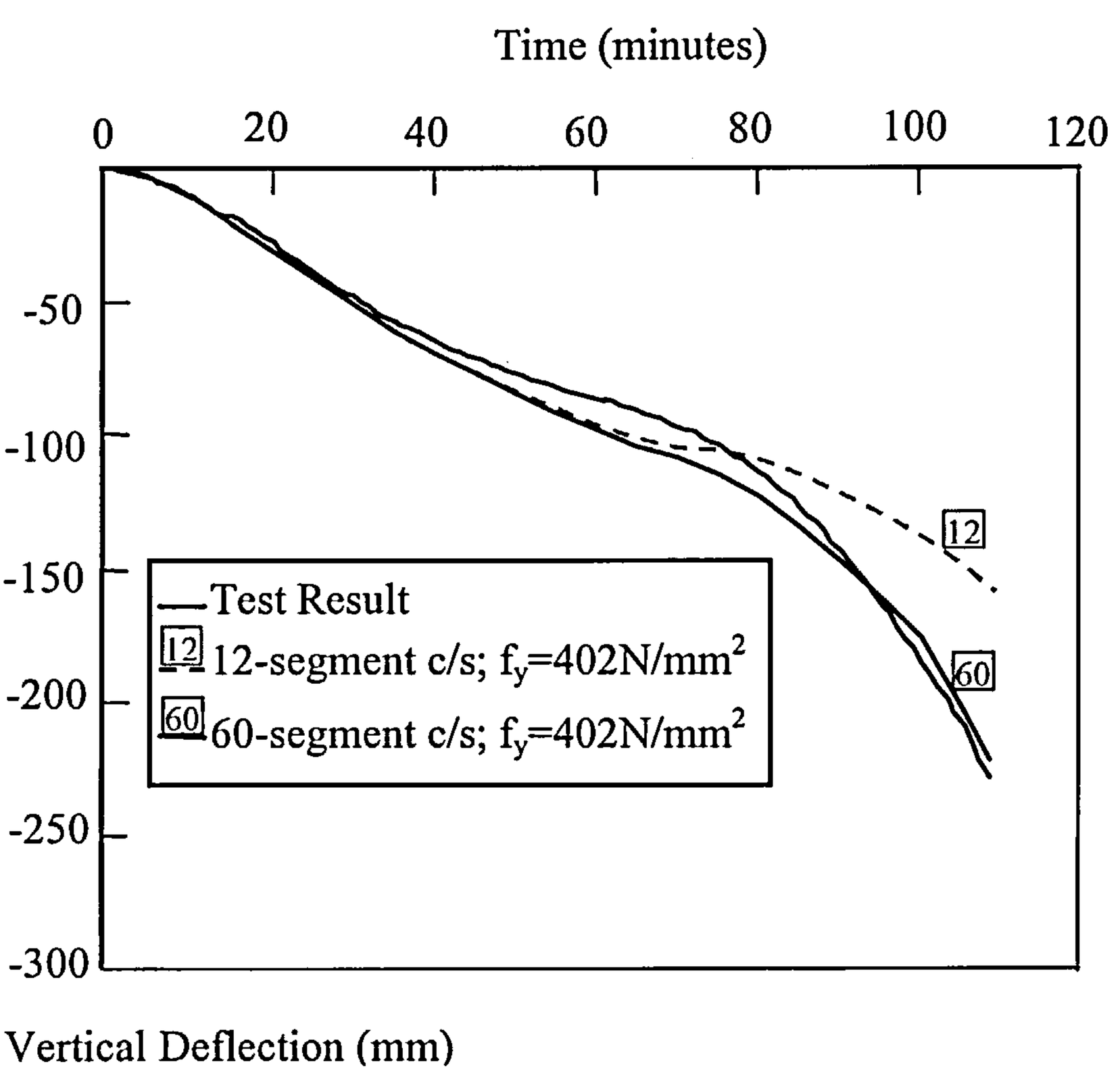

Fig. 6-23 Displacement-time plot for the deep-deck ASB composite beam at mid-span.

These figures indicate the importance of composite action between the ASB and the concrete slab, and show that the asymmetric steel beam cross-section really needs to be represented by more than 12 segments (N=2). Analyses with more segments, such as 18 segments (N=3), show a distinct improvement in correlation with test results. Another standard ASB fire test was also conducted at the Warrington Fire Research Centre, but the data could not be obtained for comparison. From the collection Figs 6-21 to 6-23, the results suggest that VULCAN is capable of modelling the behaviour of simply supported deep-deck slim-floor systems using the asymmetric beam formulation developed in this chapter.

6.4.2.2 COMPARISONS OF ASB BEAMS FROM FULL SCALE FIRE TEST AND COMPUTER PREDICTIONS

The final comparison is with a full-scale fire test conducted by the Building Research Establishment (BRE) on a composite Slimdek floor system[88] extending across two bays in both directions. The slab was supported on a steel structure with two spans of 6109mm (Fig. 6-24). One quarter of the structure was used for the analysis. The steel structure consisted of 254x254UC73 columns, 280ASB100 asymmetric beams and T-section (191x229x49) beams. The steel grade throughout was BSEN10025 S355 and concrete was grade C30 NWC in accordance with BS8110. The 295mm deep composite slab was cast on top of a SD225 deck. A single 20mm diameter reinforcing bar (Grade 460) was placed in each rib. The details of sections have been illustrated in Fig 6-25 and Table 6-2. A uniformly distributed load of 6.88kN/m² was applied; recorded test temperatures were used in this analysis. Fig 6-26 shows the average atmosphere temperature during the test and Fig 6-27 shows the temperature distribution along the cross-section at midspan for one of ASB beams (beam 2). The cross-section of the asymmetric beam was divided into 60 segments and 10 finite

elements were used along its length. 10x10 finite elements were assigned to the slab with each element 610.9x 610.9mm. Semi-rigid connection characteristics were calculated using the component method[89]. Huang's effective-stiffness slab model[90] was used to model the concrete slab.

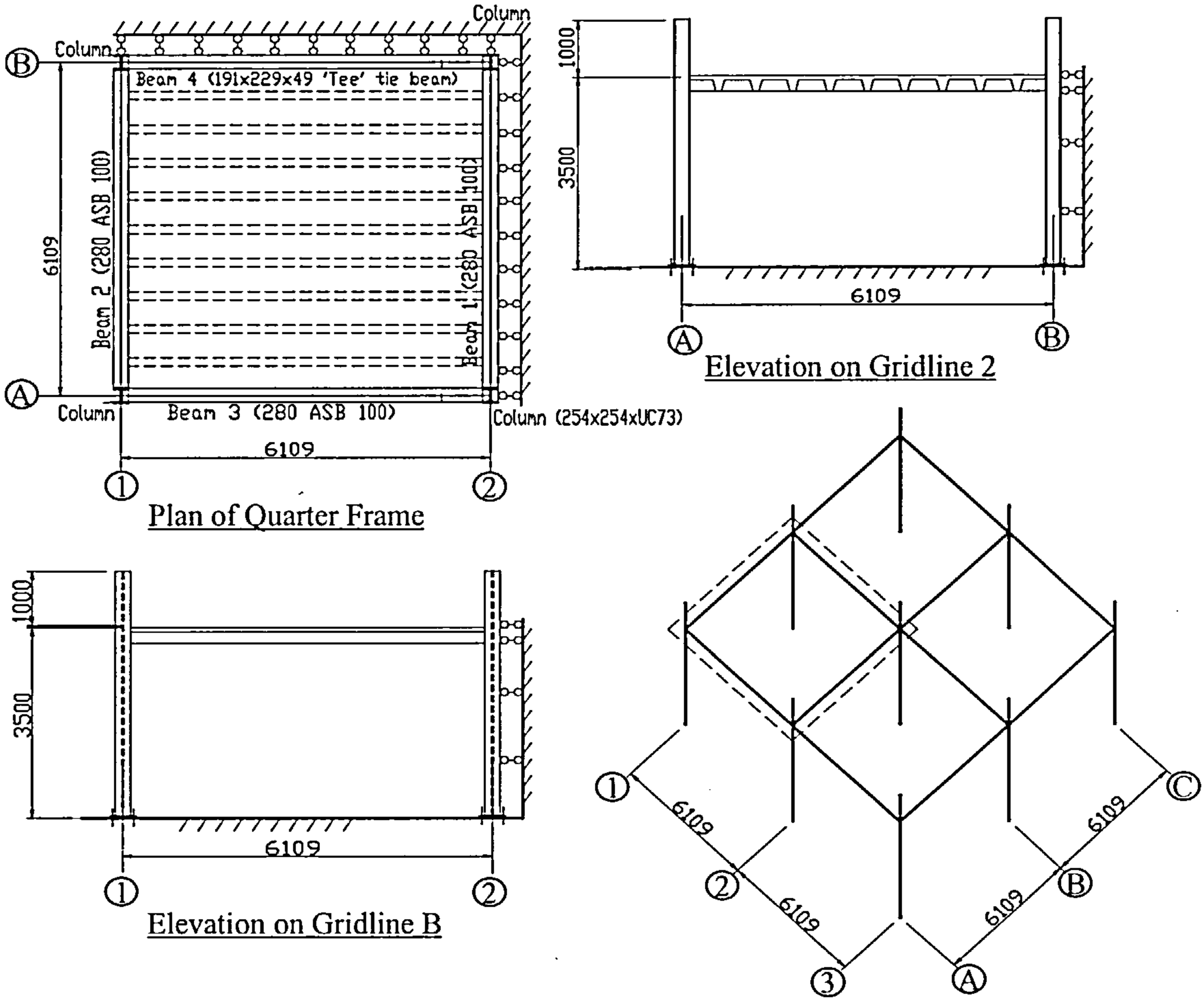

Fig. 6-24 Details of one quarter of full-scale fire test on a Slimdek Floor System (All dimensions in mm).

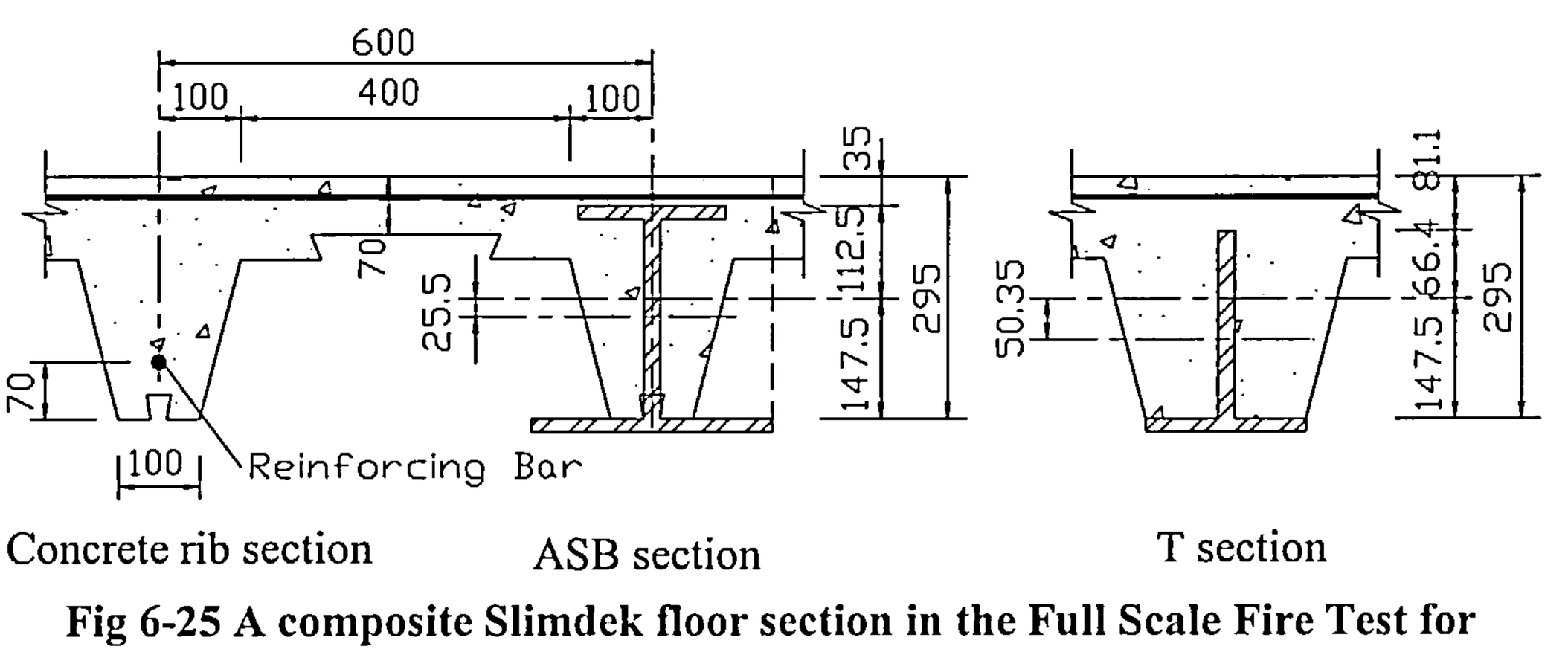

Concrete rib section ASB section T section

Fig 6-25 A composite Slimdek floor section in the Full Scale Fire Test for computing.

Member No.	Designation	Depth h (mm)	Flange Width (mm)		Flange t1/t2 (mm)	Web t3 (mm)	Note
			Top	Bottom			
Beam 1	280 ASB 100	276	184	294	16	19	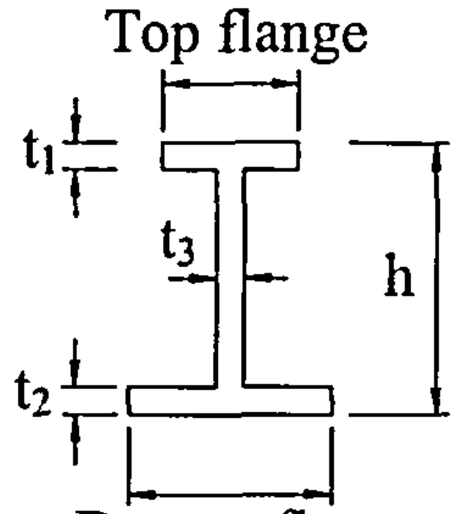
Beam 2	280 ASB 100	276	184	294	16	19	
Beam 3	280 ASB 100	276	184	294	16	19	
Beam 4	T191x229x49	233.5	--	192.8	19.6	11.4	
Column	254x254xUC73	254.1	254.6	254.6	14.2	8.6	

Table 6-2 Dimensional Data for the Steel Section Used in the Full Scale Fire Test at the Building Research Establishment (BRE).

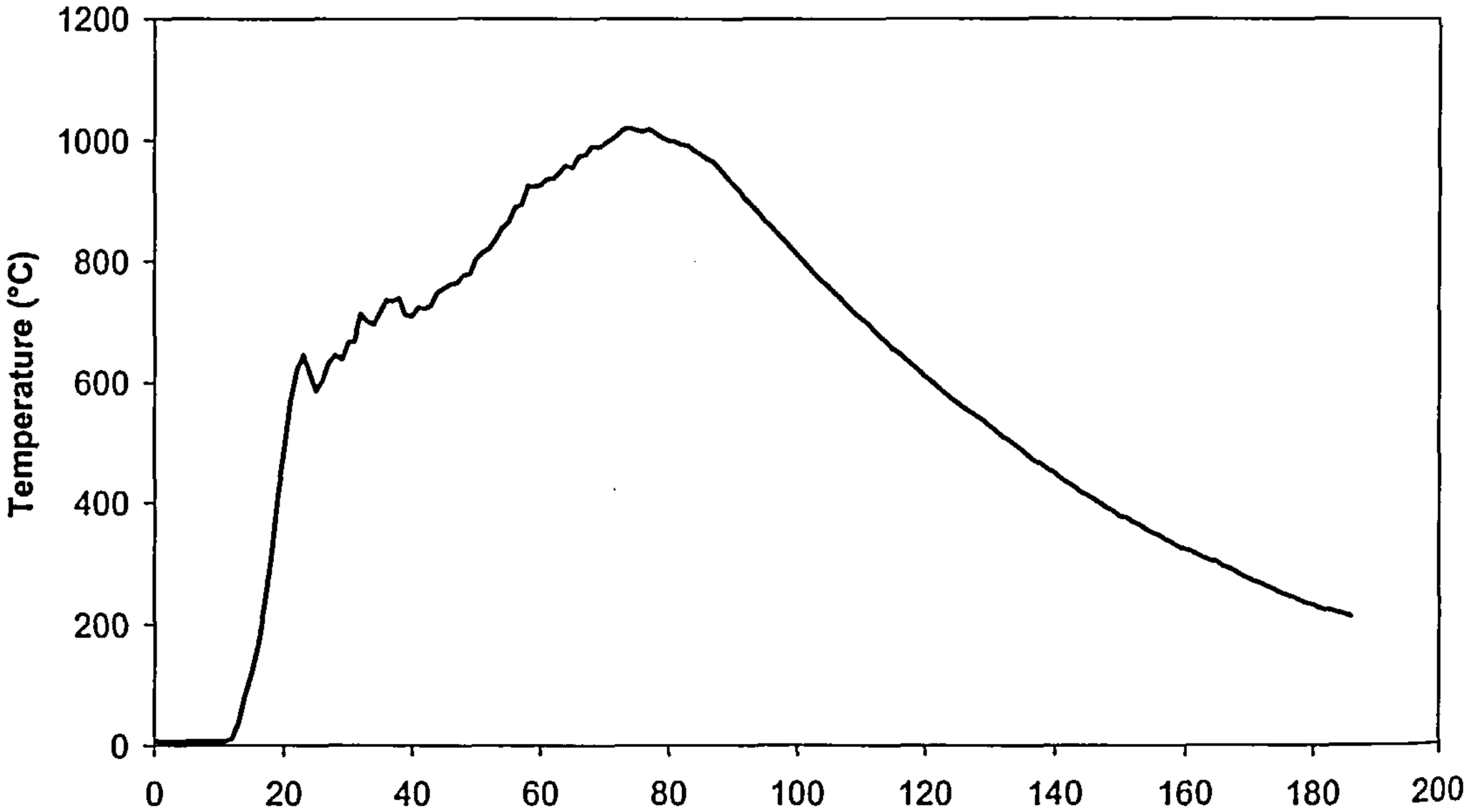

Fig. 6-26 Average atmosphere temperature

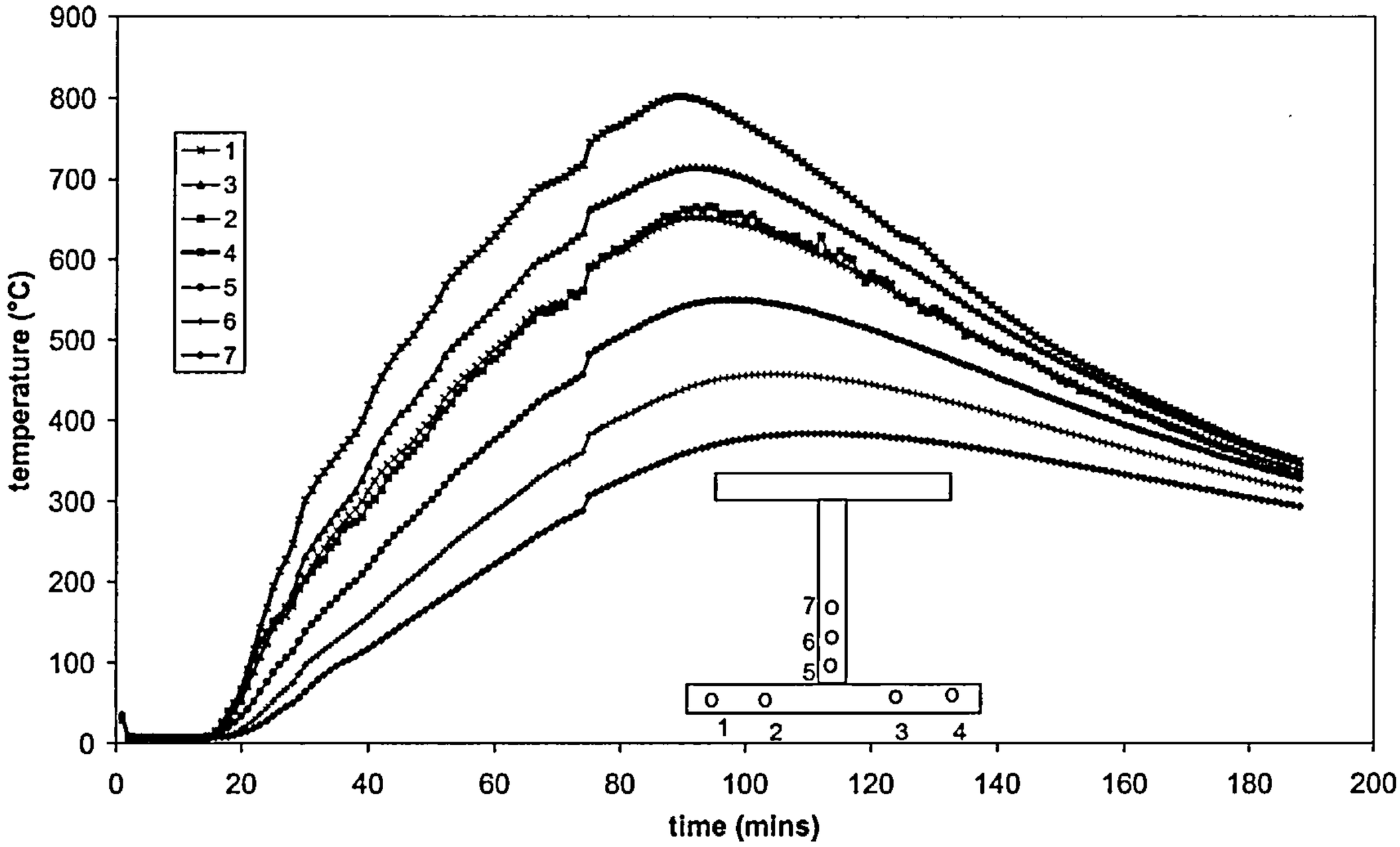

Fig. 6-27 Temperature distribution at centre of the ASB beam (beam 2)

The analytical results for Beams 1 and 2 are compared with the test results in Figs. 6-28 to 6-30. The maximum average atmosphere temperature recorded in the test was approximately 1017°C after 75 minutes of heating. It can be seen from the figures that the comparisons between computer predictions and test results are very good for both beams. At the peak temperature the vertical deflection at mid-span of Beam 1 deviated from the test result by about 18% and for beam 2 by 4.6%. In the cooling phase, it can be seen that the beam deflection reverses although it does not fully recover because of permanent mechanical strains. This is well modelled by the software.

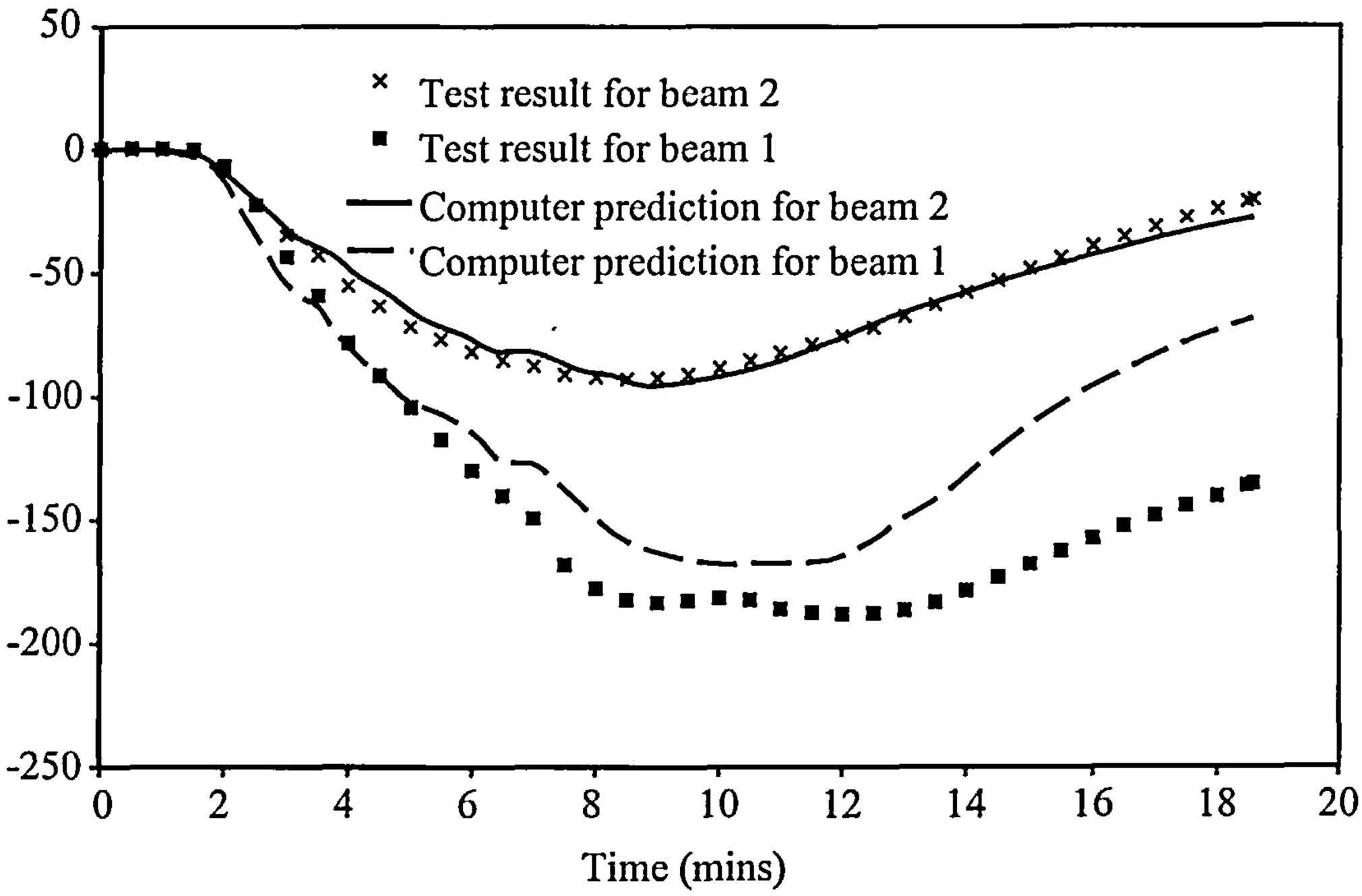

Fig. 6-28 Comparison of test results with computer predictions for Slimdek Fire Test.

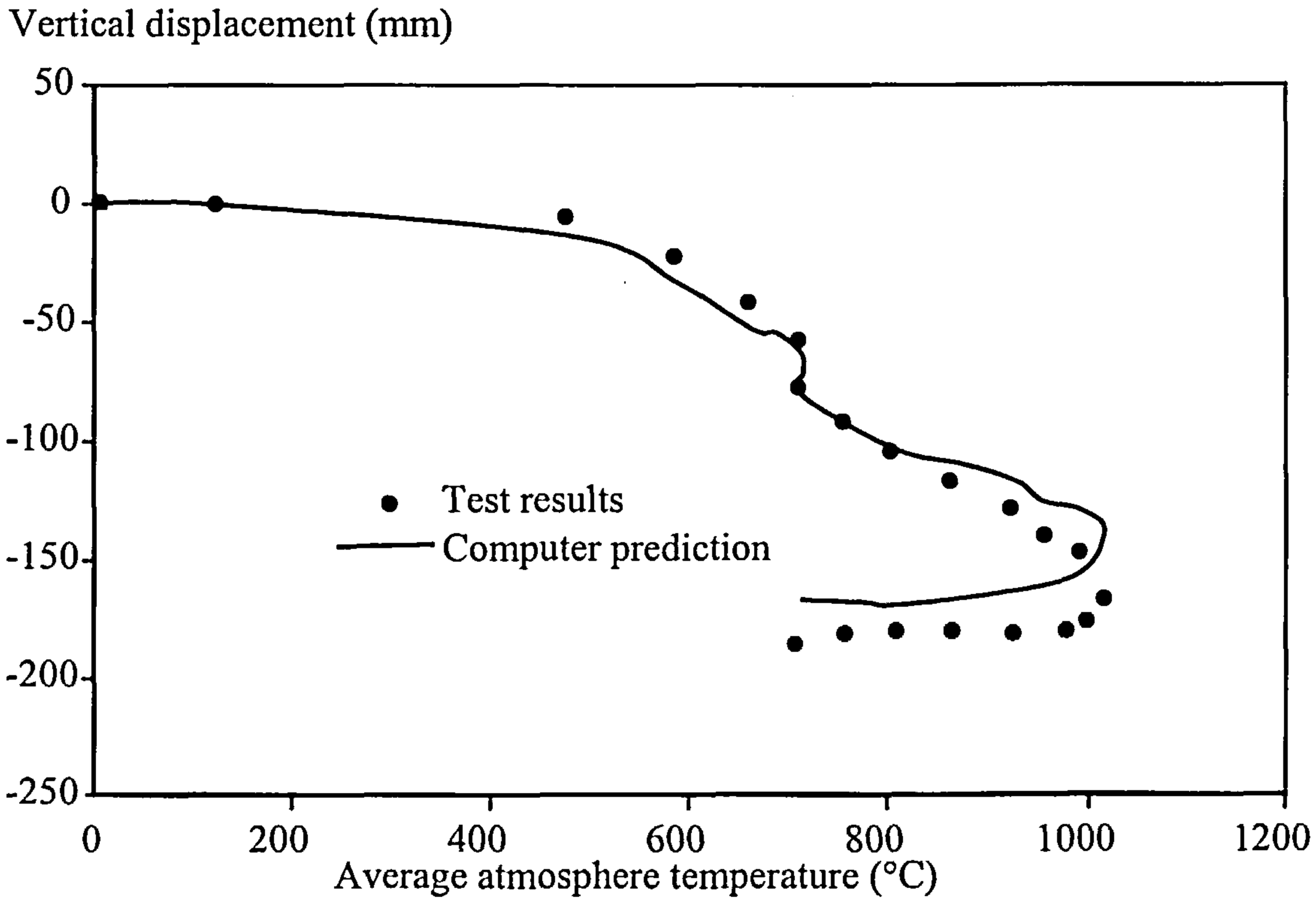

Fig. 6-29 Displacement-temperature comparisons for Beam 1.

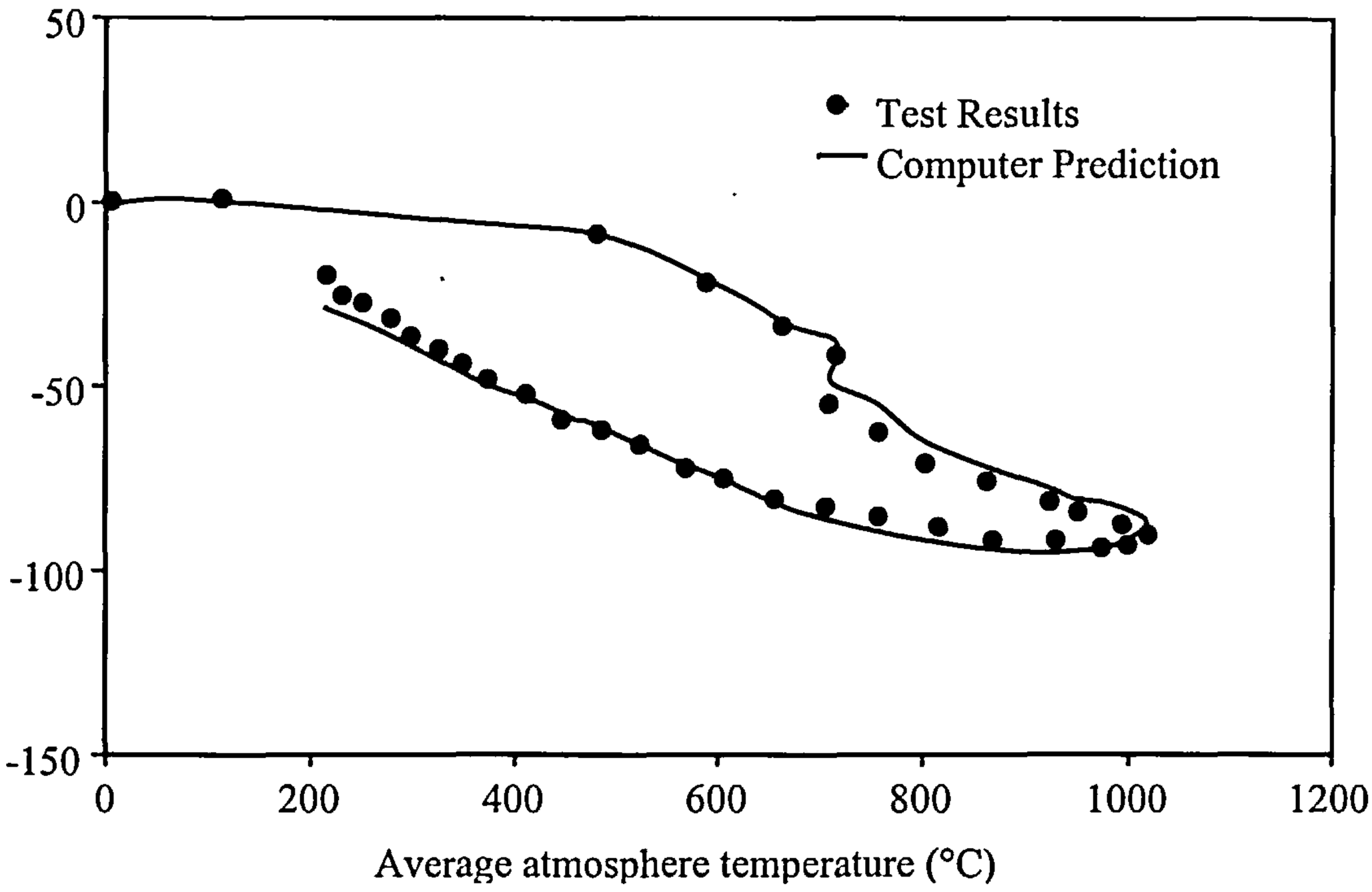

Fig. 6-30 Displacement-temperature comparisons for Beam 2.

6.5 CONCLUSIONS

A new type of steel beam element, the so-called asymmetric beam (ASB), has been introduced into the program VULCAN. The comparisons between computer predictions and classical solutions at ambient temperature and the results from high temperature tests indicate that the modified program is capable of predicting the behaviour of such members with good accuracy. However, due to the limited amount of test data available at present this study is at an early stage and further investigation is needed, especially in relation to composite action in slim-floor beams. In this chapter the main principles and details which relate to asymmetric members have been presented. Two-noded one-dimensional beam elements have been used to minimise computer memory and processing time, whilst refinement of the cross-section ensures sufficient accuracy. The latest development currently allows the structural analysis of

full three-dimensional composite buildings with symmetric and asymmetric beam cross-sections subjected to fire. At present, a new concrete beam model is being developed to model the behaviour of the concrete ribs of Slimdek floor systems, instead of using Huang's effective stiffness model[90] which is suitable for ribbed floors with shallower ribs at closer spacings and was already adopted in predicting the last full scale fire test case. This new model is more suited to ribbed floors with deep ribs and will be introduced in the next chapter.

7. GENERALISED STEEL/REINFORCED CONCRETE BEAM/COLUMN ELEMENT MODEL FOR FIRE CONDITIONS

In this chapter a generalised beam-column element, which can model not only reinforced concrete sections but also steel sections of different shapes, is presented, The formulation is used to further develop the software VULCAN which is then validated by comparing with some theoretical and experimental results.

7.1 INTRODUCTION

Since 1996 when Najjar[34] extended the software to three-dimensions, the beam element in VULCAN has been further developed by others[10,91]. However, to model a composite beam, the current method is to combine a steel beam element with a concrete slab[68,91]. This is not always convenient and may cause some errors because of using different shape functions and the reference axes for the beam and slab elements. Furthermore it is difficult to model beam cross-sections other than steel I-sections, such as concrete filled hollow members. A new generalised beam element has therefore been developed to deal with those problems, and to model the concrete ribs of Slimdek floor systems. Details of the main principles and program development for this generalised beam element are given in this chapter. Different material models have also been considered in the software, especially for tension in concrete, which may significantly affect the results. Validation of this new beam model has been carried out for single members and more complicated structures. The results demonstrate the capability of modelling alternative cross-sections in fire.

7.2 PRINCIPLES AND FORMULATIONS

As for the steel beam element, the concrete beam element is a two-noded line element, each node having eight degrees of freedom in local coordinates (as shown in Fig. 2-2). Before we formulate the governing equations for the generalised beam, the following assumptions should be established:

- The member is straight, prismatic and plane cross-sections remain plane under flexural deformations.
- There is no slip between different materials, for example the steel reinforcement and surrounding concrete.
- The twist (θ_z) of the beam member is relatively small, and there is no distortion in cross-section.

The calculations for the deformations of the generalised beam element are based on Lagrangian description with displacements of any point within the element specified in relation to its initial position. Therefore, the displacements at any point on the reference axis can be expressed by

$$\{u_0\} = [N]\{q\} \tag{7-1}$$

where,

$$\{q\}^T = \langle u_i, u_i', u_j, u_j', v_i, v_i', v_j, v_j', w_i, w_i', w_j, w_j', \theta_i, \theta_i', \theta_j, \theta_j' \rangle,$$

$$\{u_0\}^T = \langle u_0, v_0, w_0, \theta_z \rangle,$$

[N] is a cubic shape function matrix

$$[N] = \begin{bmatrix} \langle N_a \rangle & \langle 0 \rangle & \langle 0 \rangle & \langle 0 \rangle \\ \langle 0 \rangle & \langle N_a \rangle & \langle 0 \rangle & \langle 0 \rangle \\ \langle 0 \rangle & \langle 0 \rangle & \langle N_a \rangle & \langle 0 \rangle \\ \langle 0 \rangle & \langle 0 \rangle & \langle 0 \rangle & \langle N_a \rangle \end{bmatrix}$$

where,

$\langle 0 \rangle = \langle 0,0,0,0 \rangle$;

$\langle N_a \rangle = \langle N_1, N_2, N_3, N_4 \rangle$

in which $N_1 = \frac{1}{4}(\bar{z}+2)(\bar{z}-1)^2$, $N_2 = \frac{L}{8}(\bar{z}+1)(\bar{z}-1)^2$, $N_3 = \frac{1}{4}(2-\bar{z})(\bar{z}+1)^2$,

$N_4 = \frac{L}{8}(\bar{z}-1)(\bar{z}+1)^2$, L is length of element, $\bar{z} = \frac{2z}{L}$, $-1 \le \bar{z} \le 1$.

The derivatives can be similarly expressed

$$\{u_0'\} = [N']\{q\} \tag{7-1a}$$

$$\{u_0''\} = [N'']\{q\} \tag{7-1b}$$

where

$\{u_0'\} = \langle u_0', v_0', w_0', \theta_z' \rangle$, $\{u_0''\} = \langle u_0'', v_0'', w_0'', \theta_z'' \rangle$,

$$[N'] = \begin{bmatrix} \langle N_a' \rangle & \langle 0 \rangle & \langle 0 \rangle & \langle 0 \rangle \\ \langle 0 \rangle & \langle N_a' \rangle & \langle 0 \rangle & \langle 0 \rangle \\ \langle 0 \rangle & \langle 0 \rangle & \langle N_a' \rangle & \langle 0 \rangle \\ \langle 0 \rangle & \langle 0 \rangle & \langle 0 \rangle & \langle N_a' \rangle \end{bmatrix}$$

and

$$[N''] = \begin{bmatrix} \langle N_a'' \rangle & \langle 0 \rangle & \langle 0 \rangle & \langle 0 \rangle \\ \langle 0 \rangle & \langle N_a'' \rangle & \langle 0 \rangle & \langle 0 \rangle \\ \langle 0 \rangle & \langle 0 \rangle & \langle N_a'' \rangle & \langle 0 \rangle \\ \langle 0 \rangle & \langle 0 \rangle & \langle 0 \rangle & \langle N_a'' \rangle \end{bmatrix}$$

in which

$\langle N_a' \rangle = \langle N_1', N_2', N_3', N_4' \rangle$;

$\langle N_a'' \rangle = \langle N_1'', N_2'', N_3'', N_4'' \rangle$;

where

$N_1' = \frac{1}{2L}(\bar{z}-1)(3\bar{z}+3)$, $N_2' = \frac{1}{4}(\bar{z}-1)(3\bar{z}+1)$,

$$N_3' = \frac{1}{2L}(\bar{z}+1)(3-3\bar{z}),\ N_4' = \frac{1}{4}(\bar{z}+1)(3\bar{z}-1),$$

$$N_1'' = \frac{6\bar{z}}{L^2},\ N_2'' = \frac{1}{L}(3\bar{z}-1),\ N_3'' = -\frac{6\bar{z}}{L^2},\ N_4'' = \frac{1}{L}(3\bar{z}+1).$$

L is length of element, $\bar{z} = \frac{2z}{L}$, $-1 \le \bar{z} \le 1$.

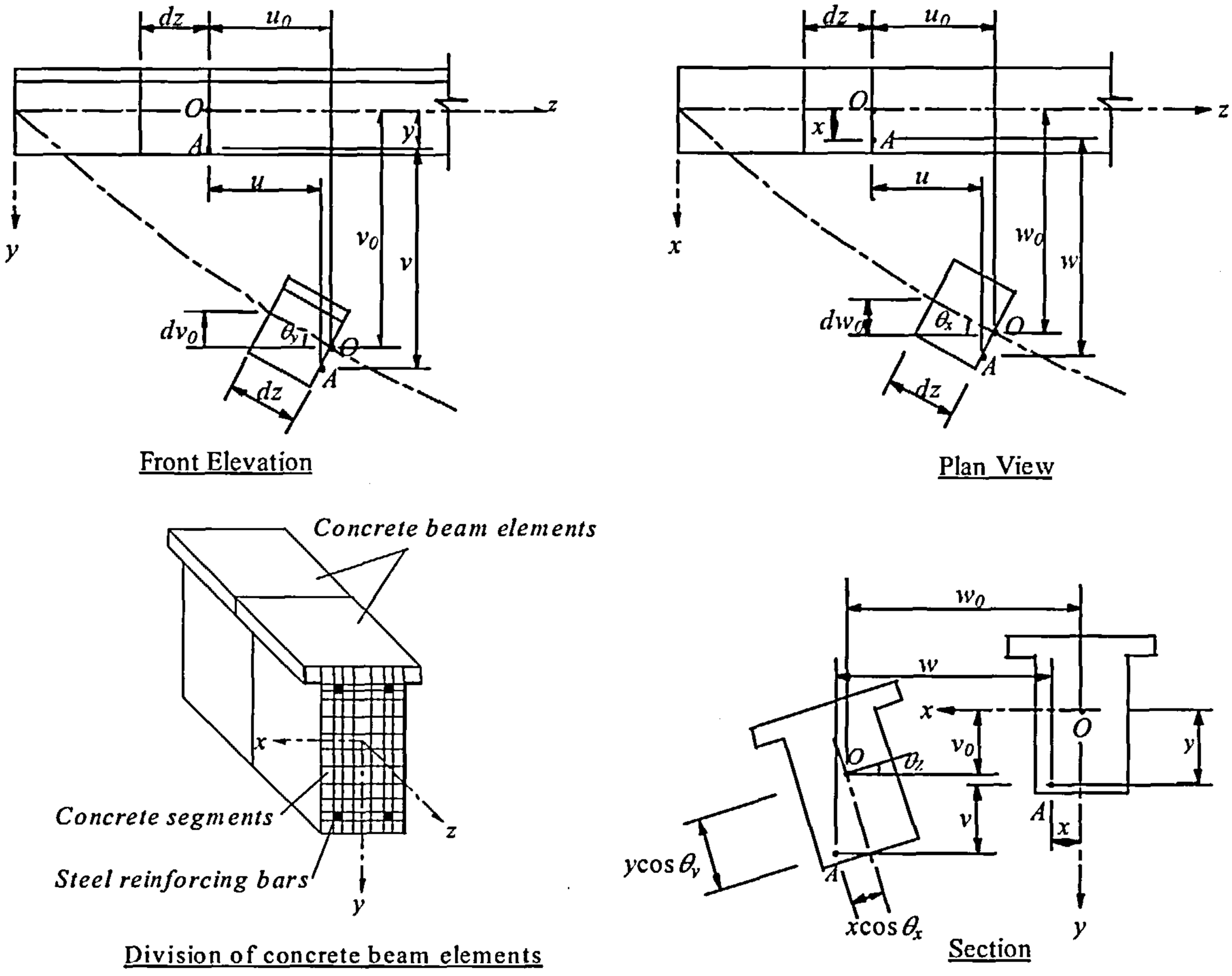

Fig. 7-1 The deformations of concrete beam element

As shown in Fig. 7-1, the displacements of an arbitrary point A on any cross-section can be expressed in terms of the reference axis displacements by

$$u = u_0 - (y\sin\theta_y + x\sin\theta_x) \tag{7-2a}$$

$$v = v_0 - y + (y\cos\theta_y\cos\theta_z + x\cos\theta_x\sin\theta_z) \tag{7-2b}$$

$$w = w_0 - x + (x\cos\theta_x\cos\theta_z - y\cos\theta_y\sin\theta_z) \tag{7-2c}$$

in which x and y are the co-ordinates of point **A**. The reference axis for displacements is based on the undeformed elements.

It can be seen from Fig. 7-1 that the slopes of the member in the x and y-directions respectively are:

$$sin\theta_x = \frac{dw_0}{dz} = w_0' \tag{7-3a}$$

$$sin\theta_y = \frac{dv_0}{dz} = v_0' \tag{7-3b}$$

Although the slopes could be represented by tangents, the sine function gives a better representation for large-displacement problems. Eqn. (7-3a,b) also give us the implicit expression for cosine as

$$cos\theta_x = \sqrt{1 - sin^2\theta_x} = \sqrt{1 - (w_0')^2} \tag{7-3c}$$

$$cos\theta_y = \sqrt{1 - sin^2\theta_y} = \sqrt{1 - (v_0')^2} \tag{7-3d}$$

The series expressions for $sin\theta_z$ and $cos\theta_z$ can be obtained by using Maclaurin's (or Taylor's) series:

$$sin\theta_z = \theta_z - \frac{\theta_z^3}{3!} + \frac{\theta_z^5}{5!} - \frac{\theta_z^7}{7!} + \cdots$$

$$cos\theta_z = 1 - \frac{\theta_z^2}{2!} + \frac{\theta_z^4}{4!} - \frac{\theta_z^6}{6!} + \cdots$$

Since the twist angle θ_z is assumed to be small, we can disregard all terms containing powers of θ_z and therefore have

$$sin\,\theta_z = \theta_z \quad \text{and} \quad cos\,\theta_z = 1 \tag{7-3e}$$

Then Eqns. (7-2) can be rewritten as:

$$u = u_0 - (yv_0' + xw_0') \tag{7-4a}$$

$$v = v_0 - y + (y\sqrt{1 - (v_0')^2} + x\theta_z\sqrt{1 - (w_0')^2}) \tag{7-4b}$$

$$w = w_0 - x + (x\sqrt{1-(w_0')^2} - y\theta_z\sqrt{1-(v_0')^2}) \qquad (7\text{-}4c)$$

Eqn. (7-4a) is based on the assumption (Bernoulli's hypothesis) that plane cross-sections remain plane after deformation so that it only represents the axial deformation. It will be satisfied for solid or hollow members of circular cross-sections, since there is negligible effect from warping. However for thin-walled open beams, such as steel I-sections, it is necessary to include the effect of warping[79,92]. Adding the warping term ($\omega\theta_z'$) to Eqn. (7-4a), we have another equation for thin-walled open beams:

$$u = u_0 - yv_0' - xw_0' + \omega\theta_z' \qquad (7\text{-}4d)$$

where ω is the sectorial co-ordinate of the arbitrary point **A** as illustrated in Fig. 7-2. It should be noted that in some books the term ($\omega\theta_z'$) may have a minus sign, because the different sign convention is used of the sign for the sectorial co-ordinate (ω).

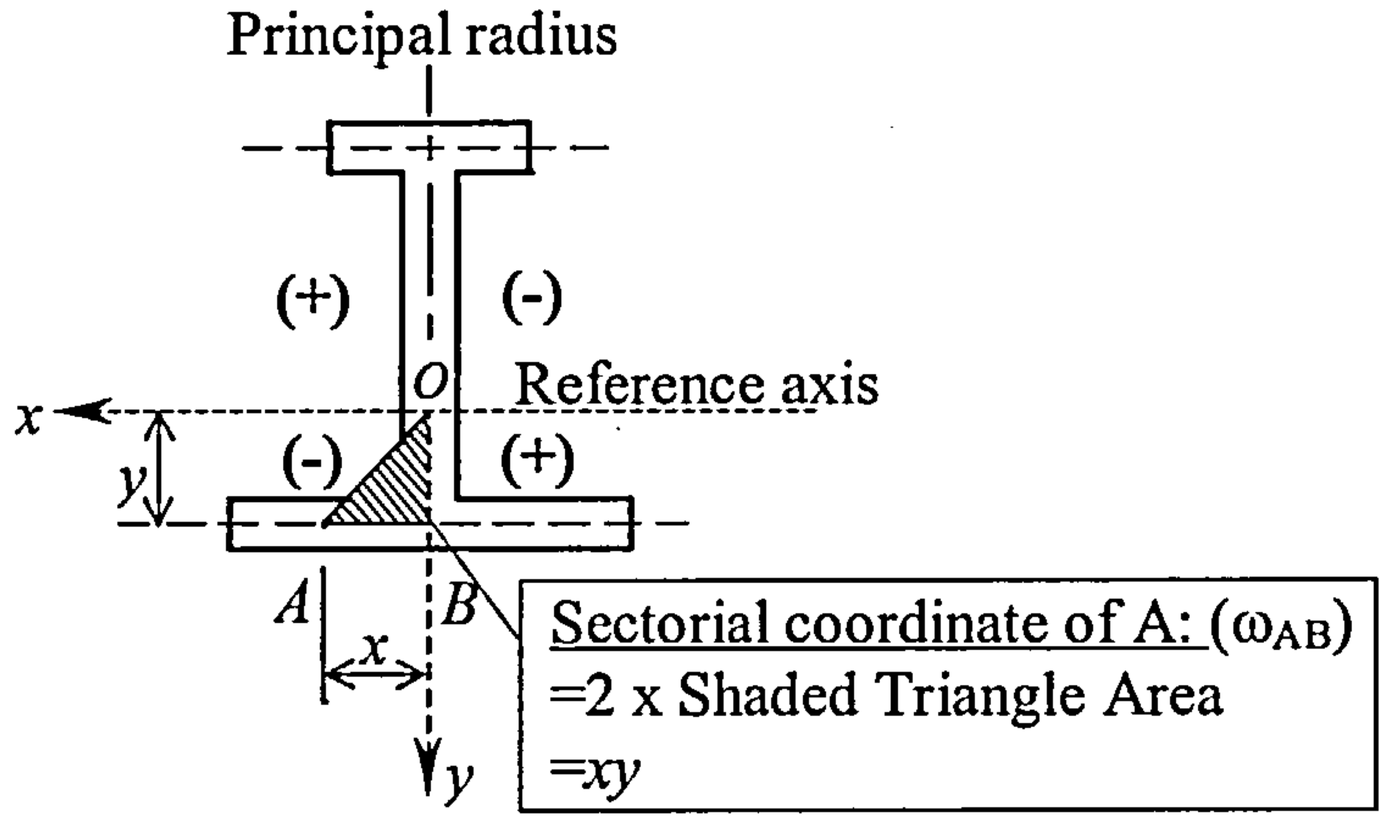

Fig. 7-2 Definition of sectorial co-ordinate of the arbitrary point *A*

The generalised equation can be obtained by applying an effective coefficient ($\alpha_{(x,y)}$) for the warping term.

$$u = u_0 - yv_0' - xw_0' + \alpha\omega\theta_z' \qquad (7\text{-}4e)$$

where α is a reduction factor; in the software, for thin-walled open section members a constant value of one will be used, but for solid or hollow members the value of zero should be applied to eliminate the effect of warping.

The equations (Eqns. (7-4)) can be put into matrix form as follows:

$$\begin{Bmatrix} u \\ v \\ w \end{Bmatrix} = \begin{bmatrix} 1 & -y\frac{\partial}{\partial z} & -x\frac{\partial}{\partial z} & \alpha\omega\frac{\partial}{\partial z} \\ 0 & 1 & 0 & 0 \\ 0 & 0 & 1 & 0 \end{bmatrix} \begin{Bmatrix} u_0 \\ v_0 \\ w_0 \\ \theta_z \end{Bmatrix} + \begin{Bmatrix} 0 \\ -y \\ -x \end{Bmatrix} + \left(\begin{bmatrix} 0 & 0 \\ y & 0 \\ 0 & x \end{bmatrix} + \begin{bmatrix} 0 & 0 \\ 0 & x \\ -y & 0 \end{bmatrix} \left(\begin{Bmatrix} 0 \\ 0 \\ 0 \\ 1 \end{Bmatrix}^T \begin{Bmatrix} u_0 \\ v_0 \\ w_0 \\ \theta_z \end{Bmatrix} \right) \right)$$

$$\begin{bmatrix} \sqrt{(\ )} & 0 \\ 0 & \sqrt{(\ )} \end{bmatrix} \left(\begin{Bmatrix} 1 \\ 1 \end{Bmatrix} - \left(\begin{bmatrix} 1 & 0 \\ 0 & 0 \end{bmatrix} \left(\begin{Bmatrix} 0 \\ \frac{\partial}{\partial z} \\ 0 \\ 0 \end{Bmatrix}^T \begin{Bmatrix} u_0 \\ v_0 \\ w_0 \\ \theta_z \end{Bmatrix} \right) + \begin{bmatrix} 0 & 0 \\ 0 & 1 \end{bmatrix} \left(\begin{Bmatrix} 0 \\ 0 \\ \frac{\partial}{\partial z} \\ 0 \end{Bmatrix}^T \begin{Bmatrix} u_0 \\ v_0 \\ w_0 \\ \theta_z \end{Bmatrix} \right) \right)$$

$$\begin{bmatrix} 0 & \frac{\partial}{\partial z} & 0 & 0 \\ 0 & 0 & \frac{\partial}{\partial z} & 0 \end{bmatrix} \begin{Bmatrix} u_0 \\ v_0 \\ w_0 \\ \theta_z \end{Bmatrix} \Bigg) \qquad (7\text{-}5a)$$

where $\sqrt{(\ )} = \sqrt{(\ )}$, and a pair of bold parenthesises "( )" has the highest priority compared with other operators.

If we create a new operator that $\sqrt{^2}(\ ) = \sqrt{1-(\ )^2}$, the tidy form of Eqn. (7-5a) can be given by:

$$\begin{Bmatrix} u \\ v \\ w \end{Bmatrix} = \Bigg(\begin{bmatrix} 1 & -y\frac{\partial}{\partial z} & -x\frac{\partial}{\partial z} & \alpha\omega\frac{\partial}{\partial z} \\ 0 & 1+y\sqrt{^2}\left(\frac{\partial}{\partial z}\right) & 0 & 0 \\ 0 & 0 & 1+x\sqrt{^2}\left(\frac{\partial}{\partial z}\right) & 0 \end{bmatrix} + \Big(\langle 0 \quad 0 \quad 0 \quad 1 \rangle \begin{Bmatrix} u_0 \\ v_0 \\ w_0 \\ \theta_z \end{Bmatrix} \Big)$$

$$\begin{bmatrix} 0 & 0 & 0 & 0 \\ 0 & 0 & x\sqrt{^2}\left(\frac{\partial}{\partial z}\right) & 0 \\ 0 & -y\sqrt{^2}\left(\frac{\partial}{\partial z}\right) & 0 & 0 \end{bmatrix} \Bigg) \begin{Bmatrix} u_0 \\ v_0 \\ w_0 \\ \theta_z \end{Bmatrix} + \begin{Bmatrix} 0 \\ -y \\ -x \end{Bmatrix} \qquad (7\text{-}5b)$$

In symbolic form, we have

$$\{u\} = [\overline{A}]\{u_0\} + \{k_c\} \qquad (7\text{-}5c)$$

in which $[\overline{A}]$ is the geometric description matrix and contains displacements, $\{k_c\}^T = \{0,-y,-x\}^T$.

The general definition of axial strain at any arbitrary point of a concrete beam element can be found by using large displacement equations (Green's strain tensor)[69,97] as

$$\varepsilon_z = u' + \frac{1}{2}\{(u')^2 + (v')^2 + (w')^2\} \tag{7-6a}$$

Eqn (7-6a) can also be written in matrix form by:

$$\varepsilon_z = \langle H_1 \rangle \{u\} + \frac{1}{2}\{u\}^T [H]^T [H] \{u\} \tag{7-6b}$$

in which $[H] = \begin{bmatrix} \frac{\partial}{\partial z} & 0 & 0 \\ 0 & \frac{\partial}{\partial z} & 0 \\ 0 & 0 & \frac{\partial}{\partial z} \end{bmatrix}$, $\langle H_1 \rangle = \left\langle \frac{\partial}{\partial z}, 0, 0 \right\rangle$ and $\{u\}^T = \langle u, v, w \rangle$.

or in symbolic form

$$\varepsilon_z = < \overline{S} > \{u\} \tag{7-6d}$$

where $\langle \overline{S} \rangle$ is a suitable operator vector, and the bar indicating non-linearity.

Differentiating Eqn. (7-4),

$$u' = u_0' - yv_0'' - xw_0'' + \alpha\omega\theta_z'' \tag{7-7a}$$

$$v' = v_0' + (-y\frac{v_0' v_0''}{\sqrt{1-(v_0')^2}}) + x\theta_z' \sqrt{1-(w_0')^2} + (-x\theta_z \frac{w_0' w_0''}{\sqrt{1-(w_0')^2}}) \tag{7-7b}$$

$$w' = w_0' + (-x\frac{w_0' w_0''}{\sqrt{1-(w_0')^2}}) - y\theta_z' \sqrt{1-(v_0')^2} - (-y\theta_z \frac{v_0' v_0''}{\sqrt{1-(v_0')^2}}) \tag{7-7c}$$

Ignoring the smaller terms containing $\theta_z v_0'$, $\theta_z w_0'$, and assuming the twist angle θ_z is small, Eqns. (7-7b,c) becomes

$$v' = v_0' - y\frac{v_0' v_0''}{\sqrt{1-(v_0')^2}} + x\theta_z'\sqrt{1-(w_0')^2} \qquad (7\text{-}7d)$$

$$w' = w_0' - x\frac{w_0' w_0''}{\sqrt{1-(w_0')^2}} - y\theta_z'\sqrt{1-(v_0')^2} \qquad (7\text{-}7e)$$

Substituting Eqns. (7-7a,d,e) into Eqn. (7-6a) produces

$$\varepsilon_z = u_0' - yv_0'' - xw_0'' + \alpha\omega\theta_z'' + \frac{1}{2}\{[(u_0')^2 + (yv_0'')^2 + (xw_0'')^2 + (\alpha\omega\theta_z'')^2 - 2yu_0'v_0'' -$$

$$2xu_0'w_0'' + 2\alpha\omega\theta_z''u_0' + 2xyv_0''w_0'' - 2yv_0''\alpha\omega\theta_z'' - 2xw_0''\alpha\omega\theta_z''] + [(v_0')^2 + (\frac{yv_0'v_0''}{\sqrt{1-(v_0')^2}})^2$$

$$+ (x\theta_z'\sqrt{1-(w_0')^2})^2 - \frac{2yv_0''(v_0')^2}{\sqrt{1-(v_0')^2}} + 2xv_0'\theta_z'\sqrt{1-(w_0')^2} - \frac{2xyv_0''v_0'}{\sqrt{1-(v_0')^2}}\theta_z'\sqrt{1-(w_0')^2}]$$

$$+ [(w_0')^2 + (\frac{xw_0'w_0''}{\sqrt{1-(w_0')^2}})^2 + (y\theta_z'\sqrt{1-(v_0')^2})^2 - \frac{2xw_0''(w_0')^2}{\sqrt{1-(w_0')^2}} - 2yw_0'\theta_z'\sqrt{1-(v_0')^2}$$

$$+ \frac{2xyw_0''w_0'}{\sqrt{1-(w_0')^2}}\theta_z'\sqrt{1-(v_0')^2}]\} \qquad (7\text{-}8a)$$

Discarding higher order terms, which may be negligible with respect to other terms, produces

$$\varepsilon_z = u_0' - yv_0'' - xw_0'' + \alpha\omega\theta_z'' + \frac{1}{2}(u_0')^2 - yu_0'v_0'' - xu_0'w_0'' + \alpha\omega\theta_z''u_0' + \frac{1}{2}(v_0')^2 - \frac{yv_0''(v_0')^2}{\sqrt{1-(v_0')^2}}$$

$$+ xv_0'\theta_z'\sqrt{1-(w_0')^2} + \frac{1}{2}(w_0')^2 - \frac{xw_0''(w_0')^2}{\sqrt{1-(w_0')^2}} - yw_0'\theta_z'\sqrt{1-(v_0')^2} \qquad (7\text{-}8b)$$

Furthermore, according to Taylor's series, $\sqrt{1-(v_0')^2}$ and $\frac{1}{\sqrt{1-(v_0')^2}}$ can be written

in infinite series forms by

$$\sqrt{1-(v_0')^2} = 1 - \frac{(v_0')^2}{2} - \frac{(v_0')^4}{8} - \cdots$$

$$\frac{1}{\sqrt{1-(v_0')^2}} = 1 + \frac{(v_0')^2}{2} + \frac{3(v_0')^4}{8} + \cdots$$

and similarly:

$$\sqrt{1-(w_0')^2} = 1 - \frac{(w_0')^2}{2} - \frac{(w_0')^4}{8} - \cdots$$

$$\frac{1}{\sqrt{1-(w_0')^2}} = 1 + \frac{(w_0')^2}{2} + \frac{3(w_0')^4}{8} + \cdots$$

For concrete beams v_0' and w_0' are relatively small, therefore Eqn. (7-8b) can be simplified by ignoring high order terms, producing

$$\varepsilon_z = u_0' - yv_0'' - xw_0'' + \alpha\omega\theta_z'' + \frac{1}{2}(u_0')^2 - yu_0'v_0'' - xu_0'w_0'' + \alpha\omega\theta_z''u_0' + \frac{1}{2}(v_0')^2 + \frac{1}{2}(w_0')^2 + xv_0'\theta_z' - yw_0'\theta_z' \qquad (7\text{-}8c)$$

It is noted that, because the beam element is a two-noded line element, the strains (ε_x, ε_y) in the **x**- and **y**-axes, which are perpendicular to beam z-axis, are free strains. In Eqn. (7-8c) the first four terms on the right hand side represent small linear-displacement strains and the rest are caused by non-linear displacement, thus Eqn. (7-8c) can be rewritten in terms of the infinitesimal and non-linear displacement components by

$$\varepsilon_z = \varepsilon_0 + \varepsilon_L \qquad (7\text{-}8d)$$

Since we have

$$d\varepsilon_0 = du_0' - ydv_0'' - xdw_0'' + \alpha\omega d\theta_z''$$

and

$$d\varepsilon_L = u_0'du_0' - yv_0''du_0' - yu_0'dv_0'' - xw_0''du_0' - xu_0'dw_0'' + \alpha\omega\theta_z''du_0' + \alpha\omega u_0'd\theta_z'' + v_0'dv_0' + w_0'dw_0' + x\theta_z'dv_0' + xv_0'd\theta_z' - y\theta_z'dw_0' - yw_0'd\theta_z'$$

then writing in matrix form there is

$$d\varepsilon_z = d\varepsilon_0 + d\varepsilon_L = \langle B_0 \rangle \{dq\} + \langle \overline{B}_L \rangle \{dq\} \qquad (7\text{-}9a)$$

where,

$$\langle B_0 \rangle = \langle \langle N_a' \rangle, -y\langle N_a'' \rangle, -x\langle N_a'' \rangle, \alpha\omega\langle N_a'' \rangle \rangle$$

and only $\langle \overline{B}_L \rangle$ depends on the displacements,

$$\langle \overline{B}_L \rangle = \langle (u_0' - yv_0'' - xw_0'' + \alpha\omega\theta_z'')\langle N_a' \rangle, (v_0' + x\theta_z')\langle N_a' \rangle - yu_0'\langle N_a'' \rangle,$$
$$(w_0' - y\theta_z')\langle N_a' \rangle - xu_0'\langle N_a'' \rangle, (xv_0' - yw_0')\langle N_a' \rangle + \alpha\omega u_0'\langle N_a'' \rangle \rangle$$

or

$$\{\overline{B}_L\} = \begin{bmatrix} \{N_a'\} & \{0\} & \{0\} & \{0\} & \{0\} & \{0\} & \{0\} \\ \{0\} & \{N_a'\} & \{0\} & \{0\} & \{N_a''\} & \{0\} & \{0\} \\ \{0\} & \{0\} & \{N_a'\} & \{0\} & \{0\} & \{N_a''\} & \{0\} \\ \{0\} & \{0\} & \{0\} & \{N_a'\} & \{0\} & \{0\} & \{N_a''\} \end{bmatrix} \begin{bmatrix} \langle N_a' \rangle & -y\langle N_a'' \rangle & -x\langle N_a'' \rangle & \alpha\omega\langle N_a'' \rangle \\ \langle 0 \rangle & \langle N_a' \rangle & \langle 0 \rangle & x\langle N_a' \rangle \\ \langle 0 \rangle & \langle 0 \rangle & \langle N_a' \rangle & -y\langle N_a' \rangle \\ \langle 0 \rangle & x\langle N_a' \rangle & -y\langle N_a' \rangle & \langle 0 \rangle \\ -y\langle N_a' \rangle & \langle 0 \rangle & \langle 0 \rangle & \langle 0 \rangle \\ -x\langle N_a' \rangle & \langle 0 \rangle & \langle 0 \rangle & \langle 0 \rangle \\ \alpha\omega\langle N_a' \rangle & \langle 0 \rangle & \langle 0 \rangle & \langle 0 \rangle \end{bmatrix} \{q\}$$

$$= \begin{bmatrix} \{N_a'\}\langle N_a' \rangle & -y\{N_a'\}\langle N_a'' \rangle & -x\{N_a'\}\langle N_a'' \rangle & \alpha\omega\{N_a'\}\langle N_a'' \rangle \\ -y\{N_a''\}\langle N_a' \rangle & \{N_a'\}\langle N_a' \rangle & [0] & x\{N_a'\}\langle N_a' \rangle \\ -x\{N_a''\}\langle N_a' \rangle & [0] & \{N_a'\}\langle N_a' \rangle & -y\{N_a'\}\langle N_a' \rangle \\ \alpha\omega\{N_a''\}\langle N_a' \rangle & x\{N_a'\}\langle N_a' \rangle & -y\{N_a'\}\langle N_a' \rangle & [0] \end{bmatrix} \{q\}$$

$$= \begin{bmatrix} [N_{a2}] & -y[N_{b2}] & -x[N_{b2}] & \alpha\omega[N_{b2}] \\ -y[N_{b2}]^T & [N_{a2}] & [0] & x[N_{a2}] \\ -x[N_{b2}]^T & [0] & [N_{a2}] & -y[N_{a2}] \\ \alpha\omega[N_{b2}]^T & x[N_{a2}]^T & -y[N_{a2}]^T & [0] \end{bmatrix} \{q\}$$

$$= \begin{bmatrix} [N_{a2}] & -y[N_{b2}] & -x[N_{b2}] & \alpha\omega[N_{b2}] \\ & [N_{a2}] & [0] & x[N_{a2}] \\ & \textit{symmetric} & [N_{a2}] & -y[N_{a2}] \\ & & & [0] \end{bmatrix} \{dq\} = [B_L]\{q\}$$

in which,

$$[N_{a2}]=\{N_a'\}\langle N_a'\rangle=\begin{bmatrix} N_1'N_1' & N_1'N_2' & N_1'N_3' & N_1'N_4' \\ & N_2'N_2' & N_2'N_3' & N_2'N_4' \\ & \textit{symmetric} & N_3'N_3' & N_3'N_4' \\ & & & N_4'N_4' \end{bmatrix}$$

$$[N_{b2}]=\{N_a'\}\langle N_a''\rangle=\begin{bmatrix} N_1'N_1'' & N_1'N_2'' & N_1'N_3'' & N_1'N_4'' \\ N_2'N_1'' & N_2'N_2'' & N_2'N_3'' & N_2'N_4'' \\ N_3'N_1'' & N_3'N_2'' & N_3'N_3'' & N_3'N_4'' \\ N_4'N_1'' & N_4'N_2'' & N_4'N_3'' & N_4'N_4'' \end{bmatrix}, [0]=\begin{bmatrix} 0 & 0 & 0 & 0 \\ 0 & 0 & 0 & 0 \\ 0 & 0 & 0 & 0 \\ 0 & 0 & 0 & 0 \end{bmatrix};$$

Since matrix $[B_L]$ is symmetric, i.e. $[B_L]=[B_L]^T$, Eqn. (7-9a) may by rewritten as

$$d\varepsilon_z = d\varepsilon_0 + d\varepsilon_L = \langle B_0\rangle\{dq\}+\langle \overline{B}_L\rangle\{dq\}=\langle B_0\rangle\{dq\}+\langle q\rangle[B_L]\{dq\} \qquad (7\text{-}9b)$$

Denoting $\langle \overline{B}\rangle=\langle B_0\rangle+\langle \overline{B}_L\rangle$ Eqn. (7-9a) becomes

$$d\varepsilon_z=\langle \overline{B}\rangle\{dq\} \qquad (7\text{-}9c)$$

in which $\langle \overline{B}\rangle$ is a strain-displacement vector and contains displacements.

The non-linear shear strains at any arbitrary point of a concrete beam element may be expressed by[69]

$$\gamma_{xz}=\frac{\partial u}{\partial x}+\frac{\partial w}{\partial z}+(\frac{\partial u}{\partial x}\cdot\frac{\partial u}{\partial z}+\frac{\partial v}{\partial x}\cdot\frac{\partial v}{\partial z}+\frac{\partial w}{\partial x}\cdot\frac{\partial w}{\partial z}) \qquad (7\text{-}10a)$$

and

$$\gamma_{yz}=\frac{\partial u}{\partial y}+\frac{\partial w}{\partial z}+(\frac{\partial u}{\partial y}\cdot\frac{\partial u}{\partial z}+\frac{\partial v}{\partial y}\cdot\frac{\partial v}{\partial z}+\frac{\partial w}{\partial y}\cdot\frac{\partial w}{\partial z}) \qquad (7\text{-}10b)$$

It is evident that since we assumed no distortion over the cross-section the shear strain γ_{xy} is equal to zero.

Substituting Eqns. (7-4b,c,e) into Eqn. (7-10a,b) and ignoring higher order terms

$$\gamma_{xz}=v_0'\theta_z \text{ and } \gamma_{yz}=-w_0'\theta_z \qquad (7\text{-}10c)$$

and we also have their infinitesimal increments form

$$d\gamma_{xz} = \langle \overline{B}_{xz} \rangle \{dq\} \text{ and } d\gamma_{yz} = \langle \overline{B}_{yz} \rangle \{dq\} \qquad (7\text{-}11a)$$

where

$$\langle \overline{B}_{xz} \rangle = \langle \langle 0 \rangle, \theta_z \langle N_a' \rangle, \langle 0 \rangle, v_0' \langle N_a \rangle \rangle$$

or

$$\{\overline{B}_{xz}\} = \begin{bmatrix} \{0\} & \{0\} \\ \{N_a'\} & \{0\} \\ \{0\} & \{0\} \\ \{0\} & \{N_a\} \end{bmatrix} \begin{bmatrix} \langle 0 \rangle & \langle 0 \rangle & \langle 0 \rangle & \langle N_a \rangle \\ \langle 0 \rangle & \langle N_a' \rangle & \langle 0 \rangle & \langle 0 \rangle \end{bmatrix} \{q\}$$

$$= \begin{bmatrix} [0] & [0] & [0] & [0] \\ [0] & [0] & [0] & \{N_a'\}\langle N_a \rangle \\ [0] & [0] & [0] & [0] \\ [0] & \{N_a\}\langle N_a' \rangle & [0] & [0] \end{bmatrix} \{q\} = \begin{bmatrix} [0] & [0] & [0] & [0] \\ & [0] & [0] & [N_{c2}] \\ & \textit{symmetric} & [0] & [0] \\ & & & [0] \end{bmatrix} \{q\}$$

$$= [B_{xz}]\{q\}$$

and,

$$\langle \overline{B}_{yz} \rangle = \langle \langle 0 \rangle, \langle 0 \rangle, -\theta_z \langle N_a' \rangle, -w_0' \langle N_a \rangle \rangle$$

or

$$\{\overline{B}_{yz}\} = -\begin{bmatrix} \{0\} & \{0\} \\ \{0\} & \{0\} \\ \{N_a'\} & \{0\} \\ \{0\} & \{N_a\} \end{bmatrix} \begin{bmatrix} \langle 0 \rangle & \langle 0 \rangle & \langle 0 \rangle & \langle N_a \rangle \\ \langle 0 \rangle & \langle 0 \rangle & \langle N_a' \rangle & \langle 0 \rangle \end{bmatrix} \{q\}$$

$$= -\begin{bmatrix} [0] & [0] & [0] & [0] \\ [0] & [0] & [0] & [0] \\ [0] & [0] & [0] & \{N_a'\}\langle N_a \rangle \\ [0] & [0] & \{N_a\}\langle N_a' \rangle & [0] \end{bmatrix} \{q\} = \begin{bmatrix} [0] & [0] & [0] & [0] \\ & [0] & [0] & [0] \\ & \textit{symmetric} & [0] & -[N_{c2}] \\ & & & [0] \end{bmatrix} \{q\}$$

$$= [B_{yz}]\{q\}$$

in which,

$$[N_{c2}] = \{N_a'\}\langle N_a\rangle = \begin{bmatrix} N_1'N_1 & N_1'N_2 & N_1'N_3 & N_1'N_4 \\ N_2'N_1 & N_2'N_2 & N_2'N_3 & N_2'N_4 \\ N_3'N_1 & N_3'N_2 & N_3'N_3 & N_3'N_4 \\ N_4'N_1 & N_4'N_2 & N_4'N_3 & N_4'N_4 \end{bmatrix}$$

Since matrixes $[B_{xz}]$ and $[B_{yz}]$ are symmetric, Eqn. (7-11a) may be rewritten as

$$d\gamma_{xz} = \langle q\rangle[B_{xz}]\{dq\} \text{ and } d\gamma_{yz} = \langle q\rangle[B_{yz}]\{dq\} \quad (7\text{-}11b)$$

Therefore the infinitesimal generalised strain increments can be expressed by

$$\{d\varepsilon\} = [\overline{B}]\{dq\} \quad (7\text{-}12)$$

where $\{d\varepsilon\}^T = \langle d\varepsilon_z, d\gamma_{xz}, d\gamma_{yz}\rangle$ and $[\overline{B}]_{3x16} = \begin{bmatrix} \langle \overline{B} \rangle \\ \langle \overline{B}_{xz} \rangle \\ \langle \overline{B}_{yz} \rangle \end{bmatrix}$

Based on the stain-displacement relationship, Eqn. (7-12), and applying the principle of virtual work

$$\delta W = \int_V \{\delta\varepsilon\}^T \{\sigma\} dV - \{\delta q\}^T \{Q\} = 0 \quad (7\text{-}13)$$

where $\{\sigma\} = \{\sigma_z, \tau_{xz}, \tau_{yz}\}$ and $\{\varepsilon\}^T = \langle \varepsilon_z, \gamma_{xz}, \gamma_{yz}\rangle$ in which ε_z expresses the mechanical axial strain and is given by $\varepsilon_{zm} = \varepsilon_{zt} - \varepsilon_{zth} - \varepsilon_{zr}$, where ε_{zm} is mechanical axial strain, ε_{zt} is total axial strain, ε_{zth} is thermally-induced axial strain, and ε_{zr} is residual axial strain. Since the concrete beam element is a two-noded line element of isotropic material, the stress-strain relationship will be

$$\{\delta\sigma\} = [C]\{\delta\varepsilon\} \quad (7\text{-}14)$$

where $[C] = \begin{bmatrix} E & 0 & 0 \\ 0 & G & 0 \\ 0 & 0 & G \end{bmatrix}$ in which $G = \frac{E}{2(1+\nu)}$. G for steel is typically $G = \frac{E}{2.6}$, and for concrete in compression $G = \frac{E}{2.2}$.

It may be observed from Eqn. (7-13) that twisting is not considered, but nevertheless the total internal twisting moment can be found by[92]

$$T = T_w + T_\sigma + T_{sv} \tag{7-15a}$$

in which,

T_w is the twisting moment due to the warping shear stress and is given by $T_w = M_\omega^{'}$;

T_σ is known as the Wagner effect and $T_\sigma = \overline{K}\theta_z^{'}$; here $\overline{K}$ is called the Wagner coefficient which is given by $\overline{K} = \int_A \sigma_z (x^2 + y^2)dA$;

T_{sv} is the twisting moment due to St. Venant shear stress and is given by $T_{sv} = GJ\theta_z^{'}$.

The first two terms on the right hand side of Eqn. (7-15a) are caused by warping deformation, and they are both higher order effects; these effects may be ignored especially for solid or closed sections, for which warping is very small. Thereby Eqn. (7-15a) can be simplified as

$$T = T_{sv} = GJ\theta_z^{'} \tag{7-15b}$$

where **J** is the St. Venant torsional constant (or torsion constant). The product of **G** and **J** is known as torsional rigidity. Procedures for calculating the torsion constant are given in appendix B. It is to be noted that the twisting moment is acting about the shear centre, and for I-sections and rectangular sections the shear centre coincides with the centroid.

If we now consider the twisting effect from Eqn. (7-15), Eqn. (7-13) becomes

$$\delta W = \int_V \{\delta\varepsilon\}^T \{\sigma\} dV + \int_L T\delta\theta_z^{'} dz - \{\delta q\}^T \{Q\} = 0 \tag{7-16}$$

On substitution and rewriting Eqn. (7-16) we have,

$$\delta W = \int_L \left(\int_A \{\delta q\}^T \left[\overline{B}\right]^T \{\sigma\} dV + \{\delta q\}^T \langle B_t \rangle^T T \right) dz - \{\delta q\}^T \{Q\} = 0 \tag{7-17}$$

where $\langle B_t \rangle = \langle \langle 0 \rangle, \langle 0 \rangle, \langle 0 \rangle, \langle N_a^{'} \rangle \rangle$

Because of equilibrium, we have

$$\psi_i = \frac{\partial W}{\partial q_i} = 0$$

where i has the range of the number of local degrees of freedom for the beam element,

Thus

$$\{\psi\} = \int_L \left(\int_A \left[\overline{B}\right]^T \{\sigma\} dA + \left\langle B_t \right\rangle^T T \right) dz - \{Q\} = \{0\} \qquad (7\text{-}18)$$

Eqn. (7-18) may be rearranged as

$$\{\psi\} = \int_L \left(\int_A \left(\{B_0\}\sigma_z + \{\overline{B}_L\}\sigma_z + \{\overline{B}_{xz}\}\tau_{xz} + \{\overline{B}_{yz}\}\tau_{yz} \right) dA + \{B_t\}T \right) dz - \{Q\} \qquad (7\text{-}19a)$$

or

$$\{\psi\} = \int_L \left(\int_A \left(\{B_0\}\sigma_z + [B_L]\{q\}\sigma_z + [B_{xz}]\{q\}\tau_{xz} + [B_{yz}]\{q\}\tau_{yz} \right) dA + \{B_t\}T \right) dz - \{Q\} \qquad (7\text{-}19b)$$

where $\{\psi\}$ represents the sum of external loads and internal generalised forces.

Since Eqn. (7-19) is highly non-linear, it may be not satisfied exactly, and the Newton-Raphson method can be employed to yield[69]

$$\Delta\psi_i = \frac{\partial \psi_i}{\partial q_j} \Delta q_j = -\psi_i \qquad (7\text{-}20)$$

so that

$$\int_L \left(\int_A \left(\left[\overline{B}\right]^T [C] \left[\overline{B}\right] + [B_L]\sigma_z + [B_{xz}]\tau_{xz} + [B_{yz}]\tau_{yz} \right) dA + \left\langle B_t \right\rangle^T GJ \left\langle B_t \right\rangle \right) dz \cdot \{\Delta q\}$$
$$= \{Q\} - \int_L \left(\int_A \left[\overline{B}\right]^T \{\sigma\} dA + \left\langle B_t \right\rangle^T T \right) dz \qquad (7\text{-}21)$$

Eqn. (7-21) can be extended as

$$\int_L \left(\int_A \left(\{B_0\} E_t \{B_0\}^T + \{B_0\} E_t \{\overline{B}_L\}^T + \{\overline{B}_L\} E_t \{B_0\}^T + \{\overline{B}_t\} E_t \{\overline{B}_L\}^T + \{\overline{B}_{xz}\} G \{\overline{B}_{xz}\}^T + \right.\right.$$
$$\left.\left. \{\overline{B}_{yxz}\} G \{\overline{B}_{yxz}\}^T + [B_L]\sigma_z + [B_{xz}]\tau_{xz} + [B_{yz}]\tau_{yz} \right) dA + \{B_t\} GJ \{B_t\}^T \right) dz \cdot \{\Delta q\}$$
$$= \{Q\} - \int_L \left(\int_A \left(\{B_0\}\sigma_z + \{\overline{B}_L\}\sigma_z + \{\overline{B}_{xz}\}\tau_{xz} + \{\overline{B}_{yz}\}\tau_{yz} \right) dA + \{B_t\}T \right) dz \qquad (7\text{-}22)$$

Rearranging produces

$$\left(\int_L\left(\int_A\{B_0\}E_t\{B_0\}^T dA+\{B_t\}GJ\{B_t\}^T\right)dz+\int_L\int_A\left(\{B_0\}E_t\{\overline{B}_L\}^T+\{\overline{B}_L\}E_t\{B_0\}^T+\{\overline{B}_l\}E_t\{\overline{B}_L\}^T\right.\right.$$
$$\left.\left.+\{\overline{B}_{xz}\}G\{\overline{B}_{xz}\}^T+\{\overline{B}_{yxz}\}G\{\overline{B}_{yxz}\}^T\right)dAdz+\int_L\int_A\left([B_L]\sigma_z+[B_{xz}]\tau_{xz}+[B_{yz}]\tau_{yz}\right)dAdz\right)\cdot\{\Delta q\}$$
$$=\{Q\}-\int_L\left(\int_A\left(\{B_0\}\sigma_z+\{\overline{B}_L\}\sigma_z+\{\overline{B}_{xz}\}\tau_{xz}+\{\overline{B}_{yz}\}\tau_{yz}\right)dA+\{B_t\}T\right)dz \qquad (7\text{-}22)$$

In symbolic form we have

$$\left([K_0]+[K_L]+[K_\sigma]\right)\cdot\{\Delta q\}=\{Q\}-\{Q^R\} \qquad \text{or} \qquad [K_t]\{\Delta q\}=\{\Delta Q\} \qquad (7\text{-}23)$$

in which,

$\{Q^R\}$ is the internal (resisting) force,

$$\{Q^R\}=\int_L\left(\int_A\left(\{B_0\}\sigma_z+\{\overline{B}_L\}\sigma_z+\{\overline{B}_{xz}\}\tau_{xz}+\{\overline{B}_{yz}\}\tau_{yz}\right)dA+\{B_t\}T\right)dz;$$

$[K_t]$ is known as the tangential stiffness matrix for an element in local coordinates,

defined by

$$[K_t]=[K_0]+[K_L]+[K_\sigma] \qquad (7\text{-}24)$$

where,

$[K_0]$ is the small (linear) displacement stiffness matrix given by

$$[K_0]=\int_L\left(\int_A\{B_0\}E_t\{B_0\}^T dA+\{B_t\}GJ\{B_t\}^T\right)dz \qquad (7\text{-}25a)$$

$[K_L]$ represents the large displacement stiffness matrix

$$[K_L]=\int_L\int_A\left(\{B_0\}E_t\{\overline{B}_L\}^T+\{\overline{B}_L\}E_t\{B_0\}^T+\{\overline{B}_L\}E_t\{\overline{B}_L\}^T+\{\overline{B}_{xz}\}G\{\overline{B}_{xz}\}^T+\right.$$
$$\left.\{\overline{B}_{yz}\}G\{\overline{B}_{yz}\}^T\right)dAdz \qquad (7\text{-}25b)$$

$[K_\sigma]$ represents the geometric matrix

$$[K_\sigma]=\int_L\int_A\left([B_L]\sigma_z+[B_{xz}]\tau_{xz}+[B_{yz}]\tau_{yz}\right)dAdz \qquad (7\text{-}25c)$$

If we denote the section properties and stress resultants as

- Section and sectorial properties

$$A=\int_A dA, \qquad I_x=\int_A x dA,$$

$$I_y = \int_A y dA, \qquad I_{x2} = \int_A x^2 dA,$$

$$I_{y2} = \int_A y^2 dA, \qquad I_{xy} = \int_A xy dA,$$

$$I_\omega = \int_A \omega dA, \qquad I_{\omega x} = \int_A \omega x dA,$$

$$I_{\omega y} = \int_A \omega y dA, \qquad I_{\omega 2} = \int_A \omega^2 dA.$$

- Stress resultants:

$$n = \int_A \sigma_z dA\ , \qquad m_x = \int_A \sigma_z y dA,$$

$$m_y = \int_A \sigma_z x dA, \qquad m_\omega = \int_A \sigma_z \omega dA,$$

$$V_x = \int_A \tau_{xz} dA, \qquad V_y = \int_A \tau_{yz} dA,$$

$$T_{sv} = GJ\theta_z'$$

the small displacement stiffness matrix, large displacement stiffness matrix and geometric matrix can be expressed as follows:

The small displacement stiffness matrix ($[K_0]$):

Denoting $[K_{01}] = \int_L \int_A \{B_0\} E_t \{B_0\}^T dA dz$ and $[K_{02}] = \int_L \{B_t\} GJ \{B_t\}^T dz$ produces

$$[K_{01}] = E_t \begin{bmatrix} \int_L A[N_{a2}]dz & -\int_L I_y[N_{b2}]dz & -\int_L I_x[N_{b2}]dz & \int_L \alpha I_\omega [N_{b2}]dz \\ & \int_L I_{y2}[N_{d2}]dz & \int_L I_{xy}[N_{d2}]dz & -\int_L \alpha I_{\omega y}[N_{d2}]dz \\ & \textit{symmetric} & \int_L I_{x2}[N_{d2}]dz & -\int_L \alpha I_{\omega x}[N_{d2}]dz \\ & & & \int_L \alpha^2 I_{\omega 2}[N_{d2}]dz \end{bmatrix}$$

$$[K_{02}] = GJ \begin{bmatrix} [0] & [0] & [0] & [0] \\ & [0] & [0] & [0] \\ & \textit{symmetric} & [0] & [0] \\ & & & \int_L [N_{a2}]dz \end{bmatrix}$$

From Eqn. (7-25a) we have,

$$[K_0]_{16x16} = [K_{01}] + [K_{02}] =$$

$$\begin{bmatrix} \int_L E_t A[N_{a2}]dz & -\int_L E_t I_y[N_{b2}]dz & -\int_L E_t I_x[N_{b2}]dz & \int_L \alpha E_t I_\omega[N_{b2}]dz \\ & \int_L E_t I_{y2}[N_{d2}]dz & \int_L E_t I_{xy}[N_{d2}]dz & -\int_L \alpha E_t I_{\omega y}[N_{d2}]dz \\ & \textit{symmetric} & \int_L E_t I_{x2}[N_{d2}]dz & -\int_L \alpha E_t I_{\omega x}[N_{d2}]dz \\ & & & \int_L (\alpha^2 E_t I_{\omega 2}[N_{d2}] + GJ[N_{a2}])dz \end{bmatrix} \quad (7\text{-}26a)$$

where,

$$[N_{d2}] = \{N_a''\}\langle N_a''\rangle = \begin{bmatrix} N_1''N_1'' & N_1''N_2'' & N_1''N_3'' & N_1''N_4'' \\ & N_2''N_2'' & N_2''N_3'' & N_2''N_4'' \\ & \textit{symmetric} & N_3''N_3'' & N_3''N_4'' \\ & & & N_4''N_4'' \end{bmatrix}$$

The large displacement stiffness matrix ($[K_L]$):

Denoting $[K_{L1}] = \int_L \int_A \{\overline{B}_L\} E_t \{\overline{B}_L\}^T dAdz$, $[K_{L2}] = \int_L \int_A \{B_0\} E_t \{\overline{B}_L\}^T dAdz$,

$[K_{L3}] = \int_L \int_A \{\overline{B}_L\} E_t \{B_0\}^T dAdz$, $[K_{L4}] = \int_L \int_A \{\overline{B}_{xz}\} G \{\overline{B}_{xz}\}^T dAdz$,

$[K_{L5}] = \int_L \int_A \{\overline{B}_{yz}\} G \{\overline{B}_{yz}\} dAdz$ produces

$$(1)\quad [K_{L1}] = \begin{bmatrix} [K_{L1a}] & [K_{L1b}] & [K_{L1c}] & [K_{L1d}] \\ & [K_{L1e}] & [K_{L1f}] & [K_{L1g}] \\ & \textit{symmetric} & [K_{L1h}] & [K_{L1i}] \\ & & & [K_{L1j}] \end{bmatrix}$$

in which

$$[K_{L1a}] = \int_L E_t(A(u_0')^2 + I_{y2}(v_0'')^2 + I_{x2}(w_0'')^2 + \alpha^2 I_{\omega 2}(\theta_z'')^2 - 2I_y u_0' v_0'' - 2I_x u_0' w_0'' + 2\alpha I_\omega u_0' \theta_z'' + 2I_{xy} v_0'' w_0'' - 2\alpha I_{\omega y} v_0'' \theta_z'' - 2\alpha I_{\omega x} w_0'' \theta_z'')[N_{a2}]dz$$

$$[K_{L1b}] = \int_L E_t((Au_0' v_0' - I_y v_0' v_0'' - I_x v_0' w_0'' + \alpha I_\omega v_0' \theta_z'' + I_x u_0' \theta_z' - I_{xy} v_0' \theta_z' - I_{x2} w_0'' \theta_z' + \alpha I_{\omega x} \theta_z' \theta_z'')[N_{a2}] - (I_y(u_0')^2 - I_{y2} u_0' v_0'' - I_{xy} u_0' w_0'' + \alpha I_{\omega y} u_0' \theta_z'')[N_{b2}])dz$$

$$[K_{L1c}]=\int_L E_t((u_0'w_0'-I_y w_0'v_0''-I_x w_0'w_0''+\alpha I_\omega w_0'\theta_z''-I_y u_0'\theta_z'+I_{y2}v_0''\theta_z'+I_{xy}w_0''\theta_z'-\alpha I_{\omega y}\theta_z'\theta_z'')[N_{a2}]-(I_x(u_0')^2-I_{xy}u_0'v_0''-I_{x2}u_0'w_0''+\alpha I_{\omega x}u_0'\theta_z'')[N_{b2}])dz$$

$$[K_{L1d}]=\int_L E_t((I_x u_0'v_0'-I_{xy}v_0'v_0''-I_{x2}v_0'w_0''+\alpha I_{\omega x}v_0'\theta_z''-I_y u_0'w_0'+I_{y2}w_0'v_0''+I_{xy}w_0'w_0''-\alpha I_{\omega y}w_0'\theta_z'')[N_{a2}]+(\alpha I_\omega(u_0')^2-\alpha I_{\omega y}u_0'v_0''-\alpha I_{x\omega}u_0'w_0''+\alpha^2 I_{\omega 2}u_0'\theta_z'')[N_{b2}])dz$$

$$[K_{L1e}]=\int_L E_t((A(v_0')^2+2I_x v_0'\theta_z'+I_{x2}(\theta_z')^2)[N_{a2}]-(I_y u_0'v_0'+I_{xy}u_0'\theta_z')([N_{b2}]+[N_{b2}]^T)+I_{y2}(u_0')^2[N_{d2}])dz$$

$$[K_{L1f}]=\int_L E_t((Av_0'w_0'-I_y v_0'\theta_z'+I_x w_0'\theta_z'+I_{xy}(\theta_z')^2)[N_{a2}]-(I_x u_0'v_0'+I_{x2}u_0'\theta_z')[N_{b2}]-(I_y u_0'w_0'-I_{y2}u_0'\theta_z')[N_{b2}]^T+I_{xy}(u_0')^2[N_{d2}])dz$$

$$[K_{L1g}]=\int_L E_t((I_x(v_0')^2-I_y v_0'w_0'+I_{x2}v_0'\theta_z'-I_{xy}w_0'\theta_z')[N_{a2}]+(\alpha I_\omega u_0'v_0'+\alpha I_{\omega x}u_0'\theta_z')[N_{b2}]-(I_{xy}u_0'v_0'-I_{y2}u_0'w_0')[N_{b2}]^T-\alpha I_{\omega y}(u_0')^2[N_{b2}])dz$$

$$[K_{L1h}]=\int_L E_t((A(w_0')^2-2I_y w_0'\theta_z'+I_{y2}(\theta_z')^2)[N_{a2}]-(I_x u_0'w_0'-I_{xy}u_0'\theta_z')([N_{b2}]+[N_{b2}]^T)+I_{x2}(u_0')^2[N_{d2}])dz$$

$$[K_{L1i}]=\int_L E_t((I_x v_0'w_0'-I_y(w_0')^2-I_{xy}v_0'\theta_z'+I_{y2}w_0'\theta_z')[N_{a2}]+(\alpha I_\omega u_0'w_0'-\alpha I_{\omega y}u_0'\theta_z')[N_{b2}]-(I_{x2}u_0'v_0'-I_{xy}u_0'w_0')[N_{b2}]^T-\alpha I_{\omega x}(u_0')^2[N_{d2}])dz$$

$$[K_{L1j}]=\int_L E_t((I_{x2}(v_0')^2-2I_{xy}v_0'w_0'+I_{y2}(w_0')^2)[N_{a2}]+(\alpha I_{\omega x}u_0'v_0'-\alpha I_{\omega y}u_0'w_0')([N_{b2}]+[N_{b2}]^T)+\alpha^2 I_{\omega 2}(u_0')^2[N_{d2}])dz$$

$$(2)\quad [K_{L2}]=[K_{L3}]^T=\begin{bmatrix}[K_{L2a}] & [K_{L2b}] & [K_{L2c}] & [K_{L2d}]\\ [K_{L2e}] & [K_{L2f}] & [K_{L2g}] & [K_{L2h}]\\ [K_{L2i}] & [K_{L2j}] & [K_{L2k}] & [K_{L2l}]\\ [K_{L2m}] & [K_{L2n}] & [K_{L2o}] & [K_{L2p}]\end{bmatrix}$$

in which,

$$[K_{L2a}]=\int_L E_t(Au_0'-I_y v_0''-I_x w_0''+\alpha I_\omega\theta_z'')[N_{a2}]dz$$

$$[K_{L2b}]=\int_L E_t((Av_0'+I_x\theta_z')[N_{a2}]-I_y u_0'[N_{b2}])dz$$

$$[K_{L2c}]=\int_L E_t((Aw_0'-I_y\theta_z')[N_{a2}]-I_x u_0'[N_{b2}])dz$$

$$[K_{L2d}] = \int_L E_t((I_x v_0' - I_y w_0')[N_{a2}] + \alpha I_\omega u_0'[N_{b2}])dz$$

$$[K_{L2e}] = \int_L E_t(-I_y u_0' + I_{y2} v_0'' + I_{xy} w_0'' - \alpha I_{\omega y} \theta_z'')[N_{b2}]^T dz$$

$$[K_{L2f}] = \int_L E_t(-(I_y v_0' + I_{xy} \theta_z')[N_{b2}]^T + I_{y2} u_0'[N_{d2}])dz$$

$$[K_{L2g}] = \int_L E_t((-I_y w_0' + I_{y2} \theta_z')[N_{b2}]^T + I_{xy} u_0'[N_{d2}])dz$$

$$[K_{L2h}] = \int_L E_t((-I_{xy} v_0' + I_{y2} w_0')[N_{b2}]^T - \alpha I_{\omega y} u_0'[N_{d2}])dz$$

$$[K_{L2i}] = \int_L E_t(-I_x u_0' + I_{xy} v_0'' + I_{x2} w_0'' - \alpha I_{\omega x} \theta_z'')[N_{b2}]^T dz$$

$$[K_{L2j}] = \int_L E_t(-(I_x v_0' + I_{x2} \theta_z')[N_{b2}]^T + I_{xy} u_0'[N_{d2}])dz$$

$$[K_{L2k}] = \int_L E_t((-I_x w_0' + I_{xy} \theta_z')[N_{b2}]^T + I_{x2} u_0'[N_{d2}])dz$$

$$[K_{L2l}] = \int_L E_t((-I_{x2} v_0' + I_{xy} w_0')[N_{b2}]^T - \alpha I_{\omega x} u_0'[N_{d2}])dz$$

$$[K_{L2m}] = \int_L E_t(\alpha I_\omega u_0' - \alpha I_{\omega y} v_0'' - \alpha I_{\omega x} w_0'' - \alpha^2 I_{\omega 2} \theta_z'')[N_{b2}]^T dz$$

$$[K_{L2n}] = \int_L \alpha E_t((I_\omega v_0' + I_{\omega x} \theta_z')[N_{b2}]^T - I_{\omega y} u_0'[N_{d2}])dz$$

$$[K_{L2o}] = \int_L \alpha E_t((I_\omega w_0' - I_{\omega y} \theta_z')[N_{b2}]^T - I_{\omega x} u_0'[N_{d2}])dz$$

$$[K_{L2p}] = \int_L E_t(\alpha(I_{\omega x} v_0' - I_{\omega y} w_0')[N_{b2}]^T + \alpha^2 I_{\omega 2} u_0'[N_{d2}])dz$$

(3) $$[K_{L4}] = \begin{bmatrix} [0] & [0] & [0] & [0] \\ & \int_L GA\theta_z^2[N_{a2}]dz & [0] & \int_L GAv_0'\theta_z[N_{c2}]dz \\ & symmetric & [0] & [0] \\ & & & \int_L GA(v_0')^2[N_{e2}]dz \end{bmatrix}$$

$$= \begin{bmatrix} [0] & [0] & [0] & [0] \\ & [K_{L4a}] & [0] & [K_{L4b}] \\ & symmetric & [0] & [0] \\ & & & [K_{L4c}] \end{bmatrix}$$

$$(4)\quad [K_{L5}]=\begin{bmatrix} [0] & [0] & [0] & [0] \\ & [0] & [0] & [0] \\ & \textit{symmetric} & \int_L GA\theta_z^2[N_{a2}]dz & \int_L GAw_0'\theta_z[N_{c2}]dz \\ & & & \int_L GA(w_0')^2[N_{e2}]dz \end{bmatrix}$$

$$=\begin{bmatrix} [0] & [0] & [0] & [0] \\ & [0] & [0] & [0] \\ & \textit{symmetric} & [K_{L5a}] & [K_{L5b}] \\ & & & [K_{L5c}] \end{bmatrix}$$

Therefore, from Eqn. (7-25b) we have

$$[K_L]_{16x16}=[K_{L1}]+[K_{L2}]+[K_{L3}]+[K_{L4}]+[K_{L5}]$$

$$=\begin{bmatrix} [K_{L1a}]+2[K_{L2a}] & [K_{L1b}]+[K_{L2b}]+[K_{L2e}]^T & [K_{L1c}]+[K_{L2c}]+[K_{L2i}]^T & [K_{L1d}]+[K_{L2d}]+[K_{L2m}]^T \\ & [K_{L1e}]+[K_{L2f}]+[K_{L2f}]^T+[K_{L4a}] & [K_{L1f}]+[K_{L2g}]+[K_{L2j}]^T & [K_{L1g}]+[K_{L2h}]+[K_{L2n}]^T+[K_{L4b}] \\ & \textit{symmetric} & [K_{L1h}]+[K_{L2k}]+[K_{L2k}]^T+[K_{L5a}] & [K_{L1i}]+[K_{L2l}]+[K_{L2o}]^T+[K_{L5b}] \\ & & & [K_{L1j}]+2[K_{L2p}]+[K_{L4c}]+[K_{L5c}] \end{bmatrix}$$

(7-26b)

The geometric matrix ($[K_\sigma]$):

Denoting $[K_{\sigma 1}]=\int_L\int_A[B_L]\sigma_z dAdz$, $[K_{\sigma 2}]=\int_L\int_A[B_{xz}]\tau_{xz}dAdz$, $[K_{\sigma 3}]=\int_L\int_A[B_{yz}]\tau_{yz}dAdz$

produces

$$[K_{\sigma 1}]=\begin{bmatrix} \int_L n[N_{a2}]dz & -\int_L m_x[N_{b2}]dz & -\int_L m_y[N_{b2}]dz & \int_L \alpha m_\omega[N_{b2}]dz \\ & \int_L n[N_{a2}]dz & [0] & \int_L m_y[N_{a2}]dz \\ & \textit{symmetric} & \int_L n[N_{a2}]dz & -\int_L m_x[N_{a2}]dz \\ & & & [0] \end{bmatrix}$$

$$[K_{\sigma 2}]=\begin{bmatrix} [0] & [0] & [0] & [0] \\ & [0] & [0] & \int_L V_x [N_{c2}]dz \\ & \textit{symmetric} & [0] & [0] \\ & & & [0] \end{bmatrix}$$

$$[K_{\sigma 3}]=\begin{bmatrix} [0] & [0] & [0] & [0] \\ & [0] & [0] & [0] \\ & \textit{symmetric} & [0] & -\int_L V_y [N_{c2}]dz \\ & & & [0] \end{bmatrix}$$

From Eqn.(7-25c) we have

$$[K_{\sigma}]_{16x16}=\begin{bmatrix} \int_L n[N_{a2}]dz & -\int_L m_x[N_{b2}]dz & -\int_L m_y[N_{b2}]dz & \int_L \alpha m_\omega [N_{b2}]dz \\ & \int_L n[N_{a2}]dz & [0] & \int_L m_y[N_{a2}]dz + \int_L V_x[N_{c2}]dz \\ & \textit{symmetric} & \int_L n[N_{a2}]dz & -\int_L m_x[N_{a2}]dz - \int_L V_y[N_{c2}]dz \\ & & & [0] \end{bmatrix} \quad (7\text{-}26c)$$

The internal forces vector will be,

$$\{Q^R\}=\{Q_0^R\}+\{Q_L^R\} \quad (7\text{-}27)$$

where

$$\{Q_0^R\}=\int_L\left(\int_A\{B_0\}\sigma_z dA+\{B_t\}T\right)dz=\int_L\begin{Bmatrix} n\{N_a'\} \\ -m_x\{N_a''\} \\ -m_y\{N_a''\} \\ \alpha m_\omega\{N_a''\}+T\{N_a'\}\end{Bmatrix}dz;$$

$$\{Q_L^R\}=\int_L\int_A(\{\overline{B}_L\}\sigma_z+\{\overline{B}_{xz}\}\tau_{xz}+\{\overline{B}_{yz}\}\tau_{yz})dAdz$$

$$=\int_L\begin{Bmatrix} (nu_0'-m_xv_0''-m_yw_0''+\alpha m_\omega\theta_z'')\{N_a'\} \\ (nv_0'+m_y\theta_z'+V_x\theta_z)\{N_a'\}-m_xu_0'\{N_a''\} \\ (nw_0'-m_x\theta_z'-V_y\theta_z)\{N_a'\}-m_yu_0'\{N_a''\} \\ (m_yv_0'-m_xw_0')\{N_a'\}+\alpha m_\omega u_0'\{N_a''\}+V_xv_0'\{N_a\}-V_yw_0'\{N_a\}\end{Bmatrix}dz$$

so that

$$\{Q^R\}=\begin{Bmatrix} \int_L (n(1+u_0')-m_x v_0''-m_y w_0''+\alpha m_\omega \theta_z'')\{N_a'\}dz \\ \int_L ((nv_0'+m_y\theta_z'+V_x\theta_z)\{N_a'\}-m_x(1+u_0')\{N_a''\})dz \\ \int_L ((nw_0'-m_x\theta_z'-V_y\theta_z)\{N_a'\}-m_y(1+u_0')\{N_a''\})dz \\ \int_L ((m_y v_0'-m_x w_0'+T)\{N_a'\}+\alpha m_\omega(1+u_0')\{N_a''\}+(V_x v_0'-V_y w_0')\{N_a\})dz \end{Bmatrix}$$

It is interesting to see that for linear problems the Eqn. (7-23) can be simplified by ignoring non-linear terms, thus

$$[K_0]\{\Delta q\}=\{Q\}-\{Q_0^R\}=\{Q\}-[K_0]\{q_0\} \qquad (7\text{-}28a)$$

Eqn. (7-28a) may be rewritten as

$$[K_0]\{\Delta q+q_0\}=\{Q\} \qquad \text{or} \qquad [K_0]\{q\}=\{Q\} \qquad (7\text{-}28b)$$

for linearly small deflection beam. The above equation can also be obtained from Eqn. (7-19) directly by ignoring non-linear terms.

We can use the transformation matrix [T] which was given in detail by Najjar[34] to transform the local equilibrium equation into global coordinates, thus:

$$[K_T]\{\Delta r\}=\{\Delta R\} \qquad \text{or} \qquad [K_T]\{\Delta r\}=\{R\}-\{R^R\} \qquad (7\text{-}29)$$

where,

$$[K_T]=[T]^T[K_t][T]$$

$$\{R^R\}=[T]^T\{Q^R\}$$

We also define $\{q\}=[T]\{r\}$.

Once Eqn. (7-29) has been established for each structural member, the structural equilibrium equation can be obtained by assembling the stiffness matrixes in global coordinates. The unknown displacements are obtained by solving these equations.

7.3 CROSS-SECTION PROPERTIES AND STRESS RESULTANTS

The section and sectorial properties are defined, with reference to Fig. 7-3, by the following expressions:

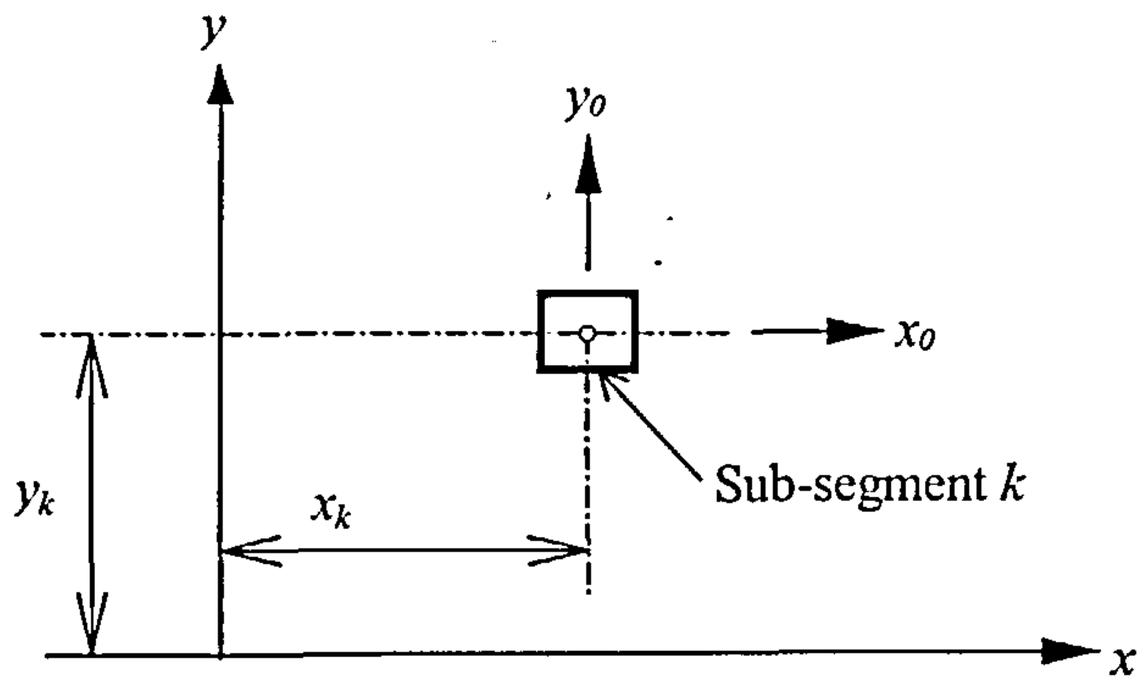

Fig. 7-3 Co-ordinate system for segments

$$A = \int_A dA = \sum_{k=1}^{n} A_k \,, \qquad I_x = \int_A (x_0 + x_k)dA = \sum_{k=1}^{n} b_k h_k x_k \,,$$

$$I_y = \int_A (y_0 + y_k)dA = \sum_{k=1}^{n} b_k h_k y_k \,, \qquad I_{x2} = \int_A (x_0 + x_k)^2 dA = \sum_{k=1}^{n} (I_{x0} + b_k h_k x_k^2) \,,$$

$$I_{y2} = \int_A (y_0 + y_k)^2 dA = \sum_{k=1}^{n} (I_{y0} + b_k h_k y_k^2) \,,$$

$$I_{xy} = \int_A (x_0 + x_k)(y_0 + y_k)dA = \sum_{k=1}^{n} b_k h_k x_k y_k \,,$$

$$I_\omega = \int_A \omega dA = \sum_{k=1}^{n} \omega b_k h_k \,, \qquad I_{\omega x} = \int_A \omega x dA = \sum_{k=1}^{n} b_k h_k \omega x_k \,,$$

$$I_{\omega y} = \int_A \omega y dA = \sum_{k=1}^{n} b_k h_k \omega y_k \,, \qquad I_{\omega 2} = \int_A \omega^2 dA = \sum_{k=1}^{n} \omega^2 b_k h_k \qquad (7\text{-}30)$$

The stress resultants can be defined by

$$n = \int_A \sigma_z dA = \sum_{k=1}^{n} \sigma_{zk} b_k h_k \,, \qquad m_x = \int_A \sigma_z y dA = \sum_{k=1}^{n} \sigma_{zk} b_k h_k y_k \,,$$

$$m_y = \int_A \sigma_z x dA = \sum_{k=1}^{n} \sigma_{zk} b_k h_k x_k \,, \qquad m_\omega = \int_A \sigma_z \omega dA = \sum_{k=1}^{n} \sigma_{zk} b_k h_k \omega \,,$$

$$V_x = \int_A \tau_{xz} dA = \sum_{k=1}^{n} \tau_{xzk} b_k h_k \ , \qquad V_y = \int_A \tau_{yz} dA = \sum_{k=1}^{n} \tau_{yzk} b_k h_k \ ,$$

$$T_{sv} = GJ\theta_z' \tag{7-31}$$

The physical meaning of these stress resultants is shown in Fig. 7-4.

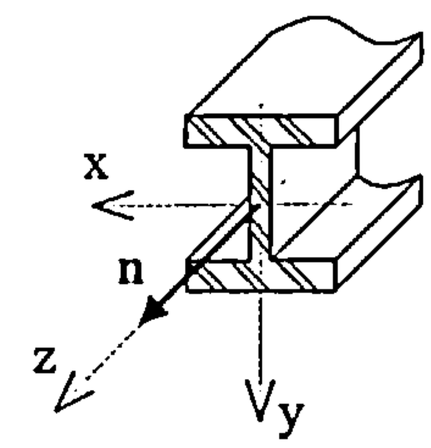

(a) Axial force (**n**)

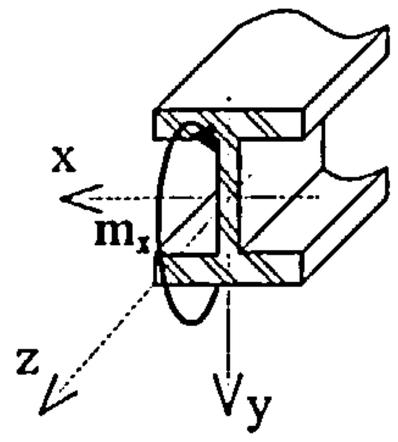

(b) Bending moment about the x-axis ($\mathbf{m_x}$)

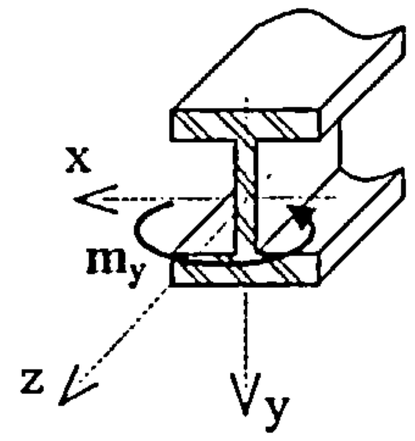

(c) Bending moment about the y-axis ($\mathbf{m_y}$)

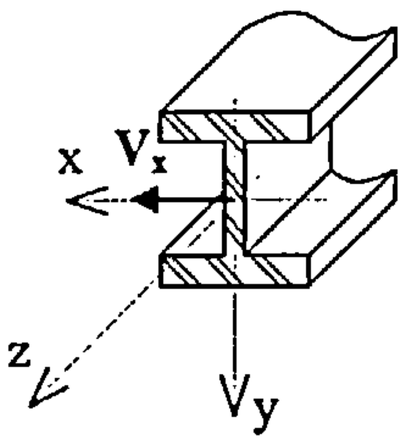

(d) Shear force parallel to the x-axis ($\mathbf{V_x}$)

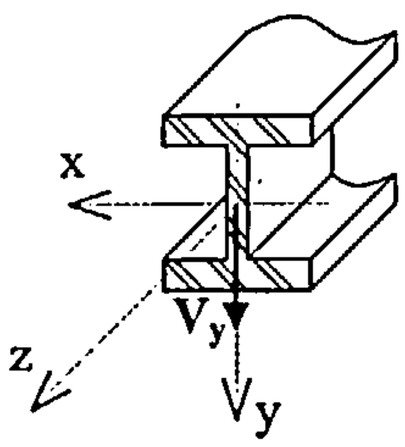

(e) Shear force parallel to the x-axis ($\mathbf{V_y}$)

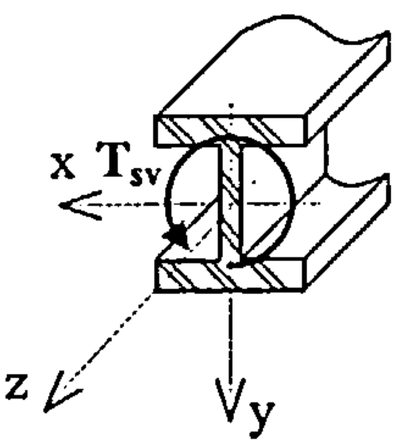

(f) Torsional moment due to St. Venant shear stress ($\mathbf{T_{sv}}$)

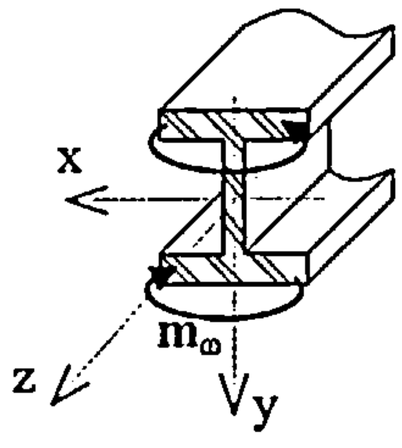

(g) Warping moment or bimoment ($\mathbf{m_\omega}$) for open cross-section

Fig. 7-4 Generalised stress

Note that, since the warping deformation of a closed-section is generally small and can be ignored, m_ω represents the warping moment for open cross-sections only, for I-shaped cross-section

$$m_{\omega} = h_1 \int_{A_1} \sigma_z x dA - h_2 \int_{A_2} \sigma_z x dA = h_1 m_{y(top\ flange)} - h_2 m_{y(bottom\ \text{flange})} \qquad (7\text{-}32)$$

where h_1 is the distance between top flange and reference axis, and h_2 is the distance from bottom flange to the reference axis.

7.4 MECHANICAL PROPERTIES AT ELEVATED TEMPERATURE

In the generalised concrete beam model, the materials are considered as temperature-dependent. Since any element may include two different materials, two uniaxial material models are required.

7.4.1 MATHEMATICAL MODEL OF CONCRETE

The mathematical material model used for concrete is according to EC4 Part 1.2[93]. In this model, the thermal elongation for normal weight and lightweight concrete is different as shown in Fig. 7-5. The temperature-dependent stress-strain relationships for concrete in compression given in Fig. 7-6 from EC4. Two stress-strain curves, one was suggested by Vecchio and Collins, et al.[58,68] and another by Rots, et al.[59,94], have been employed here for concrete in tension. Both curves have the same linear ascending branch with an initial stiffness equal to that in compression but different descending branches as shown in Fig. 7-7. Vecchio and Collins's curve simulates the tensile strain-softening and is more stiff. The tensile strength is assumed to be $f_t = 0.3321\sqrt{f_c}$ and the corresponding strain is $\varepsilon_{cr} = f_t / E_c$. At tensile strains greater than this value of ε_{cr} the concrete is assumed to follow the descending branch of the stress-strain curve (Fig. 7-7). Once tensile strains exceed ε_{cu} the concrete is ignored, although it is still assumed to be capable of carrying compression. However, once the concrete has crushed, it is assumed to have no residual strength in either compression or tension. Both the physical loss of moisture and shrinkage at high temperature cause

a decrease in the coefficient of expansion, but these effects have not been considered in the present model. The model also does not attempt to model spalling, the concrete cross-section being assumed to remain intact.

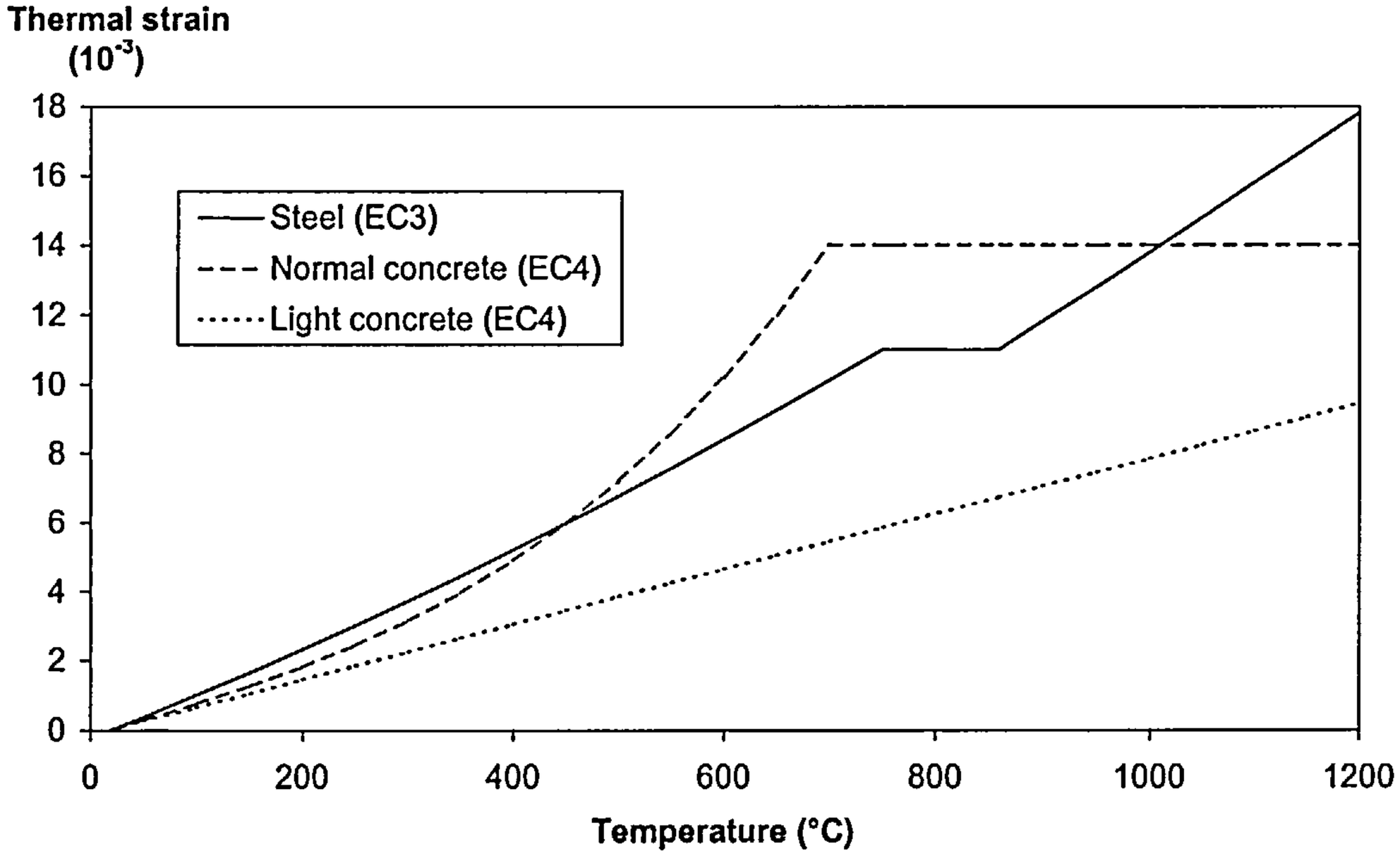

Fig. 7-5 Thermal strain of concrete and steel

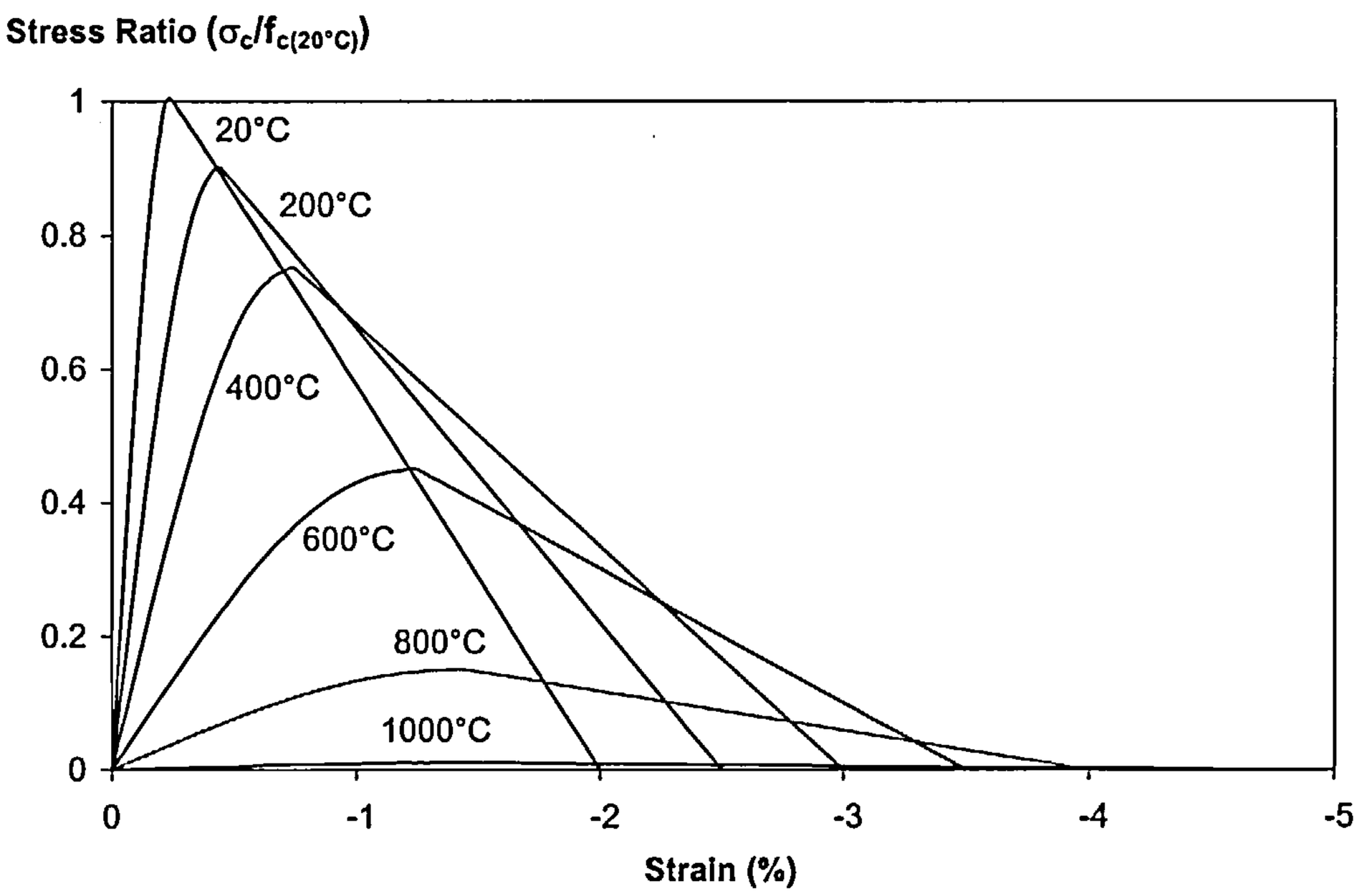

Fig. 7-6 Stress-strain relationships of concrete under compression at elevated temperature. (Note: $f_{c(20°C)}$) is compressive strength at ambient temperature)

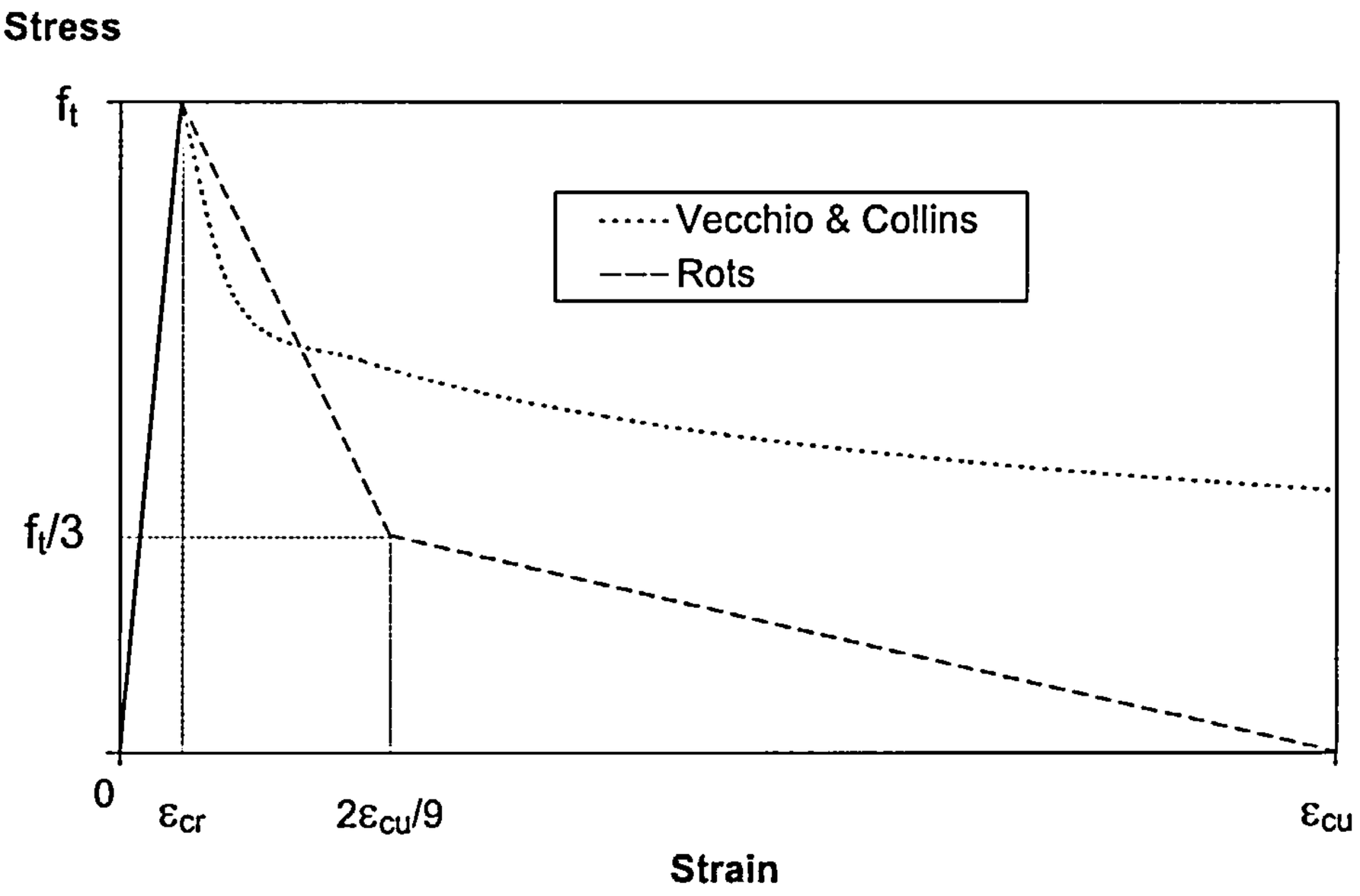

Fig. 7-7 Stress-strain relationships of concrete under tension at elevated temperature. (Note: f_t is tensile strength and ε_{cr} is tensile strain at peak stress)

7.4.2 MATHEMATICAL MODEL OF STEEL

The thermal expansion of steel has been taken according to EC3: Part 1.2[46], and is shown in Fig 7-5. For the stress-strain relationship two temperature-dependent constitutive models are available. The first one is called the smoothed Ramberg-Osgood (**SR-O**) model[66], which was based on a fit of experimental results to a Ramberg-Osgood type of expression[10,95] with continuous functions for its temperature-dependent parameters ($\mathbf{A_t}$ and $\mathbf{B_t}$). The second is that defined in EC4: Part 1.2[93] for both cold worked and hot rolled reinforcing steel, the differences being represented by different parameters ($\mathbf{E_s/E_{s(20°C)}}$, $\mathbf{\sigma_{spr}/f_{sy(20°C)}}$ and $\mathbf{\sigma_{smax}/f_{sy(20°C)}}$). Properties in tension and compression are assumed to be identical. Both the constitutive models can model the unloading of steel, as illustrated in Fig. 7-8 and Fig. 7-9 respectively.

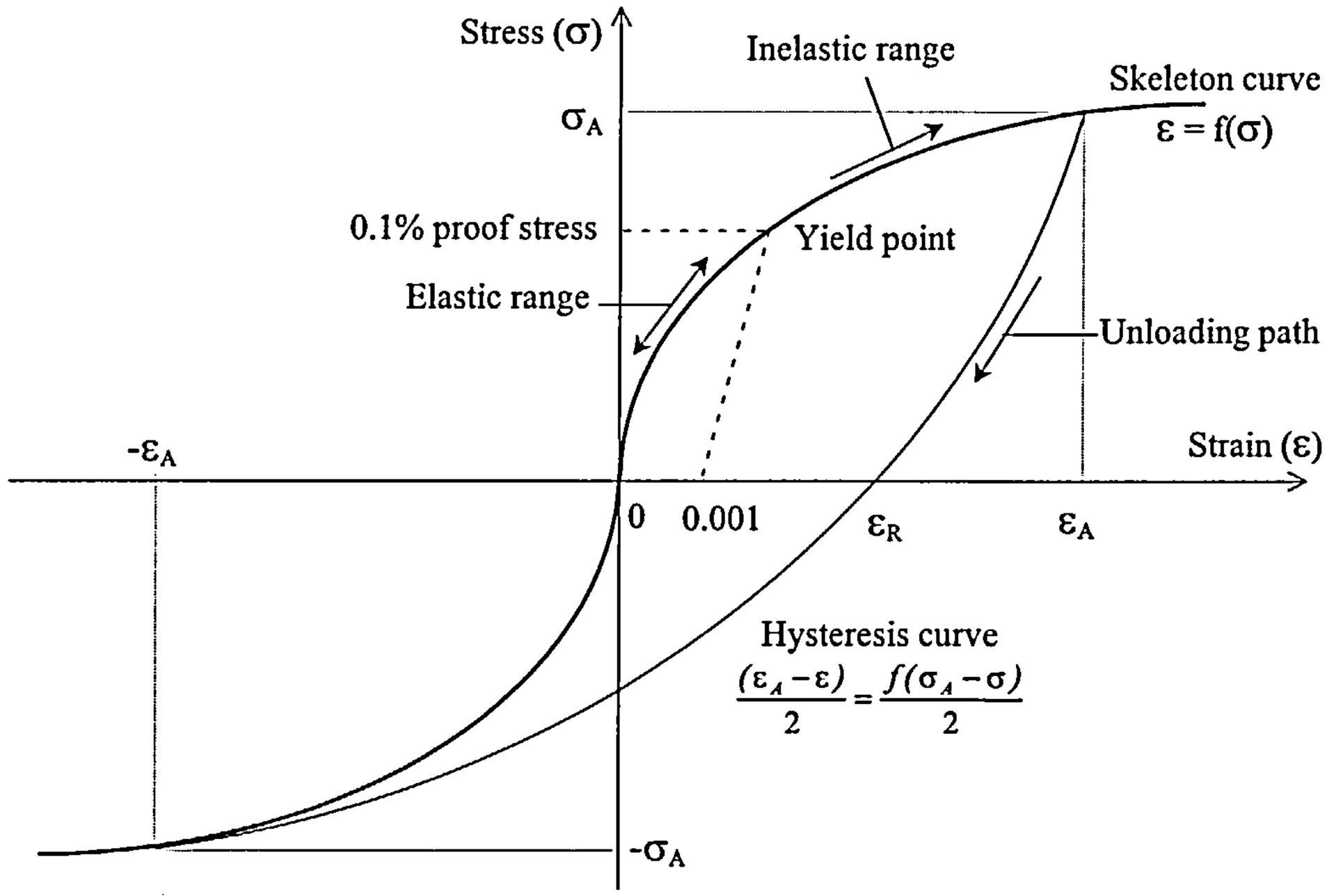

Fig. 7-8 Definition of unloading of smoothed Ramberg-Osgood model for steel

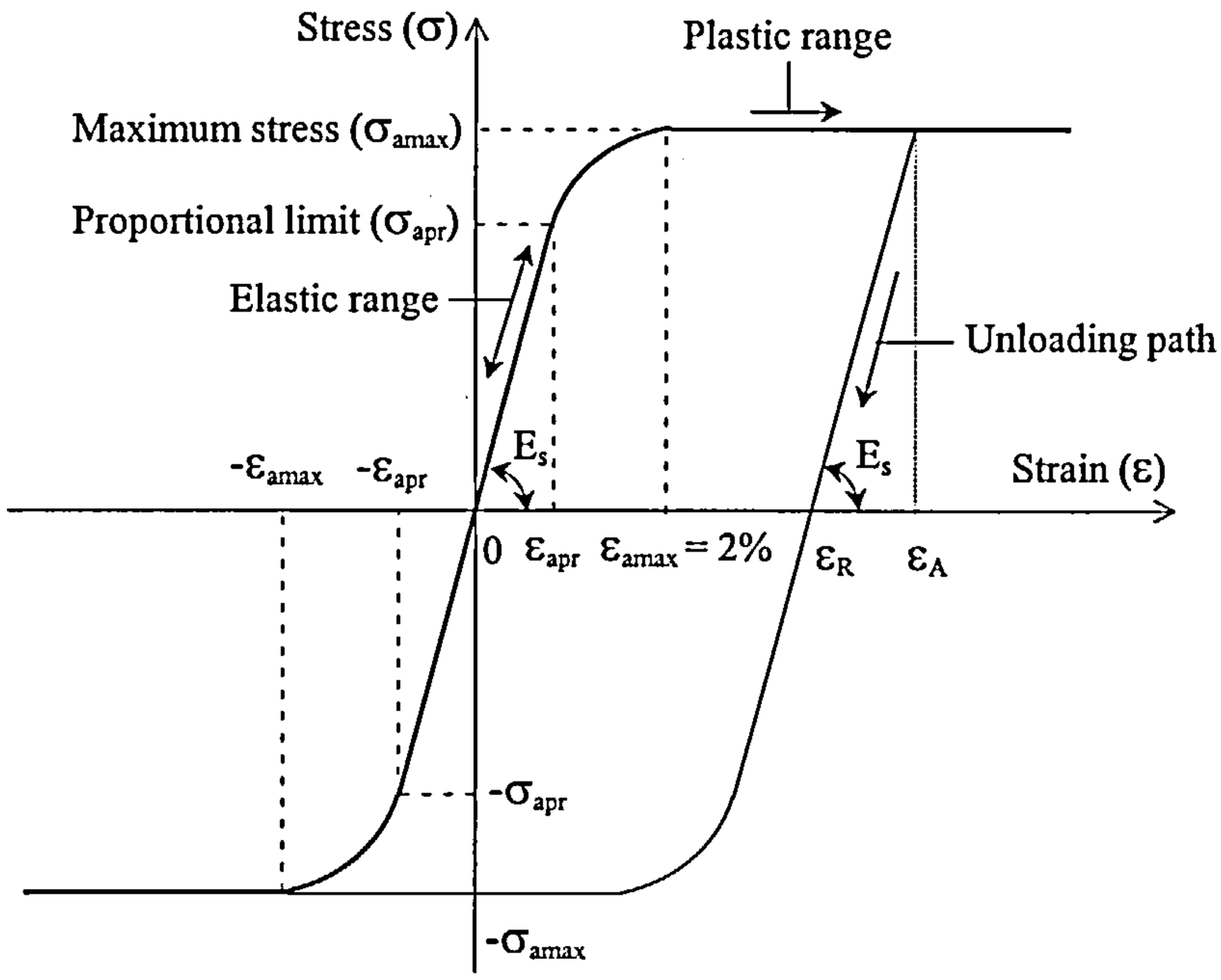

Fig. 7-9 Definition of unloading of EC3's model for steel

7.5 DIVISION OF THE MEMBER

In order to represent variations of strain and stress, the cross-section is divided into a number of segments (**n**) as shown in Fig. 7-10. Each segment is considered to have a central sampling point at which the displacement is defined. As illustrated in Fig. 7-10 the temperatures, strains and stresses within each segment are assumed to be uniform but by using a sufficiently large number of segments non-uniform distributions of these parameters through the cross-section can be approximated. Different material properties can also be specified for different segments. At present standard materials included are steel (structural steel, hot rolled and cold formed reinforcement) and concrete (normal and light weight concrete) materials. To allow for more general sections, a new "none" segment, which has free strain but no stress, has been developed. This none segment is so versatile that it can enable VULCAN to model almost any structural cross-sections. Fig. 7-10 also shows a typical section division.

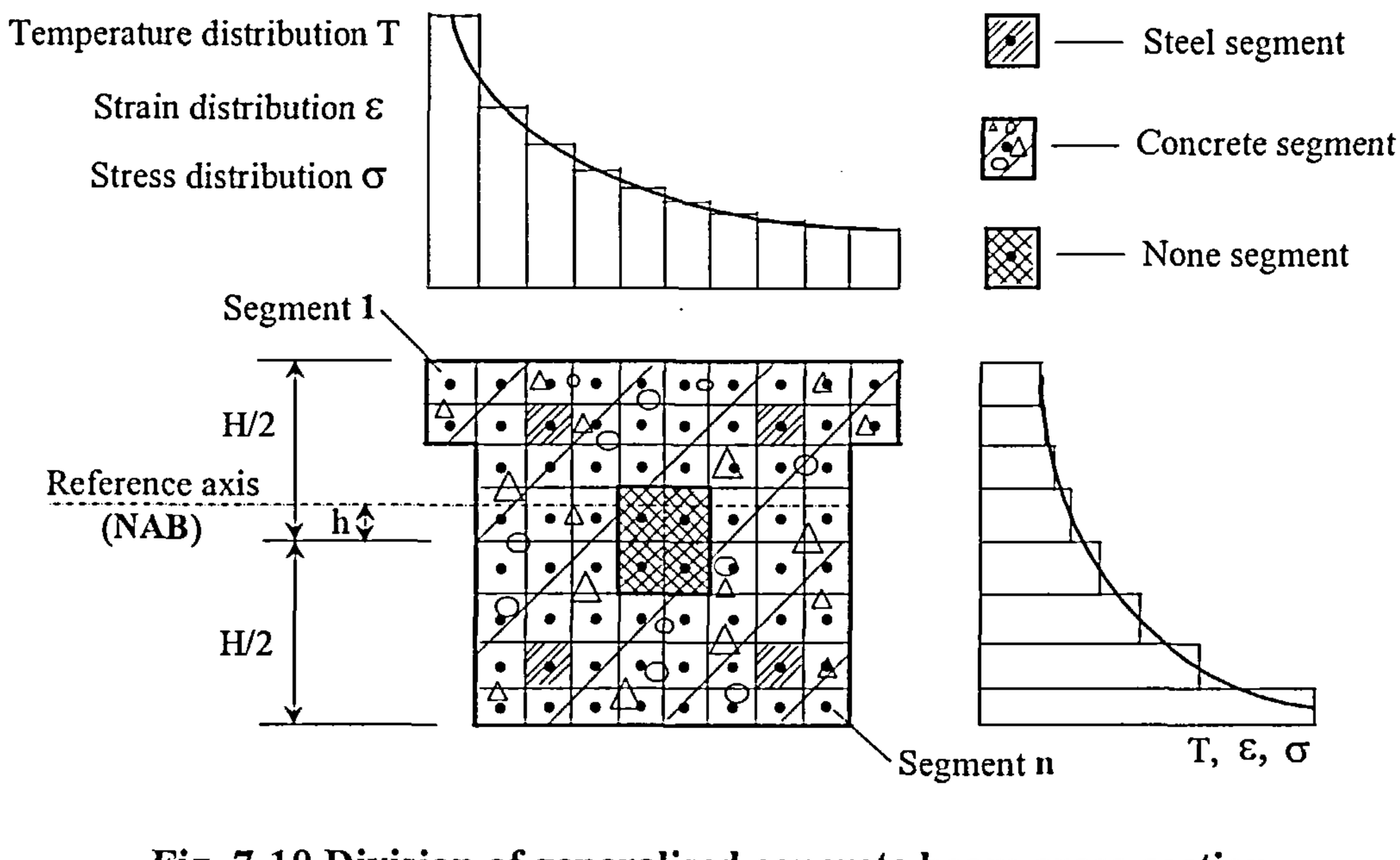

Fig. 7-10 Division of generalised concrete beam cross-section

The reference axis of the concrete beam element is normally defined as the neutral axis for elastic bending (**NAB**). However when combined with a concrete slab, its position is usually set at the mid-surface of the concrete slab. Some studies have been carried

using different reference axis positions for the same simply supported beam cases, including concrete beams and steel beams. These showed that the assumed position of the reference axis had no effect on the calculated deflections, indicating that for simply supported beams the position of the reference axis is not important. The following equations define the **NAB** position as show in Fig. 7-10.

From the equilibrium for the resultant axial force due to bending stresses, it requires

$$E_a \int_{A_a} y_a dA_a + E_b \int_{A_b} y_b dA_b = 0 \tag{7-33}$$

Then, produces

$$E_a \sum_{i=1}^{l} A_{ai}(y_{ai} - h) + E_b \sum_{j=1}^{m} A_{bj}(y_{bj} - h) = 0 \tag{7-34}$$

The distance (**h**) between the mid-depth of the cross-section and **NAB** then will be

$$h = \frac{\sum_{k=1}^{n} E_k b_k h_k y_k}{\sum_{k=1}^{n} E_k b_k h_k} \tag{7-35}$$

where,

E_k, b_k, h_k are the modulus of elasticity, breadth and depth of segment **k** respectively;

y_k is the distance from mid-depth of the cross-section to the centre of segment **k**.

If the member only contains one material or the area of one material is much bigger than another one, the above equation can be simplified as

$$h = \frac{\sum_{k=1}^{n} b_k h_k y_k}{A} \tag{7-36}$$

7.6 PROGRAM DEVELOPMENT

The software VULCAN has been modified to incorporate the numerical model presented above. Since two materials may exist in a single beam element, in order to

facilitate the programming, the transformed section concept has been employed with the performance based on one material at ambient temperature. Because the model contains highly non-linear formulations, the Newton-Raphson solution procedure is used, as detailed in chapter 2. The non-linear formulations also require integration over the length and this is achieved by using four-point Gauss quadrature formula. To improve computational efficiency, a beam element is subdivided into three sub-elements with the central sub-element being 80% of the length of the element. A static condensation scheme is then used to eliminate the internal degrees of freedom. At each temperature or load step the previous nodal displacements are used as the initial trial displacements. After repeating several cycles, the convergence criterion may be reached defining the unknown nodal displacements and internal forces. In this procedure, structural failure is defined by finding zero or negative element on the leading diagonal of the stiffness matrix. The subroutines, which have been developed in the modification of VULCAN, are:

(1) SUBROTINE MAINMG;
(2) SUBROTINE STIFF;
(3) SUBROTINE GET_CONBM;
(4) SUBROTINE CALDIS;
(5) SUBROTINE CONSTEPF;
(6) SUBROTINE CONTEMRD;
(7) SUBROTINE THERMEP;
(8) SUBROTINE CONBEAMN;
(9) SUBROTINE CONREIN;
(10) SUBROTINE SECARE;
(11) SUBROTINE SHEMOD;
(12) SUBROTINE JCONS0;
(13) SUBROTINE JCONS1;
(14) SUBROTINE JCONS2;
(15) SUBROTINE TORCON;
(16) SUBROTINE UNLDST.

7.7 VALIDATIONS

The modified version of VULCAN, incorporating the generalised concrete beam element has been validated for single structural members and more complicated structures subjected to fire conditions. Since the original version of VULCAN has

been well validated[62,65,91] for bi-symmetric thin-walled I-section steel beams, it is convenient to compare the original and modified software for such cases. A number of analyses were carried out at both ambient and high temperatures and indicated that the two versions of the software gave almost identical results. A typical case was a cantilever beam at ambient temperature with a point load **P,** which was gradually increased up to $\frac{1.5L^2}{EI}$, applied at the free end. The beam length was 1000mm, the cross-section was a 127x76x13 UB, and the material was S355 steel which was assumed to remain elastic. Both models had ten elements along the beam length whist their cross-section was divided into twelve segments. The results are shown in Figs. 7-11 to 7-13 together with the theoretical solutions for this classic problem[84]. It is clear that the two predictions are very close and demonstrate excellent correlation with th large deflection curve, indicating the important of geometrical non-linear effects at high deformations.

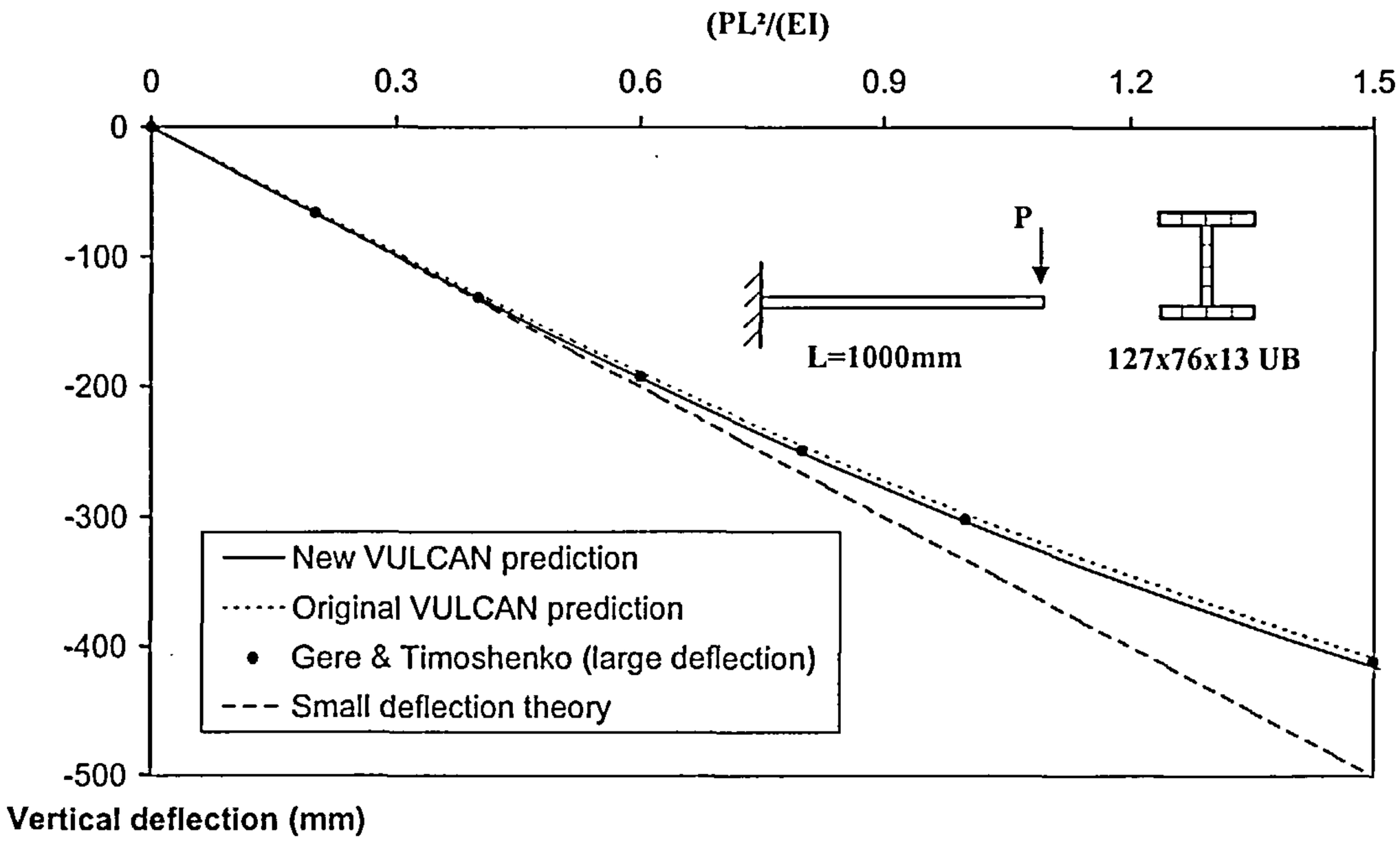

Fig. 7-11 Vertical deflection at free end of elastic cantilever beam

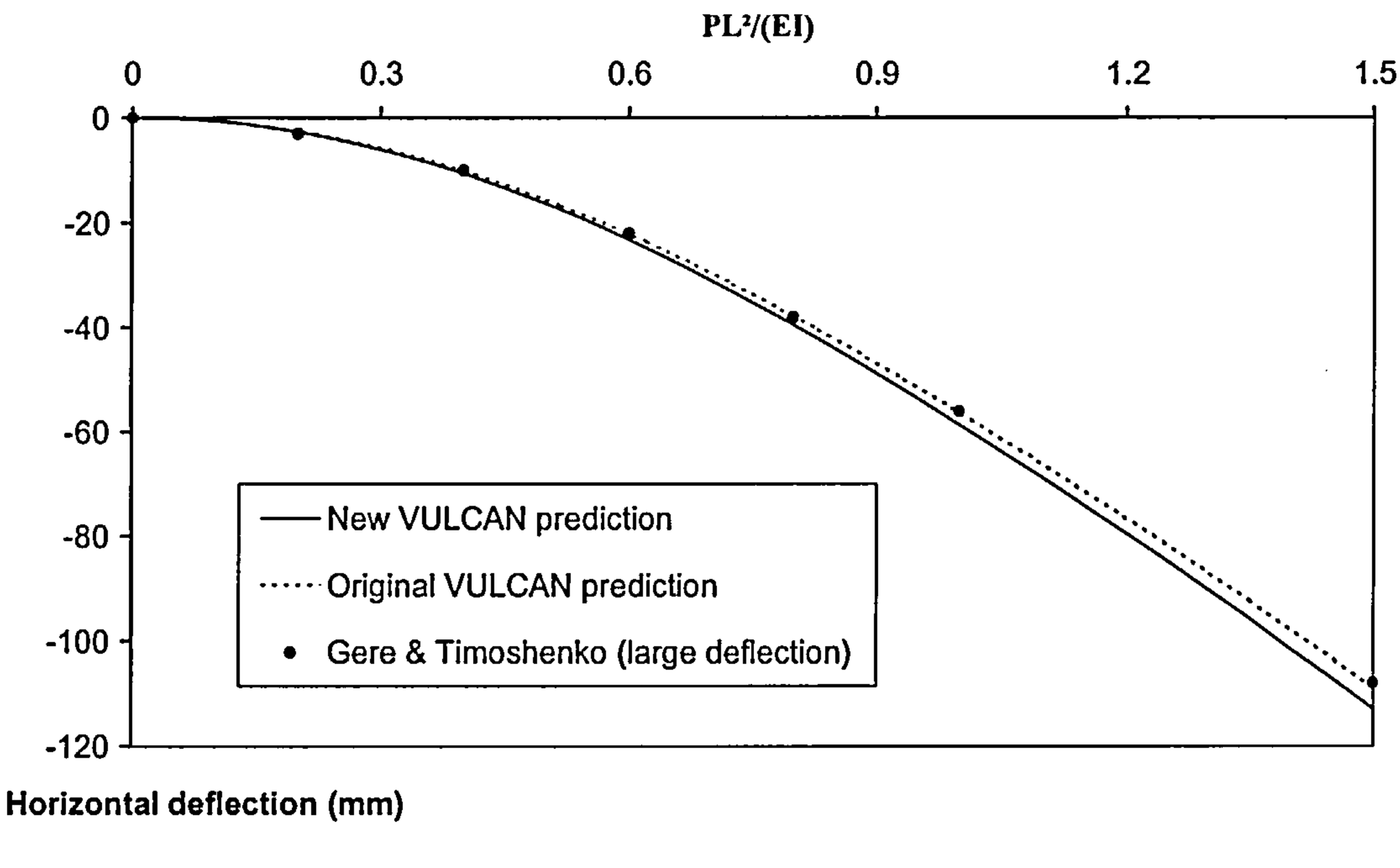

Fig. 7-12 Horizontal deflection at free end of elastic cantilever beam

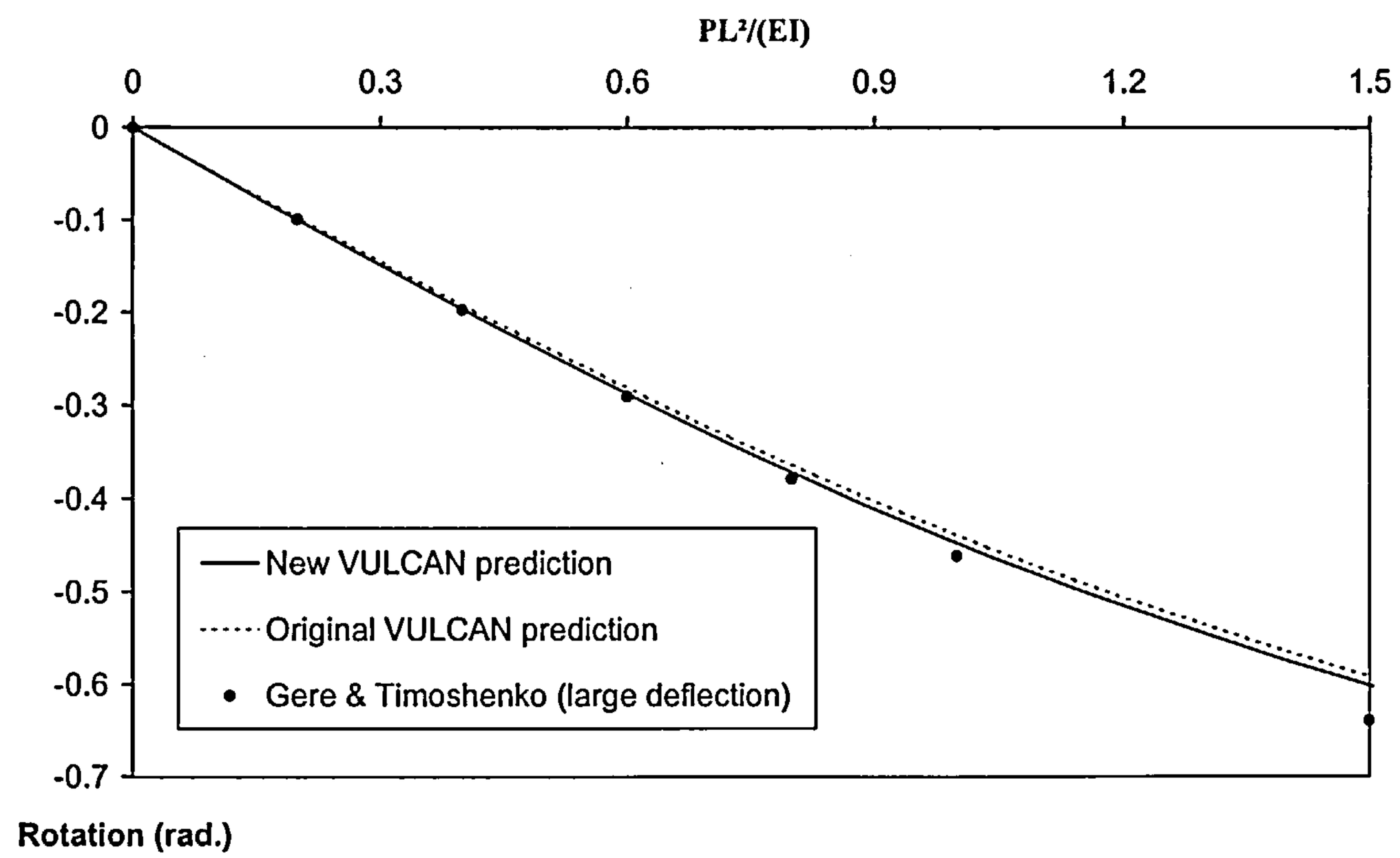

Fig. 7-13 Rotation angle at free end of elastic cantilever beam

In order to validate the software for members other than I cross-sections or consisting of two materials, two schemes have been adopted. One compares with classical analyses performed manually, excluding material non-linearity and the thermal effects.

Another approach was to compare with elevated temperature test data including both geometric and material non-linearities. Unfortunately this was restricted by the limited test data available.

7.7.1 VALIDATION WITH THEORETICAL SOLUTIONS AT AMBIENT TEMPERATURE FOR COMPOSITE BEAM

Theoretical solutions for small and large deflections are well established for a wide range of members. Three cases have been analysed in this chapter, involving hollow and solid rectangular beams and a nonprismatic beam in which the materials were assumed to be concrete and remained elastic.

(a) Large deflection check on hollow box cantilever beam:

A hollow box section cantilever beam at ambient temperature was analysed by VULCAN for comparison with theoretical solutions. The length of beam was 1000mm with a concentrated load **P** acting on the free end. The cross-section, which was 110mm x 110mm with a uniform wall thickness of 13.731mm, was divided into 7x7 segments, including 5x5 '**none**' elements, whilst twenty elements were allocated along the beam length. The material was assumed to be elastic normal weight concrete so that the modulus of elasticity **E** was 18000N/mm^2. The results are compared in Figs. 7-14 and 7-15, indicating that VULCAN is able to model hollow section beams at ambient temperature very accurately.

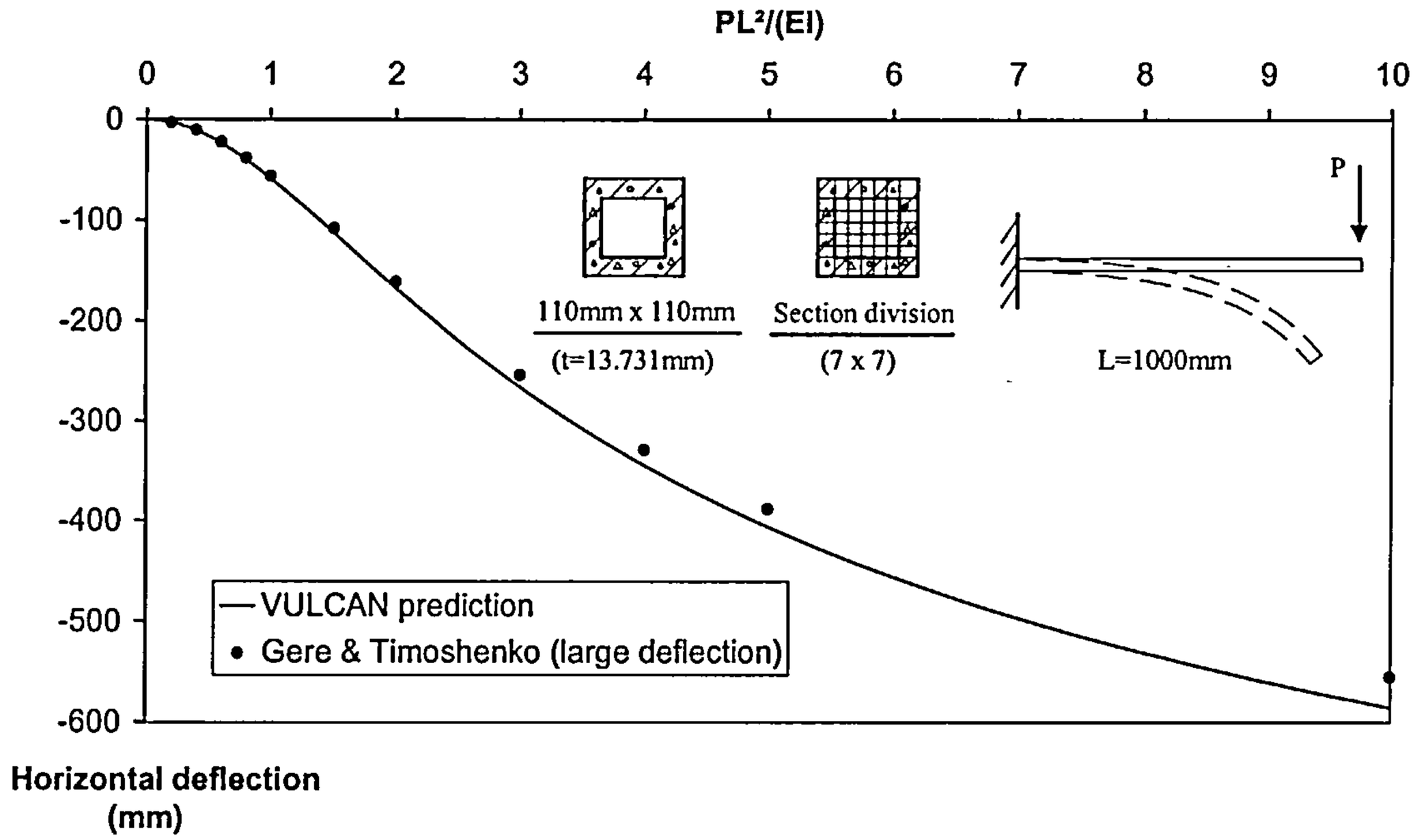

Fig. 7-14 Horizontal deflection at free end of elastic cantilever beam(Hollow Section)

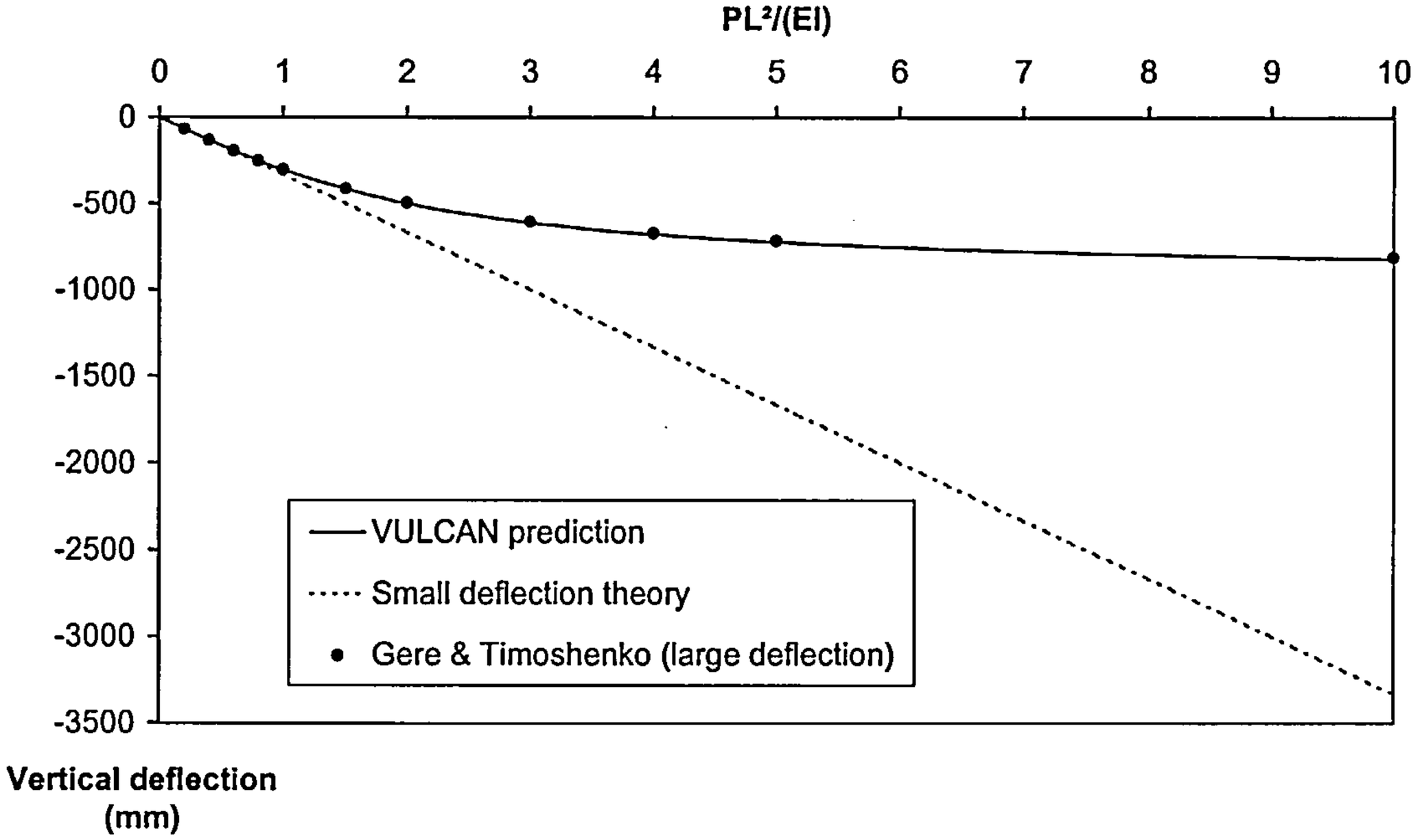

Fig. 7-15 Vertical deflection at free end of elastic cantilever beam (Hollow Section)

(b) Large deflection check on solid rectangle concrete cantilever beam:

The above comparison was repeated for a solid rectangular cross-section as shown in Fig. 7-16. In this analysis the cross-section was divided into 2 x 2 segments, 4 x 4 segments and 10 x 10 segments respectively. The material still remained elastic. Figs. 7-17 and 7-18 show the deflections at the free end of the cantilever. It can be seen that the results from VULCAN show good agreements with large deflection theory even when the cross-section is represented by 2 x 2 segments. Clearly a larger number of segments gives improved results, but 4 x 4 segments should be sufficiently accurate.

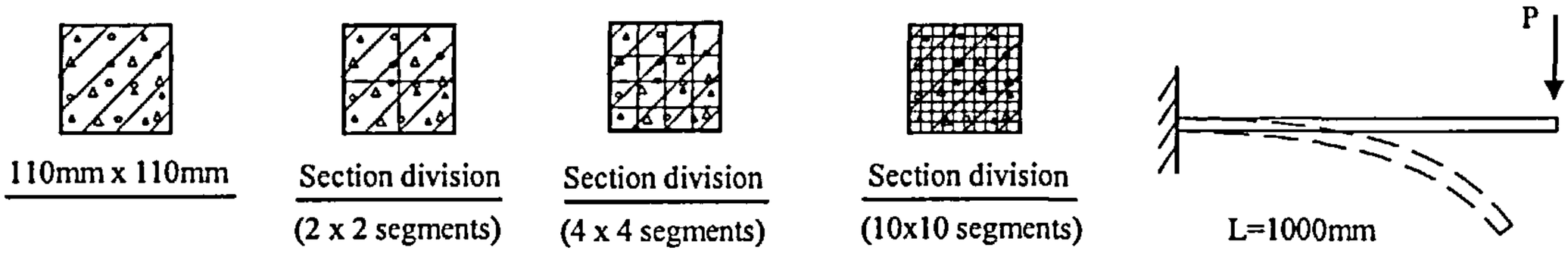

Fig. 7-16 Solid rectangle cantilever beam example

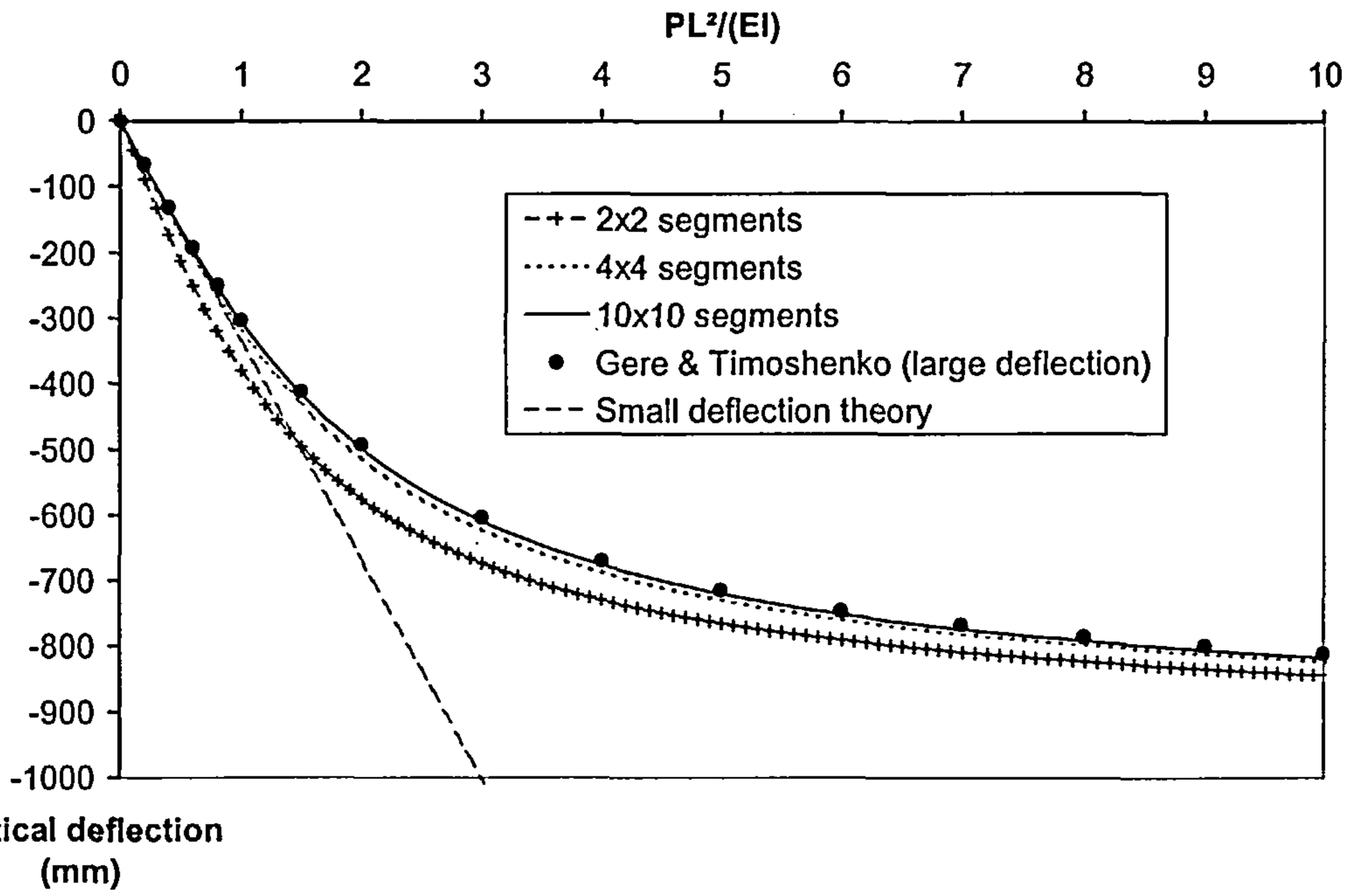

Fig. 7-17 Vertical deflection at free end of elastic solid rectangle cantilever beam

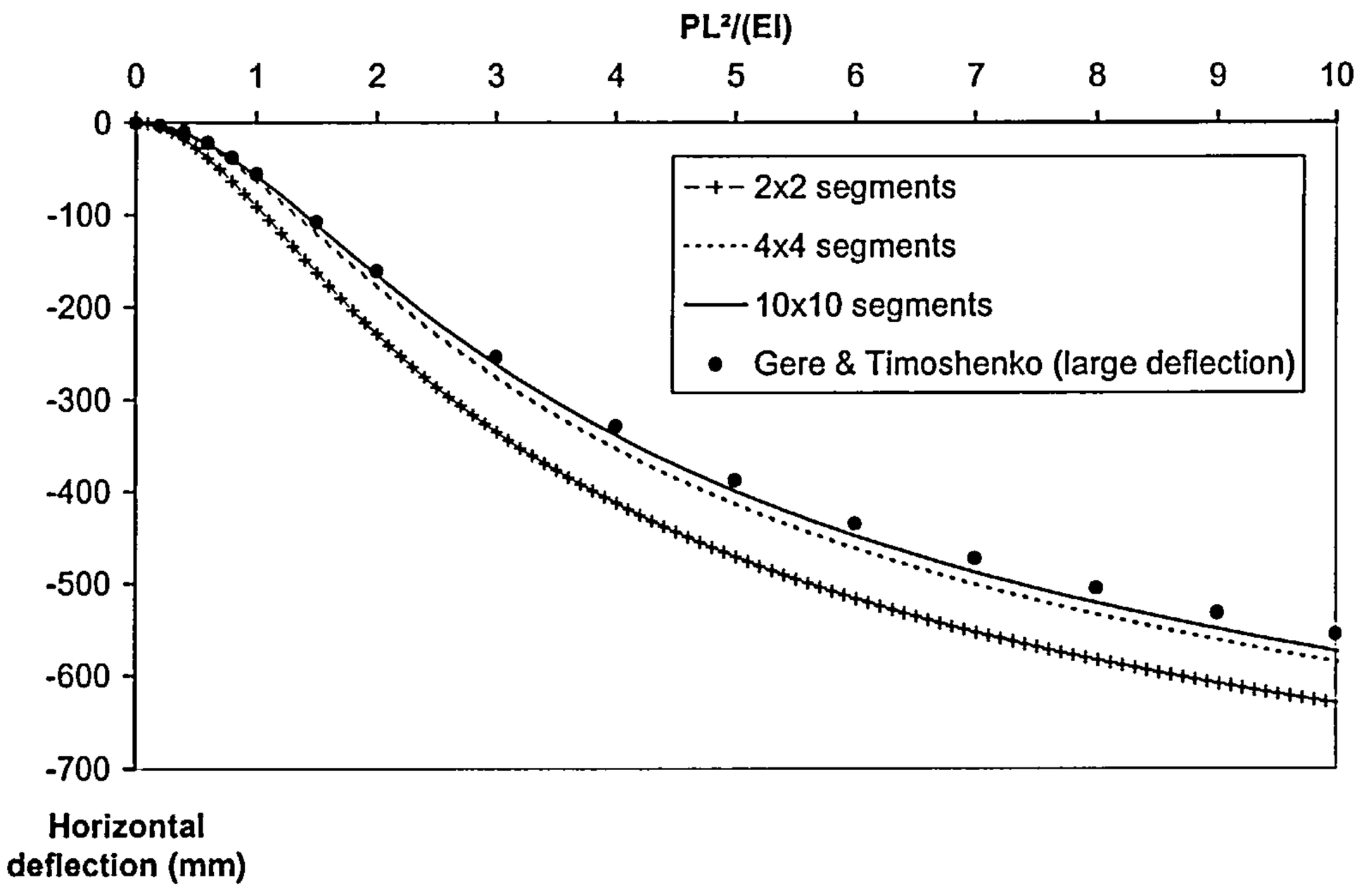

Fig. 7-18 Horizontal deflection at free end of solid rectangle cantilever beam

(c) Simply supported non-prismatic concrete beam -- small deflections:

In this example a simply supported non-prismatic concrete beam spanning 1000mm was analysed under a central point load (**P**) of 100kN. The cross-section size and division are shown in Fig. 7-19 and the concrete beam was divided into twenty elements along its length. The material was assumed to remain elastic (**E**=18000 N/mm²). Since the vertical deflection was expected to be small, small deflection theory was employed giving a theoretical solution for the vertical deflection as[84]

$$\begin{cases} y = -\dfrac{Px^3}{12EI_1} + \dfrac{PL^2x}{64E}\left(\dfrac{1}{I_1} + \dfrac{3}{I_2}\right) & \left(0 \le x \le \dfrac{L}{4}\right) \\ y = -\dfrac{Px^3}{12EI_2} + \dfrac{PL^2x}{16EI_2} + \dfrac{PL^2}{384E}\left(\dfrac{1}{I_1} - \dfrac{1}{I_2}\right) & \left(\dfrac{L}{4} \le x \le \dfrac{L}{2}\right) \end{cases} \tag{7-37}$$

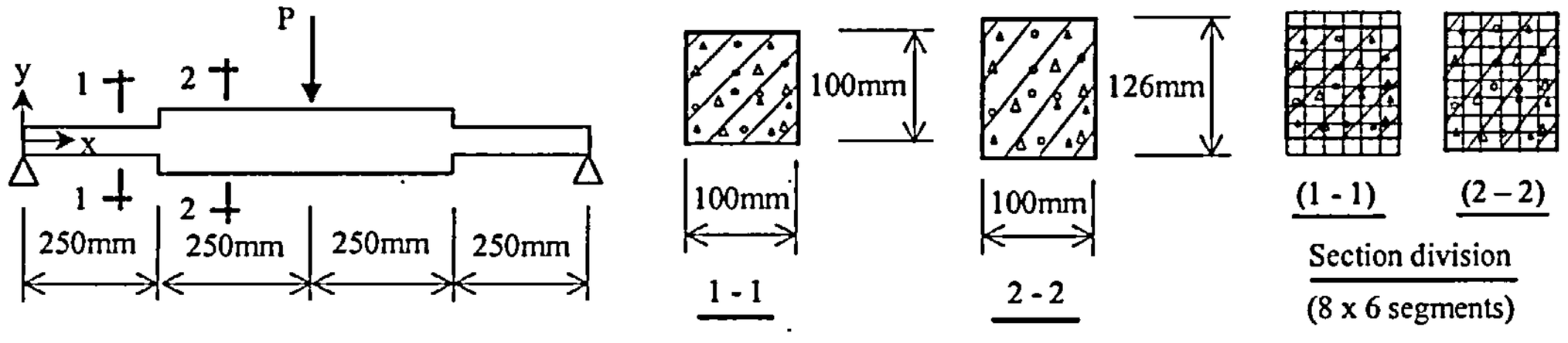

Fig. 7-19 Simply supported non-prismatic concrete beam at ambient temperature

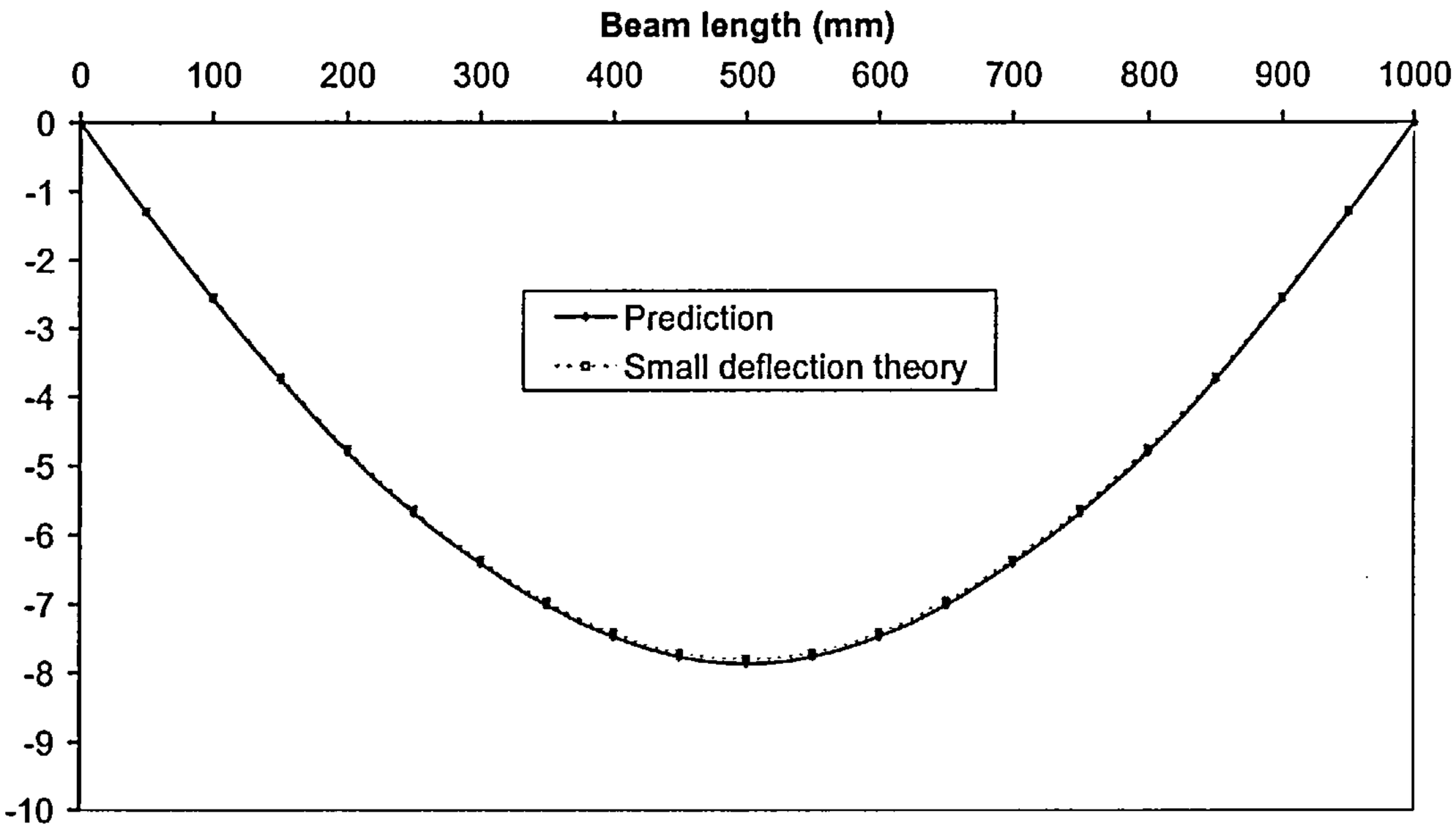

Fig. 7-20 Vertical deflection of elastic non-prismatic concrete beam at ambient temperature

The comparisons given in Fig. 7-20 show almost identical deflections for VUCAN and classical analysis.

(d) Validations on reinforced concrete beam at ambient temperature:

The above three cases were for a single elastic material -- concrete. To test the modified version of VULCAN for reinforced concrete members comparisons have been made with theoretical solutions for a simply supported reinforced concrete beam at ambient temperature. This was first assumed to remain elastic, then based on more

realistic material properties non-linearly considering different concrete tension patterns. Huang's concrete slab model[68], which considers the slab as several layers, was also used to do the extended comparisons. In this study the concrete beam was rectangular and reinforced as illustrated in Fig. 7-21. The beam was 4500mm in length (L) with a concentrated load (**P**) acting at its centre, and the cross-section was 200mm x 150mm (**B** x **H**). Reinforcement was equivalent to a smeared steel layer 0.252mm thick with a concrete cover (**a**) of 25mm. The following material properties were assumed:

$\mathbf{E_s} = 210000 N/mm^2$; $\mathbf{E_c} = 18000 N/mm^2$. Both the steel reinforcement and the concrete remained elastic in the first analysis. In the second analysis the material properties were represented using the EC4 model for the steel, with a yield strength of $460 N/mm^2$ and using Figs. 7-6 and 7-7 for concrete with a strength of $30 N/mm^2$.

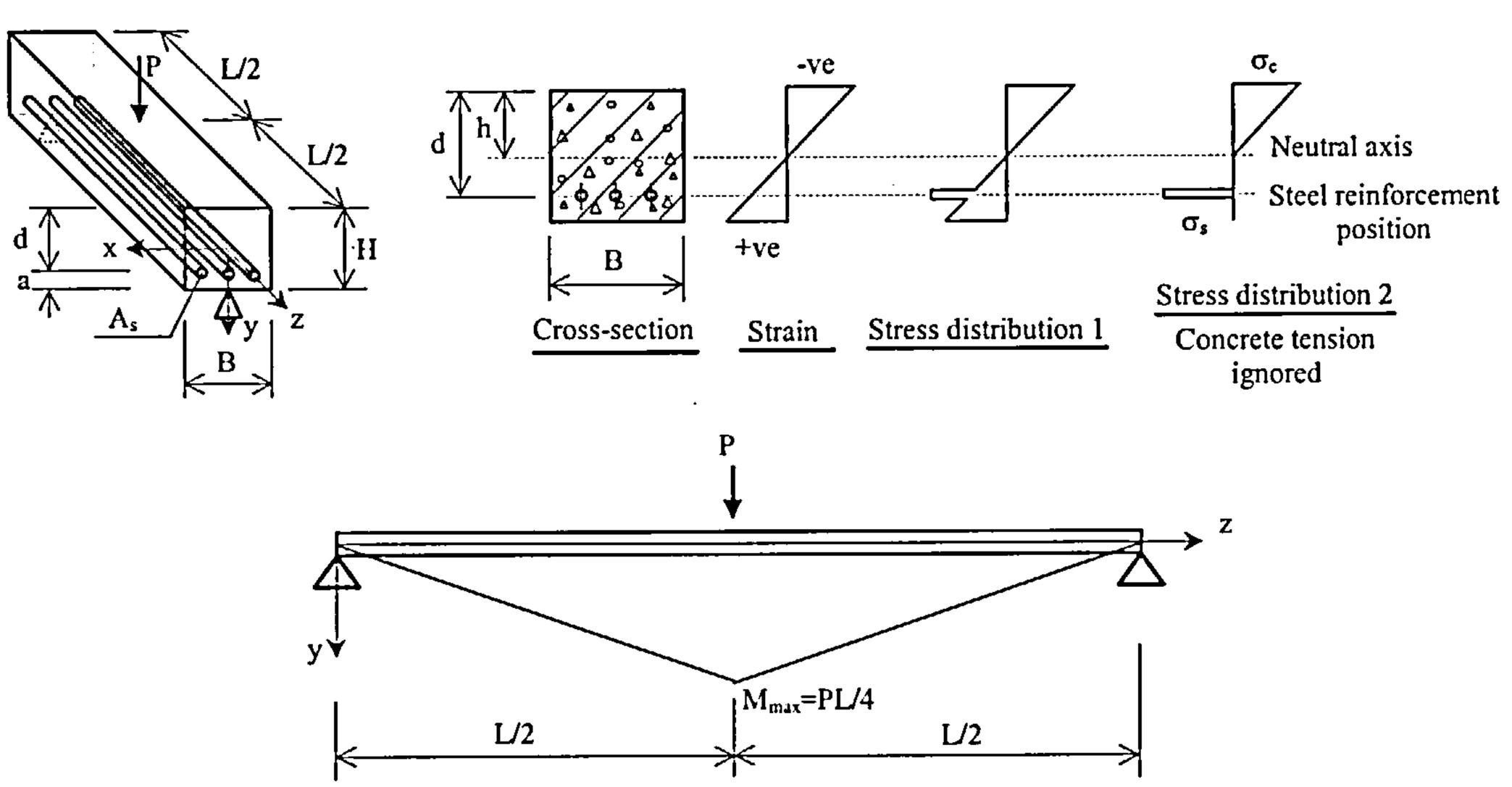

Fig. 7-21 Simply supported reinforced concrete beam under a central point load P

The theoretical solutions for this simply supported reinforced concrete beam can be obtained by employing the energy theorem, based on Fig. 7-21, as follows

For a linear strain distribution, both materials (concrete and steel) deform to a circular arc, yielding

$$-\frac{1}{R}=\frac{\varepsilon_c}{y_c}=\frac{\varepsilon_s}{y_s} \tag{7-38}$$

and the stresses at distance y from neutral axis will be,

$$\sigma_c = E_c\varepsilon_c = -\frac{E_c y_c}{R} \text{ and } \sigma_s = E_s\varepsilon_s = -\frac{E_s y_s}{R} \tag{7-39}$$

We also have,

$$\frac{1}{R}=-\frac{\sigma_c}{E_c y_c}=-\frac{\sigma_s}{E_s y_s} \tag{7-40}$$

For longitudinal equilibrium it requires,

$$\int_{A_c}\sigma_c dA_c + \int_{A_s}\sigma_s dA_s = 0 \qquad \text{or} \qquad \frac{E_c}{R}\int_{A_c} y_c dA_c + \frac{E_s}{R}\int_{A_s} y_s dA_s = 0 \tag{7-41}$$

If we ignore the tension effect of concrete, Eqn. (7-41) becomes

$$E_c B\int_{-h}^{0} y_c dy + E_s(d-h)A_s = 0 \tag{7-42}$$

then,

$$h=\sqrt{(\frac{E_s A_s}{E_c B})^2+\frac{2E_s A_s d}{E_c B}}-\frac{E_s A_s}{E_c B} \tag{7-43}$$

otherwise, from Eqn. (7-41) we have

$$E_c B\int_{-h}^{H-h} y_c dy + E_s(d-h)A_s = 0 \tag{7-44}$$

then,

$$h=\frac{E_c BH^2+2E_s A_s d}{2E_c BH+2E_s A_s} \tag{7-45}$$

The bending moments (**M**) caused by the external concentrated load (**P**) are

$$M=\frac{1}{2}Pz \qquad (z\le\frac{L}{2})$$

$$M = \frac{1}{2}P(L-z) \qquad (\frac{L}{2} < z \le L) \tag{7-46}$$

For moments equilibrium it requires

$$M = \int_{A_c} \sigma_c y_c dA_c + \int_{A_s} \sigma_s y_s dA_s = -\frac{E_c}{R}\int_{A_c} y_c^2 dA_c - \frac{E_s}{R}\int_{A_s} y_s^2 dA_s$$
$$= -\frac{E_c I_c + E_s (d-h)^2 A_s}{R} \tag{7-47}$$

in which $I_c = \int_{A_c} y_c^2 dA_c$.

Substituting $\frac{1}{R}$ from Eqn. (7-40) into Eqn. (7-47) and rearranging produces

$$\sigma_c = \frac{M y_c E_c}{E_c I_c + E_s (d-h)^2 A_s} \quad \text{and} \quad \sigma_s = \frac{M y_s E_s}{E_c I_c + E_s (d-h)^2 A_s} \tag{7-48}$$

The elastic strain energy stored in the concrete beam is

$$U = \int_V \frac{\sigma^2}{2E} dV = \int_{V_c} \frac{\sigma_c^2}{2E_c} dV_c + \int_{V_s} \frac{\sigma_s^2}{2E_s} dV_s$$
$$= \frac{1}{2\left(E_c I_c + E_s (d-h)^2 A_s\right)^2}\left(\int_{V_c} E_c M^2 y_c^2 dV_c + \int_{V_s} E_s M^2 y_s^2 dV_s\right)$$
$$= \frac{1}{2\left(E_c I_c + E_s (d-h)^2 A_s\right)^2}\left(E_c I_c + E_s (d-h)^2 A_s\right)\left(\int_0^{\frac{L}{2}} \frac{1}{4}P^2 z^2 dz + \int_{\frac{L}{2}}^{L} \frac{1}{4}P^2 (L-z)^2 dz\right)$$
$$= \frac{P^2 L^3}{96\left(E_c I_c + E_s (d-h)^2 A_s\right)} \tag{7-49}$$

The vertical displacements can be obtained by using Castigliano's second theorem:

$$\delta_i = \frac{\partial U}{\partial P_i} \tag{7-50}$$

Hence,

$$y = \frac{PL^3}{48(E_c I_c + E_s (d-h)^2 A_s)} \tag{7-51}$$

where I_c is the moment of inertia about the neutral axis of the concrete cross-sectional area. If we ignore the tension effect of concrete $I_c = \frac{1}{3}Bh^3$, otherwise,

$$I_c = \frac{1}{3}BH^3 - BH^2h + BHh^2 .$$

These results are compared with those from VULCAN in Figs. 7-22 and 7-23, where the reinforced concrete beam was subdivided into seven layers using Huang's layer model and 10 x 13 segments using the current generalised beam element. From Fig. 7-22 it can be seen that, for small deflections, the predictions are identical. However due to the effect of geometric non-linearity, the solutions gradually diverge as the deflections increase. This is because the theoretical solutions are based on Castigliano's second theorem which assumes geometrical linearity. In Fig. 7-23 the differences between the theoretical results and those from VULCAN are due to the material non-linearity. Geometric non-linearity is not significant in this case because the deflections are much smaller than those shown in Fig 7-22. Predictions 1 to 4 use the following different tension patterns for concrete as introduced in Section 7.4:

1, Vecchio and Collins's tension model[58]; **2**, Rots' tension curve[59]; **3**, neglecting the descending part of the tension curve; **4**, totally neglecting the tension.

It is interesting to see from Fig. 7-23 that prediction 1 is very close to the layer model results which uses Vecchio's model for concrete in tension. The other concrete tension models show big differences. These results show that VULCAN is capable of modelling reinforced concrete beams at ambient temperature but the analysis is very sensitive to concrete tension patterns.

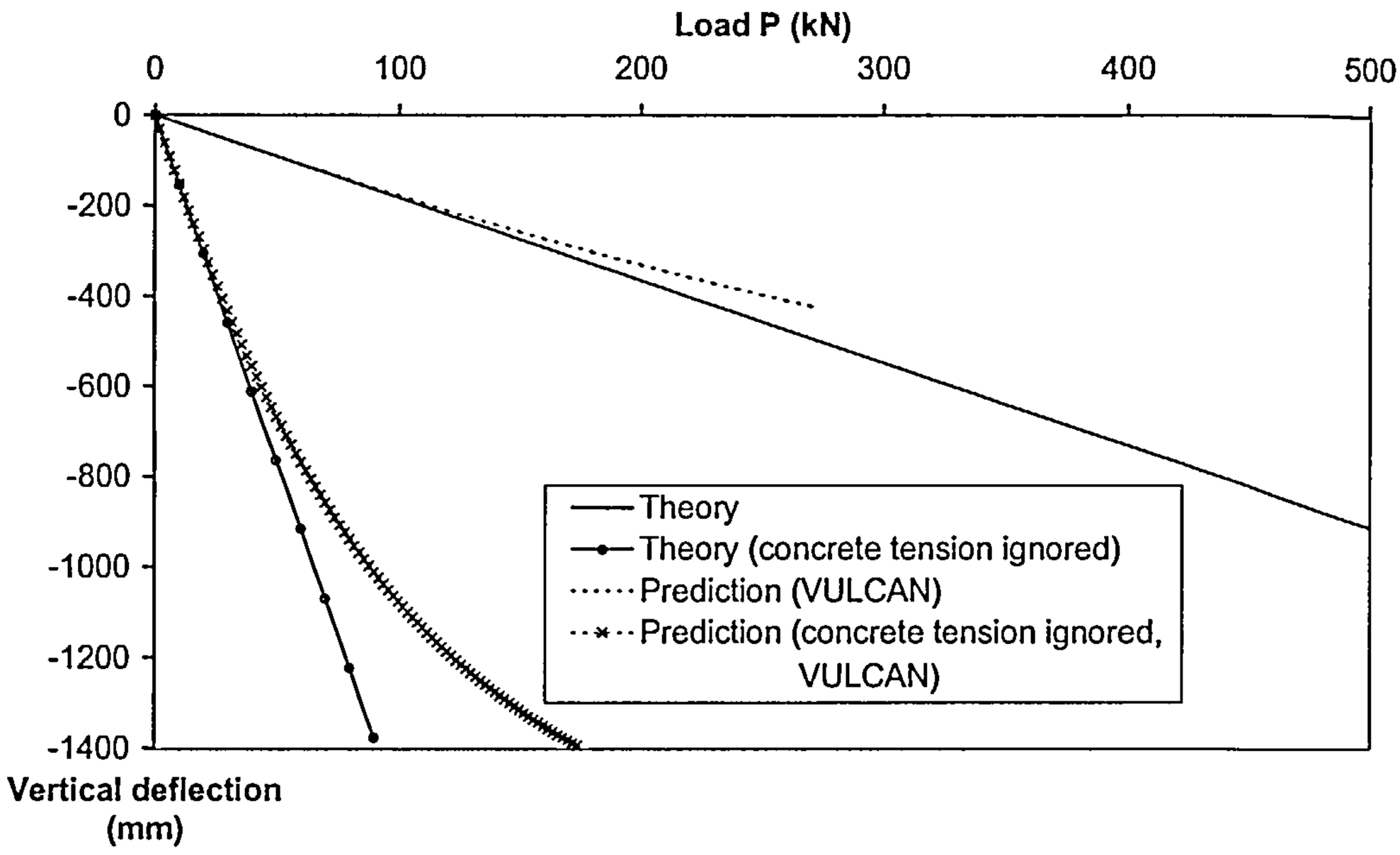

Fig. 7-22 Vertical deflection at the central point of reinforced concrete beam

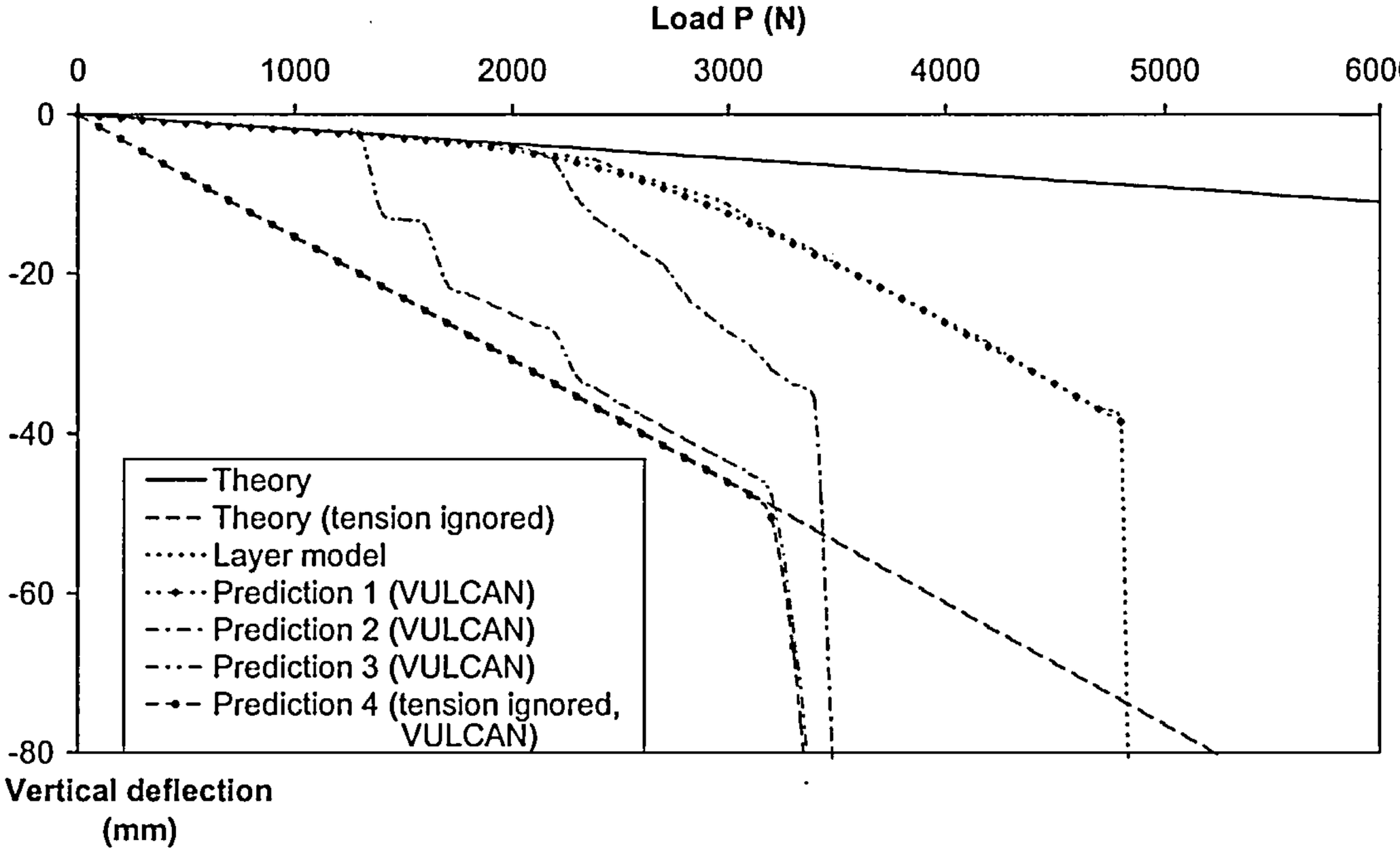

Fig. 7-23 Comparison with layer slab model for mid-span vertical deflection at ambient temperature

(e) Torsion deflection of a composite beam at ambient temperature:

In order to examine the effect of torsion, a cantilever beam, 5000mm long, with a torque (T) applying at the free end was analysed. Since the twisting angle in the software VULCAN is assumed to be small, the torsion equation for the cantilever beam can be given by [84]: $\phi = TL/(GJ)$

Table 7-1 Torsion at the free end of cantilever beam

Cross-section description 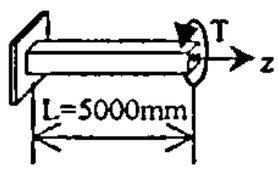	Torque T (kNm)	Material properties	Analysis (rad.)	Theory (rad.)	Note
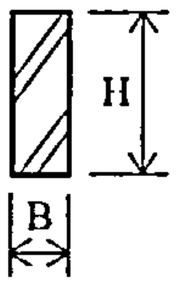 B=5mm, H=100mm	0.01	Steel: G = E/2.6, E = 210000N/mm²	0.1484	0.1486	Steel strip
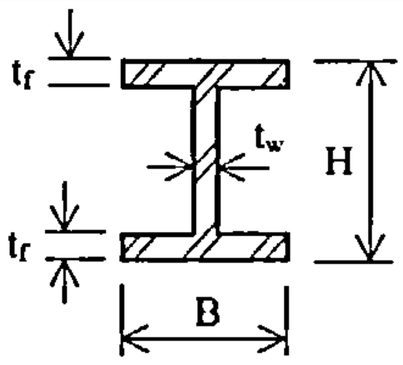 B=H=100mm, t_f= t_w =5mm	0.01	Steel: G = E/2.6, E = 210000N/mm²	0.0449	0.0492	I shape steel beam
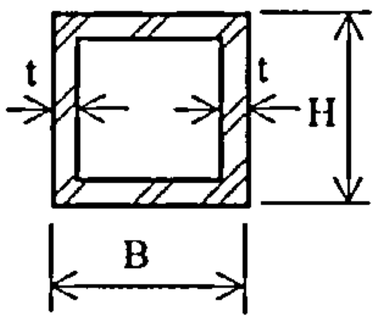 B=H=100mm, t=5mm	10	Steel: G = E/2.6, E = 210000N/mm²	0.1423	0.1444	Hollow box steel beam
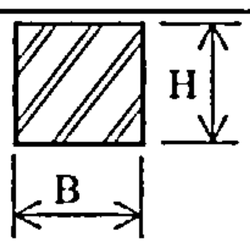 B=H=100mm	10	Steel: G = E/2.6, E = 210000N/mm²	0.0436	0.0439	Rectangular steel beam
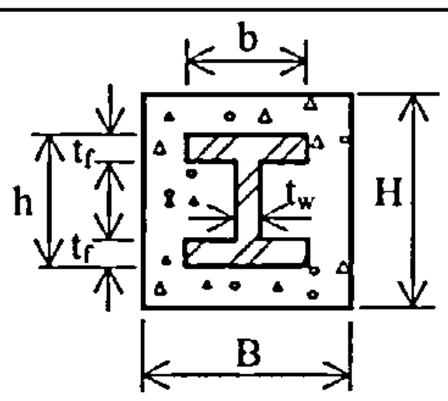 B=H=120mm, b=h=100mm, t_f= t_w =5mm	10	Steel: G = E_s/2.6, E_s = 210000N/mm² Concrete: G = E_c/2.4, E_c = 18000N/mm²	0.2255	0.2269	Concrete encased composite section
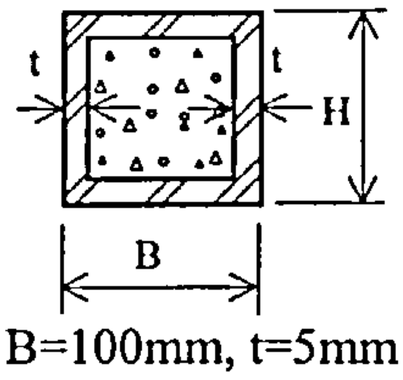 B=100mm, t=5mm	10	Steel: G = E_s/2.6, E_s = 210000N/mm² Concrete: G = E_c/2.4, E_c = 18000N/mm²	0.1188	0.1203	Concrete filled hollow section

Table 7-1 illustrates the results for some different cross-section beams, indicating good agreement with theoretical solutions.

The final ambient temperature validation was for a "T" cross-section reinforced concrete member which was compared with the results from Huang's effective-stiffness slab model[90]. A simply supported "T" beam spanning 6100mm was analysed to simulate the concrete ribs as presented in chapter 6. The cross-section and layout of the beam are shown in Fig. 7-24.

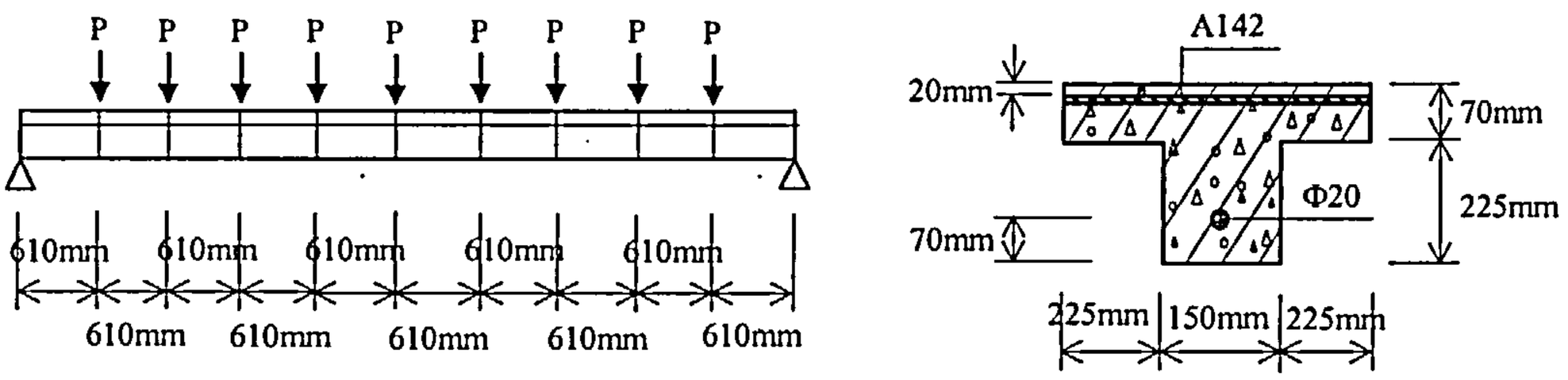

Fig. 7-24 Reinforced concrete beam as used to model the concrete rib of a Slimdek floor system at ambient temperature

In this case, the steel reinforcement was grade 460 in accordance with BS 4449 and concrete was grade C30 NWC in accordance with BS8110. The "T" beam was modelled using ten two-noded beam elements by concrete beam model or twenty nine-noded shell elements by effective-stiffness slab model, respectively. Nine point loads (**P**) of 1.8576kN were applied at each beam approximating to a uniformly distributed load of 6.88kN/mm².

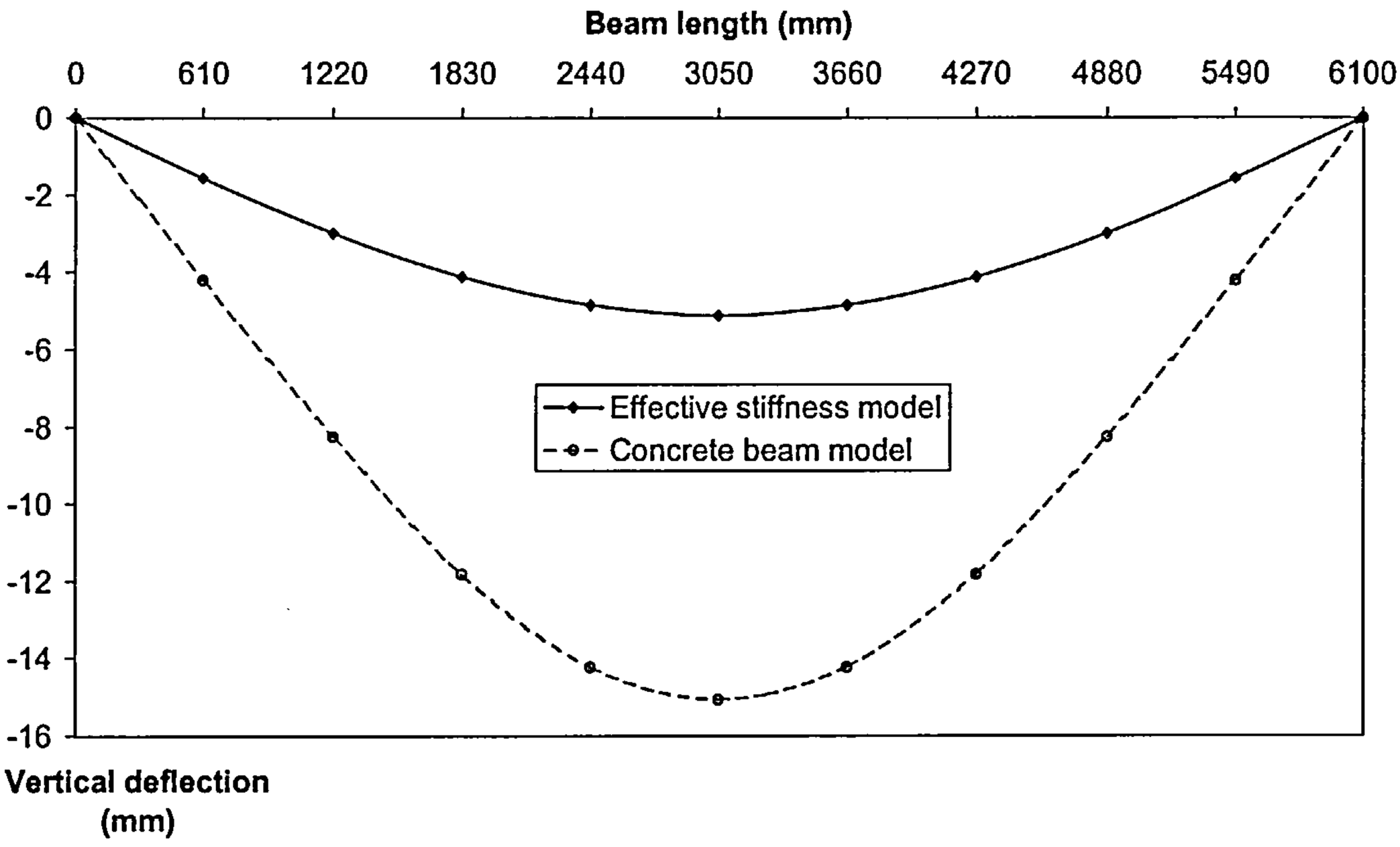

Fig. 7-25 Vertical deflections for the reinforced concrete beam under nine point loads of 1.8576kN by using generalised concrete beam and effective stiffness models at ambient temperature

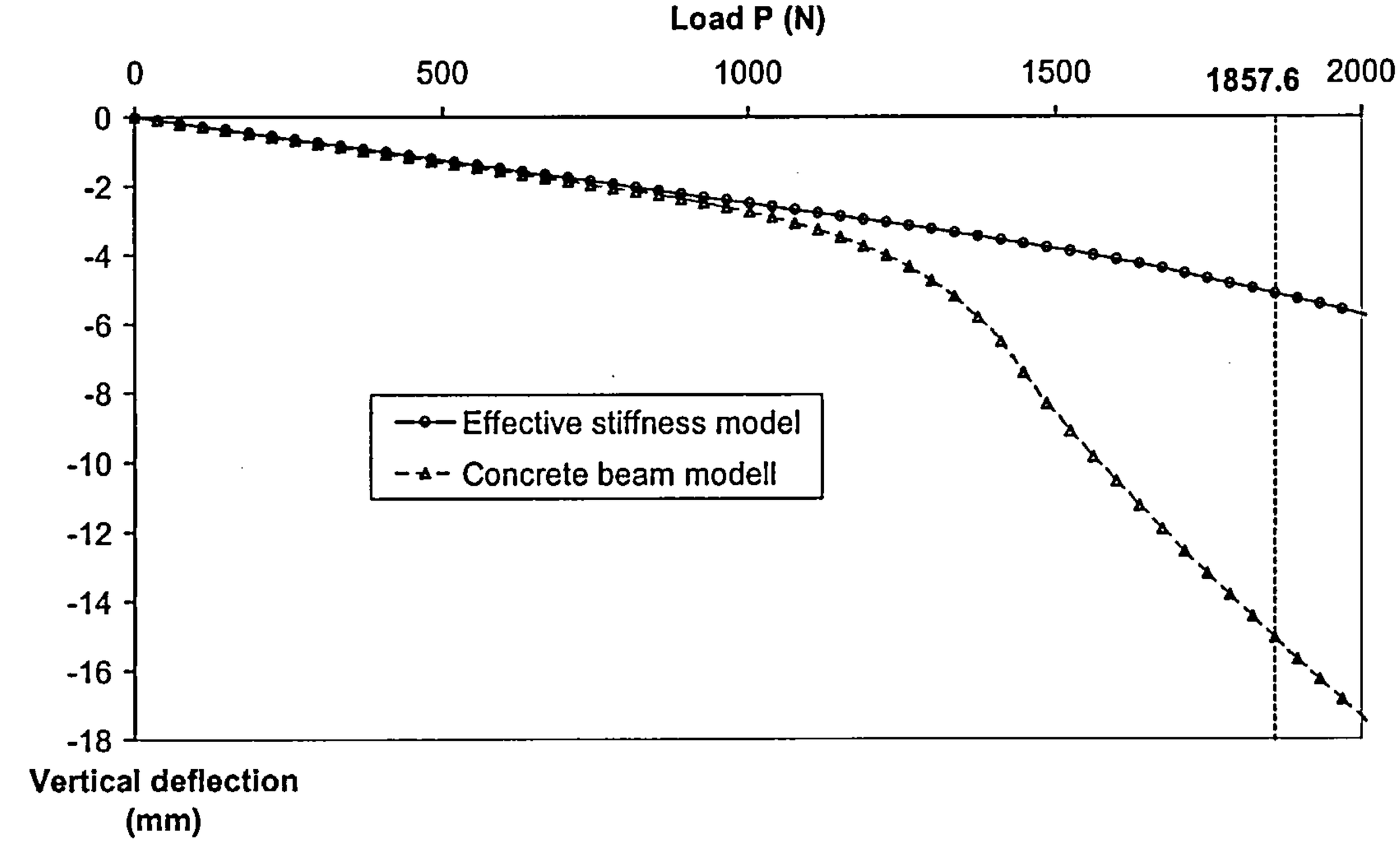

Fig. 7-26 Vertical deflection history at the central point of the reinforced concrete beam

The results of the comparisons are given in Fig. 7- 25 and Fig. 7-26. It can be seen from Fig. 7-26 that, the two models are in very close agreement for loads up to about 1000N but then diverge significantly at higher load levels. It is evident that the effective stiffness slab model is stiffer than the generalised concrete beam model. The reason for this is that, the effective stiffness model uses the effective-stiffness factors to modify the material stiffness matrices of plain concrete assuming that the stiffness in each direction is based on an elastic un-cracked concrete section. The cracking of the concrete ribs will in reality reduce the effective-stiffness factor. However, at present within the effective-stiffness model this factor is kept constant.

7.7.2 COMPARISON WITH TEST DATA SUBJECTED TO HIGH TEMPERATURE

A series of fire tests carried out at Construction Technology Laboratory of the Portland Cement Association according to ASTM E119 and SDHI fires and reported by Ellingwood and Lin[17], have been used to validate the computer predictions for reinforced concrete beam at high temperature. In these fire tests, six reinforced concrete beams were cast according to ACI Standard 318 (building 1983) with a 20-ft (6.1m) span and a 6-ft (1.8m) cantilever each beam. The central span of the beam was exposed to fire whilst the cantilevers were kept cool. Beams 1-4 were tested using the ASTM E119 fire exposure and beams 5 and 6 were exposed to a short-duration SDHI (high intensity) fire. Each beam was subjected to six concentrated loads (**P**) on the central span and a variable concentrated load, initially from $\mathbf{P_0}$ on the cantilever part. All the beams were of normal-weight concrete and Grade 60 deformed reinforcing bars. Three of the beams were analysed using VULCAN and the results are shown in Fig. 7-27. Other details for the beams are given in table 7-2. All these measured properties were adopted as input data.

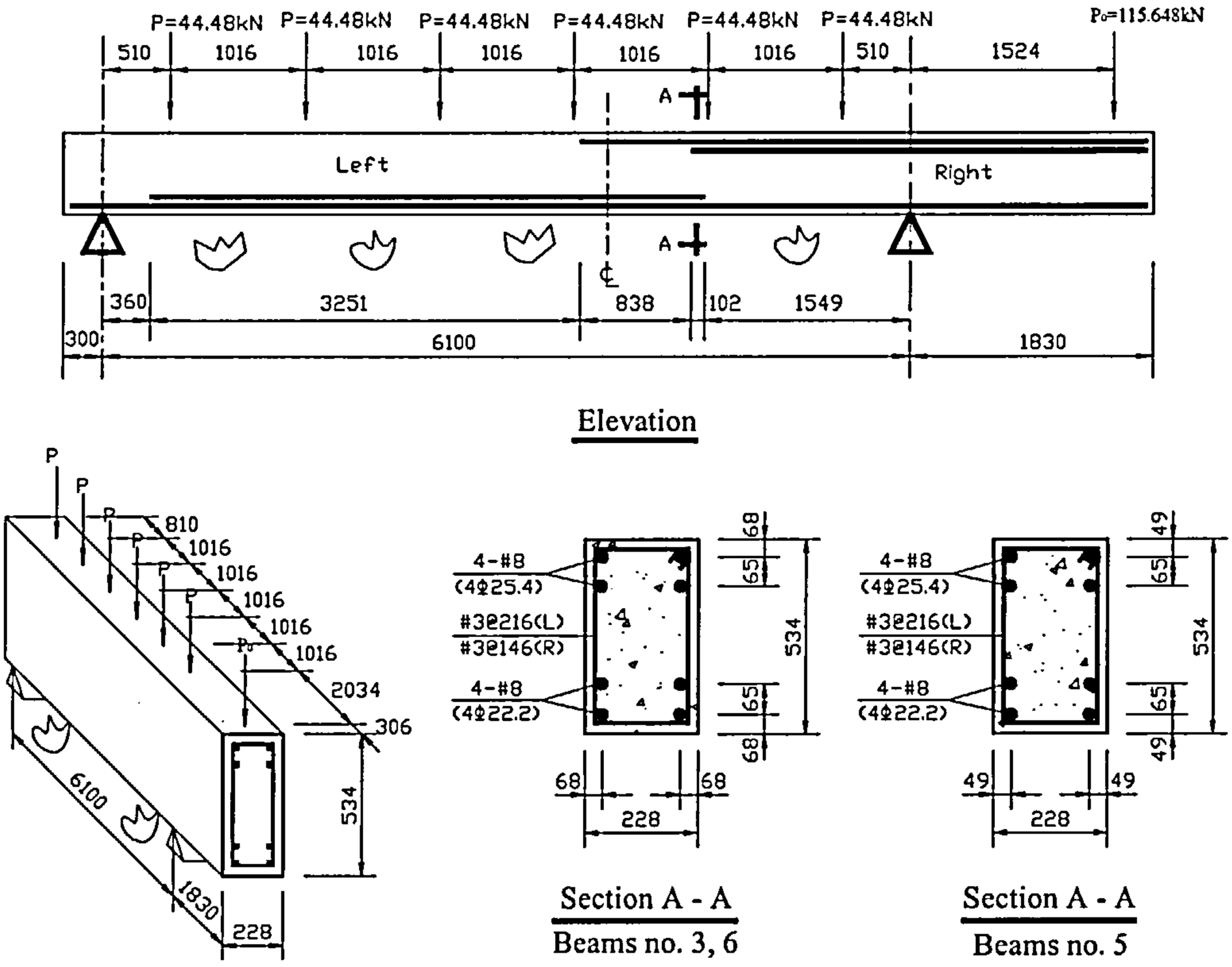

Fig. 7-27 Details of fire tests on reinforced concrete beams (All dimensions in mm)

Table 7-2 Details of beam tests

Beam no.	Reinforcement f_y (Mpa), ε_y (mm/mm)			Concrete f_c' at test (Mpa)	Load P (kN)	Load P_0 (kN)	Fire exposure	Test duration (hr:min)
	#3	#7	#8					
3	f_y=483.34	f_y=481.27	f_y=509.54	29.65	44.48	111.2	ASTM	4:03
5	ε_y=0.0028	ε_y=0.0025	ε_y=0.0028	33.72	44.48	115.65	SDHI	4:03
6				34.54	44.48	111.2	SDHI	4:03

For the computer analysis, the concrete beam was divided into twenty elements along its length and 12 x 6 segments over the cross-sections. Steel segments were used at the reinforcing bar positions. In order to model the temperature distributions across the cross-section, Huang's thermal analysis program FPRCBC-T[96], which is capable of simulating non-linear temperature histories within reinforced concrete members in

fires (including ASTM E119 fire and SDHI fire as shown in Fig. 7-28), was used. The results of maximum vertical deflections are shown in Figs. 7-29 to 7-31. The figures also include Ellingwood's analyses[17].

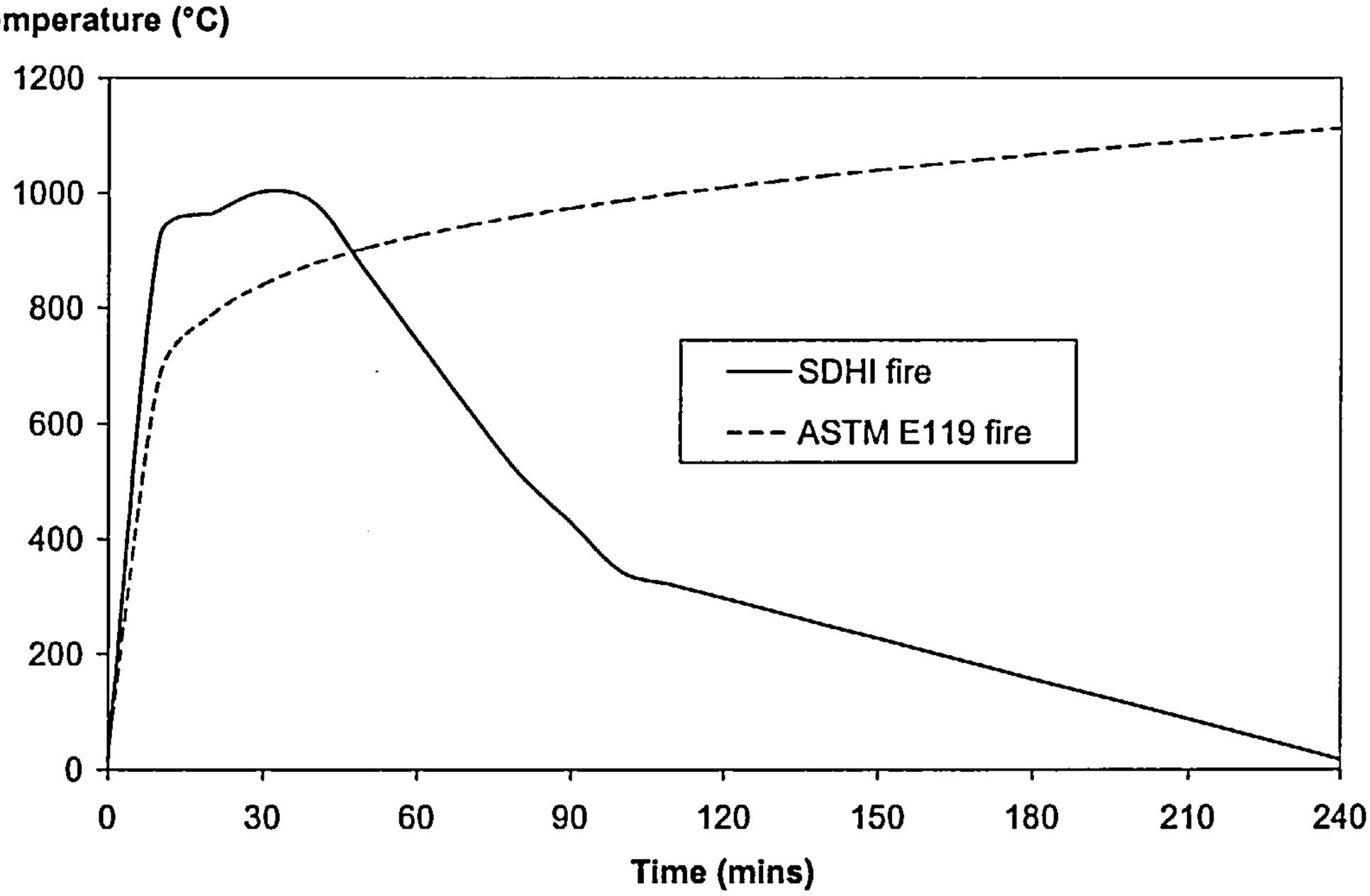

Fig. 7-28 Simulated atmosphere temperature for SDHI and ASTM fire

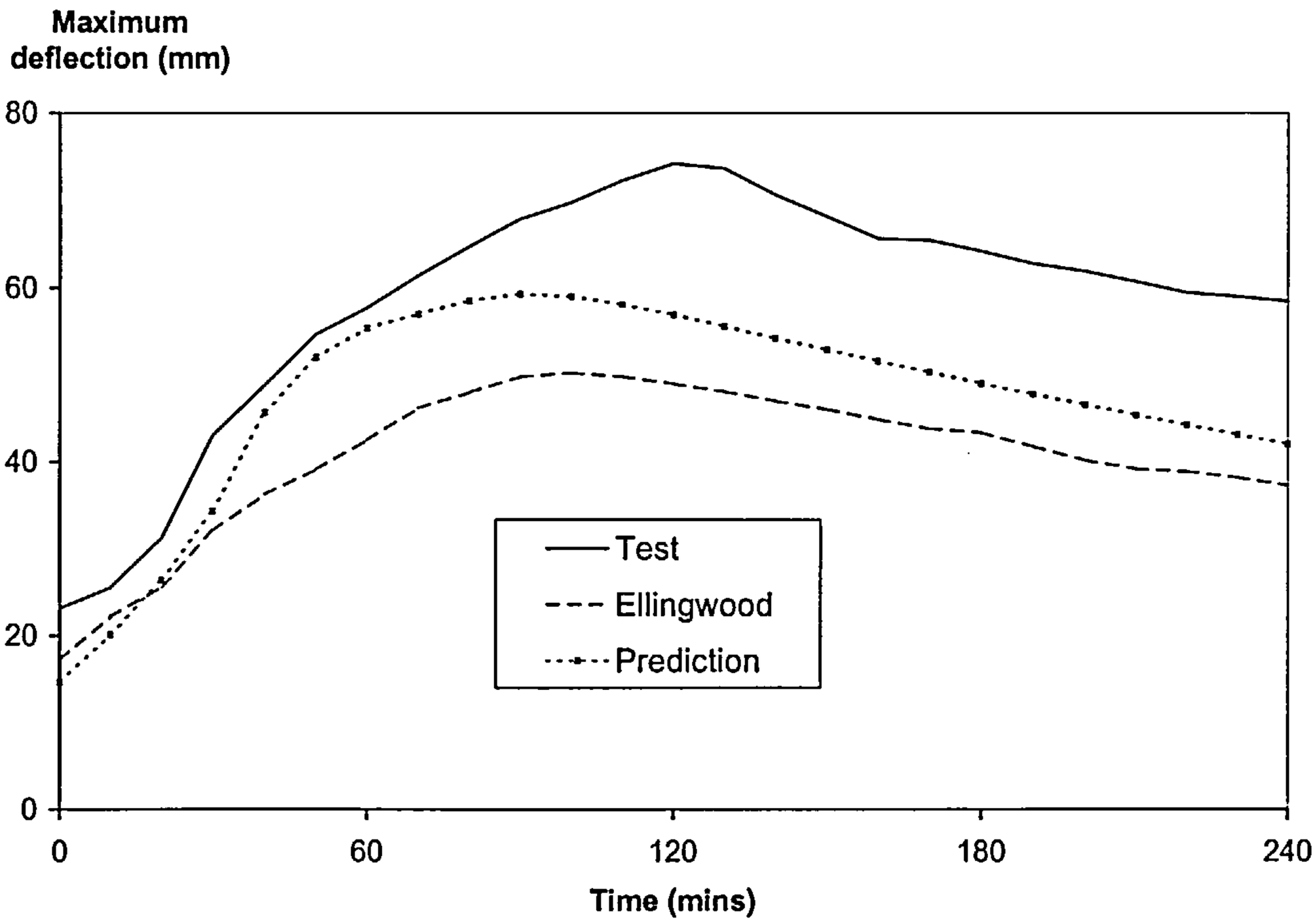

Fig. 7-29 Maximum deflection of beam 5 under SDHI fire

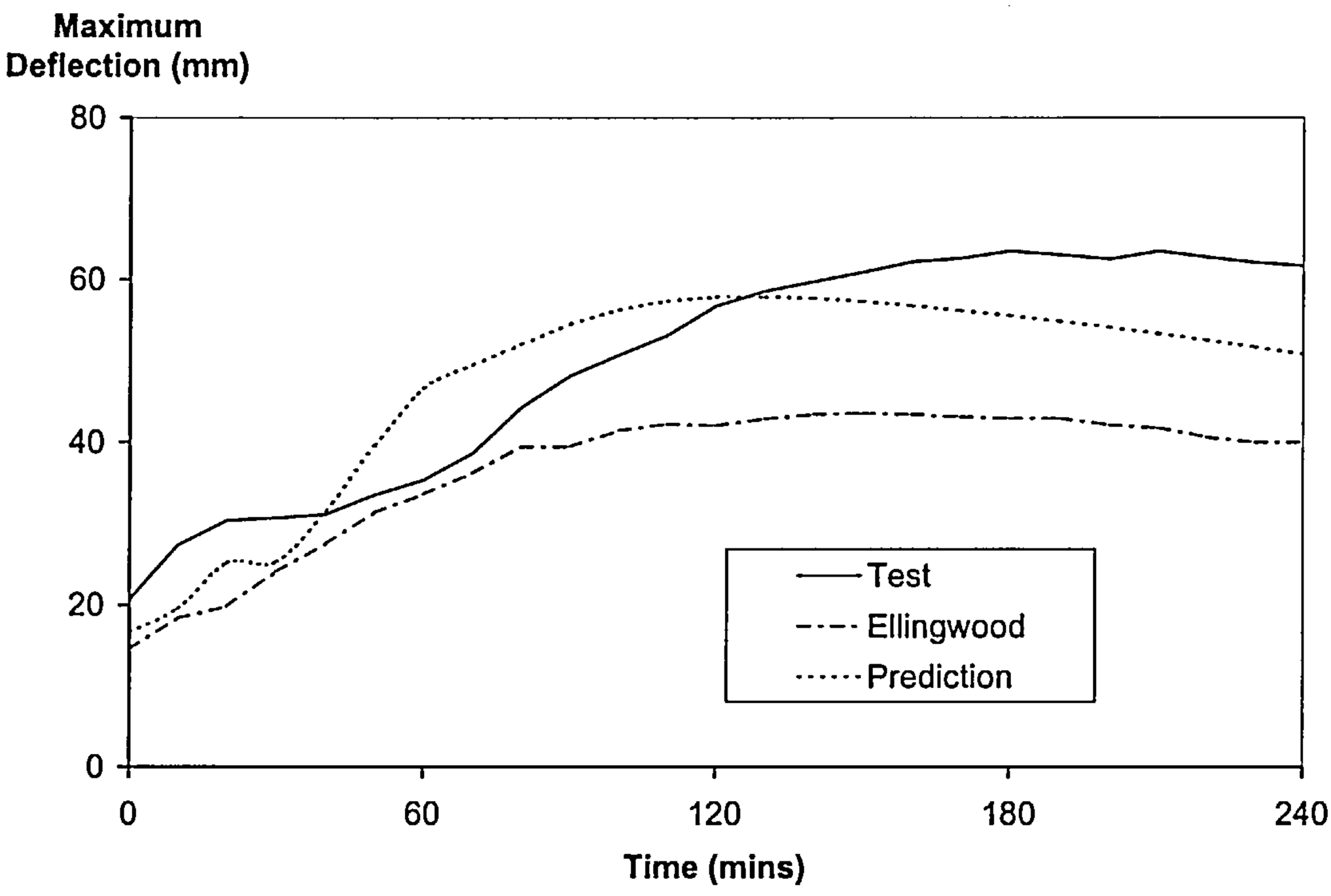

Fig. 7-30 Maximum deflection of beam 6 under SDHI fire

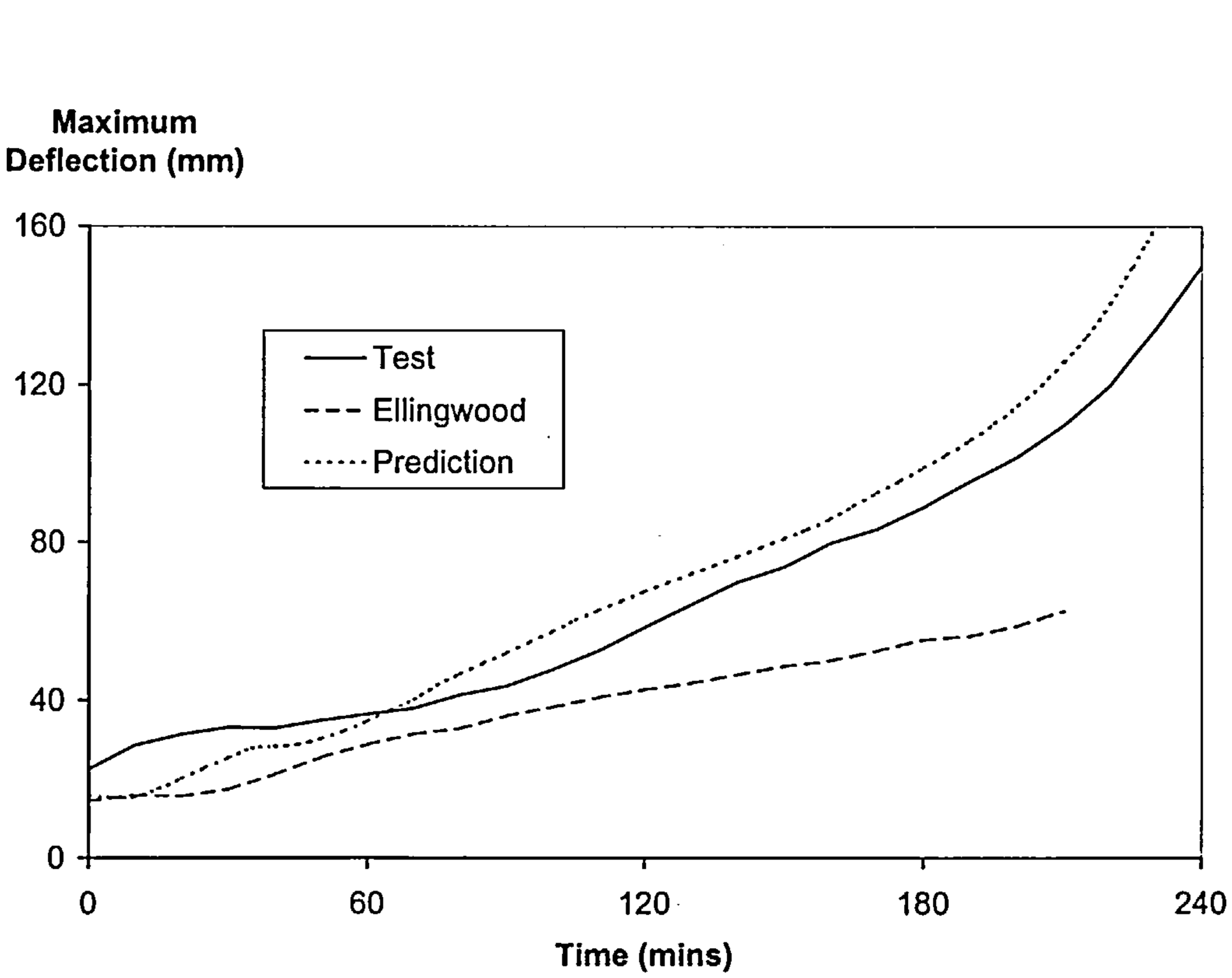

Fig. 7-31 Maximum deflection of beam 3 under ASTM E119 fire

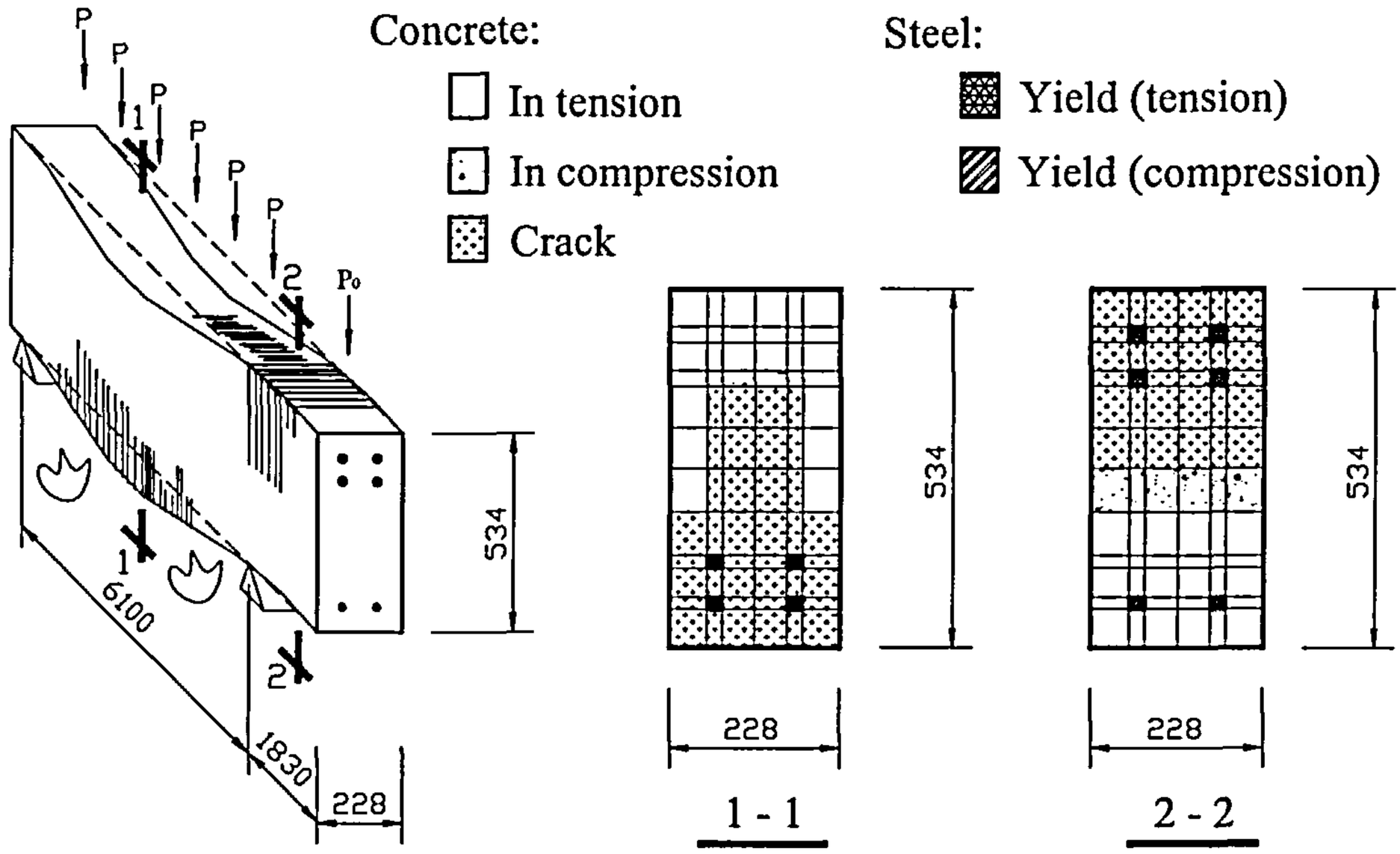

Fig. 7-32 Predicted Cracking patterns for beam 3 under ASTM E119 fire at the end of test (240 minutes)

The comparisons shown in Figs. 7-29 to 7-31, show that the proposed model is in very good agreement with the test results for all three cases. In particular the predicted results for beam 3 which is exposed to the standard ASTM E119 fire follow similar pattern to the test data, and give much closer predictions than Ellinwood's own analysis throughout the heating history. Fig. 7-32 illustrates the extent of cracking for beam 3 at the end of test (240 minutes), and it is interesting to see that there is no crushing.

7.8 CONCLUSIONS

In this chapter, the 3D finite element software VULCAN has been extended to enable modelling of generalised composite beam sections in fire. Not only pure steel or concrete members can be analysed but also composite members with two materials, such as a reinforced concrete beam or a concrete filled column. The cross-section is divided into a number of segments allowing variations of temperatures and stresses

over the section. Thermal expansion and material degradation for both concrete and steel are considered. Since the formulations are highly non-linear, a numerical iteration solution procedure is required, and the Newton-Raphson method is used for this. Comparisons with results indicate that the modified VULCAN is clearly capable of modelling composite elements in fire. However there is still a need for further investigations on more extensive structures, including for example Slimdek floor systems and the behaviour of the concrete ribs.

8. CONCLUSIONS

This chapter discusses the main research work presented in the thesis, and presents conclusions and recommendations for further studies.

8.1 INTRODUCTION

The research work in this thesis has mainly concerned:

- the analysis of corner columns subjected to push-out by the connected beams,
- refinement of the steel beam cross-section,
- modelling of asymmetrical beam sections,
- the development of a generalised concrete beam element, all for fire conditions.

Because columns play a key role in carrying loads back to foundations they become more important than other members, and are usually protected by applying thermal insulation. However, in the special case of perimeter building columns, an additional bending moment caused by the push-out of unprotected connected beams due to thermal expansion may be induced, and this may lead to a column buckling even through it is protected. For internal columns such effects are less pronounced, since the thermal expansions on opposite sides are to some extent balanced. The existing fire design codes do not consider this beam push-out effect. In order to investigate the potential effects of column push-out a series of parametric studies, based on a column sub-frame of the Cardington BRE Corner Fire Test, have been carried out. The finite element analysis software VULCAN has been used throughout these studies, together with an alternative generalised simplified approach, based on the classical methods of structural mechanics, which is suitable for hand calculation, enabling a quick assessment of perimeter building columns.

Full-scale fire tests are very expensive, so computer models are very important for investigating structures under different fire conditions. One such finite element software, VULCAN, has been developed at University of Sheffield to assess three-dimensional frames and sub-frames subjected to fire conditions, and is continually being developed by research workers in the Steel in Fire Research Group. Recently a new composite floor system, known as the Slimdek® floor system, has been introduced into building construction. Such floor systems offer very significant potential advantages compared with conventional composite floors, and the availability of validated software capable of modelling their behaviour in fire will be very important if the full advantages of these new systems are to be realised. The computer software VULCAN has been extended to include these requirements. The ASB beam and the generalised beam models have been developed to simulate respectively the Asymmetric Slimfor® Beam and the concrete ribs of these floor systems. In these models, two-noded one-dimensional elements are used and the Newton-Raphson method is adopted for solving the non-linear problems efficiently. The analysis has been validated against available test results, generally indicating good agreement. However, a limited number of fire tests are still necessary because the development of performance-based fire engineering design guidance should be based on both theory and experimental evidence.

The major conclusions and recommendations for this research work are reviewed below.

8.2 THE BEHAVIOUR OF CORNER SUB-FRAMES IN FIRE

In current fire design practice the structure is normally treated as an assembly of isolated individual members. This is a conservative treatment in most cases, because

the continuity of the structure has not been taken into account. However, this method may give un-conservative results in some special situations. One of these cases occurs on heating when the perimeter building columns are connected to unprotected beams. In this case additional bending moments may be induced in the columns due to thermal expansion of the beams, and ignoring this effect may give an unsafe result. A typical corner sub-frame, in which two orthogonal beams, both of 356x171x51UB Grade 50 section, one 6000mm long and the other 9000mm, are pinned to the mid-point of a 305x305x137UC Grade 50 column of 8370mm total length, was used to carry out a series of parametric studies. This analytical model is intended to simulate a corner frame of the Cardington test building, representing the worst case of column push-out. The software VULCAN was used to model this type of sub-frame, indicating that the **P-Δ** effect and thermal expansion are indeed important factors which are not normally considered in column design.

In order to enable a quick assessment of the problem of column push-out without using complex finite element analysis a generalised formulation, based on a simple 2D model, was developed using classical theory. This enables the maximum bending moment to be estimated, and a simple check to be performed to ensure that the column stresses in combined bending and compression do not exceed yield.

Several conclusions are drawn from these studies:

(1) The analyses show that existing fire design codes, such as BS5950: Part 8, can be unsafe since the **P-Δ** effect due to thermal expansion of unprotected beam are not normally considered in column design.

(2) The induced column moments are mainly caused by the second-order "**P-Δ**" effect, linking the thermal expansion of the beams and the column axial force.

(3) To calculate the critical temperature of a column within a corner sub-frame when column and beam sizes are similar to those in the corner frames of the Cardington test building, an effective length factor multiplied by 1.2 should be used, and whether the structure is braced or not, the factor for a sway frame should be used.

(4) The deflection of the column and the associated bending moment are proportional to the thermal effect (thermal elongation or force) of the beam, which in turn depends on the beam stiffness.

(5) It is clear that the thermal push-out effect is controlled mainly by the relation between the stiffnesses of the beam and column -- the smaller the relative stiffness of the beam then the less the effect.

(6) The thermal expansion of unprotected beams induces extra lateral force onto the column. As the failure temperature of the column is approached this force reverses and becomes a restraining force.

(7) Each imperfection can be regarded as an equivalent initial out-of-straightness, which may have negligible effect in the normal case.

(8) The slab has a significant influence in reducing the effect of beam expansion.

(9) It is suggested that designers use a simplified calculation (the generalised formulation) in two dimensions to model the structural instability approximately. This can be implemented on spreadsheet software.

(10) The pull-in effect at high temperature is of benefit to the survival temperature of the column, but is relatively small compared with the effect of thermal expansion which is the primary **P-Δ** effect.

(11) It would be helpful to carry out further work in the form of a series of parametric studies based on the generalised equation, and to tabulate the results for convenient use by engineers.

8.3 DEVELOPMENT OF SOFTWARE VULCAN

The structural software VULCAN has been developed over many years and has proved to be capable of performing non-linear analysis of three-dimensional frames and sub-frames subjected to fire conditions. The finite element approach currently includes both beam-column and flat-shell slab elements.

A new kind of steel beam – the Asymmetric Slimflor Beam (ASB) -- which forms part of a composite slim-floor system with deep decking, has been introduced into VULCAN. The section of the ASB beam normally has a web of greater thickness than that of the flange, and this Slimdek floor system provides good fire resistance.

The development described in this thesis allows the structural analysis of full three-dimensional composite buildings with symmetric and asymmetric beam cross-sections subjected to fire, together with a section refinement which enables the cross-section to be divided as finely as is required to achieve sufficient accuracy. The modified software has been validated by comparison with both classical analytical results and test results, indicating good simulation.

To model the behaviour of the concrete ribs of the Slimdek floor system, a generalised concrete beam model has been developed and incorporated into the software. Both geometric and material non-linearities have been included. The cross-section is divided into a number of segments, allowing two-dimensional variation of temperatures and stresses over the section. Thermal properties are taken into account in accordance with current codes. Uniaxial temperature-dependent mathematical

models are considered for two different materials -- one for steel and another for concrete. Because two different materials may exist in a single two-noded one-dimensional beam element the transformed section concept is applied, with the performance related to one material at ambient temperature for programming convenience. The Newton-Raphson solution procedure is used since the model contains high non-linearity. Validations of this new beam model have been carried out, and the results demonstrate its capability of modelling alternative cross-sections at elevated temperature. This development also allows the modelling of a member composed of one or two materials -- typically steel and concrete -- with different section shapes. Examples include concrete-filled hollow sections or partially encased open sections. In comparison with Huang's effective-stiffness slab model[90], which has been used to simulate the ribbed floor in VULCAN, this concrete beam model predicts greater deformations and is believed to be more suitable for deep ribs. For this reason this concrete beam element, together with a normal flat slab element[68], is recommended for modelling the deep ribbed floor system instead of using the effective-stiffness model[90]. Composite structures constructed with members which are not I-sections can also be simulated using the latest developed software. Further developments might include more material models, such as brick and timber. Another further development would be to extend the existing concrete material model, especially in the tension range, and to incorporate spalling, which mainly depends on the moisture pressure inside the concrete at elevated temperature. Based on the development of the software, the following conclusions can be reached:

(1) The modified VULCAN is capable of modelling the behaviour of composite buildings in fire, which include not only pure steel or concrete members but also members composed of two materials or alternative cross-sections.

(2) The cross-section of the beam element is divided into a number of segments so that variations of strains, stresses and temperatures can be simulated. The analytical results indicate that division of the cross-section into 12 segments gives sufficiently accurate results for most analytical purposes with symmetric cross-section members. However for members of non-symmetric cross-sections, such as the Asymmetric Slimflor Beam (ASB), with highly non-linear temperature distributions, the cross-section really needs to be represented by more than 18 segments. Increasing the number of sub-segments increases the accuracy of the results, but costs more in computing time.

(3) Two uniaxial temperature-dependent material models for steel and concrete are available in the software. The mathematical models for steel are based on EC3: Part1.2 or Ramberg-Osgood expressions representing the EC3 test data. Both are able to model the unloading of steel in the cooling phase. The concrete mathematical model conforms to EC4: Part1.2, and the cracking and crushing behaviours can be simulated in "smeared" form. The analyses indicate that the computer predictions are very sensitive to the assumed concrete tension model. This tension model may need to be further developed.

(4) It is assumed that a member is straight and prismatic, and that its plane cross-sections remain plane and intact during deflection. This explicitly means that spalling of the concrete has not been simulated. Also there is no slip between different materials in the cross-section. The effects of high-temperature creep for both steel and concrete are implicitly taken into account by the present material models.

(5) To model the composite floor systems, Huang's effective stiffness model is suited to ribbed floors with shallow ribs at close spacings. When ribbed floors

with deep ribs are present, it is necessary to use the concrete beam element together with a normal flat slab element[68] to model these floor system.

8.4 Recommendations for the future work

The latest version of VULCAN enables both steel and RC structures to be analysed in fire, using two-noded line elements for the beams and columns. The highly non-linear formulation includes 8 degrees of freedom at each node in local coordinates (including two unusual degrees of freedom – 'strain' and 'warping'). These degrees of freedom transform into 11 global degrees of freedom, and some doubts have been expressed about the need for their inclusion, particularly since they must waste computation time and may cause the software to become numerically unstable, also because transformation of "strain" leads to 3 additional apparent degrees of freedom in global coordinates which are not logical. Further research is being carried out at Sheffield to remove these extra degrees of freedom. Although the number of nodal degrees of freedom will be reduced, the basic method and formulations will be unchanged except for the transformation matrix. However, the detailed equations may need to be modified. Accordingly, the basic assumption that the twist angle of the beam member is relatively small would no longer be a restriction and the equations which relate to twist, for example the basic geometric equations, should be modified. This development could improve both program stability and computational efficiency.

REFERENCES

[1] *International Fire Engineering Design for Steel Structures: State of the Art*, International Iron and Steel Institute, Brussels, 1993.

[2] *Steel and fire safety: A global approach, Steel promotion Committee of Eurofer*, Square de Meeûs, 5, bte 9, B-1040 Brussels, Belgium, 1990.

[3] John Dowling, Jef Robinson and Euan Crouch of British Steel, 'Fire Prevention: The use of Sprinkler Systems', *Journal of the Fire Protection Association*, March 1993.

[4] El-Rimawi, J.A., 'The Behaviour of Flexural Memebers under Fire Conditions', *PhD thesis*, University of Sheffield, 1989.

[5] Simms, I. And Newman, G., '*The behaviour of Structures in Fire*', Steel Construction Institute, 1999.

[6] Lennon, T., '*Cardington Fire Tests: Survey of Damage to the Eight Storey Building*', Building Research Establishment, 1997.

[7] Newman, G. and Simms, I., '*A New Approach to the Design of Multi-storey Steel Framed Building in Fire*', Steel Construction Institute, 1998.

[8] Bailey, C.G., Moore, D.B. and Lennon, T., 'The Structural Behaviour of Steel Columns During a Compartment Fire in a Multi-storey Braced Steel-frame', *Journal of Constructional Steel Research*, **52**, 1999: pp 137-157.

[9] Uddin, T. and Culver, C.G., 'Effect of Elevated Temperature on Structural members', *Journal of the Structural Division ASCE*, **101** (ST7), 1975: pp 1531-1549.

[10] Bailey, C. G., 'Simulation of the Structural Behaviour of Steel-framed Buildings in Fire', *PhD Thesis*, University of Sheffield, 1995.

[11] Culver, C.G., 'Steel Column Buckling under Thermal Gradients', *Journal of the Structural Division ASCE*, **98** (ST8), 1972: pp 1853-1865.

[12] Culver, C.G., Aggarwal, V. and Ossenbruggen, R.J., 'Buckling of Steel Columns at Elevated Temperature', *Journal of the Structural Division ASCE*, **99** (ST4), 1973: pp 715-726.

[13] Ossenbruggen, R.J., Aggarwal, V. and Culver, C.G., 'Steel Column Failure under Thermal Gradients', *Journal of the Structural Division ASCE*, **99** (ST4), 1973: pp 727-739.

[14] Newmark, N.M., 'Numerical Procedure of Computing Deflections, Moments and Buckling Loads', *Transactions ASCE*, **180**, 1943, p1161.

[15] Becker, J.M. and Bresler, B., 'FIRES – RC: a Computer Program for the Fire Response of Structures – Reinforced Concrete Frames', *Report No. UCB FRG 74-3*, University of California, Berkeley, July 1974.

[16] Bizri, H., 'Structural Capacity of Reinforced Concrete Columns Subjected to Fire Induced Thermal Gradients', *REPORT NO. UC SESM 73-1*, University of California, Berkeley, January 1973.

[17] Ellingwood, B. and Lin, T.D., 'Flexure and Shear Behaviour of Concrete Beams During Fires', *Journal of Structural Engineering ASCE*, **117** (2), February 1991: pp 440-458.

[18] Cheng, W. and Mak, K., 'Computer Analysis of Steel Frames in Fire', *Journal of the Structural Division ASCE*, **101** (ST4), 1975: pp 855-867.

[19] Jain, P. and Rao, R., 'Analysis of Steel Frames under Fire Envitoment', *International Journal for Numerical Methods in Engineering*, **19**, 1983: pp 1467-1478.

[20] Cheng, W.C., 'Theory and Application on the Behaviour of Steel Strructures at Elevated Temperatures', *Computers and Structures*, **16** (1-4), 1983: pp 27-35.

[21] Lie, T.T. and Chabot, M., 'A method to Predict the Fire Resistance of Circular Concrete Filled Hollow Steel Columns', *Journal of Fire Protection Engineering*, **2** (4), 1990: pp 111-126.

[22] Lie, T.T., 'Fire Resistance of Circular Steel Columns Filled with Bar-Reinforced Concrete', *Journal of Structural Engineering ASCE*, **120** (5), 1994: pp 1489-1509.

[23] Kodur, V.K.R. and Lie, T.T., 'Fire Resistance of Circular Steel Columns Filled with Fibre-Reinforced Concrete', *Journal of Structural Engineering ASCE*, **122** (7), 1996: pp 776-782.

[24] Cheung, Y.K., 'Finite Strip Method in Structural Analysis', *Pergamon Press*, Oxford, 1976.

[25] Uy, B. and Bradford, M.A., 'Local Buckling of Cold Formed Steel in Composite Structural Elements at Elevated Temperatures', *Journal of Constructional Steel Research*, **34**, 1995: pp 53-73.

[26] Wang, Y.C. and Moore, D.B., 'Steel Frames in Fire: Analysis', *Engineering Structures*, **17** (6), 1995: pp 462-472.

[27] Liu, T.C.H., 'Finite Element Modelling of Behaviour of Steel Beams and Connections in Fire', *Journal of Constructional Steel Research*, **36** (2), 1996: pp 181-199.

[28] Bailey, C.G., 'The behaviour of Asymmetric Slim Floor Dteel Beams in Fire', *Journal of Constructional Steel Research*, **50**, 1999: pp 235-257.

[29] Forsen, N.E., 'Steel Fire – A finite element program for non-linear analysis of steel frames exposed to fire', *Users manual*, Multi Consult A/s, Oslo, Norway, 1983.

[30] Schleich, J.B., 'CEFICOSS, a computer program for the fire engineering of steel structures', *Proceedings of International Conference on Mathematical Models for Metals and Material Applications*, London, 1987.

[31] Van Foeken, R. J. and Snijder, H.H., 'Steel Column and frame stability analysis using finite element technique', H*eron*, **30** (4), 1986, pp 3-29.

[32] Liew, R.J.Y., Tang, L.K., Holmaas, T. and Choo, Y.S., 'Advanced analysis for the assessment of steel frames in fire', *Journal of Constructional Steel Research*, **47**, 1998: pp 19-45.

[33] Weeks, N.J., 'Lateral Instability of Slander Reinforced Concrete columns in a Fire Environment', *PhD Thesis*, Aston University, 1985.

[34] Najjar, S.R., 'Three-dimensional Analysis of Steel Frames and Subframes in Fire', *PhD Thesis*, University of Sheffield, 1994.

[35] '*ISO834: Fire Resistance Tests – Elements of Building Construction*', International Organisation for Standardisation, Switzerland, 1975.

[36] '*BS 476: Fire Tests on Building Material and Structures, Part 20: Method of Determination of the Fire Resistance of Elements of Construction (General Principles)*', BSI, London, 1987.

[37] '*ASTM-E.199: Standard Methods of Fire Test of Building Construction and Materials*', American Society for Testing and Materials, Philadelphia, USA, 1983.

[38] '*JIS A 1304: Method of Fire Resistance Test for Structural Parts of Buildings*', Japanese Standard Association, Japan, 1976.

[39] '*BS 476: Fire Tests on Building Material and Structures, Part 21: Method of Determination of the Fire Resistance of Load Bearing Elements of Construction*', BSI, London, 1987.

[40] Wainman, D.M. and Martin, D.M., 'Preliminary Assessment of the Data Arising from a Standard Fire Resistance Test Performed on a Slimflor Beam at the Warrington Fire Research Centre on 14th February, 1996', *Technical Note SL/HED/TN/S2440/4/96/D*, British Steel Swinden Technology Centre, March 1996.

[41] Ali, F., O'Connor, D.J., Simms, W.I., Randall, M.J., Shepherd, P.G. and Burgess, I.W., 'The Effect of Axial Restraint on the Fire Resistance of Steel Columns', Second World Conference on Structural Steel Design, San Sebastian, *Journal of the Constructional Steel Research*, **46** (1-3), 1998, Paper No. 71.

[42] Franssen, J.M. and Dotreppe, J.C., 'Fire Resistance of Columns in Steel Frames', *Fire Safety Journal*, **19** (2&3), 1992: pp 159-175.

[43] Gere, J.M. and Timoshenko, S.P., '*Mechanics of Materials*', Third Edition, PWS-KENT Publishing Company, 1984.

[44] Timoshenko, S.P. and Gere, J.M., '*Theory of Elastic Stability*', McGraw-Hill Book Company, Inc., 1961.

[45] Li, G.Q., Jiang, S.Ch. and Lin, G.X., '*Fire Resistance Calculation and Design for Steel Structure*', ISBN 7-112-03585-6, Construction Publishing Company, P. R. China, 1999.

[46] Eurocode 3: *Design of Steel Structures. Part 1.2: Structural Fire Design*, Commission of the European Communities, Brussels, 1993.

[47] BS5950: *Structural Use of Steelwork in Buildings. Part 8: Code of Practice for Fire Resistant Design*, British Standards Institution, London, 1990.

[48] Eurocode 4: *Design of Steel and Composite Structures. Part 1.2: Structural Fire Design*, Commission of the European Communities, Brussels, 1993.

[49] ECCS (European Convention for Constructional Steelwork), *European recommendations for the fire safety of steel structures*, Elsevier, Amsterdam, 1983.

[50] Franssen, J.-M., 'Etude du comportement au feu des structures mixtes acier-béton', *PhD thesis*, Université de liège, 1987.

[51] CTICM (Centre Technique Industriel de la Construction Métallique), *Méthode de prévision par le calculdu comportement au feu des structures en acier*, Construction Métallique, 3, 1982: pp 39-79

[52] Purkiss, J.A., 'Developments in the Fire Safety Design of Structural Steelwork', *J. Construct. Steel Research*, **11** (3), 1988: pp 149-173.

[53] Harmathy, T.Z., 'A Comprehensive Creep Model', *Journal of Basic Engineering*, ASTM, September 1967: pp 496-502.

[54] Ellingwood, B. and Shaver, J.R., 'Analysis of Reinforced Concrete Beams Subjected to Fire', *NBS Building Science Series 76*, U.S. DEPARTMENT OF COMMERCE, National Bureau of Standards, July 1970.

[55] Petzold, A. and Röhrs, M., '*Concrete for high Temperatures*', ACLAREN AND SONS LTD, LONDON, 1970.

[56] Khennane, A. and Baker G., 'A Uniaxial Model for the Thermo-Mechanical Behaviour of Concrete at Elevated Temperature', *Research Report No. CE104*, University of Queensland, June 1989.

[57] Bazant, Z.P. and Kaplan, M.F., '*Concrete at High Temperatures: Material Properties and Mathematical Models*', Longman Group Limited, England, 1996.

[58] Vecchio, F.J., and Collins, M.P., 'The Modified Compression-Field Theory for Reinforced Concrete Element Subject to Shear', *ACI JOURNAL, Proceedings* V. 83, No. 2, March – April (1986): pp 219-231.

[59] Rots, J.G., et al., 'The Need for Fracture Mechanics Options in Finite Element Models for Concrete Structures', *Proc. International Conference on Computer Aided Analysis and Design of Concrete Structures, Part 1, F. Damjanic, et al., eds.*, Pineridge Press, Swansea, 1984: pp 19-32.

[60] Olawale, A.O. and Plank, R.J., 'The collapse analysis of steel columns in fire using a finite strip method', *International Journal for Numerical Methods in Engineering*, **26**, 1988: pp2755-2764.

[61] Saab, H.A., 'Nonlinear finite element analysis of steel frames in fire', *PhD Thesis*, University of Sheffield, 1990.

[62] Saab, H.A. and Nethercot, D.A., 'Modelling Steel Frame Behaviour under Fire Conditions', *Engineering Structures*, **13** (4), 1991: pp 371-382.

[63] EI-Zanaty, M. H., and Murray, D. W., 'Inelastic Behaviour of Multistory Steel Frames ', *PhD Thesis*, University of Alberta, 1980.

[64] EI-Zanaty, M. H., and Murray, D. W., 'Nonlinear Finite element analysis of steel frames', *ASCE J. Struct. Div.*, **109** (2), 1983: pp 353-368.

[65] Najjar, S.R. and Burgess, I.W., 'A non-linear analysis for three-dimensional steel frames in fire conditions', *Engineering Structures*, **18** (1), 1996: pp 77-89.

[66] Shepherd, P., 'The Performance in Fire of Restrained Columns in Steel-Framed Construction', *PhD Thesis*, University of Sheffield, 1999.

[67] Huang, Z., Burgess, I.W. and Plank, R.J., 'Layered Slab Elements in modelling of Composite Frame Behaviour in Fire', *Second International Conference on Concrete under Severe Conditions*, Tromsö, Norway, 1998: pp 785-794.

[68] Huang, Z., Burgess, I.W. and Plank, R.J., 'Nonlinear Analysis of Reinforced Concrete Slabs Subjected to Fire', *ACI Structural Journal*, **96** (1), January-February 1999: pp 127-135.

[69] Zienkiewicz, O.C., and Taylor, R.L., *The Finite Element Method. Vol. 2: Solid and Fluid Mechanics Dynamics and Non-linearity*, Fourth Edition, McGraw-Hill Book Company, 1991.

[70] Yam L.C.P., Chapman J.C., 'The inelastic behaviour of simply supported composite beams of steel and concrete', *J. Instit. Civ. Engrs.*, **41** (1), 1968: pp 651-683.

[71] Yam L.C.P., Chapman J.C., 'The inelastic behaviour of continuous composite beams of steel and concrete', *J. Instit. Civ. Engrs.*, **53** (12), 1972: pp 487-501.

[72] Huang, Z., Burgess, I.W. and Plank, R.J., 'The influence of shear connectors on the behaviour of composite steel-framed buildings in Fire', *Journal of Constructional Steel Research*, **51**, 1999: pp 219-237.

[73] Bathe, K.-J. and Dvorkin, *Finite Element Procedures*, Prentice-Hall Inc., Englewood Cliffs, N.J., 1996.

[74] Huang, Z., Burgess, I.W. and Plank, R.J., 'Modelling Membrane Action of Concrete Slabs in Composite Buildings in Fire. Part I: Theoretical Development', Research Report DCSE/00/F/4, University of Sheffield, 2000.

[75] Huang, Z., Burgess, I.W. and Plank, R.J., 'Modelling Membrane Action of Concrete Slabs in Composite Buildings in Fire. Part II: Validations', Research Report DCSE/00/F/5, University of Sheffield, 2000.

[76] Cai, J., Burgess, I.W. and Plank, R.J., "The Effect of Push-out of Perimeter Building Columns on Their Survival in Fire", Paper 09.08, *Proc. International Conference on Steel Structures of the 2000's*, Istanbul, 2000: pp345-350

[77] Wang, C.M., Kitipornchai, S. and Ai-bermani, F.G.A., "Buckling of Columns: Allowance for Axial Shortening", *Research Report No. CE115*, Department of Civil Engineering, The University of Queensland, August 1990.

[78] Gere, James M. and Timoshenko, Stephen P., "Mechanics of Materials", Van Nostrand Reinhold, New York, 1972.

[79] Vlasov, V.Z., *'Thin-Walled Elastic Beams'*, Second Edition, Israel Program for Scientific Translations Ltd., 1963.

[80] Fung, Y.C., *'Foundations of Solid Mechanics'*, Prentice-Hall, Inc., Englewood Cliffs, N.J., 1965.

[81] Hartley Grandin, Jr., *'Fundamentals of the Finite Element method'*, Collier Macmillan Publishers, 1986.

[82] Zienkiewicz, O.C. and Taylor, R.L., *'The Finite Element Method'*, Vol. 1, Fourth Edition, McGraw-Hill Book Company, 1991.

[83] Ramberg W. and Osgood W., 'Description of Stress-Strain Curves by Three Parameters,' National Advisory Committee for Aeronautics, Technical Note#902, 1942.

[84] Gere, J.M. and Timoshenko, S.P., *'Mechanics of Materials'*, Third Edition, PWS-Kent Publishing Company, 1984.

[85] Huang, Z., Burgess, I.W. and Plank, R.J., 'Three-dimensional Analysis of Composite Steel-Framed Building in Fire', *J. Struct. Eng ASCE*, **126** (3), 2000: pp389-397.

[86] Rojahn, C., 'Large Deflections of Elastic Beams', Thesis for the Degree of Engineer, Stanford University, June 1968.

[87] Mills, G.M., *'Theory of Structures'*, Macmillan, London, 1963.

[88] Lennon, T., 'Full Scale Fire Test on a Slimdek Floor System,' BRE Client Report TCR 30/99, November 1998.

[89] Eurocode 3: Annex J: Beam-to-column connections, Commission of the European Communities, 1993.

[90] Huang, Z., Burgess, I.W. and Plank, R.J., 'Effective Stiffness Modelling of Composite Concrete Slabs in Fire', *Engineering Structures*, **22**, 2000: pp1133-1144.

[91] Cai, J., Burgess, I.W. and Plank, R.J., 'Modelling of Asymmetric Cross-section Members for Fire Conditions', *Research Report DCSE/00/F/6*, University of Sheffield, 2000. (currently submitted for publication--J. construct. Steel Research)

[92] Chen, W. and Atsuta, T., *Theory of beam-columns, Vol. 2: Space Behaviour and Design*. McGraw-Hill Book Company. 1977.

[93] Eurocode 4: *Design of Composite Steel and Concrete Structures. Part 1.2: Structural Fire Design*, CEN/TC250/SC4 N39, 1993.

[94] Huang, Z., and Platten, A., 'Nonlinear Finite Element Analysis of Planar Reinforced Concrete Members Subjected to Fires', *ACI Structural Journal*, **94** (3), May – June (1997): pp 272-282.

[95] Burgess, I.W., Ei-Rimawi, J.A. and Plank, R.J., 'A Secant Stiffness Approach to the Fire Analysis of Steel Beams', *J. Construct. Steel Research*, **11**, 1988: 105-120.

[96] Huang, Z., Platten, A. and Roberts, J., 'No-linear Finite Element Model to Predict Temperature Histories within Reinforced Concrete in Fires', *Building and Environment*, **31** (2), 1996: pp 109-118.

[97] Crisfield, M.A., *'Non-linear Finite Element Analysis of Solids and Structures'*, John Wiley & Sons Ltd, 1997.

APPENDIX A:

Post-processing Program for Extracting Data from Output File (S.1)

A.1 Introduction

Recently the structural analysis software VULCAN, which can perform non-linear analysis of three-dimensional frames and sub-frames subjected to fire conditions, has been developed at University of Sheffield. It will record analytical results for all the nodes and members, in the form of nodal displacements and member forces, into an output file (S.1) for the complete temperature heating history. However, the output file is normally very large, and the process of selecting certain data from it becomes extremely difficult, even though all the information required is in the output file. In order to solve this problem, two versions of a program have been written using C++ and standard Fortran languages. This program helps to extract the required data from the output file and then put them in a specially appointed file.

A.2 Programming

Since the output file is formed as numbers of blocks, and those blocks are recorded in the sequence of temperature, displacement and force, a program was written to find and output the required data by using and distinguishing these specified blocks. Two versions of the program, one written in Fortran code and the other in C++ code, are available for this work. The main flowchart used by the Fortran code is shown in Fig. A-1. However, the C++ version is more compact and efficient. Its base class, class **General_file**, is firstly created, and derived classes, such as classes **Displacement_file** and **Force_file**, can then be built by inheriting the attributes and methods from the base class. An Object Modelling Technique (OMT) style diagram

illustrates these relationships for classification hierarchy in Fig A-2. Both codes are listed in the following section.

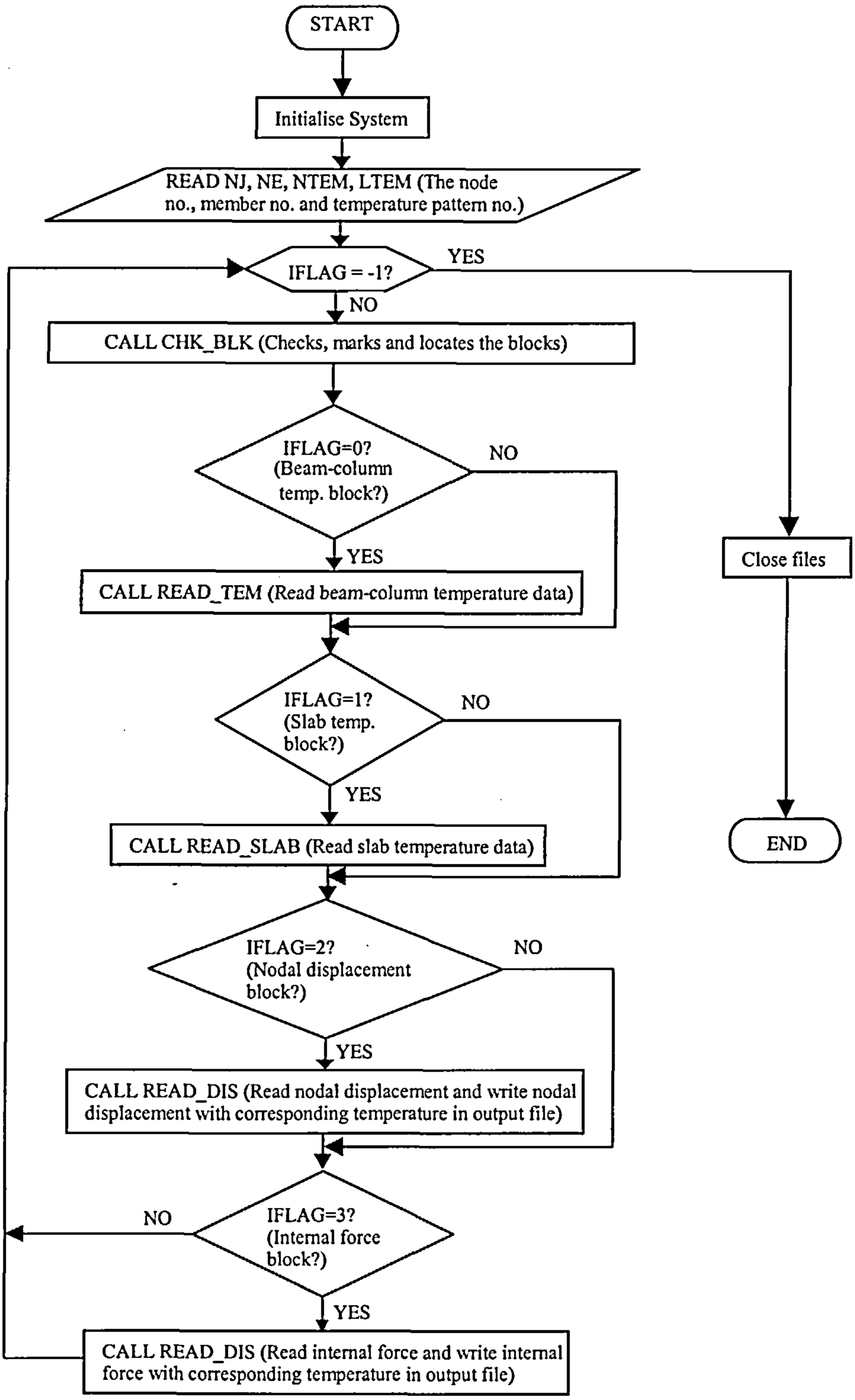

Fig. A-1 Flowchart for the main program used by Fortran code

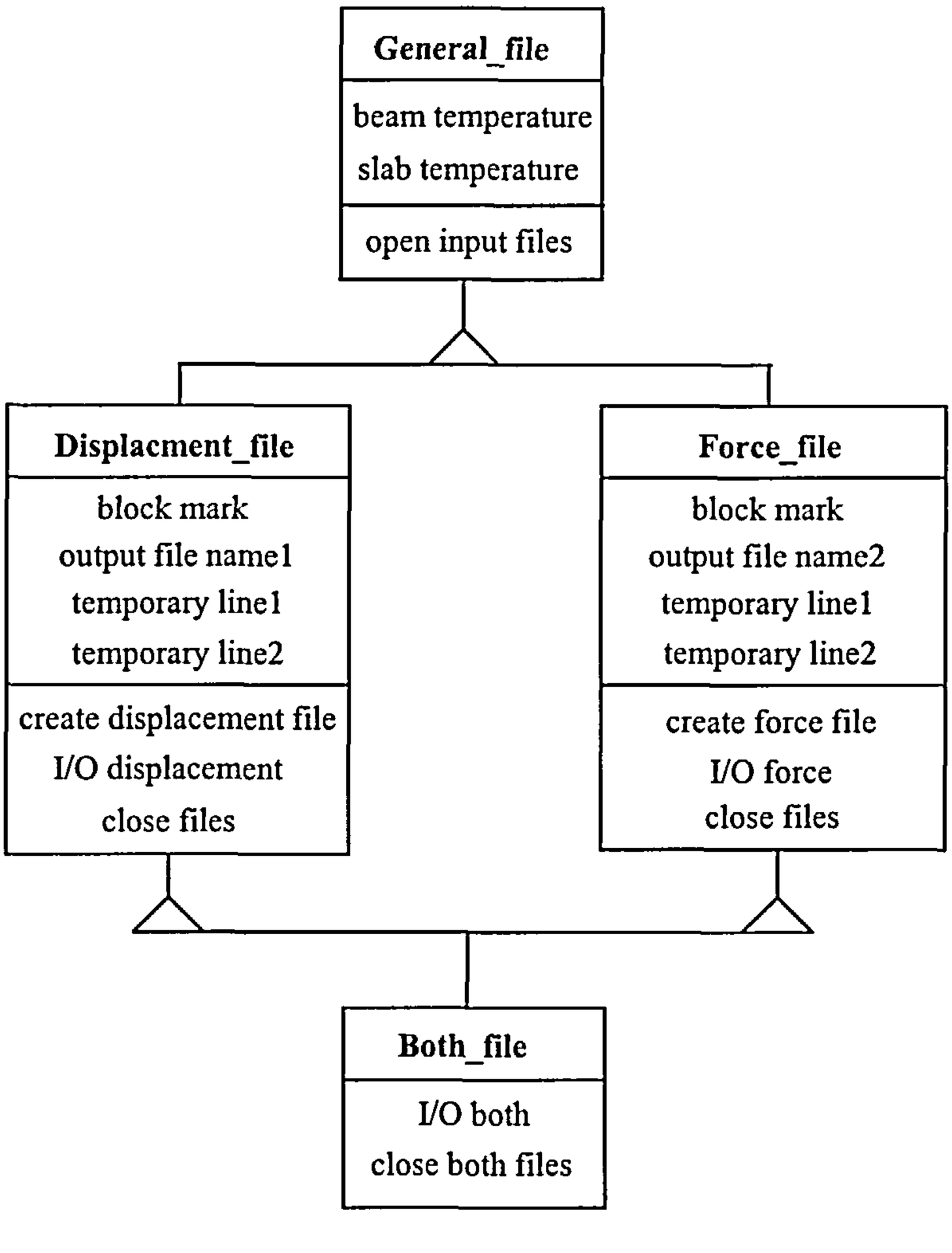

Fig. A-2 An OMT style diagram showing the classes, attributes and methods in the C++ program

A.3 Program list:

(a) Standard FORTRAN

```
C*************************************************************************
C                                                                        *
C  THIS PROGRAM READS THE OUTPUT FILE OF VULCAN ( S.1) AND OUTPUTS       *
C  DISPLACEMENTS AND/OR FORCES.                                          *
C                                                  by Jun Cai ---- 26/11/1998  *
C                                                                        *
C*************************************************************************
C
      IMPLICIT REAL*8(A-H,O-Z)
      IMPLICIT INTEGER*4(I-N)
      PARAMETER (ISHOWDEF=1)
      PARAMETER (LAYER1 = 1)
      PARAMETER (NUMTEM1 = 11)
      COMMON /TEMPO1/ NJ,NE,LAYER,NUMTEM,TEMP(13),TSLAB(100)

      CHARACTER*12 TEXT
```

```
C
C  OPEN FILES
      OPEN (UNIT=3, FILE='S.1', STATUS='OLD', IOSTAT=NERR)

C  IBEGIN ---- It is a flag to mark output file if  it is beginning.
      IBEGIN=1
C  SLAB PARAMETER, LTEM -- SLAB TEMPERATURE PATTERN.
      LTEM = 1
      LAYER = LAYER1
C  BEAM AND COLUMN PARAMETER,NTEM – TEMPERATURE PATTERN
      NTEM = 1
      NJ = 1
      NE = 1
      NUMTEM = NUMTEM1
      WRITE (*,'(/1X,A54,A21)')
     * 'Input: Node No.(DEF); Member No.(FRC); Temp. pattern; ',
     * '& Slab Temp. Pattern?'
      READ *, NJ,NE,NTEM,LTEM
C  Chooses output type: Nodal displacement (1) , Member force (2) , or Both (0).
      IF (NJ.EQ.0.AND.NE.EQ.0) THEN
         STOP 'No Nodal displacement or Member force output!'
      ELSEIF (NJ.EQ.0) THEN
         NTYPE=2
      ELSEIF (NE.EQ.0) THEN
         NTYPE=1
      ELSE
         NTYPE=0
      ENDIF
      IF (NTYPE.EQ.1) THEN
         DO I = 1,ISHOWDEF
            CALL MAKETEXT ('NODE',NJ,'DEF',TEXT)
            OPEN (UNIT=20+I,FILE=TEXT)
            WRITE (20+I,'(10X,A4,9X,2(A5,7X),A5,3X,3(A8,4X))') 'TEMP',
     *                 'Z(mm)','Y(mm)','X(mm)','Rx(rad.)','Ry(rad.)','Rz(rad.)'
         ENDDO
       ELSEIF (NTYPE.EQ.2) THEN
         DO I = 1,ISHOWDEF
            CALL MAKETEXT ('MEMB',NE,'FRC',TEXT)
            OPEN (UNIT=30+I,FILE=TEXT)
            WRITE (30+I,'(10X,A4,9X,3(A6,10X),3(A7,9X))') 'TEMP',
     *                'Fz(KN)','Fy(KN)','Fx(KN)','Mx(KNm)','My(KNm)','Mz(KNm)'
         ENDDO
       ELSE
         DO I = 1,ISHOWDEF
            CALL MAKETEXT ('NODE',NJ,'DEF',TEXT)
            OPEN (UNIT=20+I,FILE=TEXT)
            WRITE (20+I,'(10X,A4,9X,2(A5,7X),A5,3X,3(A8,4X))') 'TEMP',
     *                    'Z(mm)','Y(mm)','X(mm)','Rx(rad.)','Ry(rad.)','Rz(rad.)'
         ENDDO
         DO I = 1,ISHOWDEF
            CALL MAKETEXT ('MEMB',NE,'FRC',TEXT)
            OPEN (UNIT=30+I,FILE=TEXT)
            WRITE (30+I,'(10X,A4,9X,3(A6,10X),3(A7,9X))') 'TEMP',
     *                   'Fz(KN)','Fy(KN)','Fx(KN)','Mx(KNm)','My(KNm)','Mz(KNm)'
         ENDDO
       ENDIF

C   IFLAG ---- It is a flag for marking block.
      IFLAG=4
      DO WHILE (IFLAG.NE.-1)
```

```
C  Locates and marks block.
      CALL CHK_BLK(IFLAG)
      IF (IFLAG.EQ.0) THEN
C  If it is beam-column temp. block, put out temp.
         CALL READ_TEM(NTEM)
      ELSEIF (IFLAG.EQ.1) THEN
C  If it is slab temp. block, put out slab temp.
         CALL READ_SLAB(LTEM)
      ELSEIF ((IFLAG.EQ.2.AND.NTYPE.EQ.1).OR.
     *        (IFLAG.EQ.2.AND.NTYPE.EQ.0)) THEN
C  If it is nodal displacement, put out displacement.
         CALL READ_DIS()
      ELSEIF ((IFLAG.EQ.3.AND.NTYPE.EQ.2).OR.
     *        (IFLAG.EQ.3.AND.NTYPE.EQ.0)) THEN
C  If it is member force block, put out member force.
         CALL READ_FRC(IBEGIN)
      ENDIF
    ENDDO

    IF (NERR.NE.0) THEN
      PRINT *,'ERROR : S.1 File Failed To Open'
      STOP
    ENDIF

    CLOSE (3)
    IF (NTYPE.EQ.1) THEN
      CLOSE (21)
    ELSEIF (NTYPE.EQ.2) THEN
      CLOSE (31)
    ELSE
      CLOSE (21)
      CLOSE (31)
    ENDIF

    END
C  ***********************************************************
    SUBROUTINE CHK_BLK (IFLAG)
C
C  CHECKS AND MARKS BLOCK
C  ***********************************************************
    IMPLICIT REAL*8(A-H,O-Z)
    IMPLICIT INTEGER*4(I-N)
    CHARACTER*27 MARK

    IN=3
    READ (IN,'(A27)') MARK
    IF (MARK(1:14).EQ.'<TEMPERATURES>') THEN
      IFLAG=0
    ELSEIF (MARK(1:19).EQ.'<SLAB TEMPERATURES>') THEN
      IFLAG=1
    ELSEIF (MARK(1:21).EQ.'<NODAL DISPLACEMENTS>') THEN
      IFLAG=2
    ELSEIF (MARK(1:17).EQ.'<INTERNAL FORCES>') THEN
      IFLAG=3
    ELSEIF (MARK(1:10).EQ.' CPU TIME=') THEN
      WRITE(*,*) MARK
      IFLAG=-1
      WRITE(*,*) 'END'
    ELSE
      IFLAG=4
```

```
      ENDIF

      RETURN
      END
C     ***************************************************
      SUBROUTINE READ_TEM (NTEM)
C
C     READS TEMPERATURE DATA (if available)
C     ***************************************************
      IMPLICIT REAL*8(A-H,O-Z)
      IMPLICIT INTEGER*4(I-N)
      COMMON /TEMPO1/ NJ,NE,LAYER,NUMTEM,TEMP(13),TSLAB(100)
      IN=3
      IF (NTEM.EQ.0) THEN
        DO I=1,13
          TEMP(I)=0.0
        ENDDO
      ELSEIF (NTEM.EQ.1) THEN
        READ (IN,*) NO,(TEMP(I),I=1,NUMTEM)
      ELSE
        DO I=1,NTEM-1
          READ(IN,*)
        ENDDO
        READ (IN,*) NO,(TEMP(I),I=1,NUMTEM)
      ENDIF
      WRITE(*,*) TEMP(NUMTEM)

      RETURN
      END
C     ***************************************************
      SUBROUTINE READ_SLAB (LTEM)
C
C     READS SLAB TEMPERATURE DATA (if available)
C     ***************************************************
      IMPLICIT REAL*8(A-H,O-Z)
      IMPLICIT INTEGER*4(I-N)
      COMMON /TEMPO1/ NJ,NE,LAYER,NUMTEM,TEMP(13),TSLAB(100)

      IN=3
      IF (LTEM.EQ.0) THEN
        DO I=1,LAYER
          TSLAB(I)=0.0
        ENDDO
      ELSEIF (LTEM.EQ.1) THEN
        READ (IN,*) NO,(TSLAB(I),I=1,LAYER)
      ELSE
        DO I=1,LTEM-1
          READ(IN,*)
        ENDDO
        READ (IN,*) NO,(TSLAB(I),I=1,LAYER)
      ENDIF
      WRITE (*,*) TSLAB(LAYER)

      RETURN
      END
C     ***************************************************
      SUBROUTINE READ_DIS ()
C
C     READS NODAL DISPLACEMENTS DATA (if available).
```

```
C  ***************************************************
      IMPLICIT REAL*8(A-H,O-Z)
      IMPLICIT INTEGER*4(I-N)
      COMMON /TEMPO1/ NJ,NE,LAYER,NUMTEM,TEMP(13),TSLAB(100)
      DIMENSION DIS(11)

      IN=3
      IO=21
C     Locates the position of node.
      CALL LOCATE (NJ,IDEN)
      IF (IDEN.EQ.2) THEN
        READ (IN,*) NO,(DIS(I),I=1,11)
      IF (INT(TSLAB(LAYER)).EQ.0.AND.
     *      INT(TEMP(NUMTEM)).EQ.0) THEN
        STOP 'No temperature output!'
      ELSEIF (INT(TSLAB(LAYER)).EQ.0) THEN
        WRITE (IO,'(2X,A,3X,F9.3,6(2X,F10.4))') ' ',
     *        TEMP(NUMTEM),(DIS(I),I=1,3),DIS(4),DIS(5),DIS(9)
      ELSEIF (INT(TEMP(NUMTEM)).EQ.0) THEN
        WRITE (IO,'(1X,A4,1X,F9.3,6(2X,F10.4))') 'SLAB',
     *        TSLAB(LAYER),(DIS(I),I=1,3),DIS(4),DIS(5),DIS(9)
      ELSE
        WRITE (IO,'(F8.3,1X,F8.3,6(2X,F10.4))') TEMP(NUMTEM),
     *        TSLAB(LAYER),(DIS(I),I=1,3),DIS(4),DIS(5),DIS(9)
      ENDIF
     ENDIF
     WRITE(6,*) 'OUTPUT DISPLACEMENT'

     RETURN
     END
C  ***************************************************
      SUBROUTINE READ_FRC (IBEGIN)
C
C  READS INTERNAL FORCES data (if available)
C  ***************************************************
      IMPLICIT REAL*8(A-H,O-Z)
      IMPLICIT INTEGER*4(I-N)
      COMMON /TEMPO1/ NJ,NE,LAYER,NUMTEM,TEMP(13),TSLAB(100)
      DIMENSION FRC(11),SL_FRC(4,11),NO(4)

      IN=3
      IO=31
C     Locate the position of the member.
      CALL LOCATE(NE,IDEN)
C     If it is beam-column, put out.
      IF (IDEN.EQ.0) THEN
        READ (IN,*) NOO,NO1,(FRC(I),I=1,11)
        IF (INT(TEMP(NUMTEM)).EQ.0) THEN
          STOP 'No temperature output!'
        ENDIF
        WRITE (IO,'(2X,A,3X,F9.3,6(1X,F15.6))') ' ',TEMP(NUMTEM),
     *        (FRC(I)/1000,I=1,3),
     *        FRC(4)/1000000,FRC(5)/1000000,FRC(9)/1000000
        WRITE (*,*) 'OUTPUT BEAM-COLUMN INTERNAL FORCE'
C     If it is slab, put out.
      ELSEIF (IDEN.EQ.1) THEN
        READ (IN,*) NOO,NO(1),(SL_FRC(1,I),I=1,11)
        DO N=2,4
          READ (IN,*) NO(N),(SL_FRC(N,I),I=1,11)
        ENDDO
```

```
      IF (INT(TSLAB(LAYER)).EQ.0) THEN
          STOP 'No temperature output!'
      ENDIF
C   If it is at the head of output file, re-mark with the slab title.
      IF (IBEGIN.EQ.1) THEN
          IBEGIN=IBEGIN+1
          REWIND IO
          WRITE (IO,'(1X,A10,2X,A4)')
     *                    'SLAB TEMP.','NODE'
      ENDIF
      WRITE (IO,'(2X,F8.3,2X,I4,11(2X,F15.3))')
     *                TSLAB(LAYER),NO(1),(SL_FRC(1,I),I=1,11)
      DO M=2,4
          WRITE (IO,'(12X,I4,11(2X,F15.3))')
     *                NO(M),(SL_FRC(M,I),I=1,11)
      ENDDO
      WRITE (*,*) 'OUTPUT SLAB INTERNAL FORCE'
    ENDIF

    RETURN
    END
C   ***********************************************************
    SUBROUTINE LOCATE(NDAT,IDEN)
C
C   MARKS AND LOCATES THE POSITION OF DATA.
C   ***********************************************************
    IMPLICIT REAL*8(A-H,O-Z)
    IMPLICIT INTEGER*4(I-N)

    IN=3
    ICHK=0
    IDEN=10
    DO WHILE(ICHK.NE.1)
      CALL CHK_DAT(IDEN)
C   at end of a block.
      IF (IDEN.EQ.-1) THEN
          STOP 'Cannot find the node or member'
C    at the beginning of a beam-column internal force.
      ELSEIF (IDEN.EQ.0) THEN
          READ(IN,*) NUMDAT
          IF (NUMDAT.EQ.NDAT) THEN
              BACKSPACE IN
              ICHK=ICHK+1
          ELSE
              READ(IN,*)
          ENDIF
C   at the beginning of a slab internal force.
      ELSEIF (IDEN.EQ.1) THEN
          READ(IN,*) NUMDAT
          IF (NUMDAT.EQ.NDAT) THEN
              BACKSPACE IN
              ICHK=ICHK+1
          ELSE
              DO I=1,3
                  READ(IN,*)
              ENDDO
          ENDIF
C   at the beginning of a nodal displacement.
      ELSEIF (IDEN.EQ.2) THEN
          READ(IN,*) NUMDAT
```

```
      IF (NUMDAT.EQ.NDAT) THEN
         BACKSPACE IN
         ICHK=ICHK+1
      ENDIF
   ELSEIF (IDEN.EQ.3) THEN
      READ(IN,*)
   ENDIF
ENDDO

RETURN
END
C  ***********************************************************
   SUBROUTINE CHK_DAT(IDEN)
C
C  TO CHECK WHAT THE DATA IS.
C  ***********************************************************
   IMPLICIT REAL*8(A-H,O-Z)
   IMPLICIT INTEGER*4(I-N)
   CHARACTER*27 TEXTX1,TEXTX2,TEXTX3

   IN=3
   ISLAB=-10
   READ (IN,'(A27)') TEXTX1
   READ (IN,'(A27)') TEXTX2
   READ (IN,'(A27)') TEXTX3
   DO I=1,3
      BACKSPACE 3
   ENDDO
   IF (TEXTX1(1:1).EQ.'{') THEN
C  It is the end of block.
      IDEN = -1
   ELSEIF (TEXTX1(1:9).EQ.'        ') THEN
C  It is the title.
      IDEN = 3
   ELSEIF (TEXTX2(1:9).NE.'        ') THEN
C  It is displacement.
      IDEN = 2
   ELSEIF (TEXTX3(1:9).EQ.'        ') THEN
C  It is slab data of internal force block.
      IDEN = 1
   ELSE
C  It is beam data of internal force block.
      IDEN = 0
   ENDIF

   RETURN
   END
C  ***********************************************************
   SUBROUTINE MAKETEXT (TEXT1,NUMBER,TEXT2,TEXT)

C  CONVERTS AN INTEGER INTO A FILENAME
C  ***********************************************************
   IMPLICIT REAL*8(A-H,O-Z)
   IMPLICIT INTEGER*4(I-N)
   CHARACTER TEXT1*4, TEXT2*3, TEXT*12

   TEXT(1:4) = TEXT1
   TEXT(5:9) = '0000.'
   TEXT(10:12) = TEXT2
   IDEF = NUMBER
```

```
IF (IDEF.GT.999) THEN
   TEXT(5:5) = CHAR(48+INT(IDEF/1000))
   IDEF = IDEF - (1000*INT(IDEF/1000))
ENDIF
IF (IDEF.GT.99) THEN
   TEXT(6:6) = CHAR(48+INT(IDEF/100))
   IDEF = IDEF - (100*INT(IDEF/100))
ENDIF
IF (IDEF.GT.9) THEN
   TEXT(7:7) = CHAR(48+INT(IDEF/10))
   IDEF = IDEF - (10*INT(IDEF/10))
ENDIF
   TEXT(8:8) = CHAR(48+IDEF)
   RETURN
   END
```

(b) C++ version

```
/*************************************************************
*        This program reads the output file (S.1) produced by VULCAN        *
*        and outputs the required displacements and/or forces                *
*                                                    by Jun Cai              *
*************************************************************/
#include <iostream.h>
#include <stdio.h>
#include <string.h>
#include <stdlib.h>

//Converts integer into characters
char *intochar(int number1)
{
        int tem1;
        char *charater1 = "0000";

        if (number1 > 999)
        {
                tem1 = number1/1000;
                number1 = number1-1000*tem1;
                charater1[0] = 48+tem1;
        }
        if (number1 > 99)
        {
                tem1 = number1/100;
                number1 = number1-100*tem1;
                charater1[1] = 48+tem1;
        }
        if (number1 > 9)
        {
                tem1 = number1/10;
                number1 = number1-10*tem1;
                charater1[2] = 48+tem1;
        }
        charater1[3] = 48+number1;
        return charater1;
}

// Checks and marks block.
int check_block(FILE *in)
{
```

```
int block = 0;
char *mark1 = "<TEMPERATURES>", *mark2 = "<SLAB TEMPERATURES>";
char *mark3 = "<NODAL DISPLACEMENTS>";
char *mark4 = "<INTERNAL FORCES>", *mark5 = " CPU TIME=", mark[500];

do
{
        fgets(mark,500,in);
        if (strncmp(mark, mark1, 12) == 0)    block = 1;
        else if (strncmp(mark, mark2, 17) == 0) block = 2;
        else if (strncmp(mark, mark3, 19) == 0) block = 3;
        else if (strncmp(mark, mark4, 15) == 0) block = 4;
                else if (strncmp(mark, mark5, 7) == 0) block = 5;
        } while (block == 0);
        return block;
}

float read_temperature(FILE *in, int num1)
{
        int i,m;
        float templine;
        char string1[500];

        for (i = 1; i <= num1; i++)
        {
                fscanf(in, "%d %f", &m, &templine);
                fgets(string1, 500, in);
        }
        return templine;
}

void read_write(FILE *in, FILE *out, int flag1)
{
        int m;
        float line1[6];
        char string1[500];

        fscanf(in, "%d %f %f %f %f %f %*f %*f %*f %f", &m, &line1[0], &line1[1],
                &line1[2], &line1[3], &line1[4], &line1[5]);
        fgets(string1, 500, in);
        if (flag1 == 0) fprintf(out, "%11.4f%11.4f%11.4f%11.4f%11.4f%11.4f\n", line1[0],
                line1[1], line1[2], line1[3], line1[4], line1[5]);
        else if (flag1 == 1) fprintf(out,"%5d%11.4f%11.4f%11.4f%11.4f%11.4f%11.4f\n",
                m, line1[0]/1000, line1[1]/1000, line1[2]/1000, line1[3]/1000000,
                line1[4]/1000000, line1[5]/1000000);
}

class General_file
{
protected:
        int i,m;
        long offset;
        char *T1, *T2, string[500];
        FILE *in;
public:
        General_file();
        ~General_file() {cout << "Output is finished" << endl;}
        FILE *open_in();
};
General_file :: General_file()
```

```
{
        offset = 10L;
        T1 = "Beam Temp";
        T2 = "Slab Temp";
}
FILE *General_file :: open_in()
{
        if (in = fopen("s.1","r") == NULL)
        {
                printf("ERROR:S.1 File Failed To Open\n");
                void exit();
        }
        return in;
}
class Displacement_file: virtual public General_file
{
protected:
        int block;
        char name1[13];
        float line1, line2;
        FILE *out1;
public:
        FILE *open_displacement_out(char *njj, char *tem_name1, char *tem_name2);
        void IO_displacement(int nj, int ntem, int ltem);
        void close_displacement_file();
};
class Force_file: virtual public General_file
{
protected:
        int block;
        char name2[13], tem_string[11];
        float line1, line2;
        FILE *out2;
public:
        FILE *open_force_out(char *nee, char *tem_name1, char *tem_name2);
        void IO_force(int ne, int ntem, int ltem);
        void close_force_file();
};
class Both_file : public Displacement_file, public Force_file
{
public:
        void IO_both(int nj, int ne, int ntem, int ltem);
        void close_both_file();
};

FILE *Displacement_file :: open_displacement_out(char *njj, char*tem_name1,
                                                 char *tem_name2)
{
        strcpy (name1, tem_name1);
        strcat (name1, njj);
        strcat (name1, tem_name2);
        if (out1 = fopen(name1, "w") == NULL)
        {
                printf("ERROR: Output File Failed (.DEF) To Open\n");
                void exit();
        }
        fprintf(out1, "%10s%10s%11s%11s%11s%11s%11s%11s\n", T1, T2, "Z(mm)",
                "Y(mm)", "X(mm)", "Rx(rad)", "Ry(rad)", "Rz(rad)");
        return out1;
}
```

```
FILE *Force_file :: open_force_out(char *nee, char *tem_name1, char *tem_name2)
{
        strcpy (name2, tem_name1);
        strcat (name2, nee);
        strcat (name2, tem_name2);
        if (out2 = fopen(name2,"w") == NULL)
        {
                printf("ERROR: Output File (.FRC) Failed To Open\n");
                void exit();
        }
        fprintf(out2, "%10s%10s%5s%11s%11s%11s%11s%11s%11s\n", T1, T2, "Node",
                "Fz(kN)", "Fy(kN)", "Fx(kN)", "Mx(kNm)", "My(kNm)", "Mz(kNm)");
        return out2;
}

void Displacement_file :: IO_displacement(int nj, int ntem, int ltem)
{
        do
        {
                block = check_block(in);
                if (block == 1)
                {
                        line1 = read_temperature(in, ntem);
                        cout << "Beam tempertature=" << line1 << endl;
                }
                else if(block == 2)
                {
                        if (ltem > 0)
                        {
                                line2=read_temperature(in, ltem);
                                cout << "Slab tempertature=" << line2 << endl;
                        }
                }
                else if (block == 3)
                {
                        if (ltem > 0)  fprintf(out1, "%10.3f%10.3f", line1, line2);
                        else if (ltem == 0) fprintf(out1, "%10.3f%10s", line1, "****");
                        if (nj >= 2) for (i = 1; i <= (nj-1); i++) fgets(string, 500, in);
                        read_write(in, out1, 0);
                        cout << " Output displacement." << endl;
                }
        } while (block != 5);
}
void Force_file :: IO_force(int ne, int ntem, int ltem)
{
        do
        {
block = check_block(in);
if (block == 1)
{
        line1 = read_temperature(in, ntem);
        cout << "Beam tempertature=" << line1 << endl;
}
else if (block == 2)
{
        if (ltem > 0)
        {
                line2 = read_temperature(in, ltem);
                cout << "Slab tempertature=" << line2 << endl;
```

```
                }
        }
        else if (block == 4)
        {
                do
                {
                        fgets(tem_string, 10, in);
                        if (ne != atoi(tem_string)) fgets(string, 500, in);
                } while (ne != atoi(tem_string));
                if (ltem > 0)  fprintf(out2, "%10.3f%10.3f", line1, line2);
                else if (ltem == 0) fprintf(out2, "%10.3f%10s", line1, "****");
                read_write(in, out2, 1);
                        cout << " Output force." << endl;
                }
        } while (block != 5);
}
void Both_file :: IO_both(int nj, int ne, int ntem, int ltem)
{
        Displacement_file :: IO_displacement(nj, ntem, ltem);
        fseek(in, 0, 0);
        Force_file :: IO_force(ne, ntem, ltem);
}

void Displacement_file :: close_displacement_file()
{
        fclose(in);
        fclose(out1);
}
void Force_file :: close_force_file()
{
        fclose(in);
        fclose(out2);
}
void Both_file :: close_both_file()
{
        fclose(in);
        fclose(out1);
        fclose(out2);
}

void main()
{
        int nj, ne, ntem, ltem;
        int flag = 0;
        char *njj = "0000", *nee = "0000";
        Displacement_file file1;
        Force_file file2;
        Both_file file3;

cout << "Input: Node No.(DEF); Member No.(FRC); "
        << "Temp. Pattern; Slab Temp. Pattern." << endl
        << "(Separated by space)" << endl;
cin >> nj >> ne >> ntem >> ltem;
if (nj > 0  &&  ne > 0)
{
        strcpy(njj, intochar(nj));
        nee = intochar(ne);
        flag = 3;
}
else if (nj == 0  &&  ne > 0)
```

```
{
        nee = intochar(ne);
        flag = 2;
}
else if (nj > 0  &&  ne == 0)
{
        njj = intochar(nj);
        flag = 1;
}
else
{
        cout << "No node or member output!";
        void exit();
    }
    if (ntem < 0  ||  ltem < 0  ||  (ntem == 0  &&  ltem == 0))
    {
        cout << "No temperature output!";
        void exit();
    }
    switch(flag)
    {
// Output displacements.
        case 1:  file1.open_in();
                 file1.open_displacement_out(njj, "NODE", ".DEF");
                 file1.IO_displacement(nj, ntem, ltem);
                 file1.close_displacement_file();
                 break;
// Output forces.
        case 2:  file2.open_in();
                 file2.open_force_out(nee, "MEMB", ".FRC");
                 file2.IO_force(ne, ntem, ltem);
                 file2.close_force_file();
                 break;
// Output displacements and forces.
        case 3:  file3.open_in();
                 file3.open_displacement_out(njj, "NODE", ".DEF");
                 file3.open_force_out(nee, "MEMB", ".FRC");
                 file3.IO_both(nj, ne, ntem, ltem);
                 file3.close_both_file();
                 break;
    }
}
```

APPENDIX B:

Calculation of Torsion Constant "J "

The Torsion Constant, or St. Venant torsional constant, **J** can be defined as follows

(B.1) Thin-wall closed section:

For a thin walled hollow tube, the torsion constant **J** is

$$J = \frac{4A_m^2}{\int_0^{L_m} \frac{ds}{t}}$$

If the cross-section has constant thickness **t**, the torsion constant **J** can be simplified as

$$J = \frac{4tA_m^2}{L_m}$$

where,

$\mathbf{L_m}$ is the entire length of median line of the tube section,

$\mathbf{A_m}$ is the area enclosed by the median line of the tube section.

(B.2) Thin-wall open section:

For a section consisting of **n** flat, thin elements, the torsion constant **J** is

$$J = \frac{1}{3}\sum_{i=1}^{n} b_i t_i^3$$

where,

$\mathbf{b_i}$ is the width of the i-th plate element, and $\mathbf{t_i}$ is the thickness of the i-th plate element.

(B.3) Solid rectangular or square section:

For a solid rectangular or square section, the torsion constant **J** is

$$J = \beta b h^3$$

where,

b and **h** are the longer and shorter side respectively,

β is a factor dependent on the geometry, which is given by:

b/h	1	1.5	2	2.5	3	4	6	10	∞
β	0.141	0.196	0.229	0.249	0.263	0.281	0.299	0.312	0.333

(B.4) Composite member:

Within a composite member, we have the equations:

$$T = T_a + T_b \text{ and } \phi = \frac{T_a L}{G_a J_a} = \frac{T_b L}{G_b J_b}$$

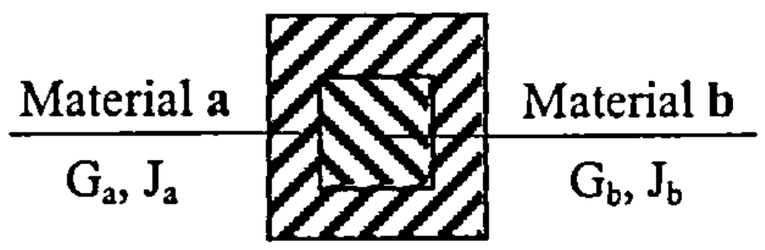

Composite cross-section

then producing

$$T_a = T\left(\frac{G_a J_a}{G_a J_a + G_b J_b}\right) \text{ and } T_b = T\left(\frac{G_b J_b}{G_a J_a + G_b J_b}\right),$$

the twisting angle becomes $\phi = \dfrac{TL}{G_a J_a + G_b J_b}$

Therefore, the total torsional rigidity **GJ** is

$$GJ_{total} = G_a J_a + G_b J_b$$

APPENDIX C:

VULCAN Input File Format

The format of the parts of the input file which have been used to input ASB beam, generalised beam and spring connector data, are described as follows:

<SECTION SIZES>

n, h(n), w(n), tf(n), tw(n)

{SECTION SIZES}

<SECTION SIZES (ASB)>

notal

no, h(no), wns1(no), wns2(no), tfns1(no), tfns1(no), tw(no) } *Repeat **notal** times for all ASB members*

.....

{SECTION SIZES (ASB)}

<MATERIAL PROPERTIES>

n, ey(n), ep(n), eult(n), ys(n), yps(n), ults(n)

{MATERIAL PROPERTIES}

.....

<CONCRETE BEAM>

numcon, nummat, nctemp, nctype, noutcb, icurve, icurve1

mmat, stley(1), stlep(1), stleult(1), stlys(1), conys(1) } *Repeat **nummat** times for all materials*

.....

To define a section {

mmo, nscon, nconh, nconb(1), nconb(2), ...

conh(1), conb(1,1), conb(1,2), ... } *Repeat **nconh** times*

conh(2), conb(2,1), conb(2,2), ...

.....

mmo1, nsteel

nsl, nsc, nstlf } *Repeat **nsteel** times*

.....

.....

*Repeat **numcon** times for all sections* }

{CONCRETE BEAM}

.....

<ROTATIONAL STIFFNESS>

nnsr

aconec, bconec, expoec, contemr } *Repeat **nnsr** times*

.....

{ROTATIONAL STIFFNESS}

<SEMI-RIGID>

nnsr1

semirigd } *Repeat **nnsr1** times*

.....

{SEMI-RIGID}

<AXIAL STIFFNESS>

nnsr2

axisrigd } *Repeat **nnsr2** times*

.....

{AXIAL STIFFNESS}

.....

<TEMPERATURE>

slab_no, 2, slab_temperature, …

.....

concrete_beam_no, 3, concrete_beam_temperature, …

.....

beam_no, 1, beam_temperature, …

.....

.....

slab_no, 0, slab_temperature, …

.....

concrete_beam_no, 0, concrete_beam_temperature, …

.....

beam_no, 0, beam_temperature, ...

{TEMPERATURE}

The notation used in the listing is as follows:

notal = total number of ASB beams;

h, wns1, wns2, tfns1, tfns1, tw = section properties for ASB beam;

numcon = total number of section types;

nummat = total number of material types;

nctemp = total number of different temperature patterns;

nctype = the temperature profile, where

= 1 uniform distribution,

= 7 to specify the temperature for each segment;

noutcb = a flag for output information control;

icurve, icurve1 = concrete tension and compression curve pattern;

stley, stlep, stleult, stlys = steel properties for concrete beam;

conys = compressive strength of concrete;

nscon = a section flag for torsion constant calculation, where

= 0 closed section,

= 1 opened section,

= 2 rectangular solid section,

= 3 concrete encased composite section,

= 4 concrete filled hollow section;

nconh, nconb = section division properties as illustrated in Fig. C-1;

conh, conb = the thickness and width of a segment as illustrated in Fig. C-1;

nsteel = number of segments which are not normal concrete (if 0 <**nsteel**< 10000),

= 0 if all segments are normal concrete,

= 10001 if all segments are lightweight concrete,

= 10002 if all segments are hot rolled steel bar,

= 10003 if all segments are cold worked steel bar,

= 10004~5 if all segments are steel;

nsl, nsc = the location of a segment;

nstlf = a flag to identify a segment material, where

= -1 none,

= 0 normal concrete,

= 1 light-weight concrete,

= 2 hot rolled steel bar,

= 3 cold worked steel bar,

= 4, 5 steel;

nnsr, nnsr1, nnsr2 = total number of temperature-dependent connectors, semi-rigid rotational connectors and axial spring connectors, respectively;

aconec, bconec, expoec = temperature-dependent factors which have been described by Ramberg-Osgood expression as **A**, **B**, **n**;

contemr = temperature reduction factor for connector;

semirigd = rotational stiffness;

axisrigd = axial spring stiffness.

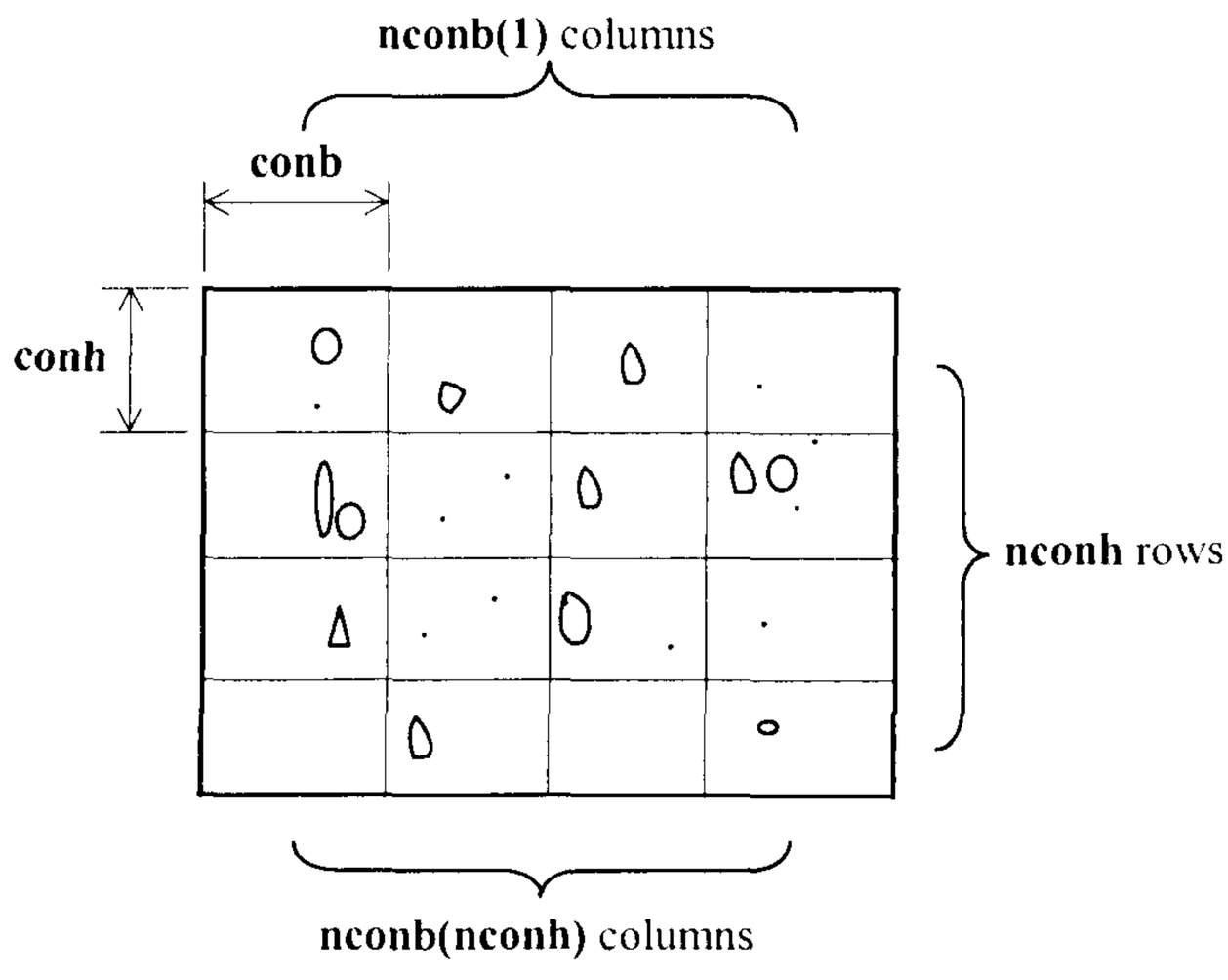

Fig. C-1 Section division for a concrete beam member